Transport and Shielding of Ionising Radiation

25 September 2015

Transport and Shielding of Ionising Radiation

Compiled by:

Johann van Rooyen
Radiation and Reactor Theory (RRT) Section
Building P-1900
Necsa (South African Nuclear Energy Corporation)
PO Box 582
PRETORIA
0001
SOUTH AFRICA

johann.vanrooyen@necsa.co.za
tjvanrooyen01@gmail.com

012-305-5029 (w)
082-829-8734 (m)
012-305-5166 (f)

Table of Contents

Chapter	Title	Page
1.	Introduction to Radiation Transport and Shielding	1
2.	Radiation Transport: The Boltzmann Transport Equation	49
3.	The Interaction of Ionising Radiation with Matter	60
4.	Radioactivity	174
5.	Sources of Ionising Radiation Frequently Encountered in Radiation Shielding Projects	219
6.	The Shielding of Neutrons	303
7.	The Shielding of Ionising Photons	340
8.	Complementary Shielding Materials; Principles of Shield Optimisation	368
9.	Monte Carlo Methods in Radiation Transport	378
10.	Introduction to the Practical Use of the Monte Carlo Radiation Transport Code, MCNP	386
11	Preparatory skills for using MCNP	401
12.	Case Studies: Radiation Shielding & Dose Distribution	405
13.	Case Studies: Nuclear Criticality Safety	490
14.	Case Studies: Nuclear Reactor Modelling	497
Annexure A	Reference Material	499
Annexure B	The Amount of Boron Carbide (B_4C) to Mix into Hydrogenous Shielding Materials	505

Annexure C
Approximate, Semi-Analytical Methods in Radiation Transport:
Point Kernel Integration.....515

Bibliography..... 530

Abbreviations

A.....Mass number of a nucleus, i.e. the number of protons Z plus the number of neutrons N in its nucleus.

A_0.....Total radionuclide inventory in a single fuel plate at EOL, i.e. 60 % burnup.

$A(t)$.....Activity of a radionuclide as a function of time t.

ANS.....American Nuclear Society

ANSI.....American National Standards Institute

AOI.....Area Of Interest

BOL.....Beginning Of Life (of a fuel assembly)

BTE.....Boltzmann Transport Equation

BTO.....Boltzmann Transport Operator

$\mathcal{C}$.....Centre-of-mass system of reference

CA.....Control Assembly

CL.....CentreLine

CLNT.....Coolant

CN.....Compound Nucleus

Cr.....Chromium

DEMIN.....Demineralisation system

DFN.....Delayed Fission Neutron

DR.....Dose Rate

ENDF/B-7.1.....Evaluated Nuclear Data File, type B, Release 7.1 (example).

EOL.....End Of Life (of a fuel assembly)

FA.....Fuel Assembly

Fe.....Iron

FP..... Fuel Plate

γ.....Photon, specifically a photon having an energy high enough to excite and ionise atoms and molecules. Ionising photon.

HWR..... Heavy Water Reactor

ID.....Inner Diameter

IR.....Inner Radius

$\mathcal{L}$..... The Laboratory system of reference

LANL..... Los Alamos National Laboratories, USA

LCS..... Low-Carbon Steel

LOCA.....Loss of Coolant Accident

LWR.....Light Water Reactor

MC.....Monte Carlo

MCNP..... Monte Carlo N-Particle transport code

Mn..... Manganese

Mo..... Molybdenum

MTR..... Materials Testing Reactor

n..... Neutron

NDR..... Neutron Dose Rate

Necsa..... South African Nuclear Energy Corporation

Ni.....Nickel

OD.....Outer Diameter

OR.....Outer Radius

ORIGEN.....**O**ak **R**idge **I**sotope **GEN**eration and Depletion Code

ORNL.....Oak Ridge National Laboratories, USA

p.....Ionising Photon

Pb.....Lead

PDR.....Photon Dose Rate

PE.....PolyEthylene

PFN.....Prompt Fission Neutron

PP.....PolyPropylene

PPS.....Photons Per Second

PWax.....Paraffin Wax

RCC.....Right Circular Cylinder

RPP.....Rectangular ParallelePiped.

RSICC.....Radiation Safety Information Computational Center (at ORNL, USA)

RTPT.....Radiation Transport

PVC.....PolyVinylChloride

SOI.....Structure-of-Interest

SS.....Stainless Steel

SS-304.....Stainless Steel type 304. An additional postfix designation L signifies a low-carbon alloy

SS-316.....Stainless Steel type 316 An additional postfix designation L signifies a low-carbon alloy

SSC.....Structures, Systems & Components

STP.....Standard Temperature and Pressure

TDR.....Total Dose Rate contributed by all ionising radiation types

TEM..... Tissue-Equivalent Material

TMF.....Tally Multiplication Factor

$TMF_{F1F2F4F5}$..... Tally Multiplication Factor for F1, F2, F4 and F5 type tallies in MCNP

TMF_{F6F8}..... Tally Multiplication Factor for F6 and F8 type tallies in MCNP

TPT.....(Radiation) Transport

1-D.....One-dimensional radiation transport, i.e. material variation & specification is only allowed in 1 of the 3 spatial variables

2-D.....Two-dimensional radiation transport, i.e. material variation & specification is allowed in 2 of the 3 spatial variables

3-D.....Three-dimensional radiation transport, i.e. material variation & specification is allowed in all 3 of the 3 spatial variables

Values of Fundamental Physical Constants

The values of the Fundamental Physical Constants are updated at least once per decade; the latest set of values are listed in
http://physics.nist.gov/PhysRefData/

The MathCAD reference worksheet,
C:\REFERENCE\Library of Constants and Units and Functions.xmcd
which is referenced by all MathCAD calculations presented in these lecture notes, is updated by the author at least once every decade to reflect the latest recommended set of values of the fundamental physical constants. At present (2015), the 2014 set of Fundamental Physical Constants are used in this book.

When solving physics, chemistry and engineering problems, always use the latest, recommended set of values of the fundamental physical constants. For accurate calculations, do NOT mix values from different evaluated sets, because the values within a given evaluated set are carefully "tuned" to each other by regression techniques that will minimise overall calculational errors.

The NIST (US National Institute of Standards and Technology) recently issued the following statement early in 2015:

> There will be an adjustment of the Fundamental Physics Constants to provide the values for a revision of the International System of Units (the SI system) in 2018. The 2018 CODATA adjustment of the fundamental constants will be based on the revised SI System, which will significantly affect the uncertainties of many constants.

Scientists and engineers will have to update the values of the Fundamental Physics Constants that they use, towards the end of 2018. Updated, revised values are released at least every 5 years on average.

Prescribed books

At present (2015) there are no "ideal" textbooks on the subject of the contemporary practice of the discipline of radiation shielding. The following textbook is a useful reference work, but is, alas, not suited as a stand-alone text for mastering the art of practical radiation shield design:

SHULTIS KJ & FAW, ER. 2000. *Radiation Shielding.* American Nuclear Society.

Chapter 1: Introduction to Radiation Transport and Shielding

1.1 Radiation safety system

The concept of a radiation safety system is developed here on the basis of a {challenge : response}-model.

Challenges

- Ionising radiation presents a health risk;
- Deontological ethics: The duty to protect people & the environment from excessive radiation health risk;
- Radiation protection recommendations by the ICRP; radiation protection standards set by the IAEA;
- National radiation protection legislation;
- The "international best practice" principle;
- Ionising radiation and radioactivity are emotional subjects that are politically sensitive — people fear invisible hazards.

The **response** to this challenge: A ***radiation safety system.***

1.1.1 Three pillars of a radiation safety system

A radiation protection programme must be based on:

- An engineered radiation safety system;
- Management controls;
- Fostering a safety culture in an organisation.

1.1.2 Engineered radiation safety system

The more intense and dangerous the sources of ionising radiation that are used, the higher the reliance on engineered radiation safety systems must be. The two pillars of engineered radiation safety systems are:

- A radiation containment system;

- An access control system to control access to radiation areas, e.g. prevent human entry into radiologically dangerous areas.

Radiation containment system

A radiation containment system has passive and active features:

- Passive radiation containment system features: Fixed/static radiation shielding, e.g. thick concrete walls, entrance labyrinths, shielding doors, are typically used to reduce dose rates to acceptable levels in areas where free access is permitted.

- Active radiation containment system features: Source reduction in the event of the detection of excessive radiation levels or other unsafe conditions.
  Example at a particle accelerator facility: If installed radiation measuring instruments detect unacceptably high radiation levels in an irradiation vault that is not formally cleared, intense radiation sources are shut down or moved to shielded positions; movable shielding structures such as plug-doors and neutron shutters can also be moved into place.
  Example at a nuclear reactor facility: When safe radiation levels are exceeded, a reactor may be scrammed.

Access control system

The function of an access control system is to prevent unauthorised people from entering a radiation area at all, and to prevent operating personnel, who are radiation workers, from ever being in a radiation area where unsafe, high dose rates prevail. A safety interlock system and area clearance system is vital wherever strong sources are used. In addition, there must be an independent radiation level measurement system, with effective visual and audible warning measures such as strobe lights and loud audible alarms. Furthermore, personnel that enter potentially high dose rate areas, must carry a calibrated, check-source-tested dose rate meter as well as wear Electronic Personal Dosimeters (EPDs). This gives defence-in-depth — multiple, independent, redundant safety systems having multiple catch-nets.

Note: The two other facets of a radiation safety system — management controls and safety culture — fall beyond the scope of this course.

1.2 A criterion for judging the efficacy of radiation shielding: Dose attenuation factor

For a given application, a radiation shield has a *dose attenuation factor* (DAF), defined as

$$\mathrm{DAF} = \frac{\text{Transmitted dose rate with shield in place}}{\text{Transmitted dose rate without shield in place}} \tag{1.1}$$

If a shield has a DAF of $1/150$, it means that we gain a factor 150 by having the shield in position, i.e. the shield decreases the dose rate to a value $1/150$ of what the radiation level would have been without the shield.

Note that it is usually clearer to express the DAF as a fraction $\frac{1}{n}$ than as a decimal number.

Assignment 1.1

1. The total dose rate 100 cm from an unshielded source of neutrons and ionising photons, is measured to be 1.3×10^{-2} Sv/h. Because this dose rate is dangerously high, a biological shield is constructed and interposed between source and detector. The new dose rate is measured as 1.7×10^{-6} Sv/h. Calculate the dose attenuation factor (DAF) and express it as a fraction $\frac{1}{n}$.

1.3 Educational approach

Most textbooks on the topic of radiation transport derive, with great travail of soul, a bewildering succession of hundreds to thousands of simplified and hence highly approximate, analytical formulas to facilitate "approximate hand-calculations" of radiation transport problems. In end-of-chapter exercises, students are then required to use this plethora of approximate and rather inaccurate analytical expressions, to solve a large variety of problems using manual calculations, in order to gain experience in the subject and to develop a "feeling" for radiation transport.

The real-life situation in the 21st century, is that shielding analysts use powerful codes running on powerful digital computers to solve radiation transport, nuclear criticality safety and shielding problems. The practicing shielding analyst therefore requires the following knowledge and skills:

- A broad, encyclopedic mastery of the ***scientific concepts*** that govern ionising radiation emission, radiation transport and radiation dosimetry;
- The ability to model radiation transport problems using a range of state-of-the-art ***radiation transport codes,*** e.g. the SCALE system and MCNP.

The details of the numerical techniques used in radiation transport codes, belong to the subject of numerical analysis; because this is a course in *applied radiation physics* or *nuclear engineering,* we shall not delve deeply into the detail of the numerical techniques. Because (1) powerful and accurate radiation transport codes are available, and (2) nuclear safety regulators only accept safety cases and licensing applications if state-of-the-art codes were used, it is not considered meaningful to teach students a series of approximate analytical calculational techniques. The methodology followed in this text is therefore as follows:

- To guide the student to understand and become skilled in the foundational concepts of the transport of ionising radiation. A conceptual mastery of the subject is required to guide the practicing shielding analyst.

- To present a clear formulation of the physics principles underlying radiation transport and the characteristic shielding abilities of important materials;

- To expose students to radiation transport codes used internationally to prepare *safety cases* and *license applications* to Nuclear Safety Regulators.

- To teach the student to build up a "toolbox" of calculational techniques, using e.g. MathCAD, Maple, MatLAB, Mathematica, Fortran code, etc. Such a calculational "toolbox" is one mark of a professional scientist. The moment an important technical topic is mastered, the calculations involved in the analysis should be coded in e.g. MathCAD and be added to the scientists' calculational "toolbox." If this essential "life-skill" and "habit of highly effective scientists" is neglected, the scientist may possibly struggle to develop into a professional, fast & accurate worker.

Nuclear scientists who develop radiation transport codes, of course need to master the numerical techniques required to solve radiation transport problems, in detail. This course does not directly address this field of endeavour.

1.4 The transport of ionising radiation

1.4.1 Ionising radiation

Ionising radiation has energy quanta large enough to cause ionisation and excitation in matter. Ionisation is the removal of electrons from atoms or molecules, leading to the formation of ion pairs. Excitation is the excitation of electrons to higher energy levels in atoms and molecules.

1.4.2 Directly ionising and indirectly ionising radiation

Ionising radiation may be classified as (1) directly ionising and (2) indirectly ionising.

Directly ionising radiations are charged particles, e.g. electrons, positrons, protons, alpha-particles and heavy ions, having sufficient energy to ionise or excite atoms and molecules.

Indirectly ionising radiations are uncharged particles, e.g. ionising photons and neutrons, that set in motion directly ionising radiation, i.e. charged particles. Ionising photons produce secondary electrons via three chief mechanisms: The interaction of the ionising photon with an atom may e.g. cause the photo-electric emission of electrons, knock out electrons via Compton scattering, and produce electron-positron pairs via pair production. All these ionising photon interactions set in motion secondary charged particles, which subsequently deposit their energy in matter. Neutrons are also indirectly ionising — neutron scattering produces recoiling nuclei which are stripped of some or all of their electrons and then deposit their kinetic energy by high-LET ionisation, i.e. the linear density of their energy deposition, expressed in a

convenient unit such as $\frac{\text{keV}}{\mu\text{m}}$, is quite high on account of their high electrical charge and their relatively slow movement. Neutrons can also set in motion charged particles by producing nuclear reactions characterised by the presence of a charged particle in the exit channel. It is evident that neutron-induced nuclear reactions such as (n, p) (n, α), (n, d), (n, t) and (n, np) reactions, all produce charged particles in the exit channel. The result of neutron interactions that produce a charged particle, is that part of the energy of the incident neutron is transferred to charged particles in the exit channel. When a neutron interaction creates an ionising photon in the exit channel, the photon will eventually interact to release electrons, and these light charged particles will deposit the photon energy in matter. The charged particles released by neutron interactions interact far more intensely than the uncharged parent particle, and will transfer their energy to the medium within a distance that is far shorter than the mean free path of the uncharged neutron.

We see that neutral particles such as neutrons and photons are indirectly ionising: they release charged particles in matter, and energy deposition is then via these charged particles, which directly cause ionisation. One can state that indirectly ionising particles such as neutrons and ionising photons effectively deposit their energy "by proxy" via charged particles which they release in matter.

Indirectly ionising radiation types have long ranges in matter and substantial thicknesses of shielding material may be required to attenuate indirectly ionising particles such as neutrons and ionising photons to acceptably low levels. In contrast, directly ionising radiation, i.e. charged particles, interact intensely and are therefore easily attenuated — they continually interact with their environment via the electromagnetic force. The electron density in solids and liquids is quite high, and every ionisation event requires an ionisation energy ranging between e.g. 35 eV and 200 eV, and therefore decreases the energy of the charged particle by that amount, step by step. The range in typical solids and liquids of charged particles, is typically in the order of a few μm to a few cm. As a result of their short ranges, the incident, i.e. primary charged particles usually present little difficulty to a shield designer. In some reactions, however, directly ionising, short-ranged charged particles produce secondary uncharged types of ionising radiation such as neutrons and ionising photons, which are far more penetrating than the primary charged particles. Examples are (α, n) reactions as well as the production of *bremsstrahlung* x-rays when electrons are decelerated in matter, as well as the production of neutrons in target materials hit by e.g. a beam of high-energy protons at a particle accelerator facility. Example: A 100 μA, 66 MeV incident proton beam is fully stopped in only 0.8 cm Cu, but concrete shielding walls that are at least 300 cm thick are required to attenuate the secondary neutrons and ionising photons generated by the proton beam by e.g. (p, Xn) nuclear reactions.

1.4.3 Kerma — the sum of the initial kinetic energies of all the charged particles liberated by uncharged ionising radiation

Kerma is the sum of the initial kinetic energies of all the charged particles liberated by uncharged ionising radiation (i.e., indirectly ionising radiation such as photons and neutrons) in a sample of matter, divided by the mass of the sample. It is defined by the quotient $\frac{d\epsilon}{dm}$.

Kerma dose is different from absorbed dose. Whilst roughly equal at low energies, kerma is much higher than absorbed dose at higher energies, because some of the energy escapes from the absorbing volume in the form of bremsstrahlung photons or fast moving electrons.

The unit for kerma is $\frac{\text{joule}}{\text{kg}}$ i.e. gray (Gy), which is the same as for absorbed dose.

The word "kerma" originally was an acronym for "kinetic energy released in material" or "kinetic energy released in matter." It is, however, better to think of kerma as an initialism for ***K****inetic* ***E****nergy* ***R****eleased in matter per unit* ***MA****ss.*

The energy of an ionising photon is transferred to matter in a two-step process. First, energy is transferred to charged particles in the medium through various photon interactions (e.g. photoelectric effect, Compton scattering and pair production). Next, these secondary charged particles transfer the energy to the medium through atomic excitation and ionisations.

For low energy ionising photons, kerma is numerically approximately the same as absorbed dose. However, for higher energy photons it starts to differ, because energetic electrons produced by the photon interaction may deposit some of their energy outside the region of interest, or some may lose their energy through bremsstrahlung that escape the region of interest. In this case, kerma will be larger than absorbed dose. For low x-ray energies, there is usually a negligible difference between kerma and absorbed dose.

Kerma K has two parts to it: Collision kerma k_{col} and radiative kerma k_{rad},

$$K = k_{\text{col}} + k_{\text{rad}}.$$

Collision kerma k_{col} results in the production of electrons that dissipate their energy as ionisation and excitation by interactions between the charged particle and the atomic electrons. Radiative kerma k_{rad} results in the production of bremsstrahlung ionising photons via interaction between the charged particle and the atomic nuclei, but can also result from annihilation.

Collision kerma k_{col} is usually expressed as

$$k_{\text{col}} = K(1 - g)$$

where g is the average fraction of energy transferred to electrons that is lost through bremsstrahlung.

The kerma concept is primarily important in the **experimental detection of ionising radiation.** The radiation transport code MCNP calculates the absorbed dose, and not kerma.

1.4.4 The purpose of radiation shield design calculations

A typical purpose of radiation shield design calculations is to design shields that can attenuate the fluence-rate of all ionising radiations that are harmful to humans and sensitive materials, to levels low enough so that *response* rates — e.g. absorbed dose rates, effective dose rates, damage rates, activation rates, etc., — on the "personnel side" or "detector/receiver side" of the

shield are lower than acceptable limiting values, which have been derived from e.g. (1) dose limits, dose constraints and (2) maximum annual occupancy times.

Response rates R can be expressed mathematically as functionals, conveniently written using inner-product notation, $R = \langle \phi, \mathfrak{R} \rangle$, where $\mathfrak{R}$ denotes the response function, ϕ the fluence-rate and the inner-product brackets $\langle \rangle$ denote integration over the continuous variables and summation over the discrete variables of phase-space.

1.4.5 The source-term

The first step in shield design, is to determine the type, energies and yield of the primary ionising radiation originating within the source volume. We have to know the properties of these particles, specifically their *energy spectrum, production rate* (and, seldomly, the dependence of emission on the polar angle θ). (Note that the azimuthal angle φ is only of importance in the case of polarised particle beams.) Secondly, we should know the energy dependence of the dosimetric response function for every type of radiation and, in the event of material damage studies, for every type of material. Thirdly, we need to have a good grasp of the laws of nature which control the attenuation of these types of radiation. This is very important in the initial conceptual design of shields. The shield designer uses his or her "broad, encyclopædic grasp" of the principles of radiation shielding to choose an initial shield configuration, i.e. the choice of shield materials and the placement of these materials, and then uses numerical radiation transport methods to perform detailed parametric shield optimisation studies.

Powerful radiation transport codes and their associated cross-section libraries contain an immense amount of physics, and this fact radically simplifies the generation of the source-term required for transport calculations. Consider the case of a 66 MeV proton beam incident upon a radionuclide production target. Before the advent of codes such as MCNP6, one had to use experimentally measured neutron and photon yields as well as the neutron and ionising photon spectra at different angles from the incident direction, to construct an approximate source-term. Numerical integration over the energy partition of the multigroup cross-section library that was used, was necessary to generate this source-term in multigroup format. With the code MCNP6, source term specification has become much simpler — the shielding analyst simply models the primary beam of incident, mono-energetic, mono-directional protons. The code MCNP6 uses cross-section tables and nuclear models that contain (p, nX) and $(p, \gamma X)$ cross-sections, i.e. the cross-sections for nuclear reactions with protons in the entrance channel and neutrons and ionising photons in the exit channel. That is, the production of neutrons and ionising photons are modelled by the code, using information in cross-section libraries and in nuclear reaction models. Whenever tabular cross-section data is not available, nuclear models are used by MCNP6. In this way, the production of secondary types of ionising radiation such as neutrons and ionising photons, with accurate energy spectra and angular distributions, are accounted for seamlessly, and these particles are then transported by the code.

1.4.6 Absorbed dose

The effects of ionising radiation on matter are initiated by processes in which atoms and molecules of the medium are ionised or excited. Over a wide range of conditions, it is an

excellent approximation to assume that the average number of ionisations and excitations is proportional to the amount of energy imparted to the medium by ionising radiation in the volume of interest. The **absorbed dose, that is, the average amount of energy imparted to the medium per unit mass,** is therefore of central importance for the production of radiation effects, and the calculation of absorbed-dose distributions in irradiated media is the focus of interest of the present course material. It should be pointed out, however, that even though absorbed dose is useful as an index relating absorbed energy to radiation effects, it is almost never sufficient; it may have to be supplemented by other information, such as the distributions of the amounts of energy imparted to small sites, the correlation of the amounts of energy imparted to adjacent sites, and so on. Such quantities are termed stochastic quantities. Unless otherwise stated, all quantities considered here, are non-stochastic.

Stochastic quantities are characterised by probability distribution functions, can be measured accurately, are determined in an infinitesimal volume and are calculated using Monte Carlo simulation methods. Many non-stochastic quantities used in radiation protection and dosimetry are expectation values of stochastic quantities. These non-stochastic quantities are continuous, differentiable point functions of time and space, and may be calculated by deterministic radiation transport techniques. (A more detailed discussion concerning stochastic quantities is given in ICRU Report 33 (ICRU, 1980).)

The absorbed dose, D, is defined (ICRU, Report 33) as the quotient of $d\bar{\epsilon}$ by dm:

$$D = \frac{d\bar{\epsilon}}{dm} \tag{1.2}$$

where $d\bar{\epsilon}$ is the *mean* energy imparted by ionising radiation to matter of mass dm contained in an infinitesimal volume. The SI unit of absorbed dose is joule per kg, and its special name is the gray.

The absorbed dose $D(\vec{\boldsymbol{x}})$ is a function of the spatial variable $\vec{\boldsymbol{x}}$, and this spatial variation is termed the dose distribution. A second important aspect refers to the temporal pattern of dose accumulation. The *absorbed-dose rate* is defined as

$$\dot{D}(\vec{\boldsymbol{x}}, t) = \frac{dD(\vec{\boldsymbol{x}}, t)}{dt} \tag{1.3}$$

and its SI unit is gray per hour, written as Gy/h.

1.4.7 Dose measurement and dose calculation

The absorbed dose of ionising radiation may be determined by two entirely different methods: measurement and calculation.

Measurement has the decided advantage in that it requires — at least in principle — only one auxiliary quantity — the calibration factor of the instrument employed. The construction of the instrument from materials of suitable atomic composition can largely obviate even the need to identify the incident radiation. The experimental determination is also often simpler and more rapid than a calculation.

Calculations, on the other hand, usually require extensive subsidiary information, including configuration of sources, the configuration and atomic composition of matter between sources and the points of interest, and corresponding data for objects that are merely in the vicinity of source and receptor if they produce significant scattered or secondary radiation. Information is also needed on the nature and energy distributions of the primary radiations, on the cross sections for the production of secondary radiation (or on the magnitude of material constants such as attenuation coefficients and stopping powers, if we employ simplified transport models). These must again be known for each type and as a function of energy for all significant primary and secondary radiations. Errors or uncertainties in any of the variables in this lengthy database can result in incorrect dose assessment; further inaccuracies may also be caused by numerous simplifications that must often be made. Even with such simplifications, the calculations tend to be complex.

Theoretical assessments are nevertheless essential in a number of cases:

- Measurements can be made only when dose is actually received. Retrospective determinations of doses that have been received, or evaluations of the doses to be received, as well as the design of shields that have not been built yet, require calculations.

- Calculations are also necessary when it is impractical to place a dosimeter at the point of interest as in most instances of radiotherapy or the dosimetry of internal emitters.

- Calculations can be performed when the required spatial resolution cannot be attained with a physical device or when radiation intensities are too high or too low to permit measurements with available equipment.

1.4.8 Dose calculations: Deterministic and Stochastic approaches

The calculation of dose and dose rates require a description of the radiation fields in terms of sources of particles, of the physics of their interactions, and of receptors i.e. radiation detectors. With this description, one is able to predict the flow of energy in and out of volumes of interest, and to calculate the dose.

Two general methods, not always equivalent, are used in radiation transport calculations. From the viewpoint of deterministic radiation transport techniques, the transport of neutrons and photons are described by the linear Boltzmann transport equation (BTE). As a consequence of the mathematical complexity of the BTE, it can not be solved analytically for problems of practical interest; we have to resort to numerical techniques. The two rigorous generic methods for radiation transport calculations, then, are (1) deterministic solutions of a transport equation such as the Boltzmann transport equation, and (2) Monte Carlo simulations of individual particle tracks and interactions.

In the so-called ***deterministic*** approach to radiation transport, the radiation field is characterised by functions describing the phase-space density of particles at a given point and its distributions with respect to energy, angle and particle type. The term “deterministic” refers to the fact that these density functions (or their distributions) are subject to mathematical

laws termed *transport equations,* and, therefore, given the sources, boundary conditions and interaction coefficients, one can calculate their values at each point and time.

In the second approach, the particle trajectories are simulated individually according to the stochastics of the physical interactions. The treatment is in terms of probability distributions, for instance the probability that a given number of particles (in an energy and solid angle interval) traverse an element of area. The ***stochastic*** approach (e.g. a Monte Carlo method) allows the calculation of any deterministic quantity as the average of the corresponding stochastic one over its probability distribution, (although, of course, a large body of additional information is available). The simulation of particle trajectories is performed with Monte-Carlo techniques.

1.4.9 Particle density in phase space

The central problem of neutron/photon radiation transport can be stated quite simply. It is to compute, for any time t, the characteristics of the free-neutron and ionising photon population throughout an extended region of space containing an arbitrary, but known, mixture of materials. Specifically we wish to know the number of radiation quanta in any infinitesimal volume dV around the point $\vec{\boldsymbol{x}}$ that have kinetic energies between E and $E + dE$ and are travelling in directions within an infinitesimal angle $d\Omega$ of a fixed direction specified by the unit vector $\widehat{\boldsymbol{\Omega}}$.

Note: The solid angle is defined as

$$\frac{\text{Subtended area on surface of sphere}}{\text{radius}^2}.$$

Working in a spherical co-ordinate system, with polar angle θ and azimuthal angle φ, the infinitesimal solid angle

$$d\Omega = \frac{(r\sin(\theta)\,d\varphi)(r\,d\theta)}{r^2} = \sin\theta\,d\theta\,d\varphi.$$

The unit vector $\widehat{\boldsymbol{\Omega}} = \frac{\vec{v}}{v}$, where $\vec{\boldsymbol{v}}$ is the velocity of the particle and v is the magnitude of $\vec{\boldsymbol{v}}$.

If this number of radiation quanta is known, we can use basic cross-section and dosimetry data (obtained experimentally and theoretically in nuclear physics, atomic physics, radiobiology & radio-epidemiology) to predict the rates at which all possible nuclear and atomic reactions will take place throughout the region, and we would be able to calculate reaction rates, heat release rates, dose rates, displacements-per-atom-rates, etc. at any given time at any location in the region.

The problem of determining the characteristics of the free particle population is greatly simplified by the fact that, in most cases of interest, that population is so large that it can be treated as a fluid. Hence, just as with an ordinary gas, we can speak of the *particle "density in phase space"* and do not have to face the problem of following the life history of each individual radiation quantum. The quantity of prime interest then becomes the particle density distribution in phase space, $M(\vec{\boldsymbol{x}}, \widehat{\boldsymbol{\Omega}}, E, t)$, which is defined by the statement that $M(\vec{\boldsymbol{x}}, \widehat{\boldsymbol{\Omega}}, E, t)\,dV\,dE\,d\Omega$ is the (expected) number of *free* neutrons/photons which, at time t, are located in an infinitesimal volume element dV containing the point $\vec{\boldsymbol{x}}$, have kinetic energy

in an infinitesimal energy range dE about E, and are travelling in a direction contained in the infinitesimal solid angle cone of directions dΩ about the unit vector $\widehat{\boldsymbol{\Omega}}$.

As we shall only concern ourselves with steady-state, i.e. time-independent, radiation fields[1], we shall henceforth drop the time variable t. Let $M(\vec{\boldsymbol{x}}, \widehat{\boldsymbol{\Omega}}, E)$ be the steady-state *particle density distribution* with respect to E and $\widehat{\boldsymbol{\Omega}}$. The particle density at the point $\vec{\boldsymbol{x}}$ is then given by the integral,

$$M(\vec{\boldsymbol{x}}) = \int dE \int d\Omega \, M(\vec{\boldsymbol{x}}, \widehat{\boldsymbol{\Omega}}, E).$$

When the neutron/photon "fluid" is present inside a material medium, the neutrons/photons will interact with that material, and it is by describing such interactions mathematically that we derive an equation which the function $M(\vec{\boldsymbol{x}}, \widehat{\boldsymbol{\Omega}}, E)$ must obey. Specifically, by writing down in mathematical terms a statement of the physical fact that the rate of increase of $M(\vec{\boldsymbol{x}}, \widehat{\boldsymbol{\Omega}}, E)$ at time t is the difference between the rate at which neutrons/photons are added to the phase volume $dV\, dE\, d\Omega$ (by being born in e.g. a fission or a nuclide transmutation process, by being scattered from other energies and directions, or by crossing the boundary from outside to inside dV) and the rate at which they are removed from the phase volume $dV\, dE\, d\Omega$ (by being absorbed in material inside dV, by scattering to other energies and directions, or by crossing the boundary from inside to outside dV), we can derive an integro-differential equation for $M(\vec{\boldsymbol{x}}, \widehat{\boldsymbol{\Omega}}, E)$. This equation is the Boltzmann transport equation — abbreviated as the BTE. If we were able to solve it, we could then design radiation shields (and nuclear reactors, etc.) with an accuracy limited only by uncertainties of the basic nuclear and dosimetric data that prescribe the probabilities of what will happen to a neutron/photon of a given energy when it interacts with an atom of a given material.

1.4.10 Cross-section σ, linear interaction coefficient μ, directional fluence-rate ψ, scalar fluence rate ϕ and reaction rate

The *microscopic interaction cross-section* $\sigma_i^{\omega}(E)$ is defined as:

> The probability that interaction of type ω will happen at the position defined by the vector $\vec{\boldsymbol{x}}$, when a *single* particle having kinetic energy E moves through a distance dx in a medium in which there are $N_i(\vec{\boldsymbol{x}})$ atoms of nuclide i per unit volume, is $N_i(\vec{\boldsymbol{x}})\, \sigma_i^{\omega}(E)\, dx$.

(To be more rigorous, E should be taken as the relative kinetic energy between the impinging particle and the target atom. This consideration is quite important in nuclear reactor core design & fuel management calculations as a result of the Doppler broadening of cross-sectional resonance peaks, i.e. peaks in the resonance region of $\sigma_i^{\omega}(E)$.)

Based on this definition of the microscopic cross-section as a quantity that specifies the probability of the occurrence of a specific interaction by a *single* radiation quantum, we can now express what will happen when a distribution of radiation quanta move through matter.

---

[1] Warning: Time-dependent radiation transport is used in the design of nuclear weapons.

The following is not a rigorous proof, but a heuristic motivation based on a specific geometry & orientation for the active volume and a specific direction of movement of the incident radiation.

View a rectangular circular cylinder (RCC) having a frontal area dS, located in a radiation field that is perpendicularly incident thereon:

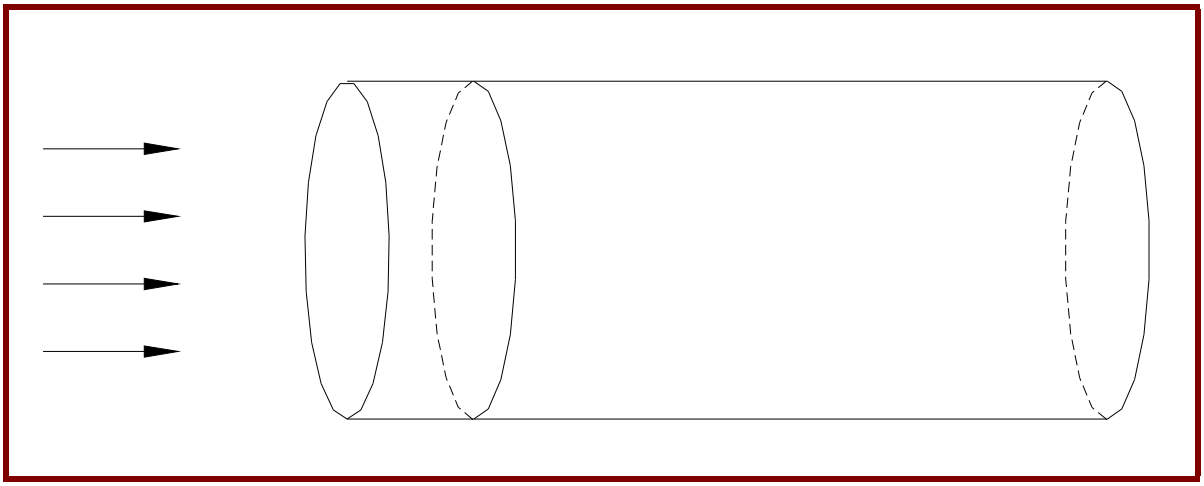

The number of radiation quanta within an energy band dE around E and within a cone $d\Omega$ of directions around $\widehat{\mathbf{\Omega}}$, that will cross the surface with area dS per unit time, is

$$v(E)\,\Big[M(\vec{\boldsymbol{x}},\widehat{\mathbf{\Omega}},E)\,d\Omega\,dE\Big]\,dS.$$

The probability that 1 radiation quantum in the energy band dE around E and the range $d\Omega$ of travelling directions around $\widehat{\mathbf{\Omega}}$, will undergo an interaction of type ω when it travels an infinitesimal distance dx, is

$$N_i(\vec{\boldsymbol{x}})\,\sigma_i^{\omega}(E)\,dx.$$

The total number of interactions of type ω that will take place inside the volume $dV = dx\,dS$ will therefore be the product of the number of particles crossing the surface dS per unit time, and the probability of interaction. This product is the reaction rate per unit volume per unit time:

$$\begin{aligned}\text{Reaction rate} &= \Big[v(E)\,M(\vec{\boldsymbol{x}},\widehat{\mathbf{\Omega}},E)\,d\Omega\,dE\,dS\Big]\,[N_i(\vec{\boldsymbol{x}})\,\sigma_i^{\omega}(E)\,dx]\\ &= N_i(\vec{\boldsymbol{x}})\,\sigma_i^{\omega}(E)\,v(E)\,M(\vec{\boldsymbol{x}},\widehat{\mathbf{\Omega}},E)\,dV\,d\Omega\,dE \qquad (1.4)\end{aligned}$$

Products of the type $N_i(\vec{\boldsymbol{x}})\,\sigma_i^{\omega}(E)$ are found in all expressions of radiation-induced reaction rates, so that it is convenient to introduce a special symbol to depict it:

$$\mu_i^{\omega}(\vec{\boldsymbol{x}},E) = N_i(\vec{\boldsymbol{x}})\,\sigma_i^{\omega}(E). \qquad (1.5)$$

The function $\mu_i^{\omega}(\vec{\boldsymbol{x}}, E)$ in the *linear interaction coefficient* at the position $\vec{\boldsymbol{x}}$ for interaction type ω between radiation quanta E, and atoms of type i. The term *linear* interaction coefficient is used because its units is [length]$^{-1}$.

Note: the historical name for the linear interaction coefficient is *macroscopic* cross-section, and its historical symbol was Σ. Both name and symbol are somewhat awkward, so that the term linear interaction coefficient and symbol μ should be used — except where the symbol μ conflicts with the customary symbol for the direction cosine of the scattering angle — in these cases, we shall revert to the symbol Σ.

Many different types of nuclides may be present inside the volume dV. The total rate of reaction type ω, between atoms in dV and radiation particles in the beam described by $v(E)$ $M(\vec{\boldsymbol{x}}, \widehat{\boldsymbol{\Omega}}, E)$ will be a linear combination of the cross-sections σ of the constituent nuclide i, weighted by the nuclide number densities N_i of nuclide i, so that the total linear interaction coefficient for reactions of type ω will be

$$\mu^{\omega}(\vec{\boldsymbol{x}}, E) = \sum_i N_i(\vec{\boldsymbol{x}})\, \sigma_i^{\omega}(E). \tag{1.6}$$

The total reaction rate for interactions of type ω in $dV\, d\Omega\, dE$ can now be written as:

$$\text{Reaction rate} = \mu^{\omega}(\vec{\boldsymbol{x}}, E)\, v(E)\, M(\vec{\boldsymbol{x}}, \widehat{\boldsymbol{\Omega}}, E)\, dV\, d\Omega\, dE. \tag{1.7}$$

Products of the type $v(E)\, M(\vec{\boldsymbol{x}}, \widehat{\boldsymbol{\Omega}}, E)$ are found in all expressions of radiation-induced reaction rates. This product of the particle speed and the particle density in phase-space is called the directional fluence-rate distribution function (or simply: directional fluence-rate), ψ:

$$\psi(\vec{\boldsymbol{x}}, \widehat{\boldsymbol{\Omega}}, E) = v(E)\, M(\vec{\boldsymbol{x}}, \widehat{\boldsymbol{\Omega}}, E). \tag{1.8}$$

The function $\psi(\vec{\boldsymbol{x}}, \widehat{\boldsymbol{\Omega}}, E)$ is a density function, i.e. a distribution function in $\widehat{\boldsymbol{\Omega}}$ and E at the spatial point $\vec{\boldsymbol{x}}$.

Whereas the *transport* of radiation quanta is intimately related to the directional aspect of particle movement, the *interaction,* and therefore physical effects such as reaction rates & heat release rates, as well as biological effects of radiation quanta in an infinitesimal volume-element dV, is normally independent of the direction of travel of the particles. Therefore the linear interaction coefficient $\mu^{\omega}(\vec{\boldsymbol{x}}, E)$ will be practically independent of the direction of movement, $\widehat{\boldsymbol{\Omega}}$, of the radiation quanta. This means that we can simplify the expression for the total rate of interactions of type ω taking place within the infinitesimal element of phase-space $dV\, dE$ by integrating over all directions of movement, $\widehat{\boldsymbol{\Omega}}$. This yields the result that the *total* number of interactions of type ω per unit time between radiation quanta inside the infinitesimal energy interval dE around E and atoms in the infinitesimal volume-element dV around $\vec{\boldsymbol{x}}$, is given by:

$$\int_{\widehat{\Omega}} \Big[\mu^{\omega}(\vec{\boldsymbol{x}}, E)\, v(E)\, M(\vec{\boldsymbol{x}}, \widehat{\boldsymbol{\Omega}}, E)\, d\Omega \Big]\, dV\, dE$$

$$= \int_{\widehat{\Omega}} \Big[\psi(\vec{\boldsymbol{x}}, \widehat{\boldsymbol{\Omega}}, E)\, d\Omega \Big]\, \mu^{\omega}(\vec{\boldsymbol{x}}, E)\, dV\, dE\,.$$

We now define the *scalar fluence-rate* distribution function as the integral of the directional fluence-rate over all directions of movement of radiation quanta:

$$\phi(\vec{\boldsymbol{x}}, E) = \int_{\widehat{\Omega}} \psi(\vec{\boldsymbol{x}}, \widehat{\boldsymbol{\Omega}}, E)\, d\Omega. \tag{1.9}$$

The scalar fluence-rate function $\phi(\vec{\boldsymbol{x}}, E)$ is a distribution function in energy E at the spatial point $\vec{\boldsymbol{x}}$.

In terms of the scalar fluence-rate distribution function $\phi(\vec{\boldsymbol{x}}, E)$, the reaction rate of type-ω interactions between radiation quanta within the infinitesimally small energy interval dE about E, and atoms in the volume-element dV around $\vec{\boldsymbol{x}}$, may be written as $\mu_i^{\omega}(\vec{\boldsymbol{x}}, E)\, \phi(\vec{\boldsymbol{x}}, E)\, dV\, dE$. Therefore the total number of interactions of type ω per unit volume per unit time at the point $\vec{\boldsymbol{x}}$ is found by integrating over the energy variable E:

$$\text{Reaction-rate}(\vec{\boldsymbol{x}}) = \int_0^{\infty} dE\; \mu^{\omega}(\vec{\boldsymbol{x}}, E)\, \phi(\vec{\boldsymbol{x}}, E) \tag{1.10}$$

In the above expression, the integration limits have been chosen as 0 and ∞. In practice, however, radiation quanta in a system always have a well-defined maximum energy, E^{max}. In practice, therefore, we are not interested in the energy region $E \in [0, \infty)$, but rather $E \in [E^{\text{min}}, E^{\text{max}}]$.

Rigorous radiation transport codes use the directional fluence-rate ψ; Radiation effects depend only on the scalar fluence-rate ϕ

At this point, the student may wonder why we bother to work with the directional fluence-rate ψ at all, seeing that reaction rates, including reactions that inflict damage to the human body, are independent on the (microscopic) direction of movement of radiation quanta, and is only a function of the scalar fluence-rate, ϕ. The answer is that there is no accurate transport equation for the calculation of the scalar fluence-rate, ϕ; the Boltzmann transport equation (BTE) describes the transport of the *directional* fluence-rate, ψ. In other words, the only way to calculate ϕ accurately is first to solve the Boltzmann transport equation numerically to determine ψ, and then to integrate the latter result over all directions of particle movement, $\widehat{\boldsymbol{\Omega}}$, to obtain the scalar fluence-rate ϕ.

1.4.11 Exponential attenuation of uncollided radiation

Consider a uniform, isotropic, homogenous medium of infinite dimensions, having a linear interaction coefficient μ. A single radiation quantum is produced at the origin ($x = 0$) and moves in the $+x$ direction.

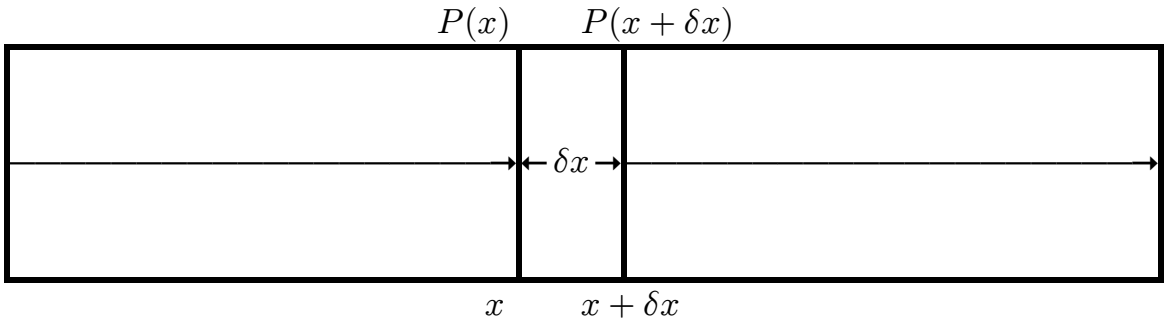

Let $P(x)$ be the probability that the quantum will move a distance x without any interaction. The probability that the quantum of radiation will react the point $x + \delta x$ without interaction is $P(x + \delta x)$, where δx is small. Let μ_t be the linear interaction coefficient for the medium at the particle energy under consideration.

We shall ignore scattering and consider the medium to be purely absorbing in nature.

According to the definition of linear interaction coefficient μ, the probability for the interaction of a single particle in the infinitesimal distance δx, is $\mu\,\delta x$. The probability of a reaction not taking place, is therefore $(1 - \mu\,\delta x)$. The probability of the quantum reaching $x + \delta x$ without interaction, is the product of the probability that it will reach x without interaction, multiplied by the probability that the particle will traverse the additional infinitesimal distance δx without interaction. Accordingly,

$$P(x + \delta x) = [P(x)]\,(1 - \mu\delta x).$$

By using the definition of a derivative, we obtain the differential equation

$$\frac{dP(x)}{dx} = -\mu P(x). \tag{1.11}$$

Next, integrate both sides, using the initial condition $P(0) = 1$. It follows that the number of particles that will penetrate to depth x without interaction, is

$$P(x) = e^{-\mu x}. \tag{1.12}$$

We see that the uncollided radiation is attenuated exponentially.

This expression was derived for a single particle. We now apply this result to 1 a parallel beam and 2 a point source.

If a **mono-energetic parallel beam of neutral radiation quanta** moves in the $+x$-direction, crossing the y–z plane with initial fluence-rate $\phi_{\text{uncoll}}(0)$, the fluence-rate that will penetrate to depth x with no interaction (i.e. uncollided), will be,

$$\begin{aligned}\phi_{\text{uncoll}}(x) &= \phi_{\text{uncoll}}(0)\, P(x) \\ &= \phi_{\text{uncoll}}(0)\, e^{-\mu x}\end{aligned} \tag{1.13}$$

Important: In pre-graduate physics courses, it is usually assumed that neutral radiation such as ionising photons and neutrons are attenuated exponentially. The above treatment makes it clear that this approximation is only rigorously true for uncollided radiation quanta. Once non-absorbing interactions such as scattering is considered, radiation transport is nearly as simple as sometimes set forth in introductory textbooks.

We now apply the result in Eq. (1.13) to a point source in a homogenous medium. Consider a **mono-energetic, isotropic point source of neutral particles** having a source strength of S quanta per unit time. The fluence-rate $\phi_{\text{uncoll}}(r)$ of particles at radius r that will move through a unit surface of a sphere with radius r, multiplied by the probability that the radiation quanta will traverse the distance r without interactions, will be

$$\begin{aligned}\phi_{\text{uncoll}}(r) &= \frac{S}{4\pi r^2}\, P(r) \\ &= \frac{S}{4\pi r^2} \exp(-\mu r)\end{aligned} \tag{1.14}$$

If the point source is in a vacuum, $\mu = 0$, so that $e^{-\mu r} = 1$, and we obtain a simple analytical expression for the uncollided fluence-rate at a distance r from a mono-energetic, isotropic point source in a vacuum

$$\phi_{\text{uncoll}}(r) = \frac{S}{4\pi r^2}.$$

Let the fluence-rate to response-rate conversion factor at the particle energy be $\mathfrak{R}$. Then the response rate at a distance r from a mono-energetic, isotropic point source in a vacuum, will be

$$R_{\text{uncoll}}(r) = \frac{S\,\mathfrak{R}}{4\pi r^2}.$$

Notice that the fluence-rate and dose rate decrease as $\left(\frac{1}{4\pi r^2}\right)$ with distance r from the point source in a vacuum. The decrease of the fluence-rate and dose-rate with increasing distance from a source, is termed *geometric attenuation.* For the special case of an isotropic point source, the *geometric attenuation* has a $\left(\frac{1}{4\pi r^2}\right)$ form. The attenuation of radiation in a medium that is a function of the attenuating properties of *matter,* and not merely of the spatial separation between the source and receiver, is termed *material attenuation.*

The total number of mean free path-lengths of a given radiation type and energy, between the source and the detector, is a dimensionless quantity termed the *total optic path length,* ξ.

1.4.12 Mean free path

Next, an expression for the mean free pathlength that a radiation quantum moves, is derived.

The probability that a particle will have a path-length between x and $x + dx$, is

$$P(x) - P(x + dx) = \mu e^{-\mu x}\, dx.$$

This is a probability distribution or probability density function. The mean free path λ of a radiation quantum in an infinite homogenous medium will be the expectation value of x, with weighting function the probability density function for path length:

$$\langle x \rangle = \frac{\int_0^\infty dx\, x\, (\mu e^{-\mu x})}{\int_0^\infty dx\, (\mu e^{-\mu x})}$$

$$\Rightarrow \lambda = \frac{1}{\mu} \tag{1.15}$$

The mean free path is an information-rich, convenient unit of length in the discipline of neutral particle transport. The physical distance can e.g. be expressed in terms of

$$\frac{x}{\lambda} = x\mu,$$

i.e. the number of mean free paths, also called the *optical path length.*

We have seen that the inverse of the total linear interaction coefficient μ is the total *mean free path,* $\lambda_t(\vec{\boldsymbol{x}}, E)$, of a radiation quantum having energy E, moving in matter with the composition it has at the point $\vec{\boldsymbol{x}}$:

$$\lambda_t(\vec{\boldsymbol{x}}, E) = \frac{1}{\mu_t(\vec{\boldsymbol{x}}, E)} \tag{1.16}$$

This concept may be generalised — we can, e.g., define the mean free path pertaining to particular interactions, such as absorption (subscript a), scattering (subscript s) and fission

(subscript f):

$$\lambda_a(\vec{\boldsymbol{x}}, E) = \frac{1}{\mu_a(\vec{\boldsymbol{x}}, E)}$$

$$\lambda_s(\vec{\boldsymbol{x}}, E) = \frac{1}{\mu_s(\vec{\boldsymbol{x}}, E)}$$

$$\lambda_f(\vec{\boldsymbol{x}}, E) = \frac{1}{\mu_f(\vec{\boldsymbol{x}}, E)}$$

Assignment 1.2

1. Consult the NIST database (http://www.nist.gov/pml/data/xraycoef/index.cfm) to calculate the linear interaction coefficient of a 3 MeV ionising photon with Fe ($\rho = 7.86\,\mathrm{g\,cm^{-3}}$). Next, calculate the mean free path of a 3 MeV photon in solid iron.

2. Consult the NIST database (http://www.nist.gov/pml/data/xraycoef/index.cfm) to calculate the linear interaction coefficient of a 5 MeV ionising photon with ordinary concrete ($\rho = 7.86\,\mathrm{g\,cm^{-3}}$). Next, calculate the mean free path of 5 MeV photons in ordinary concrete.

3. Consult the NIST database (http://www.nist.gov/pml/data/xraycoef/index.cfm) to calculate the linear interaction coefficient of 1 MeV ionising photons with dry air near sea level. Next, calculate the mean free path of 1 MeV photons in dry air near sea level.

4. A point source of a radionuclide emits one 1 MeV ionising photon per radioactive transition, and has an activity of 10^{10} Bq. It is suspended in mid-air. Ignore the attenuation and the scattering of ionising photons in the air, i.e. approximate the air as a vacuum. Calculate the fluence rate at $r = 100$ cm, $r = 200$ cm and $r = 300$ cm from the source.

5. A point source of ^{252}Cf has a total activity of $A = 10^{10}$ Bq. The branching ratio for spontaneous fission is 0.03092, i.e. 3.092% of radioactive transitions are spontaneous fissions, while the balance occur via by α-particle emissions. The total fission neutron yield is $\nu = 3.7676$ neutrons per fission. Ignore the emission of delayed neutrons.
   The point source is suspended in mid-air. Ignore attenuation and scattering of neutrons in the air, i.e. approximate the surrounding air medium as a vacuum and ignore scattering of radiation off structures. Give an the expression for the neutron fluence-rate at the distance r.

1.5 Functionals and operators in a Hilbert-space

1.5.1 Definitions

Our next step will be to generalise the definition of reaction rate to the concept *response.* To do so, we introduce the concept *functional* and the concept *operator.* The definitions are that of Akhiezer & Glazman (1961: 30).

Definition: *Functional (linear)*

Let $\mathcal{D}$ be a linear subspace of the Hilbert-space $\mathcal{H}$. A function Ψ that maps every point $f \in \mathcal{D}$ onto a specific complex number $\Psi(f)$, is called a *functional* in the space $\mathcal{H}$, with domain $\mathcal{D}$.

In simple language, we can describe a functional as a function that maps functions to numbers. Consider as an example a continuous, real, bounded function $f(x)$, which is defined on the interval $x \in [a, b]$, where a and b are real numbers. The definite integral

$$\int_a^b f(x)\, dx$$

is a real number; the definite integral (an inner product) is a real functional. Another example is the dot-product of vectors — it maps two vectors onto a scalar.

We now define the concept operator.

Definition: *Operator (linear)*

Let $\mathcal{D}$ be a subspace of the Hilbert-space $\mathcal{H}$. A Function $\mathbb{T}$ that maps every element $f \in \mathcal{D}$ onto a specific element $\mathbb{T}f = g$, where $g \in \mathcal{H}$, is called an *operator* on the space $\mathcal{H}$ having domain $\mathcal{D}$.

In a later chapter we shall see that the linear, non-homogenous Boltzmann transport equation (BTE) can be written in the operator-form,

$$\mathbb{B}\psi = Q$$

where $\mathbb{B}$ is the linear Boltzmann transport operator, Q is the source-term and ψ is the directional fluence-rate function. For all source-term functions, $Q(E, \vec{\boldsymbol{x}}, \widehat{\boldsymbol{\Omega}})$, met in practice, there exists a unique solution to this operator equation, namely the directional fluence-rate function, $\psi(E, \vec{\boldsymbol{x}}, \widehat{\boldsymbol{\Omega}})$. Both $Q(E, \vec{\boldsymbol{x}}, \widehat{\boldsymbol{\Omega}})$ and $\psi(E, \vec{\boldsymbol{x}}, \widehat{\boldsymbol{\Omega}})$ are functions in a Hilbert-space, while $\mathbb{B}$ is an operator defined in this linear space.

1.6 Generalisation of reaction rate to response

Suppose a point-detector is located at the point $\vec{\boldsymbol{x}}_d$ in a radiation field characterised by the directional fluence-rate distribution function, $\psi(\vec{\boldsymbol{x}}, \widehat{\boldsymbol{\Omega}}, E)$. From Eqs. (1.9) and (1.10), and the

definition of the Dirac delta function[2] $\delta(\vec{\boldsymbol{x}} - \vec{\boldsymbol{x}}_d)$, it follows that the reaction rate at the detector position, $\vec{\boldsymbol{x}}_d$, depends as follows on the linear interaction coefficient:

$$\begin{aligned}\text{Reaction-rate}(\vec{\boldsymbol{x}}_d) &= \int_0^\infty dE \int_{\widehat{\boldsymbol{\Omega}}} d\Omega \int_V dV\, \mu(\vec{\boldsymbol{x}}, E)\, \psi(\vec{\boldsymbol{x}}, \widehat{\boldsymbol{\Omega}}, E)\, \delta(\vec{\boldsymbol{x}} - \vec{\boldsymbol{x}}_d)\, dV \\ &= \int_0^\infty dE \int_{\widehat{\boldsymbol{\Omega}}} d\Omega\, \mu(\vec{\boldsymbol{x}}_d, E)\, \psi(\vec{\boldsymbol{x}}_d, \widehat{\boldsymbol{\Omega}}, E).\end{aligned}$$

We now introduce a more general definition of the effect of a radiation field on matter. The *response* R of a radiation field characterised by the directional fluence-rate function $\psi(\vec{\boldsymbol{x}}, \widehat{\boldsymbol{\Omega}}, E)$, is given by the linear functional of the fluence-rate and a *response function,* $\mathfrak{R}(\vec{\boldsymbol{x}}, \widehat{\boldsymbol{\Omega}}, E)$:

$$R = \int_0^\infty dE \int_{\widehat{\boldsymbol{\Omega}}} d\Omega \int_V dV\, \psi(\vec{\boldsymbol{x}}, \widehat{\boldsymbol{\Omega}}, E)\, \mathfrak{R}(\vec{\boldsymbol{x}}, \widehat{\boldsymbol{\Omega}}, E) \tag{1.17}$$

Suppose, e.g., that the response of interest is the effective dose, R_{effdos} at the point $\vec{\boldsymbol{x}}_d$. Then (ignore the factor 4π),

$$\begin{aligned}R_{\text{effdos}}(\vec{\boldsymbol{x}}_d) &= \int_0^\infty dE \int_{\widehat{\boldsymbol{\Omega}}} d\Omega \int_V dV\, \psi(\vec{\boldsymbol{x}}, \widehat{\boldsymbol{\Omega}}, E) \{\mathfrak{R}_{\text{effdos}}(E)\, \delta(\vec{\boldsymbol{x}} - \vec{\boldsymbol{x}}_d)\} \\ &= \int_0^\infty dE\ \phi(\vec{\boldsymbol{x}}_d, E)\, \mathfrak{R}_{\text{effdos}}(E).\end{aligned}$$

The concept of a ***response function*** $\mathfrak{R}$ can be viewed as a generalisation and abstraction of interaction coefficient. The concept ***response*** *can be seen as* a generalisation and abstraction of reaction rate.

It is convenient to introduce the notation employed in the description of inner-product spaces. This allows us to write the above functional very concisely as

$$R = \langle \psi, \mathfrak{R} \rangle$$

where the inner product brackets denote integration over all continuous variables and summation over all discrete variables of phase space.

Because the effect of radiation on matter is, on a microscopic scale, quite independent of the direction of movement of the radiation, the response function $\mathfrak{R}$ will be practically independent of the angular variable. Accordingly we have that (ignore the factor 4π),

$$R = \langle \phi, \mathfrak{R} \rangle \tag{1.18}$$

---

[2]See Appendix B.6 in Shultis & Faw (2000: 443-445) for an overview of the use of the Dirac delta function in the mathematical description of radiation sources and point-detectors.

The inner product $\langle \mu, \phi \rangle$, i.e.

$$\int_0^\infty dE \int_V dV \{\phi(E, \vec{\boldsymbol{x}})\, \mu(E, \vec{\boldsymbol{x}})\}$$

is seen to be the number of interactions per unit volume per unit time, i.e. the reaction rate per unit volume.

1.7 The response functional

Introduction

In its most general form, the volume-integrated effect of radiation in a volume V is given by the functional

$$R = \int_0^\infty dE \int_{4\pi} d\Omega \int_V dV \, \psi(\vec{\boldsymbol{x}}, E, \widehat{\boldsymbol{\Omega}}) \, \mathfrak{R}(\vec{\boldsymbol{x}}, E, \widehat{\boldsymbol{\Omega}}) \tag{1.19}$$

where ψ is the angular fluence-rate solution of the Boltzmann transport equation, and $\mathfrak{R}$ is the detector response function for the physical effect of interest. In virtually all applications, the effect of radiation in any infinitesimal volume is independent of its direction of movement, i.e. $\mathfrak{R}$ is independent of $\widehat{\boldsymbol{\Omega}}$; the reaction rate for the interaction of ionising radiation with matter, normally does not depend on the particular direction in which the radiation moves. The *transport* of radiation can only be modelled in terms of the directional fluence-rate distribution function, $\psi(\vec{\boldsymbol{x}}, E, \widehat{\boldsymbol{\Omega}})$; however, the *effect* of the radiation on matter normally depends only on the scalar fluence-rate distribution function, $\phi(\vec{\boldsymbol{x}}, \widehat{E})$, where $\psi(\boldsymbol{x}, E, \widehat{\boldsymbol{\Omega}})$ had been integrated over the full range of the angular variables. Accordingly, the scalar fluence-rate ϕ, and not the angular fluence-rate ψ, is used in the calculation of the response. The desired end-result of radiation shielding calculations is usually not the function $\phi(\vec{\boldsymbol{x}}, \widehat{E})$ or a discretised approximation thereof as such, but a *response*, $\boldsymbol{R}$, of the function $\phi(\vec{\boldsymbol{x}}, \widehat{E})$. These responses $\boldsymbol{R}$ are real numbers, while $\phi(\vec{\boldsymbol{x}}, \widehat{E})$ is a function in a continuous phase space. From Chapter 1 it in known that the response is a functional of the scalar fluence-rate distribution function, $\phi(\vec{\boldsymbol{x}}, \widehat{E})$, and a response function, $\mathfrak{R}(\vec{\boldsymbol{x}}, E)$:

$$R = \langle \phi, \mathfrak{R} \rangle \tag{1.20}$$

where the inner product brackets denote integration over all continuous variables of phase-space and summation over all the discrete variables of phase-space.

Response theory in a continuous function space

Two classes of detector response functions are used in practice. Dosimetric response functions represent the response properties of the human body to ionising radiation, and are accordingly postulated to be material-independent. As a result, such a response function will be independent of the spatial variable. This is quantified by using point-isotropic detector response functions of the following type:

$$\mathfrak{R}(\vec{\boldsymbol{x}}, E, \widehat{\boldsymbol{\Omega}}) = \mathfrak{R}(E) \, \delta(\vec{\boldsymbol{x}} - \vec{\boldsymbol{x}}_d) \tag{1.21}$$

where δ denotes the Dirac delta function and $\vec{\boldsymbol{x}}_d$ is the detector position — i.e. the spatial position of interest to the shield designer. Examples of response functions that may be written in the above form, are the absorbed dose rate and the effective dose rate response functions. Analytical fitting functions (over a limited energy range) may be fitted to calculated fluence-to-dose response conversion factor data. For this class of response functions, the response at the detector position $\vec{\boldsymbol{x}}_d$ is

$$R(\vec{\boldsymbol{x}}_d) = \int_0^\infty dE\, \phi(\vec{\boldsymbol{x}}_d, E)\, \Re(E) \tag{1.22}$$

where $\phi(\vec{\boldsymbol{x}}, E)$ is the scalar fluence-rate

$$\phi(\vec{\boldsymbol{x}}, E) = \int_{4\pi} d\Omega\, \psi(\vec{\boldsymbol{x}}, E, \widehat{\boldsymbol{\Omega}}). \tag{1.23}$$

The second category of response functions met in practice, gives material dependent responses such as the rate of displacements per atom, reaction rates and heating rates, when folded with ϕ. These response functions are essentially linear interaction coefficients, i.e. nuclide number-density weighted sums of the microscopic cross-sections at the point of interest in the material medium. The point-isotropic detector response function for these response functions has the form

$$\Re(\vec{\boldsymbol{x}}, E, \widehat{\boldsymbol{\Omega}}) = \Re(\vec{\boldsymbol{x}}, E)\, \delta(\vec{\boldsymbol{x}} - \vec{\boldsymbol{x}}_d) \tag{1.24}$$

and the reaction rate per unit time per unit volume at the detector position is

$$R(\vec{\boldsymbol{x}}_d) = \int_0^\infty dE\, \phi(\vec{\boldsymbol{x}}_d, E)\, \Re(\vec{\boldsymbol{x}}_d, E)\,. \tag{1.25}$$

In this course, the focus is on dosimetric responses of the human body. In the theoretical treatment below, it will therefore be assumed that the function $\Re$ *is independent of position (and therefore of material composition), i.e. that it is a dosimetric response function.* All the expressions that are derived may easily be extended to encompass the more general category of position-dependent response functions.

Important dosimetric response functions

Important dosimetric response functions for neutrons and photons are given in:

CODE-FREE CALCULATIONS FOR SIMPLE SOURCES OF PHOTONS, NEUTRONS, ELECTRONS AND PROTONS IN VACUUM.xmcd

Example 1.1

Question:
You have solved the Boltzmann transport equation (BTE), in spherical symmetry, using an accurate transport code, and have determined a close approximation to the continuous fluence-rate function $\phi(r, E)$. Construct a response function $\Re(E, r)$ that will cause the response functional $\langle \phi, \Re \rangle$ to evaluate to the fluence-rate of neutrons with energies in the range $E_n \in [2.4\text{ MeV}; 5.2\text{ MeV}]$, at a radius of $r = 100$ cm.

Hint: Use the Heaviside unit step function H to define the energy window, and the Dirac delta function to select the radial distance. It is convenient to define the "window-function" $W(a,b,x) = H(x-a) - H(x-b)$, where H is the Heaviside unit step function.

Answer:
$\mathfrak{R}(E,r) = W(2.4\text{ MeV}, 5.2\text{ MeV}, E)\,\delta(r - 100\,\text{cm})$.

Assignment 1.3

Refer to the 2010 ICRP-116 specification of the fluence to dose factors for ionising photons as well as neutrons. This is coded in the following worksheet:

CODE-FREE CALCULATIONS FOR SIMPLE SOURCES OF PHOTONS, NEUTRONS, ELECTRONS AND PROTONS IN VACUUM.xmcd

1. Determine the fluence-rate to dose-rate conversion factors, expressed in the unit $\left(\frac{(\text{Sv/h})}{(\text{cm}^{-2}\,\text{s}^{-1})}\right)$, for ionising photons with energies:
   $E_\gamma = 0.01$ MeV
   $E_\gamma = 0.1$ MeV
   $E_\gamma = 1$ MeV
   $E_\gamma = 5$ MeV and
   $E_\gamma = 10$ MeV.

2. Determine the fluence-rate to dose-rate conversion factors, expressed in the unit $\left(\frac{(\text{Sv/h})}{(\text{cm}^{-2}\,\text{s}^{-1})}\right)$, for neutrons with energies:
   $E_\gamma = 10^{-6}$ MeV
   $E_\gamma = 0.001$ MeV
   $E_\gamma = 1$ MeV
   $E_\gamma = 5$ MeV and
   $E_\gamma = 15$ MeV.

3. How much more biologically dangerous is the same fluence-rate of ionising photons with $E_\gamma = 14$ MeV compared to ionising photons having $E_\gamma = 0.01$ MeV?

4. How much more biologically dangerous is the same fluence-rate of neutrons at $E_n = 18$ MeV, compared to thermal neutrons at $E_n = 2.53 \times 10^{-8}$ MeV?

1.8 Effective dose

Before we proceed, it is vital to introduce the protection quantities, *equivalent dose* and *effective dose.*

Ionising radiation can have two general categories of health effects: deterministic tissue reactions, and stochastic effects. The dominant stochastic effect, is radiation-related cancer. The two main categories of cancer, are solid tumours and leukaemia (blood cancer). At low, legally permitted doses of ionising radiation, deterministic tissue reactions are impossible, and the dominant health concern is radiation-related cancer. The quantity effective dose and its unit, the sievert, was designed to accurately quantify the risk of radiation-related cancer.

Note that the concept effective dose should only be used when one focuses on the risk of radiation-related cancer and when dose rates are low. At higher dose rates, and when the health effect in question is deterministic tissue reactions, one should work with the quantity absorbed dose and its SI unit, the gray.

For the same absorbed dose, D, some radiations R are more damaging than ionising photons, and stochastic effects are more likely in some tissues T than in other parts of the human anatomy. In order to improve the correlation between dose quantities applied in radiation protection, and the effects considered, two types of weighting factors have been introduced: the radiation weighting factor, w_R, and the tissue weighting factor, w_T. These weighting factors are needed for the calculation of the effective dose, E.

The definition of the protection quantities is based on the mean absorbed dose, $D_{T,R}$, contributed by ionising radiation of type R and averaged over the volume of a specified organ or tissue T. Let:

$D_{T,R}$ = Average absorbed dose deposited in organ or tissue T by ionising radiation of type R;

w_R = Radiation weighting factor for ionising radiation type R

H_T = Average equivalent dose in organ or tissue T.

The protection quantity *equivalent dose* in an organ or tissue, H_T, is defined as

$$H_T = \sum_R w_R D_{T,R} \tag{1.26}$$

The sum is performed over all types R of radiations involved.

When, as is usual, more than one tissue T is exposed, it is necessary to use tissue weighting factors. The application of both the radiation and the tissue weighting factors to the tissue absorbed doses leads to the effective dose. The effective dose E is defined as

$$E = \sum_T [w_T \, H_T]$$

$$E = \sum_T w_T \left[\sum_R [w_R D_{T,R}] \right] \tag{1.27}$$

where w_R is the radiation weighting factor and w_T the tissue weighting factor, and $D_{T,R}$ is the mean absorbed dose in tissue or organ T from incident ionising radiation of type R. The unit of effective dose is the sievert (Sv). Since the effective dose is derived from mean absorbed doses in tissues and organs of the human body, a dosimetric model must be specified or implied in any statement of the magnitude of the effective dose; effective dose is a dosimetric quantity. Effective dose is a protection quantity that is not directly measurable with instruments.

Note that effective dose E is not a pure physics quantity, and that its and its SI unit, the sievert, is not a physics unit either. The definition for E weighs the physics quantity $D_{T,R}$ by weighting factors derived from radiobiology and radio-epidemiology. The effective dose is a protection quantity, a convolution of physics, radiobiology and radio-epidemiology. The radiation weighting factor w_R quantifies the effect of the microdeposition of radiation energy in tissue, on its carcinogenic potential, and is intimately related to the structure of DNA, and the fact that carcinogenesis is related to unrepaired or misrepaired radiation insult to DNA. The tissue weighting factor w_T quantifies the empirically determined radiosensitivities of tissues, based on clinical observation and results from radiobiology and radio-epidemiology. The values of the radiation weighting factors w_R for radiation type R, rely on the fact that life is organised in cells, that cells contain DNA, that DNA insult by ionising radiation is carcinogenic, that the DNA molecule has two strands, and that the carcinogenic potential of ionising radiation is related to the relationship between the mean distance between ionisation events and the distance between the strands in the DNA molecule, because double-strand breaks in DNA are far less repairable and more carcinogenic than single-strand breaks in DNA. For this reason, effective dose can in no way be classified as a physics quantity.

The values of the weighting factors w_R and w_T and, consequently, dosimetric quantities such as the protection quantities equivalent dose and effective dose, which are calculated using the ICRP's recommended values for w_R and w_T, only relate correctly to stochastic health risks. For deterministic tissue reactions caused by ionising radiation, all values of radiation weighting and tissue weighting factors are smaller than the corresponding values for stochastic effects. Use of the tabulated ICRP values of w_R and w_T in dose calculations, will overestimate the severity of tissue reactions.

Radiation weighting factors

The radiation weighting factors in Table 1.1 are recommended for general use in radiological protection.

Table 1.1: *Radiation weighting factors for different radiation types.*

Type and energy range	w_R
Photons	1
Electrons and muons	1
Protons	2
Alpha particles, fission fragments, heavy nuclei	20
Incident neutrons	See Eq. (1.28) and Figure (1.1)

The selection of the values for radiation weighting factors is mainly a judgement based on the results of radiobiological experiments.

Radiation weighting factors for neutrons: For neutrons the function $w_R(E_n)$ is

$$w_R(E_n) = \begin{cases} 2.5 + 18.2 \exp\left[-\dfrac{\{\ln(E_n)\}^2}{6}\right] & \text{for } E_n < 1 \text{ MeV} \\ 5.0 + 17.0 \exp\left[-\dfrac{\{\ln(2E_n)\}^2}{6}\right] & \text{for } 1 \text{ MeV} \leq E_n \leq 50 \text{ MeV} \\ 2.5 + 3.25 \exp\left[-\dfrac{\{\ln(0.04E_n)\}^2}{6}\right] & \text{for } E_n > 50 \text{ MeV} \end{cases} \tag{1.28}$$

where E_n is the incident neutron energy in MeV. The radiation weighting factor for neutrons is illustrated in Figure 1.1. This radiation weighting factor must be applied to the mean absorbed doses in the relevant tissues and organs. The dose is that from both the neutron-induced charged particles and the secondary ionising photons produced in the body.

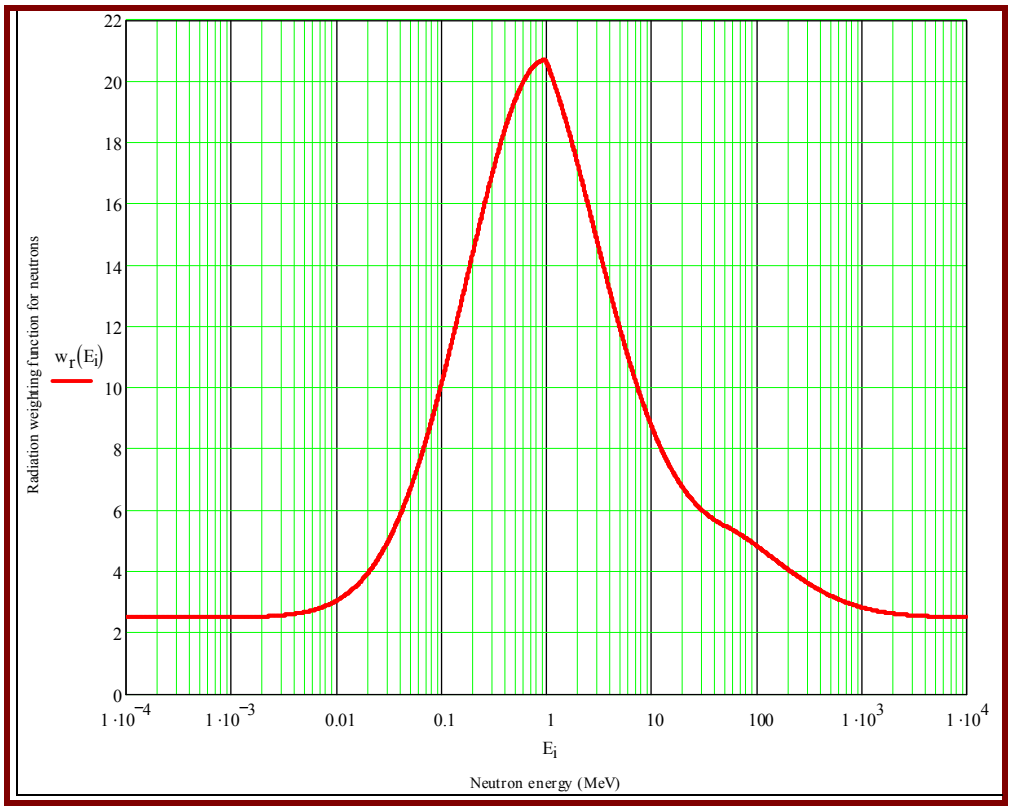

Figure 1.1: *Energy dependence of the radiation weighting factor w_R for neutrons, given by Eq. (1.28).*

At very low incident neutron energies, the radiation weighting for neutrons is 2.5. It rises to a maximum of approximately 20 at 1 MeV, and then slowly falls off to a value of 2.5 at high incident neutron energies.

Tissue weighting factors

The values of the tissue weighting factors w_T, as prescribed in the 2007 Recommendations of the ICRP (ICRP, 2007), are listed in Table 1.2.

Table 1.2: *Tissue weighting factors, as recommended by the ICRP (2007).*

Tissue	w_T	$\sum_T w_T$
Bone marrow, Breast, Colon, Lung, Stomach	0.12	0.60
Gonads	0.08	0.08
Bladder, Oesophagus, Liver, Thyroid	0.04	0.16
Bone surface, Brain, Salivary glands, Skin	0.01	0.04
Summed value for 14 remainder tissues		0.12

The values of the tissue weighting factors are a quantification of the susceptibilities of different tissues to the development of primary radiation-related cancers. Tissue weighting factors w_T are based on cancer incidence data, and takes account of the lethality rate, the years of life lost and of a weighted contribution from the non-fatal cancers and from hereditary disorders. The values of w_T are normalised to add up to 1, i.e. values have only relative meanings and no absolute meaning.

Table 1.2 indicates that bone marrow, the colon, the (young) female breast, the stomach and the lungs are the organs most susceptible to the development of primary radiation-related cancers, whereas the bone surface, brain, salivary glands, skin & the remainder tissues are relatively insensitive.

1.9 Operational dosimetric quantities

Measurable, operational dosimetric quantities are defined by the International Commission on Radiation Units and Measurements (ICRU). For measurement purposes the operational quantities, (1) ambient dose equivalent, (2) directional dose equivalent and (3) personal dose equivalent, are defined. Where doses are estimated from area monitoring results, the relevant operational quantities are (1) ambient dose equivalent and (2) directional dose equivalent.

- The ambient dose equivalent, $H^*(d)$, at a point, is the dose equivalent that would be produced by the corresponding expanded and aligned ionising radiation field, in the ICRU sphere at a depth d millimetres below the sphere's surface on the radius vector antiparallel to the direction of the aligned ionising radiation field. For measurement of strongly penetrating radiations the reference depth used is $d = 10$ mm, and this quantity is denoted as $H^*(10)$. For measurement of the skin dose, the reference depth used is $d = 0.07$ mm, and this quantity is denoted as $H^*(0.07)$.

- The personal dose equivalent, $H_p(d)$, is the dose equivalent in soft tissue, at an appropriate depth d below a specified point on the human body. $H_p(d)$ is measured with a personal radiation detector worn at the surface of the body and covered with an appropriate thickness of tissue-equivalent material. $H_p(d)$ is evaluated at $d = 10$ mm to quantify the deep dose equivalent from strongly penetrating ionising radiation, and at $d = 0.07$ mm to quantify the skin dose equivalent. $H_p(d)$ may be evaluated at $d = 3$ mm to quantify the dose equivalent to the lens of the eye.

- Directional dose equivalent — refer to relevant ICRU reports.

1.10 Response functions

1.10.1 Some response functions for non-biological effects

Reaction rates as responses

Response functions that are essentially linear interaction coefficients (i.e. macroscopic cross-sections), are used to calculate reaction rates and heat release rates. Suppose that the response of interest is the reaction rate of the neutron activation reaction,

$$^{55}\text{Mn} + n \rightarrow {}^{56}\text{Mn} \underset{T_{½}=2.58\,\text{h}}{\overset{\beta^-}{\longrightarrow}} \boxed{\text{Stable } {}^{56}\text{Fe}}$$

in a neutron field with fluence-rate distribution $\phi(E, \vec{\boldsymbol{x}})$. (This neutron activation reaction is often problematic in situations where a high thermal neutron fluence-rate moves through mild steel, which contains up to 2% Mn, i.e. ^{55}Mn. The neutron activation product, ^{56}Mn, which has a half-life $T_{½} = 2.58\,\text{h}$, can make subsequent maintenance work difficult for e.g. about 15 hours following beam-on-target conditions, as a result of high prevailing dose rates.)

The response rate is the reaction rate of the nuclear reaction, which is given by

$$R = \int_{\text{Volume}} dV \int_0^\infty dE\, \phi(E, \vec{\boldsymbol{x}})\, [N(\vec{\boldsymbol{x}})\sigma(E)]$$

where $N(\vec{\boldsymbol{x}})$ is the spatial distribution of the number-density of the target nuclide, and $\sigma(E)$ is the cross-section for the nuclear reaction $^{55}\text{Mn} + n \rightarrow {}^{56}\text{Mn}$. The response function $\mathfrak{R}(E, \vec{\boldsymbol{x}})$ is therefore the linear interaction coefficient function,

$$\mathfrak{R}(E, \vec{\boldsymbol{x}}) = \mu(E, \vec{\boldsymbol{x}}) = [N(\vec{\boldsymbol{x}})\, \sigma(E)],$$

and the response functional R is written as the inner product of the response function $\mathfrak{R}$ and the fluence-rate function, ϕ,

$$R = \langle \phi, \mathfrak{R} \rangle.$$

Note that the units of the variables in the above expressions are as follows:

N	$\text{barn}^{-1}\,\text{cm}^{-1}$
σ	barn
μ	cm^{-1}
$\mathfrak{R}$	cm^{-1}
ϕ	$\text{cm}^{-2}\,\text{cm}^{-1}$
R	$\text{cm}^{-3}\,\text{s}^{-1}$

.

It is seen that when the response R of interest is the reaction rate, its units will be $(\text{volume})^{-1}.(\text{time})^{-1}$, which will be $\boxed{\text{cm}^{-3}\,\text{s}^{-1}}$ in cgs units.

Materials-damage response functions

Materials-damage response functions are a special subset of the above. For hydrogen-rich polymers and lubricants, the absorbed dose is a good measure of material damage; for metals, the "DPA response function" (DPA ≡ displacements per atom) may be used as a measure of radiation-induced material degradation. The empirical "absolute damage" response function may be a better measure of radiation-induced damage to metals than the DPA response function. For some electronic components, absorbed dose is the limiting factor, and for others, the neutron fluence-rate is the limiting factor. Material-damage response functions are available for many materials and many classes of material damage — see e.g. the DAMSIG damage cross-section compilation, which is available from the NEA Data Bank (**www.nea.fr**).

Figure 1.2 shows the displacement-damage response function for displacement-damage on silicon (Si) by neutrons.

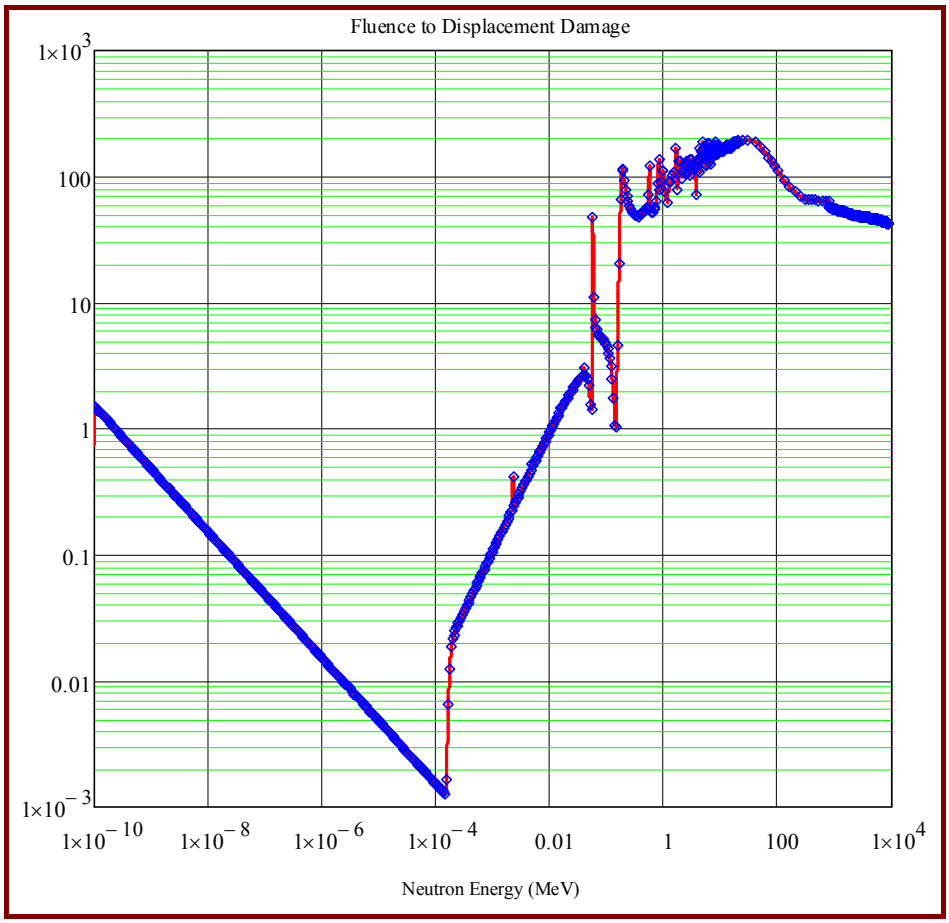

Figure 1.2: *The displacement-damage response function for displacement-damage on silicon (Si) by neutrons.*

See Van Rooyen (2004) for a practical example of combining materials damage data with fluence-rate and dose rate calculations.

1.10.2 Response functions for the radiation protection of materials and human beings

The absorbed dose response function

The absorbed dose for neutrons as well as for photons, can be measured using calibrated radiation detectors. These absorbed doses may also be calculated with a code such as MCNP. By using tissue-equivalent material in the volume of the *calculational detector,* called the *tally volume* in MCNP, the absorbed dose to biological material may be calculated.

In MCNP, absorbed dose is calculated with e.g. an F6 tally, which calculates energy deposition in a material-cell volume, in the dose unit MeV/g; this is easily converted to joule/kg, which is the SI unit for absorbed dose, and has a special name, the gray. The conversion factor necessary to convert from the default dose-rate unit in the code MCNP, $\left(\frac{\text{MeV}}{\text{g.s}}\right)$ to the unit that is used in the practice of radiation protection, namely gray/h, is

$$\frac{\left(\frac{(\text{MeV})}{(\text{g s})}\right)}{\left(\frac{\text{Gy}}{\text{h}}\right)} = \boxed{5.7678 \times 10^{-7}}. \tag{1.29}$$

In an MCNP calculation, an F6 tally that calculates the absorbed dose rate, will give a good indication of the rate of material damage to hydrogenous carbon-chain polymers, because the radiation-induced damage of such polymers tends to correlate well with the absorbed dose, i.e. the energy deposition by ionising radiation, per unit mass of material.

To be accurate, MCNP6 calculations of the spatial distribution of absorbed dose rates, need to be run in `MODE P E` for ionising photon sources. Suppose a collimated beam of ionising photons from a ^{60}Co source is used in radiotherapy. Should the radiation transport calculation be performed in the simplistic `MODE P`, the gradual build-up of the dose rate in the first circa 5 mm of tissue, will be completely miscalculated; the calculation needs to be done in `MODE P E` to observe the skin-sparing spatial dose distribution, because charged particle equilibrium will only be established approximately 4 to 5 mm inside the human tissue.

Suppose that MCNP6 is used to calculate the power distribution in a nuclear reactor, by means of `+F6` tallies. If the code is run in its simplest form, with no sampling of ionising photons emitted by fission products, and in `MODE N`, all prompt fission gamma-rays and secondary photons will not be transported, but will be assumed to deposit all their energy locally, i.e. at the point where the photon is generated. This is a simplification, and to calculate a more realistic power distribution in the reactor, sampling of ionising photons emitted by fission products must be switched on in the `PHYS:P` card, (γ, n)-reactions must be switched on in the `PHYS:P` card, the isotopes having low threshold energies for (γ, n)-reactions, usually ^{2}H, ^{13}C and ^{9}Be, must be explicitly specified in material cards, and the code must be run in

MODE N P to simulate the spatial detail of energy deposition more accurately. Note that most versions of MCNPX will crash with memory allocation errors if detailed nuclear reactor calculations are performed in MODE N P. Instead, MCNP6 must be used for such calculations.

The ambient dose equivalent response function

The ICRU (International Commission on Radiation Units and Measurements) has defined a series of operational dose quantities; refer to ICRU reports for more information.

Response functions for operational dose quantities defined by the ICRU, such as $H^*(10)$, $H^*(3)$ and $H^*(0.07)$, may be obtained using dose measurements or Monte Carlo simulations of radiation transport and energy deposition. These response functions are then available for the evaluation of chosen response functionals.

The *effective dose* response function

The *effective dose* response function, $\mathfrak{R}_{\text{effdos}}(E)$ may be evaluated using a realistic anthropomorphic phantom for measurements, or a realistic anthropomorphic calculational voxel-phantom in Monte Carlo simulations of radiation transport and energy deposition.

Graphic representations of commonly used response functions for the effective dose are given in Figure 1.3.

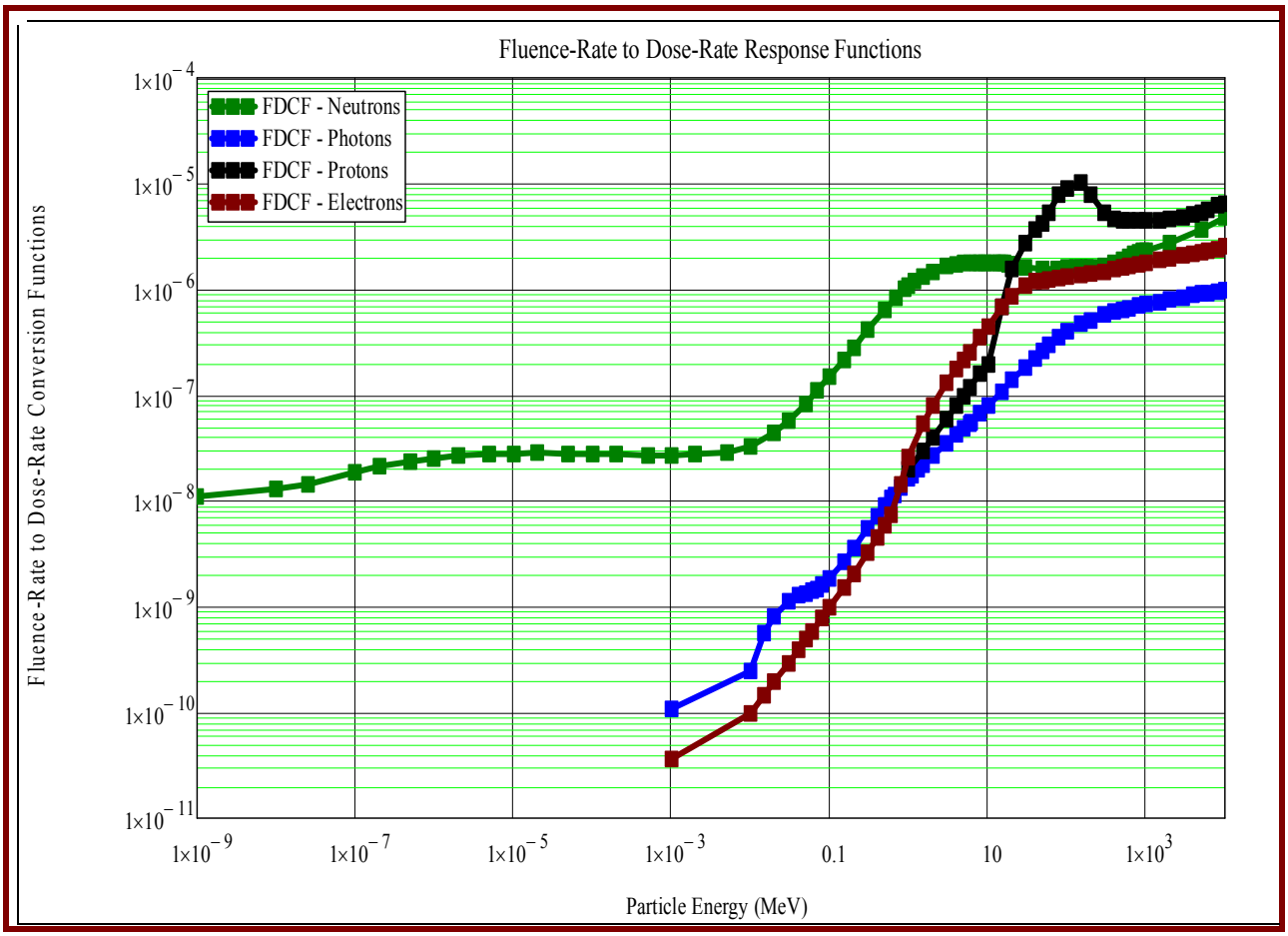

Figure 1.3: *The ICRP-116 (2010) response functions for converting from fluence-rate (unit: $cm^{-2}\,s^{-1}$) to effective dose-rate (unit: Sv/hr), for neutrons, protons, electrons and ionising photons.*

The response function for effective dose may be determined in two ways: experimentally or by calculations employing accurate radiation transport methods. An anthropomorphic phantom is placed in a radiation field, e.g. in a uniform, parallel field that is incident onto the front of the phantom. This is called an anterior-posterior or AP-exposure geometry. A known fluence-rate of mono-energetic radiation quanta having an energy E_0 is incident on the phantom as a parallel beam:

$$\psi(\vec{\boldsymbol{x}}, \widehat{\boldsymbol{\Omega}}, E) = \psi_0\, \delta(E - E_0)\, \delta(\widehat{\boldsymbol{\Omega}} - \widehat{\boldsymbol{\Omega}}_0)$$

where ψ_0 is the particle fluence-rate (unit: $\mathrm{cm}^{-2}\,\mathrm{s}^{-1}$) and $\widehat{\boldsymbol{\Omega}}_0$ is the direction of movement of the radiation quanta. This function describes a perfectly collimated, perfectly mono-energetic incident beam in a vacuum. The average absorbed dose in every organ is now experimentally measured or calculated. Equivalent doses to the organs are determined by weighting with the ICRP's latest set of recommended radiation weighting factors, w_R. Finally, the effective dose to the human body is determined by adding the equivalent doses to the different organs, weighing the sum with the ICRP's latest set of recommended tissue-weighting factors, w_T. The experiment (whether using a physical anthropomorphic phantom or an anthropomorphic calculational phantom used in a Monte Carlo simulation) is now repeated for different incident energies, E_0, and possibly also for different exposure geometries. The "calibration function" $\mathfrak{R}_{\mathrm{effdos}}(E)$ that satisfies the relationship

$$R = \langle \psi, \mathfrak{R}_{\text{effdos}} \rangle,$$

represents the response function for effective dose, for the exposure geometry of choice.

Dosimetric response functions are usually calculated for several standard exposure geometries: anterior-to-posterior (AP), posterior-to-anterior (PA), lateral from the right side to the left side (RLAT), lateral from the left side to the right side (LLAT), rotational around the vertical axis (ROT), and isotropic incidence from all directions (ISO). Note, however, that in certain locations at particle accelerators, radiation may impinge predominantly from above or from below. Therefore it is useful to extend the calculations to these special geometries as well. In practice, it is almost always found that $\mathfrak{R}_{\text{AP}}(E)$ is the most conservative response function. In some cases, accurate dose assessment may call for placing a calculational phantom at the position of interest and calculating the effective dose and equivalent doses to organs in this detailed fashion.

Ferrari & Pelliccioni (1998) deal with the determination of response functions for effective dose, using anthropomorphic phantoms in radiation transport calculations with the Monte Carlo radiation transport code FLUKA.

Note that calculations to determine the response function for effective dose, such as the above by Ferrari[3] & Pelliccioni, must be repeated every circa 20 years, because (1) the ICRP recommends new sets of radiation weighting factors w_R and tissue weighting factors w_T every ± 20 years, (2) because calculational phantom models steadily improve, and because (3) Monte Carlo codes and cross-section libraries also improve every decade. Monte Carlo codes under active development, e.g. MCNP, GEANT4, PENELOPE and FLUKA, improve quite significantly every decade and it is wise to obtain the latest version twice per decade.

The following MathCAD worksheet illustrates effective dose response functions for protons, neutrons, photons and electrons, calculated with Monte Carlo simulations of radiation fields incident upon anthropomorphic calculational phantoms.

CODE-FREE CALCULATIONS FOR SIMPLE SOURCES OF PHOTONS, NEUTRONS, ELECTRONS AND PROTONS IN VACUUM.xmcd

[3] The first author, Dr Alfredo Ferrari, is also one of the chief developers of the FLUKA Monte Carlo radiation transport code. A fully integrated particle physics Monte Carlo simulation package, FLUKA has many applications in high energy experimental physics and engineering, shielding, detector and telescope design, cosmic ray studies, dosimetry, medical physics and radio-biology. FLUKA is largely developed at the CERN particle accelerator facility in Europe; FLUKA is widely used in Europe, whereas MCNPX is widely used in the USA. The FLUKA code may be downloaded for free from the FLUKA website, http://www.fluka.org/. FLUKA courses are presented from time to time, usually in Europe and India — see the FLUKA website. Recently, many young scientists seem to favour the newer GEANT4 code over the older FLUKA. To use GEANT4, one must be an expert C++ programmer.

Application

At a Pebble-Bed Nuclear Reactor, carbon dust containing fission products as well as neutron activation products, form a thin deposit or coating inside the pipelines carrying the helium coolant. It is necessary to calculate the effective dose to a maintenance worker who have to work for e.g. 1 hour working close to such a pipeline, during a maintenance shutdown. The radionuclides such as ^{110}Ag that are present in the carbon dust, emit ionising photons and electrons.

The wrong methodology will be to calculate the contact dose rate on the pipe's exterior surface, and equate this with the effective dose rate to a maintenance worker[4]. Effective dose is a dosimetric quantity, and a reasonably accurate method will be to place a cylindrical phantom composed of tissue-equivalent material (TEM) at a representative position of the body of a maintenance worker. Such a phantom must have a height of approximately 170 cm; to keep the weight close to a realistic 70 kg, for a mass-density of $\rho = 1\ \mathrm{g\,cm^{-3}}$, the radius of the rectangular circular cylinder (RCC) must be about 12 cm. The problem is now modelled with MCNP — this amounts to the accurate modelling of the placement of materials in space, as well as the realistic modelling of the source details. The absorbed dose rate in the simple cylinder-phantom is now calculated by means of a `+F6` MCNP tally, with radiation transport performed in `mode p` or, for higher accuracy and for the accurate calculation of skin dose, in `mode p e`. Because the radiation weighting factor w_R for ionising photons has the value 1 (ICRP-103, 2007), the absorbed dose rate over the entire phantom volume will approximate the effective dose rate to a human at the exposure position.

[4] Such an error of judgement was actually made in 2007 by a consultant to PBMR, South Africa.

1.11 Calculating nuclide number-densities; specifying material compositions to radiation transport codes

Introduction

The quantity microscopic cross-section, σ, is expressed in the unit barn, which is 10^{-24} cm^2 or 10^{-28} m^2. The cgs-unit for the linear interaction coefficient, μ, also called the macroscopic cross-section Σ, is cm^{-1}. Because nuclear data compilations cite cross sections σ in the unit barn, it follows that it is most practical to express atomic number densities per unit volume, N, in the volume unit barn.cm, because then the calculation of the linear interaction coefficient, $\mu = N\sigma$ will be computationally simplified, because

$$[\text{barn}] \times \left[\text{barn}^{-1}\,\text{cm}^{-1}\right] = \left[\text{cm}^{-1}\right].$$

Example 1.2

The chemical formula for polyethylene is $(\text{CH}_2)_n$ and its mass-density is $\rho \approx 0.95$ g cm^{-3}. Calculate the nuclide number densities of ^{1}H and ^{12}C in polyethylene. Ignore the existence of all other isotopes of H and C.

Solution:
1 mole CH_2 weighs M_r gram (where M_r is the relative molar mass).

There will be N_A units of CH_2 in M_r gram CH_2.
M_r gram CH_2 has a volume of $V = \frac{\text{mass}}{\text{density}} = \frac{M_r}{\rho}$ cm^3.
Therefore there will be N_A formula-units CH_2 per $\frac{M_r}{\rho}$ cm^3 CH_2.
Therefore the number per unit volume of CH_2 will be $\left(\frac{N_A}{\frac{M_r}{\rho}}\right) = \left(\frac{\rho N_A}{M_r}\right)$ per cm^3.
Therefore there will be $\left(\frac{10^{-24}\rho N_A}{M_r}\right) = \left(\frac{0.6022\,\rho}{M_r}\right)$ formula-units CH_2 per barn.cm.

Therefore there will be $1 \times \left(\frac{0.6022\,\rho}{M_r}\right)$ ^{12}C-isotopes per barn.cm,

and there will be $2 \times \left(\frac{0.6022\,\rho}{M_r}\right)$ ^{1}H-isotopes per barn.cm.

(Note: Avogadro's constant $N_A = 6.022 \times 10^{23}$ mol^{-1}, and $\left(10^{-24} N_A\right) = 0.6022$.)

For CH_2, $M_r = [(1 \times 12.0) + (2 \times 1.008)] \approx 14$ g.mole^{-1}. Therefore the nuclide number density of ^{1}H will be $\left(\frac{2 \times 0.6022 \times 0.95}{14}\right) = 8.243\text{E-}2$ barn^{-1} cm^{-1} while the nuclide number density of ^{12}C will be 4.121E-2 barn^{-1} cm^{-1}.

The easiest way is to specify the material polyethylene, i.e. $\left(CH_2\right)_n$ to MCNP, is simply as

```
m1      1000  +2
        6000  +1
```

One can also define the material by specifying the nuclide number densities

```
m1      1000  +8.243E-2
        6000  +4.121E-2
```

Finally, one can specify the mass-fractions of the H and C in $\left(CH_2\right)_n$ as

```
m1      1000  -0.143
        6000  -0.857
```

or, equivalently, as mass percentages,

```
m1      1000  -14.3
        6000  -85.7
```

In all these material-card specifications, only the ratios between the number-fractions or mass-fractions of the constituent elements or nuclides are important. The code MCNP reads the mass-density or number-density of the bulk material in the cell cards, and uses this in conjunction with an internally normalised form of the materials specification in the material cards, to calculate the nuclide number density of each element or nuclide in the bulk material, in the unit $\text{barn}^{-1}\,\text{cm}^{-1}$. The number density N_i and the cross-section $\sigma_i(E)$ of each of the I nuclides present in the bulk material are then used to calculate the linear interaction coefficient μ, also called the macroscopic cross-section Σ, of the bulk material, as

$$\mu = \sum_{i=1}^{I} N_i\,\sigma_i \tag{1.30}$$

Calculating atom number densities

Case 1: Single material of a given mass-density

$$N = \left(\frac{\rho}{M}\right) 0.6022\ \text{barn}^{-1}\,\text{cm}^{-1}$$

where

N = atoms per barn.cm

ρ = mass-density of the material (g cm^{-3})

M = relative atomic mass of the isotope.

Case 2: Two materials, given mass-fractions & mixture density

Where there is a mixture of materials with a known mixture density and individual weight fractions, the atom number density equation becomes

$$N_i = \frac{0.6022\,\rho_{\text{mix}}\,w_i}{M_i}$$

where

N_i = atoms of material i per barn.cm

ρ_{mix} = mass-density of the mixture (g cm^{-3})

$(w)_i$ = weight fraction of material i

M_i = atomic mass number of the isotope i.

Note: There is a difference between *weight fraction* and *number fraction.*
Example: In 3% enriched uranium,

$$N_{U235} = 1.4527 \times 10^{-3} \text{ atoms.barn}^{-1}\,\text{cm}^{-1}$$

$$N_{U235} = 4.6377 \times 10^{-2} \text{ atoms.barn}^{-1}\,\text{cm}^{-1}$$

The number fractions are then

$$NF\left(^{235}\text{U}\right) = \frac{1.4527 \times 10^{-3}}{1.4527 \times 10^{-3} + 4.6377 \times 10^{-2}} = 0.0303$$

and

$$NF\left(^{238}\text{U}\right) = \frac{4.6377 \times 10^{-2}}{4.6377 \times 10^{-2} + 1.4527 \times 10^{-3}} = 0.9697$$

The difference between the mass fraction and atomic number fraction is small for ^{235}U and ^{238}U, because the ratio of their masses are close to unity. In the case of light isotopes such as ^{10}B and ^{11}B, the difference between the mass fraction and atomic number fraction is substantial.

As long as mixture density and individual weight functions are given, the above method applies.

The following MathCAD worksheets calculate the nuclide number densities, the mass-fractions and the number fractions of ^{235}U, ^{238}U and O in UO_2 nuclear fuel with a given mass-density, ρ, and a given enrichment mass-fraction for ^{235}U.

UO_2 NND Calculator.xmcd

Dry UO_2 Isotopic Composition Calculator.xmcd

UO_2.xmcd

U3Si2 Wet - Isotopic Composition Calculator.xmcd

Case 3: Several materials, given weight fractions, and individual material densities.

If the individual weight fractions and individual material densities ρ_i are known, then the net density of the mixture is given by,

$$\frac{1}{\rho_{\text{mix}}} = \frac{w_1}{\rho_1} + \frac{w_2}{\rho_2} + \ldots + \frac{w_i}{\rho_i} = \sum_i \frac{w_i}{\rho_i}$$

Other, more complex cases:

Refer to pages 127 – 147 in Tim Goorley (ed.), 2004, *MCNP Criticality Primer II: Criticality Calculations with MCNP5: A Primer.* Los Alamos National Laboratory, X-5. Report LA-UR-04-0294.

1.12 Isotopic number densities or mass-fractions of some materials

Boron carbide (B_4C)

Mass-density: $\rho = 2.52\ \mathrm{g\,cm^{-3}}$. The simplest MCNP input specification for this substance, is:

```
m1      5000   +4   $ B in B4C
        6000   +1   $ C in B4C
```

Paraffin wax ($C_{25}H_{52}$)

Typical mass-density: $\rho = 0.92\ \mathrm{g\,cm^{-3}}$. Representative chemical formula: $C_{25}H_{52}$. The simplest MCNP input specification for this substance, is:

```
m1      1000   +52    $ H in wax
        6000   +25    $ C in wax
```

Water (H_2O)

Mass-density: $\rho = 1.0\ \mathrm{g\,cm^{-3}}$ at 4 °C. The simplest MCNP input specification for this substance, is:

```
m1      1000   +2  $ H in water
        8000   +1  $ O in water
```

Concrete, Ordinary, ANSI Type 04 (mass-fractions; MCNP input format)

Typical mass-density: $\rho = 2.35\ \mathrm{g\,cm^{-3}}$.

For neutron transport problems at a particle accelerator, where the proton energy incident upon a target is e.g. 200 MeV, neutrons with energies up to 200 MeV will be produced. In an MCNP calculation for this neutron energy range, it is vital that the cross-section data compilation used, extends to as high an energy as possible, because the use of evaluated cross-section data is more accurate than the use of physics models in transport calculations. To perform an accurate MCNP6 calculation for neutron transport with maximum neutron energy well into the "model physics" energy region, specific cross-section sets with energies extending to e.g. 150 MeV, must be specified because their use will give more accurate results compared to when cross-section sets that extend only to e.g. 20 MeV are used, because the latter choice will entail that "model physics" be used for all neutron energies above 20 MeV. The following material specification for ordinary concrete, is suited for neutron transport runs with MCNP, for cases where neutron energies will exceed 20 MeV.

```
c Ordinary Concrete, ANSI type 04; Partial Density
m1     1001    -0.012997          $ Type 04 Ordinary Concrete
       1002    -2.98736E-06       $ Type 04 Ordinary Concrete
       8016    -1.165             $ Type 04 Ordinary Concrete
      11023    -0.040             $ Type 04 Ordinary Concrete
      12000    -0.010             $ Type 04 Ordinary Concrete
      13027    -0.108             $ Type 04 Ordinary Concrete
      14000    -0.740             $ Type 04 Ordinary Concrete
      16000    -0.003             $ Type 04 Ordinary Concrete
      19000    -0.045             $ Type 04 Ordinary Concrete
      20000    -0.196             $ Type 04 Ordinary Concrete
      26054    -1.7400E-03        $ Type 04 Ordinary Concrete
      26056    -2.7510E-02        $ Type 04 Ordinary Concrete
      26057    -6.4200E-04        $ Type 04 Ordinary Concrete
      26058    -9.3000E-05        $ Type 04 Ordinary Concrete
```

For photon and electron transport problems (MODE P or MODE P E calculations in MCNP), specification of the isotope is not needed, and the material specification for ordinary concrete will simply be by element:

```
c Ordinary Concrete, ANSI type 04; Partial Density
m1     1000   -0.013             $ Type 04 Ordinary Concrete
       8000   -1.165             $ Type 04 Ordinary Concrete
      11000   -0.040             $ Type 04 Ordinary Concrete
      12000   -0.010             $ Type 04 Ordinary Concrete
      13000   -0.108             $ Type 04 Ordinary Concrete
      14000   -0.740             $ Type 04 Ordinary Concrete
      16000   -0.003             $ Type 04 Ordinary Concrete
      19000   -0.045             $ Type 04 Ordinary Concrete
      20000   -0.196             $ Type 04 Ordinary Concrete
      26000   -0.030             $ Type 04 Ordinary Concrete
```

Air, dry (mass-fractions; MCNP input format)

For modelling high-energy neutron transport problems with MCNP, a good specification of the composition of dry air is:

Density: $\rho = 1.205\text{E}{-}03$ g/cc.

```
m1     6000    -1.24E-4          $ Air, dry
       7014    -0.755267         $ Air, dry
       8016    -0.231781         $ Air, dry
      18000    -0.012827         $ Air, dry
```

For modelling photon/electron transport problems in MCNP, the specification of the composition of air is simpler, because only the element and not the specific isotopes, must be specified. It is also not necessary to specify the cross-section set to be used.

Density: $\rho = 1.205\text{E-}03$ g/cc

```
m1      6000    -1.24E-4        $ Air, dry
        7000    -0.755267       $ Air, dry
        8000    -0.231781       $ Air, dry
       18000    -0.012827       $ Air, dry
```

Gypsum

Chemical formula: $\left(CaSO_4 \cdot 2H_2O\right)$
Mass-density: $\rho = 2.32\ \mathrm{g\,cm^{-3}}$.

The simplest MCNP input specification for this substance, is:

```
m1      20000    +1    $ calcium
        16000    +1    $ sulphur
         8000    +6    $ oxygen
         1000    +4    $ hydrogen
```

for photon/electron transport problems. The mass-density ρ is be specified in the cell-cards.

Inconel (standard)

Mass-density: $\rho = 8.3\ \mathrm{g\,cm^{-3}}$. MCNP material-card specification:

```
m1      14000   -0.025  $ Si mass-fraction
        22000   -0.025  $ Ti mass-fraction
        24000   -0.150  $ Cr mass-fraction
        26000   -0.070  $ Fe mass-fraction
        28000   -0.730  $ Ni mass-fraction
```

Inconel X

Mass-density: $\rho = 8.5\ \mathrm{g\,cm^{-3}}$. MCNP material-card specification:

```
m1      24000   -0.15   $ Cr mass-fraction
        26000   -0.07   $ Fe mass-fraction
        28000   -0.78   $ Ni mass-fraction
```

Nylon

Chemical formula: $C_{12}H_{22}N_2O_2$; mass-density: $\rho = 1.14\ \mathrm{g\,cm^{-3}}$. The MCNP material-card specification for nylon is:

```
m1      6000   +12  $ Number-fraction of C
        1000   +22  $ Number-fraction of H
        7000    +2  $ Number-fraction of N
        8000    +2  $ Number-fraction of O
```

Plexiglas, Lucite, Perspex

Chemical formula: $C_5H_8O_2$; mass-density: $\rho = 1.18\ \mathrm{g\,cm^{-3}}$; materials-card specification in MCNP:

```
m1      6000  +5  $ C in Perspex
        1000  +8  $ H in Perspex
        8000  +2  $ O in Perspex
```

Poly-ethylene

Representative chemical formula: $\left(CH_2\right)_n$; mass-density: $\rho = 0.96\ \mathrm{g\,cm^{-3}}$ (approximate); Materials-card specification in MCNP:

```
m1      6000  +1  $ C in Perspex
        1000  +2  $ H in Perspex
```

Polyvinyl chloride (PVC)

Representative chemical formula: $C_2H_3Cl_1$; Mass-density: $\rho \in [1.35; 1.45]\ \mathrm{g\,cm^{-3}}$. Materials specification in MCNP:

```
m1      6000    +2   $ C  in PVC
        1000    +3   $ H  in PVC
       17000    +1   $ Cl in PVC
```

Pyrex glass

Materials specification in MCNP:

```
m1      5000   -0.037  $ B  in Pyrex glass
       13000   -0.010  $ Al in Pyrex glass
       11000   -0.041  $ Na in Pyrex glass
        8000   -0.535  $ O  in Pyrex glass
       14000   -0.377  $ Si in Pyrex glass
```

Stainless steel 304L (Mass-fractions, MCNP input format, for neutron transport problems)

```
m1      6000     -0.03          $ SS-304L
       14028     -0.5532        $ SS-304L
       14029     -0.0282        $ SS-304L
       14030     -0.0186        $ SS-304L
       15031     -0.02          $ SS-304L
       16000     -0.03          $ SS-304L
       24050     -0.827         $ SS-304L
       24052    -15.920         $ SS-304L
       24053     -1.805         $ SS-304L
       24054     -0.448         $ SS-304L
       25055     -1.70          $ SS-304L
       26054     -3.980         $ SS-304L
       26056    -62.925         $ SS-304L
       26057     -1.468         $ SS-304L
       26058     -0.213         $ SS-304L
       28058     -6.776         $ SS-304L
       28060     -2.642         $ SS-304L
       28061     -0.116         $ SS-304L
       28062     -0.371         $ SS-304L
       28064     -0.095         $ SS-304L
```

Stainless steel 304L (Mass-fractions, MCNP input format, for photon/electron transport problems)

Element	Atomic number Z	Mass fraction in SS-316L	Mass fraction in SS-304L
C	6	0.03	0.03
Si	14	0.60	0.60
S	15	0.02	0.02
P	16	0.03	0.03
Cr	24	17.50	19.00
Mn	25	1.70	1.70
Fe	26	64.52	68.62
Ni	28	13.00	10.00
Mo	42	2.60	0.00
	Checksum	100.00	100.00

Stainless steel 316L (Mass-fractions, MCNP input format, for neutron transport problems)

```
m1      6000     -0.03          $ SS-316L
       14028     -0.5532        $ SS-316L
       14029     -0.0282        $ SS-316L
       14030     -0.0186        $ SS-316L
```

```
      15031   -0.02            $ SS-316L
      16000   -0.03            $ SS-316L
      24050   -0.76125         $ SS-316L
      24052  -14.66325         $ SS-316L
      24053   -1.6625          $ SS-316L
      24054   -0.413           $ SS-316L
      25055   -1.70            $ SS-316L
      26054   -3.742           $ SS-316L
      26056  -59.165           $ SS-316L
      26057   -1.381           $ SS-316L
      26058   -0.200           $ SS-316L
      28058   -8.809           $ SS-316L
      28060   -3.435           $ SS-316L
      28061   -0.151           $ SS-316L
      28062   -0.482           $ SS-316L
      28064   -0.124           $ SS-316L
      42000   -2.60            $ SS-316L
```

Tissue-equivalent material (TEM) — MCNP input format, for neutron transport problems

It is not necessary to specify the isotopic composition of elements such as Fe, because the impact on the accuracy of the result will be negligible.

c

```
c Tissue Equivalent Material (average for entire human body; WIKIPEDIA)
M5      8016       -6.5414E+01          $ O  in TEM
        6000       -1.8115E+01          $ C  in TEM
        1001       -1.0064E+01          $ H  in TEM
        7014       -3.0191E+00          $ N  in TEM
       20000       -1.4089E+00          $ Ca in TEM
       15031       -1.1070E+00          $ P  in TEM
       19000       -2.5159E-01          $ K  in TEM
       16000       -2.5159E-01          $ S  in TEM
       11023       -1.5095E-01          $ Na in TEM
       17000       -1.5095E-01          $ Cl in TEM
       12000       -5.0318E-02          $ Mg in TEM
       26000       -6.0382E-03          $ Fe in TEM
       30000       -3.2204E-03          $ Zn in TEM
       14000       -2.0127E-03          $ Si in TEM
       40000       -6.0382E-04          $ Zr in TEM
       82000       -1.7108E-04          $ Pb in TEM
       29000       -1.0064E-04          $ Cu in TEM
       48000       -7.2458E-05          $ Cd in TEM
       23000       -2.6165E-05          $ V  in TEM
       50000       -2.4153E-05          $ Sn in TEM
       80000       -1.9121E-05          $ Hg in TEM
       28000       -1.4089E-05          $ Ni in TEM
       22000       -1.3083E-05          $ Ti in TEM
```

```
        42000       -1.3083E-05          $ Mo in TEM
        51000       -1.1070E-05          $ Sb in TEM
        24000       -2.4153E-06          $ Cr in TEM
        47000       -1.0064E-06          $ Ag in TEM
        92238       -1.3083E-07          $ U  in TEM
         4009       -5.0318E-09          $ Be in TEM
MT4     LWTR.10T
```

c

Tissue-equivalent material (TEM) — MCNP input format, for photon/electron transport problems

```
c
c TEM for Photon Problems (Wikipaedia):
M5      1000       -1.000E-01       $ H          in Tissue Equivalent Material (TEM)
        3000       -3.100E-08       $ Lithium    in Tissue Equivalent Material (TEM)
        4000       -5.000E-11       $ Beryllium  in Tissue Equivalent Material (TEM)
        5000       -6.900E-07       $ Boron      in Tissue Equivalent Material (TEM)
        6000       -1.800E-01       $ Carbon     in Tissue Equivalent Material (TEM)
        7000       -3.000E-02       $ Nitrogen   in Tissue Equivalent Material (TEM)
        8000       -6.500E-01       $ Oxygen     in Tissue Equivalent Material (TEM)
        9000       -3.700E-05       $ Fluorine   in Tissue Equivalent Material (TEM)
       11000       -1.500E-03       $ Sodium     in Tissue Equivalent Material (TEM)
       12000       -5.000E-04       $ Magnesium  in Tissue Equivalent Material (TEM)
       13000       -8.700E-07       $ Aluminium  in Tissue Equivalent Material (TEM)
       14000       -2.000E-05       $ Silicon    in Tissue Equivalent Material (TEM)
       15000       -1.100E-02       $ Phosphorus in Tissue Equivalent Material (TEM)
       16000       -2.500E-03       $ Sulfur     in Tissue Equivalent Material (TEM)
       17000       -1.500E-03       $ Chlorine   in Tissue Equivalent Material (TEM)
       19000       -2.500E-03       $ Potassium  in Tissue Equivalent Material (TEM)
       20000       -1.400E-02       $ Calcium    in Tissue Equivalent Material (TEM)
       22000       -1.300E-07       $ Titanium   in Tissue Equivalent Material (TEM)
       23000       -2.600E-07       $ Vanadium   in Tissue Equivalent Material (TEM)
       24000       -2.400E-08       $ Chromium   in Tissue Equivalent Material (TEM)
       25000       -1.700E-07       $ Manganese  in Tissue Equivalent Material (TEM)
       26000       -6.000E-05       $ Iron       in Tissue Equivalent Material (TEM)
       27000       -2.100E-08       $ Cobalt     in Tissue Equivalent Material (TEM)
       28000       -1.400E-07       $ Nickel     in Tissue Equivalent Material (TEM)
       29000       -1.000E-06       $ Copper     in Tissue Equivalent Material (TEM)
       30000       -3.200E-05       $ Zinc       in Tissue Equivalent Material (TEM)
       33000       -2.600E-07       $ Arsenic    in Tissue Equivalent Material (TEM)
       34000       -1.900E-07       $ Selenium   in Tissue Equivalent Material (TEM)
       35000       -2.900E-06       $ Bromine    in Tissue Equivalent Material (TEM)
       37000       -4.600E-06       $ Rubidium   in Tissue Equivalent Material (TEM)
       38000       -4.600E-06       $ Strontium  in Tissue Equivalent Material (TEM)
       40000       -6.000E-06       $ Zirconium  in Tissue Equivalent Material (TEM)
       41000       -1.600E-06       $ Niobium    in Tissue Equivalent Material (TEM)
       42000       -1.300E-07       $ Molybdenum in Tissue Equivalent Material (TEM)
       47000       -1.000E-08       $ Silver     in Tissue Equivalent Material (TEM)
       48000       -7.200E-07       $ Cadmium    in Tissue Equivalent Material (TEM)
       50000       -2.400E-07       $ Tin        in Tissue Equivalent Material (TEM)
       51000       -1.100E-07       $ Antimony   in Tissue Equivalent Material (TEM)
       52000       -1.200E-07       $ Tellurium  in Tissue Equivalent Material (TEM)
```

```
      53000       -1.600E-07       $ Iodine     in Tissue Equivalent Material (TEM)
      55000       -2.100E-08       $ Caesium    in Tissue Equivalent Material (TEM)
      56000       -3.100E-07       $ Barium     in Tissue Equivalent Material (TEM)
      57000       -1.370E-06       $ Lanthanum  in Tissue Equivalent Material (TEM)
      58000       -5.700E-07       $ Cerium     in Tissue Equivalent Material (TEM)
      79000       -1.400E-07       $ Gold       in Tissue Equivalent Material (TEM)
      80000       -1.900E-07       $ Mercury    in Tissue Equivalent Material (TEM)
      82000       -1.700E-06       $ Lead       in Tissue Equivalent Material (TEM)
      83000       -1.000E-15       $ Bismuth    in Tissue Equivalent Material (TEM)
      90000       -1.000E-14       $ Thorium    in Tissue Equivalent Material (TEM)
      92000       -1.300E-09       $ Uranium    in Tissue Equivalent Material (TEM)
c
```

Note

For neutron transport problems, especially high-energy transport problems at particle accelerator facilities, it is always best to convert the elemental composition to an isotopic composition, using an accurate utility code[5] or a spreadsheet. One reason is that nuclides such as ${}^{2}_{1}\mathrm{H}$ and ${}^{13}_{6}\mathrm{C}$ have non-negligible (γ, n) reaction cross-sections. The small amount of ${}^{2}\mathrm{H}$ in a LWR will therefore produce a small amount of additional neutrons via (γ, n)-reactions. In reactor calculations in MCNP, run in KCODE mode, (1) modelling all ionising photon production reactions (2) modelling (γ, n) photonuclear reactions, plus (3) explicitly specifying the isotopic ${}^{2}\mathrm{H}$ content of the water, may increase the calculated value of k_{eff} by a small yet non-negligible amount.

[5] Beware of "freeware" utility codes claiming to supply nuclear data, because there is typically no quality assurance and no accountability built into "freeware" software. These codes are usually abandoned student's projects.

Chapter 2:
Radiation Transport Methods;
The Boltzmann Transport Equation

Introduction

Even for shielding analysts who mainly use Monte Carlo codes, which do not directly solve a discretised rendering of the Boltzmann transport equation (BTE), knowledge of the BTE is vital for a conceptual grasp of radiation transport.

Under circumstances encountered in radiation transport problems of practical interest, neutral particles such as neutrons and photons obey a Boltzmann-type transport equation. The transport equation may be derived with great travail of soul from the theory of quantum statistical mechanics (Williams, 1971: 1-10). Very few rigorous derivations of the Boltzmann transport equation (BTE) are found in the scientific literature. Examples of derivations are Osborn & Yip (1966) and Pázsit (1992). Because the rigorous derivation of the radiation transport equation is conceptually and mathematically very advanced, the "proofs" encountered in most educational textbooks are actually only heuristical motivations. We now present such a semi-classical "heuristical motivation" of the Boltzmann transport equation (BTE).

2.1 Semi-classical "heuristic motivation" of the Boltzmann transport equation (BTE)

We shall only consider steady-state, time-independent radiation transport, in which the time variable t does not figure.

The energy variable, the three spatial co-ordinates and the two direction cosines that describe the orientation of the unit vector $\widehat{\boldsymbol{\Omega}}$, constitute the co-ordinates of the 6-dimensional phase space in which radiation quanta are transported. We seek an equation that describes the directional fluence-rate $\psi(\vec{\boldsymbol{x}}, E, \widehat{\boldsymbol{\Omega}})\, dV\, d\Omega\, dE$ at all positions $\vec{\boldsymbol{x}}$, E, and $\widehat{\boldsymbol{\Omega}}$ in phase space, inside a differential "volume" element $dV\, d\Omega\, dE$ of phase space.

In the case of a stationary (time-invariant) radiation field, the fluence-rate within the volume element of phase space will be constant, because the number of radiation quanta that enters will be equal to the number of quanta leaving the infinitesimally small "volume" element $dV\, d\Omega\, dE$ of phase space.

Contribution processes whereby quanta enter into $dV\, d\Omega\, dE$, are:

(C_1) Radiation quanta are born within $dV\, d\Omega\, dE$ by a source $Q(\vec{\boldsymbol{x}}, E, \widehat{\boldsymbol{\Omega}})$ per unit time per unit element of phase space (unit: $\text{cm}^{-3}\ \text{MeV}^{-1}\ \text{sterad}^{-1}\ \text{s}^{-1}$). The number of source quanta

originating per unit time within $dV\,d\Omega\,dE$, is therefore

$$\text{Source} = Q(\vec{\boldsymbol{x}}, E, \widehat{\boldsymbol{\Omega}})\,dV\,d\Omega\,dE\,.$$

(C_2) The linear interaction coefficient $\mu_s(\vec{\boldsymbol{x}}, E)$ for particles having energy E is defined to mean that the product $\mu_s(E, \vec{\boldsymbol{x}})\,\psi(\vec{\boldsymbol{x}}, E, \widehat{\boldsymbol{\Omega}})\,dV\,d\Omega\,dE$ is the number of scattering events per unit time within the element of phase space, $dV\,d\Omega\,dE$. The number of particles scattered per unit time from any initial energy E' to the final energy E, and from any initial direction of movement $\widehat{\boldsymbol{\Omega}}'$ to the final direction $\widehat{\boldsymbol{\Omega}}$ within dV, is given by:

$$\text{Inscattering} = \left[\int_0^\infty dE' \int_{\widehat{\Omega}'} d\widehat{\boldsymbol{\Omega}}'\,\mu_s(\vec{\boldsymbol{x}}, E')\,p(E' \to E, \widehat{\boldsymbol{\Omega}}' \to \widehat{\boldsymbol{\Omega}})\,\psi(E', \vec{\boldsymbol{x}}, \widehat{\boldsymbol{\Omega}}')\right] dV\,d\Omega\,dE$$

where $p(E' \to E, \widehat{\boldsymbol{\Omega}}' \to \widehat{\boldsymbol{\Omega}})$ is the probability distribution for the change in direction of movement $\widehat{\boldsymbol{\Omega}}' \to \widehat{\boldsymbol{\Omega}}$ and the energy change $E' \to E$ when a scattering event occurs within volume dV.
(Note that: $\mu_s(\vec{\boldsymbol{x}}, E')\,p(E' \to E, \widehat{\boldsymbol{\Omega}}' \to \widehat{\boldsymbol{\Omega}}) \equiv \mu_s(\vec{\boldsymbol{x}}, E' \to E, \widehat{\boldsymbol{\Omega}}' \to \widehat{\boldsymbol{\Omega}})$.)

(C_3) Particles having an energy within dE around E and direction of movement within $d\Omega$ around $\widehat{\boldsymbol{\Omega}}$ spatially stream into dV from the surrounding space.

Removal processes whereby radiation quanta leave $dV\,d\Omega\,dE$ are:

(R_1) Radiation quanta are absorbed within dV and are scattered to directions of movement outside the infinitesimal cone $d\Omega$ around $\widehat{\boldsymbol{\Omega}}$ and to energies outside the infinitesimally small energy interval dE around E. In the case of an infinitesimally small differential element of phase space, any interaction will lead to such losses, so that

$$\text{Outscattering} = \mu_t(\vec{\boldsymbol{x}}, E)\,\psi(\vec{\boldsymbol{x}}, E, \widehat{\boldsymbol{\Omega}})\,dV\,d\Omega\,dE.$$

(R_2) Particles with energy within dE around E and direction within $d\Omega$ around $\widehat{\boldsymbol{\Omega}}$ spatially leak/migrate/stream out of dV to surrounding space.

The net spatial leakage from dV per unit time is given by the difference between removal term R_2 and contribution term C_3, and is given by the divergence of $\psi(\vec{\boldsymbol{x}}, E, \widehat{\boldsymbol{\Omega}})$, i.e.

$$\textit{Net leakage} = \vec{\nabla} \cdot \widehat{\boldsymbol{\Omega}}\,\psi(\vec{\boldsymbol{x}}, E, \widehat{\boldsymbol{\Omega}})\,dV\,d\Omega\,dE$$

In the case of a stationary, time-independent radiation field, the following relation should hold:

$$\textit{Rate of particle gain} = \textit{Rate of particle loss}$$

so that

$$\textit{Inscattering gain} + \textit{Source production gain} = \textit{Leakage loss} + \textit{Outscattering loss}.$$

The time independent, linear Boltzmann transport equation (BTE) follows from the above considerations:

$$\overbrace{\left\{\begin{array}{l}\textit{Spatial leakage term}\\ \textit{Spatial streaming term}\\ \textit{Ballistic term}\end{array}\right\}}^{\vec{\nabla}\cdot\widehat{\boldsymbol{\Omega}}\,\psi\left(\vec{\boldsymbol{x}},E,\widehat{\boldsymbol{\Omega}}\right)} \quad \overbrace{+\,\mu_t(\vec{\boldsymbol{x}},E)\,\psi\left(\vec{\boldsymbol{x}},E,\widehat{\boldsymbol{\Omega}}\right)}^{\textit{Outscattering term}} \;=$$

$$\overbrace{\int_0^\infty dE' \int_{\widehat{\Omega}'} d\widehat{\boldsymbol{\Omega}}'\,\mu_s\left(\vec{\boldsymbol{x}},E'\rightarrow E,\widehat{\boldsymbol{\Omega}}'\rightarrow\widehat{\boldsymbol{\Omega}}\right)\psi\left(\vec{\boldsymbol{x}},E',\widehat{\boldsymbol{\Omega}}'\right)}^{\textit{Inscattering term}} \;+\; \overbrace{Q\left(\vec{\boldsymbol{x}},E,\widehat{\Omega}\right)}^{\textit{Source-term}}. \qquad (2.1)$$

Viewed from left to right, the four terms in the BTE are:

(1) The spatial leakage removal term, also called the ballistic term;

(2) The outscattering or collision removal term;

(3) The inscattering contribution term;

(4) The source-term — a contribution term.

The source-term, Q, only pertains to primary or genuine sources, e.g. prompt fission neutrons and prompt gamma-photons from nuclear fission, while the inscattering term models scattered particles as well as the formation of secondary radiation quanta by, e.g., (n,γ) and $(n,n\gamma)$ reactions.

If the Boltzmann transport equation is multiplied by $dV\,d\Omega\,dE$, the transport equation becomes a statement of particle balance for the phase-space differential element $dV\,d\Omega\,dE$. The first term on the left represents the net spatial streaming of particles out of the differential element. The second term on the left represents the loss of particles from the element by collision (e.g. absorption and scattering). The first term on the right represents the gain of particles into the differential phase-space element by scattering events. Finally, the last term on the right represents particles gained into the element from "fixed" or "external" sources.

In essence, the Boltzmann transport equation (BTE) is seen to be a balance equation that is a statement of particle conservation in a stationary (time-independent) radiation field.

2.2 Quantum-Statistical Derivation of the Boltzmann Transport Equation (BTE)

The rigorous quantum-statistical derivation of the Boltzmann transport equation (BTE) for neutrons and photons is done in the following manner. From within the conceptual framework of quantum statistical mechanics, one starts with a so-called "master function," i.e. the phase space distribution function for radiation quanta. Four simplifying assumptions, based on four postulates, are now made (Williams, 1971: 4). The four postulates are:

- All collisions are between 2 particles;
- There exists no correlation between the moving radiation quanta, so that the movement is fully chaotic;
- The duration of a collision is much shorter than the time that elapses between collisions;
- Over the range of the forces of interaction, the gradient of inhomogeneities in the transport medium may be ignored.

These four postulates will hold well if the free neutron and free photon density is not excessively high (Williams, 1971: 4). Under these conditions, which hold for all shielding problems met in practice (Williams, 1971: 4), the steady-state distribution of the directional fluence-rate of neutrons and photons in a source-driven system is described by the non-homogeneous, time-independent, linear Boltzmann transport equation.

2.3 Operator form of the Boltzmann transport equation

In operator notation, the Boltzmann transport equation (BTE), which is an integro-differential equation, may be written as a non-homogeneous operator equation,

$$\boxed{\mathbb{B}\psi = Q}, \tag{2.2}$$

where the linear Boltzmann transport operator (BTO), $\mathbb{B}$, is:

$$\mathbb{B} \equiv \vec{\nabla} \cdot \widehat{\mathbf{\Omega}} + \mu_t(\vec{\boldsymbol{x}}, E) - \int_0^\infty dE' \int_{\widehat{\Omega}'} d\widehat{\mathbf{\Omega}}' \; \mu_s(\vec{\boldsymbol{x}}, E' \to E, \widehat{\mathbf{\Omega}}' \to \widehat{\mathbf{\Omega}}), \tag{2.3}$$

and $Q(\vec{\boldsymbol{x}}, E, \widehat{\mathbf{\Omega}})$ is the source-term *driving* the system.

The following **heuristical interpretation** can be given to the BTE, cast in the operator form, $\mathbb{B}\psi = Q$:

- The source-term Q of the BTE "drives" the system;
- The BTO, $\mathbb{B}$, of a system incorporates the placement of isotopes in space, as well the physics laws of radiation transport. In this way, the BTO determines the phase-space dependence of the directional fluence-rate "reaction", $\psi(\vec{\boldsymbol{x}}, E, \widehat{\mathbf{\Omega}})$, of the system on Q.

Physically, the Boltzmann transport equation is a particle balance equation in phase space; mathematically, it is an operator equation in a Hilbert space.

Mathematical note: A homogeneous operator equation has the form

$$\mathbb{A}f = 0$$

while a non-homogeneous operator equation has the form

$$\mathbb{A}f = B$$

where $B \not\equiv 0$. The Boltzmann transport equation (BTE) is a non-homogeneous operator equation — this is characteristic of a source-driven system.

Conclusion

By inspecting the Boltzmann transport equation (BTE), $\mathbb{B}\psi = Q$, it is evident that the specification of a radiation transport problem involves:

- Interaction cross-sections, $\sigma_t(E)$ and $\sigma_s(\vec{\boldsymbol{x}}, E' \rightarrow E, \widehat{\boldsymbol{\Omega}}' \rightarrow \widehat{\boldsymbol{\Omega}})$ of materials must be available in a suitable database;
- The placement of isotopes in space must be specified, i.e. $N(\vec{\boldsymbol{x}})$ must be known, in order to calculate linear interaction coefficients, $\mu(\vec{\boldsymbol{x}}, E) = N(\vec{\boldsymbol{x}})\,\sigma(E)$;
- The source-term, $Q\left(\vec{\boldsymbol{x}}, E, \widehat{\boldsymbol{\Omega}}\right)$ must be specified accurately.

2.4 Formalism for a general radiation shielding problem

In radiation transport, one explicitly or implicitly solves Boltzmann-type radiation transport equation,

$$\boxed{\mathbb{B}\boldsymbol{\psi} = \boldsymbol{Q}}$$

where $\mathbb{B}$ is the Boltzmann transport operator, Q the source-term which drives the non-homogenous operator equation, leading to the fluence-rate "reaction" of the system, ψ. The operator $\mathbb{B}$ encompasses the laws of radiation transport, the details of the placement of materials in space, and the detailed energy and angular dependence of the total cross-section and inscattering transfer cross-sections of materials that are present in the system.

Next, one obtains the scalar fluence-rate $\phi(E, \vec{\boldsymbol{x}}) = \int d\widehat{\boldsymbol{\Omega}}\, \psi\left(E, \vec{\boldsymbol{x}}, \widehat{\boldsymbol{\Omega}}\right)$ (this step is built into practically all radiation transport codes).

The response functional R of interest is now

$$\boxed{\boldsymbol{R} = \langle \boldsymbol{\phi}, \boldsymbol{\mathfrak{R}} \rangle}$$

where $\mathfrak{R}(E)$ is the response function, and the inner product bracket notation signifies integration over all the continuous variables and summation over all the discrete variables of phase-space.

It follows that a typical radiation transport code will always require the following foundational input data:

- The source term specification;
- Detailed microscopic cross-section databases, which can be as large as 200 GByte (2015);
- Geometry & material cards, which specify where which materials are located in space, and gives information necessary for the code to internally compute nuclide number densities N;
- A specification of one or more response functions $\mathfrak{R}(E)$, so that the code can calculate the desired quantity, e.g. a reaction rate, the absorbed dose rate (unit Gy/h) or the effective dose rate (unit Sv/h).

Besides the above foundational input, subsidiary input such as variance reduction parameters, physics cards and job execution control cards are typically also required.

Example 2.1

At a given spatial point in a nuclear reactor facility, the calculated scalar fluence-rate is $\phi(E)$. To obtain the effective neutron dose rate there, the integral

$$\int_0^\infty dE\, \phi(E)\, \mathfrak{R}_{\text{effdose}}(E)$$

is evaluated, where $\mathfrak{R}_{\text{effdose}}(E)$ is the response function for effective dose.

Example 2.2

At a given spatial point in a nuclear reactor facility, the calculated scalar fluence-rate of neutrons is $\phi(E)$. To obtain the activation rate for the production of ^{56}Mn from the activation of ^{55}Mn by neutrons, if a small sample of Mn should be located there, the integral

$$\int_0^\infty dE\, \phi(E)\, \mathfrak{R}(E)$$

is evaluated, where $\mathfrak{R}(E) = N\sigma(E)$, where N is the nuclide number density of ^{55}Mn in the sample, and $\sigma(E)$ is the microscopic cross-section for the nuclear reaction, $^{55}\text{Mn}(n,\gamma)^{56}\text{Mn}$.

2.5 Mathematical description of simple source terms, $Q(\vec{x}, \widehat{\Omega}, E)$

2.5.1 Separable source distribution functions

In the case of a *volume-distributed source,* the source distribution function $Q\left(\vec{\boldsymbol{x}}, \mathrm{E}, \widehat{\boldsymbol{\Omega}}\right)$ of the Boltzmann transport equation (BTE) is often simplified as a separable function,

$$Q(\vec{\boldsymbol{x}}, E, \widehat{\boldsymbol{\Omega}}) = \frac{m}{4\pi}\, S(E)\, P(\vec{\boldsymbol{x}}) \tag{2.4}$$

because it has been found empirically that the variables E and $\vec{\boldsymbol{x}}$ are independent to a good degree of approximation, and also because particle emission from a source is normally isotropic. The variables in the above expression are:

- m is a source strength normalisation factor,

$$m = \int_{4\pi} d\Omega \int dE \int_{V} dV\, Q(\vec{\boldsymbol{x}}, \widehat{\boldsymbol{\Omega}}, E);$$

- $S(E)$ is the normalised energy spectrum function. The function $S(E)$ is a probability density function, i.e. the probability that a particle will be produced having an energy between E_1 and E_2 will be $\int_{E_1}^{E_2} S(E)\, dE$.

- $P(\vec{\boldsymbol{x}})$ is the normalised power distribution function.

Physically the assumption that the source-term $Q(\vec{\boldsymbol{x}}, \widehat{\boldsymbol{\Omega}}, E)$ is separable into the functions $S(E)$ and $P(\vec{\boldsymbol{x}})$ means that it is assumed that the energy spectrum of the radiated quanta is independent of the position inside the source volume where the emission takes place.

The shape of the spatial power distribution function $P(\vec{\boldsymbol{x}})$ is normally only of importance if the source volume occupies a significant part of the volume where the radiation transport is modelled. This is the case for a nuclear reactor, where the source radius ranges between 100 cm and 200 cm. When the source is small compared to the area where the transport takes place, we make the simplifying assumption that $P(\vec{\boldsymbol{x}}) = \text{constant}$. In the case of small radioisotope sources, e.g. a ^{60}Co source with dimensions in the order of a few mm, located in a room having dimensions in the order of metres, in which the radiation transport takes place, the power distribution function P will normally assumed to be constant, i.e. independent of the spatial variable $\vec{\boldsymbol{x}}$.

In contrast with the simplicity of the treatment of the spatial power distribution function $P(\vec{\boldsymbol{x}})$ and the angular dependence of the emission of radiation in the source volume, in the case of a smallish radionuclide source, which is highly accurate assumptions, the energy spectrum function $S(E)$ should be modelled with great care and accuracy, because the cross-section terms in the BTE, and consequently the fluence-rate ψ, as well as response functions $\mathfrak{R}$, which is used to calculate response functionals, $R = \langle \psi, \mathfrak{R} \rangle$, are strongly dependent on the energy variable E.

2.5.2 Simple incident beams of radiation

Target audience: Scientists working at particle accelerator facilities.

In the case of a parallel beam of incident particles moving in the direction defined by the unit vector $\widehat{\mathbf{\Omega}}_0$, the source distribution function may be written as:

$$Q(\vec{\boldsymbol{x}}, \widehat{\mathbf{\Omega}}, E) = m\, S(E)\, P(x, y)\, \delta(\widehat{\mathbf{\Omega}} - \widehat{\mathbf{\Omega}}_0)$$

or

$$Q(\vec{\boldsymbol{x}}, \widehat{\mathbf{\Omega}}, E) = m\, S(E)\, P(r, \varphi)\, \delta(\widehat{\mathbf{\Omega}} - \widehat{\mathbf{\Omega}}_0).$$

In the above expression, δ is the Dirac delta function, and $\widehat{\mathbf{\Omega}}_0$ a unit vector in the direction of movement of the particles, and m is a normalisation factor for beam intensity.

If the radiation beam displays azimuthal symmetry, i.e. if there is no intensity-variation in the azimuthal variable, φ, and has a beam radius r_0 and a (normalised) radial beam fluence-rate profile, $P_r(r)$,

$$P(r, \varphi) = P_r(r)\, (H(r - 0) - H(r - r_0)), \tag{2.5}$$

where H is the Heaviside unit step function,

$$H(x) = \begin{cases} 1 \,\forall\, x \geq 0 \\ 0 \,\forall\, x < 0 \end{cases}.$$

Expressions such as Eq. (2.6) can be simplified by defining the "window function" $W(a, b, x)$ as follows in terms of the Heaviside unit step function,

$$W(a, b, x) = H(x - a) - H(x - b) \tag{2.6}$$

Figure 2.1 illustrates the "window function" $W(4, 8, x)$.

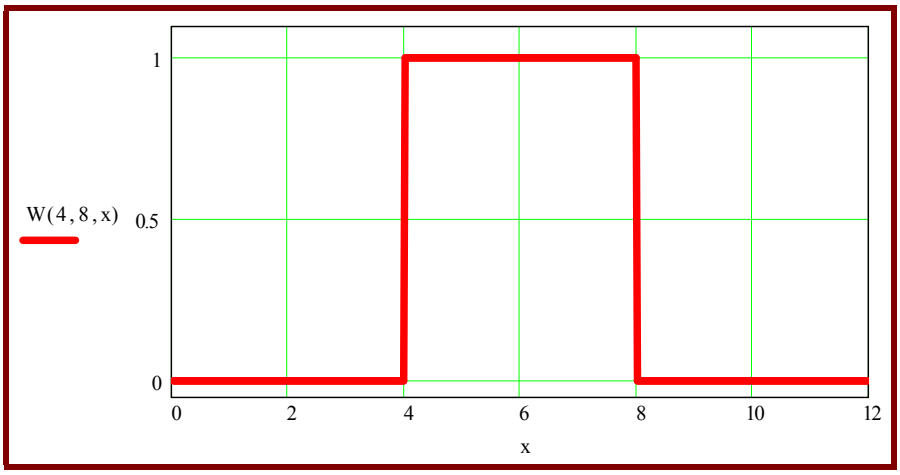

Figure 2.1: *Illustration of the "window-function", $W(a, b, x)$ for given values of a and b.*

The function W takes the value 0 to the left of a and to the right of b, and the value 1 between a and b.

In terms of the window-function W, Eq. (2.6) can now be written as

$$P(r, \varphi) = P_r(r)\, W(0, r_0, r).$$

If the radial beam profile is flat, and there is no dependence on the azimuthal angle, φ, the beam profile function P can be expressed mathematically as

$$P(r, \varphi) = c_n\, W(0, r_0, r)$$

where c_n is a normalisation constant for the particular beam and W is the "window-function".

2.5.3 Mono-energetic, isotropic point sources

A mathematical description of a point source of isotropic, mono-energetic particles is given in Eq. (2.7):

$$Q(\vec{\boldsymbol{x}}, \widehat{\boldsymbol{\Omega}}, E) = m\, \delta(E - E_0)\, \delta(\vec{\boldsymbol{x}} - \vec{\boldsymbol{x}}_0) \tag{2.7}$$

In MCNP, the "source strength" m is not specified in the SDEF source definition, but in a tally multiplication factor, i.e. an FM card.

2.5.4 Poly-energetic point sources

A mathematical description of a point source of isotropic, poly-energetic particles is given in Eq. (2.8):

$$Q(\vec{\boldsymbol{x}}, \widehat{\boldsymbol{\Omega}}, E) = m\, S(E)\, \delta(\vec{\boldsymbol{x}} - \vec{\boldsymbol{x}}_0) \tag{2.8}$$

2.6 Overview of numerical solution techniques for radiation transport

The inhomogeneous Boltzmann transport equation, $\mathbb{B}\psi = Q$, is a linear integro-differential equation that can not be solved analytically for real-world radiation transport problems of practical interest — nobody is really interested in a point-source emitting mono-energetic radiation quanta in a vacuum. We now present a brief introductory overview of numerical solution techniques for the BTE. Mathematical detail will not be treated.

Techniques for solving the BTE may be classified into 3 categories:

- **Approximate techniques:** The BTE is radically simplified to a simple deterministic model that may be solved numerically. This usually amounts to the following: The transport of particles that have not interacted — called *uncollided* or *unscattered* particles — is modelled exact by an exponential attenuation model. The total response is now obtained by multiplying the "uncollided" or "unscattered" response with a *buildup factor* which accounts for the contribution of scattered radiation quanta. Modelling is relatively simple, and execution time on a computer is fast. Approximate techniques are reasonably accurate for the transport of ionising photons, but are not acceptably accurate for neutron transport. Example: the point-kernel integration method.

- **Deterministic exact techniques.** The continuous variables of the transport equation are discretised. Integrals are replaced by averages over energy groups, or by summations. Derivatives are replaced by finite difference forms, e.g.

$$\frac{df(x)}{dx} \approx \frac{f(x+\delta x) - f(x)}{\delta x}$$

  for small δx. The continuous angular variable is represented by a Legendre series expansion or by discrete angles, each of which has a weight. In this way a set of algebraic equations is obtained which can be solved by an iterative convergence technique. Special methods to accelerate convergence, to prevent fluence-rates from becoming negative, and to dampen numerical oscillations, are used. The result is the energy group averaged directional fluence-rate ψ at the midpoint of every spatial interval and for every discrete direction of particle movement. If we make the discretisation of phase space finer, the solution tends to the exact solution of the Boltzmann transport equation. Examples of exact deterministic techniques are the method of discrete ordinates, as well as nodal techniques.

- **Monte Carlo (stochastic) methods.** These methods do not operate by solving the BTE as such, but by using principles similar to those that we used to "derive" the transport equation, to follow individual particle trajectories. Random numbers are generated, and interaction cross sections are used as probability density functions. More detail is presented later.

Deterministic radiation transport codes normally employ a *discrete partition* of the *energy variable, E*, in the solution of the BTE. We refer to this partition as *energy groups;* this fundamental simplification of the BTE is known as the *multigroup approximation.* These

transport codes use a discrete partition of the energy variable, and read energy-group-averaged cross-sections from a so-called multigroup cross-section library. Some older Monte Carlo use the multigroup approximation, but state-of-the-art Monte Carlo codes normally use continuous cross-section data, although the use of multigroup cross-section data sets remains an option in codes such as MCNP. The adjoint Boltzmann transport equation (BTE) can only be solved numerically in the multigroup formalism; the solution ψ^* to the adjoint BTE is known as the *importance function,* which is used in the calculation of optimum variance reduction parameters for Monte Carlo radiation transport calculations, as well as in certain shield optimisation algorithms.

Chapter 3:
The Interaction of Ionising Radiation with Matter

3.1 Interaction modes and penetrating abilities of charged particles

3.1.1 Introduction

Ionising radiation interacts with matter by:

- Interaction with the electron cloud of the atom, or by
- Interaction with the nucleus of the atom.

Ionising radiation can be electrically charged particles such as alpha-particles and electrons, or it can be uncharged particles & radiation quanta such as neutrons and ionising photons. The mode of interaction, range in matter and penetrating ability of charged and uncharged particles differ considerably, so that we will discuss them separately. A mono-energetic, parallel beam of charged particles has a well-defined range in a given material, whereas uncharged particles are attenuated more or less exponentially, without having a well-defined range.

When charged particles such as α-particles and free electrons interact with atoms, they lose energy in two ways — ionisation slowing down and radiative slowing down. Charged particles interact continuously and quite intensely, display a well-defined range, and do not penetrate nearly as deeply as uncharged particles.

Assignment 3.1

1. Download the charged ion transport code SRIM from www.srim.org , and install it.
2. Use SRIM to calculate the range of 8 MeV α-particles in water.
3. Use SRIM to calculate the range of 8 MeV protons in water.
4. Use SRIM to calculate the range of 200 MeV α-particles in water.
5. Use SRIM to calculate the range of 200 MeV protons in water.
6. Use MCNP to calculate the range of 8 MeV electrons in water.
7. Use MCNP to simulate the attenuation of 8 MeV ionising photons in water, and plot the attenuation curve.

8. Use MCNP to simulate the attenuation of 8 MeV neutrons in water, and plot the attenuation curve.

9. Use MCNP to graph the attenuation curve for 8 MeV ionising photons in lead, and plot the attenuation curve.

10. Use MCNP to simulate the attenuation of 8 MeV neutrons in lead, and plot the attenuation curve.

11. Draw general conclusions on the general phenomenological features of the penetrating abilities of different categories of ionising radiation, and how difficult it is to shield different types of ionising radiation.

3.1.2 Ionisation slowing down of charged particles

Coulombic interactions of charged particles with atomic electrons, can impart energy to the atom and excite it to a higher energy state. If the energy transfer of the charged particle to the atomic electrons is sufficiently high, one or more electrons may be detached from the atom — this is called ionisation. In every ionisation event, a small amount of energy is transferred from the charged particle to the atom being ionised, so that the energy of the moving particle decreases, i.e. it is slowed down. This process is called ***ionisation slowing down***. From Eq. (3.4) on page 71, it can be shown that the *linear energy transfer* (LET, i.e. the energy transferred per unit path length) of a heavy charged particle by the mechanism of ionisation slowing down, obeys the approximate relationship,

$$\left.\frac{dE}{dx}\right|_{\text{ionisation}} = \text{LET}_{\text{ionisation}} \propto \frac{z^2\,Z}{v} \tag{3.1}$$

where z is the charge of the projectile, Z is the atomic number of the medium in which the interaction takes place and v is the speed of the heavy charged particle. The linear energy transfer rate is a measure of the intensity with which the particle interacts with matter, and determines the ionisation density, i.e. the number of ion pairs produced per unit path length. Eq. (3.1) teaches us the following about ionisation and ionisation slowing down:

- The z^2 term shows that the higher the charge z on a charged particle, the more intensely it will interact, i.e. the more energy will be transferred and the more ion pairs will be produced per unit path length. A particle with charge $+3$ will e.g. interact $3 \times 3 = 9$ times more intensely than a particle with the same speed but charge $+1$.

- The Z term shows that the higher the atomic number Z of the medium in which the charged particle slows down, the more intense the interaction will be, i.e. the more energy will be transferred per unit path length.

- The $1/v$ term shows that slower-moving charged particles will interact more intensely than fast-moving charged particles.

Figure 3.1 (top part) shows the trajectories followed by 200 MeV protons in typical human tissue. The range is less than 30 cm and scattering is predominantly forward biased.

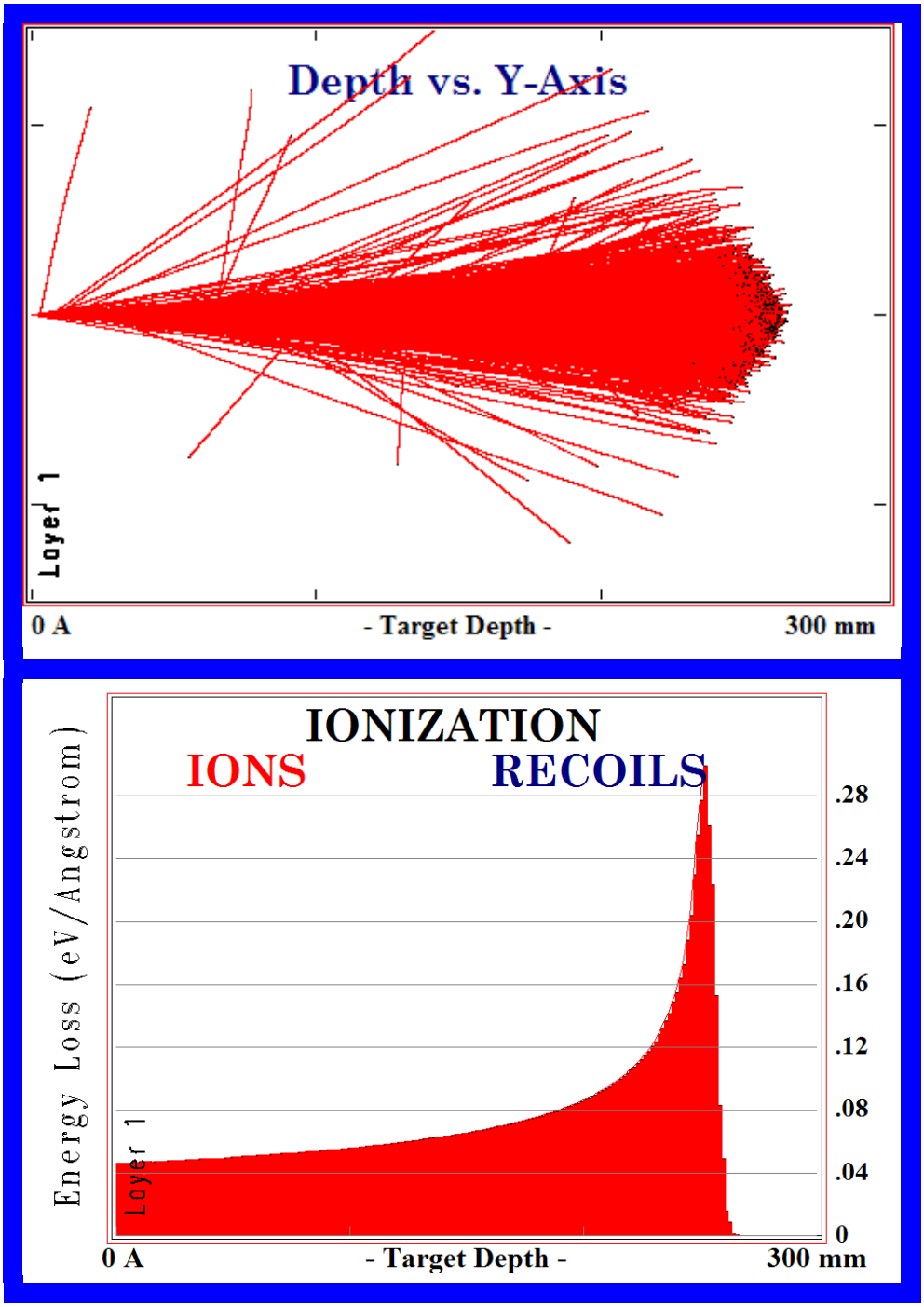

Figure 3.1: *Spatial patterns of proton transport in human tissue*[6].

In Figure 3.1, a thin beam of 200 MeV protons impinge horizontally from the left. Broadening of the beam takes place, but scattering is generally highly forward biased. The bottom graph

[6] Calculation were performed with the code SRIM — see **http://www.srim.org/** for a free download of this Monte Carlo simulation code for charged ion transport in matter. Remark: SRIM seems very "unhappy" under MS WINDOWS 7.

in Figure 3.1 shows that energy transfer by ionisation is most intense over the last ~12% of the range of the protons; this peak in the spatial pattern of energy deposition of charged particles along the beam direction, is called the *Bragg peak,* and is important in e.g. proton radiotherapy. More energy is deposited per unit path length as the speed of the charged particle decreases, up to a maximum value of energy deposition per unit path length. Also note that from Figure 3.1 that no primary particles reach beyond a specific maximum range; this range is characteristic for every combination of (1) incident particle type, (2) energy and (3) attenuating medium.

Each ionisation event causes an energy of approximately the average ionisation energy of the traversed medium, to be removed from the projectile and be deposited in the absorbing medium. The amount of energy deposited per ionisation event, is more than enough energy to cause ionisation and excitation and to disrupt chemical bonds between atoms in molecules.

3.1.3 Radiative slowing down — bremsstrahlung production

We now come to the second mechanism by which charged particles are slowed down. If a charged particle (which is free, i.e. not bound in a potential well) enters the vicinity of an atomic nucleus, it will be deflected from its original direction, by the electric field of the nucleus. (Note that the energies of matter-particles which are bound in a potential well are quantisised, whereas the energies of an unbound, free particle are not quantisised.) This causes a rapid change in the direction as well as the speed of movement of the electrically charged projectile. Keep in mind that the velocity $\vec{\boldsymbol{v}}$ of a particle is a vector quantity, and that any change in its velocity, i.e. in its speed or direction or both, amounts to acceleration, because $\vec{\boldsymbol{a}} = \frac{d\vec{\boldsymbol{v}}}{dt}$; loss of speed amounts to a negative acceleration, i.e. a deceleration. When an unbound, free, electrically charged particle is decelerated, it emits ionising photons known as *bremsstrahlung* ("braking radiation"). (In contrast, charged particles such as atomic electrons that are bound inside a potential well, have quantisised energies and do not emit *bremsstrahlung* when they are accelerated.) This process by which charged particles lose energy and slow down, is called ***radiative slowing down***. The faster the deceleration, the more *bremsstrahlung* is produced. Low-mass charged particles such as electrons are much more easily deflected and decelerated and are much more likely to undergo rapid deceleration, $\vec{\boldsymbol{a}} = \frac{d\vec{\boldsymbol{v}}}{dt}$, than heavy charged particles such as α-particles, which have a high momentum and are therefore not deflected or decelerated much in any single interaction. It is also easier for a heavy nucleus to deflect light charged particles such as electrons through large angles in a single interaction.

The intensity I of bremsstrahlung production is given by the approximate relationship (Dörschel *et al.,* 1996),

$$I \propto \frac{z^2\, Z^2}{m^2} \tag{3.2}$$

where z is the charge of the projectile, m is its mass and Z is the atomic number of the medium. Eq. (3.2) teaches us the following about *bremsstrahlung* production and radiative slowing down:

- *Bremsstrahlung* production and radiative slowing down does not play a significant role for heavy charged particles (e.g. α-particles), as a result of the $1/m^2$ term. However, radiative slowing down with associated *bremsstrahlung* production, will play an important role in the attenuation of low-mass charged particles such as electrons.

- The slowing down of charged particles in a medium with a high atomic number Z will produce much more *bremsstrahlung* compared to a medium with a low Z, on account of the Z^2 term. This explains why low-Z materials such as Be, C and Al are used to shield electrons with minimal *bremsstrahlung* production.

Assignment 3.2

1. Stopping a beam of electrons in beryllium ($Z = 4$) produces $\left(\frac{82}{\square}\right)^2 \approx \square$ times less *bremsstrahlung* than stopping the beam of electrons in lead ($Z = 82$).

2. Stopping a beam of electrons in graphite ($Z = 6$) produces $\left(\frac{82}{\square}\right)^2 \approx \square$ times less *bremsstrahlung* than stopping the beam of electrons in lead ($Z = 82$).

3. Stopping a beam of electrons in aluminium ($Z = 13$) produces $\left(\frac{82}{\square}\right)^2 \approx \square$ times less *bremsstrahlung* than stopping the beam of electrons in lead ($Z = 82$).

4. Stopping a beam of α-particles in Fe will produce [5.3E7 / 2420 / 27] times less *bremsstrahlung* than stopping a beam of electrons in Fe.

Relative importance of ionisation energy loss and radiative energy loss in the attenuation of electrons

Radiation yields for electrons of different energies, are summarised in Table 3.1, for some important materials.

Table 3.1: *Radiation yields for electrons of different energies.*

E_e (MeV)	Water	Air	Al	Fe	Pb
0.1	6×10^{-4}	7.0×10^{-3}	1.4×10^{-3}	3.1×10^{-3}	0.0116
0.2	1×10^{-3}	1.1×10^{-3}	2.2×10^{-3}	5.2×10^{-3}	0.0212
0.5	2×10^{-3}	2.2×10^{-3}	4.3×10^{-3}	0.01	0.0424
1	3.6×10^{-3}	4×10^{-3}	7.64×10^{-3}	0.017	0.0684
1.5	5.3×10^{-3}	5.8×10^{-3}	0.0110	0.0239	0.0901
2	7.1×10^{-3}	7.7×10^{-3}	0.0145	0.0310	0.1096
4	0.0149	0.0158	0.0292	0.0595	0.1761
6	0.0233	0.0242	0.0444	0.0874	0.2304
8	0.0319	0.0327	0.0596	0.1139	0.2765
10	0.0406	0.0411	0.0745	0.1389	0.3162
15	0.0622	0.0618	0.1105	0.1951	0.3955
20	0.0830	0.0817	0.1438	0.2435	0.4555
50	0.1920	0.1825	0.2959	0.4328	0.6439
100	0.3190	0.3022	0.4448	0.5848	0.7617

The data in Table 3.1 is plotted in Figure 3.1.

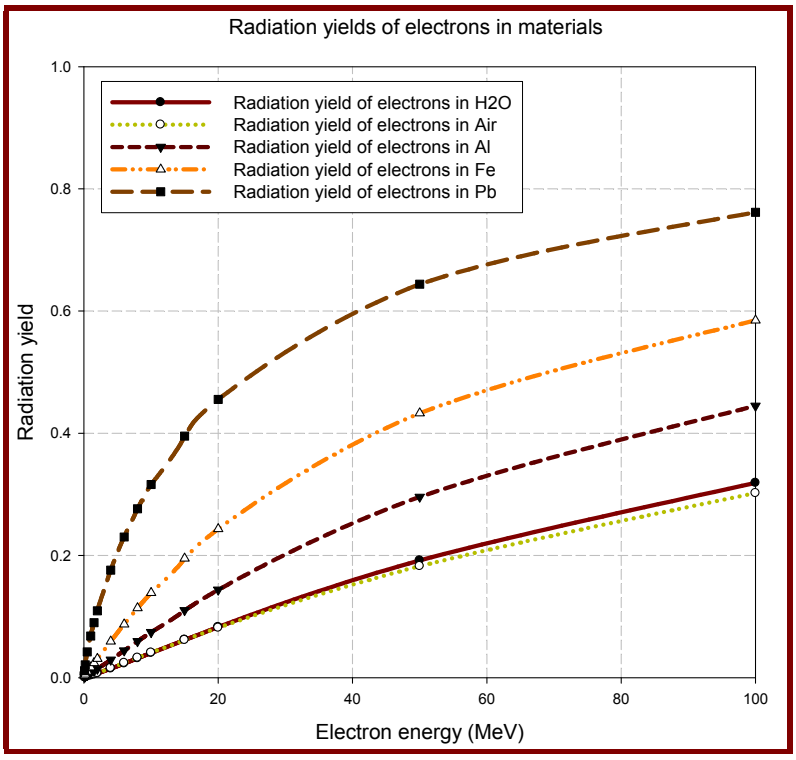

Figure 3.2: *Radiation yields for electrons of different energies, in different materials.*

It is seen that a significantly higher percentage of electron energy is converted into bremsstrahlung in high-Z materials such as Pb, compared to low-Z materials such as Al.

Example 3.1

At an electron energy $E = 6$ MeV and for Fe ($Z = 26$) as absorbing medium, about 8.7% of the energy loss of incident electrons will be by *bremsstrahlung* production, and 91.3% by ionisation slowing down.

Example 3.2

At an electron energy $E = 6$ MeV and with Pb ($Z = 82$) as absorbing medium, about 23% of the energy loss of incident electrons will be by *bremsstrahlung* production, and 77% by ionisation slowing down.

Example 3.3

At an electron energy $E = 100$ MeV and with Pb ($Z = 82$) as absorbing medium, approximately 76% of the energy loss of incident electrons will be by *bremsstrahlung* production, and 24% by ionisation slowing down.

Bremsstrahlung production in shields that stop electrons

How can we minimise *bremsstrahlung* production, and maximise the absorption of these X-rays which are produced upon the slowing down of charged particles?

Electrons are best shielded with materials with low atomic numbers to minimise the production of *bremsstrahlung X-rays,* i.e. secondary ionising photons. According to Eq. (3.2) on page 63, the cross-section for the production of Bremsstrahlung in an element with atomic number Z follows the relationship,

$$\sigma_{\text{bs}} \propto Z^2.$$

In the experimental arrangement below, we have to minimise the photon fluence-rate at the detector position. Shields A and B are just both thick enough to stop. One is made of graphite (carbon; $Z = 6$), and the other of lead ($Z = 82$). What shielding material would you use on the source and detector sides, respectively? Why?

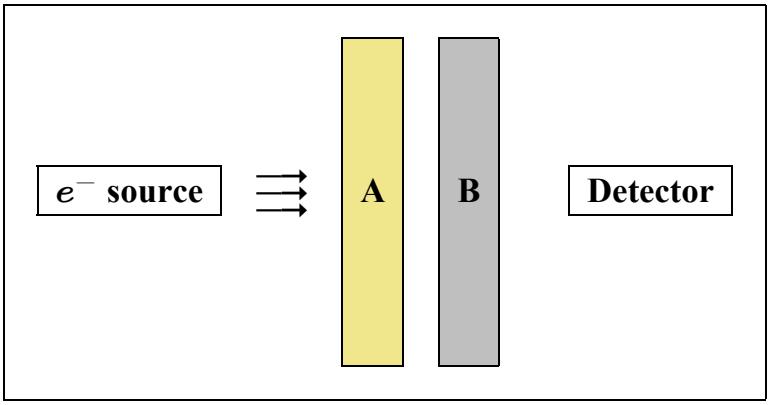

The solution is that shield A should be the carbon plate, and shield B the lead plate. Slowing down electrons in carbon ($Z = 6$) will produce $\left(\frac{82}{6}\right)^2 \approx 186$ times less *bremsstrahlung* than slowing them down in lead ($Z = 82$). The little *bremsstrahlung* produced in the carbon of shield A, will be very effectively attenuated by the lead of shield B, because high-Z materials are excellent photon shields. Note that the effectiveness of the above shield configuration can be radically "sabotaged" by simply swapping the two shielding plates around — then approximately 186 times more *bremsstrahlung* will be produced, and the graphite plate will be very inefficient at shielding the ionising *bremsstrahlung* photons, on account of its low Z-number.

3.1.4 Indirect energy deposition by neutrons and ionising photons; Charged particle equilibrium

Neutrons and ionising photons are indirectly ionising; they deposit their energy in matter indirectly, via interactions that release charged particles. These charged particles such as electrons in the case of photons, and protons and recoil nuclei in the case of neutron interactions, deposit the energy in matter. When a beam of uncharged particles such as neutrons and photons enter from a medium of low density such as air, into a medium of

significantly higher density such as the human body, it may take a few mm to establish *charged particle equilibrium.* In such situations, the entrance dose rate is lower than the dose rate at e.g. 4 mm into e.g. the human body, the polymer or the insects undergoing radiation-sterilisation. In radiotherapy, this gives a so-called skin-sparing effect.

In MCNP simulations of photon transport, this effect is seen when using an `F6:e` or a `+F6` energy deposition tally, with a run in `MODE p e`, for incident photons. If the ionising photon transport simulation is run in `MODE p`, the effect is not seen at all.

3.1.5 Charged particle range, and stopping power

A charged particle loses energy (i.e. is slowed down) as a result of both (1) Coulombic interactions with atomic electrons, and (2) radiative losses *(bremsstrahlung* production). The stopping power of a material medium, is $\frac{dE}{dx}$, i.e. the expected energy loss per unit distance travelled by the charged particle. The term stopping power is synonymous with the term Linear Energy Transfer (LET), denoted as $L(E)$ where E is the energy of the charged projectile. During the deceleration of an electrically charged particle, the stopping power generally increases until the energy of the particle is so low that charge neutralisation and quantum effects bring about an abrupt reduction. This results in a prominent Bragg peak. The distance that charged particles in an aligned beam of mono-energetic incident radiation travels before being stopped, is called its range. For a monoenergetic, parallel beam of incident particles, there is, of course, a small stochastic spread in ranges. The semi-analytical continuous slowing-down approximation (CSDA) is one widely used and quite accurate method of calculating charged particle ranges — see page 71. Monte Carlo codes such as SRIM, MCNP and, especially, EGS[7], are generally more accurate than the semi-analytical CSDA formalism.

Heavy charged particles slow down almost exclusively by Coulombic interactions; electrons slow down by a combination of Coulombic and radiative energy losses — see Table 3.1 on page 65 and Figure 3.2 on page 66.

3.1.6 Ranges of protons, α-particles and electrons in matter

[7] The EGS (Electron Gamma Shower) computer code system is a general purpose package for the Monte Carlo simulation of the coupled transport of electrons and photons in an arbitrary geometry for particles with energies from a few keV up to several TeV. It was developed at SLAC (Stanford Linear Accelerator). The SLAC version of EGS is no longer actively developed. There are two forks which are being actively maintained: (1) EGSnrc, maintained by the *Ionizing Radiation Standards Group, Institute for National Measurement Standards, National Research Council of Canada,* as well as (2) EGS, maintained by KEK, the Japanese particle physics research facility.

Assignment 3.3

1. Use SRIM and MCNP to calculate the range of protons and α-particles spanning the range from 1 MeV to 100 MeV in (1) air, (2) water and (3) copper, and construct an informative table of ranges.

Electron range in materials

Table 3.2 Table 3.2 was calculated using NIST data from the website **http://www.nist.gov/pml/data/star/ and** presents electron ranges in dry air at STD as well as in skeletal muscle.

Table 3.2: *Ranges of electrons in air and human tissue, calculated with an approximate empirical fit to electron range data (Shultis & Faw, 2000: 71).*

Electron energy (MeV)	Range in air (cm)	Range in tissue (cm)
0.1	23	0.025
0.2	67	0.074
0.3	119	0.131
0.4	174	0.192
0.5	229	0.253
0.6	284	0.314
0.7	339	0.375
0.8	392	0.436
0.9	444	0.496
1.0	496	0.555
1.1	546	0.613
1.2	596	0.671
1.3	645	0.728
1.4	693	0.785
1.5	741	0.842
1.6	788	0.898
1.7	834	0.953
1.8	880	1.008
1.9	925	1.062
2.0	970	1.116
2.5	1188	1.382
3.0	1396	1.641

An electron energy of at least 70 keV is required to penetrate the protective dead surface layer of the skin. Only electrons having energies above circa 0.5 MeV are able to reach the lens of

the eye, which is located 0.3 cm under the surface of the cornea. In general, electrons with incident energies below circa 0.05 MeV (i.e. 50 keV) are not considered to be a serious external radiation hazard.

Assignment 3.4

1. A specific radionuclide emits β^- radiation with a maximum energy of 2.99 MeV. Will any primary electrons reach you if you stand 2 m away in air from an unshielded source?

2. A specific radionuclide emits β^- radiation with a maximum energy of 2.99 MeV. Will any primary electrons reach you if you stand 12 m away in air from an unshielded source?

3. A specific radionuclide emits β^- radiation with a maximum energy of 2.99 MeV. Will any primary electrons reach you if you stand 13 m away in air from an unshielded source?

4. A specific radionuclide emits β^- radiation with a maximum energy of 2.99 MeV. Will any primary electrons reach you if you stand 15 m in air away from an unshielded source?

3.1.7 The continuous slowing-down approximation (CSDA) and the Bethe formula

Reference: Shultis & Faw (2000: 61-72).

The analytical treatment of charged particle slowing down, is conceptually and mathematically rather difficult. We therefore treat it according to the methodology that we embarked upon early in this course: "Have an outline idea of the underlying mathematical physics, but leave the detailed numerical calculations up to the radiation transport codes" such as MCNP, EGS, FLUKA or GEANT.

Under the continuous slowing-down approximation (CSDA) for heavy charged particles such as protons and alpha-particles, the range $\Lambda(T)$ of a charged particle with initial kinetic energy T, is

$$\Lambda(T) = \int_0^T \frac{1}{S(M,E,Z)} dE \tag{3.3}$$

where the ***stopping power*** S is defined as

$$S(M,E,Z) = \frac{4\pi\, q_e^4\, Q^2}{m_e\, v(M,E)^2}\, N_{\text{medium}}\, B(M,E,Z) \left(\frac{1}{4\pi\epsilon_0}\right)^2 \tag{3.4}$$

where q_e is the charge on an electron, Q is the electrical charge of the charged particle expressed as e.g. 1 for protons and 2 for α-particles, m_e is the mass of an electron and ϵ_0 is the permittivity of vacuum. The function B is given by

$$B(M,E,Z) = Z\left[\ln\left(\frac{2m_e\,(v(M,E))^2}{I}\right) - \ln\left(1 - \frac{(v(M,E))^2}{c^2}\right) - \left(\frac{(v(M,E))^2}{c^2}\right)\right] \tag{3.5}$$

where Z is the effective atomic number of the attenuating medium, I the ionisation potential of the attenuating medium, c the speed of light in a vacuum, while the speed v of a particle with mass m and kinetic energy E is given by

$$v(m,E) = c\sqrt{1 - \left[\frac{1}{\left(1 + \frac{E}{mc^2}\right)^2}\right]}$$

and the number-density N_{medium} of atoms in the stopping medium is,

$$N_{\text{medium}} = \frac{\rho N_A}{M_r}$$

where ρ is the mass-density of the attenuating medium, N_A is Avogadro's number and M_r is the relative molar mass of the attenuating medium's atoms or molecules.

Eqs. (3.4) and (3.5) constitute the Bethe formula.

The following MathCAD worksheet shows a charged particle range calculation. Note that problems with the convergence in the numerical calculation of the stopping power integral,

$$\Lambda(T) = \int_0^T \frac{1}{S(M,E,Z)} dE$$

forced the use of a non-zero lower limit for the integration — the value of 40 keV worked reasonably well. Integration right from $E = 0$ led to non-convergence of the numerical integration process in MathCAD.

Bethe Formula Charged Particle Range.xmcd

Assignment 3.5

1. Show from the Bethe formula for stopping power, i.e. Eq. (3.4) on page 71, that Linear Energy Transfer (LET) will be approximately proportional to $\frac{z^2 Z}{v}$ for charged particles, under the continuous slowing-down (CSDA) approximation.

2. Port the formulas in the above MathCAD worksheet to Mathematica, Maple or MatLAB. Does the problematic integral now converge in a more stable fashion?

We now focus on a number of important charged particles and their characteristic interaction modes.

Alpha particles

The α-particle has a charge of $+2$, and moves relatively slowly on account of its large mass, so that the variable z in Eq. (3.1) on page 61 will have the value $+2$, while v will be relatively small. It follows that α-particles will be strongly attenuated by ionisation slowing down. The linear energy transfer (LET) and ionisation density will be high. It will transmit its energy to matter over a short distance, and will have a short range. The α-particle interacts intensely with the negative electrons of atoms when it passes through matter, tearing electrons from atoms and dragging them along. During this process the α-particle continually loses energy. Atoms near the track of the α-particle are intensely ionised — an α-particle typically produces 10^7 ion pairs per cm track in tissue. Low-energy α-particles only undergo ionisation slowing down, while high-energy α-particles can also partake in nuclear reactions. Alpha particles with similar initial energies have a certain maximum *range* in a particular material.

Eq. (3.1) on page 61 shows that the α-particle, with its relatively large mass m, will undergo very little radiative slowing down and will produce practically no *bremsstrahlung*.

Alpha particles emitted by radionuclides always have energies below 10 MeV, and will therefore be completely shielded by means of a single sheet of paper or a few centimetres of air. In dense materials, the range is normally below 0.1 mm. Even the dead surface layer (thickness $\approx$ 0.07 mm) on one's skin is capable of shielding live tissue from alpha particles having an incident energy below 7.5 MeV.

Figure 3.3 shows how much slower α-particles will move compared to electrons of the same energy. Eq. (14.12) on page 500 was used to calculate particle speeds and speed ratios.

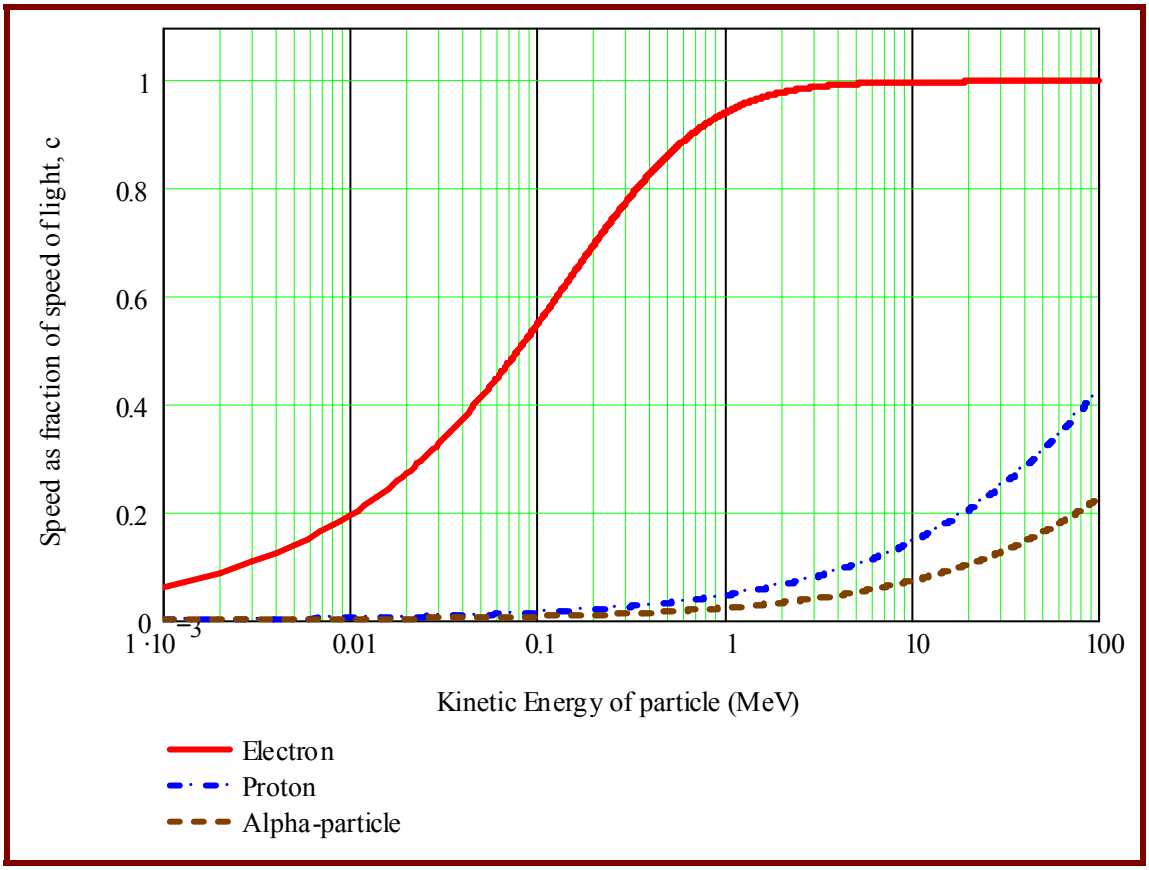

Figure 3.3: *The speed of α-particles, protons and electrons of different energies, as a fraction of the speed of light in a vacuum.*

Figure 3.4 shows that, at low energies, α-particles move about 85 times slower than electrons of the same energy. At relativistic energies, the speed ratio decreases. Alpha-particles emitted by radionuclides fall in the energy range where they will move at least 15 times slower than electrons of the same energy.

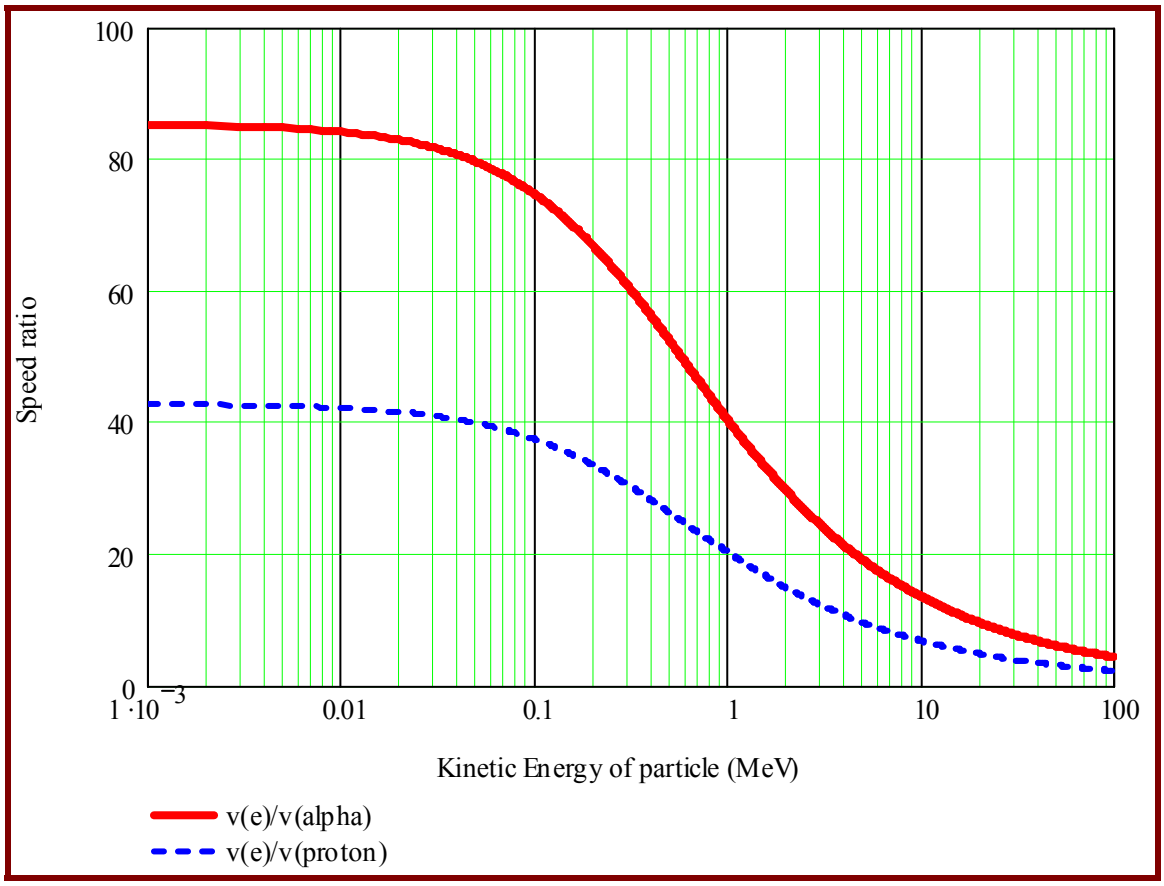

Figure 3.4: *The speed ratio of electrons to that of α-particles end protons of the same energy. In the energy range $0 \leq E \leq 100\,MeV$, the ratio $\frac{v(e^-)}{v(\alpha)}$ varies between the limits $4 < \frac{v(e^-)}{v(\alpha)} < 86$. At a low incident energy, an α-particle moves about 86 times slower than an electron of the same energy. According to Eq. (3.1) on page 61, the intensity of ionisation slowing down is proportional to $\frac{1}{v}$; this makes it clear that an alpha particle will undergo ionisation slowing down up to ~100 times more intensely than an electron.*

Protons

Attenuation of protons is analogous to that of α-particles, but interaction is less intense, Linear Energy Transfer (LET) is lower, and particle ranges somewhat larger.

Electrons

The negative electron (negatron) has a charge of -1 and a much lower mass than an α-particle. Because its mass is lower, it moves much faster (up to 85 times faster) than α-particles with the same energy. An electron gradually loses its energy in a large number of ionisation, excitation and bremsstrahlung production events. Eq. (3.1) on page 61 shows that the β-particle, with its higher velocity v than an alpha particle of similar energy, and single charge ($z = -1$), will display a **smaller LET** for ionisation slowing down than the α particle. The ionisation density produced by electrons is lower and the range of the particle is longer. Whereas a typical alpha particle produces 10^7 ion pairs per centimetre track in tissue, a typical

electron produces about 10^5 ion pairs per cm, i.e. the ionisation density produced by an electron is roughly 100 times lower than that produced by an alpha particle. Being a charged particle, the β^--particle continually loses energy; β^--particles with similar initial energies have a certain maximum range in a particular material. Because it loses less energy per unit path length, the range of an electron is considerably greater than that of an alpha particle of comparable energy.

We have seen that a charged particle which is decelerated emits *bremsstrahlung*. *Bremsstrahlung* production is proportional to $\frac{1}{m^2}$. The mass of an electron is about 7295 times lower than that of an alpha particle, so that *bremsstrahlung* production will be about 53 million times more intense when electrons are slowed down, compared to the slowing down of α-particles. An electron has a low mass m and can be rapidly decelerated when it passes close to a nucleus, as a result of interaction with the positive charge of the nucleus. Eq. (3.2) on page 63 shows that radiative slowing down will contribute appreciably to the attenuation of fast electrons, particularly when the incident energy and the atomic mass, Z, of the attenuating medium are high. *Bremsstrahlung* must be considered when working with radionuclides that emit high-energy electrons.

The **β^+-particle** is a positron. A positron will lose its kinetic energy through ionisations, excitations and *bremsstrahlung* production, in a similar fashion to a negative electron, producing essentially the same ionisation density as a β^--particle. Eventually, the positron combines with a negative electron, whereupon the positron and negatron are *annihilated,* producing two 0.511 MeV photons called *annihilation radiation.* These annihilation photons will cause further ionisation. Since positrons are electrons, the radiation hazard from the positrons themselves is very similar to the hazard from electrons. There is one important difference between β^+ and β^- emitters, though. On account of their low penetrating ability, β^- particles having energies below about 100 keV do not pose an external radiation hazard. The gamma radiation resulting from the annihilation of the positrons, however, makes all positron-emitting radionuclides potential external radiation hazards, i.e. irrespective of the energy of the β^+ particle.

Low-energy electrons only exhibit ionisation and radiative slowing down, whereas high-energy electrons, produced by particle accelerators, may also cause nuclear reactions.

Electrons have a greater penetrating power than α-particles and can, depending on the energy, move through $1-2$ cm of water or human tissue, or several metres of air.

3.2 Interaction modes and penetrating abilities of neutral particles

Whereas charged particles have an electrical charge and therefore interact continuously with the electrically charged electrons and nuclei in atoms, neutral particles like the neutron and photon do not interact continuously, but in discrete "catastrophic" collisions with atomic electrons or nuclei. In these collisions, energy is transferred to nuclei or electrons, or to charged particles produced by nuclear reactions. These charged particles subsequently interact in the manner described above.

Neutral particles such as neutrons and photons of a given incident energy do not have a fixed range in matter, but are attenuated gradually; the number of particles that penetrate to a specific depth in matter tends to approximately follow an exponential dependence similarly to that seen in half-life curves — compare Figure 4.1 on page 178.

Neutrons

The neutron is indirectly ionising — ionisation is produced by charged particles such as recoil nuclei and nuclear reaction products, produced by the neutrons. The production of secondary ionising photons by neutrons will result the release of energetic electrons, and these can deposit energy at a considerable distance from the interaction centres of the neutrons.

There is negligible interaction between neutrons and the electron cloud of atoms — the neutron is a hadron without any net charge, while electrons are leptons, and are therefore unaffected by the strong nuclear force. Because the neutron has no charge it only interacts through direct collisions with atomic nuclei. The only substantial energy loss of neutrons are through **interaction with atomic nuclei.** When neutrons impinge onto a medium, the nuclear reactions that can take place will depend on the energy of the neutron and the cross-sections for the nuclear reactions. Neutrons are scattered or absorbed by nuclei. Scattering is the deflection of neutrons from their original direction and energy. Neutrons can also be captured or absorbed by the nucleus. When a nucleus absorbs a neutron, γ-photons are, as a rule, emitted when the excited product nucleus reverts to its ground energy state. At high incident energies, neutrons produce charged particles such as alpha particles and protons, by nuclear reactions with nuclei. The secondary radiation produced in this manner causes ionisation. When a high-energy neutron is scattered by an atomic nucleus, the nucleus recoils. The recoil nucleus has a high positive charge (z is high) and moves relatively slowly (i.e. v is low); it follows from Eq. (3.1) on page 61 that it can produce very intense ionisation.

Nuclear reactions that can take place when neutrons impinge on a medium, are (n, n'), (n, np), (n, γ), (n, α), $(n, 2n)$, etc. Exit channels will open above threshold energies where the energetics of the nuclear reaction allow it.

The neutron has the greatest penetrating power of the four types of ionising radiation which we are studying in this course, and is the most difficult to shield. Neutrons also produce nuclear reactions that cause shielding material to become radioactive. In addition, secondary γ-photons are produced when neutrons are absorbed by nuclei. This complicates neutron shield design even further.

Concrete is the most practical material for neutron shields. Neutrons with very high energies are best shielded by a thick layer of steel followed by approximately 10 cm of paraffin wax or polyethylene. A shield consisting only of a hydrogen-rich material, e.g. paraffin wax or polyethylene, will in general be a poor neutron shield, especially for faster neutrons. (Note that virtually all training material on radiation protection erroneously states the exact opposite!)

Ionising photons

Like neutrons, ionising photons are indirectly ionising — their interactions will release energetic electrons, which then deposit the energy. Like the neutron, the photon carries no electric charge. Low-energy photons only interact with atomic electrons. The photons can be absorbed in photo-electric absorption, or scattered, and knock out atomic electrons in the process; (β^-, β^+) pairs are produced if $E\gamma > 1.02$ MeV. The charged electrons emitted from the atoms subsequently produce excitation and ionisation. In addition to interactions with atomic electrons, high-energy photons produce nuclear reactions that cause the emission of neutrons, α-particles, protons, β^- and β^+ particles. High-energy photons have great penetrating power and can deposit their energy in internal bodily organs. Ionising photons are best stopped by materials with high densities ρ and high atomic numbers Z.

Penetrating abilities of ionising radiation

Alpha particles, electrons, neutrons and photons do not interact with the same intensity, and have markedly different penetrating abilities, which are schematically depicted in Figure 3.5.

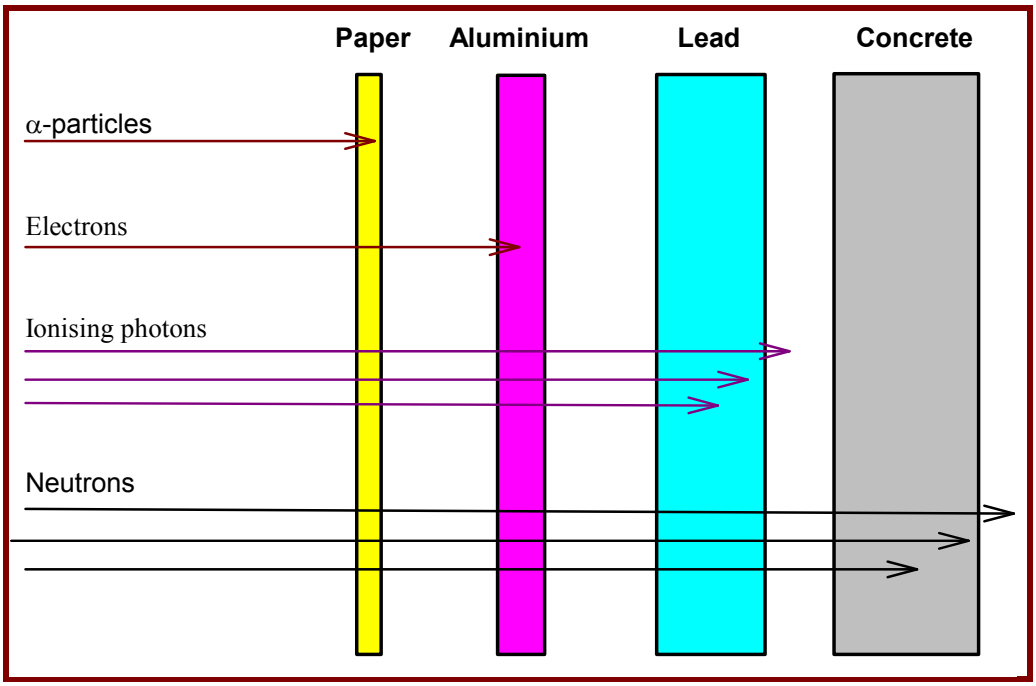

Figure 3.5: *The penetrating abilities of different types of ionising radiation. Charged particle radiation (α-, β^-- and β^+-particles) of a given energy has a fixed range in a specific material and are easily stopped because they interact intensely. In contrast, neutral particle radiations such as neutrons & ionising photons, are attenuated gradually and are far more penetrating than charged particles of the same incident energy. Neutrons cause nuclear reactions that produce secondary γ-photons as well as radionuclides in matter.*

The properties and typical ranges in air and human tissue, of important types of ionising radiation, are summarised in Table 3.3.

Table 3.3: *Important types of ionising radiation emitted by radionuclide sources, and their penetrating abilities.*
Note: high-energy charged particles produced by particle accelerators, will have much higher ranges than stated in this table; the listed ranges for charged particles only pertain to emission by radionuclides.

Radiation	Symbol	Nature	Mass (a.m.u.)	Charge	Typical range in air	Typical range in tissue
Alpha	α	Particle	4	$+2$	3 cm	0.04 mm
Electron	β^-	Particle	$\frac{1}{1823}$	-1	1 – 6 m	1-10 mm
Ionising photons	γ, X	Photon	0	0	Very large	Through body
Neutron	n	Particle	1	0	Very large	Through body

Charged particles lose their energy continuously and have fixed ranges. Heavy charged particles are mainly attenuated by ionisation slowing down, while light charged particles undergo ionisation slowing down as well as radiative slowing down (*bremsstrahlung* production). Charged particles like alpha- and electrons have a finite maximum range and can therefore be completely stopped with a sufficient thickness of absorber.

Neutral particles lose energy at discrete locations, producing secondary charged particles which causes excitation and ionisation. Neutral particles like neutrons and photons interact in a probabilistic manner, so that an individual neutron or photon will have no definite range. The fraction of neutrons or photons that passes through an absorber decreases approximately exponentially with the thickness of the absorber.

Radiation shields are used to protected, e.g., people, biota, polymers and electronic apparatus against ionising radiation, by reducing the fluence-rate ϕ of the radiation to below desired levels (neutral particles: neutrons and photons) or even stop it completely (charged particles: β^-- and α-particles). It is evident that is much easier to shield charged particles than neutral ionising radiations.

3.3 Linear Energy Transfer (LET)

The amount of energy that ionising radiation deposits per unit path length is important. The microdistribution of the ionisations and excitations produced by ionising radiation depends on the type and energy of the incident radiation. The average energy deposited along the track of the particle per unit length depends on the type of particle and its energy and is called the *linear energy transfer* (LET) of the particle,

$$\text{LET} = \frac{dE}{dl} \tag{3.6}$$

where E is the energy of the radiation and l denotes path length. Thus, a sparsely ionising radiation producing few events per micron of track, is known as a **low-LET** radiation.

Ionising photons are low-LET radiation. Radiations that produce dense ionisations along the track are known as **high-LET** radiation. Alpha particles, heavy ions, protons and recoil nuclei from neutron scattering events are all **high-LET** radiation.

Table 3.4 summarises LET values for different ionising radiation particles & energies.

Table 3.4: *Different types of ionising radiation may be classified as low-LET, medium-LET and high-LET. The microdeposition of energy, expressed as LET, is an important factor that determines the biological harmfulness of a given absorbed dose.*

Ionising radiation type	**Energy**	**LET** (keV/μm)
Photons	250 keV	3
Photons	1.25 MeV	0.3
Photons	3 MeV	0.3
Electrons	10 keV	2.3
Electrons	1 MeV	0.25
Neutrons	2.5 MeV	20
Neutrons	19 MeV	7
Protons	2 MeV	16
α-particles	5 MeV	100
Fission fragments	High	5000

Figure 3.6 illustrates different LET values for different charged particles of the same incident energy.

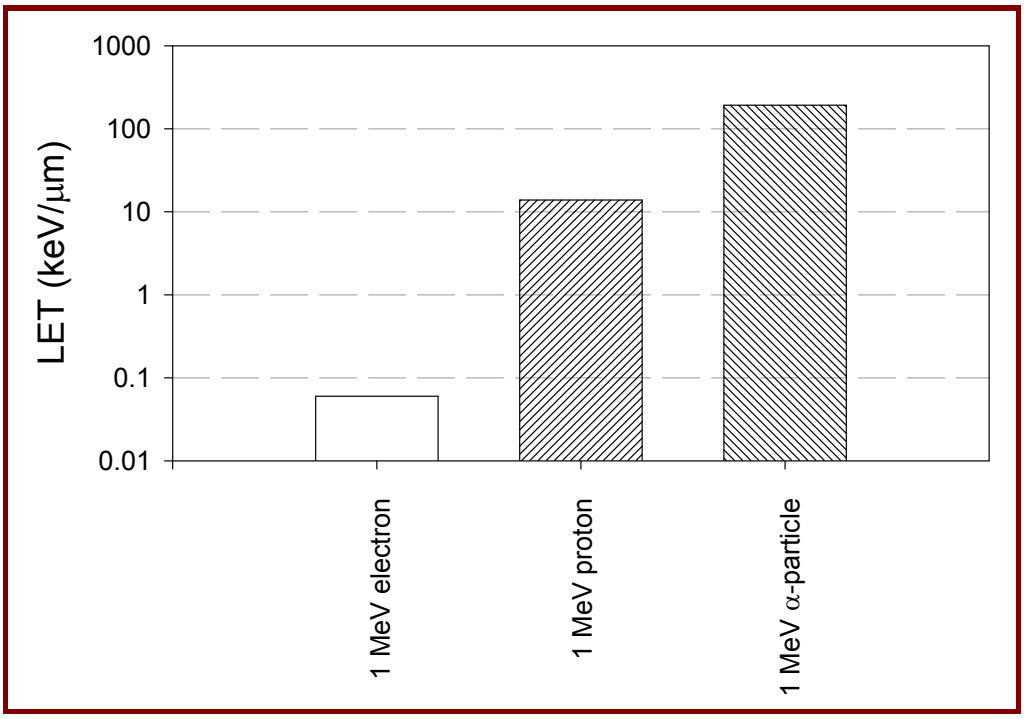

Figure 3.6: *Linear energy transfer (LET) values for different charged particles in human tissue. A 1 MeV electron has a LET of 0.06 keV/µm; a 1 MeV proton has a LET of about 14 keV/µm and a 1 MeV alpha particle has a LET of about 180 keV/µm. Alpha particles are classified as high-LET radiation while electrons are low-LET radiation. Protons could be termed medium-LET ionising radiation.*

3.4 Activation: Induced radioactivity

Ionising radiation may induce radioactivity in matter. Chapter 4 explained that a nucleus is unstable if the ratio of protons to neutrons is unfavourable. When neutrons of any energy, or high-energy protons, high-energy α-particles, high-energy β^--particles or high-energy photons, collide with a nucleus, nuclear reactions that change this $\frac{proton}{neutron}$ ratio, may take place. The product nuclei are often radionuclides, so that the material becomes radioactive. We call this process of inducing radioactivity in materials, via nuclear reactions caused by irradiation, *activation.*

Qualitative examples: Neutron activation

Example 1: Suppose we expose cobalt to neutron irradiation. Cobalt has 1 stable isotope, namely ^{59}Co, which has 27 protons and 32 neutrons in its nucleus. When a ^{59}Co nucleus absorbs a neutron, a nuclear reaction takes place. The product is still cobalt (the number of protons has not been altered), but it now has 33 neutrons and is called ^{60}Co ($27 + 33 = 60$). The activation product, ^{60}Co, has an excess of neutrons and is an unstable radionuclide with a half-life of 5.27 years. To regain a Z/N ratio that will ensure stability, ^{60}Co undergoes β^-transition. The product nucleus de-excites by emitting γ-photons.

Example 2: Suppose we expose a piece of copper to neutron irradiation. ^{65}Cu is one of the two stable isotopes of the element copper, with 29 protons and 36 neutrons in the nucleus. Suppose a neutron is absorbed by the ^{65}Cu nucleus, which then emits a proton. We call this a (n, p) reaction. A neutron was gained while a proton was lost. Because the product nucleus has 28 protons (instead of the original 29), it is now an atom of a new element — nickel. There are now $36 + 1$, i.e. 37 neutrons in the nucleus. The new isotope is ^{65}Ni $(28 + 37 = 65)$. ^{65}Ni has an excess of neutrons and is an unstable radionuclide with a half-life of 2.5 hours. To regain a Z/N ratio that will ensure stability, ^{65}Ni undergoes β^- transition. The product nucleus de-excites by emitting γ-photons.

Example 3: Suppose we bombard a zinc target in a proton beam. ^{67}Zn is a stable isotope of the element zinc, with 30 protons and 37 neutrons. Suppose a proton is absorbed by the nucleus, which then emits a neutron. A proton was gained while a neutron was lost, so that we call it a (p, n) reaction. Because the product nucleus has 31 protons (instead of the original 30), it is now an atom of the element gallium. It now has $37 - 1 = 36$ neutrons in its nucleus. The new isotope is ^{67}Ga $(31 + 36 = 67)$. ^{67}Ga has a shortage of neutrons, i.e. its Z/N ratio is too high for stability; it is a radionuclide with a half-life of 78.3 hours. It undergoes transition by electron capture, a type of beta transition. The product nucleus de-excites by emitting γ-photons. No electron is emitted in the electron capture reaction.

Quantitatively accurate examples: Neutron activation

When a fixed amount of a fixed material type having a given elemental composition, is put through a known irradiation cycle in a given neutron field, a characteristic $\{NA\}$ activation-matrix is obtained, where the N-column contains the nuclide identifier and the A-column contains the corresponding nuclide activity in a unit such as Bq. In other words, an $\{NA\}$ activation-matrix is a 2-column matrix, where column 1 contains the radio-nuclide name N, and column 2 contains the activity A in a unit such as Bq.

For a reference mass $\boxed{M\_\text{ref}_{\text{AL6082}} = 1 \text{ kg}}$ of the alloy AL-6082 irradiated in an energy-integrated total neutron fluence-rate of $\boxed{\Phi\_\text{ref} = 1.0 \times 10^{14} \text{ cm}^{-2}\,\text{s}^{-1}}$ for $T_{\text{on}} = 6$ months, and then cooled off for $T_{\text{off}} = 6$ months, with this cycle repeated a total of $\boxed{N_{\text{pulse}} = 30}$ times, i.e. for 30 years, the following $\{NA\}$ activation-matrix, Act_AL6082, is obtained:

Act_AL6082 =

Co-60	4.5894E+11
Zn-65	1.0671E+11
Fe-55	9.3970E+10
Cr-51	5.1970E+09
Ca-45	1.1359E+09
Mn-54	9.7042E+08
Fe-59	7.4360E+08
S-35	4.2963E+08
Ni-63	3.7751E+08
Sc-46	2.8976E+08
Ar-39	3.7411E+07
Ar-37	3.3957E+07
Ca-41	7.9065E+06
P-32	4.1779E+06
P-33	4.3603E+05
V-49	1.9027E+05
Cl-36	6.6186E+04
Co-58	5.7838E+04
Si-32	1.8390E+04
Al-26	6.9630E+03
Ge-71	2.6500E+03
K-40	1.9810E+03
Na-22	1.0470E+03
Fe-60	1.9330E+02
Co-60m	1.9330E+02
Ar-42	2.4110E+01
K-42	2.4110E+01
Ni-59	1.1480E+01
Mn-53	4.0050E+00

For a reference mass $\boxed{M\_\text{ref}_{\text{AL6261}} = 1\ \text{kg}}$ of the alloy Al-6261, irradiated in an integral neutron fluence-rate of $\boxed{\Phi\_\text{ref} = 1.0 \times 10^{14}\ \text{cm}^{-2}\,\text{s}^{-1}}$ for $T_{\text{on}} = 6$ months, and then cooled off for $T_{\text{off}} = 6$ months, with this cycle repeated a total of $\boxed{N_{\text{pulse}} = 30}$ times, i.e. for 30 years, the following $\{NA\}$ activation matrix, Act_AL6261, is obtained:

Act_AL6261 =

Co-60	4.5848E+11
Zn-65	1.1501E+11
Fe-55	7.6421E+10
Cr-51	2.0789E+09
Ca-45	1.1359E+09
Mn-54	7.3460E+08
Ni-63	6.9094E+08
Fe-59	5.7855E+08
S-35	4.2963E+08
Sc-46	2.8976E+08
Ar-39	3.7411E+07
Ar-37	3.3957E+07
Ca-41	7.9065E+06
P-32	4.1699E+06
P-33	4.3602E+05
V-49	7.6108E+04
Cl-36	6.6186E+04
Co-58	5.7736E+04
Si-32	1.8280E+04
Al-26	7.0650E+03
Ge-71	2.6500E+03
K-40	1.9810E+03
Na-22	1.0450E+03
Fe-60	1.5660E+02
Co-60m	1.5660E+02
Ar-42	2.4110E+01
K-42	2.4110E+01
Ni-59	1.1480E+01
Mn-53	3.2040E+00

For a reference mass $\boxed{M\_\text{ref}_{\text{SS304}} = 1 \text{ kg}}$ SS-304 irradiated in an integral neutron fluence-rate of $\boxed{\Phi\_\text{ref} = 1.0 \times 10^{14} \text{ cm}^{-2}\,\text{s}^{-1}}$ for $T_{\text{on}} = 6$ months, and then cooled off for $T_{\text{off}} = 6$ months, with this cycle repeated a total of $\boxed{N_{\text{pulse}} = 30}$ times, i.e. for 30 years, the following $\{NA\}$ activation matrix, Act_SS304, is obtained:

Act_SS304 =

Fe-55	1.3059E+13
Ni-63	1.5229E+12
Co-60	7.2493E+11
Cr-51	3.9499E+11
Mn-54	1.2007E+11
Fe-59	9.7381E+10
Co-58	4.7470E+10
Ni-59	7.7701E+09
Co-57	4.8870E+08
S-35	4.2921E+08
Zn-65	1.2765E+08
V-49	1.4461E+07
P-32	5.4549E+06
P-33	3.9010E+05
Cl-36	2.6780E+04
Si-32	2.3872E+04
Fe-60	2.3855E+04
Co-60m	2.3855E+04
Ca-45	8.5020E+03
Co-56	5.2620E+03
Sc-46	1.1990E+03
Mn-53	5.4710E+02
Ar-37	3.0950E+01
Ar-39	7.2280E+00
Be-10	1.1930E+00

It is evident that the SS-304 activates approximately 24 times worse than the Al alloys. The long-term activation of an Al alloy in a neutron field, is almost entirely driven by the alloying elements and impurities in the Al-alloy.

For a reference mass $\boxed{M\_\text{ref}_{\text{SS316}} = 1 \text{ kg}}$ SS-316 irradiated in an integral neutron fluence-rate of $\boxed{\Phi\_\text{ref} = 1.0 \times 10^{14} \text{ cm}^{-2}\,\text{s}^{-1}}$ for $T_{\text{on}} = 6$ months, and then cooled down for $T_{\text{off}} = 6$ months, with this cycle repeated a total of $\boxed{N_{\text{pulse}} = 30}$ times, i.e. for 30 years, the following $\{NA\}$ activation matrix, Act_SS316, is obtained:

Act_SS316 =

Fe-55	1.1879E+13
Ni-63	2.1321E+12
Co-60	8.5613E+11
Cr-51	3.7420E+11
Mn-54	1.0919E+11
Fe-59	8.8919E+10
Co-58	6.4260E+10
Ni-59	1.0878E+10
Mo-93	7.3804E+08
Co-57	7.0759E+08
S-35	4.2921E+08
Nb-93m	3.0985E+08
Zn-65	1.7872E+08
Tc-99	3.3391E+07
Ru-103	2.7110E+07
Rh-103m	2.6812E+07
V-49	1.3699E+07
P-32	5.4563E+06
Nb-91m	2.4930E+06
Nb-95	2.1600E+06
Nb-91	2.1460E+06
P-33	3.9010E+05
Zr-95	3.6530E+05
Nb-94	2.8090E+04
Cl-36	2.6780E+04
Si-32	2.3890E+04
Fe-60	2.1760E+04
Co-60m	2.1760E+04
Ca-45	8.0540E+03
Co-56	7.3670E+03
Y-88	6.7430E+03
Nb-92m	4.7680E+03
Nb-95m	4.1830E+03
Zr-88	2.6570E+03
Sc-46	1.1360E+03
Mn-53	4.9750E+02
Nb-92	1.6150E+02
Rh-102	1.3880E+02
Zr-93	1.3040E+02
Rh-102m	1.2690E+02
Sr-89	4.2100E+01
Y-91	3.2950E+01
Tc-97m	3.2860E+01
Ar-37	3.0950E+01
Ar-39	7.2280E+00
Tc-98	4.2950E+00
Be-10	1.1930E+00

Like SS-304, the SS-316 activates approximately 24 times worse than the Al alloys.

The long-term activation of an Aluminium alloy in a neutron field, is almost entirely driven by the alloying elements and impurities in the Al-alloy.

3.5 Introduction to neutron interactions

3.5.1 Neutron interaction cross-sections differ from isotope to isotope

The interaction of neutrons with matter is fundamentally different from those of ionising photons. In the energy range of interest, ionising photons mainly interact with atomic electrons, and almost never with nuclei. In contrast, neutrons interact essentially only with the atomic nucleus.

The cross-sections that describe neutron interactions are also very dissimilar to that of photon interaction cross-sections. Neutron cross-sections can vary very rapidly as a function of the incident neutron energy, but also drastically from one isotope of an element to another isotope of the same element. Photon interaction cross-sections for photo-electric absorption (PEA), Compton scattering (CS) and pair production (PP) on ^{10}B and ^{11}B are essentially identical, whereas there is a world of difference between the neutron interaction cross-section of ^{10}B and that of ^{11}B. Neutron interaction cross-sections differ from isotope to isotope, whereas photon interaction cross-sections for CS, PEA and PP essentially only differ from element to element and NOT from isotope to isotope of the same element.

All neutron cross-section data and models are highly empirical in nature. Nuclear models have some predictive power in energy regions where measured neutron cross-section data are not available.

Assignment 3.6

Perform the following calculations in simple spherical symmetry, with a point-source at the centre.

1. Use the code MCNP to model neutron transport through a layer of pure ^{10}B. Let the incident neutron energy be 1 eV, and let the boron layer thickness be 5 cm. Assume that the mass-density of the boron layer is $2.35\,\mathrm{g\,cm^{-3}}$. Run the problem in `MODE N P`. Calculate the neutron fluence-rate and the photon fluence-rate on the outer surface of the boron layer, using an F1 tally.

2. Repeat the above analysis, but with pure ^{11}B as the material.

3. Repeat the previous two calculations for $E_n = 1$ MeV.

4. Repeat the previous two analyses, but for incident photons, having $E_\gamma = 1\,\text{MeV}$, and a boron layer thickness of 10 cm. Run the problem in [MODE P E]. Calculate the photon fluence-rate on the outer surface of the $^{10}_{5}\text{B}$ and the $^{11}_{5}\text{B}$ layer, using an F1 tally.

5. Repeat the previous analysis, for incident photons, having $E_\gamma = 30\,\text{MeV}$ and with (γ, n)-reactions switched on in the [phys:p] card.

6. $^{10}_{5}\text{B}$ and $^{11}_{5}\text{B}$ contain the same number of [e] in the electron clouds surrounding the nucleus. Therefore QED photon-electron interactions will be practically identical for $^{10}_{5}\text{B}$ and $^{11}_{5}\text{B}$, i.e. QED photon-electron interactions will only depend on the [e] composition of a material and not on its [i] composition. In contrast to the above simple situation, $^{10}_{5}\text{B}$ and $^{11}_{5}\text{B}$ contain different numbers of [n] in their nuclei, so that all nuclear reactions will strongly depend on the isotopic composition of boron.

7. For incident photon energies below the threshold energy of (γ, n)-reactions, the transport of photons and electrons only depends on the [e] in the material regions, and not on the specific [i] that are present. In contrast, the transport of neutrons depends on the specific [i] that are present. As soon as nuclear reactions come into play, the exact [i] composition of materials become important.

8. Explain the reasons for the following input specifications in MCNP input data sets:

   - In the MCNP [MODE P E] input data file for a low-energy ($E_\gamma \leq 3\,\text{MeV}$) photon/electron transport problem, in which boron ($Z = 5$) occurs in a given material region, the ZAID for boron is specified in the material card as 5000.

   - An MCNP [MODE N H P E] input data file is written for a photon/electron transport problem, where an electron beam of 40 MeV is stopped on a 3 mm thick tungsten target. The element boron occurs in a given material region, and in the material card, the ZAID for boron is specified in terms of 5010 and 5011, i.e. by isotope and not by element.

3.5.2 ENDF neutron cross-sections

Neutron cross-section data are evaluated at a number of cross-section data centres in the world. The best-known compilation is the **E**valuated **N**uclear **D**ata **F**ile (ENDF) set, type **B**. Cross-section processing systems such as NJOY and AMPX are used to process "raw" ENDF/B cross-section data into formats that can be directly used by radiation transport codes such as MCNP. The latest release is ENDF/B-VII.1 (December 2011).

The ENDF/B-VII.0 library, made available in December 2006, was the first major release of the US nuclear reaction cross-section data library in 16 years. Intensive validation proved generally good performance of the library but a number of deficiencies were discerned. In 2008, the CSEWG[8] decided to undertake a multi-laboratory effort leading to the ENDF/B-VII.1 version, which was released in December 2011. Highlights of the new ENDF/B-VII.1 library include (i) a consistent set of covariance data, for over 180 materials, targeting explicit needs of the Advanced Fuel Cycle Initiative, (ii) new R-matrix based evaluations for several light nuclei, (iii) evaluations for reactions on structural materials in both the fast neutron region and the resonance region, (iv) improvements of resonances regions and thermal cross sections for certain fission products and neutron absorber materials (Cd, Gd), (v) improvements in minor actinide evaluations for isotopes of U, Np, Pu, and Am, (vi) adoption of JENDL-4.0 evaluations for the Cm, Bk, Cf, Es, Fm, and some other minor actinides, (vii) fission product yield advances for fission-spectrum neutrons and 14 MeV neutrons incident on ^{239}Pu, and (viii) a new Decay Data sub-library. No significant changes are expected for the major actinides ^{235}U, ^{238}U and ^{239}Pu, except reverting delayed neutron data to ENDF/B-VI.8 and adding covariances. The ENDF/B-VII.1 update concerns only the most important neutron, fission yields, and radioactive decay data sub-libraries, leaving the remaining 11 sub-libraries unchanged.

The software JANIS, available for free from the NEA Data Bank (**http://www.oecd-nea.org/janis/**), is a handy database front-end (DBFE) for viewing and extracting nuclear cross-section data.

3.5.3 TALYS: Benchmarked Nuclear Models can assist to predict cross-sections

TALYS is a computer code system for the analysis and prediction of nuclear reactions. The basic objective behind its construction is the simulation of nuclear reactions that involve neutrons, photons, protons, deuterons, tritons, ^{3}He- and α-particles, in the 1 keV – 200 MeV energy range and for target nuclides of mass 12 and heavier. To achieve this, the TALYS development team have implemented a suite of nuclear reaction models into a single code system. This enables the TALYS user to evaluate nuclear reactions from the unresolved resonance range up to intermediate energies.

There are two main purposes of TALYS, which are strongly connected. First, it is a nuclear physics tool that can be used for the analysis of nuclear reaction experiments. The interplay between experiment and theory gives insight in the fundamental interaction between particles and nuclei, and precise measurements enable the constraint of models. In return, when the resulting nuclear models are believed to have sufficient predictive power, they can give an

[8] CSEWG = Cross-Section Evaluation Working Group. The Cross Section Evaluation Working Group is a cooperative effort of the national laboratories, industry, and universities in the United States and Canada, responsible for the production of the U.S. Evaluated Nuclear Data File ENDF/B. In addition, the *Formats Committee* of CSEWG is responsible for developing and maintaining the ENDF format, in which the ENDF/B library is released.

indication of the reliability of measurements. The many examples we present at the end of this manual confirm that TALYS would be nowhere without the experimental database.

After the nuclear physics stage comes the second function of TALYS, namely as a nuclear data tool: Either in a default mode, when no measurements are available, or after re-tuning the adjustable parameters of the various reaction models using available experimental data, TALYS can generate nuclear data for all open reaction channels, on a user-defined energy and angle grid, beyond the resonance region.

The nuclear data libraries that are constructed with these calculated and experimental results provide essential information for existing and new nuclear technologies. Important applications that rely directly or indirectly on data generated by nuclear reaction simulation codes like TALYS are: conventional and innovative nuclear power reactors (GEN-IV), transmutation of radioactive waste, fusion reactors, accelerator applications, homeland security, medical isotope production, radiotherapy, single-event upsets in microprocessors, oil-well logging, geophysics and astrophysics.

3.5.4 Total cross-section

The total neutron interaction cross-section, σ_t, is the sum of the cross-sections for all possible neutron interactions, and is a measure of the probability that a neutron of a given energy will interact in some manner with the medium. At neutron energies below approximately 20 MeV, The main components of the total cross-section are the scattering cross-section σ_s and the absorption cross-section σ_a — note that (n,p), (n,α), (n,d) and (n,t) reactions are categorised as neutron absorption reactions.

3.5.5 Linear interaction coefficient μ

For a single isotope with cross-section σ and nuclide number density N, the linear interaction cross-section μ, also called the macroscopic cross-section Σ, is

$$\mu = N\sigma. \tag{3.7}$$

In a mixture of I isotopes, the net linear interaction coefficient μ is a weighted linear superposition of microscopic cross-sections σ_i, where the weighting factors are nuclide number densities, N_i,

$$\mu = \sum_{i=1}^{I} [N_i\, \sigma_i]. \tag{3.8}$$

3.5.6 Elastic and inelastic scattering of neutrons

When a neutron scatters from a nucleus, the nucleus is either left in the ground state (elastic scattering) or in an excited state (inelastic scattering). The two categories of scattering may be denoted as,

$$n + X \longrightarrow \begin{cases} X + n & \text{elastic scattering} \\ \\ X^* + n' & \text{inelastic scattering}\,. \end{cases} \tag{3.9}$$

where n denotes the incident neutron as well as an elastically scattered neutron, n' denotes an inelastically scattered neutron, X denotes the scattering nucleus in its ground state, and X^* denotes the scattering nucleus in an excited energy state.

The scattered neutron has a lower kinetic energy than the incident neutron, because (1) the target nucleus recoils, and (2) additionally absorbs energy in the event of inelastic scattering.

Mathematical expressions for neutron scattering kinetics found in almost all textbooks are non-relativistic, and suffer from other approximations too. *Code users* do not need to be able to derive and use such expressions in calculations; developers of radiation transport cross-section processing codes, on the other hand, must master this field in detail, avoiding all unnecessary simplifying assumptions.

3.5.7 Dynamics and kinematics of neutron scattering

To shield neutrons, it is necessary to first slow them down — slow neutrons are (1) significantly less dangerous to people and materials, and are also (2) easier to absorb, because neutron capture cross-sections are generally significantly higher at low neutron energies.

The term in the BTE that describes neutron slowing down via scattering, is the scattering transfer cross-section, $\sigma_s\left(E' \rightarrow E, \widehat{\mathbf{\Omega}}' \rightarrow \widehat{\mathbf{\Omega}}\right)$.

The ability of a given nuclide to lower neutron energy by scattering, depends on:

- **Scattering reaction dynamics** — the scattering cross-section, i.e. the cross-section for elastic scattering, discrete-level inelastic scattering and continuum inelastic scattering. These cross-sections are determined by the Hamiltonian of the neutron-nucleus scattering system, which is very complex as a result of the inherent complexity of strong nuclear interaction. Quark-quark interaction, as mediated by gluons, is described by Quantum ChromoDynamics (QCD), and the strong nuclear interaction between hadrons such as nucleons, is a residual effect of the QCD-interaction between the quarks that constitute the hadrons. Scattering dynamics is complex and even the best nuclear models typically use empirical fitting parameters. The scattering transfer cross-section term can be expressed as

  $$\sigma_s\left(E' \rightarrow E, \widehat{\mathbf{\Omega}}' \rightarrow \widehat{\mathbf{\Omega}}\right) = \sigma_s(E') \times p\left(E' \rightarrow E, \widehat{\mathbf{\Omega}}' \rightarrow \widehat{\mathbf{\Omega}}\right)$$

  where $\sigma_s(E')$ expresses the likelihood that the scattering reaction will take place at incident neutron energy E'. The term $\sigma_s(E')$ is wholly determined by scattering reaction dynamics.

- **Scattering kinematics** depends on the mass of the projectile being scattered, the mass of the scattering nucleus, and the specific internal energy level(s) of the nucleus that are excited by inelastic scattering, as well as the transformation from the centre-of-mass frame of reference $\mathcal{C}$, to the laboratory frame of reference $\mathcal{L}$. The mathematical treatment of scattering kinematics is mathematically reasonably simple and recipe-like. In contrast, the modelling of the quantum-mechanical dynamics of neutron scattering is complex and therefore empirical in nature. In general, it is not possible to mathematically separate the reaction dynamics term and the reaction kinematics term, i.e. it is generally *not possible* to write $p_{\text{RD\&RK}} = p_{\text{RD}} \times p_{\text{RK}}$. The joint contribution of scattering dynamics (quantum mechanics) and scattering kinematics to the lowering of the energy of neutrons as well as the change in direction of movement of neutrons, is expressed as a probability density distribution function, $p_{\text{RD\&RK}}\left(E' \rightarrow E, \widehat{\boldsymbol{\Omega}}' \rightarrow \widehat{\boldsymbol{\Omega}}\right)$.

The scattering transfer cross-section $\sigma_s\left(E' \rightarrow E, \widehat{\boldsymbol{\Omega}}' \rightarrow \widehat{\boldsymbol{\Omega}}\right)$ can be written as

$$\sigma_s\left(E' \rightarrow E, \widehat{\boldsymbol{\Omega}}' \rightarrow \widehat{\boldsymbol{\Omega}}\right) = \overbrace{\sigma_s(E')}^{\substack{\textit{Scattering}\\ \textit{dynamics}}} \times \overbrace{p\left(E' \rightarrow E, \widehat{\boldsymbol{\Omega}}' \rightarrow \widehat{\boldsymbol{\Omega}}\right)}^{\substack{\textit{Scattering}\\ \textit{dynamics}}\ \&\ \substack{\textit{Scattering}\\ \textit{kinematics}}}. \qquad (3.10)$$

The purely "scattering dynamics" term, $\sigma_s(E')$, is a measure of how likely i.e. how probable the scattering interaction is. The second term is the energy-angle transfer probability distribution function, which is a convolution of the contributions of scattering dynamics and scattering kinematics to the net ability of the nuclide to change the energy and direction of movement of neutrons. That is, the probability distribution term

$$p\left(E' \rightarrow E, \widehat{\boldsymbol{\Omega}}' \rightarrow \widehat{\boldsymbol{\Omega}}\right)$$

expresses how effective the scattering interaction will be when it happens, in its ability to lower the neutron energy and to deflect neutrons, i.e. to change their direction of movement.

The convolution of scattering dynamics and scattering kinematics is rooted in the impact of scattering dynamics on the angular distribution of the scattered neutrons. At low neutron energies, elastic scattering of neutrons is isotropic in the centre-of-mass coordinate system, $\mathcal{C}$, and this is termed s-wave scattering. At higher incident neutron energies, and especially for heavier scattering nuclides, elastic scattering quickly becomes anisotropic in $\mathcal{C}$ as a consequence of an increasing contribution from p-wave and even d-wave scattering. The degree of anisotropy of scattered neutrons is higher in the laboratory frame of reference, $\mathcal{L}$, as a result of the kinematics of the $\mathcal{C} \rightarrow \mathcal{L}$ transformation, than in the centre-of-mass reference frame, $\mathcal{C}$. Inelastic scattering remains remarkably isotropic in $\mathcal{C}$, up to neutron energies of approximately 20 MeV. The higher the degree of anisotropy of neutron scattering in $\mathcal{C}$, the more forward-biased becomes the angular distribution of scattered neutrons, and the lower becomes the kinematic ability of scattering kinematics to reduce or degrade neutron energy, because the expectation value of scattering angle will decrease. The net transfer probability distribution function may be expressed, conceptually, as

$$p(E' \rightarrow E, \theta) = f_{RK}[m_n, M, \lambda, E_\lambda, p_{RD}(E' \rightarrow E, \theta)], \tag{3.11}$$

i.e. the convolution is a function of a function, $p = f_{\text{RK}} \circ p_{\text{RD}}$, where RK denotes reaction kinematics and RD denotes reaction dynamics. In Eq. (3.11),

m_n = mass of the incident projectile, i.e. the neutron

M = mass of target nucleus

λ = number of the inelastic energy level that is excited in the target nucleus

E_λ = Excitation energy of the energy level λ that is excited in the target nucleus; 0 for elastic scattering.

3.5.8 Net ability of a nuclide to slow down neutrons — conceptual treatment

The net ability of a nuclide to slow down neutrons can be conceptualised from the expression

$$\sigma_s(E' \rightarrow E) = \sigma_s(E')\, p(E' \rightarrow E). \tag{3.12}$$

This means that neutron energies are lowered (concept: $E' \rightarrow E$) via scattering interactions (concept: σ_s), and that the transfer cross-section $\sigma_s(E' \rightarrow E)$, which quantifies the ability of a scattering nuclide to lower the neutron energy, is given by the product

$$\overbrace{\left(\begin{array}{c}\text{Cross section of}\\ \text{the scattering interaction}\end{array}\right)}^{\sigma_s(E')} \times \overbrace{\left(\begin{array}{c}\text{Net efficiency of the}\\ \text{scattering interaction}\\ \text{to lower neutron energy}\end{array}\right)}^{p(E' \rightarrow E)}. \tag{3.13}$$

This means that the ability of a scattering interaction to effect neutron slowing down, is given by the product

Term1	×	Term2
$\sigma_s(E')$	×	$p(E' \rightarrow E)$
Cross-section of the scattering interaction taking place.	×	How effective will the scattering be for lowering neutron energy, if the scattering interaction takes place.

(3.14)

From Eq. (3.14) the following conclusions can be made:

- A nuclide with a favourable "Term1" but an unfavourable "Term2" at a given incident neutron energy E', will not be good for slowing down neutrons at that energy, via elastic scattering.

- A nuclide with an unfavourable "Term1" but a favourable "Term2" at a given incident neutron energy E', will not be good for slowing down neutrons at that energy, via elastic scattering.

- Only a nuclide with a favourable "Term1" as well as a favourable "Term2" at a given incident neutron energy E', will be good for slowing down neutrons at that energy, via elastic scattering.

3.5.9 Limitations of $^{1}_{1}$H for slowing down neutrons by elastic scattering

We now have the conceptual framework in which to understand the limitations of the nuclide $^{1}_{1}$H for slowing down neutrons. The nuclide $^{1}_{1}$H can only engage in elastic scattering (ES) and not in inelastic scattering (IS), i.e. ES is the only available scattering reaction channel. For scattering that is isotropic in the centre-of-mass coordinate system C, the average kinematical energy-lowering effectiveness of elastic scattering of a neutron off ^{1}H is very high — the average neutron energy loss is 50% per scattering event, for incident neutrons in the energy range $E_n \lesssim 10$ MeV, where neutron scattering by ^{1}H is predominantly s-wave scattering, which is isotropic in the centre-of-mass system, $\mathcal{C}$. That is, for elastic scattering of neutrons by $^{1}_{1}$H,

$$\frac{\langle E\big(n, {}^{1}_{1}\text{H, ES, } 1\big)\rangle}{E'} = f(p(E' \to E)) \approx \frac{1}{2} \tag{3.15}$$

where $\langle E\big(n, {}^{1}_{1}\text{H, ES, } 1\big)\rangle$ is the expectation value of the energy E on a neutron (n) following 1 elastic scattering (ES) interaction with the isotope $^{1}_{1}$H. In other words, the fractional energy loss per elastic scattering interaction, is very favourable. The expectation value $\langle E\big(n, {}^{1}_{1}\text{H, ES, } 1\big)\rangle$ is a function of the function $p\big(E' \to E, \big(n, {}^{1}_{1}\text{H, ES, } 1\big)\big)$ for projectile n, interaction ES, and target $^{1}_{1}$H. To put it differently, the function $\boxed{p\big(E' \to E, \big(n, {}^{1}_{1}\text{H, ES, } 1\big)\big)}$ is very favourable for the argument list $\big(n, {}^{1}_{1}\text{H, ES, } 1\big)$, i.e. the fraction in Eq. (3.15) has a desired low value. However, reference to Figure 6.4 on page 308 shows that the $\sigma_s\big(E', \big(n, {}^{1}_{1}\text{H, ES, } 1\big)\big)$ becomes lower and lower as the incident neutron energy E' increases — it "nosedives" to the geometrical cross-section of the $^{1}_{1}$H nucleus, which is very low. As a result, the net ability of the reaction mechanism $\big(n, {}^{1}_{1}\text{H, ES, } 1\big)$ to slow down neutrons, becomes quite weak above an incident neutron energy of approximately 4 to 5 MeV — if the interaction occurs, the average neutron slowing down that is achieved, is quite good, but the probability of the interaction $\big(n, {}^{1}_{1}\text{H, ES, } 1\big)$ taking place at all, nosedives at neutron energies above a few MeV, and alternative nuclear reaction mechanisms must be utilised to achieve neutron slowing down in a neutron shield.

In the terminology of Eq. (3.14): The nuclide $^{1}_{1}$H has an unfavourable "Term1" but a favourable "Term2" at incident neutron energies above approximately 4 MeV, and will therefore not be good for slowing down neutrons at energies above circa 4 MeV, via elastic scattering interactions.

3.5.10 Thermal neutrons

When neutrons slow down, they eventually come into thermal equilibrium with the thermal motion of the atoms in the medium through which they are moving. The atoms of the medium are moving with a distribution of speeds, known as the Maxwellian distribution. In a state of thermal equilibrium, a neutron can gain or lose kinetic energy upon scattering with a nucleus. Neutrons in such a state of thermal equilibrium are called thermal neutrons. The average energy of thermal neutrons is $\frac{3}{2}k_BT$, while the most probable energy of thermal neutrons is k_BT, where k_B is Boltzmann's constant; at room temperature, i.e. $T = 20.5\,°\text{C}$, the most probable energy of thermal neutrons is therefore 0.0253 eV; this corresponds to a neutron speed of 2200 m/s.

Figure 3.7 shows Maxwellian thermal neutron energy distributions for a number of ambient temperatures. These spectra were obtained by using the Maxwell distribution function,

$$S(E) = \left(\frac{8\pi}{m}\right)\left(\frac{m}{2\pi k_B T}\right)^{3/2} E \exp\left(\frac{-E}{k_B T}\right) \tag{3.16}$$

where E is the neutron energy, m is the mass of a neutron, k_B is the Boltzmann constant and T is the ambient temperature in Kelvin.

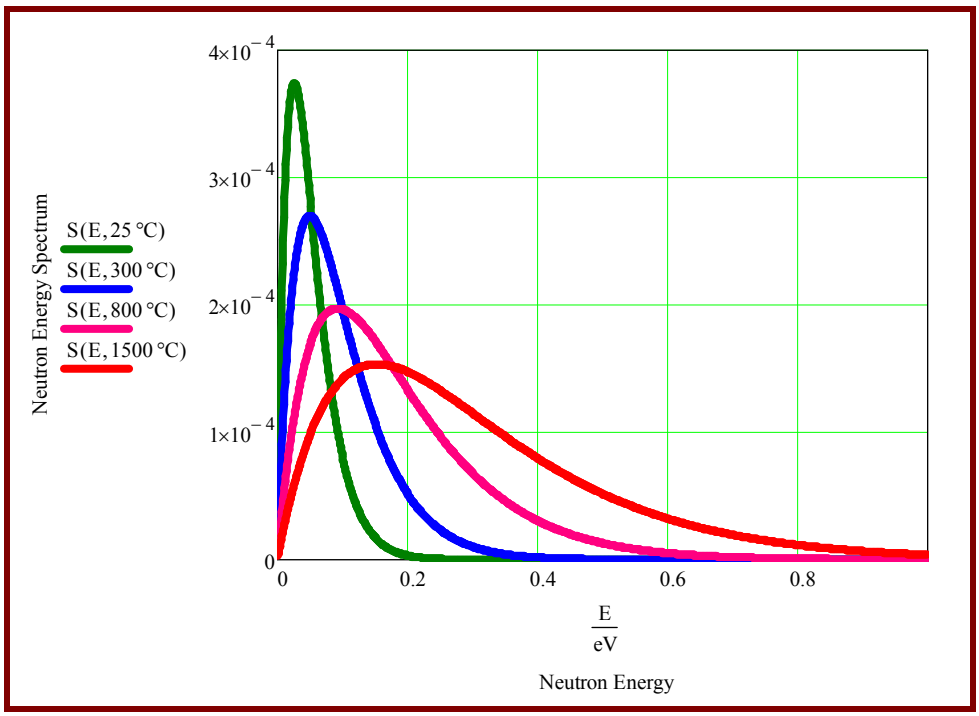

Figure 3.7: *Maxwellian thermal neutron energy distributions at a number of ambient temperatures.*

Note that — for room temperature, i.e. $T \approx 20.5\,°\text{C}$, the Maxwellian distribution peaks at the most probable neutron energy of $E_n = 0.0253$ eV, which corresponds to a neutron speed of $v_n = 2200\ \text{m}\,\text{s}^{-1}$.

The equation

$$E_{\text{av}} = \frac{3}{2} k_B T \tag{3.17}$$

is a very important link and bridge between the micro-world and the macro-world — it provides a link between the macroscopic quantity temperature (T), and the microscopic quantity namely the average energy, E_{av}, of submicroscopic particles at that temperature.

According to Eq. (3.17), thermal neutrons will have an average energy of $E_{\text{av}} = 0.035$ eV in a material at room temperature. Neutron energies and speeds are evaluated a the most probable ("mp") energy $E_{\text{mp}} = k_B T$, which yields the energy 0.0253 eV and the neutron speed of 2200 m.s^{-1}. Compilations of thermal neutron absorption cross-sections give the values of these cross-sections at the reference neutron energy 0.0253 eV, which is equivalent to the reference neutron speed of 2200 m.s^{-1}.

Assignment 3.7

1. Plot the Maxwellian energy distribution of thermal neutrons, for
   $T = 20$°C
   $T = 200$°C
   $T = 500$°C
   $T = 1000$°C
   $T = 2000$°C.

2. At room temperature, i.e. $T \approx 20.5$ °C, the Maxwellian distribution for thermal neutron energies, peaks at the most probable neutron energy of $E_n =$ [ ] eV, which corresponds to a neutron speed of $v_n =$ [ ] m s^{-1}.

3. At $T \approx 300$ °C, i.e. the temperature of typical PWR coolant, the Maxwellian distribution for thermal neutron energies, peaks at the most probable neutron energy of $E_n =$ [ ] eV, which corresponds to a neutron speed of $v_n =$ [ ] m s^{-1}.

4. At $T = 1200$ °C, i.e. typical PWR fuel temperature, the Maxwellian thermal neutron distribution peaks at the most probable neutron energy of $E_n =$ [ ] eV, which corresponds to a neutron speed of $v_n =$ [ ] m s^{-1}.

3.5.11 The kinematics of neutron scattering

Minimum, maximum and average neutron energy after a single (n, n') scattering interaction — elastic and inelastic

Let E denote the incident neutron energy. The minimum, maximum and expectation value of the energy of a scattered neutron is given by

$$E_\lambda^{\text{min}}(E, A, Q_\lambda) = \left(\frac{\Gamma_\lambda - 1}{A+1}\right)^2 \tag{3.18}$$

$$E_\lambda^{\text{max}}(E, A, Q_\lambda) = \left(\frac{\Gamma_\lambda + 1}{A+1}\right)^2 \tag{3.19}$$

$$E_\lambda^{\text{av}}(E, A, Q_\lambda) = \left(\frac{1+\alpha}{2}\right)E - A^2\left[\frac{\epsilon_\lambda}{(A+1)^2}\right] \tag{3.20}$$

when energy level λ in the target nucleus, having a Q-value of Q_λ, is excited. The excitation of energy level $\lambda = 0$ corresponds to elastic neutron scattering, for which $Q_0 = 0$. Note that this formalism incorporates elastic scattering, discrete level inelastic scattering, as well as inelastic scattering that excites the struck nucleus to the continuum, in a single formalism.

The expression for the expectation value of the energy of a scattered neutron only holds under the assumption that neutron scattering is isotropic in the centre-of-mass system $\mathcal{C}$. The symbols in Eqs. (3.18), (3.19) and (3.20) have the following definitions:

E	$=$	Energy of incident neutron		
A	$=$	$\left(\frac{\text{Mass of target nucleus}}{m_n}\right)$	(m_n = mass of neutron)	(3.21)
Q_λ	$=$	Energy of energy level number λ in the target nucleus		(3.22)
$\epsilon_\lambda(Q_\lambda, A)$	$=$	$\left[\frac{-(A+1)}{A}\right]Q_\lambda$	(threshold energy for the excitation of energy level λ by IS)	(3.23)
$Q_\lambda(\epsilon_\lambda, A)$	$=$	$\left[\frac{-A}{(A+1)}\right]\epsilon_\lambda$	(Q-value energy for the excitation of energy level λ by IS)	(3.24)
$E_{90}^{\lambda}(\epsilon_\lambda, A)$	$=$	$\left(\frac{A^2}{A^2-1}\right)\epsilon_\lambda$	Threshold energy for scattering neutrons through angles of 90 degrees or larger	
$\alpha(A)$	$=$	$\left(\frac{A-1}{A+1}\right)^2$	(collision parameter)	(3.25)
$A\left({}_1^1\text{H}\right)$	$=$	$\left(\frac{m_p}{m_n}\right) = 0.99862347821$	(m_p = mass of proton in amu; m_n = mass of neutron in amu)	(3.26)
$A\left({}_6^{12}\text{C}\right)$	$=$	11.8969142394	From Eq. (3.21)	
$A\left({}_8^{16}\text{O}\right)$	$=$	15.857510627	From Eq. (3.21)	
$A\left({}_{26}^{56}\text{Fe}\right)$	$=$	55.454434096	From Eq. (3.21)	
$\Gamma(E, A, \epsilon_\lambda)$	$=$	$A\sqrt{\left[1-\left(\frac{\epsilon_\lambda}{E}\right)\right]}$	The **effective mass number** of a nucleus which scatters a neutron of incident energy E through the excitation of discrete energy level λ having energy threshold ϵ_λ in the target nucleus. A has the value computed by using Eq. (3.21).	(3.27)

Assignment 3.8

Employ several provided MathCAD worksheets to calculate the following. Where necessary, code some of the above equations in MathCAD.

1. Show that $\Gamma(E, A, \epsilon_\lambda) = A$ for elastic scattering.

2. Evaluate $\alpha(A)$ for ${}^{1}_{1}\mathrm{H}$, ${}^{4}_{2}\mathrm{He}$, ${}^{12}_{6}\mathrm{C}$, ${}^{16}_{8}\mathrm{O}$, ${}^{56}_{26}\mathrm{Fe}$ and ${}^{208}_{82}\mathrm{Pb}$.

3. Calculate the accurate value of E_{min} for ${}^{1}_{1}\mathrm{H}$. Next, calculate E_{min} for ${}^{1}_{1}\mathrm{H}$ under the widely made but inaccurate, simplistic assumption that $A\left({}^{1}\mathrm{H}\right) = 1$.

4. A 2 MeV neutron scatters off a ${}^{1}\mathrm{H}$ nucleus, and it is known that only elastic scattering ($\lambda = 0$) can take place for this nuclide. Calculate E_{min}, E_{av} and E_{max} under the (valid) assumption of isotropic scattering in $\mathcal{C}$.

5. A 10 MeV neutron scatters off a ${}^{1}\mathrm{H}$ nucleus, and it is known that only elastic scattering ($\lambda = 0$) can take place for this nuclide. Calculate E_{min}, E_{av} and E_{max} under the rather simplistic assumption of isotropic scattering in $\mathcal{C}$.

6. A 10 MeV neutron scatters off a ${}^{56}\mathrm{Fe}$ nucleus. Calculate E_λ^{min}, E_λ^{av} and E_λ^{max} of the scattered neutron, for the range of values that λ can take.

7. A 5 MeV neutron scatters off a ${}^{56}\mathrm{Fe}$ nucleus. Calculate E_λ^{min}, E_λ^{av} and E_λ^{max} of the scattered neutron, for the range of values that λ can take.

8. A 10 MeV neutron scatters off a ${}^{208}\mathrm{Pb}$ nucleus. Calculate E_λ^{min}, E_λ^{av} and E_λ^{max} of the scattered neutron, for the range of values that λ can take.

9. A 5 MeV neutron scatters off a ${}^{208}\mathrm{Pb}$ nucleus. Calculate E_λ^{min}, E_λ^{av} and E_λ^{max} of the scattered neutron, for the range of values that λ can take.

10. Use your results to show that *elastic* scattering off a heavy nucleus is kinematically hopelessly ineffective as a neutron moderation mechanism, but that *inelastic* scattering off such a heavy nucleus can make a valuable contribution to the slowing down of neutrons, and can often exceed the kinematical efficiency of elastic scattering of a neutron by ${}^{1}_{1}\mathrm{H}$.

Expectation-value of the scattering angle

The expectation value of the scattering angle θ_{av} in the laboratory frame of reference, $\mathcal{L}$, expressed in degrees, through which a neutron is scattered in a single scattering interaction, under the assumption that neutron scattering is isotropic in the centre-of-mass system $\mathcal{C}$, is given by

$$\theta_{\mathrm{av}}(E, A, \epsilon_\lambda) = \left(\frac{180}{\pi}\right) \arccos\left(\frac{2}{3\,\Gamma_\lambda}\right) \tag{3.28}$$

where $\Gamma(E, A, \epsilon_\lambda)$ is given by Eq. (3.27) on page 97.

Assignment 3.9

1. Code Eq. (3.28).

2. A 5 MeV neutron scatters off a ^{1}H nucleus, and it is known that only elastic scattering ($\lambda = 0$) can take place for this nuclide. Calculate the expectation value for the scattering angle in $\mathcal{L}$ (implicit assumption: isotropic scattering in $\mathcal{C}$).

3. Show, formally or heuristically, that the $\mathcal{C} \rightarrow \mathcal{L}$ transformation introduces "$\mathcal{C} \rightarrow \mathcal{L}$ transformation anisotropy" to neutron scattering. That is, show that for isotropic scattering in $\mathcal{C}$, scattering in $\mathcal{L}$ will be anisotropic.

4. For isotropic scattering in $\mathcal{C}$, will the $\mathcal{C} \rightarrow \mathcal{L}$ transformation introduce more scattering anisotropy for a light or a heavy scattering nucleus?

5. Under the assumption of isotropic scattering in $\mathcal{C}$, calculate the expectation value for the scattering angle in $\mathcal{L}$, for elastic scattering of neutrons off ^{1}H. At which incident neutron energies will your calculated value for the average scattering angle begin to become inaccurate? Explain why. (Hint: refer to partial waves, s-waves, p-waves, the centrifugal barrier and quantum-mechanical tunneling; consult a textbook dealing with nuclear reactions.)

6. Under the assumption of isotropic scattering in $\mathcal{C}$, calculate the expectation value for the scattering angle in $\mathcal{L}$, for elastic and inelastic scattering of neutrons off ^{56}Fe.

7. Under the assumption of isotropic scattering in $\mathcal{C}$, calculate the expectation value for the scattering angle in $\mathcal{L}$, for elastic scattering of neutrons off ^{9}Be and ^{12}C.

8. Prompt fission neutrons are "born" in a thermal-spectrum nuclear reactor at an average energy of 2 MeV and must then slow down to thermal energies. A 2 MeV neutron scatters off a ^{9}Be nucleus. Calculate the minimum, maximum and average energies of the scattered neutron, for elastic scattering.

9. Prompt fission neutrons are "born" in a thermal-spectrum nuclear reactor at an average energy of 2 MeV and must then slow down to thermal energies. A 2 MeV neutron scatters off a ^{12}C nucleus. Calculate the minimum, maximum and average energies of the scattered neutron, for elastic scattering.

10. Explain why expensive Be, and not cheap H_2O, is used as a neutron reflector in many Material Testing Reactor (MTR) designs.

Average number of elastic scattering events necessary to slow down 2 MeV neutrons to the thermal energy, 0.0253 eV

In nuclear reactors, neutrons are produced or "born" at an average energy of approximately $E_{\text{initial}} \approx 2$ MeV, and then need to slow down to thermal neutron energies, i.e. to approximately $E_{\text{final}} \approx 0.0253$ eV. The effectiveness of various neutron moderator materials in slowing down 2 MeV neutrons to a final energy of approximately 0.0253 eV, are summarised in Table 3.6.

Table 3.5: *Kinematical effectiveness of some materials to slow down neutrons by elastic scattering. Here n is the average number of elastic scattering events necessary to slow down 2 MeV neutrons to 0.0253 eV.*

Material	n
H_2O	19.8
D_2O	35.7
He	42.8
Be	88.1
C	115

In fission nuclear reactors, neutrons are produced or "born" at a maximum energy of approximately 20 MeV, and then need to slow down to thermal neutron energies, i.e. to approximately $E_{\text{final}} \approx 0.05$ eV in the coolant which has a temperature of about 310 °C. The effectiveness of various neutron moderator materials in slowing down 20 MeV neutrons to a final energy of approximately 0.05 eV, are summarised in Table 3.6.

Table 3.6: *Kinematical effectiveness of some materials to slow down neutrons by elastic scattering. Here n is the average number of elastic scattering events necessary to slow down 20 MeV neutrons to 0.05 eV, which is the most probable value for the energy of thermal neutrons in the coolant of a typical PWR power reactor.*

Material	n
^{1}H	29
^{2}H	34
^{4}He	52
^{9}Be	100
^{12}C	130

3.5.12 Neutron capture reactions

After several scattering interactions, free neutrons are typically absorbed into a nucleus; this may transmute a stable nucleus into a radioactive nucleus. Such transformations may be intentional, as in commercial radionuclide production processes, or it may be an unintended, undesired byproduct of a free neutron population moving through matter. The capture of a neutron by a nucleus adds the neutron's binding energy, which is typically between 5 MeV and 9 MeV, to the nucleus and therefore leaves the compound nucleus in a highly excited state. The excited nucleus usually transitions rapidly, emitting (inter alia) ionising photons (symbol γ) in the process. These ionising photons that are emitted when neutrons are captured, are referred to as ionising photons from (n,γ)-reactions. Another term for (n,γ)-reactions, is radiative capture reactions. These ionising photons from the radiative capture of neutrons can represent a significant radiation hazard, and therefore slow-neutron absorbers with high neutron capture cross-sections which emit either lower-energy capture gamma-photons, or no capture gamma-photons at all, are often mixed into neutron shielding materials.

3.5.13 Neutron-induced nuclear fission reactions

See page 155.

3.6 Neutron interaction cross-sections

3.6.1 Introduction

Note: Cross-sections plotted in this section were obtained from JANIS **(http://www.oecd-nea.org/janis/).**

Neutrons interact almost exclusively with atomic nuclei. Because the Hamiltonian for neutron-nucleus interactions differ from isotope to isotope, it follows that neutron interaction cross-sections differ at the isotopic level. This is in contrast to photon interaction cross-sections, which generally only vary at the atomic level. The reason is rooted in the difference between Quantum ChromoDynamics (QCD), which determine the reaction dynamics of entities having a quark substructure, and Quantum ElectroDynamics (QED), which govern photon-electron interactions. Neutron cross-section data are highly empirical in nature, with nuclear models supplying estimates of cross-sections where evaluated cross-section data are unavailable.

The best known and most widely used compilation of cross-section data is the Evaluated Nuclear Data File, Type B (ENDF/B), which is processed by cross-section processing codes such as NJOY or AMPX to produce cross-section data in a range of formats used by radiation transport codes. At present (2015), ENDF/B-7.1 is the latest release of evaluated cross-sections. Cross-section sets for radiation transport codes such as MCNP are produced from ENDF/B files by means of the cross-section processing code NJOY.

3.6.2 ENDF reaction identifiers

Important ENDF nuclear reaction identifiers are listed in Table 3.7.

Table 3.7: *Important ENDF reaction identifiers.*

1	Total cross section, σ_t.
2	Elastic scattering cross section, σ_{es}.
4	Total inelastic scattering cross-section.
16	$(n, 2n)$ XS for producing two neutrons and a residual.
18	(n, f) XS for fission.
22	$(n, n\alpha)$ XS for the production of a neutron and alpha particle plus a residual.
28	(n, np) XS for the production of a neutron and a proton plus a residual.
51	(n, n_1) XS to the 1st excited state of the residual nucleus.
52	(n, n_2) XS to the 2nd excited state of the residual nucleus.
53	(n, n_3) XS to the 3rd excited state of the residual nucleus.
54	(n, n_4) XS to the 4th excited state of the residual nucleus.
55	(n, n_5) XS to the 5th excited state of the residual nucleus.
56	(n, n_6) XS to the 6th excited state of the residual nucleus.
57	(n, n_7) XS to the 7th excited state of the residual nucleus.
58	(n, n_8) XS to the 8th excited state of the residual nucleus.
59	(n, n_9) XS to the 9th excited state of the residual nucleus.
60	(n, n_{10}) XS to the 10th excited state of the residual nucleus.
61	(n, n_{11}) XS to the 11th excited state of the residual nucleus.
62	(n, n_{12}) XS to the 12th excited state of the residual nucleus.
63	(n, n_{13}) XS to the 13th excited state of the residual nucleus.
64	(n, n_{14}) XS to the 14th excited state of the residual nucleus.
65	(n, n_{15}) XS to the 15th excited state of the residual nucleus.

66 (n, n_{16}) XS to the 16th excited state of the residual nucleus.

67 (n, n_{17}) XS to the 17th excited state of the residual nucleus.

68 (n, n_{18}) XS to the 18th excited state of the residual nucleus.

69 (n, n_{19}) XS to the 19th excited state of the residual nucleus.

70 (n, n_{20}) XS to the 20th excited state of the residual nucleus.

71 (n, n_{21}) XS to the 21th excited state of the residual nucleus.

72 (n, n_{22}) XS to the 22th excited state of the residual nucleus.

73 (n, n_{23}) XS to the 23th excited state of the residual nucleus.

74 (n, n_{24}) XS to the 24th excited state of the residual nucleus.

75 (n, n_{25}) XS to the 25th excited state of the residual nucleus.

91 (n, n_c) XS for the production of a single neutron in the continuum not included in the above discrete representation.

102 (n, γ) Radiative capture XS.

103 (n, p) XS for the production of a proton and a residual.

104 (n, d) XS for the production of a deuteron and a residual.

105 (n, t) XS for the production of a triton plus a residual.

106 $(n, {}^3\mathrm{He})$ XS for the production of a ^{3}He particle plus a residual.

107 (n, α) XS for the production of an alpha particle plus a residual.

301 Heating (Energy Balance).

443 Heating (KERMA).

444 Damage.

The above ENDF reaction identifiers can be used in MCNP tally multiplier cards in order to enable the calculation of reaction rates.

Assignment 3.10

1. Write an MCNP tally multiplier card to quantify the reaction rate of all (n, γ)-reactions in MCNP cell 8.

2. Write an MCNP tally multiplier card to quantify the reaction rate of all (n, α)-reactions in MCNP cell 8.

3. Write an MCNP tally multiplier card to quantify the reaction rate of all (n, f)-reactions in MCNP cell 8 (f denotes fission).

4. Write an MCNP tally multiplier card to quantify the reaction rate of all (n, n_c) continuum scattering reactions in MCNP cell 8.

5. Write an MCNP material card for a pseudo-material, as well as an associated tally multiplier card to quantify the reaction rate of $^{55}\text{Mn}(n, \gamma)^{56}\text{Mn}$ reactions in MCNP cell 8.

3.6.3 Magic numbers of nucleons

In nuclear physics, a magic number is a number of nucleons (either protons or neutrons) such that they are arranged into closed, complete shells within the atomic nucleus. The seven most widely recognised magic numbers are: 2, 8, 20, 28, 50, 82 and 126. The number 40 is termed a "semi magic number."

Atomic nuclei consisting of such a magic number of nucleons have a higher average binding energy per nucleon than one would expect based upon predictions such as the semi-empirical mass formula and are hence more stable against nuclear transition.

Nuclei which have neutron numbers (N) and proton numbers (Z) each equal to one of the magic numbers are called "double magic," and are especially stable against nuclear transition. Examples of double-magic isotopes include $^{4}_{2}\text{He}$, $^{16}_{8}\text{O}$, $^{40}_{20}\text{Ca}$, $^{48}_{20}\text{Ca}$, $^{48}_{28}\text{Ni}$ and $^{208}_{82}\text{Pb}$.

Double-magic effects may allow existence of stable isotopes which otherwise would not have been expected. An example is $^{40}_{20}\text{Ca}$, with 20 neutrons and 20 protons, which is the heaviest stable isotope made of the same number of protons and neutrons. Both $^{48}_{20}\text{Ca}$ and $^{48}_{28}\text{Ni}$ are double magic because $^{48}_{20}\text{Ca}$ has 20 protons and 28 neutrons while $^{48}_{28}\text{Ni}$ has 28 protons and 20 neutrons. $^{48}_{20}\text{Ca}$ is very neutron-rich for such a light element, and like $^{40}_{20}\text{Ca}$, it is made stable by being double magic. Similarly, $^{48}_{28}\text{Ni}$, only discovered in 1999, is the most proton-rich isotope known beyond $^{3}_{2}\text{He}$; the half-life of $^{48}_{28}\text{Ni}$ is in the order of 0.5 μs.

Magic number shell effects are seen in ordinary abundances of elements: it is no accident that $^{4}_{2}\text{He}$ is the second most abundant nucleus in the universe and that $^{208}_{82}\text{Pb}$ is the heaviest stable nuclide.

The number 40 is often termed a semi-magic number. The isotope $^{90}_{40}\mathrm{Zr}$ is very stable, because it has a semi-magic number of $Z = 40$ protons and a magic number of $N = 50$ neutrons.

Assignment 3.11

1. Explain why it is neutronically efficient to employ carbon (C) as a neutron moderator, and helium (He) as a heat transfer (coolant) gas in nuclear reactors.

2. Explain why it is neutronically efficient to employ a zirconium (Zr) alloy for the cladding of fuel pins in a PWR.

3. Explain why a concrete based on high-purity marble, i.e. $CaCO_3$, is an excellent low-activation concrete in applications where neutron activation may be an issue, i.e. where the reaction rates of (n, Z) reactions must be minimised.

3.6.4 The most abundant nuclei in the universe

Table 3.8: *The top-6 most abundant elements in nature.*

Order of abundance	Element	Percentage abundance
1	H	73.9%
2	He	24%
3	O	1.04%
4	C	0.46%
5	Ne	0.134%
6	Fe	0.109%

3.6.5 Total cross-sections: graphical journey

Typical form of the dependence of the total cross-section on the energy of the incident neutron

For many nuclei, the total neutron cross-section $\sigma_t(E)$ at low energies E vary as

$$\sigma_t(E) = \sigma_s(E) + \frac{\sigma_{(n,\gamma)}(E_{\text{ref}})}{\sqrt{E}} \tag{3.29}$$

where $\sigma_s(E)$ is the elastic scattering cross-section and $\sigma_{(n,\gamma)}(E_{\text{ref}})$ is the cross section for (n,γ)-reactions at a reference incident neutron energy E_{ref}. In other words, for many nuclei the main contributions to the total neutron interaction cross-section are from (n,n')-reactions and from (n,γ)-reactions. The energy dependence of $\sigma_{(n,\gamma)}(E)$ generally follows a $\frac{1}{\sqrt{E}} = \frac{1}{v}$ energy dependence.

Total cross-sections for ^{1}H and ^{2}H

The total cross-section $\sigma_t(E)$ as a function of energy E, for the lightest nuclides, ^{1}H and ^{2}H, are shown in Figure 3.8. These two isotopes are unique because their neutron interaction cross-sections display no resonance behaviour.

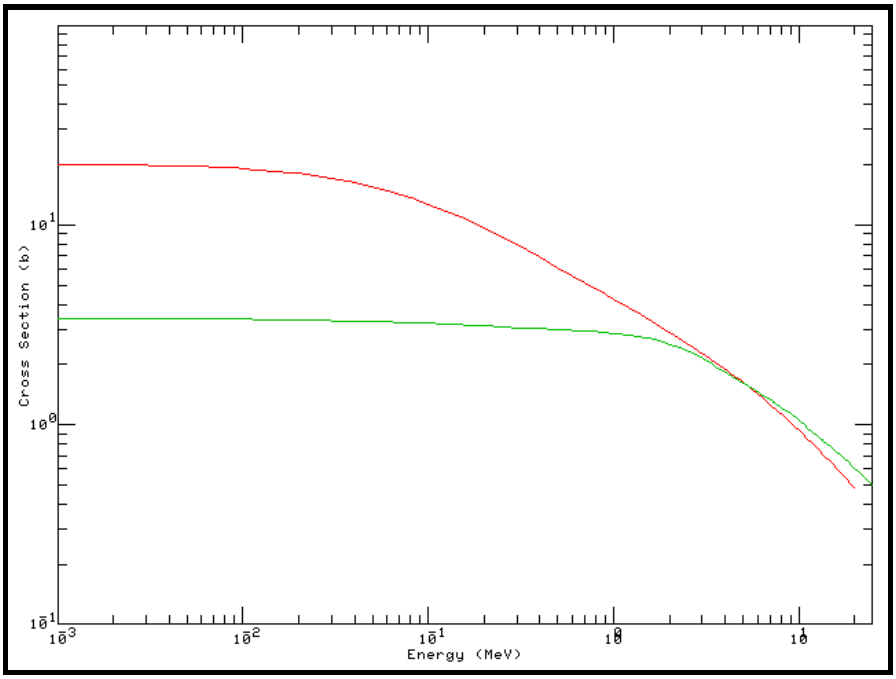

Figure 3.8: *The total neutron interaction cross-section $\sigma_t(E)$ as a function of neutron energy E, for* ^1H / ^2H.

Total cross-section for ^{4}He

In Figure 3.9 it is seen that the total neutron cross-section for ^{4}He displays a broad resonance between approximately 0.2 MeV and 20 MeV.

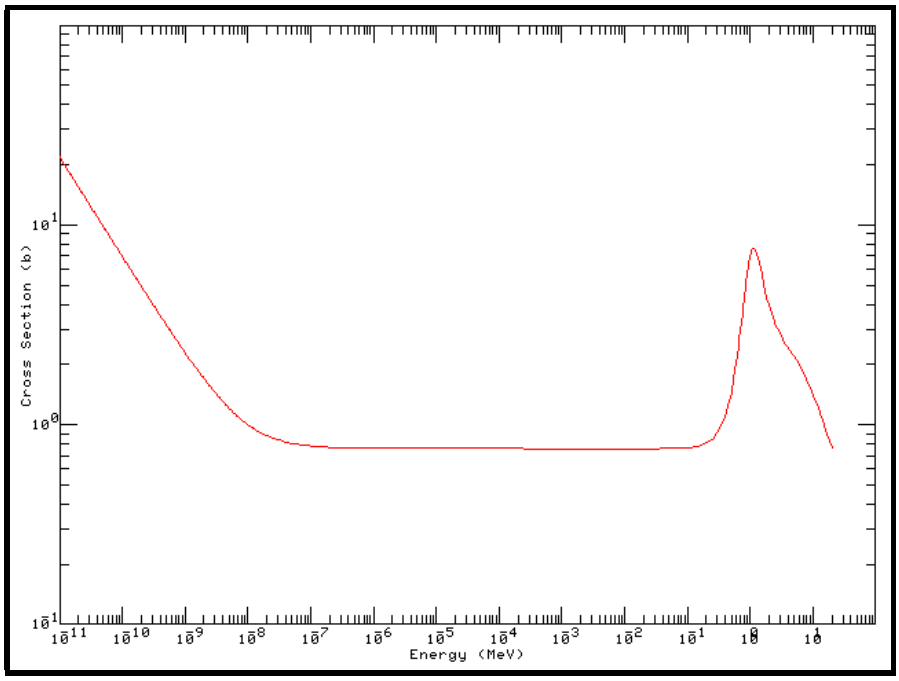

Figure 3.9: *The total neutron cross-section $\sigma_t(E)$ for ^{4}He.*

The $^{4}_{2}$He nucleus is an alpha particle, and is the most stable nucleus found in nature. In the neutron energy range up to 20 MeV, $^{4}_{2}$He only undergoes a single reaction type — elastic scattering, i.e. $\sigma_t = \sigma_{es}$. In the shell model of the nucleus, two nucleons represent a magic number, i.e. a closed shell. That is, the $^{4}_{2}$He nucleus has a closed neutron shell as well as a closed proton shell, and this accounts for its exceptional stability — it is a "double magic number" nucleus. One may say that $^{4}_{2}$He is essentially "transparent" to neutrons, because $\sigma_a = 0$ for incident neutrons, at least up to $E_n = 20$ MeV.

Total cross-section for ^{16}O

Figure 3.11 illustrates the total cross-section $\sigma_t(E)$ for the light nuclide ^{16}O.

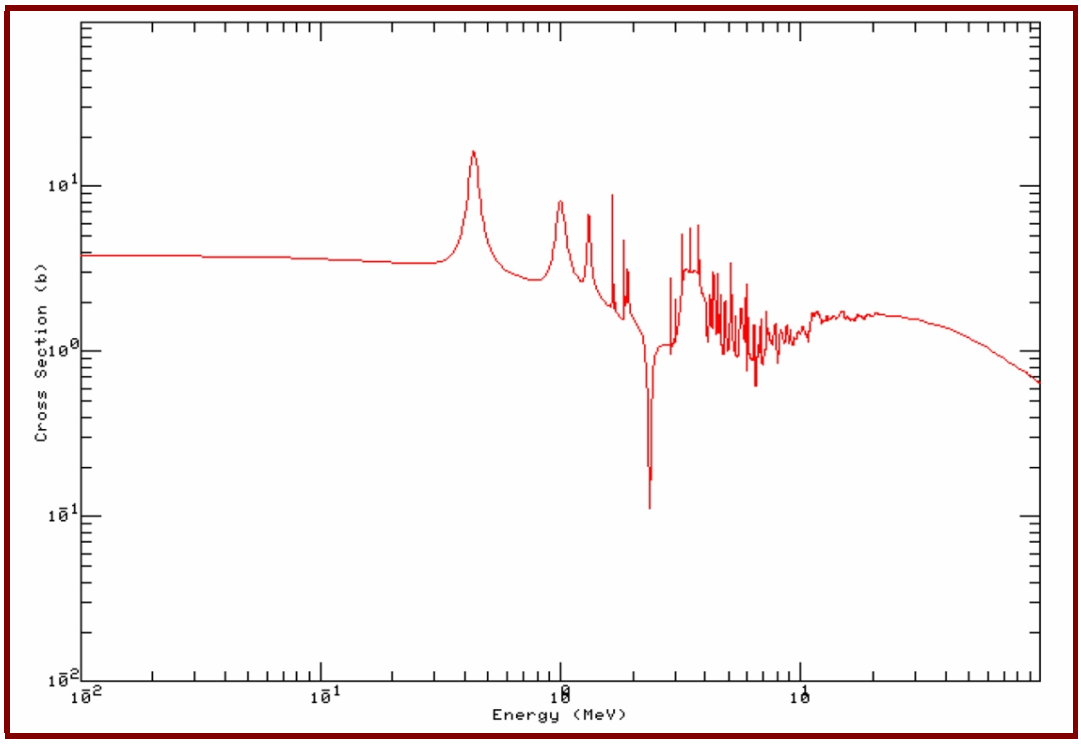

Figure 3.10: *Total neutron cross-section $\sigma_t(E)$ for ^{16}O.*

The cross-section is smooth and slowly varying up to about 0.4 MeV, from where fairly wide resonances appear. In light nuclei such as e.g. ^{16}O, the cross-section resonances are resolved, i.e. they do not overlap and can be measured as individual peaks.

The nucleus $^{16}_{8}O$ is exceptionally stable — the second most stable nucleus in nature. It has a closed shell of protons as well as a closed shell of 8 neutrons, i.e. it is a "double magic number" nucleus, as is $^{4}_{2}He$. Because $^{16}_{8}O$ is a small nucleus, a large fraction of its volume can be classified as "nuclear surface volume" having a lower nucleonic density than the interior of the nucleus. The nucleons in the "surface volume" of $^{16}_{8}O$ tend to cluster into four alpha particles $^{4}_{2}\alpha$, which adds to the stability of the $^{16}_{8}O$ nucleus.

Total cross-section for $^{12}_{6}C$

Figure 3.11 illustrates the total cross-section $\sigma_t(E)$ for the light nuclide $^{12}_{6}C$.

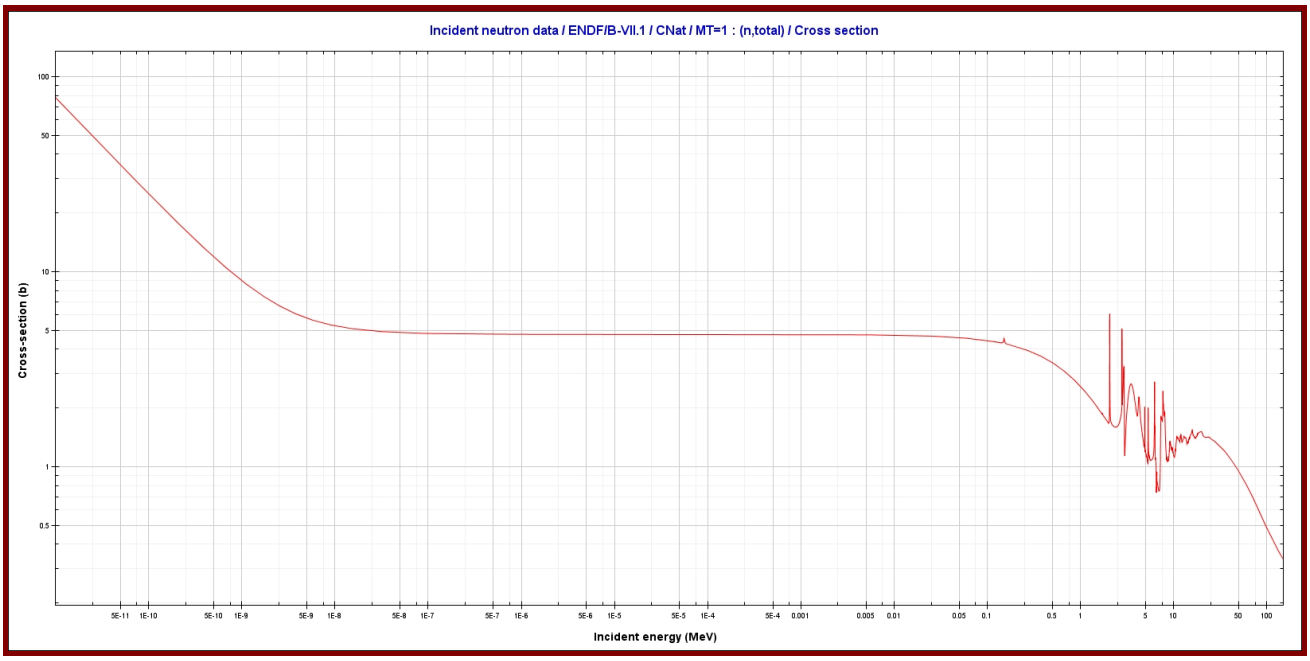

Figure 3.11: *Total neutron cross-section $\sigma_t(E)$ for ${}^{12}_{6}C$.*

The cross-section is smooth and slowly varying up to about 5 MeV, where very broad but low resonances appear. In light nuclei, neutron cross-section resonances are well resolved.

The nucleus ${}^{12}_{6}C$ is the third most stable nucleus in nature. It does not contain a magic number of protons or neutrons, but the nucleons in the "surface volume" of ${}^{12}_{6}C$ tend to cluster into three alpha particles ${}^{4}_{2}\alpha$, and this clustering phenomenon is responsible for the exceptionally high stability of the ${}^{12}_{6}C$ nucleus, because an ${}^{4}_{2}\alpha$ cluster is double-magic.

Total cross-section curve for ^{56}Fe

Figure 3.12 illustrates $\sigma_t(E)$ for an intermediate-mass nuclide, ${}^{56}Fe$.

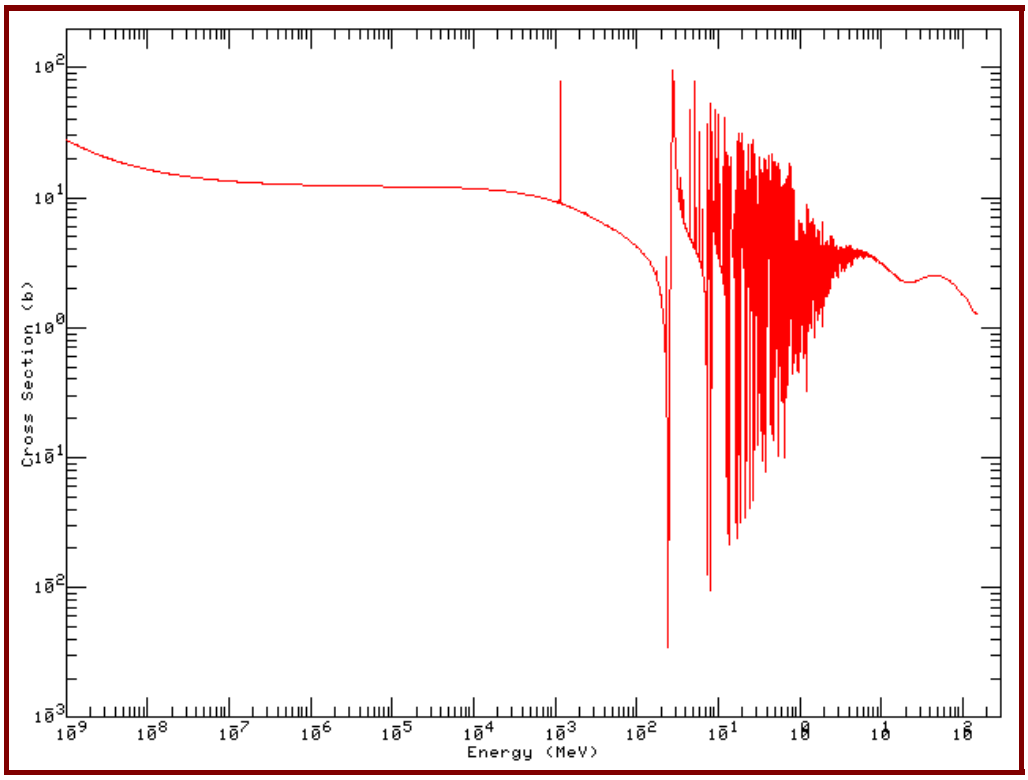

Figure 3.12: *Total neutron cross-section $\sigma_t(E)$ for ^{56}Fe.*

The cross-section is smooth and slowly varying up to approximately 10^{-2} MeV, from where narrow resonances appear. At lower energies, the resonances are resolved, but at higher energies they are so narrow and closely packed that they can not be resolved; this is the unresolved resonance region. At high incident neutron energies, giant dipole resonances are seen.

The nucleus $^{56}_{26}$Fe is one of the nuclei having the highest binding energy per nucleon. Graphs of $\left(\frac{\text{nuclear binding energy}}{\text{number of nucleons}}\right)$, abbreviated as $\left(\frac{BE}{A}\right)$, are found in practically all nuclear physics textbooks; the $\left(\frac{BE}{A}\right)$ curve reaches a peak at $^{56}_{26}$Fe. Light nuclei to the left of ^{56}Fe, can gain energy by fusion into heavier nuclei, up to $^{56}_{26}$Fe. Heavy nuclei far to the right of ^{56}Fe can release energy by fission (splitting, fragmentation) into lighter nuclei. In short: light nuclei release energy and gain stability by fusing and thereby moving towards $Z = 26$, while heavy nuclei release energy and gain stability by fragmenting and moving towards $Z = 26$.

Total cross-section curve for ^{197}Au

Figure 3.13 illustrates $\sigma_t(E)$ for a typical heavy nuclide, ^{197}Au.

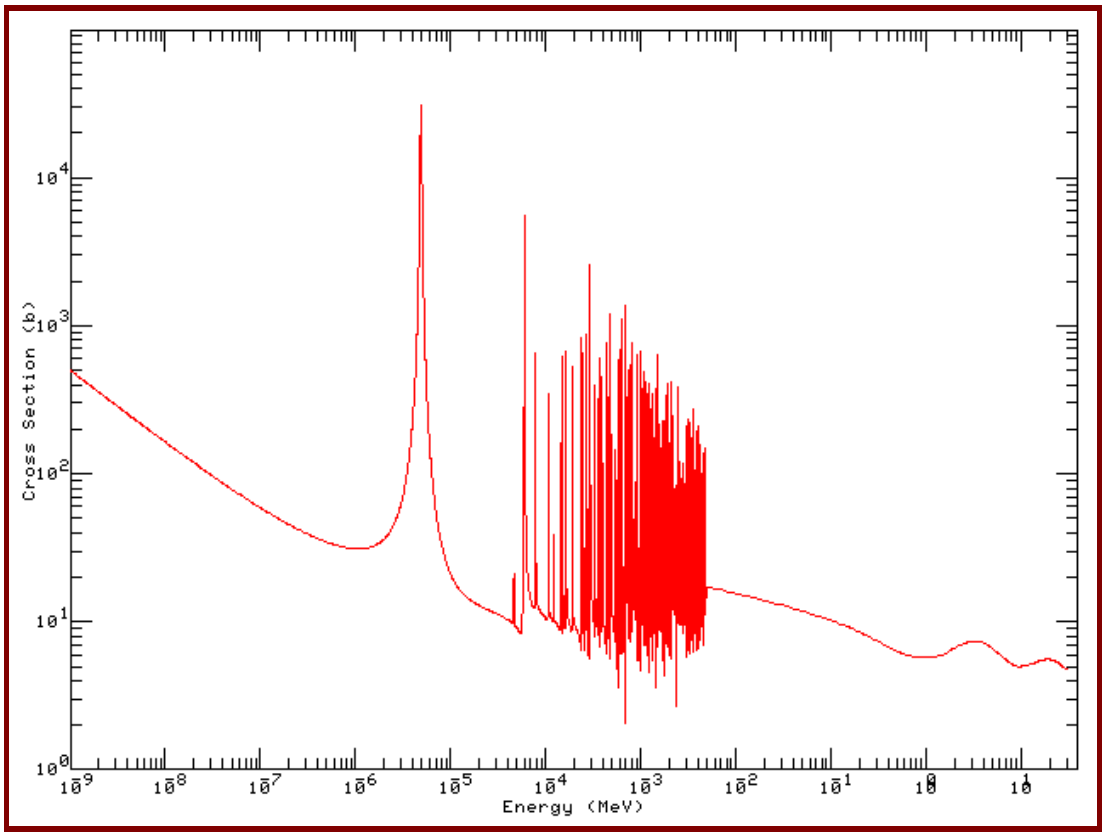

Figure 3.13: *Total neutron cross-section $\sigma_t(E)$ for the heavy nuclide ^{197}Au.*

The cross-section is smooth and slowly varying up to a few eV, from where resonances appear. At lower energies, the resonances are resolved, but at higher energies they are so narrow and closely packed that they can not be resolved any more; this is the unresolved resonance region. In the high energy region, wide, sinusoidal giant dipole resonances are clearly discernible.

The isolated and wide resonance at $1\,\text{eV} \leq E_n \leq 10\,\text{eV}$ in ^{197}Au is a (n,γ)-reaction resonance. Because ^{97}Au is the only stable gold isotope, this resonance presents an ideal method of measuring neutron fluence-rates by gold-foil or gold-wire activation.

Bismuth: An ideal filter to remove ionising photons whilst allowing neutrons to pass through

Materials-testing reactors (MTRs) are often equipped with experimental beamlines, which allow reactor neutrons to be utilised for e.g. neutron radiography and neutron diffraction studies. The beamline must allow the maximum number of neutrons through, whilst filtering out most of the ionising photons leaving the reactor core.

Figure 3.14 shows that Bismuth (^{209}Bi) is an ideal isotope to use as a filter to stop gamma-radiation and pass neutrons — its total neutron interaction cross-section is significantly lower than that of Pb over a wide energy range.

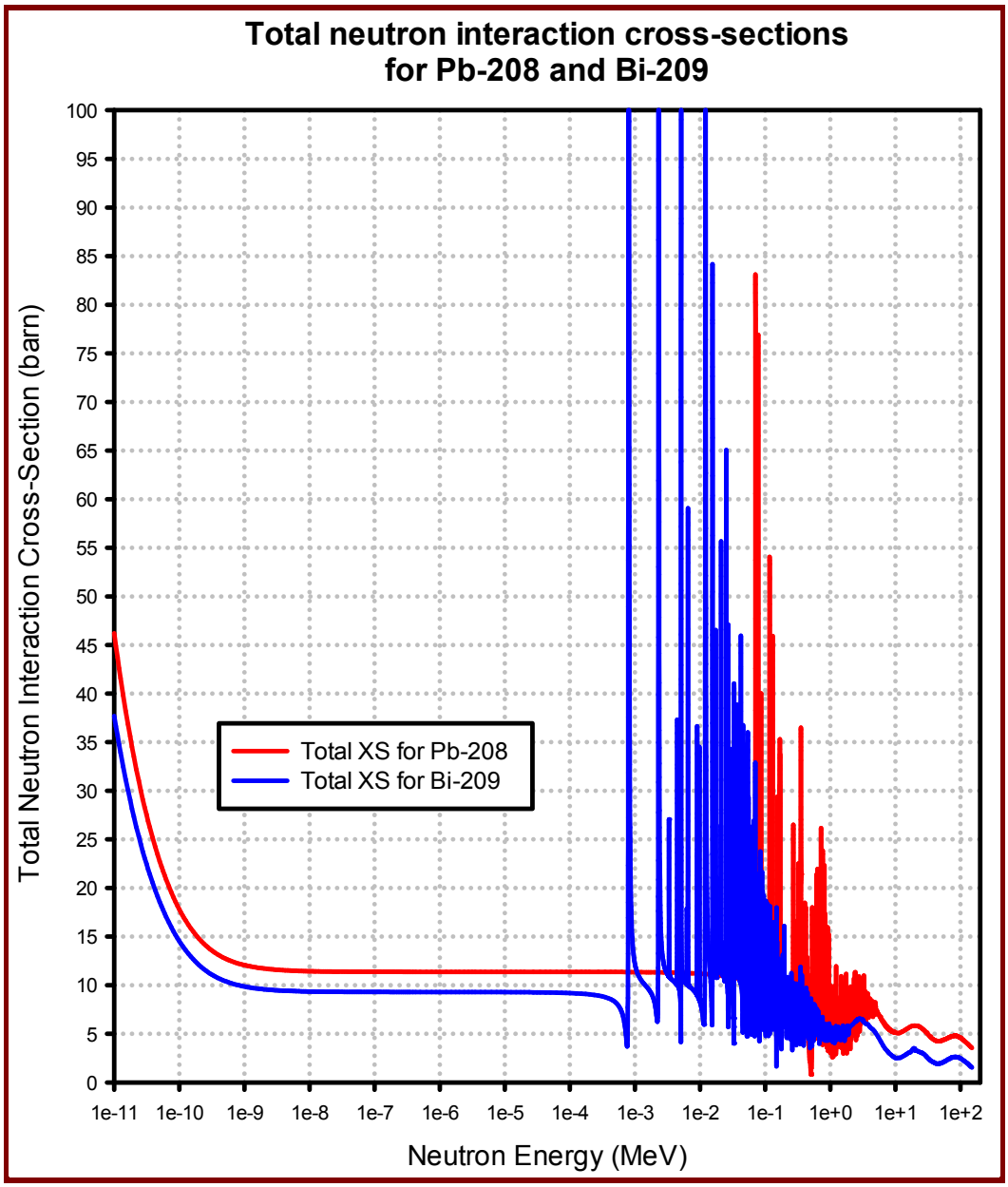

Figure 3.14: *Bismuth has a low neutron interaction cross-section, making it an ideal filter to remove ionising photons from the particle beam in experimental beamlines around Material Testing Reactors (MTRs).*

Bismuth will also not activate as much as most other materials under neutron irradiation. The product of the (n,γ) reaction with ^{209}Bi is ^{210}Bi, which has a half-life of only 5 days. This nuclide transitions to ^{210}Po, which in turn transitions to stable ^{206}Pb via α-particle emission. The effect of subsequent (n,γ)-reactions of ^{206}Pb is to first produce ^{207}Pb, which is also a stable Pb isotope. The trace amounts of ^{207}Pb formed in this way, will form stable ^{208}Pb via (n,γ) reactions. The net effect is that Bismuth will not activate much, even under quite intense irradiation by reactor neutrons.

Bismuth gamma-ray filters in MTR beamlines are typically between 8 cm and 12 cm thick. If a high thermal neutron fluence rate and a low ionising photon fluence-rate is desired, the best filtering results are obtained with single-crystal bismuth filters cryogenically cooled to

temperatures below 30 K. The colder the bismuth crystal, the more thermal neutrons pass through unperturbed.

3.6.6 Doppler broadening of cross-section resonances

There are several important effects of temperature and Doppler broadening of cross-section resonances:

1) There is the well known Doppler broadening effect in the resonance region of neutron cross-sections — as the temperature increases, cross-section resonances become broader and flatter. As temperature T increases the peaks of the resonances become lower, and the minima between resonances become flatter. At extremely high temperature the entire resonance structure disappears and the cross sections approaches a simple $\frac{1}{v}$ shape (where v is the neutron speed). Doppler-broadening of neutron cross-section resonances has a very important effect on resonance self-shielding in neutron transport calculations for, especially, fissile systems.

2) Another effect of Doppler broadening of neutron cross-section resonances is that at low neutron energies, as temperature T increases, the low-energy scattering cross-section increases and at very low energies approaches a simple $\frac{1}{v}$ shape (where v is the neutron speed). Starting from a "cold" (0 Kelvin) cross section that is constant at approximately 20 barns, as temperature increases the cross section increases. Compared to the "cold" 20 barn cross section, at thermal energy the Doppler broadened cross section is approximately 30 barns, i.e. 50 % higher. This effect extends well above thermal energy. For example, at $T = 20.5\,°\text{C}$ the thermal neutron energy is only $\langle E \rangle = 0.0253$ eV, but we can see the above effect on the cross-section up to $E \approx 1$ eV. At very low energy the cross section approaches a simple $\frac{1}{v}$ shape (where v is the neutron speed) and the cross sections at various temperatures become proportional to one another. This effect on the cross sections at low energy is important for thermal and low energy neutron systems.

3) Yet another important effect of temperature is that at lower energies neutrons do not slow down in energy as quickly and neutron scattering can even result in the upscattering of neutrons, i.e., when neutrons scatter they can gain, rather than lose, energy. This is a well known effect at low energies, where thermal scattering law data or a free gas model is used to model the interaction of neutrons with target atoms that are moving about with thermal motion. This effect can also be important at higher energies, particularly near narrow resonances, where thermal motion of the target atoms can cause neutrons to slightly upscatter. Even such slight upscattering can cause a neutron to scatter from below to above the energy of a very narrow cross-section resonance.

Figure 3.15 illustrates Doppler-broadening of neutron cross-section resonances.

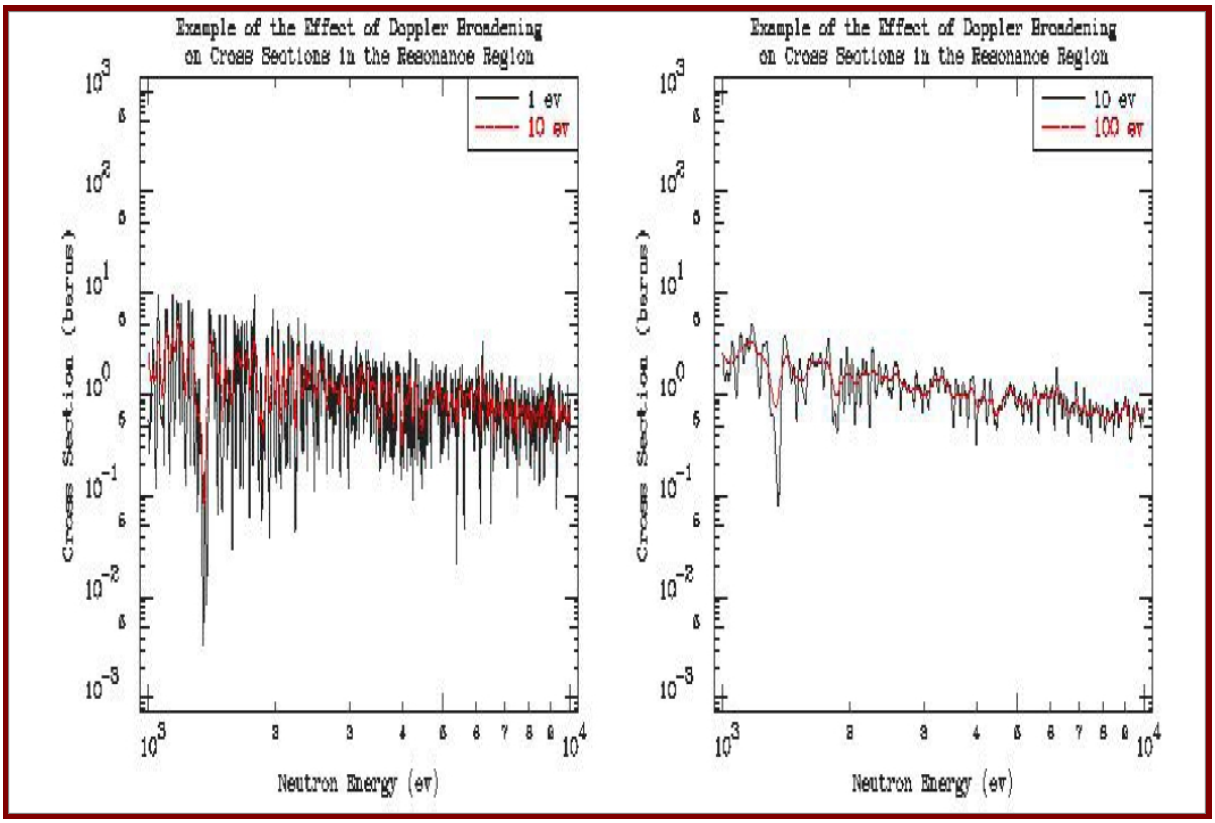

Figure 3.15: *Doppler broadening of neutron interaction cross-section resonances with temperature.*

Figure 3.16 shows the increase of low-energy cross-sections with temperature.

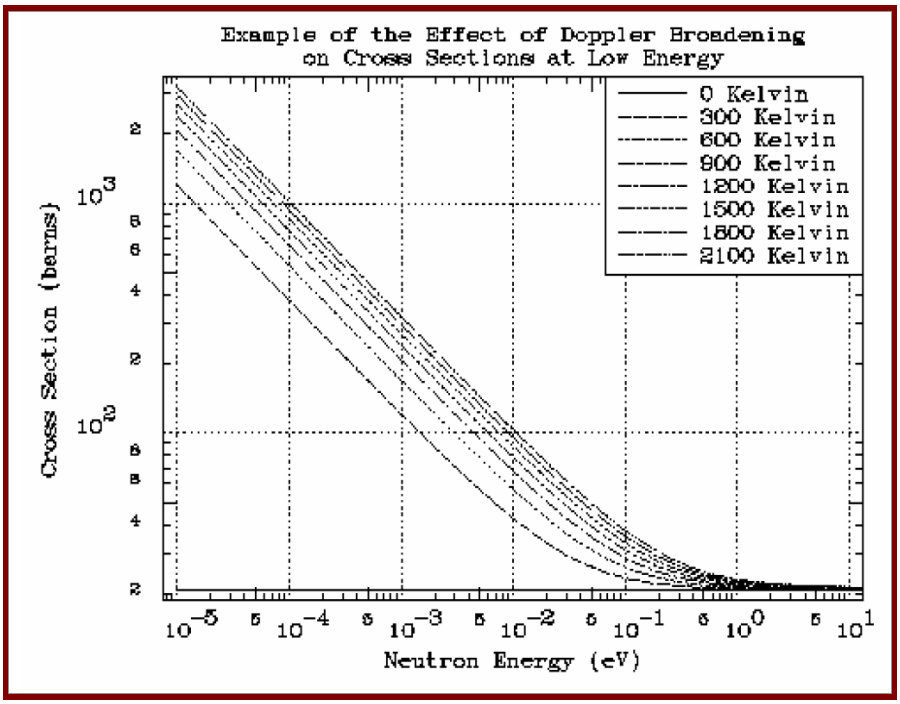

Figure 3.16: *Increase of low-energy neutron interaction cross-sections with temperature. Note that the* $\frac{1}{v}$ *part of the cross-section curve "falls flat" as* T *approaches absolute zero, i.e. 0 K.*

3.6.7 Cross-sections for radiative neutron capture, i.e. (n, γ) reactions: graphical journey

Introduction

Free neutrons can be absorbed by nuclei, and a prominent exit channel for such neutron capture nuclear reactions, is (n, γ) reactions. These reactions are exothermic (exo-ergic), and can therefore take place at all incident neutron energies. The target nucleus absorbs the neutron, a compound nucleus is produced, which then transitions to lower energy states by the emission of capture γ-rays within approximately 10^{-13} seconds. These (n, γ)-reactions are, from the perspective of radiation shielding, a very important source of secondary ionising photons. The cross-sections for (n, γ) capture reactions are usually the highest in the resonance and, especially, thermal neutron energy regions. A substantial fraction of the neutron fluence-rate in radiation shielding at a nuclear fission reactor, a nuclear fusion facility, as well as at lower energy particle accelerator facilities, is found in this energy range, so that it is often found that secondary ionising photons produced in neutron capture reactions contribute strongly to the total dose rate outside a shielded neutron source.

Cross-sections for (n, γ) reactions in ^{1}H and ^{2}H

Although ^{1}H is the most kinematically efficient material for slowing down neutrons via *elastic* scattering — see Table 3.6 on page 100 — it has two main drawbacks neutron shielding applications:

- The scattering cross-section $\sigma_s(E')$ rapidly "nose-dives" to a very low value at incident neutron energies higher than about 2 MeV, so that the likelihood of an elastic neutron scattering event with $^{1}_{1}$H taking place, becomes very low at high incident neutron energies.

- The cross-section for the nuclear reaction $^{1}\mathrm{H}(n, \gamma)^{2}\mathrm{H}$ is ~1 barn at the most probable thermal neutron energy of $E_n = k_B T \approx 0.0253$ eV at room temperature ($T = 20.5°$ C). This neutron capture cross-section of ^{1}H will lead to the production of capture γ-rays with $E_\gamma = 2.205$ MeV, which will present a further, secondary shielding problem.

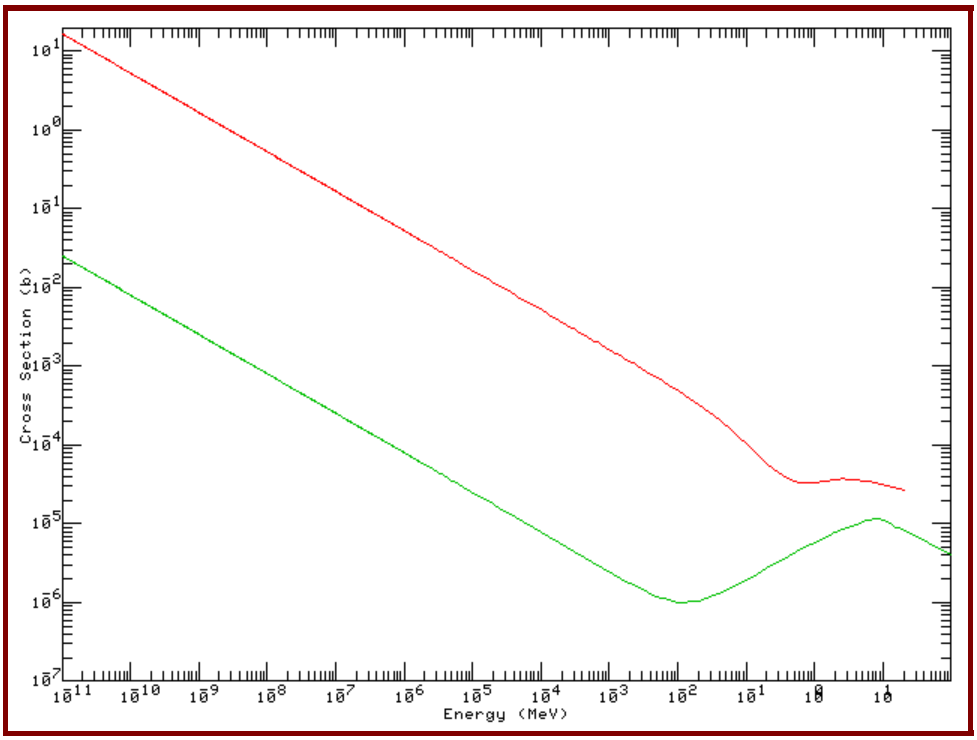

Figure 3.17: *The cross-section for the nuclear reactions* $^{1}H(n,\gamma)^{2}H$ *and* $^{2}H(n,\gamma)^{3}H$.

From sub-thermal neutron energies to $E_n \approx 0.01$ MeV, the cross-section for the neutron capture reaction $^{2}\mathrm{H}(n,\gamma)^{3}\mathrm{H}$ is almost 3 orders of magnitude lower than the cross-section for the neutron capture reaction $^{1}\mathrm{H}(n,\gamma)^{2}\mathrm{H}$. Therefore neutron economy will be significantly better in a nuclear reactor moderated by D_2O, than in a nuclear reactor moderated by H_2O.

Application: D_2O moderated nuclear reactors

Application: It is clear that the neutron capture cross-section $\sigma_{^{1}\mathrm{H}(n,\gamma)}(E)$ is orders of magnitude higher than the cross-section $\sigma_{^{2}\mathrm{H}(n,\gamma)}(E)$. Furthermore, the neutron capture cross-section $\sigma_{^{16}\mathrm{O}(n,\gamma)}(E)$ is also very low, because ^{16}O has a "magic number" of 8 neutrons and 8 protons. As a consequence, a $\left(^{1}_{1}\mathrm{H}\right)_2O$-cooled, $\left(^{1}_{1}\mathrm{H}\right)_2O$-moderated nuclear reactor using un-enriched, natural uranium can not be made critical. Such a reactor can only be operated if heavy water, D_2O, is used as moderator. In light water, i.e. H_2O, there will be too much parasitic slow-neutron absorption, on account of the fact that $\sigma_{^{1}\mathrm{H}(n,\gamma)}(E_{\mathrm{thermal}}) \approx 0.332$ barn, which is a substantial neutron absorption cross-section. For this reason, light-water (H_2O) moderated & cooled nuclear fission reactors have to use enriched uranium to become critical.

Application: Production of secondary ionising photons from neutron capture reactions — effect on shield performance

Most neutrons entering a shield are first scattered to low energies, and are then absorbed by the nuclei in the shield material — as the neutron energy decreases, neutron absorption cross-sections increase. When a nucleus absorbs a neutron, the binding energy of the neutron, which is on average $7-9$ MeV, is added to the internal energy of the nucleus that absorbed the neutron. The kinetic energy of the neutron plus its binding energy in the resulting compound nucleus, leaves the compound nucleus in a highly excited state. The excited nucleus typically transitions within about 1 ps, often through several intermediate energy states, emitting one or more gamma photons in the process. These capture gamma-photons from (n,γ)-reactions can, for specific source-shield combinations, dominate the dose rate on the "personnel side" or "detector side" of a radiation shield.

In a hydrogenous shield such as paraffin wax, polyethylene or water, the neutron capture nuclear reaction

$$^{1}\mathrm{H} + n \rightarrow {}^{2}\mathrm{H} + \gamma\ (2.205\ \mathrm{MeV})$$

produces quite energetic capture γ-photons, which can contribute a high fraction of the dose rate on the detector or personnel side of the shield.

A series of MCNP calculations, modelling an isotropic point source of mono-energetic neutrons inside a shell of paraffin wax, in spherical symmetrical geometry, was used to calculate neutron dose rates (NDR) and photon dose rates (PDR) on the personnel side of the shield. Results are summarised below.

Example 3.4

Case 1

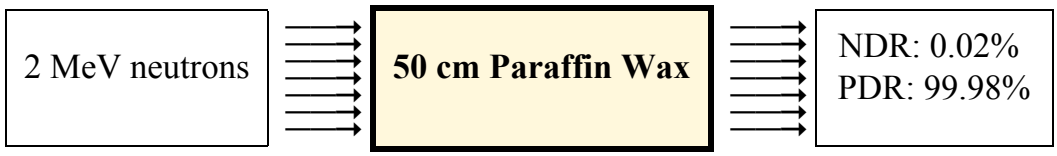

Case 2

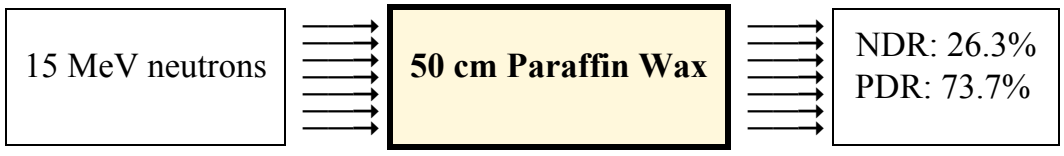

Case 3

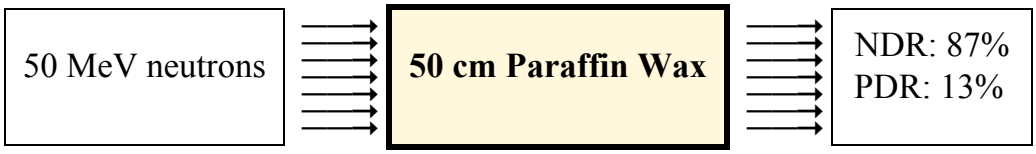

Case 4

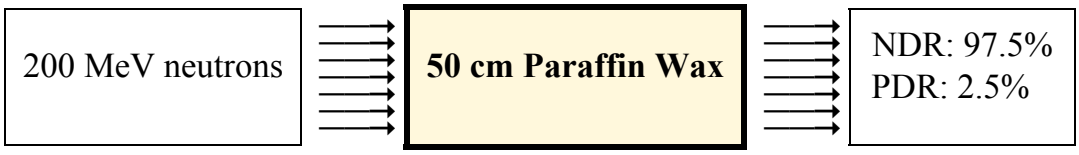

Conclusion: In paraffin wax, low energy incident neutrons are easily moderated to thermal energies, where they produce an abundance of ionising photons in hydrogenous shielding materials by $^{1}\mathrm{H}\ (n,\gamma)\ ^{2}\mathrm{H}$ radiative capture reactions, which produce ionising photons having $E_\gamma = 2.205$ MeV. For high energy incident neutrons, neutrons are not moderated well by hydrogenous shielding materials. Combined with the fact that radiative capture cross-sections for fast neutrons are extremely low, the result is that neutrons will dominate the dose rate contribution at the personnel side of the shield, for high energy neutrons incident on a 50 cm thick paraffin-wax shield.

Assignment 3.12

1. Model Example 3.4, Case 1 on page 117 with MCNP, and graph the photon energy spectrum on the detector side of the shield. Determine at which energy the bulk of secondary gamma photons are produced. Recommended tally type: F1.

2. Use MCNP6 to model a point-source emitting mono-energetic neutrons with $E_n = 10^{-7}$ MeV, surrounded by a thin shell of 0.1 cm Fe. Plot the energy spectrum of the ionising photons produced by all photon-producing interactions in the Fe. Repeat this "experiment" for,
   (a) H_2O,
   (b) Pb,
   (c) ^{113}Cd,
   (d) ^{10}B, and
   (e) ^{6}Li.
   Compare photon yields as well as photon energies. Recommended tally type: F1.

The production of the neutron activation product ^{60}Co

Figure 3.18 shows the (n,γ) cross-section for ^{59}Co. In a neutron field, this nuclide undergoes the reaction $^{59}\text{Co}(n,\gamma)^{60}\text{Co}$; the product radionuclide, ^{60}Co, has a halflife of 5.27 years, and builds up in all materials at nuclear reactors and particle accelerator facilities that contain cobalt.

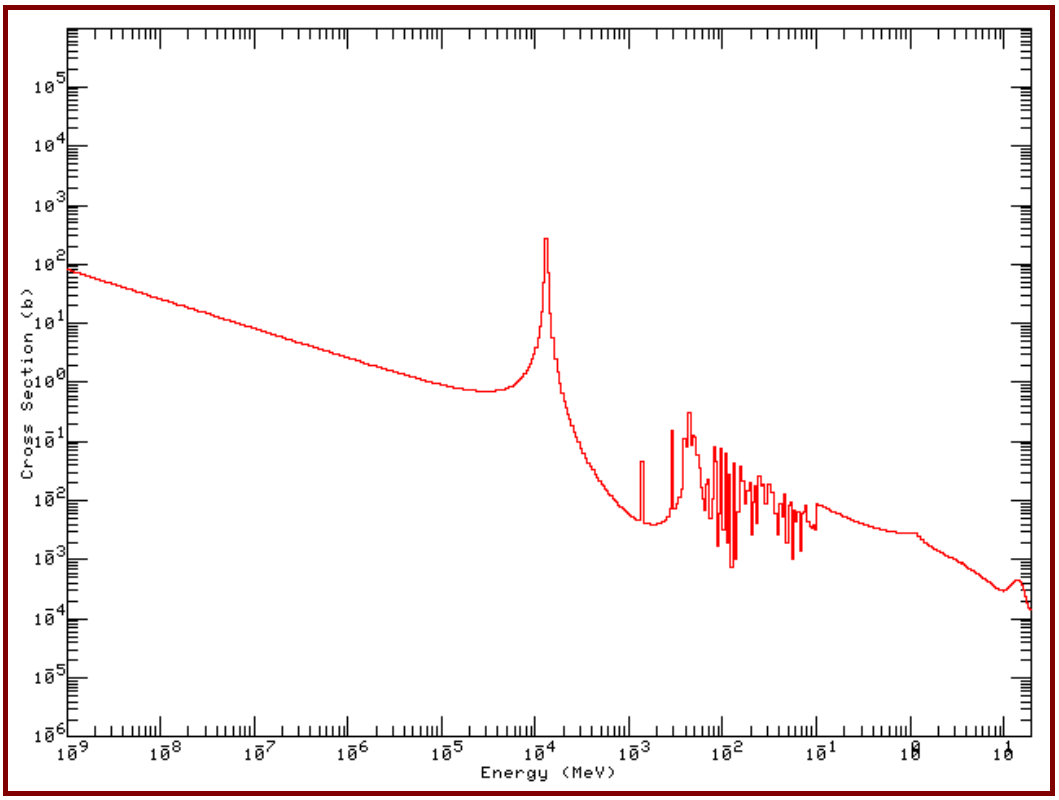

Figure 3.18: *The (n,γ) cross-section for ^{59}Co.*

In a thermalised neutron field, the stable nuclide ^{59}Co will readily undergo the nuclear reaction $^{59}\text{Co}(n,\gamma)^{60}\text{Co}$. Note the characteristic $\sigma_{(n,\gamma)} \propto \frac{1}{\sqrt{E}}$ i.e. $\sigma_{(n,\gamma)} \propto \frac{1}{v}$ shape of the cross-section curve in the low energy region, i.e. the region to the left of the lowest-energy resonance peak.

An interesting fact is that this $\frac{1}{\sqrt{E}}$ part of all (n,γ) cross-section curves becomes increasingly flat at temperatures very close to absolute zero, for all nuclides that display this $\frac{1}{\sqrt{E}}$ behaviour in $\sigma_{(n,\gamma)}$. All neutron-interaction cross-section resonance peaks also become increasingly narrow at lower temperatures.

Important: Even when there is initially practically no cobalt present in a neutron field, the radionuclide ^{60}Co will gradually build up as a result of the chain-like activation-and-decay reactions in Eq. (3.30),

$$^{54}\mathrm{Fe}(n,\gamma)^{55}\mathrm{Fe}(n,\gamma)^{56}\mathrm{Fe}(n,\gamma)^{57}\mathrm{Fe}(n,\gamma)^{58}\mathrm{Fe}(n,\gamma)^{59}\mathrm{Fe} \underset{\beta^-}{\rightarrow} {}^{59}\mathrm{Co}(n,\gamma)^{60}\mathrm{Co} \underset{\beta^-}{\rightarrow} {}^{60}\mathrm{Ni} \tag{3.30}$$

Note that, in an intense neutron field, e.g. close to or inside a reactor core, the relative abundances of the different Fe isotopes in the irradiated iron sample will be affected by, *inter alia,* the nuclear reactions in Eq. (3.30) — after several years, the isotopic composition of the sample will be measurably different from the initial natural abundances.

Accurate codes to follow neutron-induced isotopic transmutations in a known neutron fluence-rate field $\phi(t, E)$, are the following two ***activation codes***:

- ORIGEN-S, which is part of the SCALE-6.1 system (2011);
- FISSPACT, which is part of EASY — the European Activation System.

Calculations with FISPACT-2007 show that, if a Fe sample is irradiated in an intense reactor neutron spectrum for 1 year, the dominant radionuclide activities that will be present after 10 years of cooldown, will be: 99.77% Fe-55, 0.2052% Co-60 and 0.0202% Mn-54. The fractional activity of ^{60}Co will be low, but its contribution to the dose rate will be substantial, because $^{55}_{26}$Fe is an emitter of rather feeble ionising radiation.

Assignment 3.13

1. A small sample of initially 100% pure Fe is irradiated in a thermal neutron fluence-rate of $\phi_{\mathrm{th}}(t) = 1.2 \times 10^{+14}$ cm^{-2} s^{-1} inside a Material Testing Reactor (MTR) fuelled with LEU plate-type fuel. Use the activation code ORIGEN-S (part of SCALE 6.1) to calculate (1) the ^{60}Co activity following 3 years of irradiation, (2) the new isotopic composition of the irradiated sample, (3) the new elemental composition of the irradiated sample, and (4) a multigroup ionising photon source term for the activated sample.

2. A small sample of initially 100% pure Fe is irradiated in a thermal neutron fluence-rate of $\phi_{\mathrm{th}}(t) = 1.2 \times 10^{+14}$ cm^{-2} s^{-1} inside a Material Testing Reactor (MTR) fuelled with LEU plate-type fuel. Use the activation code FISSPACT (part of EASY) to calculate (1) the ^{60}Co activity following 3 years of irradiation, (2) the new isotopic composition of the irradiated sample, (3) the new elemental composition of the irradiated sample, and (4) a multigroup ionising photon source term for the activated sample.

The cross-section for the reaction $^{56}Fe(n,\gamma)^{57}Fe$

Figure 3.19 shows the (n,γ) radiative capture cross-section for ^{56}Fe, which is the Fe isotope with the highest natural abundance (91.7%).

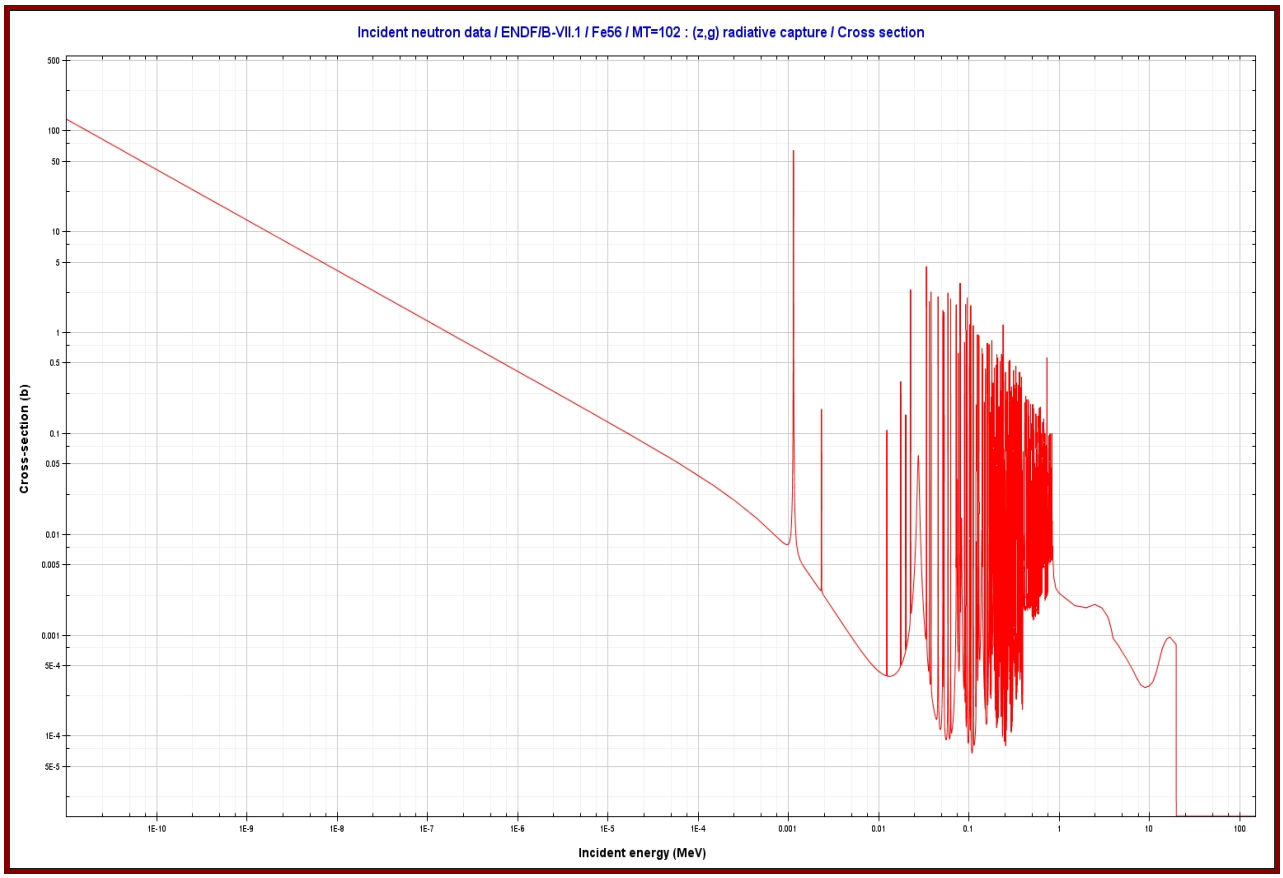

Figure 3.19: *The (n,γ) radiative capture cross-section for ^{56}Fe.*

Note the prominent $\sigma(E)_{(n,\gamma)} \propto \frac{1}{\sqrt{E}}$ trend at low incident neutron energies.

The cross-section $\sigma_{(n,\gamma)}(E)$ for the gadolinium isotope ^{157}Gd

All gadolinium (Gd) isotopes display unusually high (n,γ) cross sections; the gadolinium isotope with the highest (n,γ) cross section, is ^{157}Gd — see Figure 3.20.

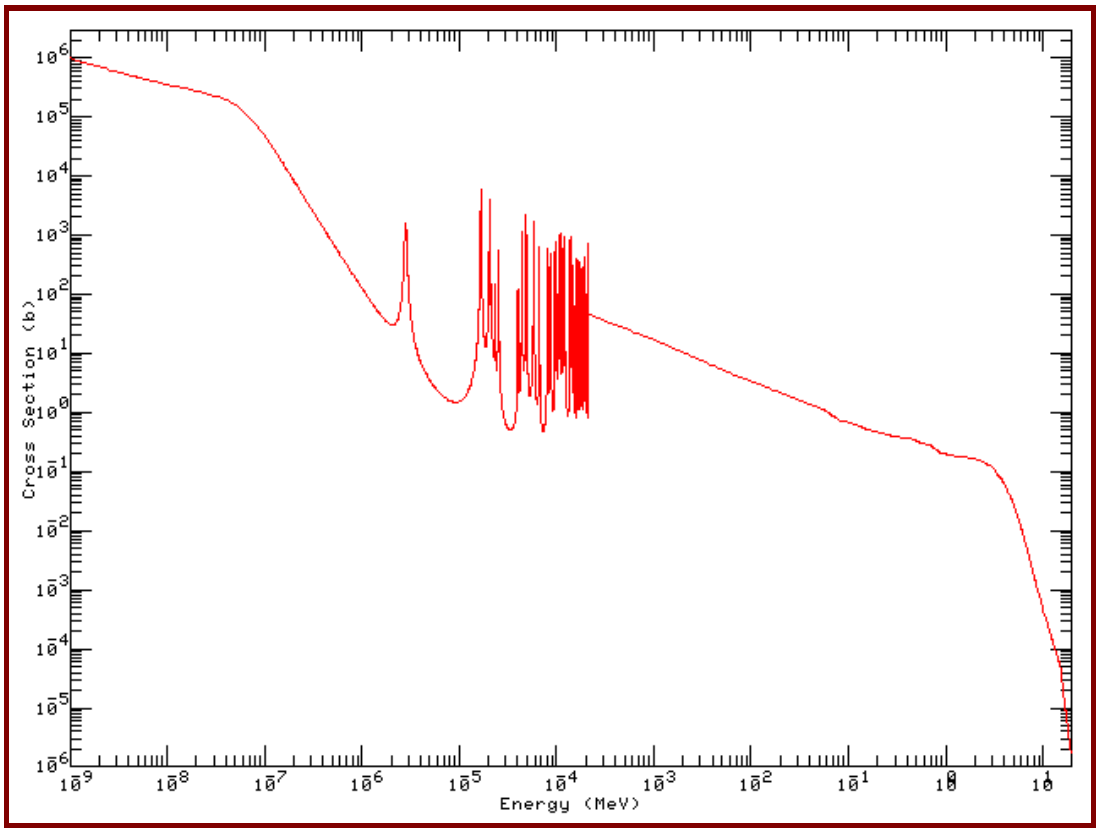

Figure 3.20: *A nuclide with a very high radiative capture, i.e. (n,γ) cross section, is an isotope of gadolinium, ^{157}Gd.*

For this reason, the strong neutron absorber gadolinium is used extensively in burnable poisons and control rods for nuclear reactor reactivity control.

(Note: The theory of nucleogenesis inside stellar interiors and during supernova explosions, presents a good explanation why the natural abundance of isotopes having high neutron capture cross-sections are very low.)

Xenon-135 and "reactor poisoning"

One of the extraordinary sequences in the operation of a fission reaction is that of the production of ^{135}I as a fission product and its subsequent transition into ^{135}Xe. The fission product ^{135}I is a rather common fission product, mounting to up to approximately 6% of the fission products. It has a rather small probability for absorbing a neutron, so it is not in itself a significant disturbing factor in reactor reactivity control. It has a half-life of approximately 6.7 hours and transitions into ^{135}Xe ($T_{½} = 9.2$ hours). The ^{135}Xe has a very large cross-section for neutron absorption — approximately 3×10^6 barns at $E_n = 0.0253$ eV — see Figure 3.21. This high (n,γ) cross-section compares to 400-600 barns for the effective ^{235}U fission cross-section in the thermal neutron energy range. The high loss-rate of neutrons that will occur when the ^{135}Xe concentration in reactor fuel rises, therefore has the potential to poison the chain reaction by absorbing too high a fraction of neutrons, rendering the effective multiplication factor of the reactor core lower than $k_{\text{eff}} = 1$.

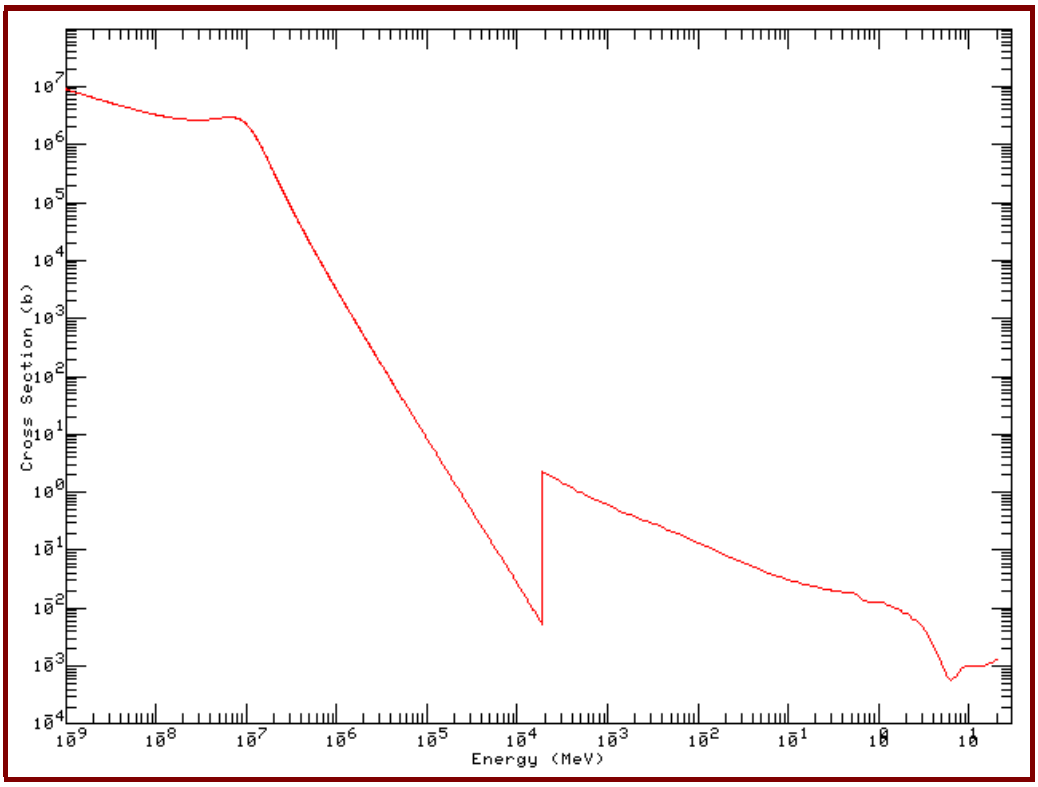

Figure 3.21: *The large (n,γ) neutron capture cross-section of ^{135}Xe for the absorption of slow neutrons.*

When a reactor is shut down, the concentration of ^{135}Xe in the fuel builds up, and this neutron poison may make it very difficult to start the core up again for a period of about 1 to 2 days.

In the normal operation of a nuclear reactor, the presence of the ^{135}Xe is naturally kept low in a reactor at power. The fission product ^{135}I is produced, transitions to ^{135}Xe which absorbs neutrons and is thereby "burned away" and kept at a low concentration which has a very low impact on core reactivity. There is an equilibrium concentration of both ^{135}I and ^{135}Xe in a reactor at steady-state power. However, when the reactor power level is drastically lowered, the ^{135}Xe concentration begins to increase because the parent ^{135}I is present at full-power equilibrium concentration, and continually feeds ^{135}Xe into the core, without the normally high neutron fluence-rate being present to "burn away" the ^{135}Xe. The concentration of the neutron-absorbing reactor poison, ^{135}Xe, will eventually peak and then decrease, but with its relatively long 9.2 hour half-life, this "xenon-poisoning" phase can be lengthy and problematic for reactor startup following a scram, and this xenon poisoning problem may persist up to 2 days.

^{149}Sm — the second most important reactor-poisoning fission product

Many of the fission products with mass 147 or greater such as Promethium-147, Samarium-149, Samarium-151, and Europium-155 have significant cross sections for neutron capture. The non-radioactive fission product, ^{149}Sm (samarium-149) is produced in an operating nuclear reactor. Because it is not radioactive, it is not removed by radioactive transition, but

almost exclusively by (n,γ)-reactions that produce ^{150}Sm. The fission product ^{149}Sm presents problems somewhat different from those encountered with ^{135}Xe. The equilibrium concentration (and thus the reactor poisoning effect) builds to an equilibrium value during reactor operation in about 500 hours of full-power operation, and since ^{149}Sm is stable, the concentration remains essentially constant during reactor operation.

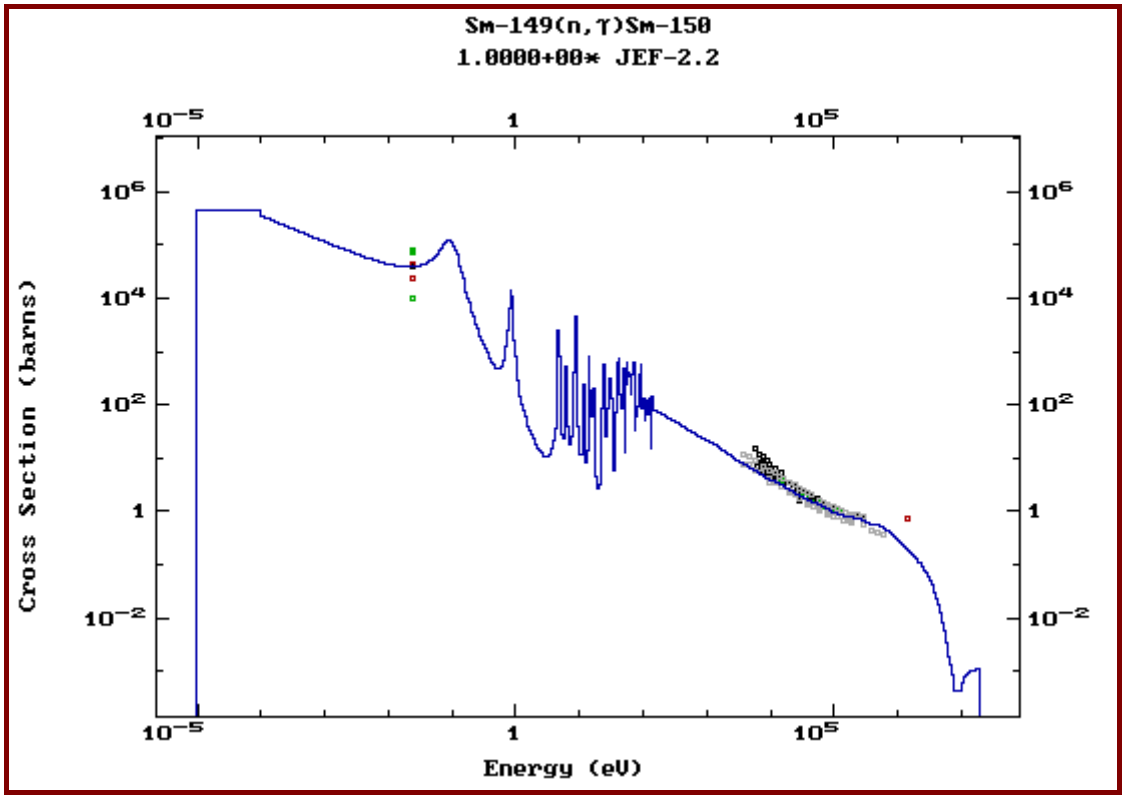

Figure 3.22: *The high (n,γ) cross-section of ^{149}Sm, which acts as a reactor poison.*

The thermal neutron capture cross-section of ^{149}Sm is approximately 4.1×10^4 barn. Upon absorbing a neutron, ^{149}Sm forms ^{150}Sm, which has an effective neutron capture cross-section of 102 barn, which is far less problematic from the viewpoint of neutron economy. The steady-state negative reactivity load as well as transient negative reactivity loads contributed by ^{149}Sm must be accommodated in reactor design and operation.

Contact the author for a simple Fortran-90 code that models ^{135}Xe and ^{149}Sm transients in reactor operation, for a user-specified core-averaged, one-group neutron fluence-rate history, $\phi(t)$.

Low (n,γ) neutron-capture cross-sections for ^{2}H, ^{9}Be, ^{nat}C and ^{16}O

Figure 3.23 displays the markedly low (n,γ) neutron-capture cross-sections for the nuclides ^{2}H, ^{9}Be, ^{nat}C and ^{16}O.

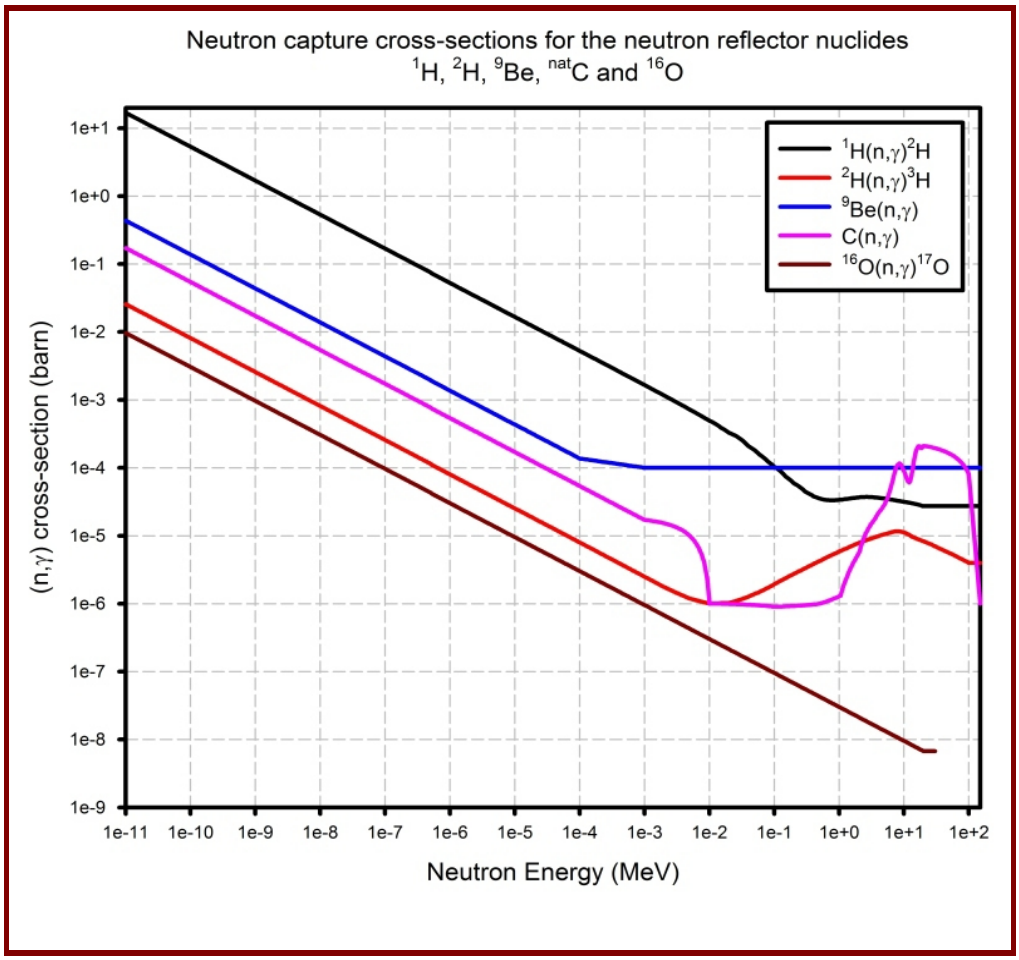

Figure 3.23: *The (n,γ) cross-sections for the nuclides ^{2}H, ^{9}Be, ^{nat}C and ^{16}O.*

Because the neutron capture cross-section for ^{2}H, ^{9}Be, ^{nat}C and ^{16}O are so low, compounds such as D_2O, high-purity Be metal, BeO, and high-purity, nuclear grade graphite, make excellent neutron reflectors. Neutron lifetimes in these materials will be relatively high. This high neutron lifetime can be clearly "seen" in MCNP neutron transport calculations in KCODE mode, through thick regions of D_2O, Be, BeO and graphite — cycle execution is remarkably slow because the neutron lifetime is relatively long in thick reflector regions having a high $\frac{\sigma_s}{\sigma_a}$ ratio.

Beryllium has a very low neutron capture cross-section and is therefore a useful neutron reflector in research reactors. Beryllium is light enough to slow neutrons down with reasonably good kinematical efficiently by elastic scattering. Its elastic scattering cross-section is significantly higher than its neutron capture cross-section. In a thick, high-purity beryllium reflector, neutron lifetime will be high.

Figure 3.24 shows $\sigma_{es}(E)$, $\sigma_{(n,\gamma)}(E)$ and $\sigma_{(n,2n)}(E)$ for ^{9}Be.

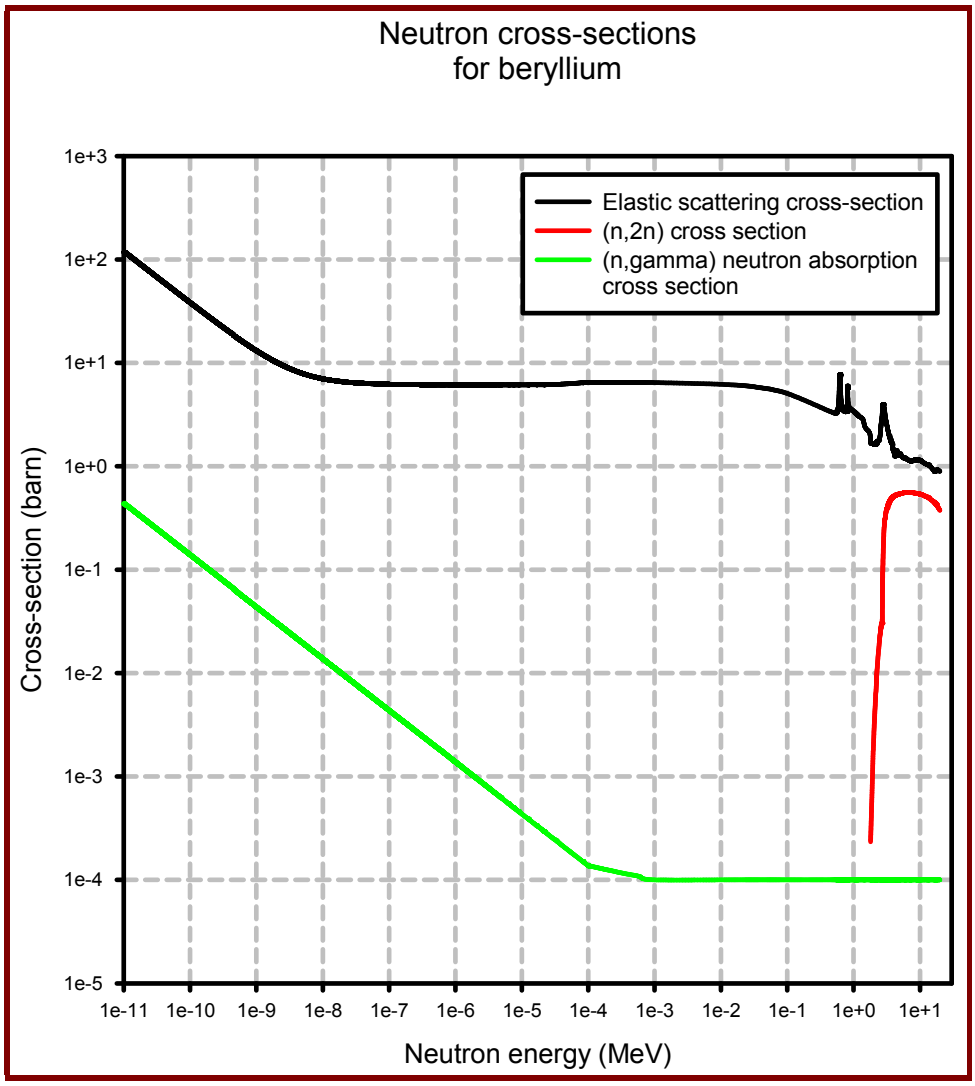

Figure 3.24: *The cross-sections $\sigma_{es}(E)$, $\sigma_{(n,\gamma)}(E)$ and $\sigma_{(n,2n)}(E)$ for ^{9}Be; (es ≡ elastic scattering).*

One characteristic of a good neutron reflector material is that the elastic scattering cross-section $\sigma_{es}(E)$ is far bigger than cross-sections for neutron absorption, i.e. $\sigma_{(n,\gamma)}(E)$, $\sigma_{(n,p)}(E)$ *and* $\sigma_{(n,\alpha)}(E)$. A substantial $\sigma_{(n,2n)}$ cross-section enhances the properties of a neutron reflector, because its leads to some degree of fast neutron multiplication inside the reflector.

The favourably high ratio $\frac{\text{neutron elastic scattering cross-section}}{\text{neutron absorption cross-section}} \approx \frac{\sigma_{es}(E)}{\sigma_{(n,\gamma)}(E)}$ for ^{9}Be, is shown in Figure 3.25.

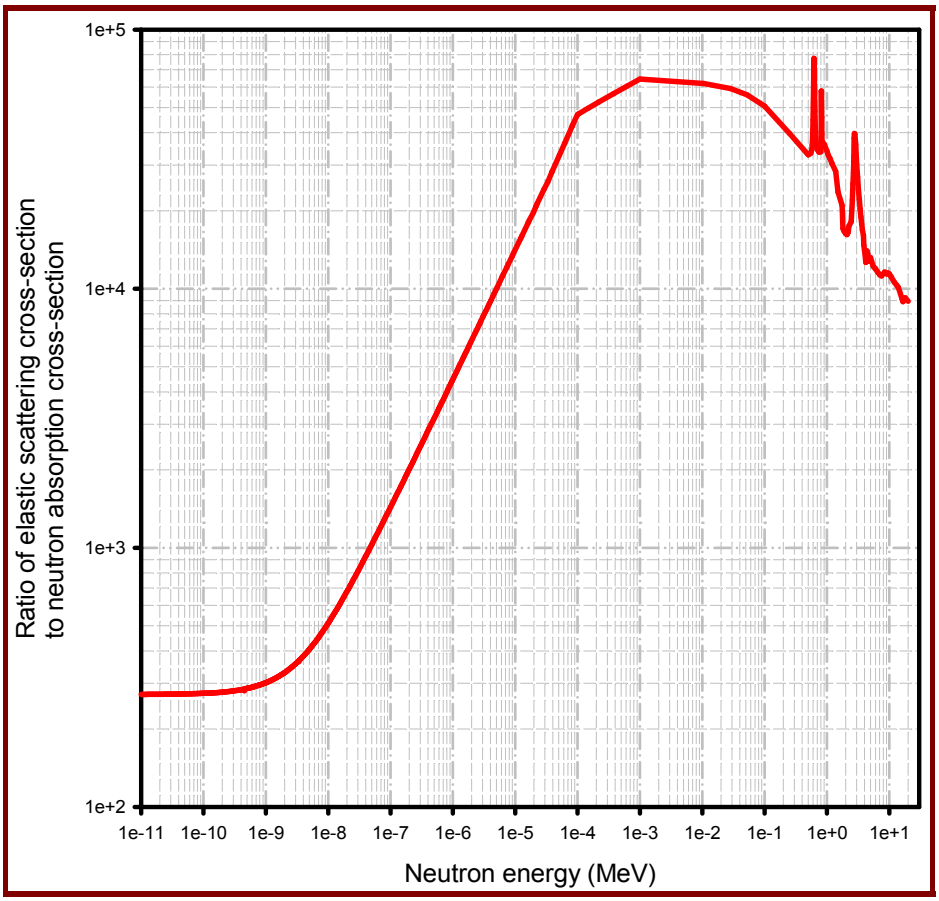

Figure 3.25: *The ratio* $\frac{\sigma_{es}(E)}{\sigma_{(n,\gamma)}(E)}$ *for* ^{9}*Be is high and makes for a good neutron reflector (es* $\equiv$ *elastic scattering).*

Summary: Be is a good neutron reflector material, because:

- $\sigma_{\text{es}}(E)$ is reasonably high over a wide energy range (es $\equiv$ elastic scattering).
- $\sigma_{\text{c}}(E)$ is low over a wide energy range (c $\equiv$ capture).
- The ratio $\frac{\sigma_{\text{es}}(E)}{\sigma_{\text{c}}(E)}$ for ^{9}Be is high; neutron losses will be low; the probability for neutron scattering is vastly higher than the probability for neutron capture.
- The kinematical effectiveness of elastic scattering by ^{9}Be is reasonably favourable, because the ^{9}Be nucleus is only ~9 times heavier than a neutron. The expectation value of the energy of a 2 MeV incident neutron will be 1.64 MeV after one elastic scattering event off ^{9}Be. A total of ~90 elastic scattering interactions are required to thermalise a neutron with incident energy $E = 2$ MeV, in beryllium.
- The mass of the ^{9}Be nucleus is high enough to scatter neutrons through large average angles — the average scattering angle is 85.8°, whereas the average scattering angle is only 48.1° for ^{1}H. ^{9}Be can scatter neutrons through all angles $\theta \in [0°; 180°]$, whereas ^{1}H can scatter a neutron only through the angles $\theta \in [0°; 90°]$.

In many Material Testing Reactors, beryllium blocks are packed around the core periphery to reflect neutrons back to the core and minimise neutron leakage — see Figure 3.26.

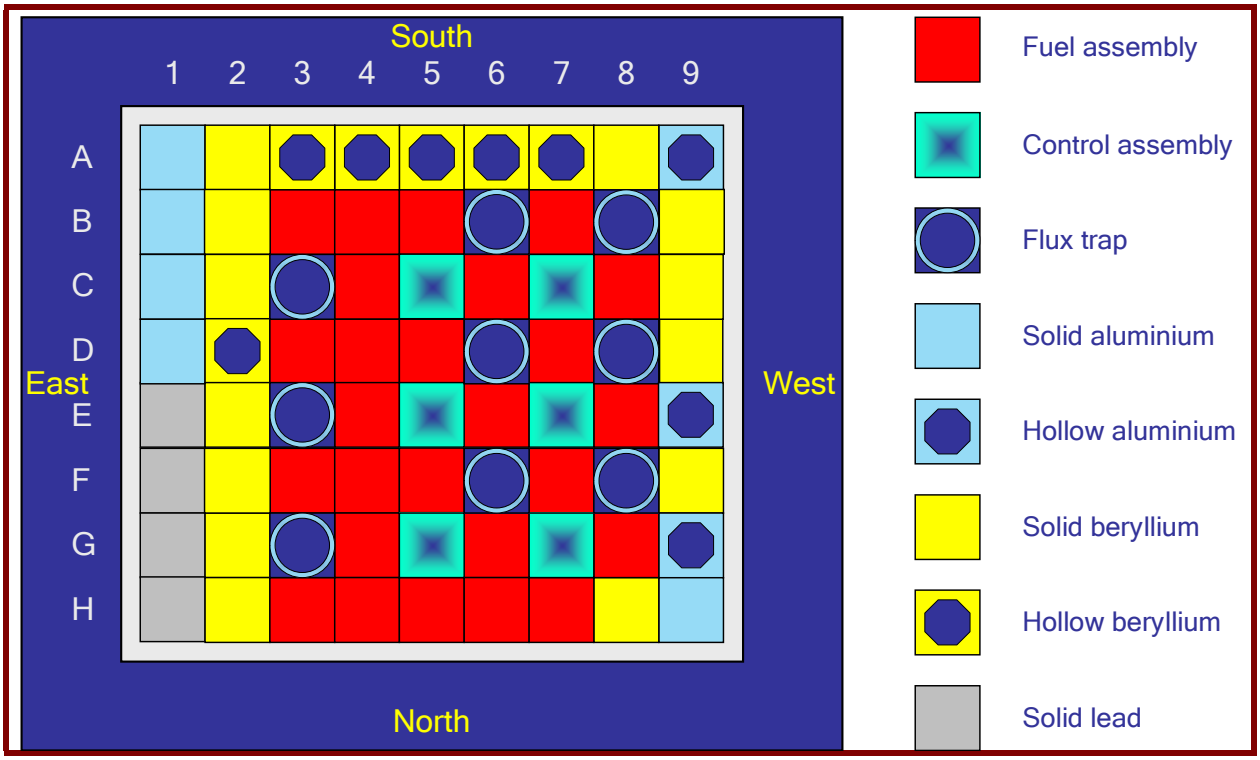

Figure 3.26: *Diagrammatic top-view of the core of an Oak Ridge type Material Testing Reactor (MTR), in which beryllium is used extensively as a neutron reflector.*

This MTR in Figure 3.26 is fuelled with 26 uranium plate-type fuel elements; the six control assemblies are of the fuel-follower type with a hollow cadmium absorber section and a fuel section beneath. There are 9 "flux-trap" positions where rigs for radioisotope production and materials research can be inserted. The abundant use of beryllium as neutron reflector in this MTR, is evident.

Assignment 3.14

1. Plot the ratio $\frac{\sigma_{es}(E)}{\sigma_{(n,\gamma)}(E)}$ for ^{nat}C and ^{2}H, and explain why these nuclides are good neutron reflectors.

2. Rate the following nuclides according to their ability to scatter neutrons through large scattering angles in the laboratory system of reference, $\mathcal{L}$: ^{9}Be, ^{nat}C and ^{2}H. Calculate the expectation value $\langle\theta\rangle$ for each nuclide, for 1 elastic scattering event.

3. Rate the following nuclides according to their ability to degrade neutron energy via elastic scattering: ^{9}Be, ^{nat}C and ^{2}H. Calculate the expectation value $\frac{\langle E\rangle}{E'}$ for each nuclide, for 1 elastic scattering event, where E' is the incident particle energy and $\langle E\rangle$ is the expectation value of the energy of the scattered neutron.

4. Model a pure ^{235}U sphere, surrounded by 100 cm air, in a spherical-symmetrical MCNP calculation, performed in KCODE mode. Vary the radius of the ^{235}U sphere as parameter until you obtain $k_{\text{eff}} \approx 1$.

5. Surround the ^{235}U sphere having a critical mass in air, by a 100 cm thick shell of $^{\text{nat}}$C, H_2O, D_2O and Be, in 4 separate MCNP calculations in KCODE mode. Report the impact of each reflector material on k_{eff} as well as on cycle execution time.

6. Surround the ^{235}U sphere that would have a critical mass in air, by a 20 cm thick shell of pure $^{10}_{5}$B having a mass-density $\rho = 3\,\text{g}\,\text{cm}^{-3}$. Run MCNP in KCODE mode. Report the impact of the neutron absorber on k_{eff} as well as on cycle execution time.

Low (n,γ) cross-section for ^{90}Zr

Figure 3.27 shows the cross-section for the neutron capture reaction $^{90}\text{Zr}(n,\gamma)^{91}\text{Zr}$. ^{90}Zr is the most abundant isotope of zirconium — its natural abundance is 51.45%.

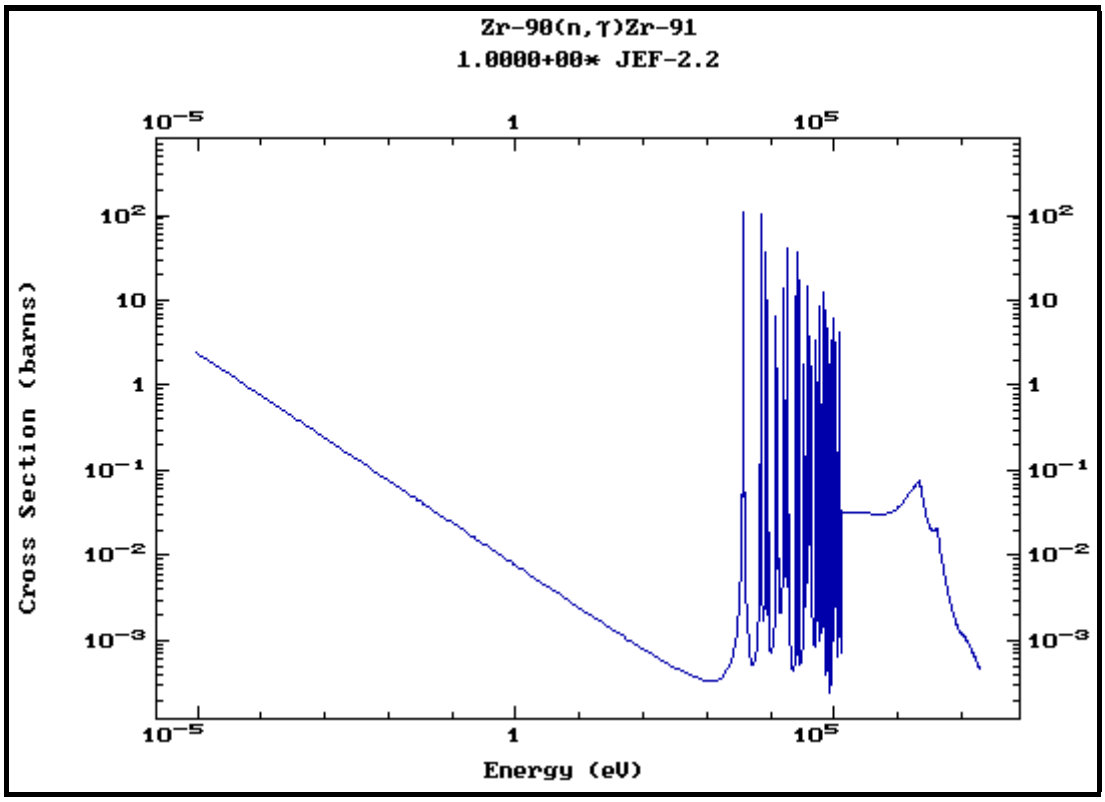

Figure 3.27: *Cross-section for the neutron capture reaction $^{90}Zr(n,\gamma)^{91}Zr$.*

The neutron capture cross-section of ^{90}Zr is low, because its nucleus contains a closed shell of 50 neutrons, i.e. a "magic number" of neutrons. The ^{90}Zr nucleus therefore has practically no "appetite" to acquire additional neutrons by absorption. The low neutron capture cross-section

of zirconium makes it suitable as the main constituent of zircalloy-2 used in BWR fuel pin cladding, and zircalloy-4 used for PWR fuel pin cladding.

Assignment 3.15

1. Model a simplified PWR core in MCNP. Keeping everything else unchanged, change the cladding material from zircalloy-4 to SS-316L, and determine the impact of this change on k_{eff}. Express the impact on the system's reactivity in the reactivity unit pcm. In other words, quantify the advantage of using zircalloy-4 instead of SS-316L as fuel-pin cladding material by giving the negative reactivity (unit: pcm) added by SS-316L cladding, relative to ZIRLOY or zircalloy-4 cladding.

High (n,γ) cross-section for europium isotopes

The two stable isotopes of europium, ^{151}Eu and ^{153}Eu, have high (n,γ) neutron-capture cross-sections, and form the radionuclides ^{152}Eu ($T_{½} = 12.4$ yr) and ^{154}Eu ($T_{½} = 8.5$ yr), respectively, by (n,γ)-reactions. If a significant fraction of the element europium is present in any material that "sees" a high fluence-rate of slow neutrons, the long-lived radionuclides ^{152}Eu and ^{154}Eu will be formed in abundance and present a radioactivity & RadWaste problem for at approximately 10 half-lives, i.e. more than a century. The (n,γ) neutron-activation cross-sections for ^{151}Eu and ^{153}Eu are shown in Figures 3.28 and 3.29.

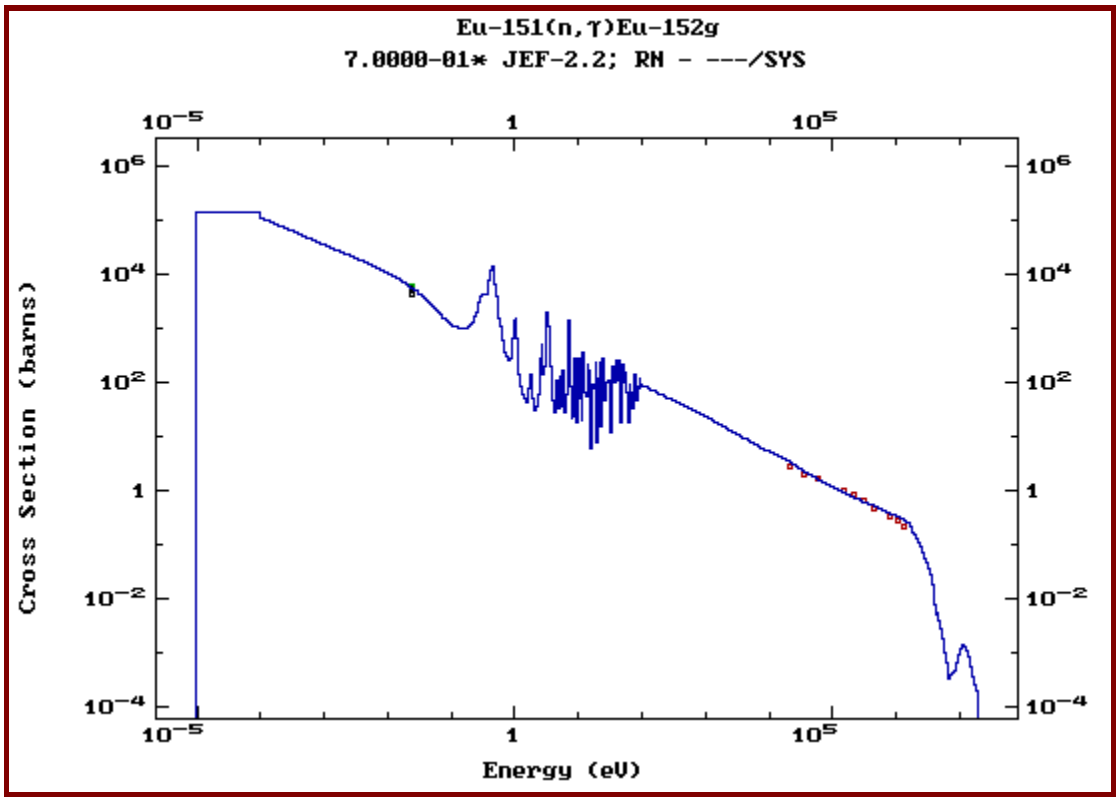

Figure 3.28: *The (n,γ) cross-section for ^{151}Eu.*

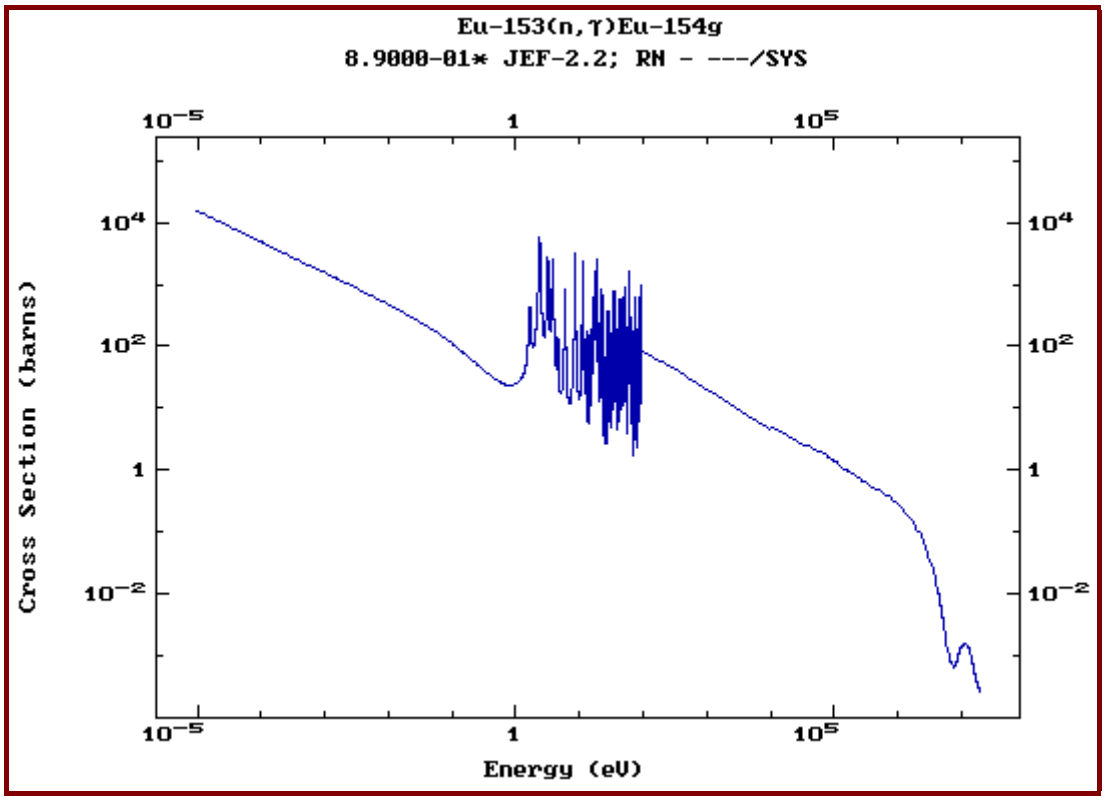

Figure 3.29: *The (n,γ) cross-section for ^{153}Eu.*

It is vital that concrete close to a nuclear power reactor, as well as in beam target station vaults at a particle accelerator facility, contain practically no cobalt or europium, because the

production of the radionuclides ^{60}Co, ^{152}Eu and ^{154}Eu in concrete is very troublesome. Every batch of raw materials from which concrete is mixed, must be tested to ensure that only low-activation concrete is used in regions in a nuclear reactor or particle accelerator facility, where the neutron fluence-rate is high.

The (n,γ) cross-section for ^{55}Mn

Mild steel may contain as much as $\sim 2\%$ manganese by mass. There is only one stable manganese isotope, namely $^{55}_{25}$Mn. This isotope has a significant (n,γ) cross-section and will activate in a neutron field to produce the radionuclide ^{56}Mn, which has a halflife of 2.58 hours, and presents an intense short-term source of ionising photons around Mn-alloy steel structures exposed to high slow-neutron fluence rates. The presence of the neutron activation product ^{56}Mn can delay the safe entry time to begin with maintenance operations, by as much as 12 to 15 hours, as a result of high prevailing dose rates caused by the presence of the neutron activation isotope ^{56}Mn.

The (n,γ) cross-section for the nuclear reaction ^{55}Mn$(n,\gamma)^{56}$Mn is shown in Figure 3.30.

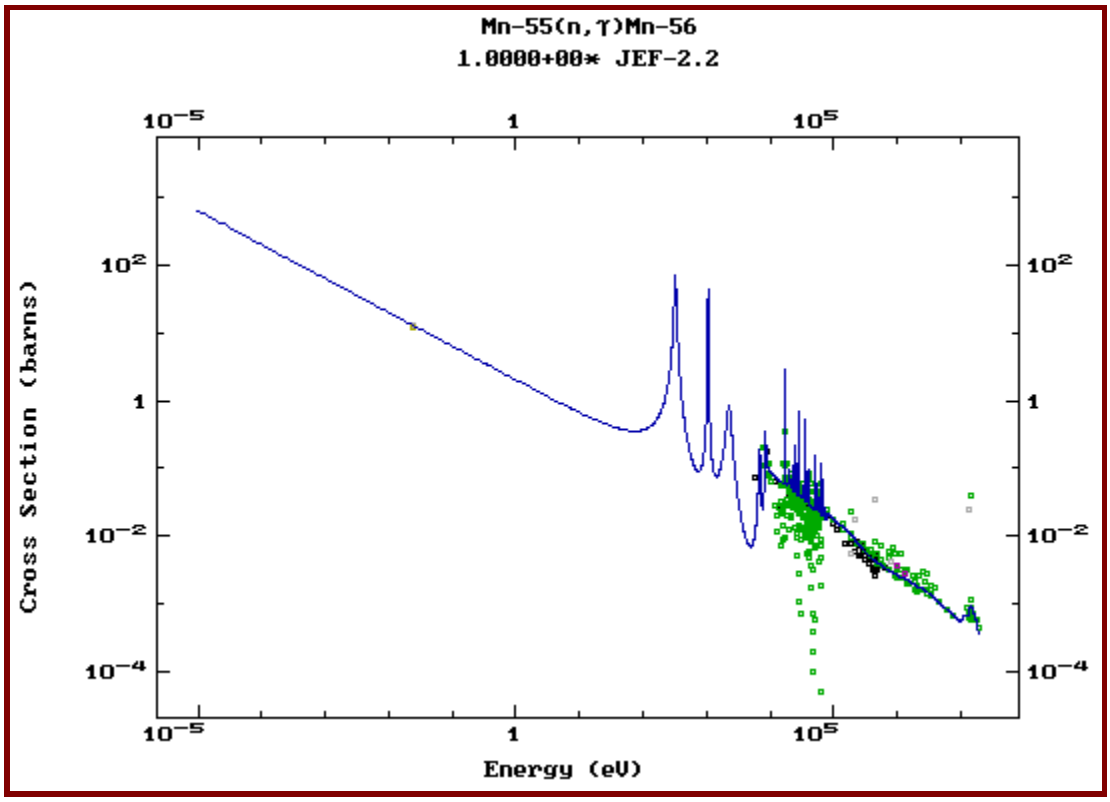

Figure 3.30: *The (n,γ) cross-section for ^{55}Mn, which is activated in a neutron field to form ^{56}Mn, which has a half-life of 2.58 hours.*

High (n,γ) cross-section for cadmium

The cadmium isotope ^{113}Cd has a high (n,γ) neutron absorption cross-section — see Figure 3.31.

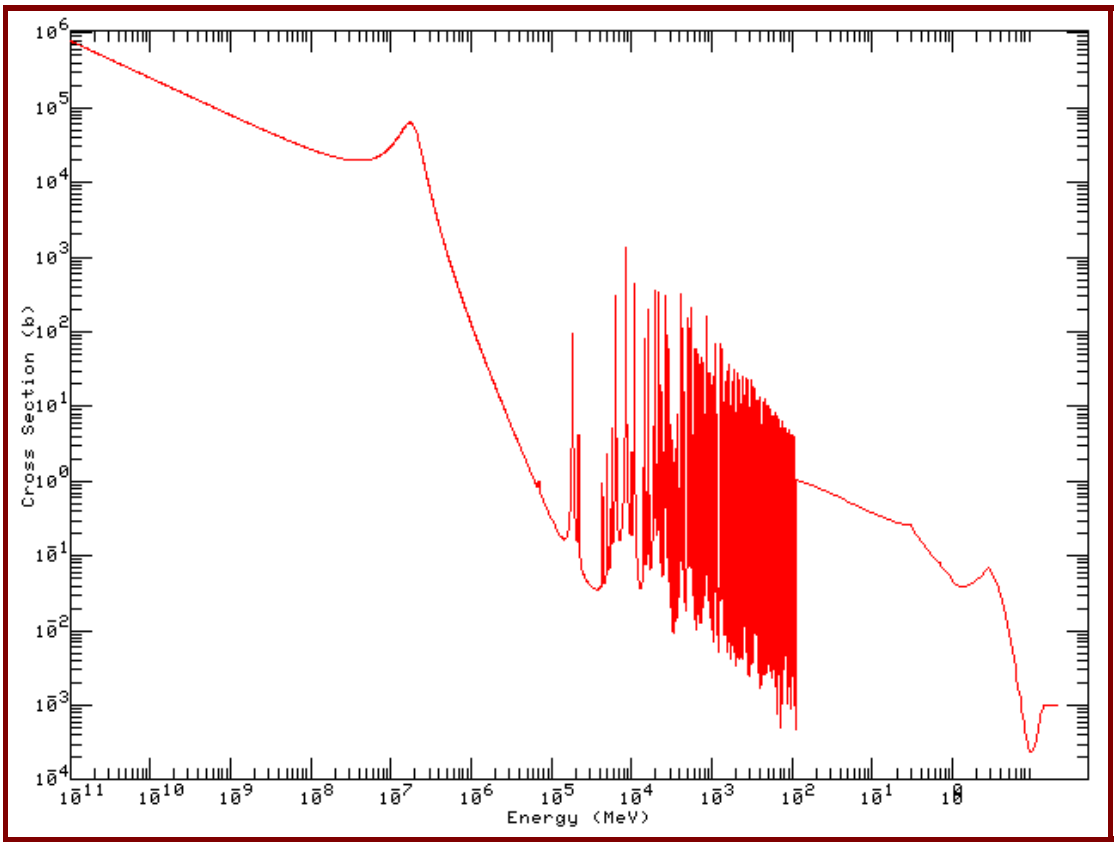

Figure 3.31: *The (n,γ) neutron-absorption cross-section for the cadmium isotope ^{113}Cd.*

The cadmium isotope, ^{113}Cd, has a high (n,γ) absorption cross-section for thermal neutrons, and a relatively low (n,γ) absorption cross-section for epi-thermal and fast neutrons. The natural abundance of ^{113}Cd is 12.3%. The "cadmium cutoff" lies at the neutron energy $E_n \approx 1$ eV.

Note that cadmium is a toxic substance[9], so that it must normally be encapsulated, sandwiched or clad inside non-toxic metals. The same holds true of beryllium. When Be is used as a neutron reflector, it is encapsulated in an Al clad.

---

[9] The main exposure pathway of humans to cadmium (Cd) is via tobacco smoke. Above age 60, cadmium deposited in the bones of long-term smokers start to leach out and poison the person. It impairs calcium metabolism, replaces calcium in the bones, and can contribute to conditions such as osteoporosis and osteomalacia, ureter and kidney stones, excessive calcium in the urine (hypercalcuria), pain in the low back and legs, rheumatoid arthritis and decreased production of metabolically active vitamin D in the liver and kidneys. It accumulates in the joints and can cause osteo-arthritis. Cadmium strongly displaces zinc from its proper sites in the body. It replaces zinc in the arteries causing stiffness, inflammation and high blood pressure. High cadmium and low zinc in the arteries can promote aneurysms. Many symptoms of cadmium poisoning are the same as those of zinc deficiency such as decreased appetite, dry scaly skin, loss of hair, loss of body weight, decreased body temperature, decreased growth, immune suppression, reduced testosterone activity and impotence, prostate cancer, loss of sense of smell, and copper toxicity. The toxic effects of cadmium are kept under control in the body and brain by the presence of zinc, its primary antagonist. Zinc is very protective against cadmium absorption in the intestines, and is required to counteract cadmium toxicity.

Assignment 3.16

1. Design and perform a calculational experiment using the code MCNP, to determine at which energies, and in what relative proportion, ^{nat}Cd emits ionising photons upon capturing thermalised neutrons.

2. Design and perform a calculational experiment using the code MCNP, to quantify the relative ability of 1 mm thick layers of ^{nat}Cd and B_4C to attenuate incident neutrons having $E_n = 0.01$ eV, 0.1 eV, 1 eV and 10 eV.

3.6.8 (n,γ) neutron capture cross-sections in fissile, fissionable and fertile isotopes

The (n,γ) neutron capture cross-section for ^{238}U

Figure 3.32 shows $\sigma_{(n,\gamma)}(E)$ for ^{238}U.

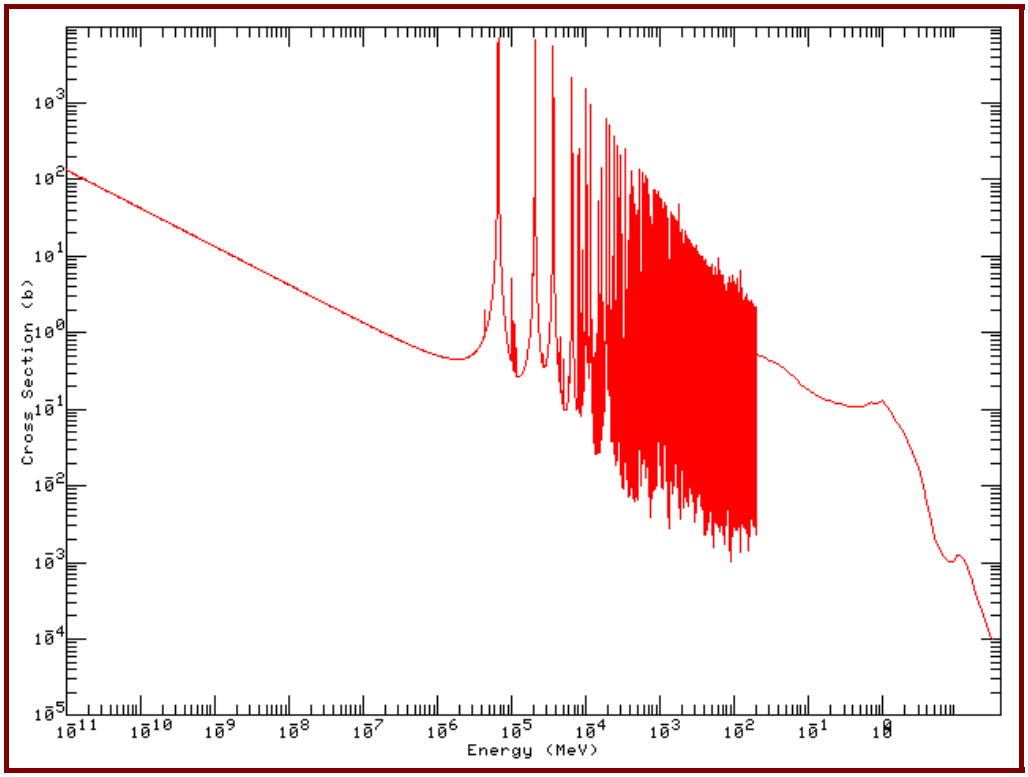

Figure 3.32: *Energy dependence of the (n,γ) neutron capture cross-section for ^{238}U.*

The lowest (n,γ) resonance peak of ^{238}U is centred at $E_n = 6.7$ eV; this is the widest and most "neutron-greedy" resonance capture peak of ^{238}U.

The use of high enrichment uranium (HEU) reactor fuel outside military applications, is actively discouraged, and will be practically phased out by circa 2011. All uranium-based reactor fuels therefore contain a high fraction of the fissionable (but not fissile) uranium isotope, ^{238}U. This uranium isotope has prominent non-fission neutron capture cross-section resonances. During fission, neutrons are "born" at an average energy of about 2 MeV. These high-energy neutrons must be thermalised by scattering interactions in order to reach the thermal neutron energy range, where neutron-induced fission cross-sections of the fissionable isotopes, chiefly ^{235}U and ^{239}Pu, are the highest. The high neutron capture resonance peaks of ^{238}U pose a problem, because neutrons will be parasitically absorbed in these capture resonances, during the slowing-down process. To counteract this by increasing the resonance-escape probability, a heterogeneous reactor design is used: fuel is bundled in thin fuel-pins or thin fuel-plates, surrounded by a moderator with a low neutron capture cross-section. The fast neutrons born in fission reactions easily escape from the thin fuel pins or plates, before entering the ^{238}U resonance capture energy region at approximately $E_n = 0.1$ MeV. Neutron moderation now largely takes place inside the moderator volume, where no neutron absorption resonances are encountered, and the moderated neutrons ideally re-enter the fuel at an energy below approximately 3 eV, which lies safely below the lowest of the ^{238}U (n, γ) neutron-capture resonances. The aim with heterogeneous reactor core design, is to have the neutron spend that part of the neutron lifetime during which its energy is lowered from circa 0.1 MeV to approximately 3 eV, largely outside the fuel region, and inside the moderator volume. In the energy range below approximately 3 eV, there are no more ^{238}U neutron capture resonances, and the fission cross-section σ_{f} for ^{235}U is consistently about 200 to 300 times higher than the non-fission (n, γ) capture cross-section of ^{238}U, so that self-sustaining reactor operation becomes possible at relatively low uranium enrichment grades, provided that the fuel-moderator configuration is heterogeneous, which will ensure a high *resonance escape probability* for neutrons.

The neutron capture resonances in $\sigma_{(n,\gamma)}(E)$ for ^{238}U, shown in Figure 3.32, contribute to reactor safety: if reactor power increases, the fuel will almost instantaneously heat up, $\sigma_{(n,\gamma)}$ neutron capture resonances will broaden, and the value of the integral $\int_0^\infty dE\, \sigma_{(n,\gamma)}\, \phi(E)$, which is proportional to the reaction rate for neutron capture in ^{238}U, will increase. This will decrease reactivity and, consequently, also decrease reactor power. A negative fuel temperature i.e. Doppler coefficient of reactivity, contributes to stable reactor operation by providing vital negative reactivity feedback.

Non-fission neutron capture cross-section for ^{236}U, which is present in reprocessed uranium fuel

In reactor fuel containing reprocessed uranium, ^{236}U will invariably be present as an unwanted contaminant isotope. Its non-fission (n, γ) capture cross-section is generally significantly higher than that of ^{238}U, especially above and below the neutron capture resonance energy region — see Figure 3.33.

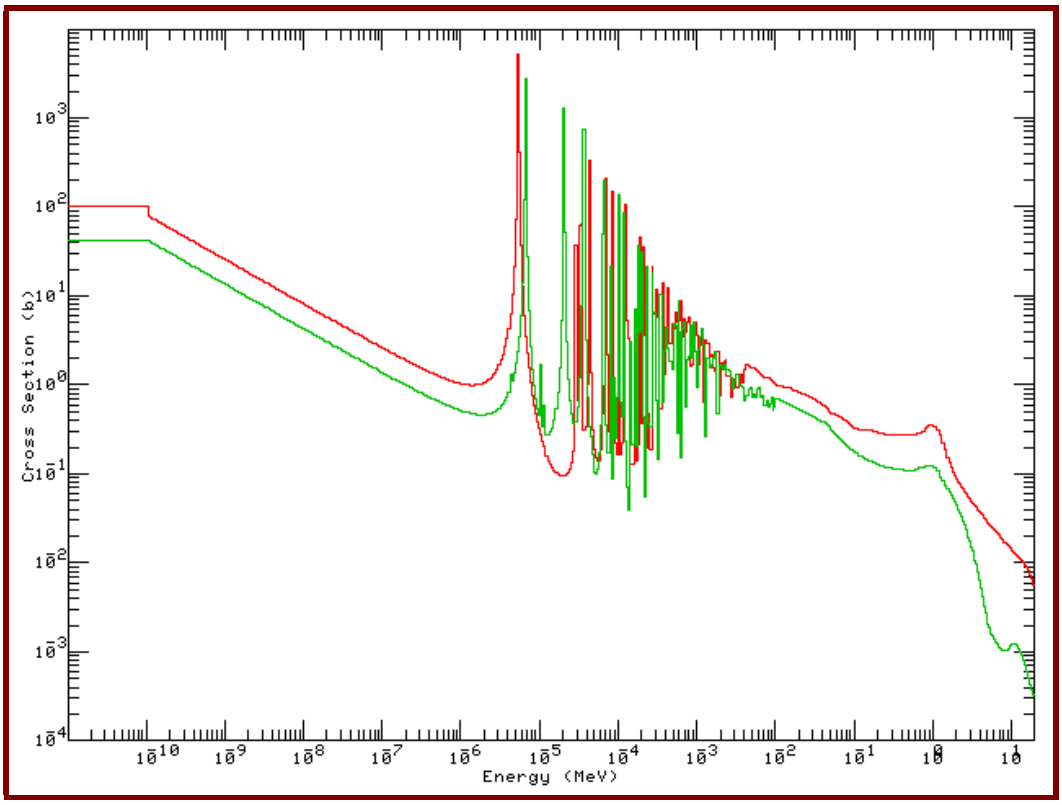

Figure 3.33: *The cross-sections* $\sigma_{^{236}U(n,\gamma)}(E)$ *and* $\sigma_{^{238}U(n,\gamma)}(E)$.

It is evident that the presence of ^{236}U in reactor fuel as well as in target-plates used for ^{99}Mo production in a Material Testing Reactor (MTR), will increase parasitic neutron capture rates. Like ^{238}U, however, its presence will provide stabilising negative reactivity feedback when fuel temperature rises.

3.6.9 Elastic scattering cross-sections: graphical journey

Elastic scattering cross-section σ_s for $^{1}_{1}H$ and $^{2}_{1}H$

Figure 3.34 shows the energy dependence of the cross-sections of $^{1}_{1}H$ and $^{2}_{1}H$ for the elastic scattering of neutrons. Both of these nuclides only scatter neutrons elastically, and never inelastically. That is, internal nuclear excitation states are never excited when $^{1}_{1}H$ and $^{2}_{1}H$ scatter neutrons.

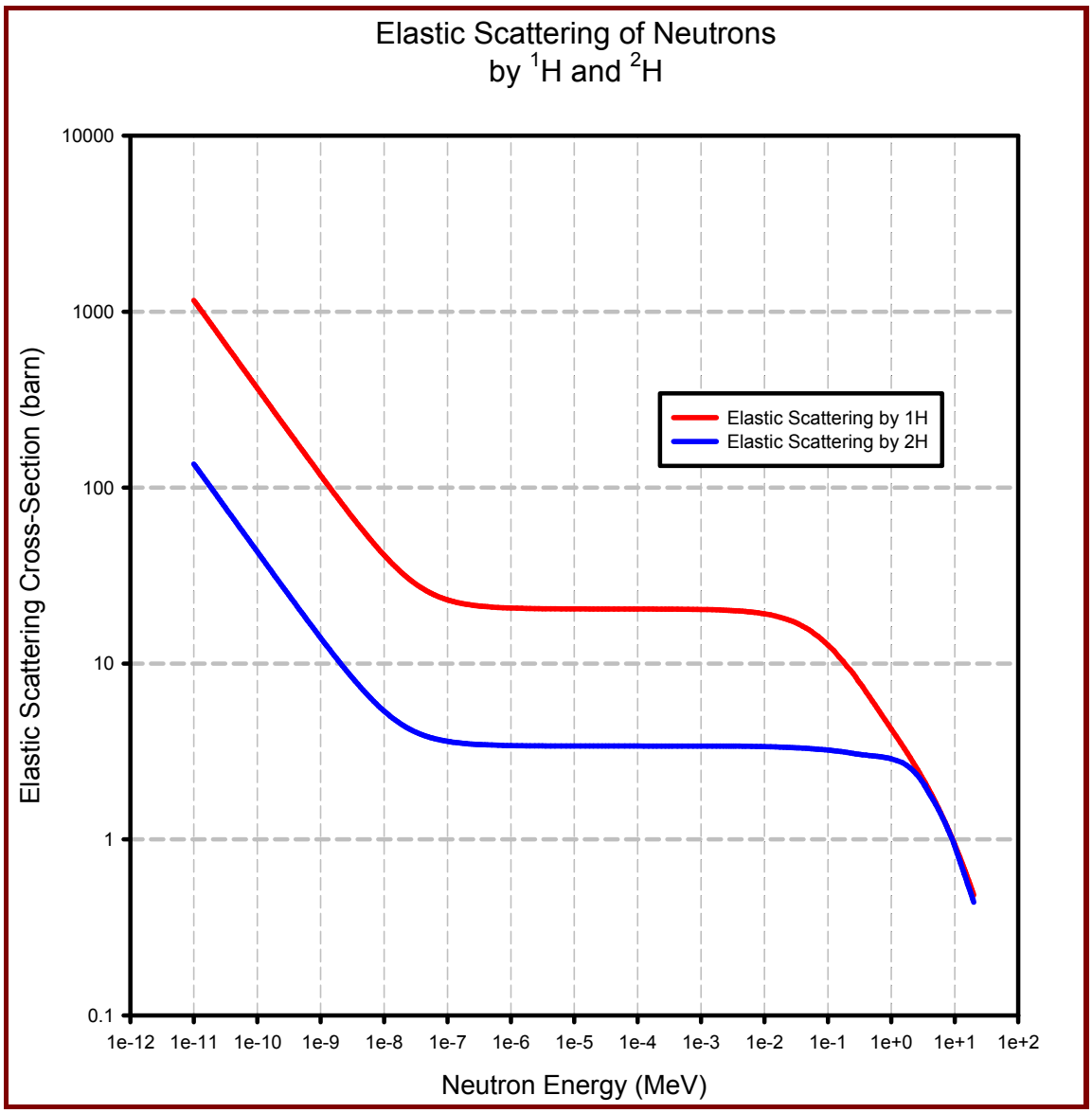

***Figure 3.34**: Elastic neutron scattering cross-sections σ_s for the hydrogen isotopes $^{1}_{1}H$ and $^{2}_{1}H$.*

Note that the energy range from 0 MeV to approximately 1 MeV, the cross-section for elastic scattering of neutrons by $^{1}_{1}H$ is between 2 and 8 times larger than that for $^{2}_{1}H$.

Application: The pitch of fuel pins in a D_2O moderated power reactor is larger than in a H_2O moderated reactor, because D_2O has a somewhat ability to slow down neutrons than H_2O — the cross-section for elastic scattering of neutrons by $^{2}_{1}H$ is between 2 and 8 times lower than that of $^{1}_{1}H$, over a wide energy range, and the kinematical effectiveness of elastic neutron scattering by $^{2}_{1}H$ is also lower than that of $^{1}_{1}H$. A heavy-water moderated nuclear reactor therefore requires a higher moderator-to-fuel ratio than a LWR, i.e. a larger fuel pin pitch.

Elastic scattering cross-section σ_s for $^{56}_{26}Fe$

Figure 3.35 shows the elastic scattering cross-section for ^{56}Fe.

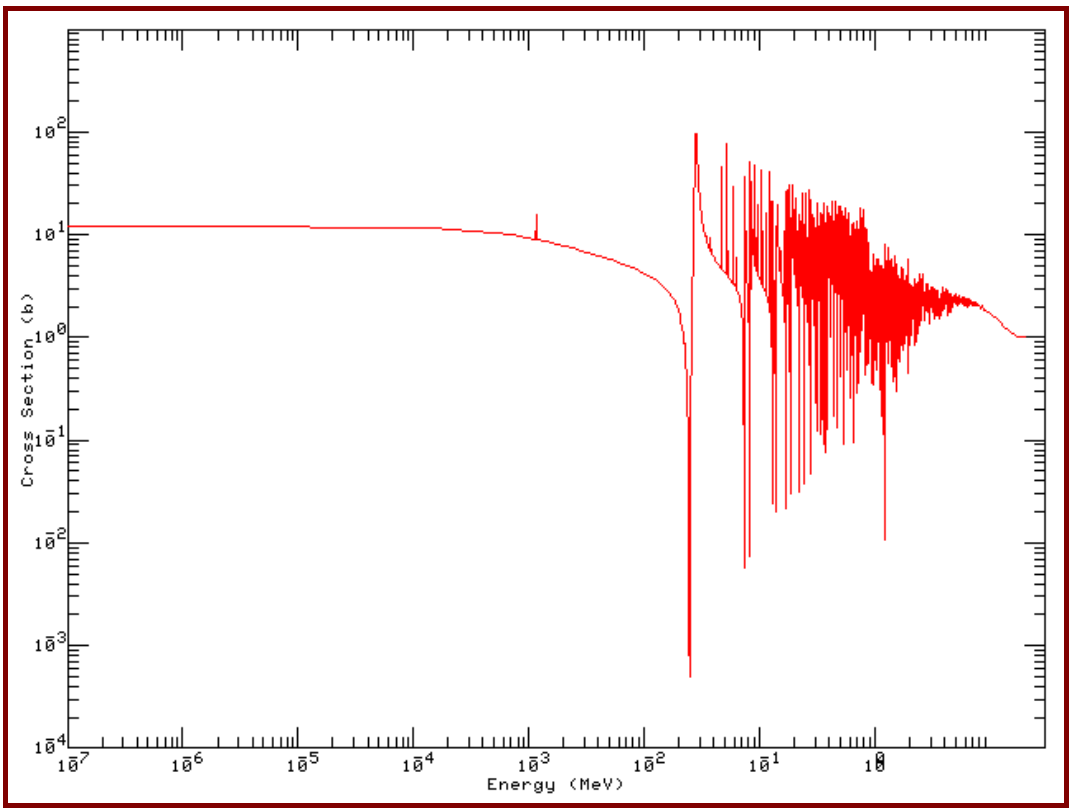

Figure 3.35: *Elastic scattering cross-section for ^{56}Fe.*

Remarks: Although σ_s for $^{56}_{26}Fe$ is reasonably high, the kinematical effectiveness of elastic scattering by Fe is quite low — the expectation value of the energy of an elastically scattered neutron will only be marginally lower than the incident neutron energy. With increasing neutron energy, elastic neutron scattering by Fe will become quite anisotropic, as depicted in Figure 3.36.

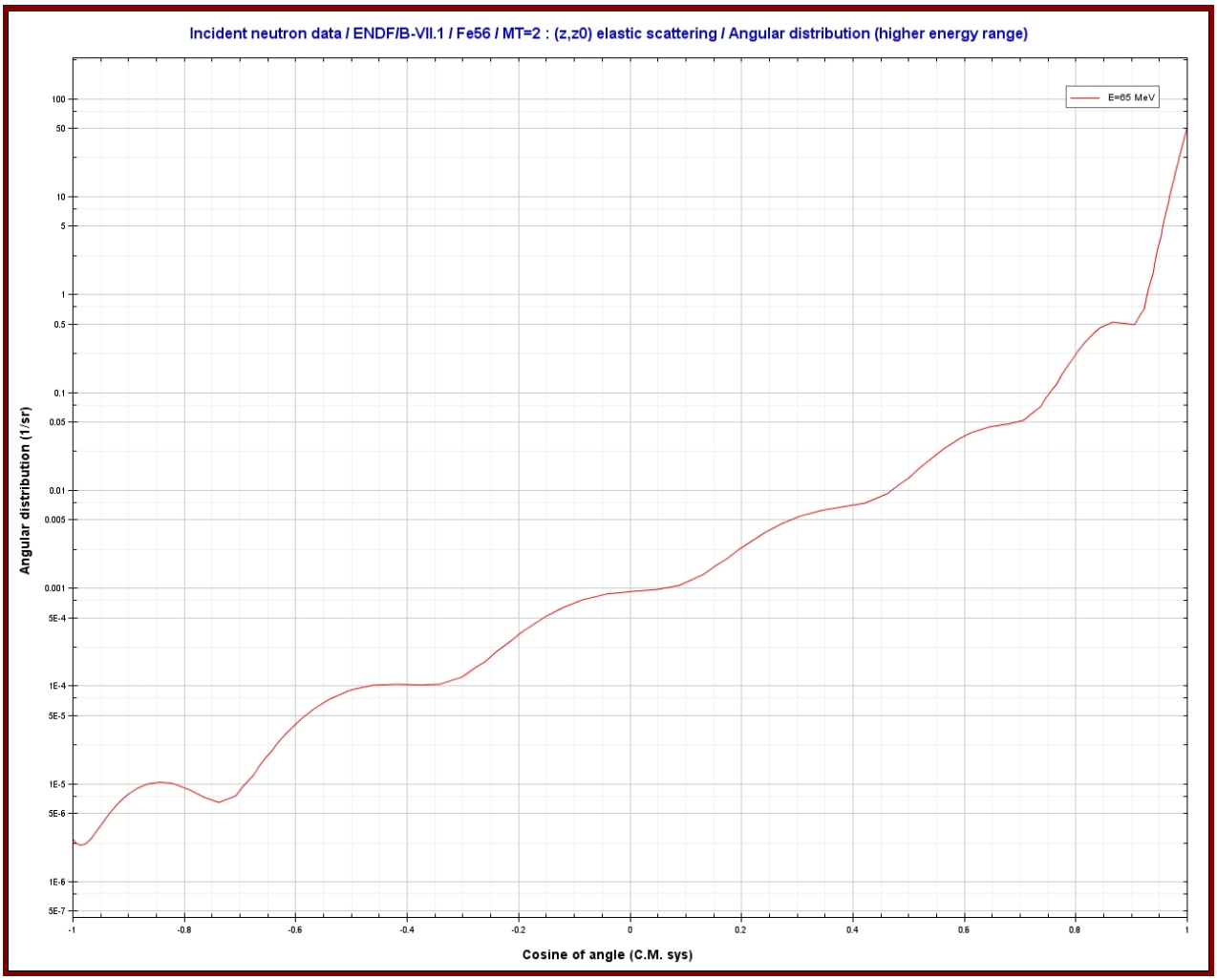

Figure 3.36: *Very high degree of scattering anisotropy for the elastic scattering of a 65 MeV incident neutron by* $^{56}_{26}Fe$.

For the same target nuclide and incident neutron energy, inelastic scattering is generally significantly less anisotropic than elastic scattering, as illustrated in Figure 3.37.

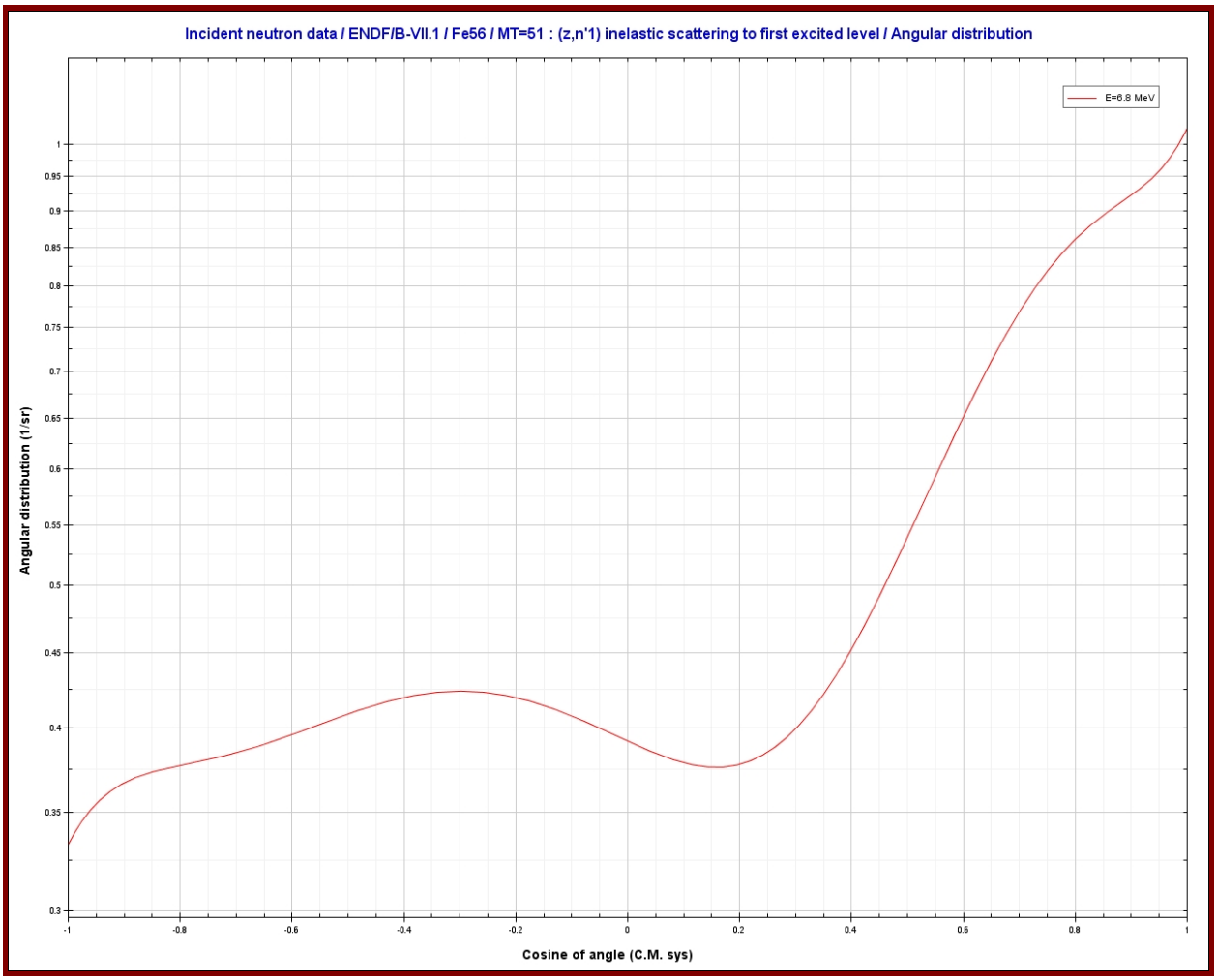

***Figure 3.37**: Lower degree of scattering anisotropy for inelastic neutron scattering of a 7 MeV incident neutron by ${}^{56}_{26}Fe$.*

Assignment 3.17

1. Point out the notable difference(s) between σ_{es} and σ_t for ${}^{56}Fe$.

2. Plot $\sigma_t(E)$ and $\sigma_{es}(E)$ for ${}^{56}Fe$, enlarging the prominent cross-section minimum between circa 22 keV and 28 keV. Pinpoint the minimum of the dip as accurately as possible. What could be practical consequences/results of this strong dip in the cross-section of the most abundant Fe isotope?

3. Investigate the angular distribution of neutron scattering for 3 important nuclides using JANIS. Is it generally true that inelastic scattering is more isotropic than elastic scattering, for the same incident neutron energy and the same scattering medium?

3.6.10 Inelastic neutron scattering cross-sections: threshold energies

Inelastic scattering takes place when an internal energy state (energy level) of a nucleus is excited by the incident neutron, and a neutron is then emitted, leaving the nucleus in the excited state. Inelastic scattering reactions always have threshold energies. Multiple energy levels may be excited; these levels may be excited simultaneously.

Energies of the first and second excited states for selected nuclei

Energies of the first and second excited states for selected nuclei are shown in Figure 3.9.

Table 3.9: *Energies of the first and second excited states for selected nuclei.*

Nuclide	**Energy of first excited state** (MeV)	**Energy of second excited state** (MeV)
${}^{1}_{1}\mathrm{H}$, ${}^{2}_{1}\mathrm{H}$, ${}^{3}_{2}\mathrm{He}$ & ${}^{4}_{2}\mathrm{He}$	none	none
${}^{12}_{6}\mathrm{C}$	4.439	7.654
${}^{16}_{8}\mathrm{O}$	6.094	6.130
${}^{40}_{20}\mathrm{Ca}$	3.352	3.736
${}^{54}_{26}\mathrm{Fe}$	1.408	2.538
${}^{56}_{26}\mathrm{Fe}$	0.847	2.085
${}^{57}_{26}\mathrm{Fe}$	0.014	0.137
${}^{206}_{82}\mathrm{Pb}$	0.803	1.167
${}^{207}_{82}\mathrm{Pb}$	0.570	0.898
${}^{208}_{82}\mathrm{Pb}$	2.615	3.198

The nuclides ${}^{1}_{1}\mathrm{H}$, ${}^{2}_{1}\mathrm{H}$, ${}^{3}_{2}\mathrm{He}$ and ${}^{4}_{2}\mathrm{He}$ have no internal energy states that can be excited by inelastic scattering, i.e. inelastic scattering is an impossible reaction mechanism for these select light nuclei. Light nuclei such as ${}^{16}_{8}\mathrm{O}$ and ${}^{40}_{20}\mathrm{Ca}$, which are double-magic, have high threshold values for nuclear excitation. The light nucleus, ${}^{12}_{6}\mathrm{C}$ in which the nucleons tend to cluster as α-particles, also has high threshold values for nuclear excitation. In the double-magic nucleus ${}^{208}_{82}\mathrm{Pb}$, the energy level of the first available excited nuclear state, as well as the

energy spacing between energy levels, is markedly higher than in the two Pb isotopes — $^{206}_{82}$Pb and $^{207}_{82}$Pb — which do not have a magic number of neutrons, i.e. which are not double-magic.

Inelastic scattering of neutrons by ^{56}Fe: threshold energies

Table 3.10 contains detail about the inelastic scattering of neutrons by the nuclide $^{56}_{26}$Fe, which is by far the most abundant isotope of Fe.

***Table 3.10**: Energy levels λ, Q-values Q_λ, energy level excitation threshold energies ϵ_λ, and backscattering threshold energy $E_{\lambda,90}$, for inelastic scattering of neutrons by the nucleus $^{56}_{26}Fe$.*

λ	Q_λ (MeV)	ϵ_λ (MeV)	$E_{\lambda,90}$ (MeV)
0	0.0	0.0	Undefined
1	-0.846996	0.862274	0.86255
2	-2.088440	2.1261	2.12679
3	-2.659836	2.7078	2.70868
4	-2.942047	2.9951	2.99607
5	-2.960022	3.0134	3.01438
6	-3.120037	3.1763	3.17733
7	-3.123001	3.179318	3.18035
8	-3.370029	3.4308	3.43192
9	-3.388005	3.4491	3.45022
10	-3.445002	3.507125	3.50827
11	-3.449005	3.5112	3.51234
12	-3.602045	3.667	3.66819
13	-3.607002	3.672046	3.67324
14	-3.756002	3.823733	3.82498
15	-3.832001	3.901103	3.90237
16	-3.857047	3.9266	3.92788
17	-4.049001	4.122016	4.12336
18	-4.100001	4.173936	4.17529
19	-4.120005	4.1943	4.19566
20	-4.298002	4.375507	4.37693
21	-4.302022	4.3796	4.38102
22	-4.395045	4.4743	4.47576
23	-4.401037	4.4804	4.48186
24	-4.458010	4.5384	4.53988
25	-4.510002	4.59133	4.59282
26 (continuum)	$\leq$ -4.539002	$\geq$ 4.539002	$\geq$ 4.62236

According to ENDF-B/7.1 (2011), there are 25 discrete energy levels in the $^{56}_{26}$Fe nucleus that may be excited by the inelastic scattering of neutrons. The values in the ϵ_λ-column in Table

3.0, were read from ENDF/B-7.1 via JANIS-4. The Q-values in column 2 were calculated using Eq. (3.24) on page 97.

Inelastic scattering of neutrons by ^{16}O: threshold energies

The $^{16}_{8}$O nucleus has 7 discrete energy levels that can be excited by inelastic scattering of neutrons. These energy levels — their Q-values, threshold energies ϵ and backscattering threshold energies $E_{\lambda,90}$, are summarised in Table 3.11.

***Table 3.11**: Inelastic scattering of neutrons by ^{16}O (ENDF/B-7.1 (2011) values: Q-values and threshold energies for excitation of levels; backscattering threshold energies.*

λ	Q_λ (MeV)	ϵ_λ (MeV)	$E_{\lambda,90}$ (MeV)
0	0.0	0.0	Undefined
1	-6.049401	6.43090	6.45656
2	-6.129900	6.51650	6.54248
3	-6.917101	7.353399	7.38266
4	-7.116851	7.565799	7.59586
5	-8.871901	9.43140	9.46903
6	-10.957013	11.64799	11.69449
7	-11.080007	11.77899	11.82576
8 (Continuum)	-9.585014	10.18999	10.23014

According to ENDF-B/7.1 (2011), there are 7 discrete energy levels in the $^{16}_{8}$O nucleus that may be excited by the inelastic scattering of neutrons. Note that the energy thresholds for the excitation of discrete levels 6 and 7 are higher than the energy threshold of scattering to the continuum. By comparing the discrete energy levels of the $^{16}_{8}$O nucleus with that of the $^{56}_{26}$Fe nucleus, and then proceeding to make more comparisons between nuclei, some general trends are observed:

- Smaller, light nuclei have less discrete energy levels than large, heavy nuclei.
- The threshold energies for the excitation of the levels of smaller, light nuclei, are higher than that of large, heavy nuclei.
- Nuclei with magic numbers of protons and neutrons, such as $^{4}_{2}$He, $^{16}_{8}$O and $^{40}_{20}$Ca, have higher discrete level energy thresholds, and a lower number of discrete levels, than

nuclei with non-magic numbers of protons and neutrons, in the same (Z, A) region of a chart of the nuclides.

Assignment 3.18

1. Repeat the above assessment for ^{nat}C — construct a table similar to Table 3.10 on page 3 for inelastic scattering of neutrons by ^{nat}C.

2. Repeat the above assessment for ^{208}Pb — construct a table similar to Table 3.10 on page 3 for inelastic scattering of neutrons by ^{208}Pb.

3.6.11 Inelastic scattering cross-sections: graphical journey

Excitation functions for the inelastic scattering of neutrons by $^{56}_{26}$Fe

Figure 3.38 shows the cross-section curves $\sigma_\lambda(E)$ ("excitation functions") for inelastic neutron scattering by $^{56}_{26}$Fe, in relation to the cross-section for elastic neutron scattering by $^{1}_{1}$H.

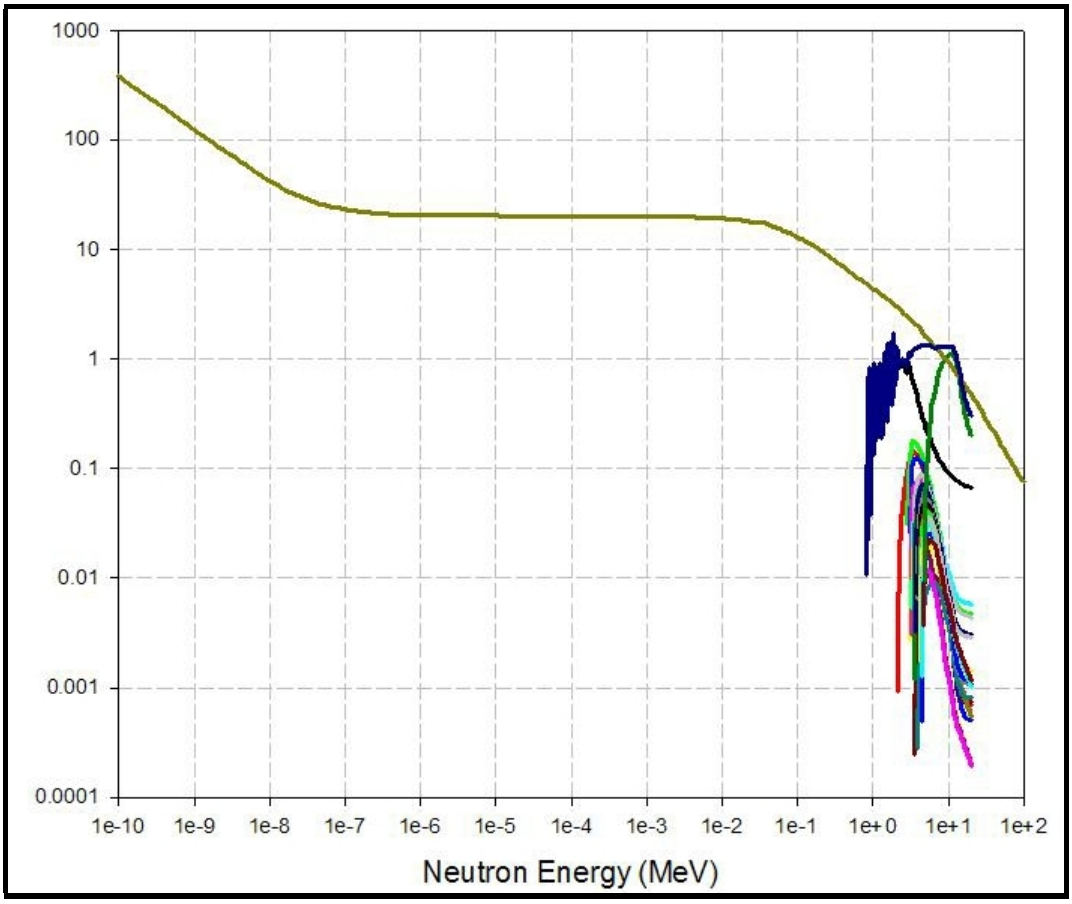

Figure 3.38: *The cross-section $\sigma(E)$ for elastic neutron scattering by $^{1}_{1}H$, and the cross-sections (excitation functions) for inelastic neutron scattering by $^{56}_{26}Fe$.*

The cross-section for neutron scattering by ^{1}H is high for neutron energies below about 0.1 MeV. Then the cross-section $\sigma(E_n)$ begins to "nose-dive" at increasing neutron energies, so that the contribution of ^{1}H to neutron slowing down at $E \gtrsim 10$ MeV, becomes very small. Inelastic scattering by an element such as iron becomes very important for the effective slowing down of neutrons with $E \gtrsim 5$ MeV.

Figure 3.39 shows greater detail of the inelastic scattering cross-sections for $^{56}_{26}$Fe in the neutron energy region where the "excitation functions" i.e. the inelastic scattering cross-sections for ^{56}Fe, start to rise. The excitation of every discrete energy level in the $^{56}_{26}$Fe nucleus by inelastic scattering of neutrons, has a characteristic threshold energy. The inelastic scattering cross-sections initially rise steeply, and then begin to fall — one reason for this is

that other nuclear reaction mechanisms with neutrons, e.g. $(n, 2n)$, $(n, 3n)$, (n, p) (n, np) and (n, α) reactions with Fe, become *energetically possible* and therefore *compete* with inelastic neutron scattering. In the language of nuclear physics: other exit channels open because they become energetically possible, and compete with inelastic scattering. Once again, the elastic scattering cross-sections for ^{1}H is shown as a reference curve.

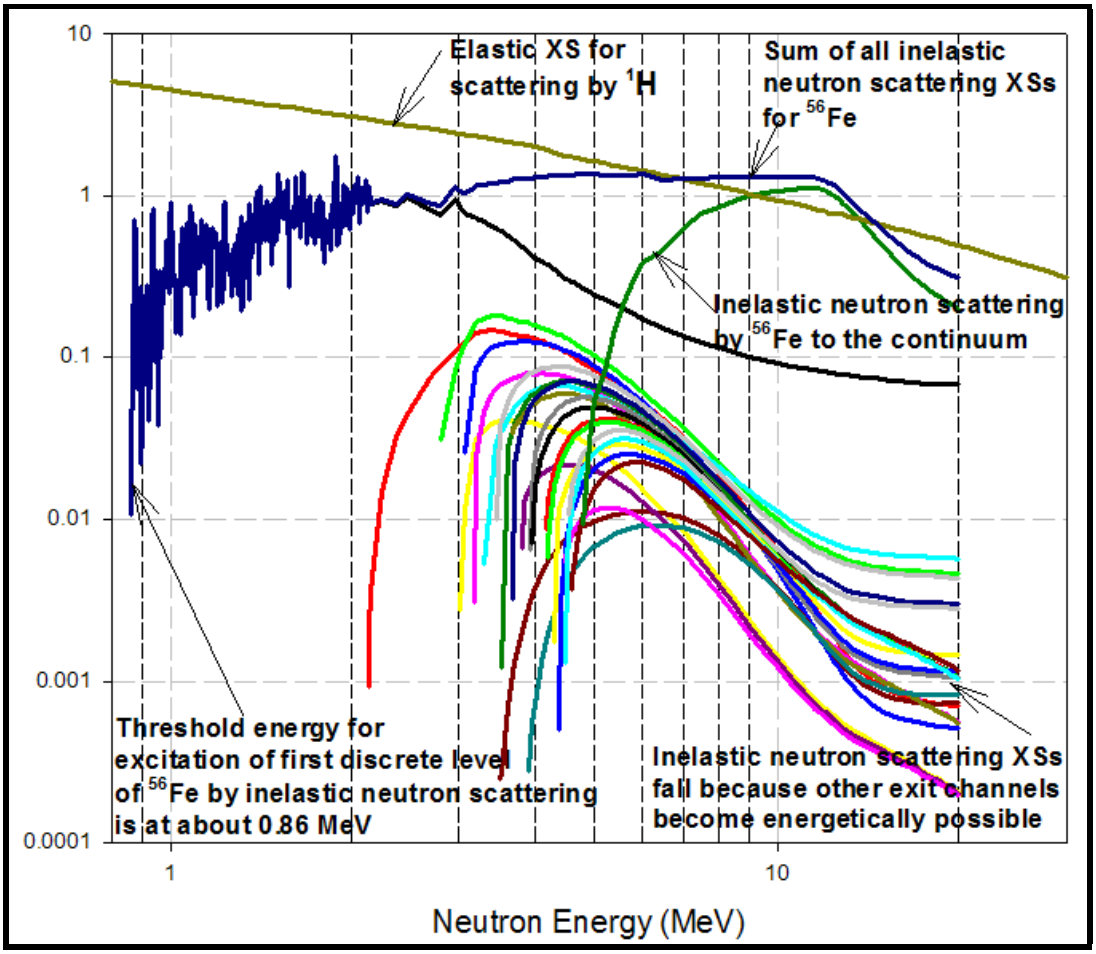

Figure 3.39: *Detail of the inelastic scattering cross-sections for $^{56}_{26}$Fe in the neutron energy region where the "excitation functions" i.e. the inelastic scattering cross-sections for ^{56}Fe, start to rise. The elastic scattering cross-section for ^{1}H (top curve starting at top left corner) is shown, for reference purposes.*

Excitation functions for the inelastic scattering of neutrons by $^{208}_{82}$Pb

Figure 3.40 shows the excitation cross-section functions for the excitation of the energy levels of the ^{208}Pb nucleus via discrete level inelastic scattering, as well as inelastic scattering to the continuum.

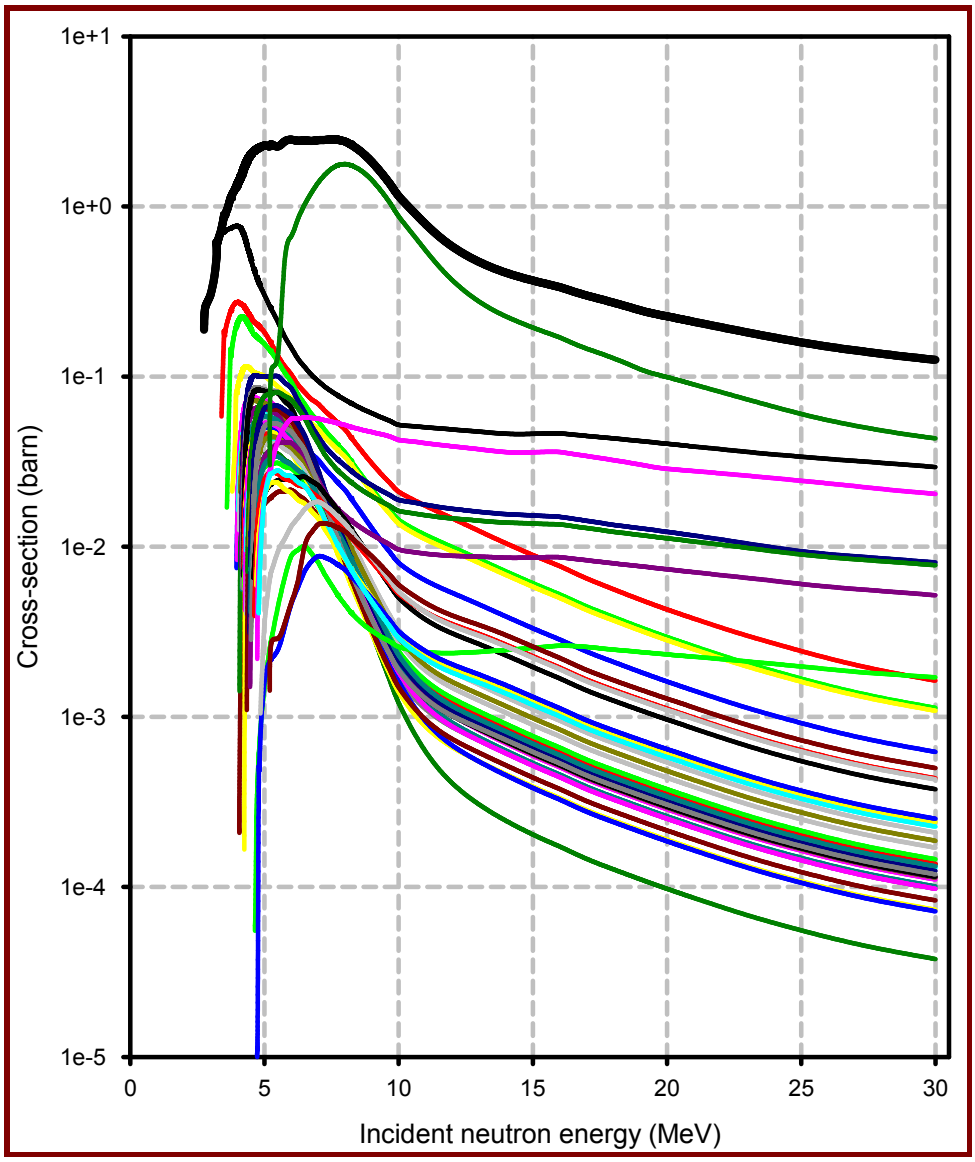

Figure 3.40: *Detail of the inelastic scattering cross-sections for ^{208}Pb in the neutron energy region where the "excitation functions" i.e. the inelastic scattering cross-sections for this nuclide, start to rise.*

The thick black line at the top of Figure 3.40 denotes the total of all inelastic scattering level excitation curves, including that for inelastic scattering to the continuum.

Note that the cross-section curves for inelastic scattering (also called the "excitation functions") of neutrons with ^{208}Pb, are generally somewhat lower than the cross-section curves for the inelastic scattering of neutrons with ^{56}Fe. This contributes to making Fe is somewhat superior compared to Pb for slowing down fast neutrons via inelastic scattering. Note, too, that the "level excitation functions" fall off faster at higher incident neutron energies for Pb than for Fe. For the most abundant Pb isotope, ^{208}Pb, the threshold energy for inelastic scattering lies at approximately 2.5 MeV, whereas the threshold energy for inelastic scattering by the most abundant Fe isotope, ^{56}Fe, is markedly lower, at 0.862274 MeV. Finally, the nuclide number density (NND; unit barn^{-1} cm^{-1}) of Fe is approximately

$$\frac{\text{NND\_Fe}}{\text{NND\_Pb}} = \frac{\left(\frac{\rho_{\text{Fe}}}{M_R(\text{Fe})}\right)}{\left(\frac{\rho_{\text{Pb}}}{M_R(\text{Pb})}\right)} \approx \frac{\left(\frac{7.86}{56}\right)}{\left(\frac{11.35}{208}\right)} \approx 2.5$$

times higher than that for Pb. All these factors contribute to make Fe somewhat superior to Pb as a neutron shielding material, mainly as a result of its better ability to lower neutron energy via inelastic scattering.

Note that multiple energy levels of a nucleus may be excited in a single inelastic scattering interaction — if the projectile energy is high enough.

Assignment 3.19

1. Model a point source of 40 MeV neutrons, surrounded by a 100 cm thickness of Fe, using MCNP. Use geometry splitting with cell importance biasing as a variance reduction technique. Calculate the neutron energy spectrum as well as the absorbed dose rates from neutrons and photons at the outer surface of the shield (using an F1 tally).

2. Model a point source of 40 MeV neutrons, surrounded by a 100 cm thickness of Pb, using MCNP. Use geometry splitting with cell importance biasing as a variance reduction technique. Calculate the neutron energy spectrum as well as the absorbed dose rates from neutrons and photons at the outer surface of the shield (using an F1 tally).

3. Conclude whether Fe or Pb is the best shielding material against incident neutrons in the $E_n \approx 40$ MeV energy range.

4. Repeat the above calculations, but for a mono-energetic neutron source with $E_n = 2$ MeV; adjust cell importances as necessary to keep variance reduction effective.

5. Analyse the exit neutron energy spectra, fluence rates and dose rates and summarise the characteristic neutron shielding ability of Fe and Pb against neutrons.

6. Conclude whether Fe or Pb is the best shielding material against incident neutrons in the $E_n \approx 2$ MeV energy range.

3.6.12 Cross-sections for (n,α), (n,p), (n,d), (n,t), $(n,{}^3\text{He})$ and (n,np), $(n,2n)$ neutron interactions

Threshold reactions

In all but a few light nuclei, neutron-induced nuclear reactions having a charged particle in the exit channel, are endo-ergic, i.e. the incident neutron energy has to exceed a threshold value before the reaction becomes energetically possible. For most of these nuclei, the cross-sections for (n,α), (n,p), (n,np), $(n,2n)$, (n,d), (n,t), $(n,{}^3\mathrm{He})$ reactions have threshold energies above approximately 2 MeV to 12 MeV, as is e.g. the case for ^{56}Fe, as shown in Figure 3.41. This contrasts significantly with (n,γ) reactions, which are always exo-ergic.

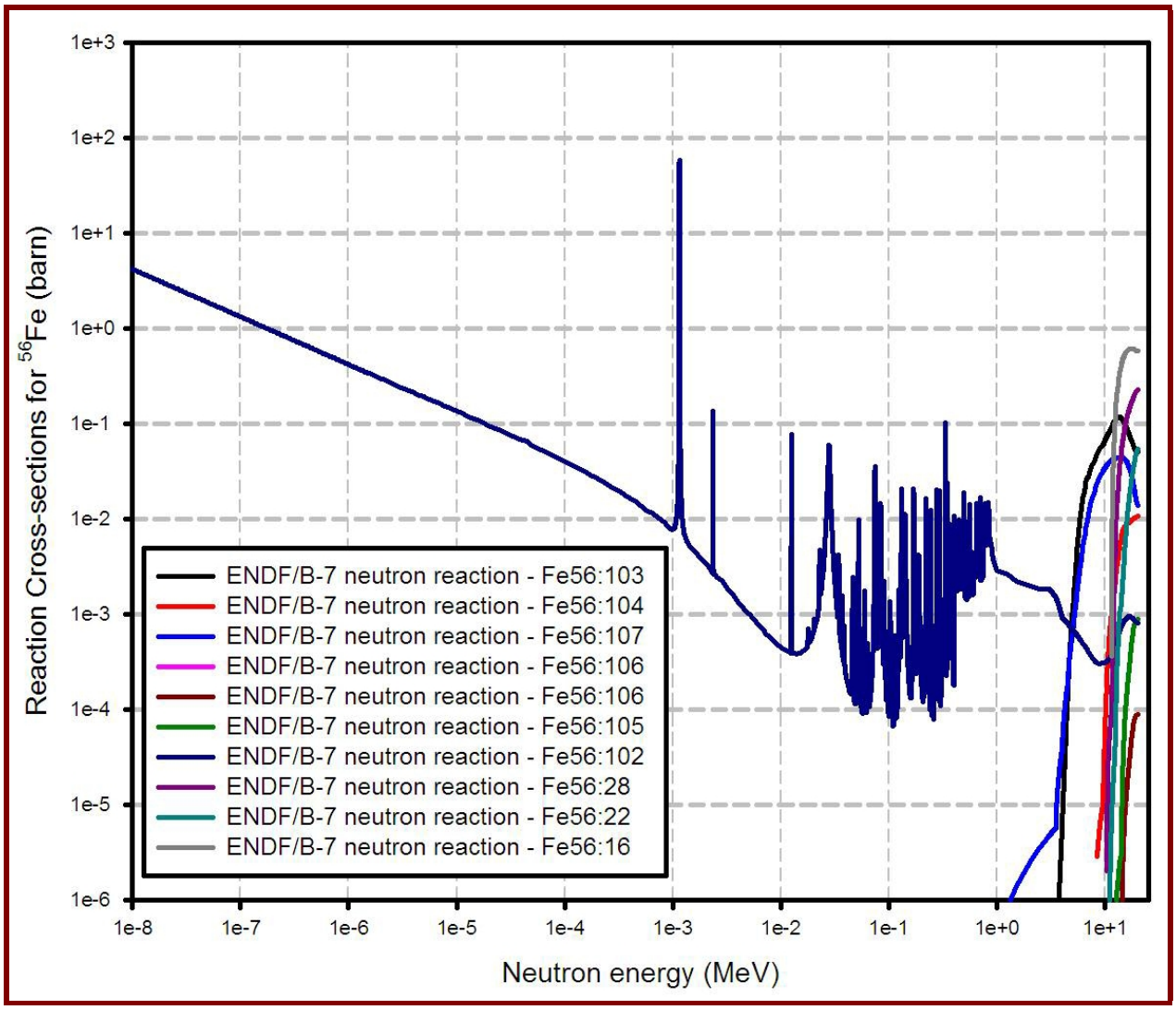

Figure 3.41: *Cross-sections for*

$(n,2n)$	$(n,n\alpha)$	(n,np)	(n,γ)	(n,p)	(n,d)	(n,t)	$(n,{}^3\mathrm{He})$	(n,α)
16	*22*	*28*	*102*	*103*	*104*	*105*	*106*	*107*

reactions with ^{56}Fe.

(Consult Table 3.7 on page 102 for ENDF/B reaction identifiers.)

Nuclear reactions (n,p), (n,d), $(n,{}^3\mathrm{He})$ and (n,t) are extremely valuable in neutron shielding, because the highly penetrating neutron is removed and in its place appears a charged particle having a very short range, which is very easily stopped in matter. Even reactions such as $(n,2n)$, $(n,n\alpha)$ and (n,np) reactions, which have a neutron or neutrons in the exit channel,

are valuable, because, as a result of energy conservation, and the high energy threshold for the endothermic nuclear reaction, the neutron(s) in the exit channel will have significantly lower energies than the neutron in the entrance channel, so that these reactions will contribute to the slowing down of neutrons.

Reaction energy thresholds for charged-particle (abbreviation: CP) emission nuclear reactions, e.g. (n, α), (n, p) and (n, np) reactions, are generally lower for light i.e. low-Z elements than for higher-Z nuclei, because the Coulomb barrier to charged particle emission is lower for low-Z nuclei, i.e. nuclei having a low positive electrical charge. In a few light nuclei such as such as ${}^{14}_{7}\text{N}$ and ${}^{10}_{5}\text{B}$, (n, CP)-reactions may even be exothermic.

We now look at an important exothermic (n, CP) nuclear reaction.

The exothermic charged-particle emission reaction, ${}^{14}\text{N}(n, p)$

The charged-particle emission reaction, ${}^{14}\text{N}(n, p)$ is exothermic, i.e. it has no energy threshold. The high cross-section at lower neutron energies for this (n, p)-reaction is largely responsible for the biological danger of slow neutrons to human tissue — via this nuclear reaction of neutrons with the ${}^{14}_{7}\text{N}$ nucleus in amino acids in proteins, thermal neutrons release protons, which deposits the radiation dose. Refer to Figure 3.42 for the cross-section of this reaction. Nitrogen is naturally present in all amino acids and, hence, proteins in the body.

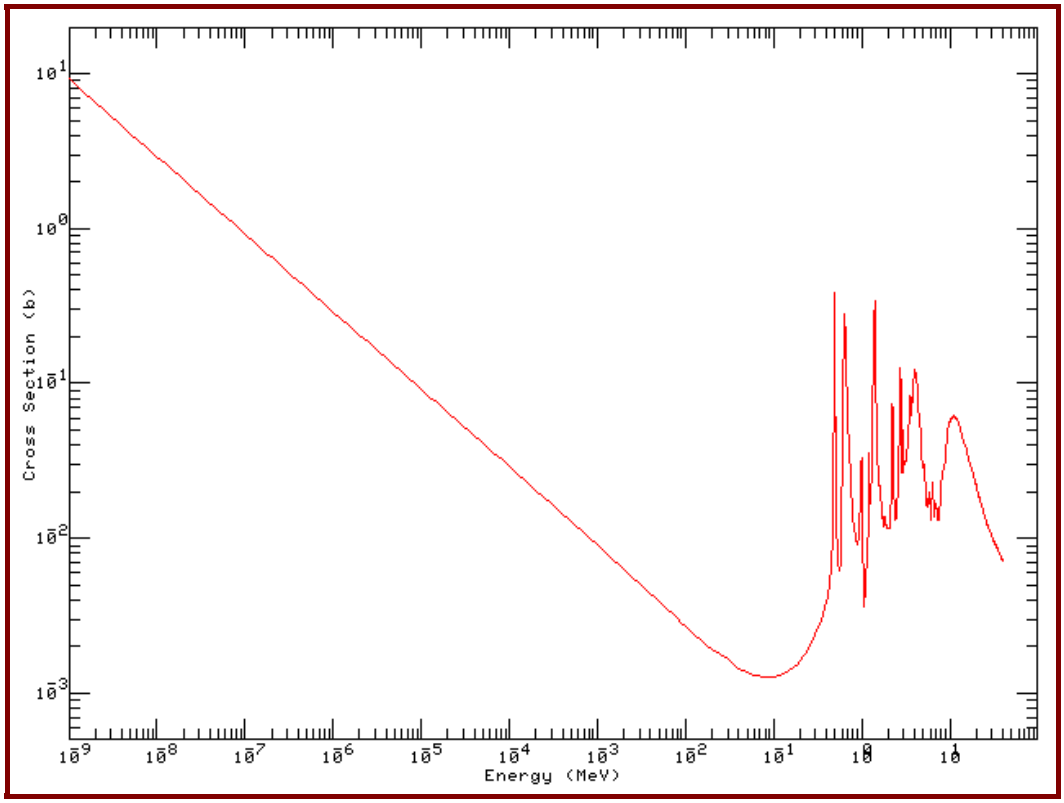

Figure 3.42: *Cross-section plot for the cross-section for ${}^{14}N(n, p)$ reactions.*

The appreciable cross-section of the ${}^{14}\text{N}(n, p)$ reaction at low neutron energies, contributes considerably to the biological hazard of thermal neutrons to human tissue; should this reaction

have had a threshold energy above a few MeV, the biological hazard of slow neutrons would have been significantly lower.

Assignment 3.20

1. Explain how and why an $(n, 2n)$ reaction with ^{9}Be will produce not only 2 neutrons, but also two α-particles.

2. Design and perform a simple calculational experiment to ascertain whether the $^{14}\mathrm{N}(n, p)$ nuclear reaction is indeed modelled in your version of MCNP and MCNP-DATA cross-section compilation. If this reaction is not modelled, have you identified a glaring gap in the abilities of the version of MCNPDATA supplied to you?

3. The following calculation can only be performed fruitfully if you have a version of MCNP capable of modelling (n, p)-reactions in the "Table Physics" neutron energy range.

   Perform an MCNP6 calculation with an F6 energy deposition tally. Run in `MODE n h p e` i.e. track neutrons, protons, photons and electrons. Use a simple cylindrical phantom, with one RCC cylinder placed inside a slightly larger RCC cylinder to simulate a skin thickness of e.g. 0.1 cm. The phantom must be 170 cm high, be composed of tissue-equivalent material and must have a mass of approximately 70 kg at a tissue-equivalent mass-density of 1 $\mathrm{g\,cm^{-3}}$; the radius is uniquely defined by these constraints and can be derived with ease. Let a wide beam of thermal energy neutrons fall onto the phantom. Calculate the absorbed dose rate in the skin, for a phantom with and without ^{14}N present in the material composition. Draw conclusions about the influence of ^{14}N in the skin, on the body's dosimetric response to low-energy neutrons. Explain the observed pattern.

The ^{10}B (n, α) reaction

The neutron capture reactions ("radiative neutron-capture reactions"),

$$^{1}\mathrm{H} + n \rightarrow {}^{2}\mathrm{H} + \gamma\ (2.205\ \mathrm{MeV})$$

and

$$^{10}\mathrm{B}\ (n, \alpha)\ {}^{7}\mathrm{Li} + \gamma\ (0.48\ \mathrm{MeV})$$

are important in the design of neutron shielding. Neutron sources require *(inter alia)* hydrogenous materials for shielding, as a result of the high kinematic efficiency of elastic scattering by ^{1}H. However, the $^{1}\mathrm{H}(n, \gamma)^{2}\mathrm{H}$ reaction produces relatively energetic 2.2 MeV capture gamma-photons. In this way, secondary gamma radiation is produced in the shield. In

thick hydrogenous shields, the ionising photon dose rate on the personnel side of the shield can easily exceed the neutron dose rate at the same position. The gamma-photons produced by the $^{10}\mathrm{B}\,(n,\alpha)\,^{7}\mathrm{Li}$ reaction have an energy of only 0.48 MeV, i.e. they are approximately 4.6 times less energetic than the capture gamma-photons produced when $^{1}\mathrm{H}$ absorbs neutrons.

At the reference neutron speed of 2200 $\mathrm{m.s^{-1}}$, the cross-section of the capture reaction $^{10}\mathrm{B}\,(n,\alpha)\,^{7}\mathrm{Li}$ is 3844 barn, while the cross-section for the reaction $^{1}\mathrm{H}\,(n,\gamma)\,^{2}\mathrm{H}$, at the same reference neutron speed, is 0.332 barn.

The cross-section for the reaction $^{10}\mathrm{B}\,(n,\alpha)\,^{7}\mathrm{Li}$, is shown in Figure 3.43.

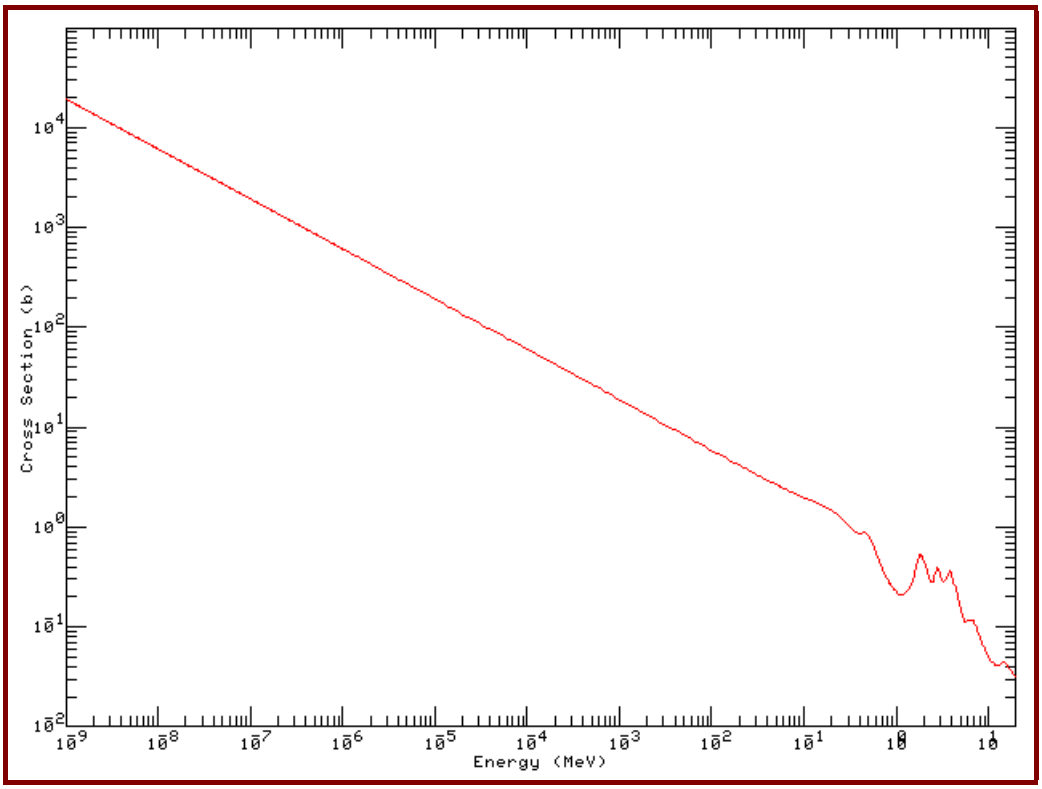

Figure 3.43: *Cross-section for the boron neutron capture reaction,* $^{10}B\,(n,\alpha)\,^{7}Li + \gamma\,(0.48\ MeV)$.

$^{10}\mathrm{B}$ is a very useful absorber of neutrons, because it is an almost perfect $\frac{1}{v}$ absorber over a very wide neutron energy range. The 0.48 MeV γ-photon emitted upon neutron capture, has a relatively low energy, and is relatively easily absorbed. Adding boron to a hydrogenous neutron shield suppresses the production rate of high-energy ionising photons from the reaction $^{1}\mathrm{H}(n,\gamma)$, and also suppresses the thermal neutron fluence rate, thereby lowering the reaction rate of all (n,γ) reactions, which is the most problematic reaction type from the viewpoint of neutron activation, i.e. the production of radionuclides in materials irradiated by neutrons.

Assignment 3.21

1. Explain why ^{10}B is more suited than ^{113}Cd for reactivity control in a fast-spectrum nuclear reactor.

2. Model the following with MCNP for sources emitting 3.7×10^{10} neutrons per second. Use point-sources enveloped by the shielding material, in spherical-symmetrical geometry. Fill in the calculated dose rates.

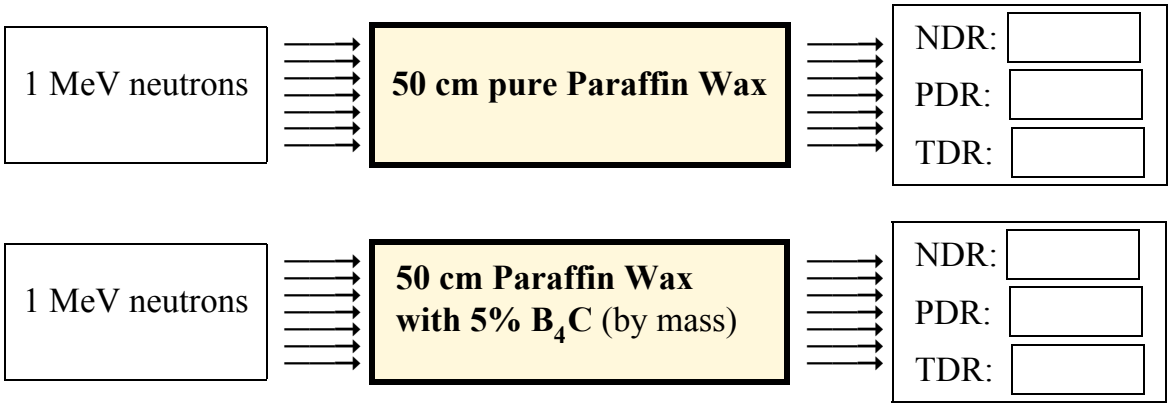

   Also plot the ionising photon spectra on the exit side of the two shields, on the same graph. What is the influence of the $^{10}_{5}$B on the prominence of the 2.205 MeV peak in the ionising photon spectrum on the exit side of the boron-containing shield, compared to the shield composed of pure paraffin wax $\left(C_{25}H_{52};\ \rho_{wax} = 0.92\ \mathrm{g\,cm^{-3}}\right)$? In your tally, place fine energy windows at $2.200 - 2.300$ MeV, as well as at $0.470 - 0.490$ MeV, and look for peaks in the exit γ-spectra. Discuss all the advantages of adding 5% B_4C to the wax layer of the radiation shield.

3. Repeat, but with a 5 cm thick Pb layer on the personnel-side of the shield.

4. Use MCNP to calculate the reaction rate of the ENDF/B nuclear reaction type 102, i.e. (n,γ)-reactions, in the wax layer of the above two shields. By what factor does the presence of the $^{10}_{5}$B lower the rate of (n,γ)-reactions?

5. Repeat the previous calculation, but use a pseudo-material[10] to specifically quantify the rate of the reaction $^{1}_{1}\mathrm{H}(n,\gamma)^{2}_{1}\mathrm{H}$. How do you have to adjust the tally multiplication factor (TMF) to achieve the calculation of a quantitatively correct reaction rate when you refer to a pseudo-material in the FM card?

6. Model the following with MCNP for neutron sources emitting 3.7×10^{10} neutrons per second. Use point-sources enveloped by the shielding material, in spherical-

[10] That is, a material card that is not referred to in the cell cards, but only in an FM card, for the calculation of reaction rates, using particle fluences calculated with real materials.

symmetrical geometry. Fill in the dose rates calculated on the outer surface of the outer Pb layer.

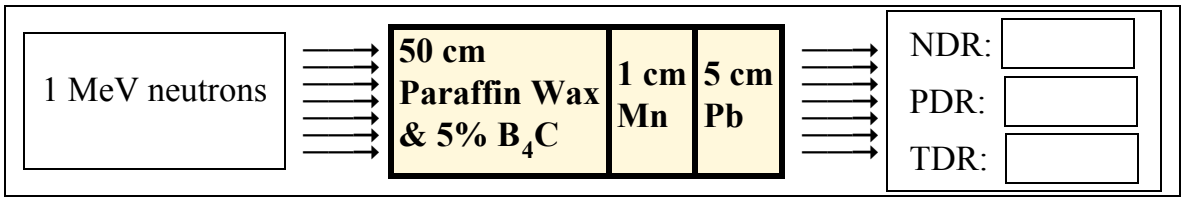

Quantify and explain the major advantages of adding approximately 5% very fine B_4C powder (m/m) to the wax layer of the radiation shield. Include the effect on the reaction rates of the nuclear reactions $^{55}\mathrm{Mn}(n,\gamma)^{56}\mathrm{Mn}$ and $^{1}_{1}\mathrm{H}(n,\gamma)^{2}_{1}\mathrm{H}$ in your discussion.

7. Use the following shield configuration as "baseline" and then place a 1 mm, a 2 mm and then a 3 mm Cd metal layer between the paraffin wax and the Mn layer. Quantify the effect on the reaction rate $^{55}\mathrm{Mn}(n,\gamma)^{56}\mathrm{Mn}$.

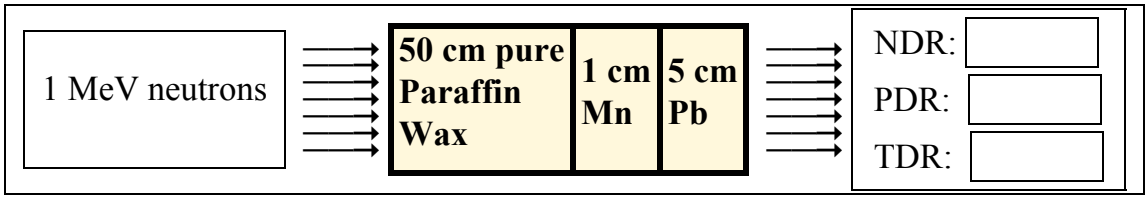

8. Use the following shield configuration as "baseline" and then place a 1 mm, a 2 mm and then a 3 mm Gd metal layer between the paraffin wax and the Mn layer. Quantify the effect on the reaction rate $^{55}\mathrm{Mn}(n,\gamma)^{56}\mathrm{Mn}$.

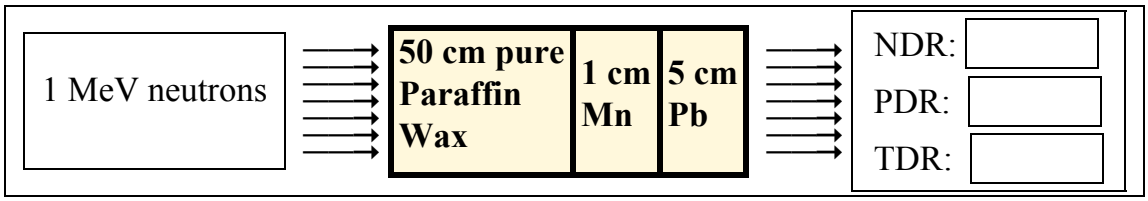

3.6.13 Cross-sections for nuclear fission, i.e. (n, f) nuclear reactions in ^{235}U and ^{238}U

Figure 3.44 shows $\sigma_{(n,f)}(E)$ for ^{235}U and ^{238}U. The top curve is the cross-section for the neutron-induced fission of ^{235}U, and the bottom curve is the cross-section for the neutron-induced fission of ^{238}U. The fission cross-section for ^{238}U only becomes appreciable at $E_n \gtrsim 1.3$ MeV. The energy dependence of the fission cross-section curve for ^{235}U shows why it is vital to slow down (moderate) neutrons in a ^{235}U-^{238}U fuelled nuclear reactor (except in fast-spectrum breeder reactors) — the ^{235}U fission cross-section for thermal neutron induced fission is approximately 3 orders of magnitude larger than the cross-section for fast neutron induced fission.

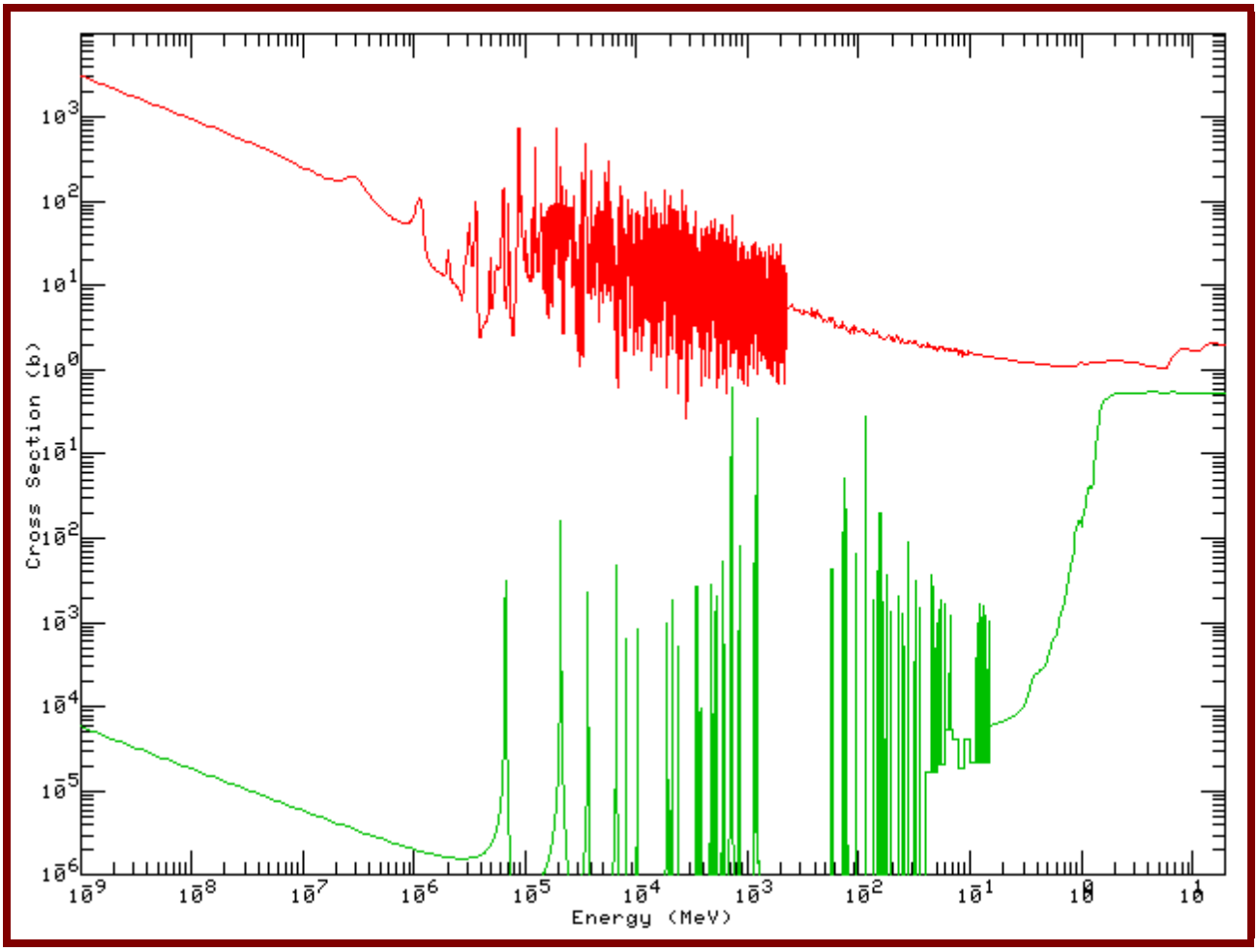

Figure 3.44: *The fission cross-sections $\sigma_{(n,f)}(E)$ for* ^{235}U / ^{238}U.

The fission cross-section $\sigma_{^{238}\mathrm{U}(n,f)}(E)$ for ^{238}U only becomes appreciable at $E_n \gtrsim 1.3$ MeV — the (n, f) resonances for ^{238}U at $E < 0.2$ MeV have no practical impact on reactor operation, because these resonances are very narrow and also low.

The "problematic" thermal-fission resonance in $\sigma_{\left[^{239}\mathrm{Pu}(n,f)\right]}(E)$ — the danger of positive reactivity feedback with a rise in fuel temperature when nuclear reactor fuel contains substantial fraction of ^{239}Pu

Figure 3.45 displays the fission cross-sections for ^{235}U, ^{238}U and ^{239}Pu on a single graph.

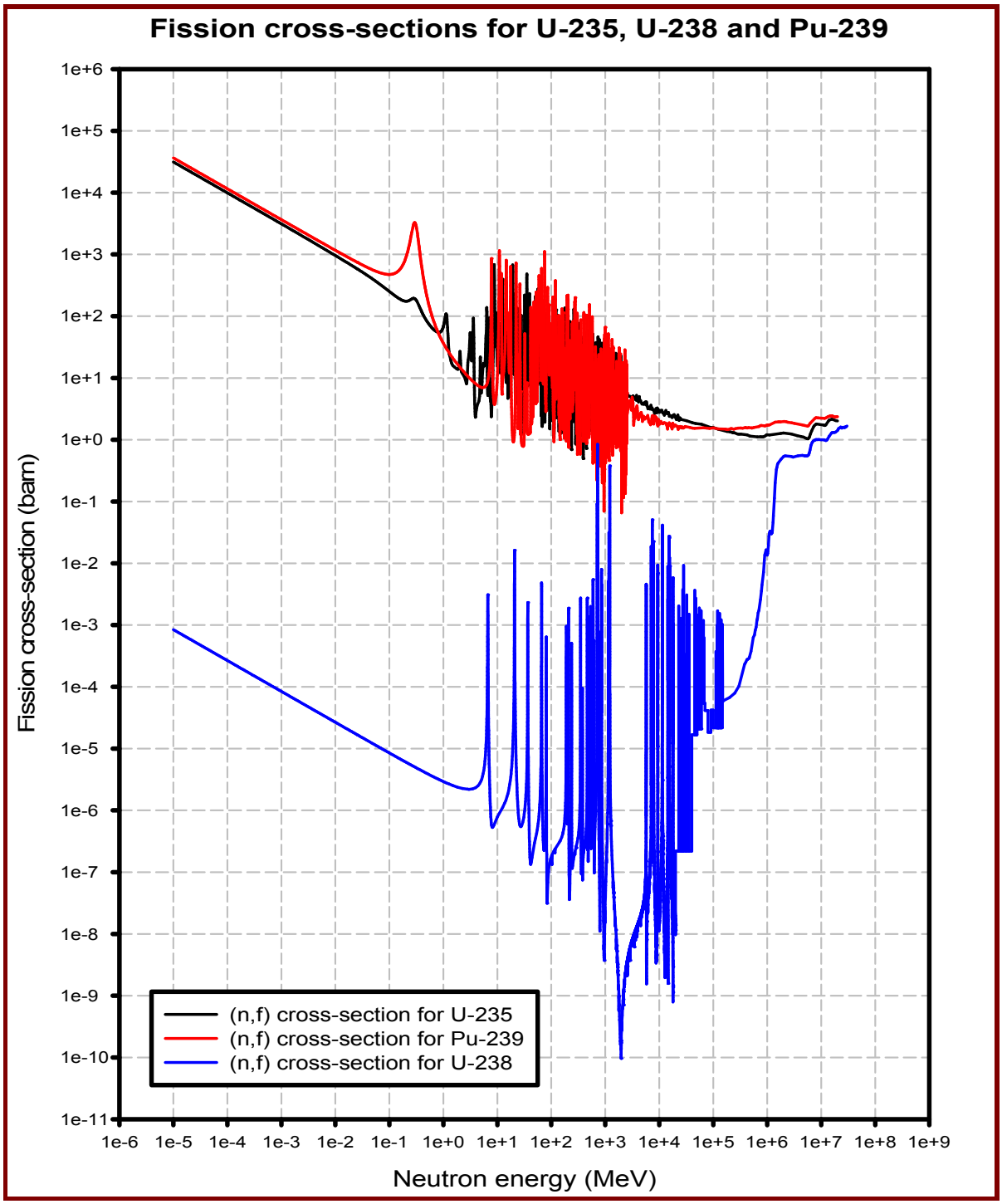

Figure 3.45: *Fission cross-sections for* ^{239}Pu, ^{235}U, ^{238}U.

Error: Neutron energy axis has units eV and not MeV.

Note the prominent resonance in the thermal neutron energy range in $\sigma_{^{239}\mathrm{Pu}(n,f)}(E)$.

When LEU reactor fuel reaches a high burnup value, the contribution of ^{239}Pu to fissions can exceed 15%, because ^{239}Pu is bred in the fuel from neutron capture by ^{238}U. When reactor

fuel that contains a significant ^{239}Pu fraction, reach unusually high temperatures in a transient, (1) the thermal neutron fission resonance cross-section of ^{239}Pu broadens via Doppler broadening, and (2) the Maxwellian peak of the thermal neutron energy spectrum shifts to higher energies, so that the fission rate increases — i.e. positive reactivity feedback takes place. A stable reactor must be characterised by negative prompt reactivity feedback. When a significant fraction of ^{239}Pu is present in reactor fuel, the core design and the reactor control system must be designed to cope with the lower prompt negative reactivity coefficient.

There is a danger that a positive reactivity coefficient of fuel temperature may develop towards End-of-Cycle (EOC) at high burnups of LEU fuel. Even without considering Doppler broadening of the thermal fission resonance of ^{239}Pu, the value of the fission-rate integral

$$\int_{10^{-4}\text{ eV}}^{1\text{ eV}} \phi(E,T)\,\sigma_{(n,\mathrm{f})}(E)dE$$

for fission of ^{239}Pu will increase by more than 300% as the fuel temperature rises from 300 K to 2000 K, as a result of the optimal overlap of the Maxwellian thermal neutron energy spectrum and the ^{239}Pu fission resonance peak in the shifted Maxwellian thermal neutron peak at the higher fuel temperature. This will add to a tendency of high-burnup LEU fuel to develop a positive fuel-temperature reactivity coefficient towards EOC. In the above fission rate integral, $\phi(E,T)$ is the neutron fluence-rate as a function of neutron energy E and temperature, T, while the function $\sigma_{(n,\mathrm{f})}(E)$ is a non-broadened representation of the energy dependence of the fission cross-section for ^{239}Pu on neutron energy, E. (The cross-section function σ_{fiss} depends on energy and temperature, but the dependence on temperature, i.e. Doppler broadening, was neglected in our simple calculation. The spatial dependence of the neutron fluence-rate, as well as the effect of the fission resonance on the energy dependence of ϕ, was also ignored.)

Figure 3.46 shows the relation between the ^{239}Pu fission cross-section and the Maxwellian thermal neutron energy spectrum at 300 K (LHS) and at 2200 K (RHS).

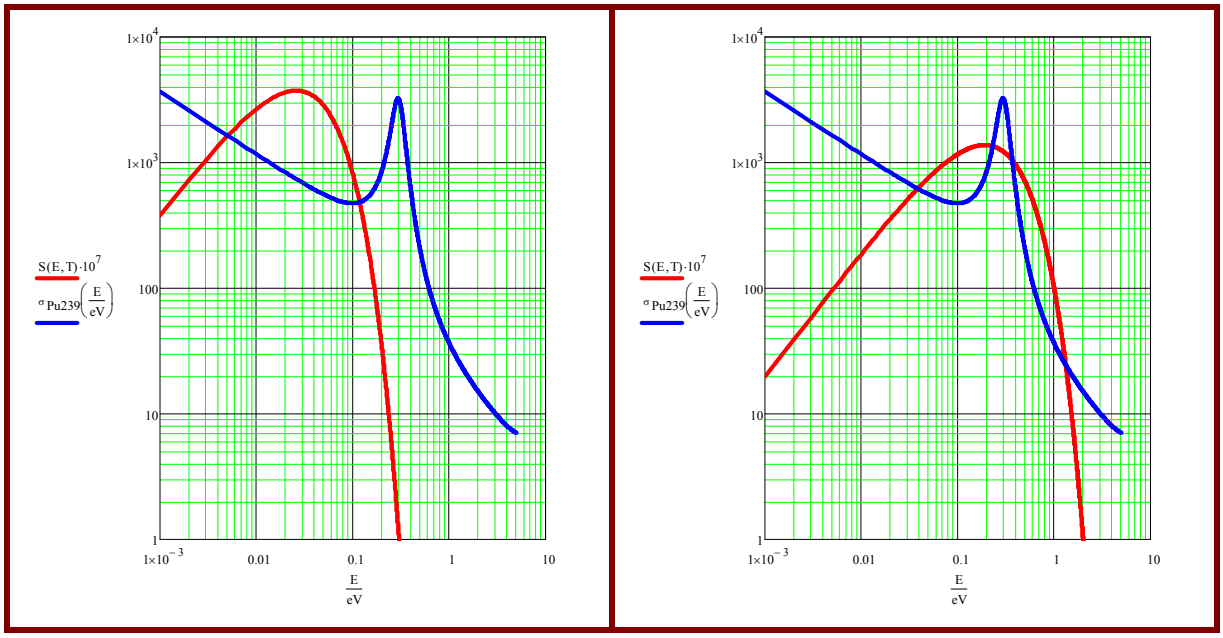

Figure 3.46: *The relation between the ^{239}Pu fission cross-section and the Maxwellian thermal neutron energy spectrum at 300 K and at 2200 K.*

At the lower fuel temperature, $\int_{10^{-4}\text{ eV}}^{1\text{ eV}} \phi(E,T)\,\sigma_{(n,\text{f})}(E)dE$ has a low value. At the higher fuel temperature, the value of $\int_{10^{-4}\text{ eV}}^{1\text{ eV}} \phi(E,T)\,\sigma_{(n,\text{f})}(E)dE$ increases by more than 300%, because the Maxwellian thermal neutron energy spectrum is "shifted" to "overlap" the thermal-region ^{239}Pu fission resonance peak. This represents a positive reactivity feedback with rising fuel temperature, which negatively impacts reactor safety. Another result from these types of analyses is that MOX[11] fuel may not contain too high a fraction of ^{239}Pu and ^{241}Pu — the latter plutonium isotope has an even more prominent and therefore problematic fission resonance in the thermal neutron energy range, which will also tend to destabilise the reactor.

The (n, f) cross-sections for ^{233}U and ^{232}Th

Figure 3.47 shows the fission cross-section for ^{233}U and ^{232}Th.

[11] MOX = Mixed Uranium-Plutonium OXide fuel. Mixed oxide fuel, commonly referred to as MOX fuel, is nuclear fuel that contains more than one oxide of fissile material, usually consisting of plutonium blended with natural uranium, reprocessed uranium, or depleted uranium. MOX fuel is an alternative to the low-enriched uranium (LEU) fuel used in the light water reactors that predominate nuclear power generation. For example, a mixture of 7% plutonium and 93% natural uranium is a viable MOX fission-reactor fuel.

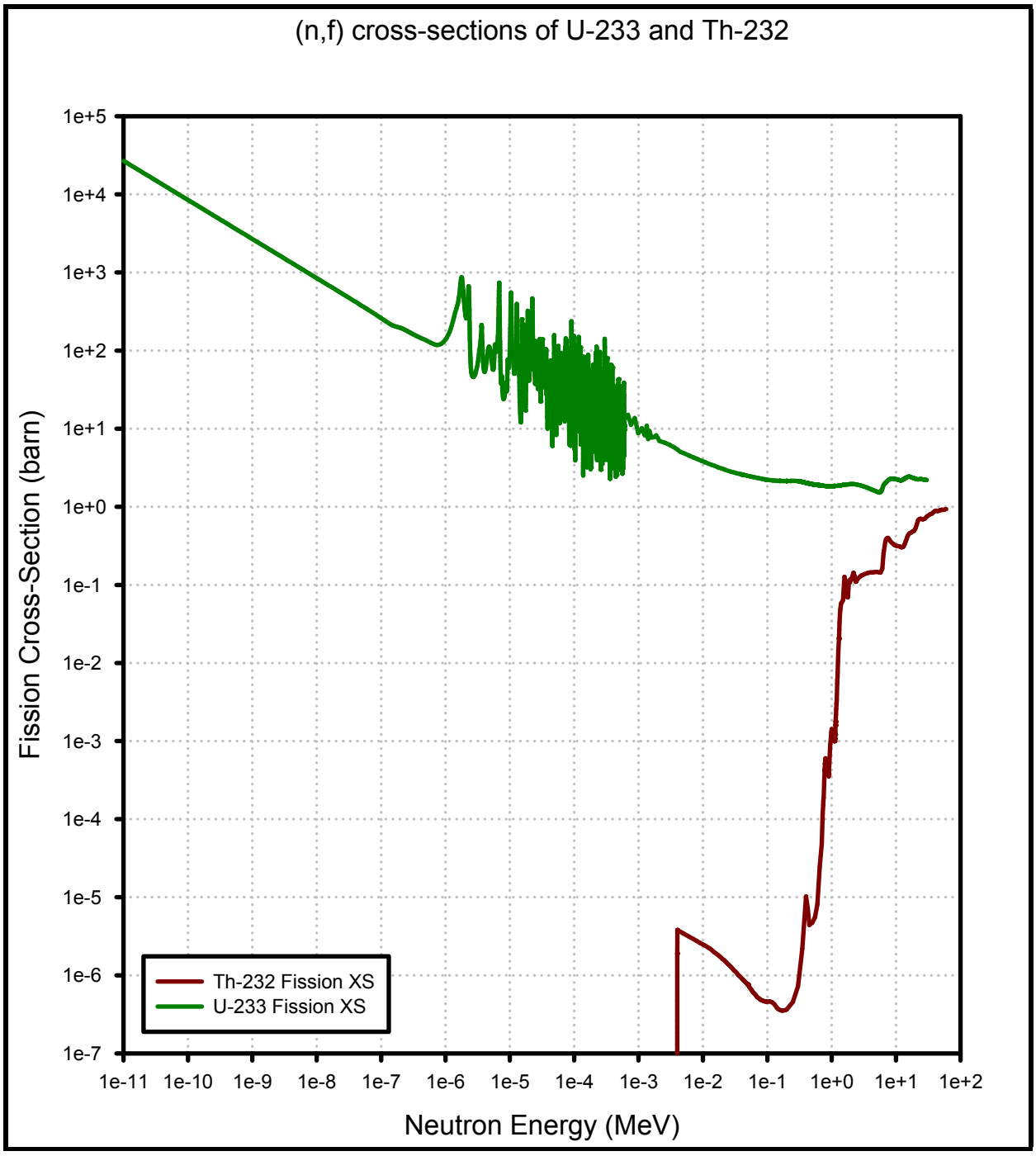

***Figure 3.47**: The fission cross-section for ^{233}U and ^{232}Th.*

^{233}U is fissile, while ^{232}Th is fissionable by fast neutrons having $E_n \geq 0.4$ MeV.

Thorium as a nuclear fuel

Thorium (i.e. Th-232) is not itself fissile and so is not directly usable in a thermal-neutron-spectrum fission reactor. However, ^{232}Th is "fertile" and upon absorbing a neutron will transmute to ^{233}U in the following manner: Neutron absorption by ^{232}Th produces ^{233}Th which beta-transitions, with a half-life of about 22 minutes, to protactinium-233 (^{233}Pa), which beta-

transitions to ^{233}U with a half-life of circa 27 days. Some of the bred ^{233}U is converted to ^{234}U by further neutron absorption; this ^{234}U is an unwanted parasitic neutron absorber. The ^{234}U produced in this way partially converts to fissile ^{235}U, the main naturally occurring fissile isotope of uranium and this fact somewhat compensates for the neutronic penalty involved with the buildup of ^{234}U. In fuel cycles involving the multi-recycle of $\{^{232}\text{Th}\text{-}^{233}\text{U}\}$ fuels, the build-up of ^{234}U over several years can be appreciable.

The isotope ^{233}U is an excellent fissile reactor fuel material — a ^{233}U nucleus yields more neutrons ν, on average, when it fissions (splits) than either a ^{235}U or ^{239}Pu nucleus. In other words, for every thermal neutron absorbed in a ^{233}U fuel, there are a greater number ν of neutrons produced and released into the surrounding fuel. This gives better neutron economy in the reactor system.

In a breeder reactor, the fissionable isotope ^{232}Th, which transmutes to the fissile isotope ^{233}U, behaves similarly to ^{238}U, which transmutes to the fissile nuclide ^{239}Pu. All thorium fuel concepts therefore require that ^{232}Th be first irradiated in a reactor by a high fluence-rate of neutrons. The ^{233}U that is produced or "bred" can either be chemically separated from the parent thorium fuel and recycled into new fuel, or the ^{233}U may be usable "in-situ" in the same fuel form, especially in molten salt reactors (MSR).

A reactor fuelled with only ^{232}Th can never become critical; thorium fuels therefore need a fissile material as a "driver" so that a chain reaction (and thus a supply of surplus neutrons) can be maintained. The only fissile driver options are ^{233}U. ^{235}U or ^{239}Pu.

It is possible — but quite difficult — to design thorium fuels that produce more ^{233}U in thermal reactors than the fissile material they consume. This is referred to as having a fissile conversion ratio of more than 1.0 and is also called breeding). Thermal breeding with thorium fuel requires that the neutron economy in the reactor has to be very good, i.e. there must be low neutron loss through spatial escape or parasitic absorption. The possibility to breed a surplus of fissile material in slow neutron-spectrum reactor systems, is a unique feature for thorium-based fuels and is not possible with uranium fuels.

Another distinct option for using thorium is as a "fertile matrix" for fuels containing plutonium that serves as the fissile driver fuel, while being consumed. This also holds for other transuranic elements like americium. Mixed thorium-plutonium oxide (Th-Pu MOX) fuel is an analog of current uranium-MOX fuel, but no new plutonium is produced from the thorium component, unlike for uranium fuels in U-Pu MOX fuel, and so the level of net consumption of plutonium is high. Production of all actinides is significantly lower for thorium fuel than with conventional LEU uranium fuel. Furthermore, the negative reactivity coefficient is better for thorium-plutonium fuels than for uranium-plutonium fuels.

In fresh thorium fuel, most of the fissions derive from the fissile driver component. As the thorium fuel evolves neutronically, the ^{233}U content gradually increases and it contributes more and more to the power output of the fuel.

An important principle in the design of thorium fuel systems is that of heterogeneous fuel arrangement, in which a high fissile (and therefore higher power) fuel-zone called the *seed region* is physically separated from the fertile (low power) thorium part of the fuel – often called the blanket. Such an arrangement is far better for supplying surplus neutrons to thorium nuclei so they can convert to fissile ^{233}U; all thermal breeding fuel designs are heterogeneous.

Some of the advantages of the ^{232}Th fuel cycle, are highlighted in Figure 3.48.

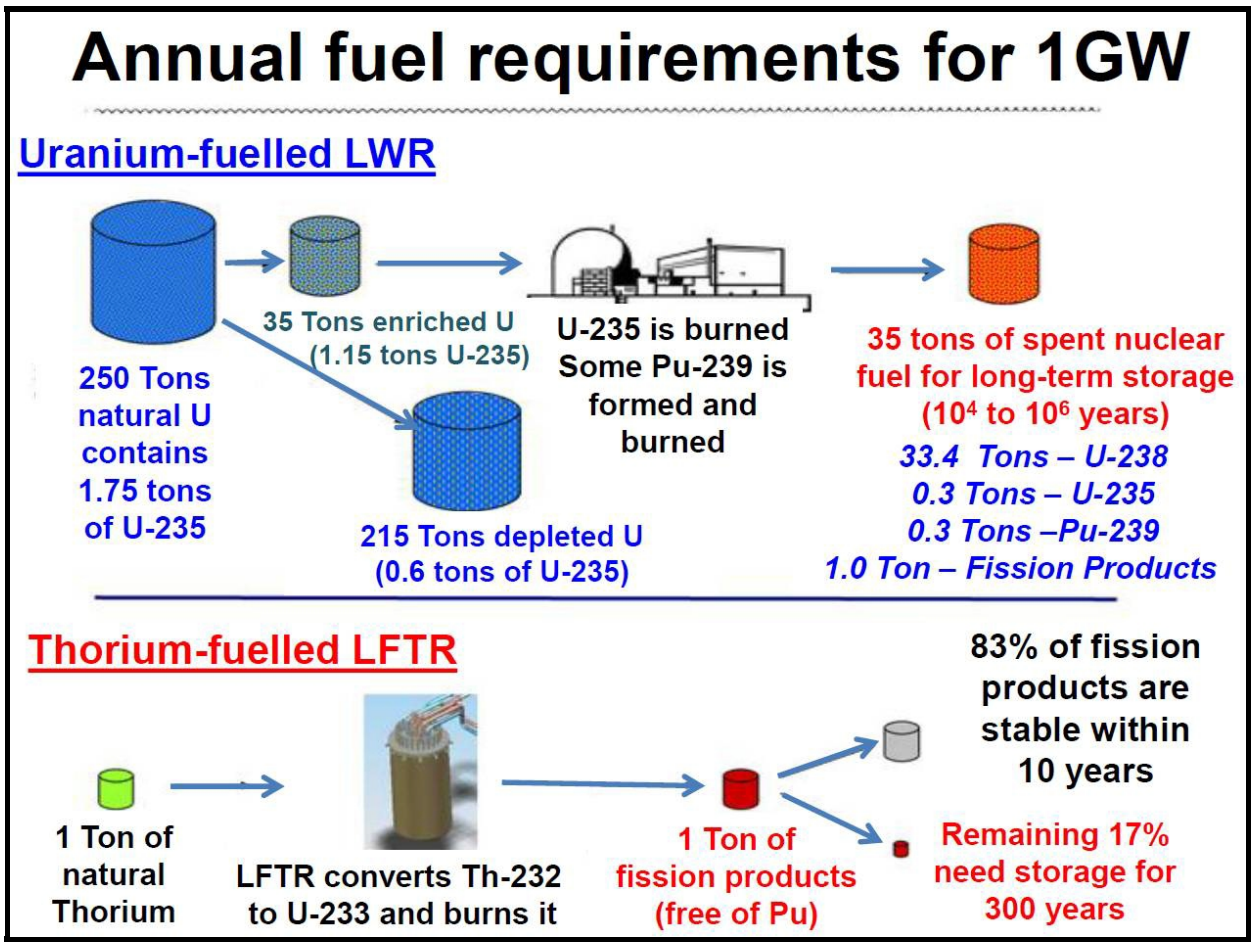

Figure 3.48: *Advantages of the ^{232}Th fuel cycle.*

The (n, f) cross-sections for ^{233}U, ^{239}Pu and ^{241}Pu

Figure 3.49 shows the fission cross-sections for the fissile nuclides ^{233}U, ^{239}Pu and ^{241}Pu.

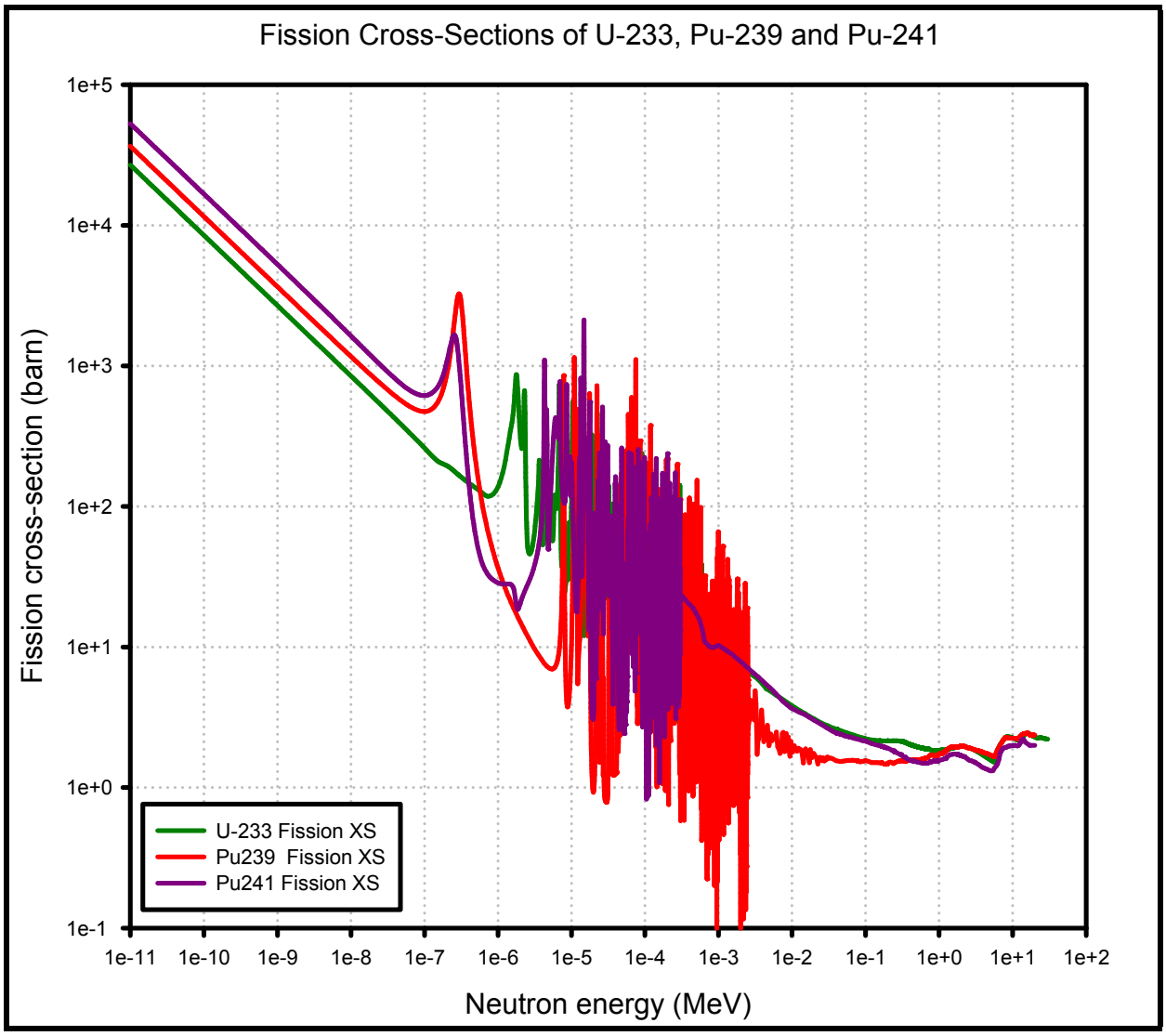

Figure 3.49: *The fission cross-sections for the fissile nuclides ^{233}U, ^{239}Pu and ^{241}Pu.*

The major difference between the ^{233}U cross-section function on the one hand, and the ^{239}Pu and ^{241}Pu cross-sections on the other hand, is the presence of high and wide fission resonance peaks at energies between 1 eV and 5 eV for ^{239}Pu and ^{241}Pu. This fission resonance peak is most prominent for ^{239}Pu.

The energy range in which these fission resonance peaks are located, is problematic from a reactor stability point of view. Consider a fission reactor fuelled by a large fraction of ^{239}Pu in the fuel. Assume that the normal fuel centreline temperature is 1200 °C, but that it is raised to 1800 °C in a power excursion. Let $S(E,T)$ be Maxwellian thermal neutron spectrum. The ratio

$$\frac{\int_{1\text{ eV}}^{5\text{ eV}} S(E, 1800°\text{C})\, dE}{\int_{1\text{ eV}}^{5\text{ eV}} S(E, 1200°\text{C})\, dE} \approx 8.5$$

i.e. there will be a significantly higher thermal neutron fluence-rate $\phi(E)$ in fission reaction rate integrals of the type

$$\int_{1\text{ eV}}^{5\text{ eV}} \phi(E)\,\sigma(E)\,dE$$

in the wide fission resonance peak ($1\text{ eV} - 5\text{ eV}$) in the case of the hotter fuel, than in the colder fuel. In other words, the fission rate will increase, and the reactor power will increase too. This is a positive reactivity feedback effect. There is a danger that reactor control can become more difficult the more ^{239}Pu is present in the fuel. The overall fuel temperature reactivity coefficient must be kept negative under all possible operational conditions, and the reactor control software and hardware must be able to cope with MOX fuel.

Assignment 3.22

1. Using cross-section data from JANIS, display the fission cross-section $\sigma_f(E)$ for ^{239}Pu and a Maxwellian thermal neutron energy spectrum on four graphs, for different reactor fuel temperatures, namely
   (a) $T = 100\,°\text{C}$,
   (b) $T = 500\,°\text{C}$,
   (c) $T = 1000\,°\text{C}$ and
   (d) $T = 1500\,°\text{C}$.
   (Note that the relationship $E_{\text{av}} = \frac{3}{2}k_B T$ relates the average energy E_{av} of the atoms in a medium to the temperature T in Kelvin.)
   Use these graphs to point out the problem of a potential positive fuel temperature reactivity feedback for reactor fuel that contains a significant proportion of the fissile nuclide ^{239}Pu.

2. Given: The relationship $E_{\text{av}} = \frac{3}{2}k_B T$ relates the average energy E_{av} of the atoms in a medium to the temperature T of the medium, in the unit kelvin.

   Using cross-section data from JANIS to display the fission cross-section $\sigma_f(E)$ for ^{239}Pu and a Maxwellian thermal neutron energy spectrum on four graphs, for different reactor fuel temperatures, namely
   (a) $T = 100\,°\text{C}$,
   (b) $T = 500\,°\text{C}$,
   (c) $T = 1000\,°\text{C}$ and
   (d) $T = 1500\,°\text{C}$.
   Use these graphs to point out and quantify the problem of a positive fuel temperature reactivity feedback for reactor fuel that contains an excessive fraction of the fissile nuclide ^{239}Pu.
   Ignore Doppler broadening (i.e. results will not be quantitatively accurate).

3.3 A certain burnable poison isotope that is added to nuclear reactor fuel, which normally operates at an average temperature of 1000 °C, has a prominent (n, γ) neutron capture cross-section between the neutron energies 0.2 eV and 0.8 eV. Can the addition of this burnable poison impart a higher negative fuel temperature reactivity to the reactor? If so, explain why and how.

3.4 Use JANIS to ascertain whether the addition of the isotope ^{167}Er as a burnable poison in reactor fuel, will be able to contribute to a greater negative value of the reactivity coefficient of fuel temperature.

3.5 Use JANIS to ascertain whether the addition of the isotope ^{152}Gd will be able to impart an enhanced negative fuel temperature reactivity coefficient to nuclear fuel operating at 1000 °C.

3.6 Use JANIS to plot the fission cross-sections of ^{239}Pu and ^{241}Pu on the same graph. Comment on the effect of the presence of these plutonium isotopes in reactor fuel, on reactor safety.

3.7 Use JANIS to plot the fission cross-section of ^{233}U, and comment on the safety of a $^{233}\mathrm{U}/^{232}\mathrm{Th}$ fuelled reactor.

3.8 The Chernobyl accident occurred near End-of-Cycle (EOC) core conditions in the $\mathrm{R_eB_aM_eK_a}$ reactor design, when the fuel's inventory of ^{239}Pu reached a maximum. Name two ways in which this added to the instability of the core and its proneness to an uncontrolled power excursion.

Maxwellian Neutron Spectrum and Pu239 Fission XS.xmcd

3.6.14 Neutron interactions in different energy regions

In the neutron energy region above roughly 0.1 MeV, the dominant neutron interaction mechanism is usually scattering. At energies below the threshold energy for the excitation of the first energy level of the target nucleus, elastic scattering is the only possible scattering mechanism. At energies above the threshold energy for the excitation of the first energy level of a nucleus, inelastic scattering becomes important and can contribute substantially to neutron slowing down. For neutron energies above circa 7 MeV, i.e. neutron energies comparable to the binding energy of a nucleon in a nucleus, multiple particles can be present in the exit channel of nuclear reactions, i.e. (n, np) and $(n, 2n)$ reactions become energetically possible. The threshold energies for $(n, 2n)$ reactions are particularly low for ^{2}H (3.3 MeV) and ^{9}Be (1.84 MeV).

Interactions such as (n, p) and (n, α) reactions, may be important for some light elements. For most nuclides, (n, p) and (n, α) reactions are endothermic, with threshold energies above a few MeV. One important exception is the exothermic reaction $^{14}\mathrm{N}(n, p)^{14}\mathrm{C}$ — the biological hazard of slow neutrons is dominated by the contribution of this exothermic $^{14}\mathrm{N}(n, p)^{14}\mathrm{C}$ nuclear reaction, which enable thermal neutrons to releases protons in materials containing nitrogen, which is present in all proteins in the body. The protons released in this (n, p) reaction deposit their energy by direct ionisation.

In the MeV neutron energy region, the endothermic (n, α) reaction cross sections for ^{14}N and ^{16}O form appreciable fractions of the total cross-section σ_{t}, and are important reactions for producing high-LET charged α-particles in human tissue, which deposit energy by direct ionisation. Figure 3.50 shows the endothermic (n, α) cross-sections for the isotopes ^{14}N and ^{16}O, which are abundant in human tissue.

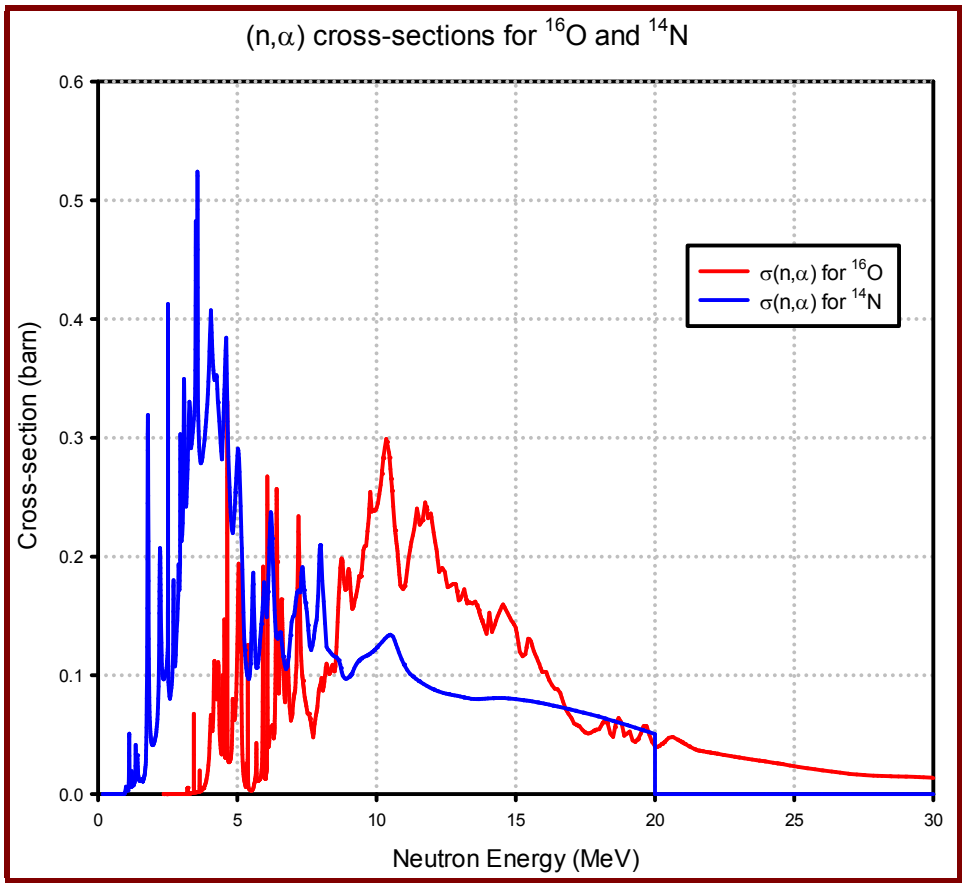

Figure 3.50: *The endothermic (n, α) cross-sections for the isotopes ^{14}N and ^{16}O.*

For heavy target nuclides, threshold neutron energies for charged particle emission reactions such as (n, p) and (n, α) reactions are high, as a result of the substantial Coulomb barrier for charged particle emission from heavy nuclei. For light target nuclides such as e.g. ^{14}N, threshold neutron energies for charged particle emission reactions such as (n, α) and (n, p) reactions are low or zero, as a result of the much lower Coulomb barrier for charged particle emission from light nuclei.

Assignment 3.23

1. Use SRIM to model the transport of $^{12}_{6}C$ and $^{16}_{8}O$ as well as $^{1}_{1}H$ through water. At which ion energy is the peak of the Bragg peak observed, i.e. at which energy is the spatial density of energy deposition into the aqueous medium most intense?
   Next, calculate the incident neutron energy that will produce $^{12}_{6}C$ and $^{16}_{8}O$ as well as $^{1}_{1}H$ at an energy, say, 10% above the above Bragg Peak energy.
   Next, attempt to correlate your finding with that neutron energy seen at the peak of the ICRP-2007 $w_R(E)$ function for neutrons — see Figure 1.1 on page 28.

2. Neutron energy deposition in the human body: Write down three (n, z) nuclear reactions, where z denotes a charged particle, through which free neutrons deposit energy in the human body.

3. A 1 MeV neutron collides elastically with $^{12}_{6}\mathrm{C}$. Calculate the expectation-value $\langle E \rangle$ of the recoiling nucleus.
A 1 MeV neutron collides elastically with $^{16}_{8}\mathrm{O}$. Calculate the expectation-value $\langle E \rangle$ of the recoiling nucleus.

4. The carbon-carbon chemical bond strength in a certain organic molecule is 5 eV. Calculate an estimate of the threshold energy at which a neutron can, via elastic scattering, break such a C-C chemical bond.

3.6.15 Consequences of cross-section minima in nuclides that are abundant in neutron shielding materials

Steel, magnetite concrete, hematite concrete and ordinary concrete are important shielding materials. These shielding materials are rich in oxygen and/or iron. The dominant oxygen isotope is $^{16}\mathrm{O}$ and the dominant Fe isotope is $^{56}\mathrm{Fe}$.

The nuclides $^{16}\mathrm{O}$ (natural abundance: 99.756%) and $^{56}\mathrm{Fe}$ (natural abundance: 91.7%) have narrow yet deep minima in their total cross-section functions, as shown in Figures 3.51 and 3.52.

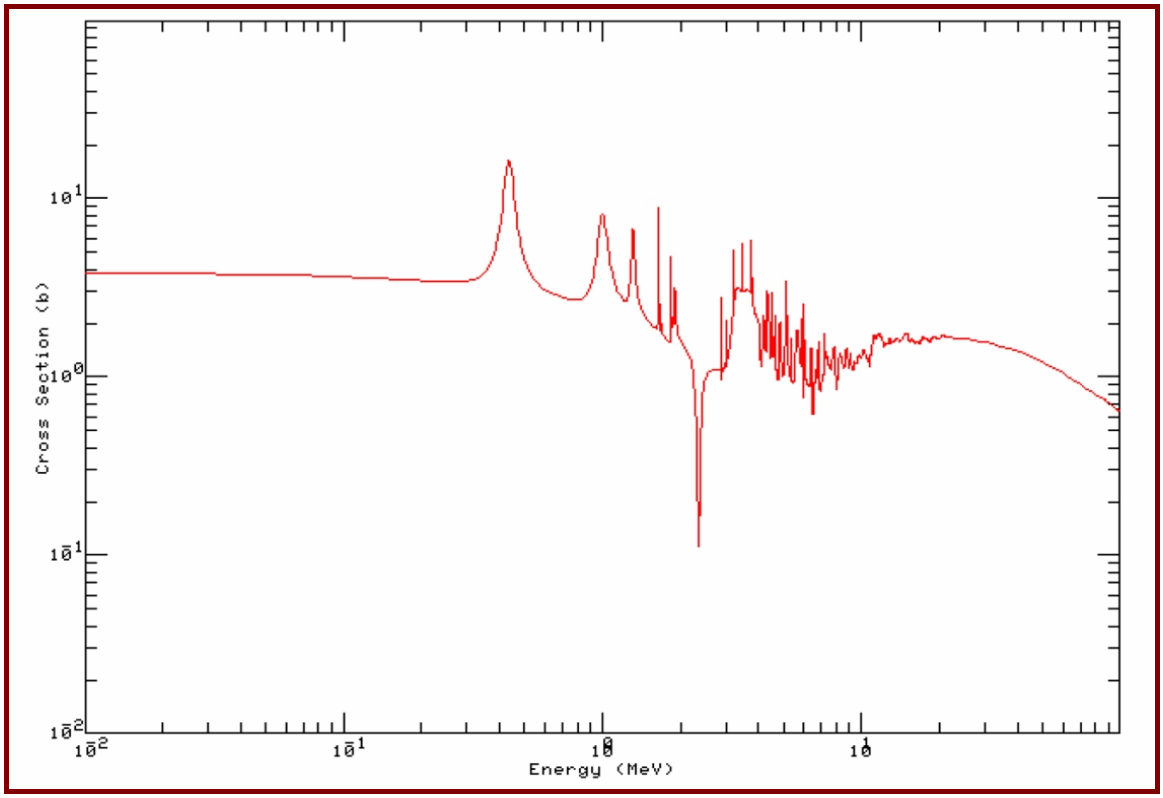

Figure 3.51: *The total neutron cross-section $\sigma_t(E)$ for ^{16}O has a pronounced minimum at $E_n \approx 2.3$ MeV.*

Consequence: For neutrons born at energies above approximately 2.5 MeV, that subsequently penetrate through thick concrete shields, which are particularly rich in oxygen, there will be a slight concentration of transmitted neutrons near $E_n \approx 2.3$ MeV as a result of the pronounced "dip" in the interaction cross-section for ^{16}O at this neutron energy. This slight "energy streaming" of neutrons through the thin $^{16}_{8}$O cross-section window, is best seen on a neutron energy spectrum expressed in "unit lethargy" i.e. where fluences ϕ_g are divided by the "lethargy interval" $[\ln(E_{\text{ref}}) - \ln(E_g)]$. (In this expression, the reference neutron energy E_{ref} is typically taken as the highest neutron energy of practical interest in the problem under analysis; in nuclear reactor analysis, the reference neutron energy for *unit lethargy* calculations, is customarily set at $E_{\text{ref}} = 10$ MeV.)

We now turn to the cross-section minimum for ^{56}Fe, the most abundant isotope of Fe — see Figure 3.52.

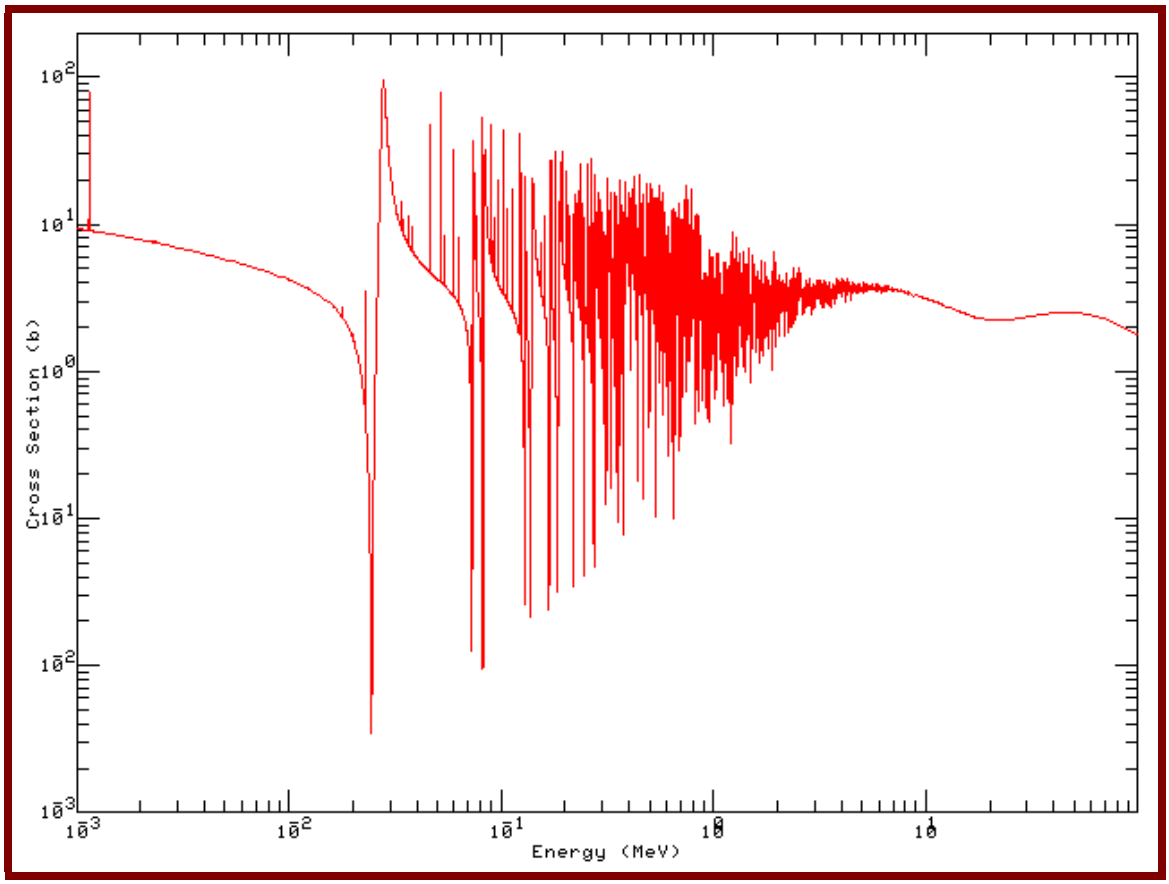

Figure 3.52: *The total neutron cross-section $\sigma_t(E)$ for ^{56}Fe has a pronounced minimum at $E_n \approx 25$ keV.*

Cross-section minima for ^{56}Fe at higher energies are very narrow, and therefore not important for "energy streaming" of neutrons.

Consequence: For neutrons born at energies above approximately 30 keV, that subsequently penetrate through thick, high-purity Fe shields, there could be an observable concentration of transmitted neutrons in a narrow band of energies around 25 keV, as a result of the "dip" in the

interaction cross-section for ^{56}Fe at this neutron energy. This "energy streaming" is best seen on a neutron energy spectrum expressed in "unit lethargy" — see page 169.

Assignment 3.24

1. Model the following with MCNP, using an F2 or F4 tally with an E tally energy-bin specification card with energy-bin boundaries suitably narrow around the neutron cross-section minima of $^{16}_{8}$O and $^{56}_{26}$Fe.

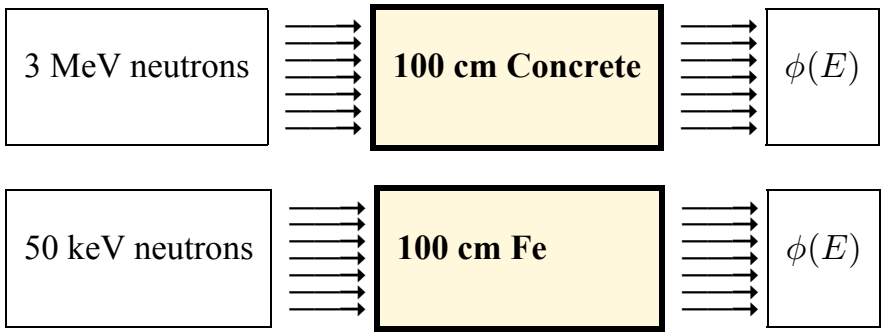

Plot the neutron spectra on the exit side of the shields, in unit lethargy. Are there any signs of "energy streaming"? In other words, attempt to detect the "fingerprint" left by the minima in the cross-sections for ^{16}O and ^{56}Fe, in the $\phi(E)$ energy spectrum on the exit side of the shield.

3.6.16 Calculating effective cross-sections

Useful effective neutron cross-sections may be calculated with the formula,

$$\langle \sigma \rangle = \frac{\int_0^\infty dE\, \sigma(E)\, \phi(E)}{\int_0^\infty dE\, \phi(E)}$$

where $\phi(E)$ is a reasonably representative neutron spectrum for the system under assessment. An example of a useful weighting spectrum $\phi(E)$ for a thermal neutron spectrum nuclear reactor, is Eq. (3.31)

$$\phi(E) = \begin{cases} E\left[\exp\left(\dfrac{-E}{2.58522 \times 10^{-8}}\right)\right] & \text{if } 0 < E < 0.125\,\text{eV} \\ \left(1.2414 \times 10^{-16}\right) \times \left(\dfrac{1}{E}\right) & \text{if } 0.125\,\text{eV} \le E < 0.8208\,\text{MeV} \\ \left(1.9228 \times 10^{-16}\right) \exp\left(\dfrac{-E}{0.965}\right) \sinh\left(\sqrt{2.29\,E}\right) & \text{if } 0.8208\,\text{MeV} \le E < 20\,\text{MeV} \end{cases} \tag{3.31}$$

which is plotted in Figure 3.53.

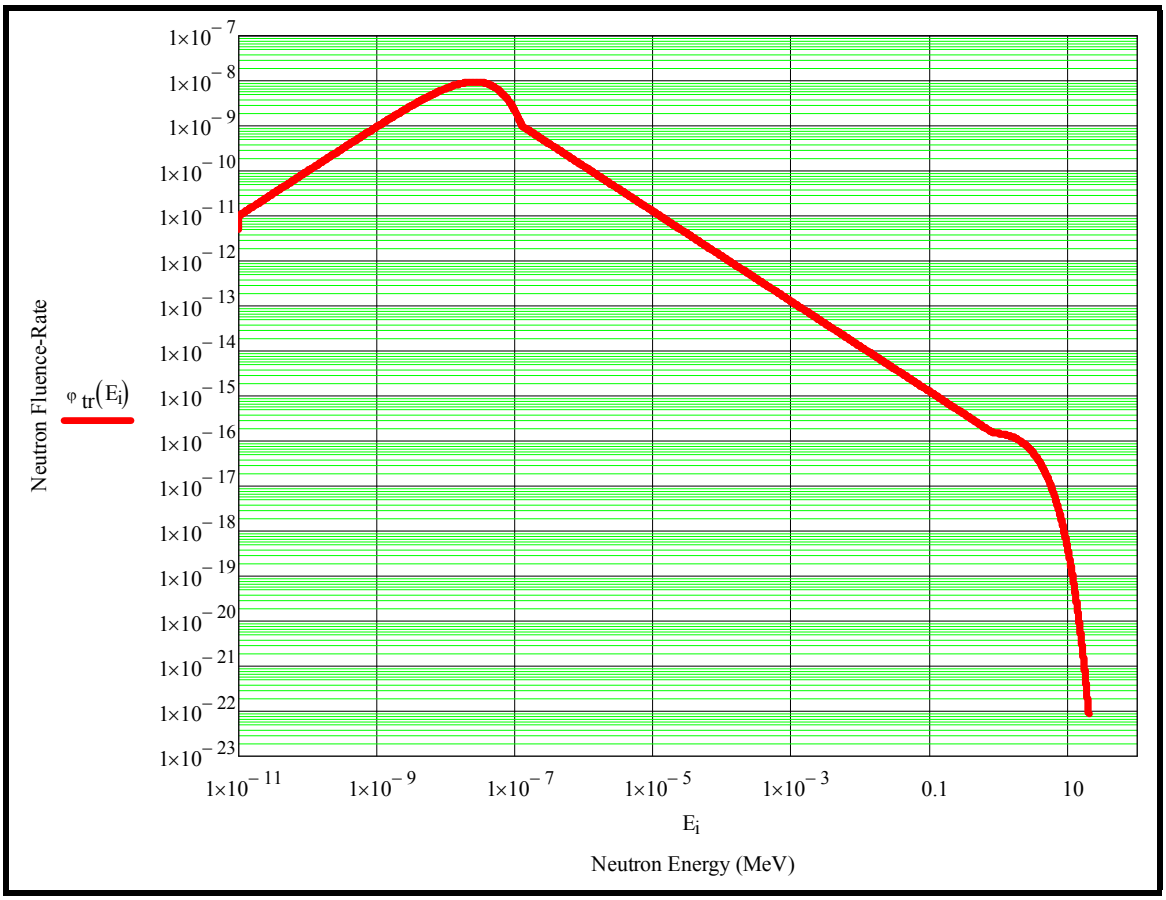

Figure 3.53: *A useful representative neutron spectrum in a thermal-spectrum nuclear reactor; this spectrum may be used as a weighting spectrum to calculate few-group cross-sections.*

From right to left in Figure 3.53: The high-energy part of the spectrum is a uncollided prompt fission neutron spectrum. To its left follows a $1/E$ "slowing-down" spectrum, followed in turn by a Maxwellian thermal neutron energy spectrum at thermal energies.

The spectrum of Eq. (3.31), as displayed in Figure 3.53, can be used as a weighting spectrum to calculate reasonably accurate effective neutron cross-sections for thermal-spectrum reactor applications.

The following MathCAD worksheet shows how effective cross-sections may be calculated by using a representative weighting spectrum. Effective cross-sections are calculated in a manner that will preserve reaction rates as accurately as possible.

Weighted Cross-Sections.xmcd

Assignment 3.25

1. Assume that the neutron spectrum in a reactor pressure vessel (RPV) is well represented by Eq. (3.31). Calculate the effective 1-group cross-section for the production of the neutron activation product ^{56}Mn from the ^{55}Mn present in the RPV steel. (Nuclear reaction: $^{55}\text{Mn}(n,\gamma)^{56}\text{Mn}$.)

2. Nickel flux-wires are irradiated in a reactor core to determine the fluence-rate, by using the $^{58}\text{Ni}\,(n,p)\,^{58}\text{Co}$ reaction. Assume that the neutron spectrum is well represented by Eq. (3.31). Calculate the effective 1-group cross-section for the $^{58}\text{Ni}\,(n,p)\,^{58}\text{Co}$ reaction in the reactor. (Hint: your answer should be between 0.1 and 0.2 barn.)

3. Copper flux-wires are irradiated in a reactor core to determine the fluence-rate, by using the $^{63}\text{Cu}\,(n,\gamma)\,^{64}\text{Cu}$ reaction. Assume that the neutron spectrum is well represented by Eq. (3.31). Calculate the effective 1-group cross-section for the $^{63}\text{Cu}\,(n,\gamma)\,^{64}\text{Cu}$ reaction in the reactor. (Hint: your answer should be between 0.002 barn and 0.008 barn.)

Use cross-section data from JANIS.

3.7 Introduction to photon interactions — photon interaction cross-sections

The interactions and shielding of ionising photons will be addressed in detail in a later chapter. Only a single graph will be displayed here.

Figure 3.54 shows linear photon interaction coefficients, $\mu = N\sigma$, for common shielding materials.

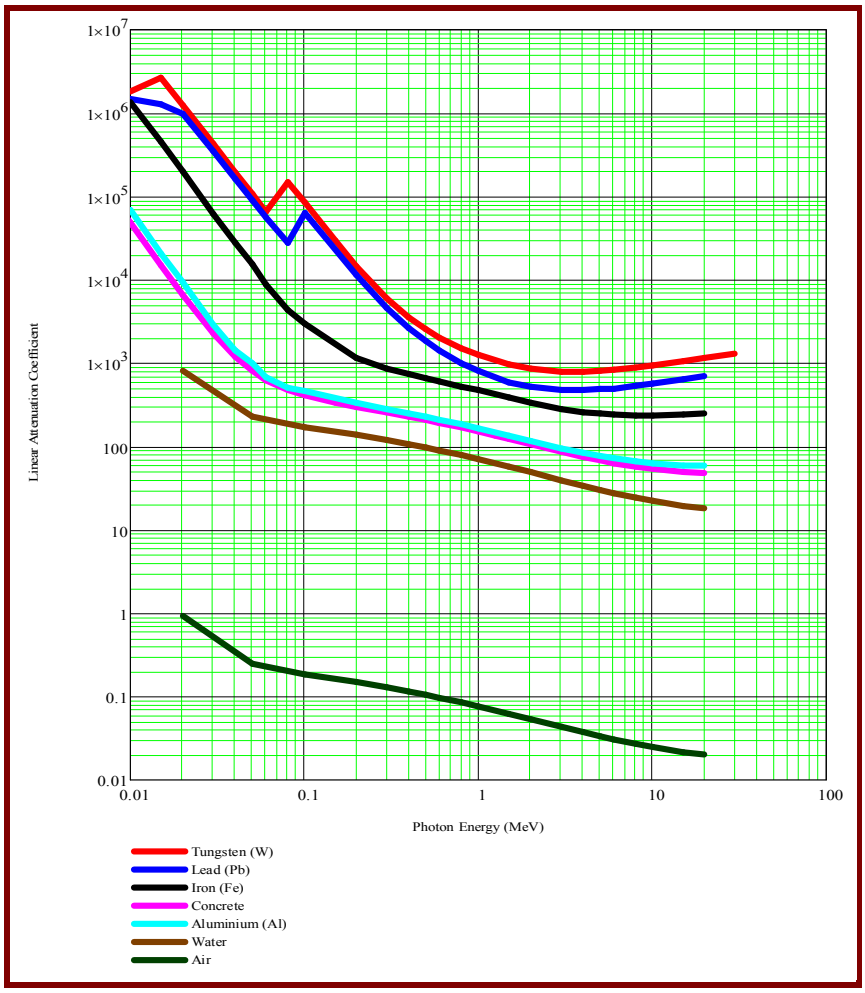

Figure 3.54: *Linear interaction coefficients μ for ionising photon interaction in some common materials.*

It is clear from Figure 3.54 that materials of high mass density ρ and high atomic number Z, will be the best shields against ionising photons. Another aspect of photon interactions in the energy range before nuclear reactions induced by photons become possible, is that such photon interaction cross-sections are (1) far simpler than neutron interactions, and (2) only depend on the element and not the isotope.

More detail on ionising photon interactions are given in Chapter 7 on page 340.

Chapter 4: Radioactivity

4.1 Characteristics of radioactivity

Radionuclides

Radioactive nuclides (radionuclides) are unstable because they have too many or too few neutrons relative to the number of protons in the nucleus. Nuclei can also be unstable if they are excessively large[12]. In a quest to reach stability, unstable nuclides undergo nuclear transitions, emitting ionising radiation in the process. This ionising radiation can be particulate and/or electromagnetic, and causes electronic excitation and ionisation when it interacts with matter.

There are in the order of 200 stable nuclides and over 1000 unstable (radioactive) nuclides known to science. A collection of a considerable number of atoms with unstable nuclei is called radioactive material (RAM).

The energy of emitted radiation

Radionuclides emit α-particles, γ-photons, characteristic x-rays, internal conversion electrons and Auger electrons with sharp, characteristic energies. The energy of the two alpha-particles emitted by ^{238}Cm, for example, will always be 6.50965 MeV and 6.46443 MeV, and the energy of the two most abundant gamma-photons emitted by ^{60}Co is always 1.33249 MeV and 1.17323 MeV.

The energy of electrons emitted during beta transition, is an exception — beta-electrons have a continuous energy spectrum. What is the reason for this phenomenon? When a beta-electron is emitted, the energy is divided between three particles: (1) the beta-electron, (2) an electron-neutrino ν_e and (3) the recoiling nucleus. The neutrino is a lepton with no charge and an exceedingly minute mass. When energy and momentum are shared between 3 particles, energies have a wide distribution, and are not sharp and unique. Consequently, a beta-electron may be emitted with an energy varying in a continuous spectrum from zero to a maximum energy, E_{max}, which is characteristic of the radionuclide. (The neutrino carries off the balance of the energy, minus a small recoil energy that is imparted to the recoiling nucleus. Accordingly, the neutrino will have an energy distribution that is close to the complement of the energy distribution of the electron.) The average energy of the beta-electron energy spectrum is generally around 40% of the maximum beta energy, E_{max}.

[12] See the lecture notes, *Nuclear Physics or Nuclear Engineers,* for an explanation — download this from website **www.radiation-shielding.co.za** free of charge.

The radioactive transition law

When a radioactive "parent" nucleus undergoes a radioactive transition, it produces another nucleus, known as the product nucleus, progeny nucleus or "daughter" nucleus. The exact detail of any individual radioactive transition process is random, so that radioactivity is described in terms of statistically averaged quantities over events in large amounts of nuclei.

If a sample contains N nuclei of a radioactive nuclide, the number δN of radioactive nuclei that will undergo a transition in time δt, will be proportional to the number of nuclei, N. If δN is the increment in the number of radioactive nuclei in time δt,

$$\begin{aligned} \delta N &\propto -N\delta t \\ &= -\lambda N \delta t \\ \therefore \frac{dN}{dt} &= -\lambda N \end{aligned} \tag{4.1}$$

The constant of proportionality, λ, is known as the radioactive transition constant, and it has a unique value for every radionuclide. We can write Eq. (4.1) as

$$\frac{dN}{N} = -\lambda\, \delta t.$$

If there are N_0 nuclei at $t = 0$, and N nuclei at the general time $t \geq 0$, integration of this differential equation gives

$$\begin{aligned} \int_{N_0}^{N} \frac{dN'}{N'} &= -\lambda \int_{t=0}^{t} dt' \\ \therefore \ln(N) - \ln(N_0) &= -\lambda\,(t-0) \\ \therefore \ln\left(\frac{N}{N_0}\right) &= -\lambda t \\ \therefore N(t) &= N_0 \exp(-\lambda t) \end{aligned} \tag{4.2}$$

Eq. (4.2) gives $N(t)$, the number of nuclei present at time t. The graph of $N(t)$ vs. t therefore follows an exponential curve, as illustrated in Figure 4.1 on page 178.

Radioactive transition series: One sometimes comes across radioactive transition series, where one radionuclide undergoes transition to another radionuclide, etc., until a final stable nuclide is formed. Examples of important radioactive series or transition cascades, include the ^{238}U and ^{232}Th series found in nature. The analytical solution $N_i(t)$ of the system of $i = 1, 2, \ldots I$ coupled ordinary differential equations (ODEs) describing series radioactive transition is rather intimidating and a general (albeit numerically unstable) formalistic analytical solution is set forth in § 4.4 on page 196.

Half-life

The transition of radioactive atoms is a gradual process — the unstable atoms do not all undergo transitions at the same time, but undergoes transitions in a random manner. Every radionuclide undergoes a transition at a characteristic average rate, so that the rate at which the number of radionuclides in a given sample decreases, is not the same for all radionuclides. Eventually, the radionuclides undergo transitions to stable final products. Accordingly, the number of radioactive atoms will decrease with time.

To quantify the rate at which radionuclides undergo transition, the concept of the *half-life* of a radionuclide is introduced. The half-life of a radionuclide is the average time it takes for one *half* of the atoms of a collection of a specific radionuclide to undergo radioactive transition. The symbol $T_{½}$ or T_{half} denotes half-life. The half-life of a radionuclide is a measure of the rate at which the nuclide undergoes radioactive transition. Each radionuclide has its own unique half-life, which is independent of its chemical or physical state. Half-lives of radionuclides range from nanoseconds to billions of years.

Radioactive transition is a random process which follows a characteristic exponential curve — as illustrated in Figure 4.1 on page 178.

We now derive the relationship between the halflife $T_{½}$ and the transition constant λ of a radionuclide. According to the definition of halflife,

$$\begin{aligned} N(t) &= \frac{1}{2}N_0 \\ &= N_0\exp(-\lambda T_{½}) \\ \therefore N_0\exp(-\lambda T_{½}) &= \frac{1}{2}N_0 \\ \therefore T_{½} &= \frac{\ln(2)}{\lambda} \\ \therefore \lambda &= \frac{\ln(2)}{T_{½}} \end{aligned} \tag{4.3}$$

Example 4.1

An atom of the element cesium (symbol ≡ Cs) has 55 protons in the nucleus. Atoms of one particular isotope of this element have 82 neutrons in the nucleus. The symbol of this radioactive isotope is ^{137}Cs $(55 + 82 = 137)$. The radionuclide ^{137}Cs has a half-life of approximately 30 years. If we start with, say, 10 000 ^{137}Cs atoms, only half, i.e. 5000 ^{137}Cs atoms, will (on average) be left after 30 years. After a further 30 years, only half of the 5000 atoms, i.e. 2500 atoms, will (on average) be left, etc. This is illustrated in Figure 4.1 on page 178.

Activity — transition rate

The activity of radioactive material is the expectation value of the transition rate, i.e. the number of transitions that occur per second. Activity is transition rate and its unit is the becquerel (Bq). The becquerel is that quantity of a radioactive material in which 1 atom undergoes a transition per second:

$$1 \text{ Bq} \equiv 1 \text{ transition per second.}$$

For most practical applications, the becquerel is a very small quantity of activity, so that we commonly employ multiples of becquerel to express the quantity of radioactive material, e.g.:

$$1 \text{ kilobecquerel (kBq)} = 10^3 \text{ Bq}$$

$$1 \text{ megabecquerel (MBq)} = 10^6 \text{ Bq}$$

$$1 \text{ gigabecquerel (GBq)} = 10^9 \text{ Bq}$$

$$1 \text{ terabecquerel (TBq)} = 10^{12} \text{ Bq}$$

The curie (Ci) is an older unit of activity: $1 \text{ Ci} = 3.7 \times 10^{10}$ transitions per second, i.e. $1 \text{ Ci} = 3.7 \times 10^{10}$ Bq. The curie is a very large amount of radioactivity, so that submultiples of this unit, e.g. microcurie (10^{-6} Ci) and millicurie (10^{-3} Ci), are often used in practice.

Because every radionuclide transitions at a characteristic average rate, the activity of radioactive material will depend directly on the number N of radionuclides in the material, and the constant of proportionality is called the radioactive transition constant λ. Because the number N of radionuclides decrease with a given half-life $T_{½}$, the activity A of radioactive material will decrease with the same half-life.

The relationship between activity, A, and the number of nuclides, N, is that activity equals the time-rate at which N changes, because A is defined as the number of transitions of a given nuclide per unit time. Because N is decreasing as a function of time, $\frac{dN}{dt}$ is negative, so that a negative sign must be introduced to keep A positive:

$$\begin{aligned} A(t) &= \frac{-dN(t)}{dt} \\ &= \frac{d}{dt}(N_0 \exp(-\lambda t)) \\ &= -N_0[-\lambda \exp(\lambda t)] \\ &= \lambda[N_0 \exp(-\lambda t)] \\ &= \lambda\, N(t) \end{aligned} \tag{4.4}$$

From Eq. (4.4) it follows that activity A is directly proportional to the number of

radionuclides, N, that are present. Further,

$$A(t) = \lambda\, N(t)$$

$$= \lambda\, N_0 \exp(-\lambda t)$$

$$\therefore A(t) = A_0 \exp(-\lambda t) \tag{4.5}$$

where

$$A_0 = \lambda N_0 \tag{4.6}$$

is the initial activity at time $t = 0$.

Radioactive decay is a stochastic process, and nuclide numbers $N(t)$ as well as activities $A(t)$ are always subject to statistical fluctuations.

Figure 4.1 shows how the activity of a source containing one specific radionuclide, will diminish by a factor 2 every $T_{½}$.

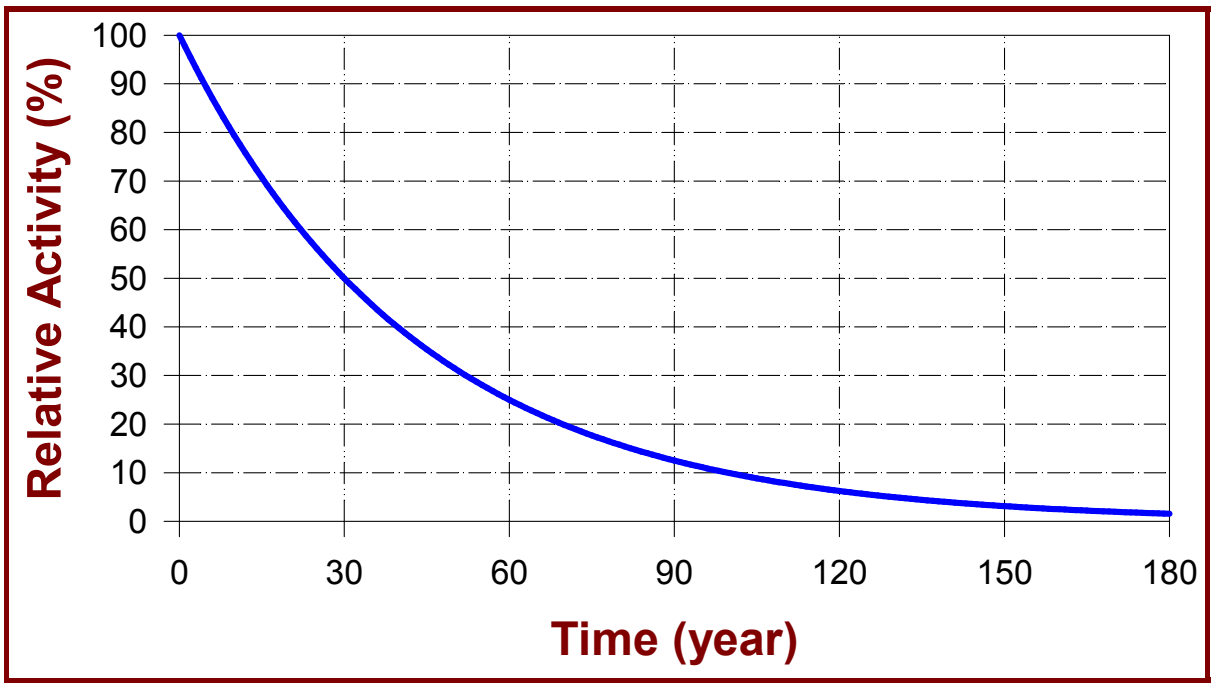

Figure 4.1: *The decrease of radioactivity with time for the radionuclide ^{137}Cs, which has a half-life of 30 years.*

In Figure 4.1 it is seen that after 30 years, 50% of the original activity will remain, after 60 years, 25% will remain, etc. The above smooth curve is the expectation value of the activity; the real activity as a function of time will be subject to statistical fluctuations, which will increase as relative percentage, as the activity diminishes.

The fraction of the original activity of a specific radionuclide that will be left after different half-lives, are summarised in Table 4.1.

***Table 4.1**: The fraction of activity of a specific radionuclide that will be left after different half-lives.*

Number of half-lives	Remaining fraction of original activity: $\frac{A}{A_0}$
1	$\left(\frac{1}{2}\right)^1 = \frac{1}{2}$
2	$\left(\frac{1}{2}\right)^2 = \frac{1}{4}$
3	$\left(\frac{1}{2}\right)^3 = \frac{1}{8}$
4	$\left(\frac{1}{2}\right)^4 = \frac{1}{16}$
5	$\left(\frac{1}{2}\right)^5 = \frac{1}{32}$
10	$\left(\frac{1}{2}\right)^{10} = \frac{1}{1024} \approx 10^{-3}$
20	$\left(\frac{1}{2}\right)^{20} = \frac{1}{1\,048\,576} \approx 10^{-6}$
N	$\left(\frac{1}{2}\right)^N = \frac{1}{2^N}$

Example 4.2

Let us consider what happens in the β^--transition of, e.g., $^{60}_{27}$Co. This nuclide is radioactive and transitions by emitting a beta-electron. This is followed by the emission of a number of γ-rays by the excited product nucleus, in its quest to reach the ground energy state. In the β-transition, the number of protons, Z, will increase by 1, so that the nucleus will contain 1 more proton than before. The atomic number of Co is $Z = 27$; the atomic number of the product nucleus will be $Z = 27 + 1 = 28$, which represents the element nickel (Ni); therefore the product nuclide will be $^{60}_{28}$Ni. Note that the mass number is still $A = 60$, since the sum of the number of protons and neutrons has not changed.

4.2 Radioactive transition calculations — single radionuclide with stable product

The information in Table 4.1 can be applied in solving practical problems.

Example 4.3

Suppose we find that the radiologically dominant nuclide in a specific activated component is ^{60}Co. The halflife of this nuclide is 5.27 years. How long do we have to wait until the activity of the activated component will fall by a factor 10^3?

Table 4.1 shows that a waiting period of 10 halflives is required for the activity to diminish by a factor ~1000, i.e. the required waiting time is 10×5.27 years, i.e. ~53 years.

Example 4.4

Suppose we find that the radiologically dominant nuclide in a specific activated component is ^{60}Co. The halflife of this nuclide is 5.27 years. How long do we have to wait until the activity of the activated component will fall by a factor 10^6?

Table 4.1 shows that a waiting period of 20 halflives is required for the activity to diminish by a factor ~10^6, i.e. the required waiting time is 20×5.27 years, i.e. ~106 years.

Example 4.5

The radionuclide ^{32}P has a half-life of 14.3 days. On January 10, the activity of a ^{32}P sample was 10 μCi. What will the activity be on February 7 of the same year?

February 7 is 28 days after January 10, and

$$A(t = 28\,\text{days}) = 10\ \mu\text{Ci} \times \exp\left(-0.693 \times \frac{28\,\text{days}}{14.3\,\text{days}}\right)$$

$$= 2.6\ \mu\text{Ci}.$$

A quick estimate could also have been made by noting that 28 days is approximately 2 half-lives. So the final activity would roughly be $\frac{1}{2} \times \frac{1}{2}$, i.e. $\frac{1}{4}$ of the original activity, i.e. roughly $\frac{10\ \mu\text{Ci}}{4} \approx 2.5\ \mu\text{Ci}$.

Time to reach a fraction of original activity

Eq. (4.5) on page 178 gives the activity $A(t)$ of a 1-member radionuclide transition series.

How long will it take to reach a specified fraction of the original activity of a radionuclide source? If, after a time t, the activity must be a fraction k of the original activity A_0, then

$$A(t) = kA_0$$

$$\therefore kA0 = A_0\exp(-\lambda t)$$

$$\therefore t = \left(-\frac{1}{\lambda}\right)\ln(k)$$

Now substitute $\lambda = \dfrac{\ln(2)}{T_{½}}$

Then

$$t = \left[-T_{½}\left(\frac{\ln(k)}{\ln(2)}\right)\right] \tag{4.7}$$

Example 4.6

How long will it will take a ^{60}Co source to reach 1.5%, i.e. a fraction 0.015 of its present activity?

$$t = -T_{½}\left(\frac{\ln(k)}{\ln(2)}\right)$$

$$= -5.27\left(\frac{\ln(0.015)}{\ln(2)}\right) \text{ years}$$

$$= 31.9 \text{ years}$$

Example 4.7

After the initial cleanup effort at TMI, approximately 1.514×10^6 litres i.e. 1514 m^3 of radioactive water remained in the basement of the containment building of TMI Unit 2. The principal sources of this activity were ^{137}Cs at 156 µCi/cm^3 and ^{134}Cs at 26 µCi/cm^3. How many atoms of these radionuclides were present per cm^3 in the water, at that time? Also calculate the masses of each radionuclide.

Given: $T_{½}$ of ^{137}Cs is 30.07 years, while $T_{½}$ of ^{134}Cs is 2.0652 years.

Answer:

Let A be the activity of a radionuclide, and let N be the number of radionuclides present. Let $\lambda = \frac{\ln(2)}{T_{½}}$ denote the decay constant for the radioactive transition (i.e. decay).

Definition of activity: $A = \lambda N$. Therefore $N = \frac{A}{\lambda} = \left(\frac{A}{\left(\frac{\ln(2)}{T_{½}}\right)}\right) = \frac{A\,T_{½}}{\ln(2)} = 1.443\,A\,T_{½}$.

Activity of ^{137}Cs in 1 cm^3 of water: 156 µCi ^{137}Cs $= 5.772 \times 10^6$ Bq.

Activity of ^{134}Cs in 1 cm^3 of water: 26 µCi ^{134}Cs $= 9.62 \times 10^5$ Bq.

Halflife of ^{137}Cs: 30.07 years $= 9.489 \times 10^8$ s.

Halflife of ^{134}Cs: 2.0652 years $= 6.517 \times 10^7$ s.

$N_{Cs137} = 1.443 A_{Cs137} \times T\_half_{Cs137} = 7.90 \times 10^{15}$ radionuclide atoms of ^{137}Cs per cc; these will have a mass of only approximately 1.8 µg.

$N_{Cs134} = 1.443 A_{Cs134} \times T\_half_{Cs134} = 9.05 \times 10^{13}$ radionuclide atoms of ^{134}Cs per cc; these will have a mass of only approximately 0.02 µg.

For the sake of interest, the total mass of ^{137}Cs in the TMI Unit 2 containment building, calculates to approximately 2.7 gram, and the total mass of ^{134}Cs in the containment sump water calculates to a mere 30.5 mg.

Half-life of a free neutron

A free neutron is not stable, and undergoes radioactive transition to form a proton, an electron and a neutrino; its halflife is in the order of 10 to 12 minutes.

Assignment 4.1

1. Model the radioactive transition of ^{60}Co ($T_{½} = 5.27124$ years) and ^{137}Cs ($T_{½} = 30.07064$ years) using MathCAD.

2. Given an initial activity of 4 kCi ^{60}Co on 14 April 2002, what will the activity of the source be on 19 October 2015?

3. Given an initial activity of 90 kCi ^{137}Cs on 24 June 2003, what will the activity of the source be on 29 September 2014?

4. Given a measured activity of 7 kCi ^{137}Cs on 24 October 2015, what was the activity of this source on 15 March 2004 (i.e. at a time in the past)?

5. Solve without using a computer: The present activity of a ^{60}Co source is 1 Ci. How long will you have to wait until the activity is 1 µCi?

6. Solve without using a computer: The present activity of a ^{60}Co source is 1 Ci. How long will you have to wait until the activity is 1 nCi?

7. Solve without using a computer: The present activity of a ^{60}Co source is 1 Ci. How long will you have to wait until the activity is 1 pCi?

8. Solve without using a computer: The present activity of a ^{137}Co source is 1 TBq. How long will you have to wait until the activity is 1 kBq?

9. The present average natural abundance of ^{235}U is 0.71% and that of ^{238}U is 99.29%. Suppose that the planet earth existed 3 billion years ago. Calculate the natural abundances of the above two uranium isotopes 3 billion years ago.

10. Tritium has a half-life of 12.5 years against β^- transition. What fraction of a sample of pure tritium will remain after 35 years?

11. One gram of ^{226}Ra (radium-226) has an activity of 1 curie. From this fact, determine the half-life of ^{226}Ra.

4.3 Radioactive transition calculations: 2 successive radionuclides

Suppose a radionuclide of which there are $N_1(t)$ units in a given sample, transitions to radionuclide 2, the number of which there is in the sample at a given time, is denoted by $N_2(t)$. Radionuclide 2 in turn transitions to a stable product nucleus with number $N_3(t)$ in the sample. This system is described by a set of 3 coupled, linear ordinary differential equations,

$$\frac{dN_1}{dt} = -\lambda_1 N_1$$

$$\frac{dN_2}{dt} = \lambda_1 N_1 - \lambda_2 N_2$$

$$\frac{dN_3}{dt} = \lambda_2 N_2$$

with initial conditions

$$N_1(t=0) = N_1(0)$$

$$N_2(t=0) = 0$$

$$N_3(t=0) = 0$$

Solving these equations leads to the solution set,

$$N_1(t) = N_1(0)\exp(-\lambda_1 t)$$

$$N_2(t) = N_1(0)\left(\frac{\lambda_1}{\lambda_2 - \lambda_1}\right)[\exp(-\lambda_1 t) - \exp(-\lambda_2 t)]$$

$$N_3(t) = N_1(0)\left[1 + \left(\frac{\lambda_1}{\lambda_2 - \lambda_1}\right)\exp(-\lambda_2 t) - \left(\frac{\lambda_2}{\lambda_2 - \lambda_1}\right)\exp(-\lambda_1 t)\right] \tag{4.8}$$

Because $A_i(t) = \lambda_i N_i(t)$, and because the last radionuclide is stable, the activities of the 3 nuclides will be given by,

$$A_1(t) = A_1(0)\exp(-\lambda_1 t)$$

$$A_2(t) = A_1(0)\left(\frac{\lambda_2}{\lambda_2 - \lambda_1}\right)[\exp(-\lambda_1 t) - \exp(-\lambda_2 t)]$$

$$A_3(t) = 0 \tag{4.9}$$

4.3.1 Secular equilibrium

If the halflife of the product radionuclide is far less than that of the parent radionuclide, secular equilibrium is established. The activity of the product nuclide "grows in" to reach that of the parent radionuclide, and subsequently their activities will be practically the same and decrease at the same rate.

As an example, we model the ^{90}Sr/^{90}Y pair. The radionuclide ^{90}Sr transitions to ^{90}Y; the halflife of ^{90}Sr is 29.1 years and the halflife of ^{90}Y is 64.2 hours. A high degree of secular equilibrium will be established within approximately 7 to 8 halflives of the product ^{90}Y, i.e. approximately 7×64 h $\approx$ 19 days; this is illustrated in Figure 4.2.

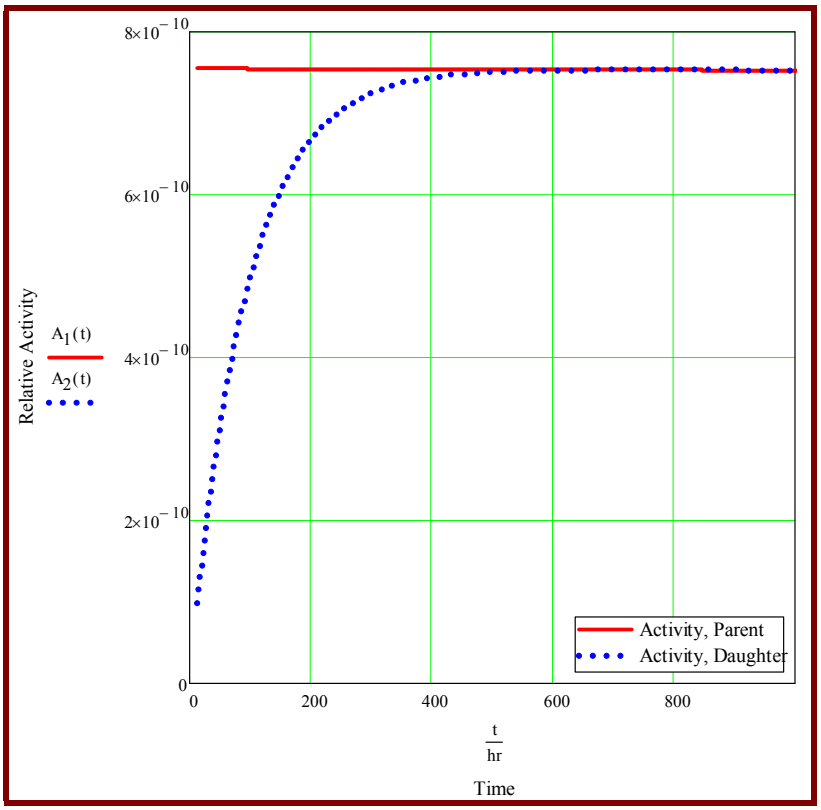

Figure 4.2: *The activities of ^{90}Sr ($T_{½} = 29.1$ years) and its transition product ^{90}Y ($T_{½} = 64.2$ hours), as a function of time.*

Mathematically, a large value of $T_{½}$ implies a very small value of λ, as a result of the reciprocal relationship between these variables. If the halflife of the product radionuclide (chain member 2) is far less than that of the parent radionuclide (chain member 1), the transition constants are related as $\lambda_2 \gg \lambda_1$, so that the expression

$$A_2(t) = A_1(0)\left(\frac{\lambda_2}{\lambda_2 - \lambda_1}\right)[\exp(-\lambda_1 t) - \exp(-\lambda_2 t)]$$

may be approximated as $A_2(t) = A_1(0)\left(\frac{\lambda_2}{\lambda_2}\right)[\exp(-\lambda_1 t) - \exp(-\lambda_2 t)]$, because $\lambda_2 - \lambda_1 \approx \lambda_2$ for $\lambda_2 \gg \lambda_1$. At large values of t, the term $\{\exp(-\lambda_2 t)\} \ll \{\exp(-\lambda_1 t)\}$, so that the activity of the daughter radionuclide will tend to the limiting value

$$A_2(t) = A_1(0)\left(\frac{\lambda_2}{\lambda_2}\right)[\exp(-\lambda_1 t) - \exp(-\lambda_2 t)]$$

$$= A_1(0)\exp(-\lambda_1 t)$$

$$= A_1(t).$$

That is, when the halflife of the daughter radionuclide is significantly shorter than that of the parent radionuclide, *secular radioactive equilibrium* is established and the activity of the daughter radionuclide grows in to reach the *same activity* as that of the parent radionuclide.

4.3.2 Transient equilibrium

If the halflife of the product radionuclide is only slightly shorter than that of the parent radionuclide, transient equilibrium is established. The activity of the product radionuclide *overshoots* that of the parent radionuclide, and then decreases more or less at the same rate as the parent radionuclide.

Example: Halflife (parent radionuclide) = 10 years; halflife (progeny radionuclide) = 8 years.

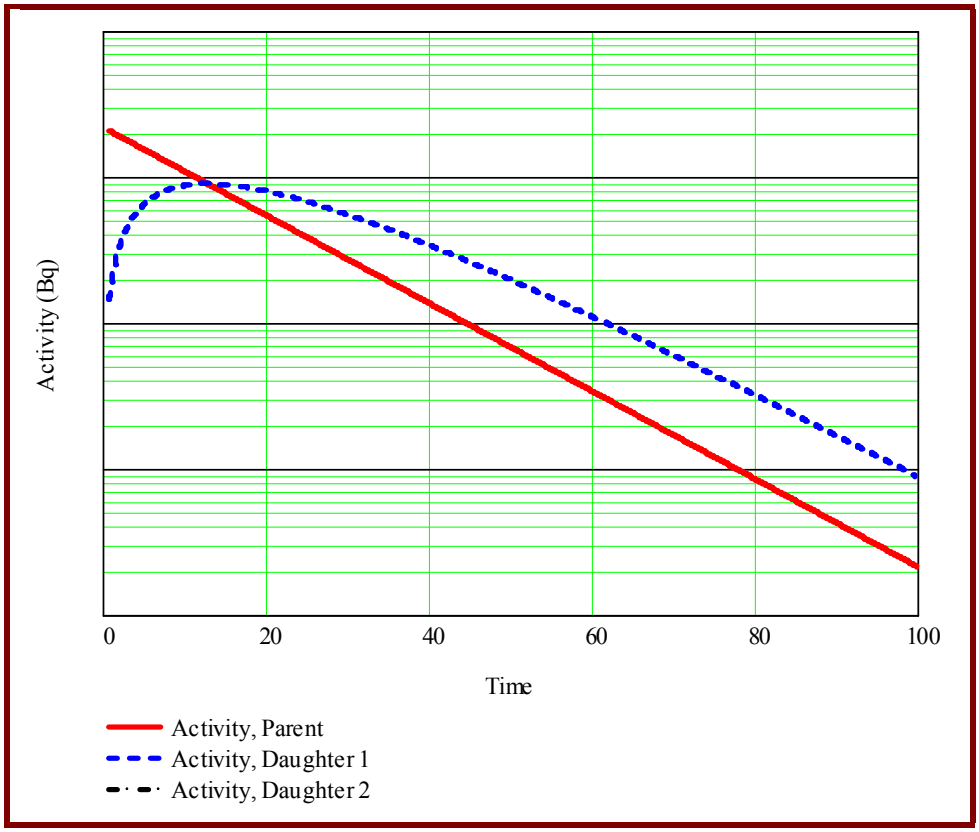

Figure 4.3: *The establishment of transient equilibrium between a radioactive nuclide and a radioactive product nucleus with a somewhat shorter halflife.*

4.3.3 No equilibrium

If the halflife of the product is larger than that of the parent nuclide, no equilibrium will ever be established.

Example: $T_{½}$(parent radionuclide) = 10 years; $T_{½}$(product radionuclide) = 100 years.

The failure to establish any equilibrium between the activities of the parent and the daughter radionuclide, is illustrated in Figure 4.4.

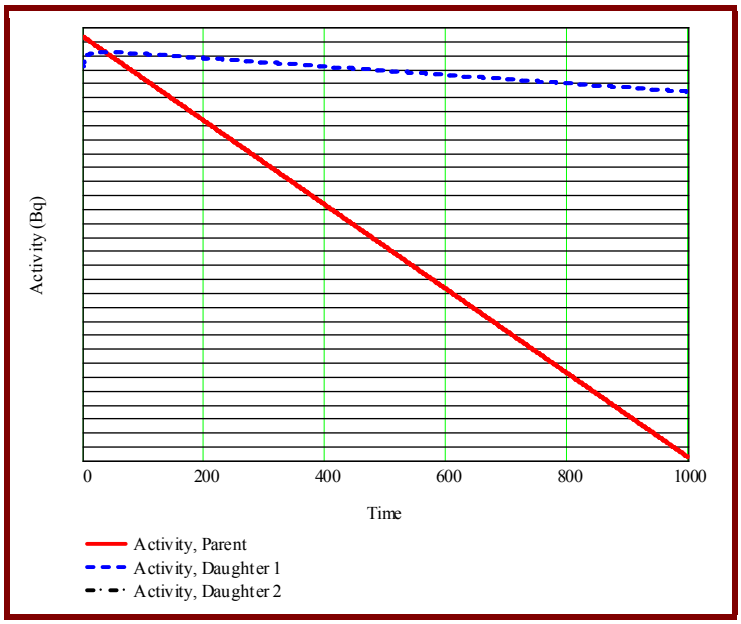

Figure 4.4: *When the halflife of a radioactive nuclide is shorter than the halflife of its radioactive product nucleus, no equilibrium is established.*

4.3.4 Source term calculation for radionuclide doublets such as $\{^{90}\text{Sr}\text{-}^{90}\text{Y}\}$, $\{^{99}\text{Mo}\text{-}^{99m}\text{Tc}\}$ and $\{^{137}\text{Cs}\text{-}^{137m}\text{Ba}\}$

General method for the generation of an EY-matrix for a radionuclide doublet

Radioactive transition equilibrium can only be established in a radioactive doublet, if the halflife of the daughter radionuclide is shorter than that of the parent nuclide. If radioactive transition equilibrium is established, the equilibrium activity ratio AR between the daughter or progeny radionuclide (subscript D) and the parent radionuclide (subscript P) will be

$$AR(R_{\text{br}}, T_P, T_D) = \lim_{t\to\infty}\left[\frac{A_D(t)}{A_P(t)}\right] = R_{\text{br}} \times \left(\frac{T_P}{T_P - T_D}\right) \tag{4.10}$$

where R_{br} is the branching ratio for the formation of the progeny nuclide from the parent, T_P is halflife of the parent radionuclide, T_D is the halflife of the daughter radionuclide, the symbol A denotes activity and the symbol t denotes time.

In the calculation of the $\{(\text{Line Energy}); (\text{Emission Yield})\}$ or EY-matrix for a radionuclide doublet, it is assumed that full equilibrium exists between the parent and the daughter radionuclide. This is, radiologically, the most conservative assumption possible.

To calculate an EY matrix (EY = photon **E**nergy; emission **Y**ield) for a radionuclide doublet, the following method is followed:

- Take ionising photon EY-matrixes for the parent nuclide P and the daughter nuclide D from ICRP-107 (2008), and delete all rows where the particle energies is below the photon energy cutoff of 1 keV (this holds for MCNP5 and MCNPX 2.7).
- Now multiply the Y-column of the EY-matrix of the daughter radionuclide D by the equilibrium activity ratio $AR(R_{\text{br}}, T_P, T_D)$ as given in Eq. (4.10).
- Next, the original $[EY_P]$ matrix and the adjusted $[EY_D]$ matrix are vertically stack-joined to form the EY matrix for the $\{P\text{-}D\}$ radionuclide doublet. It may be sorted from e.g. high to low energy, and a test should be run to make certain that each energy is unique, i.e. a duplicate-energy consolidation algorithm should be run.
- The two columns of this new EY matrix, i.e. $[EY_{\{P\text{-}D\}}]$, are used as follows in the MCNP input data set: the E-column becomes the SI card (line emission energies), while the Y-column becomes the SP card (corresponding emission probabilities).

Note that the value $AR(R_{\text{br}}, T_P, T_D) = \lim_{t\to\infty}\left[\frac{A_D(t)}{A_P(t)}\right]$ is unique for every radionuclide doublet.

Generation of the EY-matrix for the radionuclide doublet $\{^{99}\text{Mo-}^{99m}\text{Tc}\}$

It is assumed that, initially, only ^{99}Mo is present in a purified product sample. The parent radionuclide ^{99}Mo has a halflife of $T_1 = 2.7475$ days, i.e. 65.94 hours, while its radioactive progeny, ^{99m}Tc, which is formed with a branching ratio of $\boxed{R_{\text{br}} = 0.8791925}$, has a halflife of $T_2 = 6.015$ hours. After approximately eight daughter half-lives, i.e. $8 \times T_2$, i.e. circa 48 hours i.e. 2 days, a very high degree of transition equilibrium between the radioactive parent nuclide ^{99}Mo and the radioactive progeny nuclide ^{99m}Tc, will be established. In the calculation of the $\{(\text{Line Energy}); (\text{Emission Yield})\}$ i.e. the EY-matrix for the $\{^{99}\text{Mo-}^{99m}\text{Tc}\}$ radionuclide doublet, it is assumed that full equilibrium exists between the parent ^{99}Mo and the daughter radionuclide ^{99m}Tc. This is, radiologically, the most conservative assumption possible.

To calculate an EY matrix (EY = photon **E**nergy; emission **Y**ield) for the $\{^{99}\text{Mo-}^{99m}\text{Tc}\}$ radionuclide doublet, the following method is followed:

- Take ionising photon EY-matrixes for ^{99}Mo and ^{99m}Tc from ICRP-107 (2008), and delete all rows where the particle energies are below the photon energy cutoff of 1 keV (this holds for MCNP5 and MCNPX 2.7).
- Now multiply the Y-column of the EY-matrix of the daughter radionuclide ^{99m}Tc by the equilibrium activity ratio $AR(R_{\text{br}}, T_P, T_D)$ as given in Eq. (4.10), which evaluates to $AR(R_{\text{br}}, T_P, T_D) = \mathbf{0.96744}$ for the $\{^{99}\text{Mo-}^{99m}\text{Tc}\}$ radionuclide doublet.
- Next, the original $\left[EY_{(^{99}\text{Mo})}\right]$ matrix and the adjusted $\left[EY_{(^{99m}\text{Tc})}\right]$ matrix are vertically stack-joined to form the consolidated EY matrix for the $\{^{99}\text{Mo-}^{99m}\text{Tc}\}$ radionuclide doublet in full equilibrium. It may be sorted from e.g. high to low energy, and it should be verified that each energy is unique, i.e. an energy-duplicate consolidation algorithm should be run.
- The two columns of this new EY matrix, i.e. $\left[EY_{\{^{99}\text{Mo-}^{99m}\text{Tc}\}}\right]$, are used as follows in the MCNP input data set: The E-column becomes the SI card (line emission energies; L), while the Y-column becomes the SP card (corresponding emission probabilities; D).

MathCAD worksheets for the calculation of source terms for the radionuclide pairs $\{^{90}\text{Sr-}^{90}\text{Y}\}$, $\{^{99}\text{Mo-}^{99m}\text{Tc}\}$, $\{^{137}\text{Cs-}^{137m}\text{Ba}\}$, $\{^{131}\text{I -}^{131m}\text{Xe}\}$ and $\{^{123}\text{Xe-}^{123}\text{I}\}$

The above worksheets are found in the sub-folder

MCNP-SDEF-CALCULATIONS for RA PAIRS

under the folder

MCAD MathModels .

Assignment 4.2

1. Use JANIS to identify the two radionuclide pairs in the list on page 189 that will never reach equilibrium. Explain your answer.

2. Given: The radio-nuclide $^{238}_{92}\mathrm{U}$ undergoes 8 α-particle emissions as well as 6 β^--transitions before a stable nuclide is formed. Determine which stable product is formed.

3. If you start with a sample of 1 Ci pure $^{90}\mathrm{Sr}$ at $t = 0$, what activity of $^{90}\mathrm{Sr}$ and $^{90}\mathrm{Y}$ will be present at (a) $t = 1$ day, (b) $t = 10$ days and (c) $t = 1$ year?

4. If you start with a sample of 1 Ci pure $^{90}\mathrm{Sr}$ at $t = 0$, express the activity ratio $A\left(^{90}\mathrm{Y}\right)/A\left(^{90}\mathrm{Sr}\right)$ at the following times:
   (a) $t = 1\,T_{½}$
   (b) $t = 2\,T_{½}$
   (c) $t = 3\,T_{½}$
   (d) $t = 4\,T_{½}$
   (e) $t = 5\,T_{½}$
   (f) $t = 6\,T_{½}$
   (g) $t = 7\,T_{½}$
   (h) $t = 8\,T_{½}$
   (i) $t = 9\,T_{½}$
   (j) $t = 10\,T_{½}$
   where $T_{½}$ is the half-life of the daughter radionuclide. Now derive some general principles from the above answers. Also plot the above ratio.

5. Calculate an EY matrix (EY = photon **E**nergy; emission **Y**ield) for the $\left\{^{90}\mathrm{Sr}\text{-}^{90}\mathrm{Y}\right\}$ radionuclide doublet and add to your compendium of templates.

6. Calculate an EY matrix (EY = photon **E**nergy; emission **Y**ield) for the $\left\{^{99}\mathrm{Mo}\text{-}^{99\mathrm{m}}\mathrm{Tc}\right\}$ radionuclide doublet and add to your compendium of templates.

7. What unusual and therefore useful property does a $\left\{^{90}\mathrm{Sr} + {}^{90}\mathrm{Y}\right\}$-source have?

4.4 Primordial naturally occurring radionuclides

4.4.1 The most important natural radioactive transition series

In the front-end of the nuclear fuel cycle, natural radioactivity is an important issue. The naturally occurring radionuclides that are of importance in the nuclear fuel cycle, specifically in uranium mining and enrichment, are members of 3 long radioactive series transition chains. These three radioactive transition series, plus an additional unimportant fourth radioactive transition series, are summarised in Table 4.2.

Table 4.2: *Series radionuclides.*

Primordial radionuclide	Half-life (years)	Number of intermediates	Final product	$\frac{T_{½}}{\text{Age of universe}}$
^{238}U	4.46808×10^{9}	14	^{206}Pb	29%
^{235}U	7.03814×10^{8}	12	^{207}Pb	4.6%
^{232}Th	1.40503×10^{10}	10	^{208}Pb	91%
^{237}Np	2.14405×10^{6}	12	^{209}Bi	0.01%

The primordial radionuclides undergo transitions at a very slow rate, and produce several radioactive products *(progeny)* in their respective transition cascades.

Uranium consists primarily of 2 radio-isotopes: Approximately 99.2745% of naturally occurring uranium is ^{238}U, and approximately 0.72% is ^{235}U.

^{232}Th is the most abundant of all naturally occurring radionuclides.

Modern cosmology states that the universe was formed[13] around 15×10^{9} years ago. In the first 100 seconds of the initial "Big Bang," only ^{1}H, ^{2}H, ^{3}He and ^{4}He were produced, along with minute quantities of ^{7}Li. In other words, practically only hydrogen and helium were formed. After approximately 300,000 years, radiation and matter decoupled, and the first generation of stars & galaxies were then formed. In the first generation of stars, heavy elements up to Fe ($Z = 26$) were formed via thermonuclear fusion. Being massive, many of these stars exploded in supernovas. Elements heavier than Fe were formed via nucleon capture reactions, mainly neutron capture, especially during the supernova explosions. The heavy elements entered interstellar space and subsequently contracted gravitationally to form a

[13] Almost two thousand years ago, sages taught from the Hebrew text of Genesis 1 that the universe is 15.3425 billion years old (and NOT 6000 years). *Pirqei Eliezer* mentions 974 successive creations and destructions of life on earth before the present creation; these first 974 previous creations were overturned and made extinct in devastations characterised as *tohu & bohu.* Our planet is very old and composed of ancient stardust.

later generation of stars having planets revolving around them. This explains why elements heavier than Fe have significantly lower natural abundances than elements with $Z \leq 26$. Practically all the elements with $Z \geq 4$ are "stardust" formed by stellar nucleosynthesis (while practically only H, He and Li were formed at the very beginning of the universe, during Big-Bang Nucleosynthesis (BBN)). It is estimated that the solar system was formed around 4.5×10^9 years ago. The heavier elements were not formed during the big bang, but are "stardust" from the supernova explosions of the earlier generations of stars.

Reference to Table 4.2 indicates that only 3 of the 4 radioactive transition series could have survived since the formation of our home planet circa 4.54×10^9 years ago. At present, only the ^{232}Th, ^{238}U and ^{235}U transition series are found in nature. The 4th series, i.e. the ^{237}Np transition series, is not found in nature, because the half-life of ^{237}Np is so short relative to the age of the solar system, that more than 2100 half-lives would have elapsed. For this reason, the ^{237}Np transition series disappeared ages ago. However, since nuclear reactors began operating in the middle of the 20th century, ^{241}Pu ($T_{½} = 14.29031$ years) and ^{241}Am ($T_{½} = 432.60868$ years) have been produced in considerable quantities. ^{241}Pu transitions to ^{241}Am, which in turn transitions to ^{237}Np. In this way, human nuclear technology has recently re-introduced the ^{237}Np transition series to the earth. However, it is generally not found in nature.

All three radioactive transition series of present-day importance, have several characteristics in common:

- The first member of the series always has an extremely long half-life — more than approximately 5% of the estimated age of the universe, which is approximately 15×10^9 years.
- An isotope of the radioactive gas radon (Rn) is a member of every transition cascade.
- The end-product of every transition chain is a stable isotope of lead (Pb).

4.4.2 The ^{238}U transition cascade ("decay series")

The main radionuclides in the ^{238}U radioactive transition cascade or chain are summarised in Table 4.3.

Table 4.3
The radionuclides in the ^{238}U transition chain. Columns 3 and 4 jointly contain the half-life information, while column 5 contains the formation yields of the nuclides.

Number	Nuclide	Halflife	Halflife unit	Yield
1	^{238}U	4.46808×10^{9}	years	1.000000
2	^{234}Th	24.1	days	1.000000
3	^{234m}Pa	1.159	minutes	1.000000
4	^{234}Pa	6.7	hours	0.00150017
5	^{234}U	2.45505×10^{5}	years	1.000000
6	^{230}Th	7.53816×10^{4}	years	0.9989861
7	^{226}Ra	1.60004×10^{3}	years	1.0206151
8	^{222}Rn	3.8235	days	1.0206151
9	^{218}Po	3.098	minutes	1.0202771
10	^{214}Pb	26.8	minutes	1.0202771
11	^{214}Bi	19.9	minutes	1.0206151
12	^{214}Po	1.643×10^{-4}	seconds	1.0202771
13	^{210}Pb	22.20047	years	1.0202771
14	^{210}Bi	5.012	days	1.0206151
15	^{210}Tl	1.3	minutes	0.000214557
16	^{210}Po	138.37604	days	1.0206151
17	^{206}Pb	stable	N/A	1.000000

4.4.3 The ^{235}U transition cascade ("decay series")

The radionuclides in the ^{235}U transition chain are summarised in Table 4.4.

Table 4.4: *The radionuclides in the ^{235}U transition chain. Columns 3 and 4 jointly contain the half-life information, while column 5 contains the formation yields Y_{nf} of each nuclide in the series.*

Nuclide	Halflife_Number	Halflife_Unit	Y_nf = Nuclide Formation Yield
U_235	7.0381400E+08	a	1.000000
Th_231	1.0633300E+00	d	1.0000000
Pa_231	3.2760800E+04	a	1.0000000
Ac_227	2.1772470E+01	a	1.0006388
Th_227	1.8680000E+01	d	0.9868512
Fr_223	2.2000000E+01	m	0.0138089
Ra_223	1.1430000E+01	d	1.0006388
Rn_219	3.9600000E+00	s	1.0006388
Po_215	1.7810000E-03	s	1.0006388
At_215	1.0000000E-04	s	4.00266E-06
Pb_211	3.6100000E+01	m	1.0006388
Bi_211	2.1400000E+00	m	1.0006388
Po_211	5.1600000E-01	s	2.73180E-03
Tl_207	4.7700000E+00	m	0.9979239

4.4.4 The ^{232}Th transition cascade ("decay series")

The radionuclides in the ^{232}Th transition chain are summarised in Table 4.5.

Table 4.5: *The radionuclides in the ^{232}Th transition chain. Columns 2 and 3 jointly contain the half-life information, while column 4 contains the formation yields of the nuclides.*

Number	Nuclide	Halflife	Halflife unit	Yield
1	^{232}Th	1.40503×10^{10}	years	1.0000000
2	^{228}Ra	5.75012	years	0.9992777
3	^{228}Ac	6.15	hours	0.9993945
4	^{228}Th	1.91204	years	0.9997026
5	^{224}Ra	3.66	days	1.0049393
6	^{220}Rn	55.6	seconds	1.0049393
7	^{216}Po	0.145	seconds	1.0049393
8	^{212}Pb	10.64	hours	1.0049393
9	^{212}Bi	1.00917	hours	1.0049499
10	^{212}Po	2.99×10^{-7}	seconds	0.6437228
11	^{208}Tl	3.053	minutes	0.3610784

4.4.5 Calculating nuclide number concentrations and activities in radioactive transition series

The Bateman Equation

In the nuclear physics of naturally occurring primordial radionuclides, we always meet long radioactive transition series. We seek a mathematical expression for the activities of each chain member as a function of time. Let N denote the number of a specific nuclidic species that is present in a sample. Then $N(t)$, the number of nuclides as a function of time t, of the first member of such a transition series, is given by

$$N_1(t) = N_0 \exp(-\lambda_1 t) \tag{4.11}$$

where N_0 is the amount present at $t = 0$, and the transition constant $\lambda = \frac{\ln(2)}{T_{½}}$.

The problem of calculating the radionuclidic concentrations and activities of all the nuclides in a radioactive transition series was solved long ago by Bateman as a favour to Ernest Rutherford in the early days of nuclear physics. Bateman solved the system of coupled first-order linear transition equations via Laplace transforms[14]. The so-called Bateman equation for

[14] Many nuclear physics texts provide discussions of Bateman's equations but they seldom draw attention to the fact that in their full generality the solutions are numerically unstable in finite precision arithmetic. Large actinide or fission product decay chains have coupled species of disparate lifetimes. One problem with transition cascades is that radioactive transition is often accompanied by nuclide transport. In both the geosphere and cosmosphere, therefore, secular disequilibrium is the rule rather than the exception since nuclides have different transport properties even if they belong to the same transition chain. The safest way to solve for the radioactive transition of long chains of nuclides is via a stiff ODE solver in which the absolute and

the number $N_n(t)$ of the n^{th} member of a radioactive transition series, as a function of time, t, is given by

$$N_n(t) = N_0 \left(\prod_{p=1}^{n-1} \lambda_p \right) \sum_{j=1}^{n} \left(\frac{\exp(-\lambda_j\, t)}{\prod_{p=1}^{n} \begin{pmatrix} 1 \text{ if } (\lambda_p - \lambda_j)=0 \\ (\lambda_p - \lambda_j) \text{ otherwise} \end{pmatrix}} \right). \tag{4.12}$$

After having calculated the nuclide numbers, $N_n(t)$, it is very easy to calculate their activities $A_n(t)$ by the following equation,

$$A(t) = \lambda\, N(t),$$

where

$$\lambda = \frac{\ln(2)}{T_{½}}$$

Secular equilibrium in the series transition chains

It is a well known fact that, when the half-life of the first member of a radioactive transition series is considerably longer that of the other series members, secular equilibrium is established after some time. This means that the activity of the individual chain members will tend to the activity of the primordial ancestor radionuclide, which is the continuous source of their formation. Full secular equilibrium will only be reached if there is no separation of the radionuclides, e.g. by the escape of radioactive gases or by water leaching out specific chemical species. The time that it will take for equilibrium to be established, depends on the longest half-life of a chain member (excluding the primordial radionuclide heading the chain).

Let us view the establishment of secular equilibrium in the ^{238}U and ^{232}Th chains.

4.4.6 The ^{238}U transition cascade: Ingrowth, emissions, dose rates and isotopic contributions to the dose rate

Ingrowth in the ^{238}U chain

In the case of the ^{238}U chain, the longest lived series member (excluding ^{238}U itself) is, according to Table 4.3 on page 194, ^{234}U, with a half-life of approximately 0.25 million years. Near-full secular equilibrium is established after about 10 times the half-life of the longest-lived chain member, so that it will take approximately 2.5 million years for equilibrium to be established throughout the ^{238}U transition cascade. This is shown in Figure 4.5.

---

relative error tolerances are selected on the basis of the detection limits of the best analytic techniques for the experimental measurement of a nuclide's concentration.

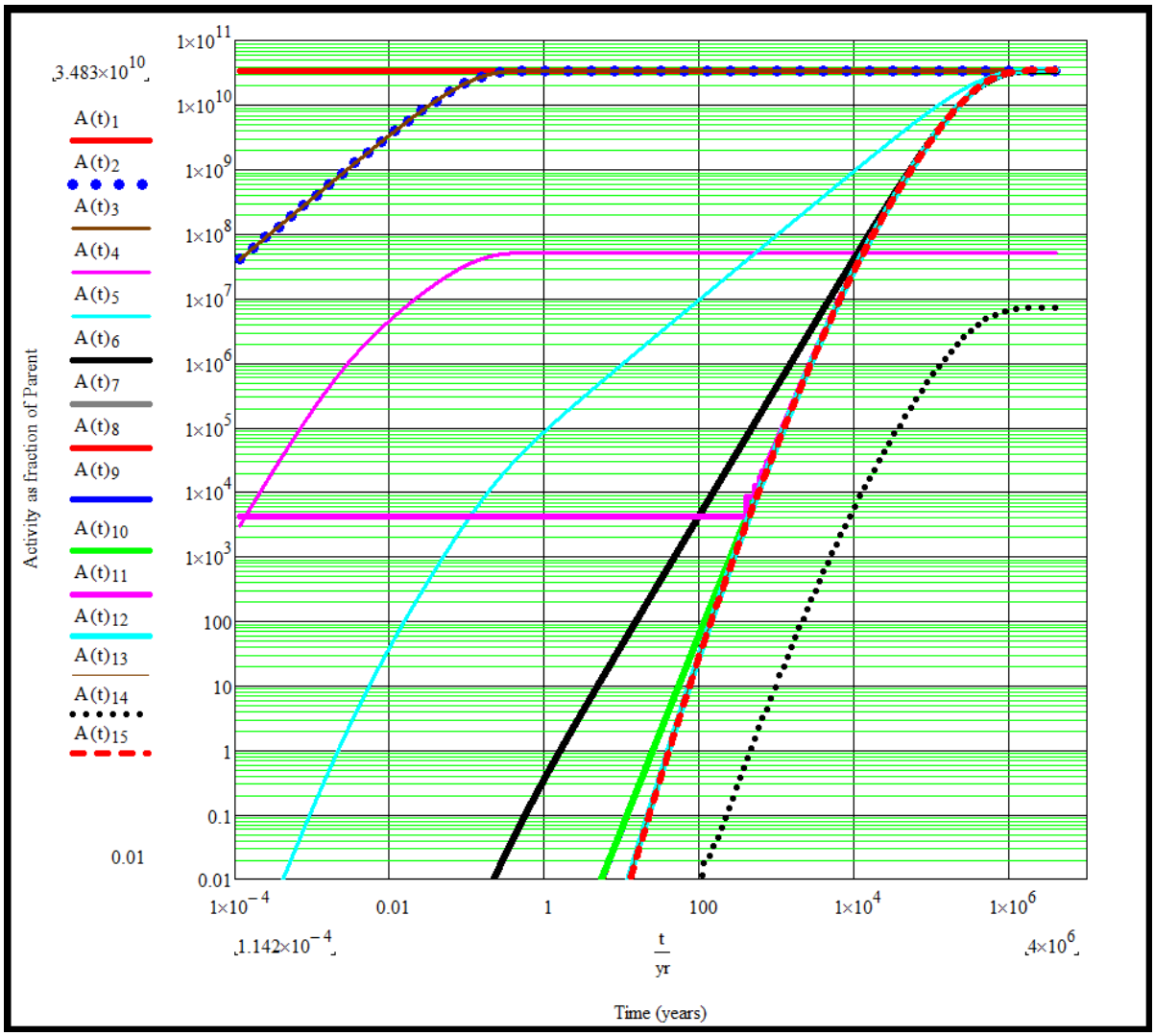

Figure 4.5: *The establishment of near-complete secular equilibrium in the ^{238}U transition chain takes approximately 2 million years — ingrowth is slow.*

The ^{238}U chain nuclides "grow in" in two distinct ingrowth groups:

- A group of radionuclides comprising ^{234}Th, ^{234m}Pa and ^{234}Pa, begins to grow in almost at once, and reaches near-complete equilibrium after 6 months. During the latter stage of ingrowth, the ingrowth rate of this group of nuclides is determined by the 24.1 day half-life of ^{234}Th. Near-complete secular equilibrium is established after approximately $8 \times T_{½}(^{234}Th) \approx 6$ months.

- A second group of radionuclides only reach near-complete equilibrium after approximately 2 million years. During the latter stage of ingrowth, the ingrowth rate of this group of nuclides is determined by the long half-life of ^{234}U. Near-complete secular equilibrium is only established after approximately $8 \times T_{½}(^{234}U) \approx 2$ million years.

Photon emission in the ^{238}U transition chain

About 1930 ionising photons are emitted by the radionuclides in the ^{238}U transition chain. The total number of photons emitted by all the radionuclides in the ^{238}U chain, per 1 transition of the parent ^{238}U, is

$$Y\left(^{238}\text{U series in full equilibrium}\right) = 3.457.$$

The photon energies and their emission yields for the ^{238}U series in full equilibrium are shown in Figure 4.6.

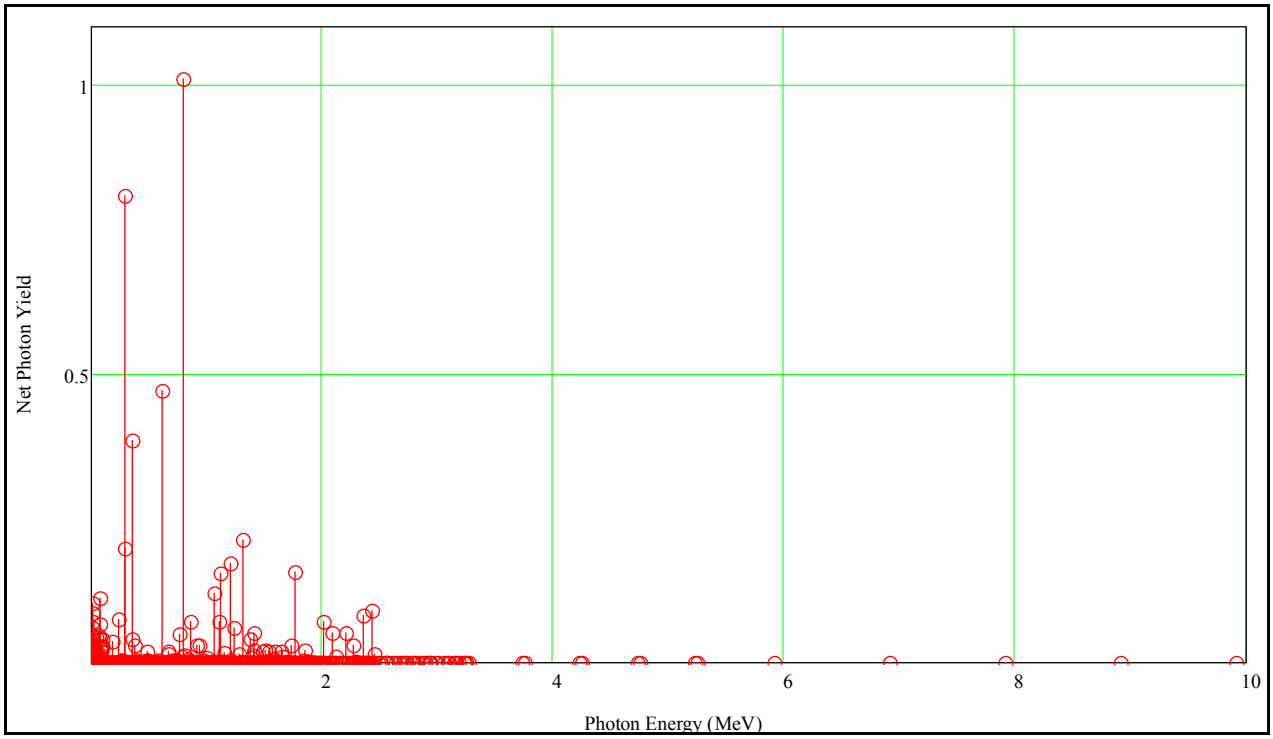

Figure 4.6: *Photons emitted by ^{238}U and its cascade progeny in secular equilibrium — energies and yields. The net yield of every photon, is the nuclide's photon emission yield multiplied by the nuclide formation yield (branching ratio).*

The {Energy, Yield} photon lines in Table 4.6 are indicative of the presence of ^{238}U in a sample.

Table 4.6: *$\{Energy, Yield\}$ photon lines that are indicative of the presence of ^{238}U in a sample.*

Photon Energy (MeV)	Photon Emission Yield per NT
0.60931	0.47068
0.35193	0.38389
0.29522	0.19705
1.76449	0.15723
1.12029	0.15417
0.07741	0.11261
0.01084	0.10325
0.24200	0.07586
0.07506	0.06735
0.01084	0.05932
1.23811	0.05912
2.20421	0.05187
0.76836	0.05044
0.06329	0.04834
0.00246	0.04750
0.04654	0.04339
0.01628	0.04180
1.37767	0.04084

Relative significance of radionuclides in the ^{238}U series, as an external radiation hazard, when secular equilibrium prevails

For a small, unshielded source of ^{238}U in equilibrium with its transition chain products, the percentage contributions of the different radionuclides to the external dose rate from ionising photons, have been calculated; results are presented in Table 4.7.

Table 4.7: *The percentage contributions of the individual cascade progeny in the ^{238}U transition chain, to the effective dose rate field around a small, unshielded, point-like source of ^{238}U in full equilibrium with its chain members.*

Nuclide	Percentage Contribution to Photon Dose Rate
U_238	0.1610
Th_234	0.8188
Pa_234m	0.9223
Pa_234	0.1294
U_234	0.2237
Th_230	0.1815
Ra_226	0.4840
Rn_222	2.4600E-02
Po_218	0.0541
Pb_214	16.461
Bi_214	79.962
Po_214	4.9692E-03
Pb_210	0.5401
Bi_210	2.0160E-05
Tl_210	0.0320
Po_210	0.0006

When viewed a source of ionising photons presenting an external radiation hazard, the ^{238}U chain is dominated by the nuclides ^{214}Pb (16.46%) and, especially, ^{214}Bi (80%). Note that this is only holds true at full ingrowth equilibrium, without any losses of progeny from the system during ingrowth.

Time-dependence of dose-rate near a ^{238}U source that retains all radioactive transition products

The contributions of the different radionuclides in the ^{238}U transition series to the dose rate near a small source of ^{238}U, will be a function of time because the daughter radionuclides "grow in" as a function of time. The time-dependence of the dose rate will depend on the ingrowth as well as the ionising photon emission characteristics (photon energy & photon yield) of each radionuclide. Figure 4.7 shows how the dose rate close to a hypothetical, small

^{238}U source from which no daughter radionuclides escape, increases as a function of time, until full equilibrium is established after approximately 2 million years of ingrowth.

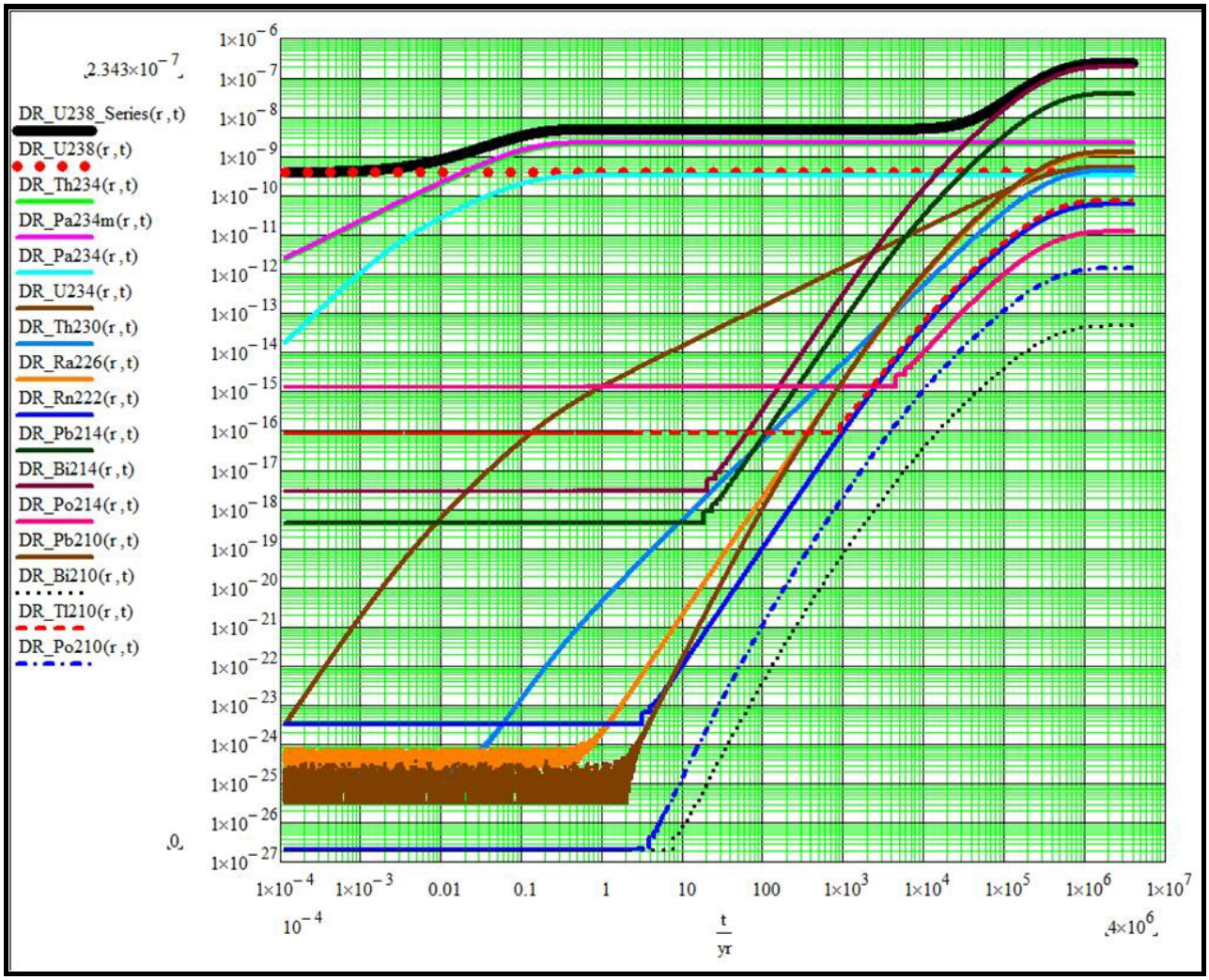

Figure 4.7: *The ionising photon dose-rate close to a hypothetical, small ^{238}U source from which no daughter radionuclides escape during ingrowth, increases as a function of time, until full equilibrium is established after approximately 4 million years of ingrowth.*

At full ingrowth of the ^{238}U series, i.e. after 4 million years, the joint dose rate from ionising photons emitted by all the series radionuclides, present in their equilibrium concentrations, will be approximately 621 times higher than for pure ^{238}U at $t = 0$.

4.4.7 The ^{235}U transition cascade: Ingrowth, emissions, dose rates and isotopic contributions to the dose rate

Ingrowth in the ^{235}U chain

In the case of the ^{235}U chain, the longest lived series member (excluding ^{235}U itself) is, according to Table 4.4 on page 195, the nuclide ^{231}Pa, having a half-life of approximately 33 000 years. Near-full secular equilibrium is established after about 10 times the half-life of the longest-lived chain member, so that it will take approximately 300 000 years for equilibrium to be established throughout the ^{235}U transition cascade. This is shown in Figure 4.8.

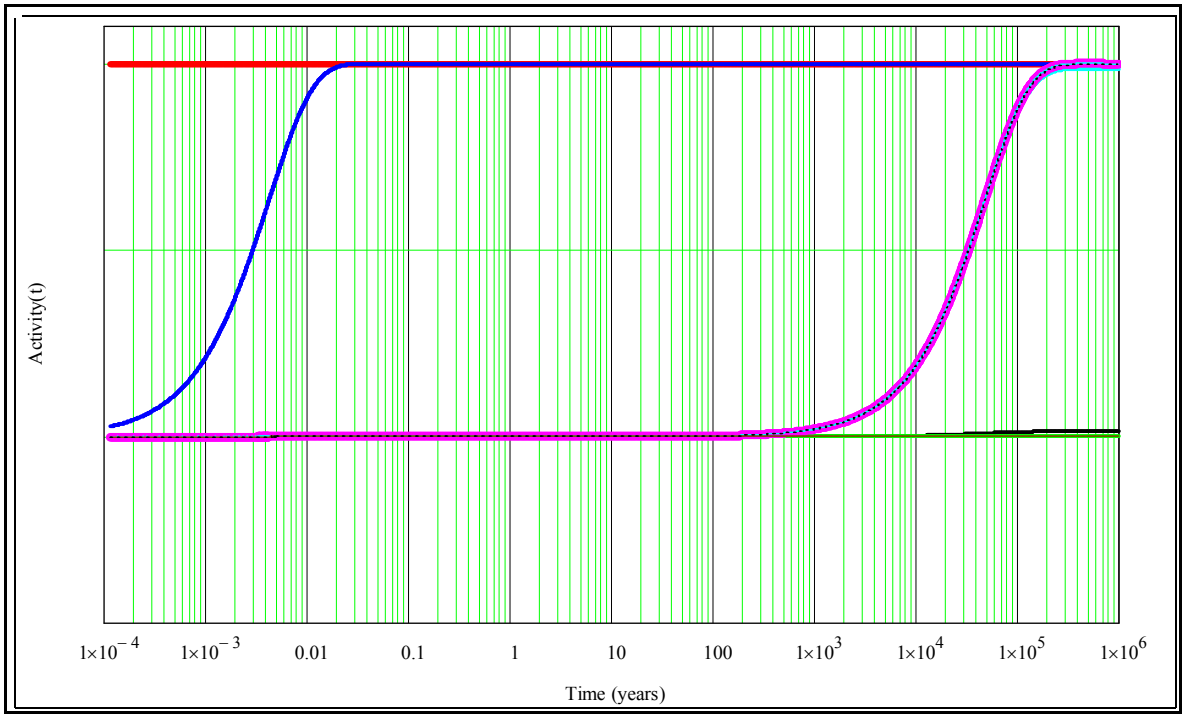

Figure 4.8: *The establishment of near-complete secular equilibrium in the ^{235}U transition chain takes approximately 300 000 years — ingrowth is slow, but not as slow as in the ^{238}U transition cascade.*

Photon emission in the ^{235}U transition chain

About 1840 ionising photons are emitted by the radionuclides in the ^{235}U transition chain. The total number of photons emitted by all the radionuclides in the ^{235}U chain, per 1 transition of

the parent ^{235}U, is

$$Y\left(^{235}\text{U series in full equilibrium}\right) = 6.2624.$$

The photon energies and their emission yields for the ^{235}U series in full equilibrium are shown in Figure 4.9.

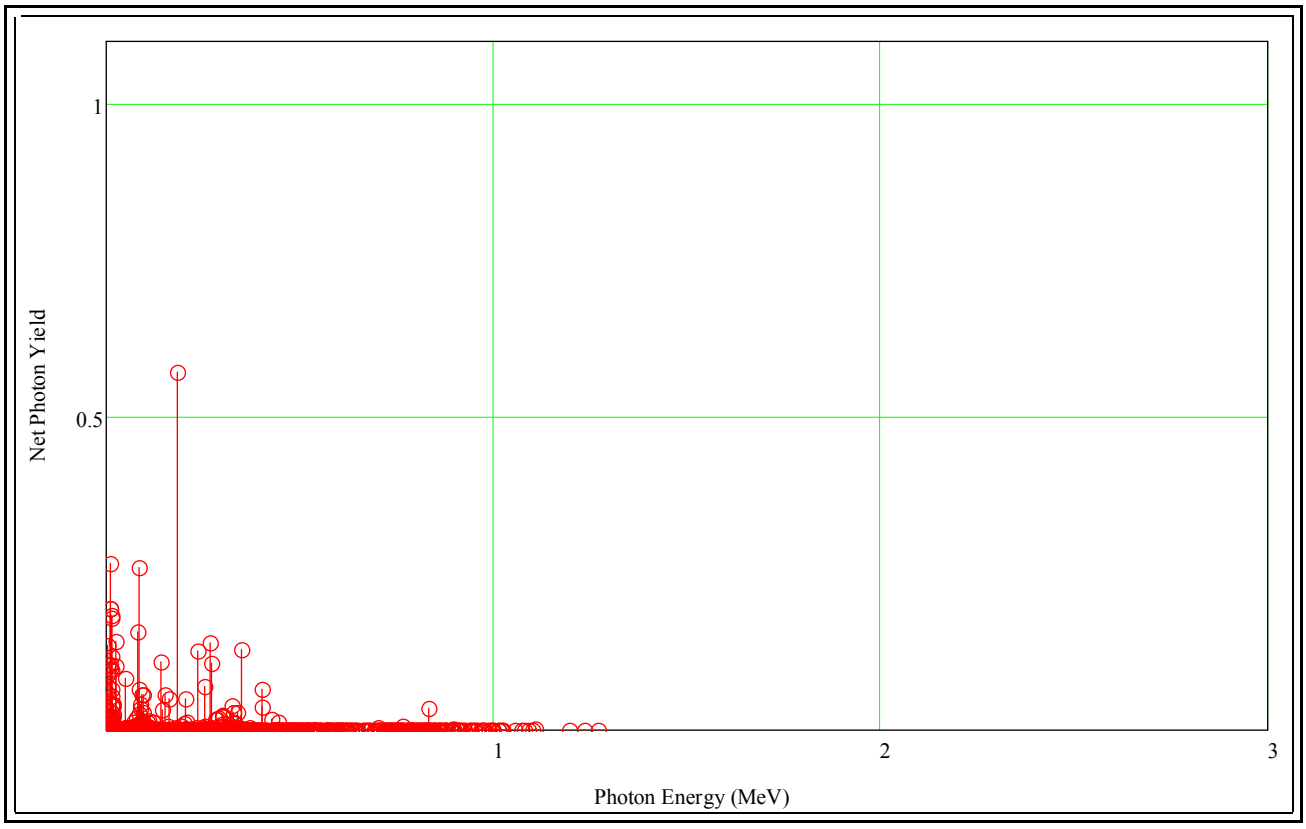

Figure 4.9: *Photons emitted by ^{235}U and its cascade progeny in secular equilibrium — energies and yields. The net yield of every photon, is the nuclide's photon emission yield multiplied by the nuclide formation yield (branching ratio).*

Note that most photons in the ^{235}U series have energies below 0.5 MeV, i.e. they are not very penetrating and are easily shielded. This is in contrast to the high yield of high energy ionising photons in the ^{232}Th series.

Photon-spectrometric fingerprints of the ^{235}U series

The $\{\text{Energy}, \text{Yield}\}$ photon lines in Table 4.8 are indicative of the presence of ^{235}U in a sample, when there is equilibrium with progeny radionuclides.

Table 4.8: *{Energy, Yield} photon lines that are indicative of the presence of ^{235}U in a sample.*

Photon Energy (MeV)	Photon Yield
1.8571500E-01	0.572
1.3299400E-02	0.265
8.4145000E-02	0.259
1.2658900E-02	0.194
1.2344700E-02	0.194
1.6785900E-02	0.183
1.5301300E-02	0.180
8.1368000E-02	0.157
2.5640000E-02	0.141
2.6946300E-01	0.139
3.1706300E-03	0.135
3.5106000E-01	0.129
2.3596000E-01	0.127
1.5783400E-02	0.118
1.4376000E-01	0.110
2.7123000E-01	0.108
2.9857800E-03	0.106
1.2976400E-02	0.105
2.7360000E-02	0.103
1.1729700E-02	0.0990
1.6277600E-02	0.0964

Relative significance of radionuclides in the ^{235}U series, as an external radiation hazard, when secular equilibrium prevails

For a small, unshielded source of ^{235}U in equilibrium with its transition chain products, the percentage contributions of the different radionuclides to the external dose rate from ionising photons, have been calculated; results are presented in Table 4.9.

Table 4.9: *The percentage contributions of the individual cascade progeny in the ^{235}U transition chain, to the effective dose rate field around a small, unshielded, point-like source of ^{235}U in full equilibrium with its chain members.*

RadioNuclide	Percentage Contribution to photon dose rate
U_235	23.5
Th_231	5.67
Pa_231	7.52
Ac_227	0.19
Th_227	19.3
Fr_223	0.14
Ra_223	20.3
Rn_219	8.10
Po_215	0.024
At_215	9.48E-08
Pb_211	8.46
Bi_211	6.55
Po_211	0.00287
Tl_207	0.295

When viewed a source of ionising photons presenting an external radiation hazard, the ^{235}U chain is dominated by the nuclides ^{235}U (23.5%), ^{223}Ra (20.3%), ^{227}Th (19.3%), ^{211}Pb (8.5%), ^{219}Rn (8.1%), ^{231}Pa (7.5%), ^{211}Bi (6.6%) and ^{231}Th (5.7%). Note that this is only holds true at full ingrowth equilibrium, without any losses of progeny from the system during ingrowth.

Time-dependence of dose-rate near a ^{235}U source that retains all radioactive transition products

The contributions of the different radionuclides in the ^{235}U transition series to the dose rate near a small source of ^{235}U, will be a function of time because the daughter radionuclides "grow in" as a function of time. The time-dependence of the dose rate will depend on the ingrowth as well as the ionising photon emission characteristics (photon energy & photon yield) of each radionuclide. Figure 4.10 shows how the dose rate close to a hypothetical, small ^{235}U source from which no daughter radionuclides escape, increases as a function of time, until full equilibrium is established after approximately 4×10^5 years of ingrowth.

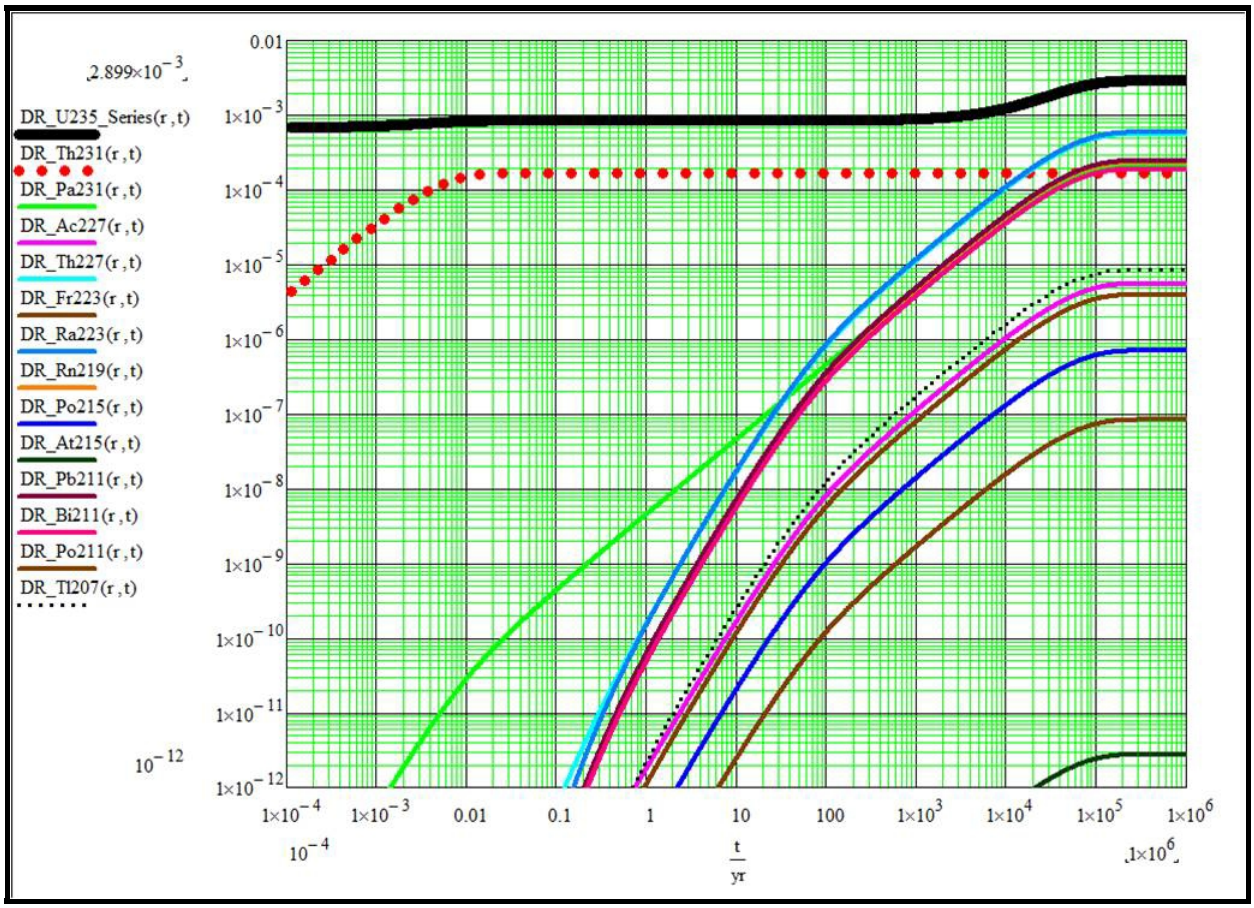

Figure 4.10: *The ionising photon dose-rate close to a hypothetical, small ^{235}U source from which no daughter radionuclides escape during ingrowth, increases as a function of time, until full equilibrium is established after approximately 4×10^5 years of ingrowth.*

At full ingrowth of the ^{235}U series, the joint dose rate from ionising photons from all the series radionuclides, present in their equilibrium concentrations, will be approximately 4.3 times higher than for pure ^{235}U. This factor is far lower than for the ^{238}U and the ^{232}Th series.

4.4.8 The ^{232}Th transition cascade: Ingrowth, emissions, dose rates and isotopic contributions to the dose rate

Ingrowth in the ^{232}Th chain

In the case of the ^{232}Th chain, the longest lived chain member (^{228}Ra) has a half-life of only 5.6 years, so that significant ingrowth will start after approximately 50 days, and near-complete secular equilibrium will be reached after approximately 7×5.6 years ≈ 40 years. This is displayed in Figure 4.11.

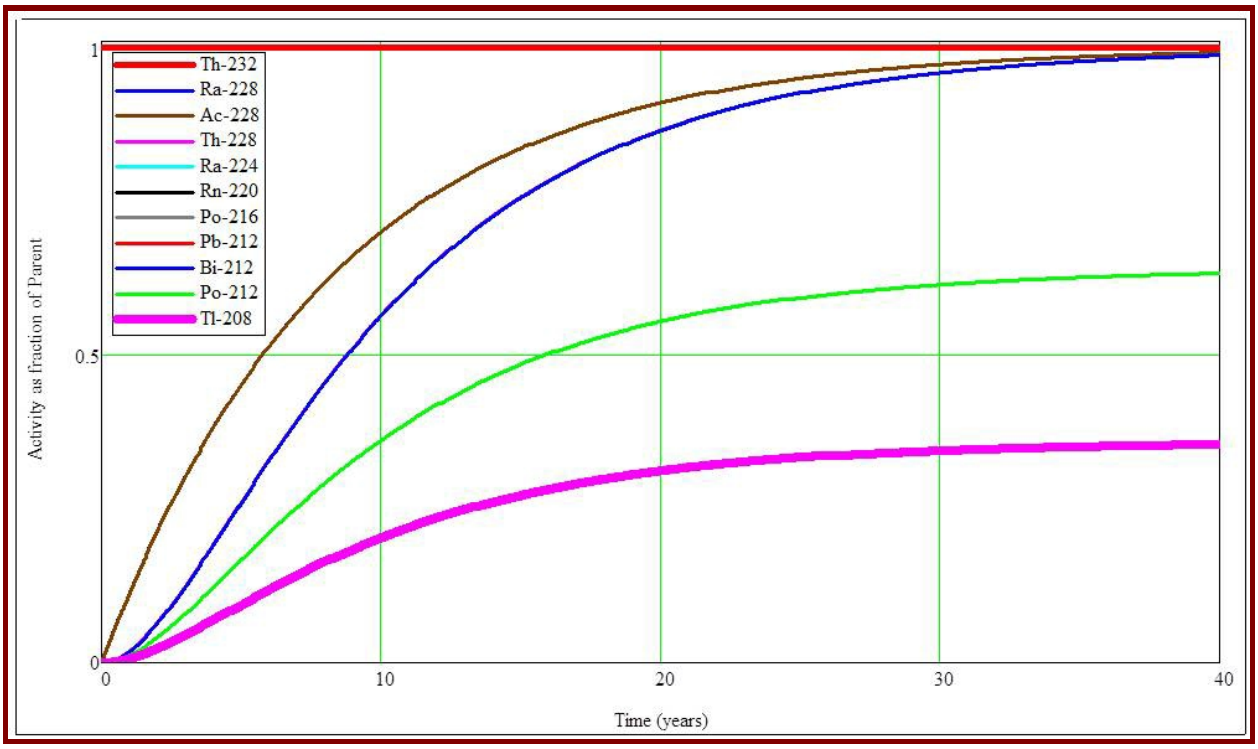

Figure 4.11: *The establishment of a high degree of secular equilibrium in the ^{232}Th chain is reached approximately 10^5 times quicker than for the ^{238}U chain.*

Because the half-life of the gaseous chain member ^{220}Rn in the ^{232}Th chain is far shorter than the gaseous chain member ^{222}Rn in the ^{238}U chain, much less radon gas will escape from ores containing ^{232}Th; this will also contribute to the establishment of a high degree of secular equilibrium in a fairly short time period — the radioactive ingrowth of the members of the ^{232}Th chain is fast — much faster than in the ^{238}U chain.

Photon emission in the ^{232}Th transition chain

The radionuclides in the ^{232}Th transition chain are given in Table 4.5 on page 196.

More than 1050 notable ionising photons are emitted by the radionuclides in the ^{232}Th transition chain. The total number of photons emitted per unit activity of the parent ^{232}Th, is

$$Y\left(^{232}\text{Th series in equilibrium}\right) = 4.1384.$$

The energies and yields of the photon emissions of the ^{232}Th transition cascade, are depicted in Figure 4.12.

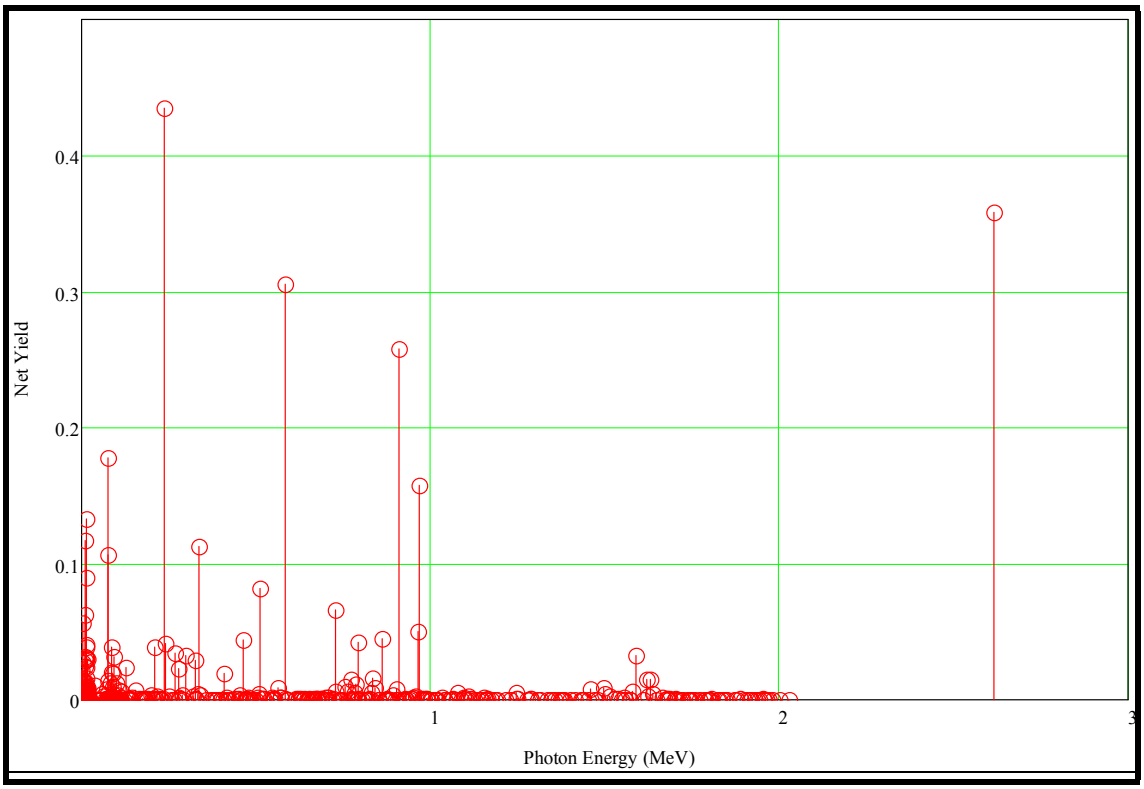

Figure 4.12: *Ionising photons emitted by ^{232}Th and its progeny, and the photon abundances.*

The $\{\text{Energy}, \text{Yield}\}$ photon lines in Table 4.10 are indicative of the presence of ^{232}Th in a sample.

Table 4.10: *{Energy, Yield} photon lines that are indicative of the presence of ^{232}Th in a sample.*

Photon Energy (MeV)	Photon Emission Yield per NT
0.23863	0.43461
2.61453	0.35761
0.58319	0.30469
0.91120	0.25754
0.07741	0.17789
0.96897	0.15772
0.01628	0.13267
0.01298	0.11653
0.33832	0.11250
0.07506	0.10638
0.01620	0.08983
0.51077	0.08154
0.72733	0.06604
0.01084	0.06230
0.00307	0.05619
0.96477	0.04981
0.86056	0.04481
0.46300	0.04392
0.79495	0.04242
0.24099	0.04115

Relative significance of radionuclides in the ^{232}Th series, as an external radiation hazard, when secular equilibrium prevails

For a small, unshielded source of ^{232}Th in equilibrium with its transition chain products, the percentage contributions of the different radionuclides to the external dose rate from ionising photons, have been calculated; results are presented in Table 4.11.

Table 4.11: *The contributions of the individual cascade progeny in the ^{232}Th transition chain, to the effective dose rate field around a small, unshielded, point-like source of ^{232}Th in full equilibrium with all its chain members.*

Nuclide	DR Contribution (%)
Th_232	0.128
Ra_228	0.274
Ac_228	40.229
Th_228	0.251
Ra_224	0.538
Rn_220	0.032
Po_216	0.001
Pb_212	7.684
Bi_212	4.810
Po_212	0.000
Tl_208	46.055

Two radionuclides clearly dominate the ^{232}Th series as a source of ionising photons, when all transition products are present in their equilibrium activities: ^{228}Ac and ^{208}Tl. Two other series radionuclides make lesser but non-negligible contributions: ^{212}Pb and ^{212}Bi.

Time-dependence of dose-rate near a ^{232}Th source that retains all radioactive transition products

The contributions of the different radionuclides in the ^{232}Th transition series to the dose rate near a small source of ^{232}Th, will be a function of time because the daughter radionuclides "grow in" as a function of time. The time-dependence of the dose rate will depend on the ingrowth as well as the ionising photon emission characteristics (photon energy & photon yield) of each radionuclide. Figure 4.13 shows how the dose rate close to a hypothetical, small ^{232}Th source from which no daughter radionuclides escape, increases as a function of time.

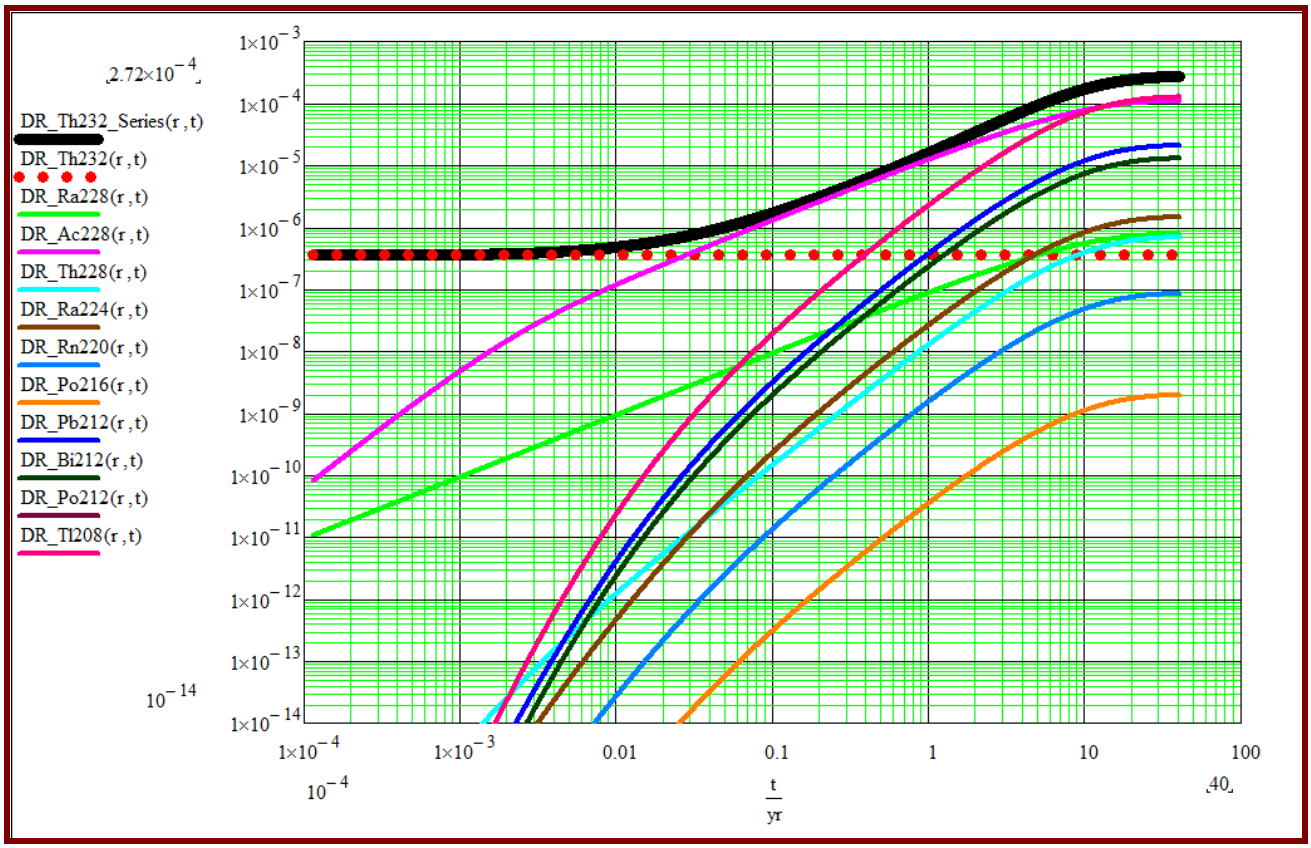

Figure 4.13: *The dose rate close to a hypothetical, small ^{232}Th source from which no daughter radionuclides escape, increases as a function of time.*

The two radionuclides, ^{228}Ac and ^{208}Tl, in the ^{232}Th transition-cascade, make dominant contributions to the dose rate, while ^{212}Pb and ^{212}Bi also make noteworthy contributions to the dose rate.

At full ingrowth of the ^{232}Th series, the dose rate from ionising photons emitted by all the series radionuclides, present at their equilibrium quantities, will be approximately 783 times higher than for pure ^{232}Th at time $t = 0$, evaluated for a point source in a vacuum.

4.4.9 Notable differences between the external photon dose-rate hazard presented by the ^{238}U and the ^{232}Th series

More high-energy photons are emitted in the ^{232}Th chain (Figure 4.12 on page 209) compared to the photon emission in the ^{238}U transition cascade (Figure 4.6 on page 199). Under the condition of full equilibrium, the nuclides of the ^{232}Th series emit approximately 30% more photons per 1 transition of the primordial parent radionuclide, compared to the ^{238}U transition chain.

The biological harm-potential of all the ionising photons emitted by the nuclides of the ^{232}Th transition chain, under full equilibrium, is approximately 40% higher than that of all the ionising photons emitted by the nuclides of the ^{238}U transition chain.

Assignment 4.3

1. A given nuclear reactor uses ^{232}Th fuel (and also ^{233}U, to enable it to operate). While in storage, its fresh, i.e. unused $^{232}ThO_2$ breeding-blanket fuel assemblies, are observed to become "more radioactive" with time, in terms of the measured ionising photon dose rate close to the fuel. Explain this phenomenon.

2. You analyse an environmental mineral sample and detect prominent ionising photon emission lines at 0.23863 MeV, 2.61453 MeV, 0.58319 MeV and 0.91120 MeV. Is it a ^{238}U or ^{235}U or ^{232}Th sample (in equilibrium with progeny) that you are dealing with?

3. You analyse an environmental mineral sample and detect prominent ionising photon emission lines at 0.609 MeV, 0.352 MeV, 0.295 MeV, 1.1765 MeV and 1.12 MeV. Is this a ^{238}U or ^{235}U or ^{232}Th sample (in equilibrium with progeny) that you are analysing with photon spectrometry?

4. You analyse an environmental mineral sample and detect prominent ionising photon emission lines at 0.18572 MeV, 0.26946 MeV, 0.35106 MeV, 0.23596 MeV, 0.14376 MeV and 0.27123 MeV. Is this a ^{238}U or ^{235}U or ^{232}Th sample (in equilibrium with progeny) that you are analysing with photon spectrometry?

4.5 Radioactivity of natural and enriched uranium

Uranium, as found in nature, contains approximately 0.72% ^{235}U, 99.2745% ^{238}U, and a trace (0.0055%) of ^{234}U, by mass.

In terms of the amount of radioactivity, natural uranium's activity is made up as summarised in Table 4.12.

***Table 4.12**: Activity percentage of the present natural abundance of uranium nuclides.*

Nuclide	Percentage activity
^{238}U	48.70 %
^{235}U	2.24 %
^{234}U	49.05 %

This is the case, because the activity A of a nuclide is given by $A = \lambda N$, where $\lambda \propto 1/T_{½}$, and N is the number of atoms of the radionuclide that is present. The halflife of ^{235}U is 6.35

times shorter than that of ^{238}U, so that a given number of ^{235}U atoms will be 6.3 times more radioactive than the same number of ^{238}U atoms. The halflife of ^{234}U is 1.82E4 times shorter than that of ^{238}U, so that a given number of ^{234}U atoms will be 18200 times more radioactive than the same number of ^{238}U atoms.

During enrichment in gas centrifuges, when the uranium is in the chemical form UF_6, enrichment of the light uranium isotope, ^{235}U, takes place. Because ^{234}U is even lighter than ^{235}U, the isotope ^{234}U will be enriched even more than ^{235}U. For example: if the ^{235}U is enriched by a factor 27.576 from approximately 0.72% to 20%, the ^{234}U may empirically be found to be enriched by a factor of e.g. 30 to 31. Therefore that the majority of the radioactivity of such enriched uranium originates from ^{234}U.

In uranium enriched to 19.75% ^{235}U (m/m), the activity makeup from different uranium isotopes, will typically be in the order of magnitude given in Table 4.13:

***Table 4.13**: Typical activity makeup from different uranium isotopes in (non-reprocessed[15]) uranium enriched to 19.75% ^{235}U.*

Nuclide	Activity %
^{238}U	2.46%
^{235}U	3.92%
^{234}U	93.62%

It is clear that the uranium isotope ^{234}U is the highest activity uranium isotope in natural uranium, and increasingly so in enriched uranium.

The radionuclide ^{234}U is the 5^{th} member of the ^{238}U series transition chain, so that the ^{234}U-sub-series will comprise the lower or last 12 radionuclides in the ^{238}U transition series.

In underground uranium-bearing ore, the members of the ^{238}U and ^{235}U transition series are typically found in a state of near-equilibrium, i.e. the activities of the daughter radionuclides are similar to that of the parent radionuclide. When uranium is chemically extracted during ore beneficiation, the equilibrium activities of the two uranium series are totally disrupted. Radionuclides with chemistries similar to that of uranium will tend to concentrate with the uranium, while other radionuclides will largely end up in waste streams. This will hold true for each chemical processing step that the uranium is put through. In other words, all ^{234}U and ^{235}U will concentrate along with ^{238}U in the chemical minerals extraction steps.

---

[15] In reprocessed uranium, ^{236}U will also be present.

4.6 Activity per unit mass; mass and volume per unit activity

Activity per unit mass

The relationship between the activity A of a radionuclide in a sample that contains N of these nuclides, is,

$$A = \lambda N = \left(\frac{\ln(2)}{T_{½}}\right) N$$

A sample with mass M_r gram contains N_A atoms, where M_r is the relative molar mass.
Therefore 1 gram will contain $\left(\frac{N_A}{M_r}\right)$ atoms.
Therefore 1 gram will have an activity of $\left(\frac{N_A}{M_r}\right) \times \left(\frac{\ln(2)}{T_{½}}\right)$, so that the activity per unit mass will be,

$$A_{\text{um}}(T_{½}, M_R) = \frac{\ln(2)\, N_A}{T_{½}\, M_R} \tag{4.13}$$

where N_A is Avogadro's constant and M_R is the relative molar mass of the nuclide. Activities per unit mass for the radionuclides ^{238}U, ^{232}Th and ^{40}K were calculated using Eq. (4.13) and are summarised in Table 4.14.

Table 4.14: *Activity per unit mass, $A_{um}(T_{½}, M_R)$, for important naturally occurring radionuclides.*

Nuclide	$T_{½}$	**Activity per unit mass** (Bq.g^{-1})
^{234}U	2.45505×10^5 years	2.302×10^8
^{235}U	7.03814×10^8 years	7.996×10^4
^{236}U	2.34205×10^7 years	2.393×10^6
^{238}U	4.468×10^9 years	1.244×10^4
^{232}Th	1.405×10^{10} years	4.06×10^3
^{40}K	1.24803×10^9 years	2.58×10^5
^{210}Po	138.376 days	1.66×10^{14}
^{208}Tl	3.07 minutes	1.1×10^{19}

Mass and volume per unit activity of radionuclides

The mass per unit activity ("ua") of a pure sample of a single radionuclide, is the reciprocal of Eq. (4.13), i.e.

$$M_{\text{ua}}(T_{½}, M_R) = \left(\frac{T_{½}\, M_R}{\ln(2)\, N_A} \right) \tag{4.14}$$

where A is the activity of the nuclide, $T_{½}$ is the halflife of the nuclide, N_A is Avogadro's constant and M_R is the relative molar mass of the nuclide. The mass per unit activity for selected naturally occurring radionuclides were calculated using Eq. (4.14) and are summarised in Table 4.15.

By combining Eq. (4.14) with the relationship between the volume, mass and mass density of a material, $\rho = \frac{M}{V}$, the volume per unit activity ("ua") of a pure sample of a single radionuclide, is

$$V_{\text{ua}}(T_{½}, M_R, \rho) = \left(\frac{T_{½}\, M_R}{\ln(2)\, N_A\, \rho} \right) \tag{4.15}$$

where N_A is Avogadro's constant and M_R is the relative molar mass of the nuclide, ρ is the mass density of the material and $T_{½}$ is the halflife of the nuclide.

Masses and volumes per unit activities for some naturally occurring radionuclides were calculated using Eqs. (4.14) and (4.15), and are summarised in Table 4.15.

Table 4.15: *Mass and volume per curie activity of some important NORM radionuclides.*

Nuclide	$T_{½}$	Mass per Ci	Volume per Ci
^{238}U	4.468×10^9 years	2.97 tonne	165 litres
^{232}Th	1.405×10^{10} years	9.12 tonne	780 litres
^{40}K	1.28×10^9 years	0.14 tonne	150 litres
^{210}Po	138.376 days	0.22 mg	~ 0.02 mm^3
^{208}Tl	3.07 minutes	3.40 ng	$\sim 3 \times 10^{-7}$ mm^3

Conclusions:

(1) When $T_{½}$ is long, the activity per unit mass is low; the mass and volume per unit activity are high;

(2) When $T_{½}$ is short, the activity per unit mass is high; the mass and volume per unit activity are low.

Assignment 4.4

1. At a specific particle accelerator facility with associated radionuclide production activities, an average activity $A = 0.45$ Ci of the radionuclide ^{65}Zn is released to an on-site waste-water pond per annum. Calculate the mass of this ^{65}Zn release.
   How can competitive mass-action be deployed to suppress the uptake of this radionuclide in biota, i.e. plants and animals?

2. At a specific particle accelerator facility with an associated radionuclide production business, approximately 0.25 Ci of the radionuclide ^{87}Rb is released to an on-site waste-water pond per annum. Calculate the mass of this ^{87}Rb release.
   How can competitive mass-action be deployed to suppress the uptake of this radionuclide in biota, i.e. plants and animals?

3. Point out the general principle for the relationship between the activity per unit mass, and the halflife $T_{½}$, in simple language that can be easily understood by a non-specialist.

4.7 Typical terrestrial radionuclide concentration

How much natural radioactivity is found in typical soil of a volume 1 km × 1 km × 1 m? Table 4.16 was calculated for this volume of 10^6 m^3. Soil mass density was assumed to be approximately 1.6 g cm^{-3}.

Table 4.16: *Amount of naturally occurring radionuclides in typical soil of a volume 1 km × 1 km, and 1 m deep.*

Nuclide	**Typical crustal activity concentration** (Bq.kg^{-1})	**Mass in 10^6 m^3**	**Activity in 10^6 m^3**
^{238}U	25 Bq/kg	2800 kg	40 GBq
^{232}Th	40 Bq/kg	15200 kg	65 GBq
^{40}K	400 Bq/kg	2500 kg	630 GBq
^{226}Ra	48 Bq/kg	2.2 g	80 GBq
^{222}Rn	10 kBq/m^3	14 µg	9.5 GBq

It is clear that substantial amounts of radionuclides are found in the earth's crust. In fact, natural radioactivity is largely responsible for the fact that the interior of the earth is hot and molten. For an average activity per unit mass of ~1000 $Bq.kg^{-1}$ in the earth, and an estimated recoverable energy of 2 MeV per nuclear transition event, it can be shown that the earth is a gigantic heater producing approximately 2×10^{15} watt. This is roughly equivalent to 10^{12} household heaters of 2 kW each, or, alternatively, to the total thermal power produced by almost 1 million AREVA EPR type nuclear reactors.

High-density chemical forms of high-density elements such as uranium and thorium are concentrated near the molten centre of the earth; there is a body of evidence pointing to the possible existence of a nuclear fission reactor at the core of the earth.

Chapter 5:
Sources of Ionising Radiation Frequently Encountered in Radiation Shielding Projects

5.1 The Source-term

Conceptually, we look at radiation shielding in terms of the Boltzmann Transport Equation (BTE). In operator notation, the Boltzmann Transport Equation (BTE), which is an integro-differential equation, may be written as a non-homogeneous operator equation,

$$\mathbb{B}\psi = Q,$$

where $\mathbb{B}$ denotes the linear Boltzmann transport operator (BTO), and Q is the source-term "driving" the system.

The following **heuristic interpretation** can be given to the BTE. The source-term Q of the BTE ***"drives"*** the system, while the material-dependent BTO, $\mathbb{B}$, determines the phase-space dependence of the directional fluence-rate "reaction", $\psi(\vec{\boldsymbol{x}}, E, \widehat{\boldsymbol{\Omega}})$, of the system on the source-term, Q.

The quantities of interest to the shield designer are usually dose rates, heating rates, material damage rates, reaction rates, etc. The generic term for these quantities-of-interest that depend on the fluence-rate ϕ or the fluence, Φ, is ***response***. The response R is determined by calculating a response functional, which is, in its most general form, the inner product of the fluence-rate function ϕ and a response function $\mathfrak{R}$, also termed a fluence-to-response conversion function.

It is convenient to introduce the notation employed in the description of functionals in inner-product spaces, because this allows us to write the response functional R very concisely as

$$R = \langle \psi, \mathfrak{R} \rangle$$

where $\mathfrak{R}$ is the response function and ϕ is the fluence-rate. In the above expression, the inner product brackets denote integration over all continuous variables and summation over all discrete variables, of phase space.

Because the *local effect* of radiation on matter is, under most circumstances encountered in radiation shielding, quite independent of the direction of movement of the radiation, the response function $\mathfrak{R}$ will be practically independent of the angular variable $\widehat{\Omega}$. Accordingly the response functional can be expressed as the inner product of the scalar fluence-rate ϕ with the response function $\mathfrak{R}$,

$$R = \langle \phi, \mathfrak{R} \rangle.$$

and it is not generally necessary to use the angular fluence-rate ψ directly to evaluate response functions.

In summary:

Radiation transport and the system-response to ionising radiation has been conceptually contracted to first obtaining the solution ψ of the BTE,

$$\mathbb{B}\boldsymbol{\psi} = \boldsymbol{Q} \tag{5.1}$$

by means of a radiation transport code whose input contains the detail of the placement of materials in space, as well as the source term of ionising radiation, Q. The code then solves for ψ and then determines the scalar fluence-rate ϕ by integrating ψ over all directions of particle movement, $\widehat{\Omega}$. The response function $\mathfrak{R}$ is also specified to the code, which uses ϕ and $\mathfrak{R}$ to determine the response R by calculating the inner product,

$$\boldsymbol{R} = \langle \boldsymbol{\phi}, \boldsymbol{\mathfrak{R}} \rangle. \tag{5.2}$$

Even when we simulate radiation transport by a Monte Carlo method, which does not actually "solve" the BTE directly, it is always fruitful to conceptualise the calculational process in terms of the above formalism.

From the operator form of the Boltzmann transport equation (BTE), $\boxed{\mathbb{B}\boldsymbol{\psi} = \boldsymbol{Q}}$, it is seen that knowledge about the source-term, $Q\left(\vec{x}, E, \widehat{\Omega}\right)$, is required before a radiation transport problem can be solved. We need to know the spatial distribution, energy spectrum, angular distribution and strength of the source.

Small radionuclide sources generally emit radiation quanta isotropically, with a "flat" emission-intensity distribution over the active source volume, so that knowledge of (1) the integral activity and (2) the EY-matrix of every type of discrete-energy radiation (such as X-rays, γ-rays, , and (3) the probability density function $P(E)$ of radiation types such as emitted with a continuous energy spectrum, must be known.

Assignment 5.1

1. In a given system, the scalar fluence-rate is $\phi(E, \vec{\boldsymbol{x}})$. The response function for the response of interest is $\mathfrak{R}(E)$. Write down an expression for the response at the detector position $\vec{\boldsymbol{x}}_{\mathrm{d}}$. (Hints: Because the given functions are continuous, the inner product will be an integral. Make use of the Dirac Delta function δ.)

2. In a given system, the scalar fluence-rate of neutrons is $\phi_n(E, \vec{\boldsymbol{x}})$ and the scalar fluence-rate of photons is $\phi_\gamma(E, \vec{\boldsymbol{x}})$. The response functions for the response of interest are $\mathfrak{R}_n(E)$ for neutrons and $\mathfrak{R}_\gamma(E)$ for photons. Write down an expression for the total response-rate, i.e. the combined response rate from neutrons and γ-rays, at the detector position $\vec{\boldsymbol{x}}_{\mathrm{d}}$.

5.2 Real-life source definition (SDEF) calculations for single radionuclides; $\{EY\}$-matrixes and $\{EP\}$-matrixes

Generating an SDEF specification for the radionuclide ^{60}Co

As an example, we construct a source definition specification for 1 mCi ^{60}Co.

In the ICRP-107 (2008) database ICRP-07.RAD, the emissions of the radionuclide ^{60}Co are given as follows:

```
Co-60       5.2713y        64
 2 1.50257E-03 1.45030E-05  X
 2 5.02051E-14 1.79600E-05  X
 2 7.90703E-09 5.95467E-05  X
 2 1.88427E-09 1.21520E-04  X
 2 8.17232E-09 1.39480E-04  X
 2 1.10137E-06 7.48381E-04  X
 2 5.82779E-07 7.66341E-04  X
 2 1.81945E-09 7.86540E-04  X
 2 1.76654E-09 7.88810E-04  X
 2 1.78285E-09 8.06771E-04  X
 2 6.78951E-08 8.52098E-04  X
 2 7.39118E-07 8.52361E-04  X
 2 2.52983E-08 8.58930E-04  X
 2 3.99531E-07 8.70064E-04  X
 2 1.38510E-08 8.76890E-04  X
 2 5.54510E-08 9.26018E-04  X
 2 8.48861E-08 9.28291E-04  X
 2 1.99386E-10 9.91581E-04  X
 2 2.61353E-10 9.91840E-04  X
 2 3.19463E-05 7.41782E-03  X
 2 6.23882E-05 7.43578E-03  X
 2 3.90686E-06 8.22229E-03  X
 2 7.66065E-06 8.22459E-03  X
 2 3.34900E-09 8.28784E-03  X
 2 4.86742E-09 8.28816E-03  X
 1 7.50000E-05 3.47140E-01  G
 1 7.60000E-05 8.26100E-01  G
 1 9.98500E-01 1.17323E+00  G
 1 9.99826E-01 1.33249E+00  G
 1 1.20000E-05 2.15857E+00  G
 1 2.00000E-08 2.50569E+00  G
 5 9.98800E-01 9.58654E-02 B-
 5 1.20000E-03 6.25925E-01 B-
 7 5.83929E-04 4.79803E-05 AE
 7 7.32775E-05 7.87867E-05 AE
 7 3.93729E-04 7.72593E-04 AE
```

```
 7 3.97670E-06 8.18380E-04 AE
 7 1.24729E-04 6.49788E-03 AE
 7 3.11916E-05 7.31362E-03 AE
 7 2.05737E-06 8.13349E-03 AE
 6 3.76876E-07 3.38837E-01 IE
 6 3.55561E-08 3.46134E-01 IE
 6 1.20411E-09 3.46255E-01 IE
 6 1.38713E-09 3.46273E-01 IE
 6 2.31404E-08 8.17797E-01 IE
 6 2.22619E-09 8.25094E-01 IE
 6 2.54225E-11 8.25215E-01 IE
 6 2.39864E-11 8.25233E-01 IE
 6 1.49950E-04 1.16493E+00 IE
 6 1.43798E-05 1.17222E+00 IE
 6 1.35110E-07 1.17234E+00 IE
 6 1.56700E-07 1.17236E+00 IE
 6 1.13537E-04 1.32419E+00 IE
 6 1.08897E-05 1.33149E+00 IE
 6 8.82547E-08 1.33161E+00 IE
 6 1.06304E-07 1.33162E+00 IE
 6 5.36789E-10 2.15027E+00 IE
 6 5.17962E-11 2.15756E+00 IE
 6 2.39562E-13 2.15769E+00 IE
 6 3.59675E-13 2.15770E+00 IE
 6 1.55807E-12 2.49739E+00 IE
 6 1.54615E-13 2.50469E+00 IE
 6 1.49361E-15 2.50481E+00 IE
 6 8.76110E-16 2.50482E+00 IE
```

The first and last of the total of 4 columns, are numerical and mnemonical codes for the type of radiation specified in that row of the database. The number 2 or the symbol X signifies an X-ray, while the number 1 and the symbol G signifies a γ-ray, etc. For the purposes of radiation transport, it is irrelevant whether a photon is an X-ray or a γ-ray — all that matters is that it is an ionising photon emitted at a characteristic, unique energy E_g and with a known average emission yield y_g. Likewise, it is immaterial whether an electron originates as an Auger-electron (AE) or in an internal conversion process (IE) — all that matters is that it is an electron emitted at a characteristic, unique energy E_g and with a known average emission yield y_g.

Column 2 is the emission yield y_g and column 3 specifies the energy Eg of the emission.

To construct an SDEF specification for e.g. ^{60}Co, columns 2 and 3 are swapped around so that emission energy is in column 2 and emission yield in column 3. Next, all ionising photons are grouped together under emission category photon. This constitutes the $\{EY\}$ matrix for photon emission. Then all electrons emitted at discrete energies, i.e. line energies, are grouped together under emission category electron. This constitutes the $\{EY\}$ matrix for electron emission. Beta-electrons can not be treated in this way, but must be treated separately. The

$\{EP\}$ matrix for the beta-negatrons ("BEN") emitted by ^{60}Co is read from the database ICRP-07.BET.

Important: The norm is to delete all line-photons and line-electrons emitted at energies below 0.001 MeV = 1 keV, because such low energy radiation is generally unimportant. All radiation emission yields given below, are therefore sums over emitted radiation quanta having $E \geq 0.001$ MeV.

The full SDEF specification for ^{60}Co, ready for use in the code MCNP6, looks as follows:

```
c
c SDEF FOR Co-60
c
mode   P  E
c
c
SDEF   POS = 0  0  0
       PAR = D7
       ERG = FPAR  = D10
c
#       SI7      SP7               DS10
         L        D                 S
         P        1.9985949E+00     22      $ Photons
         E        4.4766187E-04     23      $ Line-Electrons
         E        1.0000000E+00     24      $ Beta-Electrons (-)
c
c Co-60 Line-Photons
c
#       SI22              SP22
        L                 D
        2.505690E+00      2.000000E-08
        2.158570E+00      1.200000E-05
        1.332490E+00      9.998260E-01
        1.173230E+00      9.985000E-01
        8.261000E-01      7.600000E-05
        3.471400E-01      7.500000E-05
        8.288160E-03      4.867420E-09
        8.287840E-03      3.349000E-09
        8.224590E-03      7.660650E-06
        8.222290E-03      3.906860E-06
        7.435780E-03      6.238820E-05
        7.417820E-03      3.194630E-05
c
c Co-60 Line-Electrons
c
#       SI23              SP23
        L                 D
        2.504820E+00      8.761100E-16
        2.504810E+00      1.493610E-15
        2.504690E+00      1.546150E-13
```

```
        2.497390E+00       1.558070E-12
        2.157700E+00       3.596750E-13
        2.157690E+00       2.395620E-13
        2.157560E+00       5.179620E-11
        2.150270E+00       5.367890E-10
        1.331620E+00       1.063040E-07
        1.331610E+00       8.825470E-08
        1.331490E+00       1.088970E-05
        1.324190E+00       1.135370E-04
        1.172360E+00       1.567000E-07
        1.172340E+00       1.351100E-07
        1.172220E+00       1.437980E-05
        1.164930E+00       1.499500E-04
        8.252330E-01       2.398640E-11
        8.252150E-01       2.542250E-11
        8.250940E-01       2.226190E-09
        8.177970E-01       2.314040E-08
        3.462730E-01       1.387130E-09
        3.462550E-01       1.204110E-09
        3.461340E-01       3.555610E-08
        3.388370E-01       3.768760E-07
        8.133490E-03       2.057370E-06
        7.313620E-03       3.119160E-05
        6.497880E-03       1.247290E-04
c
c Co-60 Beta-Electrons (BEN-)
c
#       SI24               SP24
        A                  D
        0.000000E+00       6.626000E+00
        1.000000E-04       6.623000E+00
        1.000000E-03       6.597000E+00
        1.100000E-03       6.594000E+00
        1.200000E-03       6.591000E+00
        1.300000E-03       6.588000E+00
        1.400000E-03       6.586000E+00
        1.500000E-03       6.583000E+00
        1.600000E-03       6.580000E+00
        1.800000E-03       6.574000E+00
        2.000000E-03       6.568000E+00
        2.200000E-03       6.563000E+00
        2.400000E-03       6.557000E+00
        2.600000E-03       6.551000E+00
        2.800000E-03       6.545000E+00
        3.000000E-03       6.540000E+00
        3.200000E-03       6.534000E+00
        3.600000E-03       6.523000E+00
        4.000000E-03       6.516000E+00
        4.500000E-03       6.507000E+00
        5.000000E-03       6.497000E+00
        5.500000E-03       6.488000E+00
```

```
6.000000E-03       6.478000E+00
6.500000E-03       6.469000E+00
7.000000E-03       6.459000E+00
7.500000E-03       6.450000E+00
8.000000E-03       6.440000E+00
8.500000E-03       6.431000E+00
9.000000E-03       6.422000E+00
1.000000E-02       6.403000E+00
1.100000E-02       6.385000E+00
1.200000E-02       6.367000E+00
1.300000E-02       6.349000E+00
1.400000E-02       6.332000E+00
1.500000E-02       6.315000E+00
1.600000E-02       6.298000E+00
1.800000E-02       6.265000E+00
2.000000E-02       6.234000E+00
2.200000E-02       6.203000E+00
2.400000E-02       6.172000E+00
2.600000E-02       6.142000E+00
2.800000E-02       6.113000E+00
3.000000E-02       6.083000E+00
3.200000E-02       6.053000E+00
3.600000E-02       5.993000E+00
4.000000E-02       5.932000E+00
4.500000E-02       5.853000E+00
5.000000E-02       5.771000E+00
5.500000E-02       5.685000E+00
6.000000E-02       5.596000E+00
6.500000E-02       5.502000E+00
7.000000E-02       5.405000E+00
7.500000E-02       5.304000E+00
8.000000E-02       5.198000E+00
8.500000E-02       5.089000E+00
9.000000E-02       4.977000E+00
1.000000E-01       4.742000E+00
1.100000E-01       4.494000E+00
1.200000E-01       4.235000E+00
1.300000E-01       3.967000E+00
1.400000E-01       3.692000E+00
1.500000E-01       3.411000E+00
1.600000E-01       3.127000E+00
1.800000E-01       2.557000E+00
2.000000E-01       1.998000E+00
2.200000E-01       1.469000E+00
2.400000E-01       9.907000E-01
2.600000E-01       5.822000E-01
2.800000E-01       2.658000E-01
3.000000E-01       6.436000E-02
3.200000E-01       1.027000E-03
3.600000E-01       1.050000E-03
4.000000E-01       1.070000E-03
```

```
         4.500000E-01       1.089000E-03
         5.000000E-01       1.102000E-03
         5.500000E-01       1.108000E-03
         6.000000E-01       1.108000E-03
         6.500000E-01       1.102000E-03
         7.000000E-01       1.089000E-03
         7.500000E-01       1.070000E-03
         8.000000E-01       1.044000E-03
         8.500000E-01       1.010000E-03
         9.000000E-01       9.695000E-04
         1.000000E+00       8.627000E-04
         1.100000E+00       7.174000E-04
         1.200000E+00       5.296000E-04
         1.300000E+00       3.083000E-04
         1.400000E+00       9.574000E-05
         1.491390E+00       0.000000E+00
c
c END OF SDEF FOR Co-60
c
```

For line-photon emission, the total yield per nuclear transition, is $Y_{\text{LP}} = \sum_{g=1}^{G}(y_g) = 1.9985949$. The maximum photon energy emitted by ^{60}Co is 2.505690 MeV.

For line-electron emission, the total yield per nuclear transition, is $Y_{\text{LE}} = \sum_{g=1}^{G}(y_g) = 4.4766187\text{E-}04$. The maximum line-electron energy emitted by ^{60}Co is 2.504820 MeV.

For beta-electron emission (BEN $= \beta$-negatron), the total yield per nuclear transition, is $Y_{\text{BEN}} = \int P_{\text{BEN}}(E)\, dE = 1.0000000$. The maximum beta-negatron energy emitted by ^{60}Co is in the order of 1.49138 MeV.

The $\{EY\}$ matrix for line-photon emission by ^{60}Co is:

```
         2.505690E+00       2.000000E-08
         2.158570E+00       1.200000E-05
         1.332490E+00       9.998260E-01
         1.173230E+00       9.985000E-01
         8.261000E-01       7.600000E-05
         3.471400E-01       7.500000E-05
         8.288160E-03       4.867420E-09
         8.287840E-03       3.349000E-09
         8.224590E-03       7.660650E-06
         8.222290E-03       3.906860E-06
         7.435780E-03       6.238820E-05
         7.417820E-03       3.194630E-05
```

The $\{EY\}$ matrix for line-electron emission by ^{60}Co is:

```
2.504820E+00       8.761100E-16
2.504810E+00       1.493610E-15
2.504690E+00       1.546150E-13
2.497390E+00       1.558070E-12
2.157700E+00       3.596750E-13
2.157690E+00       2.395620E-13
2.157560E+00       5.179620E-11
2.150270E+00       5.367890E-10
1.331620E+00       1.063040E-07
1.331610E+00       8.825470E-08
1.331490E+00       1.088970E-05
1.324190E+00       1.135370E-04
1.172360E+00       1.567000E-07
1.172340E+00       1.351100E-07
1.172220E+00       1.437980E-05
1.164930E+00       1.499500E-04
8.252330E-01       2.398640E-11
8.252150E-01       2.542250E-11
8.250940E-01       2.226190E-09
8.177970E-01       2.314040E-08
3.462730E-01       1.387130E-09
3.462550E-01       1.204110E-09
3.461340E-01       3.555610E-08
3.388370E-01       3.768760E-07
8.133490E-03       2.057370E-06
7.313620E-03       3.119160E-05
6.497880E-03       1.247290E-04
```

The $\{EP\}$ matrix for beta-negatron (BEN) emission by ^{60}Co is:

```
0.000000E+00       6.626000E+00
1.000000E-04       6.623000E+00
1.000000E-03       6.597000E+00
1.100000E-03       6.594000E+00
1.200000E-03       6.591000E+00
1.300000E-03       6.588000E+00
1.400000E-03       6.586000E+00
1.500000E-03       6.583000E+00
1.600000E-03       6.580000E+00
1.800000E-03       6.574000E+00
2.000000E-03       6.568000E+00
2.200000E-03       6.563000E+00
2.400000E-03       6.557000E+00
2.600000E-03       6.551000E+00
2.800000E-03       6.545000E+00
3.000000E-03       6.540000E+00
3.200000E-03       6.534000E+00
```

```
3.600000E-03       6.523000E+00
4.000000E-03       6.516000E+00
4.500000E-03       6.507000E+00
5.000000E-03       6.497000E+00
5.500000E-03       6.488000E+00
6.000000E-03       6.478000E+00
6.500000E-03       6.469000E+00
7.000000E-03       6.459000E+00
7.500000E-03       6.450000E+00
8.000000E-03       6.440000E+00
8.500000E-03       6.431000E+00
9.000000E-03       6.422000E+00
1.000000E-02       6.403000E+00
1.100000E-02       6.385000E+00
1.200000E-02       6.367000E+00
1.300000E-02       6.349000E+00
1.400000E-02       6.332000E+00
1.500000E-02       6.315000E+00
1.600000E-02       6.298000E+00
1.800000E-02       6.265000E+00
2.000000E-02       6.234000E+00
2.200000E-02       6.203000E+00
2.400000E-02       6.172000E+00
2.600000E-02       6.142000E+00
2.800000E-02       6.113000E+00
3.000000E-02       6.083000E+00
3.200000E-02       6.053000E+00
3.600000E-02       5.993000E+00
4.000000E-02       5.932000E+00
4.500000E-02       5.853000E+00
5.000000E-02       5.771000E+00
5.500000E-02       5.685000E+00
6.000000E-02       5.596000E+00
6.500000E-02       5.502000E+00
7.000000E-02       5.405000E+00
7.500000E-02       5.304000E+00
8.000000E-02       5.198000E+00
8.500000E-02       5.089000E+00
9.000000E-02       4.977000E+00
1.000000E-01       4.742000E+00
1.100000E-01       4.494000E+00
1.200000E-01       4.235000E+00
1.300000E-01       3.967000E+00
1.400000E-01       3.692000E+00
1.500000E-01       3.411000E+00
1.600000E-01       3.127000E+00
1.800000E-01       2.557000E+00
2.000000E-01       1.998000E+00
2.200000E-01       1.469000E+00
2.400000E-01       9.907000E-01
2.600000E-01       5.822000E-01
```

```
        2.800000E-01        2.658000E-01
        3.000000E-01        6.436000E-02
        3.200000E-01        1.027000E-03
        3.600000E-01        1.050000E-03
        4.000000E-01        1.070000E-03
        4.500000E-01        1.089000E-03
        5.000000E-01        1.102000E-03
        5.500000E-01        1.108000E-03
        6.000000E-01        1.108000E-03
        6.500000E-01        1.102000E-03
        7.000000E-01        1.089000E-03
        7.500000E-01        1.070000E-03
        8.000000E-01        1.044000E-03
        8.500000E-01        1.010000E-03
        9.000000E-01        9.695000E-04
        1.000000E+00        8.627000E-04
        1.100000E+00        7.174000E-04
        1.200000E+00        5.296000E-04
        1.300000E+00        3.083000E-04
        1.400000E+00        9.574000E-05
        1.491390E+00        0.000000E+00
```

Note that an $\{EY\}$-matrix specifies discrete particle emission energies and associated yields per nuclear transition, whereas an $\{EP\}$-matrix is a specification of a selection of some points on a probability density function (PDF). When this PDF is sampled by the Monte Carlo code, the discrete points in the $\{EP\}$-matrix are used in an interpolation scheme.

5.3 Real-life source definition (SDEF) calculations for mixtures of radionuclides — $\{NA\}$-matrixes

The code **MCNP-SOURCE-APP**

As an example, we construct a source definition specification for 232 grams of initially pure ^{232}Th that have undergone radioactive transition for 20 years. The easiest way to calculate the $\{\text{Nuclide}, \text{Activity}\}$ matrix or $\{NA\}$ matrix, is to first calculate the number of ^{232}Th nuclei present in the given pure specimen, at $t = 0$, and then let this number of ^{232}Th atoms undergo 20 years of radioactive transition in an activation code such as FISPACT. A FISPACT-2007 input data set for this problem looks as follows:

```
NOHEAD
MONITOR 1
AINP
<< A good convergence and iteration spec >>
CONV  10  1E-6  1E-6
FISPACT
* 1 mole Th-232 decays
```

```
DENS   14.0
FUEL   1
TH232  6.022E23
HALF
MIND   1.0E-48
<< Dose rate 1 m from a 1 gram point source >>
DOSE   2   1.0
HAZARDS
LOOPS 6000
SPLIT  1
<< Cooling >>
LEVEL  1000  50
TIME   20 YEARS   ATOMS
END
* END OF RUN
/*
```

The output file will have the following $\{NA\}$-matrix at $t = 20$ years.

```
NUCLIDE    ACTIVITY (Bq)
Th-232      9.4143E+05
Ac-228      8.5706E+05
Ra-228      8.5695E+05
Pb-212      8.2147E+05
Po-216      8.2147E+05
Rn-220      8.2147E+05
Ra-224      8.2147E+05
Bi-212      8.2147E+05
Th-228      8.1719E+05
Po-212      5.2620E+05
Tl-208      2.9515E+05
```

This $\{NA\}$ matrix is given as input to the utility code MCNP-SOURCE-APP [16], which then calculates a spectroscopic MCNP SDEF specification by using the $\{EY\}$ matrices for discrete energy emissions, as well as the probability density function $\{EP\}$ matrices from a radio-nuclide emissions database such as ICRP-107 (2008). In the above ^{232}Th ingrowth example, the code MCNP-SOURCE-APP will combine the Line-Photon (LP), Line-Electron (LE), Spontaneous Fission Neutrons (N), Alpha-particle (A), Alpha-Particle Recoil (AR), Fission Fragment (FF), Beta-Negatron (BEN) and Beta-Positron (BEP) emissions of Th-232, Ac-228, Ra-228, Pb-212, Po-216, Rn-220, Ra-224, Bi-212, Th-228, Po-212 and Tl-208, into a single consolidated MCNP6 SDEF (Source DEFinition) — within a few seconds.

[16] The code MCNP-SOURCE-APP was developed by Dr Rian Prinsloo, Necsa RRT. Code specification and testing was by Johann van Rooyen, Necsa RRT.

5.4 Neutron sources

5.4.1 Introduction

Neutrons and photons are the most penetrating and usually the main radiation types that need be considered in radiation shielding. They are electrically neutral and undergo isolated interactions at specific spatial positions. Between these points of interaction, the neutral particles move unperturbed and in straight lines. The mean free path length and therefore the range of electrically neutral ionising radiation types are much larger than that of charged particles.

The shield designer has to consider all types of ionising radiation originating from processes in the nuclei or electron clouds of atoms. This daunting task is today made possible because radiation transport codes that use state-of-the-art cross-section data compilations, e.g. MCNP, contain a great amount of "physics" built into the code's physics models and into its cross-section data libraries, so that it is normally only necessary for the code user to specify the ***primary*** radiation that "drives" the system — the production of important secondary types of ionising radiation is usually accounted for in the radiation transport simulation. Prompt fission neutron spectrum formulas are available in MCNP and can be specified with ease. When run in KCODE mode, MCNP generates prompt and delayed fission neutrons as well as prompt fission gamma-photons, with the correct energy spectra. MCNP6 can also generate ionising photons from fission-products (i.e. the so-called "delayed γ-rays"). The code can generate all these spectra and associated particle yields, without the user having to supply this information.

Examples of "physics" that are be default included in MCNP6 cross-section libraries and physics models:

- Production of ionising photons from neutron interactions such as (n,γ)-reactions and inelastic scattering.
- Prompt fission neutron (PFN) spectra for important fissioning actinides, are built into MCNP and are used when the code is run in KCODE mode.
- The release of electrons and positrons by photon interactions, the production of annihilation photons from positron-electron annihilation, as well as the release of bremsstrahlung photons from electron interactions.
- Fission product γ-ray emission — only if this option is activated.

Certain "physics" options are not active be default, and must be activated

Sadly, MCNP is still (2015) incapable of modelling (α,n) reactions in the incident alpha-particle energy range below 20 MeV. As a consequence, ^{9}Be(α,n) reactions, which is the nuclear reaction that is foundational to the functioning of an important category of neutron sources, e.g. ^{241}Am-Be sources, can not be modelled with MCNP. Instead, the MCNP user must obtain measured ^{241}Am-Be neutron spectra from the literature. In the cross-section tables for interactions below 20 MeV, supplied with MCNP6, there are no cross-section data for (n,γ)

In this section, we look at selected examples of important primary neutron sources.

5.4.2 Prompt fission neutrons (PFNs)

Many heavy nuclides fission after the absorption of a neutron, or even spontaneously, producing several fission neutrons. Fission neutrons are of great importance in nuclear reactor shielding. The most important fissile nuclides, i.e. nuclides that fission in an exothermic fission reaction, so that they can be fissioned by thermal neutrons, i.e. with no energy threshold, are: ^{233}U, ^{235}U, ^{239}Pu and ^{241}Pu. The most important fissionable nuclides, i.e. nuclides with an energy threshold for fission, are: ^{238}U and ^{232}Th, as well as ^{240}Pu and ^{242}Pu.

Prompt fission neutrons and delayed fission neutrons

More than approximately 98% to 99% of fission neutrons are *prompt* fission neutrons (PFNs) — they are emitted within about 10^{-7} s of the fission event. A small fraction of the fission neutrons are emitted as *delayed neutrons,* which are produced by fission products that radioactively transition by the emission of neutrons. Delayed neutrons can be emitted many seconds or even minutes after the fission event. Delayed neutrons are not important in shield design, because they are overshadowed by the prompt fission neutrons, for the following reasons:

- Far less delayed neutrons than PFNs are released — approximately ≥ 100 times less, i.e. their relative yield is low.
- The mean energy of delayed neutrons is only circa 0.4 MeV, whereas the mean energy of PFNs is approximately 2 MeV — see Figure 5.4 on page 248.
- Unlike the spectrum of PFNs, the energy spectrum of delayed neutrons has no high energy tail — see Figure 5.4 on page 248. It is those neutrons with energies above circa 3 MeV that are biologically the more harmful, more penetrating and hence difficult to shield. The high-energy tail of PFNs extends to approximately $E_n \approx 18$ MeV.

In nuclear reactor shielding, prompt fission neutrons are much more important to the shield designer than prompt gamma radiation and gamma radiation from fission products, because these photons are strongly absorbed by the high-Z elements present in a reactor, such as uranium, as well as the steel of the reactor pressure vessel (RPV). It is an important shield design principle that one designs a shield to shield the *primary* radiation — a shield that effectively "extinguishes" the primary radiation, will also "extinguish" the secondary radiation types — because the latter are produced by the former. In nuclear reactor shielding, the prompt fission neutrons is the most important primary radiation; primary fission gamma-rays as well as ionising photons from fission products are quite easy to shield, and the most important ionising photons some distance into the biological shield around a nuclear reactor, are ionising photons produced in (1) (n, γ) reactions, in (2) the de-excitation of nuclei that scattered neutrons inelastically, as well as (3) from radionuclides formed in neutron activation reactions. By attenuating the primary neutrons to negligible fluence-rates, the production rate of secondary ionising photons will be effectively stopped. Conversely, in all regions of a shield reached by non-neglible fluence-rates of primary neutrons, secondary ionising photons

will be produced via neutron interactions. "A shield that stops the primary radiation, will also stop the secondary radiation" is indeed a valuable motto for a designer of shielding against ionising radiation.

Two observables that characterise prompt fission neutron emission

Prompt fission neutron emission from nuclear fission is characterised by two important observables: The energy spectrum $S(E)$ of the emitted neutrons, and the average number of neutrons emitted per fission. The latter observable is known as the average prompt neutron multiplicity or yield, ν. These two observables are measured before the fission fragments undergo subsequent nuclear transitions towards the valley of β-stability and are therefore called the *prompt* fission neutron spectrum and the *prompt* fission neutron yield. Accurate knowledge of these two properties are important in the design of macroscopic systems driven by nuclear fission reactions, e.g. nuclear fission reactors and their radiation shields.

Note that both the energy spectra $S(E)$ and the average prompt neutron multiplicity or yield, $\nu(E)$, of prompt fission neutrons from the fissioning isotopes ^{232}Th, ^{233}U, ^{235}U , ^{238}U and ^{239}Pu are built into MCNP.

The prompt fission neutron multiplicity or yield ν

The average prompt fission neutron multiplicity or yield, ν, depends on the fissioning nucleus as well as on the incident energy of the neutron that induces the fission. Table 5.1 lists the average yield ν of fission neutrons for some important fissionable nuclides (Shultis & Faw, 2000). Also see the MCNP code manual for values of ν.

Table 5.1: *Yield or multiplicity of fission neutrons, $\overline{\nu}(E_n)$, as a function of the incident neutron's energy E_n (Shultis & Faw, 2000).*

Nuclide	$\overline{\nu}(E_n)$	E_n range (MeV)
^{235}U	$\overline{\nu} = 2.432 + 0.066E_n$ $\overline{\nu} = 2.349 + 0.150E_n$	$0 \le E_n \le 1$ $1 < E_n < 15$
^{238}U	$\overline{\nu} = 2.304 + 0.160E_n$	$1.5 \le E < 15$
^{239}Pu	$\overline{\nu} = 2.867 + 0.148E_n$ $\overline{\nu} = 2.907 + 0.133E_n$	$0 \le E_n \le 1$ $1 < E_n < 15$

Nuclear fission mechanism

Nuclear fission and subsequent prompt fission neutron emission take place as follows. A neutron is absorbed by the fissile or fissionable nucleus, thereby adding its binding energy (circa 7 MeV) as well as practically all its kinetic energy as internal excitation energy to the compound nucleus that is formed. The compound nucleus, formed after neutron absorption, is

very unstable, with a lifetime of approximately 10^{-14} s. The "nuclear fluid" of the excited, large compound nucleus undergoes large oscillations and shape-deformations, because the repulsive Coulomb force in such a large, highly excited nucleus is very destabilising; in such nuclei, the strong nuclear interaction "struggles" to keep the violently oscillating nucleus "in one piece." If the compound nucleus is sufficiently excited, it will, during one such "pumpkin-shaped to rugby-ball-shaped" oscillation, "overshoot" and deform into an elongated dumbbell shape, the two ends of which then repel each other strongly via Coulomb repulsion. The strong nuclear interaction, being very short-ranged, is no longer able to hold the two positively charged ends together. The two dumbbell-shaped "blobs" scission within approximately 10^{-20} seconds into two positively charged nuclear fragments, which repel each other with such tremendous Coulombic repulsion that many of their orbital electrons are torn off as a result of the fierce acceleration of the two fission fragments. Two highly positively charged fission fragments are thus formed. The (usually 2) fission fragments are accelerated by the repulsive Coulomb force; they are highly excited and excessively rich in neutrons, so that neutrons evaporate from the accelerated fission fragments. The Coulomb barrier prevents charged particles from evaporating from the fission fragments; only neutrons can evaporate, because they are electrically neutral. The fission fragments also de-excite by emitting prompt gamma-photons (PGs). Following the emission of prompt fission gamma-photons, which is practically co-incident with the fission process, "delayed fission gammas" i.e. ionising photons from radioactive fission products, are emitted by the fission products — this process yields ionising photons for many years.

The nuclear fission process is shown diagrammatically in Figure 5.1.

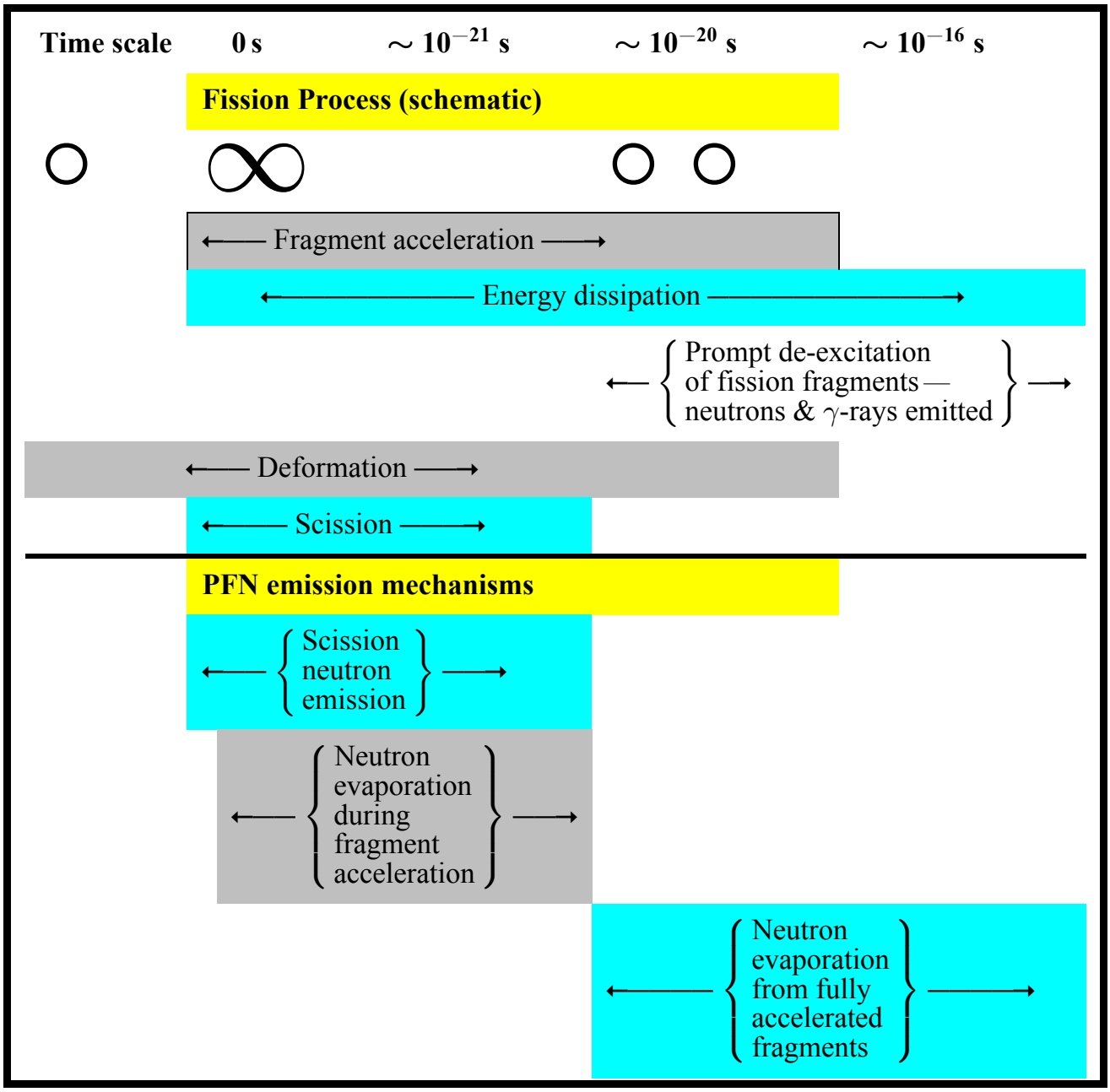

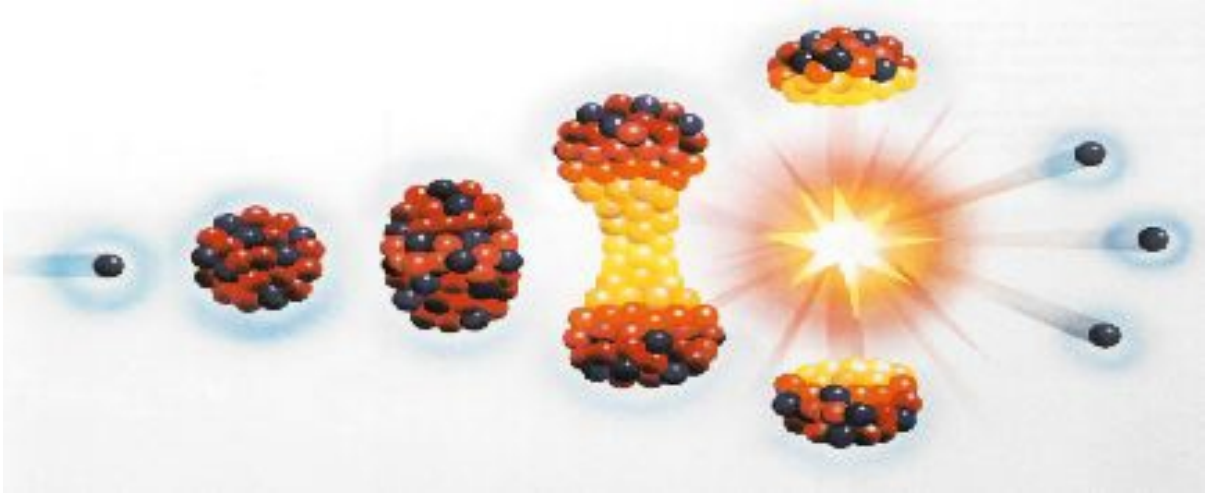

Figure 5.1: *The physics of nuclear fission and prompt fission neutron emission.*

While the fission fragments are being ripped apart and accelerated by the repulsive Coulomb force acting between the two accelerating fragments, a subcategory of prompt fission neutrons, called scission-neutrons, are More than 95% of prompt fission neutrons are emitted from fully accelerated fission fragments.

The primary fission fragments are produced in such highly excited nuclear states that neutrons "boil off" from them. Between 0 and 8 neutrons evaporate from the primary fission fragments within approximately 10^{-17} seconds of the scissioning of the compound nucleus. These neutrons are called prompt fission neutrons. The average prompt fission neutron multiplicity or yield ranges between circa 2.4 for thermal neutron induced fission of ^{235}U and 3.768 for ^{252}Cf spontaneous fission.

After prompt fission neutron emission, the fission fragments are still in excited states, but with excitation energies insufficiently high to cause particle emission. Transition to lower energy levels now take place via gamma-photon emission; these ionising photons are termed prompt gamma-photons. The emission of prompt gamma-photons is typically completed within approximately 2×10^{-14} s after the emission of the prompt fission neutrons.

Following prompt fission neutron and prompt gamma-photon emission, the fission fragments are termed *fission products*. The fission products are radioactive because they have a large neutron excess. The fission products therefore transition via β^--transitions, and so does the progeny radionuclei, until a stable (i.e. non-radioactive) terminal nuclide is reached. The half-lives of the fission product daughters range from fractions of a second to many thousands of years.

Nearly all of the fission neutrons — typically more than 99% — are emitted promptly when fission happens. Fission fragments usually have much higher excitation energy than the neutron separation energy, and therefore emit these prompt neutrons. The half-life of prompt fission neutron emission of these highly excited states is in the order of 10^{-15} s or even smaller. De-excitation by neutron emission is also accompanied by γ-emission. Not all fission fragments emit neutrons — some of them de-excite only by γ-emission.

The nuclei that are formed just after the fission process (within 10^{-14} s) are called *fission fragments*. These fast-moving nuclei slow down by colliding with the atoms of the fuel material, then pick up electrons, and finally become neutral atoms. The fission fragments suffer from a severe neutron excess in their nuclei, and are therefore radioactive, so that they undergo several nuclear transition processes to form a cascade of nuclides, along the way to the valley of beta stability. The collection of nuclides formed by the successive nuclear transitions of primary fission fragments, are collectively called **fission products** (FPs).

There are several hundred possible ways for the ^{236}U* compound nucleus to fission into fission fragments. One of these possibilities is e.g.

$$^{235}\mathrm{U} + n \rightarrow {}^{236}\mathrm{U}^* \rightarrow {}^{90}\mathrm{Kr} + {}^{143}\mathrm{Ba} + 3n$$

The number of possible fission fragments and, consequently, fission products, is very large. The mass-number distribution of the fission fragment Yield Y is a function of the isotopic mass number A, and the function $Y(A)$ has the form of a saddle-shaped curve, known as the "saddle-curve" or the "M-curve," depicted in Figure 5.2. This curve is the relative yield $Y(A)$ of primary fission fragments, as a function of the mass number A of the fission fragment.

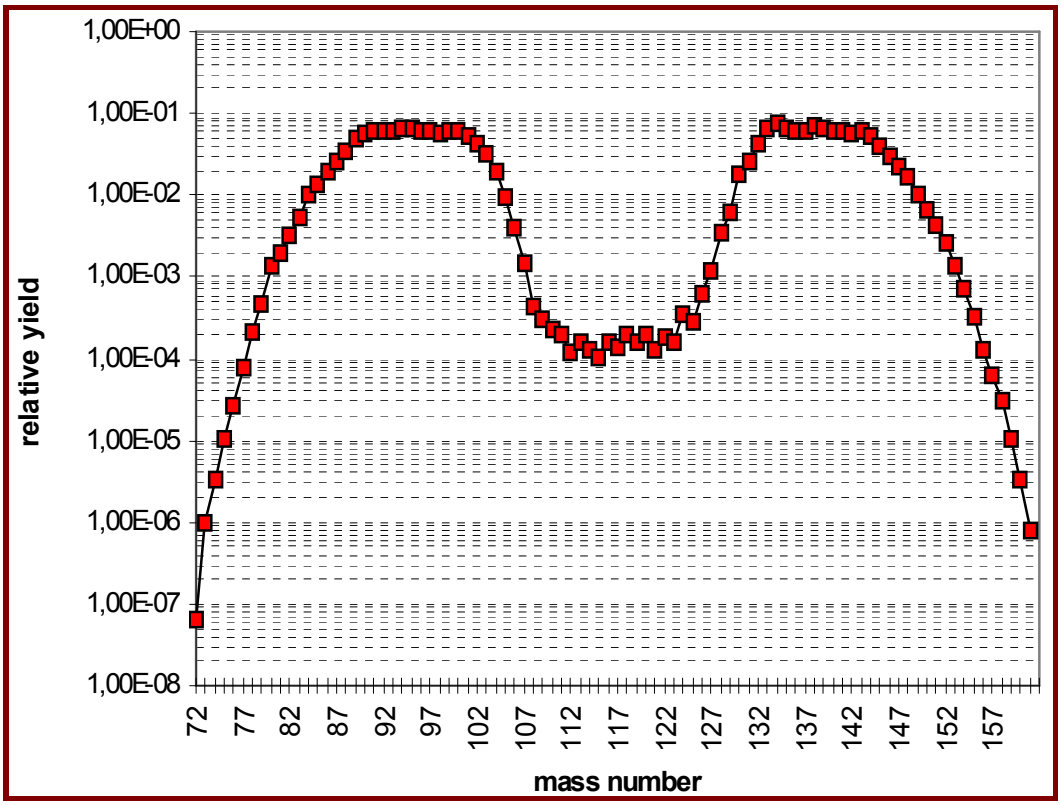

Figure 5.2: *The relative yield $Y(A)$ of primary fission fragments as a function of the mass-number A of the fission fragment, for the fission of the fissile isotope ^{235}U by thermal neutrons.*

Note that the vertical axis in Figure 5.2 uses a logarithmic scale, so that the fall-off in yield as one moves laterally away from the two maxima of $Y(A)$, is indeed very steep. The curve shows two maxima for the function $Y(A)$: one around $A \in \{90 \text{ to } 103\}$ and another for $A \in \{130 \text{ to } 145\}$. The primary fission fragments have excess neutrons as compared to stable nuclei with the same atomic number Z, i.e. the $\frac{\text{neutron}}{\text{proton}}$-ratio in the nucleus is far too large for nuclear stability. In most cases they undergo several successive β^--transitions to adjust the $\frac{\text{neutron}}{\text{proton}}$-ratio in the nucleus to a lower value that will ensure stability against β-transition.

Energy spectra of PFNs

Two widely used simple PFN spectrum formulae were obtained by fitting the free parameters of expressions derived from very simple neutron evaporation models, to experimentally measured PFN spectra. The parameters are adjusted to optimally reproduce a given experimental PFN spectrum. The two most widely used macroscopic analytical PFN spectrum models, the Maxwellian and the Watt formulae, will now be reviewed.

The Maxwell energy spectrum for evaporation neutrons may be derived from a maximum-entropy variational principle (Fröhner, 1991) and is given by

$$S(E) = \left(\frac{8\pi}{m}\right)\left(\frac{m}{2\pi\, k_B\, T_M}\right)^{3/2} E \exp\left(\frac{-E}{k_B\, T_M}\right). \tag{5.3}$$

where m is the mass of the neutron, E is the neutron energy and k_B the Boltzmann constant. The Maxwellian neutron energy spectrum is characterised by a single temperature parameter, T_M, related to the average energy of the spectrum by $E_{av} = \frac{3}{2}T_M$. The Maxwellian spectrum neglects the distribution of fission-fragment excitation energy, fragment spin and the center-of-mass motion of the heavy fission fragments emitting the neutrons. As a result of these simplifying assumptions, the Maxwellian PFN spectrum model is rather inaccurate and has no predictive power, i.e. it is unable to predict the PFN spectrum for a nuclide in the absence of experimental data.

Watt (1952) assumed a Maxwellian center-of-mass PFN spectrum and considered the movement of an *average* fission fragment in the laboratory system. A Galileo transformation to the laboratory system, yielded the following two-parameter expression for the PFN spectrum

$$S(E) = \frac{\exp\left(\frac{-E_f}{T_W}\right)}{\sqrt{\pi E_f T_W}} \exp\left(\frac{-E}{T_W}\right) \sinh\left(\frac{2\sqrt{E E_f}}{T_W}\right), \tag{5.4}$$

where E_f is the average kinetic energy per nucleon of the fission fragment and T_W is the Watt temperature parameter. The average energy of the Watt spectrum is

$$E_{av} = \frac{3}{2}T_w + E_f.$$

The Watt spectrum reduces to the Maxwellian spectrum for $E_f \to 0$. Instead of using a Galileo transformation, one may perform a relativistic (Lorentz) transformation to the laboratory system. Fröhner (1991) showed that this is an unnecessary complication, as it does not add significantly to accuracy in the energy range of PFN's. The Watt spectrum does account for the center-of-mass motion of an *average* fission fragment, and is more physical and accurate than the Maxwellian spectrum (Madland, 1989).

Based on an experimental determination of the ^{235}U PFN spectrum between 500 keV and 10 MeV, Watt calculated a set of fitting parameters for Eq. (5.4). Cranberg *et al.* (1956) measured the PFN spectrum for ^{235}U between 800 keV and 12 MeV and derived improved fitting parameters: $E_f = 0.533$ MeV and $T_W = 0.965$ MeV. This yields the well known Watt formula with Cranberg coefficients, which quickly became a virtual "industry standard" PFN spectrum for nuclear reactor shielding calculations, for many decades,

$$S(E) = 0.453 \exp\left(\frac{-E}{0.965}\right) \sinh\sqrt{2.29E}\,. \tag{5.5}$$

Figure 5.3 shows the Watt-Cranberg prompt fission neutron spectrum on a simple linear-linear system of axes.

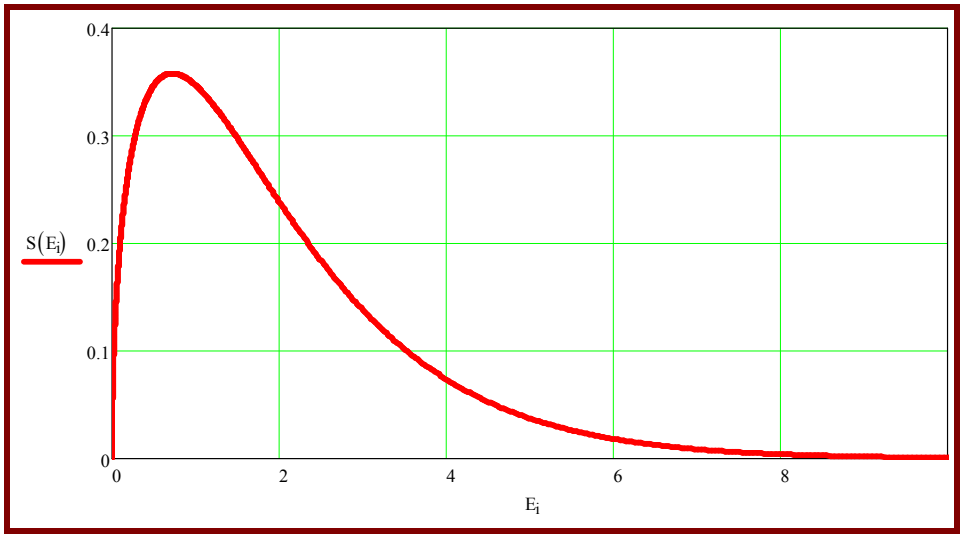

Figure 5.3: *The Watt-Cranberg prompt fission neutron (PFN) spectrum.*

Shultis & Faw (2000: 84) propose the fitting parameters listed in Table 5.2 for the Watt PFN spectrum formula,

$$S(E) = a \exp\left(\frac{-E}{b}\right) \sinh\sqrt{cE} \tag{5.6}$$

for different fissioning nuclides.

Table 5.2: *Parameters for the Watt approximation (Eq. (5.6)) of the prompt fission neutron energy spectrum, for various fissionable nuclides (Shultis & Faw, 2000: 145).*

Nuclide	***a***	***b***	***c***
^{235}U	0.5535	1.0347	1.6214
^{239}Pu	0.5710	1.1593	1.2292
^{238}U	0.5759	1.0269	1.5776
^{252}Cf	0.6400	1.1750	1.0401

Note that the fitting parameters of Table 5.2 were obtained by giving a greater statistical weight to high energy neutrons, which are of greatest importance in shielding calculations, because they are more penetrating and biologically more harmful than lower energy neutrons. The fitting parameters for the Watt spectrum, built into the code MCNP, were not derived via a greater statistical weight given to high energy neutrons.

Besides ^{235}U, the nuclides ^{238}U, ^{239}Pu and ^{241}Pu also contribute to fission in a LEU-fuelled fission reactor. The relative contribution of these isotopes to fission is a function of the burnup of the LEU fuel. The prompt fission neutron spectra of the isotopes ^{235}U, ^{238}U, ^{239}Pu and ^{241}Pu are quite close, yet not identical to, the prompt fission neutron spectrum of ^{235}U.

When run in KCODE mode, the code MCNP internally samples the fissioning isotope for every fission event, and automatically generates the appropriate energy spectrum for PFNs, DFNs as well as the correct DFN fraction and PFN yield.

Figure 5.3 shows prompt fission neutron spectra for important fissioning nuclides.

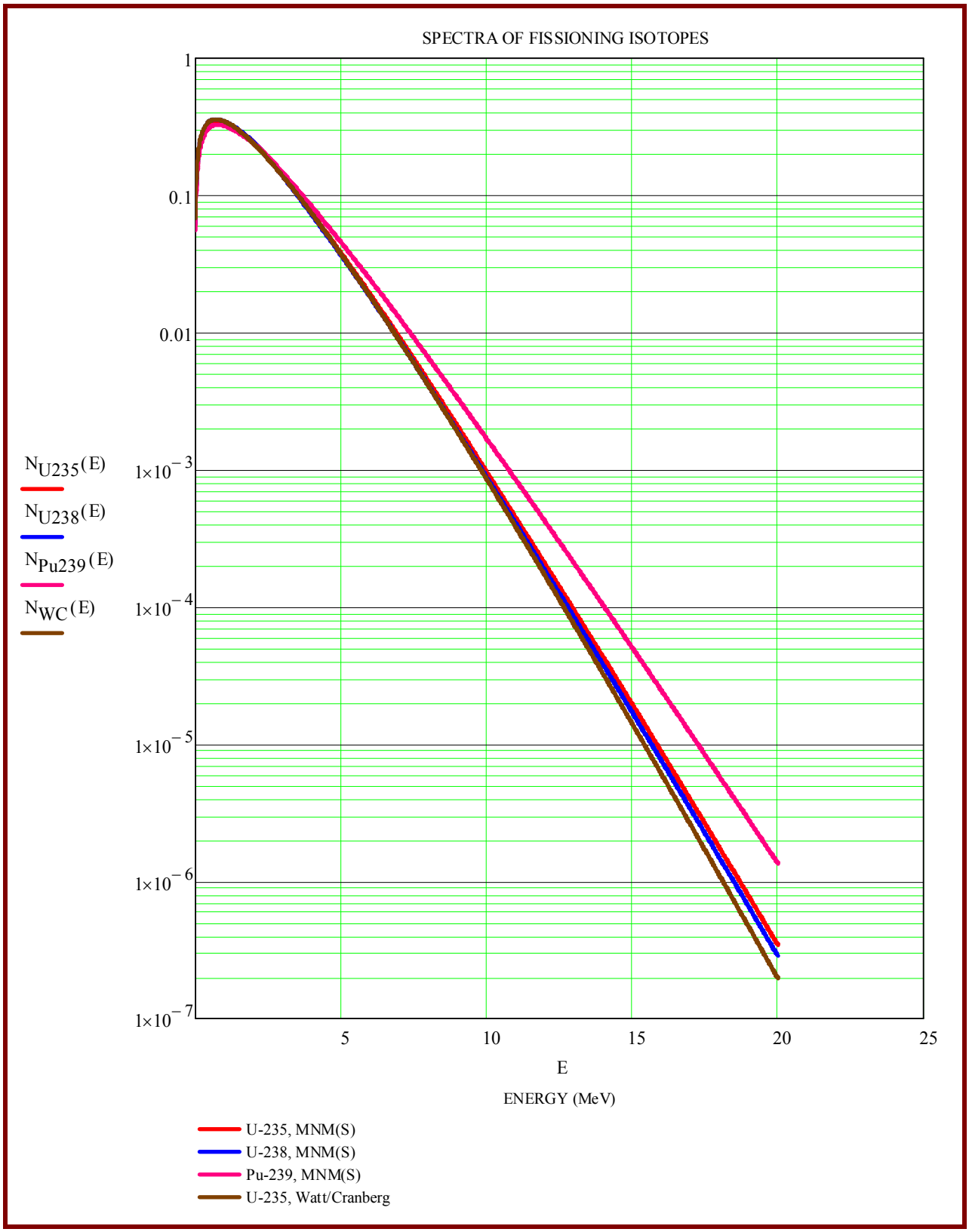

Figure 5.3: *Prompt fission neutron spectra for important fissioning nuclides in LEU fission-reactor fuel.*

Using the Watt-Cranberg prompt fission neutron (PFN) spectrum for all fissioning nuclides, will somewhat underestimate the high energy prompt fission neutron component, especially

towards End-of-Cycle (EOC) in LEU-fuelled reactors, when fission of ^{239}Pu makes a sizable contribution to fission. It is clear from Figure 5.3 that the prompt fission neutron spectrum of ^{239}Pu is significantly "harder" in the high energy range, than that of ^{235}U and ^{238}U, and that the Watt-Cranberg PFN spectrum will underestimate the high-energy neutron component in the PFN spectrum of ^{239}Pu.

Assignment 5.2

1. Plot the "classical" Watt-Cranberg prompt fission neutron (PFN) spectrum for ^{235}U on a simple linear-linear system of axes, as well as on log-log axes.

2. Plot the prompt fission neutron energy spectra for ^{235}U, ^{238}U and ^{239}Pu on the same graph, using the fitting coefficients specified in Table 2 on page 240.

3. What fraction of PFNs (prompt fission neutrons) emitted when ^{235}U fissions, is emitted with $E_n \in [1 \text{ MeV}; 3 \text{ MeV}]$?

4. What fraction of PFNs emitted when ^{239}Pu fissions, is emitted with $E_n \in [1 \text{ MeV}; 3 \text{ MeV}]$?

5. What fraction of PFNs emitted when ^{235}U fissions, is emitted with $E_n \in [5 \text{ MeV}; 20 \text{ MeV}]$?

6. What fraction of PFNs emitted when ^{239}Pu fissions, is emitted with $E_n \in [5 \text{ MeV}; 20 \text{ MeV}]$?

7. Determine the ratio of (fraction of PFNs emitted by ^{239}Pu with energies between 5 and 20 MeV)/(fraction of PFNs emitted by ^{235}U with energies between 5 and 20 MeV).

8. Will the neutron spectrum emitted by low enrichment uranium (LEU) reactor fuel "harden" or "soften" towards End-of-Cycle (EOC)? Explain your answer. What will the impact of the spectral shift be on shielding and the damage to metal structures? Explain your answer.

9. Calculate the expectation value of the energy of prompt fission neutrons emitted by each of ^{235}U, ^{238}U, ^{233}U, ^{239}Pu and ^{252}Cf. (Use the MCNP manual to find the fitting parameters for the Watt prompt fission neutron spectrum of ^{233}U.)

10. Use MathCAD to plot the prompt fission neutron energy spectra for ^{235}U, ^{238}U and ^{239}Pu on the same graph, using the fitting coefficients specified in the MCNP manual. Next, home in on the energy region between 5 and 20 MeV, and comment on your observations.

Energy released in nuclear fission

Total energy release in nuclear fission is approximately 210 MeV, of which approximately 197 MeV to 202 MeV is recoverable (depending on the fissioning isotopes involved), while the remainder is lost as the energies of neutrinos. The neutrino is an uncharged lepton that only interacts extremely weakly with matter via weak interaction (WI). The strength of weak interaction is only 10^{-14} times that of the strong nuclear interaction (SNI), and the range of weak interaction is also very short at approximately 10^{-3} fm, a range $\sim$ 1000 times shorter than the already very short range of strong nuclear interaction. This explains why neutrino energy is not recoverable — it will not be deposited inside the fissioning system such as the nuclear reactor.

Assignment 5.3

1. For a given configuration of fissile and fissionable isotopes, MCNP can be used to calculate the recoverable energy released in fission. Study Volume 2 of the MCNP5 manual and give step-by-stem instructions on how a tally must be designed to determine the average recoverable energy released in fission.

2. Use the fact that the average recoverable energy from the fission of ^{235}U is approximately 200 MeV, to calculate (a) the fission rate in a nuclear reactor producing a thermal power output of 3200 MW, and (b) the neutron production rate in the above reactor, given that $\nu = 2.46$.

3. In a BURN calculation, MCNPX 2.7 or MCNP6 calculates the values of Q and ν. A typical printout looks as follows:

step	duration (days)	time (days)	power (MW)	keff	flux	ave. nu	ave. q	burnup (GWd/MTU)	source (nts/sec)
0	0.000E+00	0.000E+00	1.308E+01	1.00812	1.325E+14	2.507	200.987	0.000E+00	1.018E+18

What are the values of $\overline{\nu}$ and that of $\overline{Q}$ for the above fissioning system?

5.4.3 Spontaneously fissioning nuclides

Some transuranic nuclides undergo spontaneous fission (SF). Most of these nuclides transition much more rapidly by α-emission than by spontaneous fission. Important spontaneously fissioning nuclides are listed in Table 5.3.

Table 5.3: *Important spontaneously fissioning (SF) nuclides.*

Nuclide	$T_{½}$	Fission probability per transition	Neutrons per fission	α-particles per fission	Neutrons per (g s)
^{248}Cm	3.4×10^5 y	8.3%	3.14	11	4.1×10^7
^{250}Cm	6900 y	61%	3.31	0.4	1.6×10^{10}
^{252}Cf	2.64 y	3.1%	3.73	31	2.3×10^{12}
^{254}Cf	60.5 d	99.7%	3.89	0.0031	1.2×10^{15}

Question:
What is practically problematic about the spontaneously fissioning (SF) nuclides listed in Table 5.3?

Answer:
The values of the half-life $T_{½}$ are either uneconomically short or dangerously long. Purchasing an expensive neutron source with $T_{½} = 2.64$ years will not be good "value for money" because it will scarcely last 15 years. On the other hand, being responsible for a neutron source with a halflife of 6900 years is dangerous, because such a source must never escape regulatory control for approximately 10 halflives, i.e. 70 000 years, which will be impossible to guarantee in practice — almost no country has been politically stable for 1000 years, let alone 70 000 years…

From the viewpoint of the security of radioactive sources, a spontaneous fission neutron source with a halflife of approximately 20 years would have been ideal but is, alas, not found. Faced with these practical problems posed by available spontaneous fission (SF) neutron sources, most researchers rather opt for ^{241}Am-Be (α, n) neutron sources, which has $T_{½} \approx 430$ yr for the ^{241}Am. Again, an alpha-particle emitter with a halflife in the order of 20 years would have been ideal, but is, alas, not found.

5.4.4 Delayed fission neutrons (DFNs)

A few highly unstable radio-nuclides transition by the emission of a neutron. Delayed fission neutrons are an example — fission products have a very substantial neutron excess in their nuclei, and some fission products such as ^{87}Br transition by the emission of delayed fission neutrons. The presence of delayed fission neutrons enable the control of reactor reactivity; without delayed fission neutrons nuclear reactors would be uncontrollable.

During the fission process the ^{235}U nucleus first absorbs a neutron, and a ^{236}U compound nucleus is formed in an excited state. This compound nucleus (CN) is unstable, and fissions

into two medium-sized fission fragments. Additionally, a few neutrons are also emitted — for ^{235}U, the average number of emitted neutrons is $\overline{\nu} \approx 2.47$. More than 99% of these neutrons are emitted promptly, within approximately 10^{-12} s after the fission, and are called prompt fission neutrons (PFNs). There are also neutrons which are emitted long after the fission process, sometimes several minutes later — these are called *delayed fission neutrons* (DFNs). Although their emission yield relative to the emission yield for prompt fission neutrons is quite small (for ^{235}U they represent only 0.64% of the total yield of fission neutrons), they are very important in enabling nuclear reactor power to be controlled in a safe, stable fashion.

Origin of the delayed fission neutrons

After the emission of the prompt neutrons there is usually no further neutron emission; the fission products undergo several successive β^--transitions to reduce their neutron-excess. However, in some cases a daughter nucleus is formed after a β^--transition, where the excitation energy is higher than the neutron-separation energy. This nucleus will emit a neutron, nearly promptly after its formation. These are the delayed neutrons. The transition chain for delayed neutron emission is as follows

$$ {}^{A}_{Z}X_{N} \xrightarrow[\beta^-]{} {}^{A}_{Z+1}Y_{N-1} \rightarrow {}^{A}_{Z+1}T_{N-2} + n. \tag{5.7} $$

The "X" nucleus is called the **delayed-neutron precursor,** and the "Y" nucleus is called the **delayed-neutron emitter.** Obviously, for DFN emission, the "delay time" is determined by the half-life of the precursor nucleus (X), which can be relatively long, since the β^--transition is governed by the weak interaction. Another interesting consequence of this transition chain is that the excitation energy of the delayed-neutron emitter nucleus is usually much lower than the excitation energies of the direct fission fragments. Therefore, the average energy of the delayed fission neutrons is also considerably lower ($E_{\text{av}}^{\text{DFN}} \approx 0.3$ MeV – 0.6 MeV) than that of the prompt neutrons ($E_{\text{av}}^{\text{PFN}} \approx 2$ MeV).

The total yield ν of the fission neutrons is the sum of the yield ν_p of prompt neutrons and the yield ν_d of delayed neutrons

$$ \nu = \nu_p + \nu_d. \tag{5.8} $$

The delayed-neutron fraction is defined as

$$ \beta = \frac{\nu_d}{\nu}. \tag{5.9} $$

The net delayed fission neutron yield is strongly dependent on the fissioning nucleus. The values shown in Table 5.4 suggest two simple rules:

- The delayed-neutron yield increases with the mass-number (A), for the same atomic number (Z);
- The delayed-neutron yield decreases with increasing atomic number, (Z).

Table 5.4: *Delayed fission neutron yields (number of delayed neutrons per 100 fission events) for thermal neutron induced fission of different fissioning nuclides.*

Fissioning nucleus	ν_d (%)	$\beta = \frac{\nu_d}{\nu}$
^{232}Th	#	#
^{233}U	0.667	0.0026
^{235}U	1.621	0.0065
^{238}U*	4.39	0.0157
^{239}Pu	0.628	0.0021
^{240}Pu*	0.95	
^{241}Pu	1.52	
^{242}Pu*	2.21	
*Data for fast-neutron induced fission.		

The delayed neutron groups

Nuclear physicists have identified so far more than 66 delayed neutron precursor nuclei — these are mainly isotopes of Ga, As, Se, Br, Kr, Rb, Sr, Y, In, Sn, Sb, Te, I, Xe, Cs, Ba, La and Tl. Their half-lives range between approximately 0.12 s and 78 s, so that their delayed neutrons appear with considerably differing delay times. A rigorous treatment of the delayed neutrons in reactor-kinetic calculations would consider each precursor nucleus with its own half-life and yield. However there are two problems when proceeding this way:

- The calculation scheme becomes complicated because of the large number of the precursor nuclei;
- The decay scheme, half-life and yield are not well known for every precursor nucleus.

In the 1950s, Dr GR Keepin from LANL in the USA, suggested an acceptable approximate method for these calculations. In his method, the experimentally determined delayed-neutrons were grouped, i.e. binned, based on the half-lives of their precursors. In the Keepin approximation, delayed fission neutrons are binned into 6 groups, each group having an effective halflife and fraction. Table 5.5 summarises the main parameters of the delayed-neutron groups for 3 different fissile nuclei — ^{235}U, ^{239}Pu and ^{233}U. The six delayed-neutron group formalism is widely used in reactor kinetics calculations.

Table 5.5: *Parameters of the delayed-neutron groups for three fissile nuclei (g ≡ energy bin/group).*

g	Possible precursor nuclei	Mean energy (MeV)	Average half-life of the precursor nuclei (s)			Delayed-neutron fraction (%)		
			^{235}U	^{239}Pu	^{233}U	^{235}U	^{239}Pu	^{233}U
1	^{87}Br, ^{142}Cs	0.25	55.72	54.28	55.0	0.021	0.0072	0.0226
2	^{137}I, ^{88}Br	0.56	22.72	23.04	20.57	0.140	0.0626	0.0786
3	^{138}I, ^{89}Br $^{(93,94)}$Rb	0.43	6.22	5.60	5.00	0.126	0.0444	0.0658
4	^{139}I, $^{(93,94)}$Kr ^{143}Xe, $^{(90,92)}$Br	0.62	2.3	2.13	2.13	0.252	0.0685	0.0730
5	^{140}I, ^{145}Cs	0.42	0.61	0.618	0.615	0.074	0.018	0.0135
6	(Br, Rb, As etc)	-	0.23	0.257	0.277	0.027	0.0093	0.0087
Total						0.64	0.21	0.26

Figure 5.4 compares the energy spectra of prompt and delayed fission neutrons.

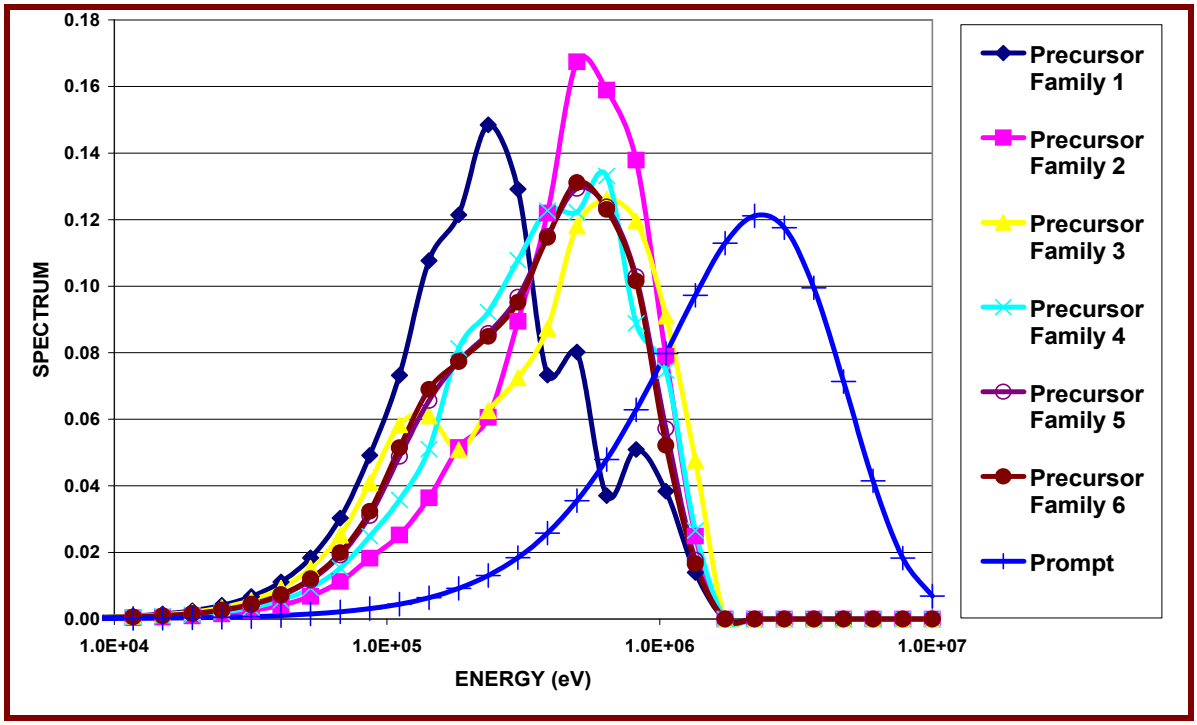

Figure 5.4: *Comparison of the energy spectra of prompt and delayed fission neutrons.*

There is a distinct difference in the energies at which prompt and delayed fission neutrons are emitted. Prompt fission neutrons are born with an average energy of approximately 2 MeV, and their energies may extend as high as ~18 MeV. In contrast, a delayed neutron is born with an average energy of ~0.5 MeV, and its maximum energy is below 2 MeV.

Because a delayed neutron is born with a significantly lower average energy than a prompt neutron (PFN), and also because its energy spectrum has no high-energy tail as is the case for PFNs, delayed neutrons will remain in the fast energy range for a significantly shorter period of time — they are significantly more easily moderated than PFNs. For this reason they are also easier to shield.

5.4.5 Fusion neutrons

When light elements fuse exothermically in nuclear reactions, energetic neutrons are released. The two neutron-producing fusion reactions of most interest are

$$\begin{aligned} &\text{D-T fusion} \quad {}^{2}\mathrm{H} + {}^{3}\mathrm{H} \longrightarrow {}^{4}\mathrm{He}\ (3.5\ \mathrm{MeV}) + {}^{1}n\ (14.1\ \mathrm{MeV}) \\ &\text{D-D fusion} \quad {}^{2}\mathrm{H} + {}^{2}\mathrm{H} \longrightarrow {}^{3}\mathrm{He}\ (0.82\ \mathrm{MeV}) + {}^{1}n\ (2.46\ \mathrm{MeV}) \end{aligned} \tag{5.10}$$

where D ≡ Deuterium and T ≡ Tritium. The cross-section plots for these reactions, as a function of incident energy, is shown in Figure 5.5.

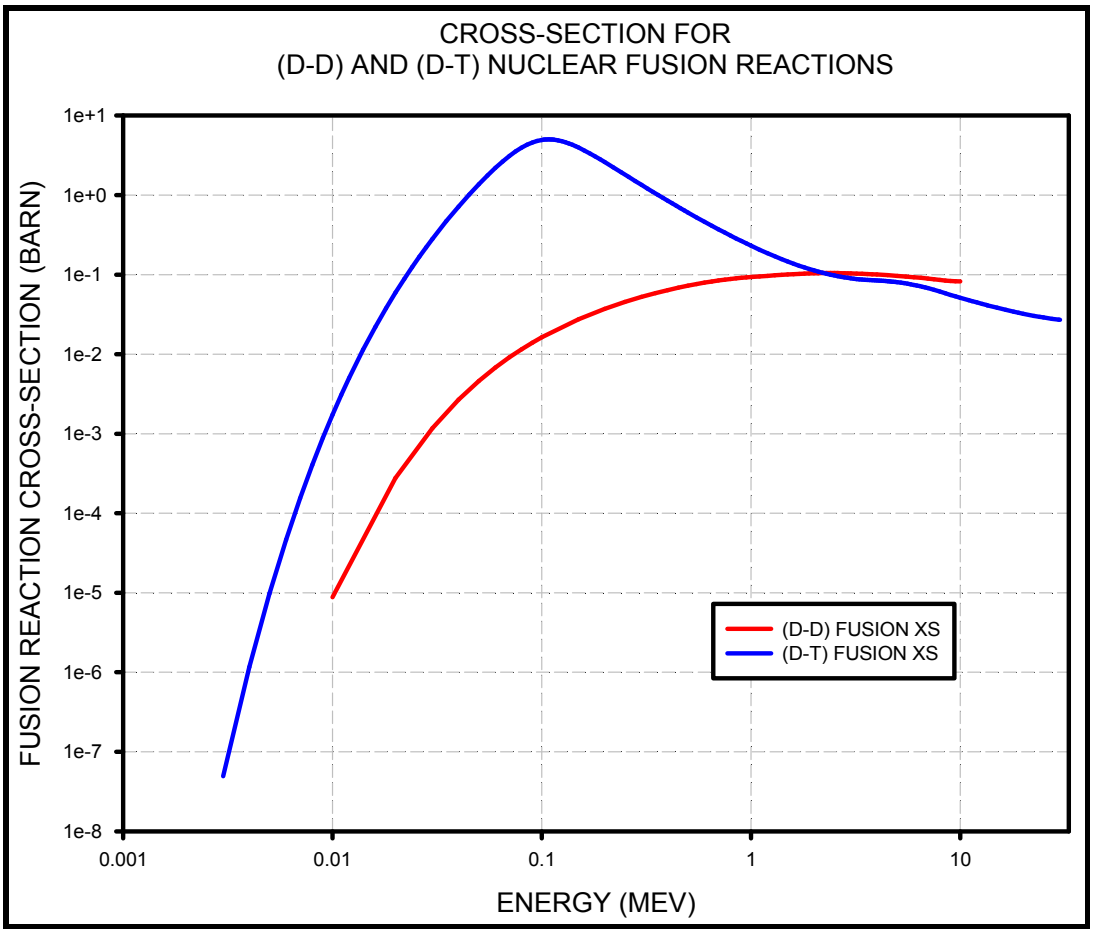

Figure 5.5: *Cross-sections for* (D-D) *and* (D-T) *nuclear fusion reactions.*

For (D-D) nuclear fusion, the incident deuteron energy must be in the range $1-10$ MeV; for (D-T) nuclear fusion, the incident deuteron energy must be close to 0.1 MeV.

For low energy incident deuterons, the velocity of the centre-of-mass is negligible, and the energy spectrum of the emitted (D-T) fusion neutrons is given by Eq. (5.11),

$$S(E) = 1.303 \exp\left[-300\left(\sqrt{E} - \sqrt{14.07}\right)^2\right] \tag{5.11}$$

and for (D-D) fusion neutrons, the energy spectrum of the emitted fusion neutrons is given by Eq. (5.12),

$$S(E) = 5.688 \exp\left[-1000\left(\sqrt{E} - \sqrt{2.46}\right)^2\right]. \tag{5.12}$$

It is especially the Deuterium-Tritium (D-T) nuclear fusion reaction that is commonly used by nuclear physicists for the production of energetic fusion neutrons. These (D-D) and (D-T) fusion neutron production reactions are harnessed in relatively compact fusion neutron-producing devices, called *neutron generators*. In a neutron generator, deuterium ions are accelerated through a high voltage and then strike a deuterium-bearing or tritium-bearing target. In this way, a (D-D) or (D-T) fusion neutrons are produced. Fusion of deuterium

atoms, i.e. $(\mathrm{D}+\mathrm{D})$, results in the formation of a ^{3}He ion and a neutron with a kinetic energy with a narrow Gaussian energy distribution around a peak at $E = 2.46$ MeV. Fusion of a deuterium and a tritium nucleus, i.e. a $(\mathrm{D}+\mathrm{T})$ reaction, results in the formation of a ^{4}He ion and a neutron with a kinetic energy of approximately 14.1 MeV. Thousands of small, relatively inexpensive (D-D) and (D-T) neutron generator systems have been built since ~1950.

A typical advanced commercial compact neutron generator has a diameter of circa 50 cm and is less than 40 cm long. A (D-D) fusion neutron output higher than 10^{13} n/s and (D-T) fusion neutron output of 10^{15} n/s are attainable with such a generator (data for year 2015).

Assignment 5.4

1. Plot the (D-T) fusion neutron spectrum of Eq. (5.12). Ascertain that it is a normalised spectrum.

2. Plot the (D-D) fusion neutron spectrum of Eq. (5.12). Ascertain that it is a normalised spectrum.

5.4.6 Photoneutrons - photonuclear reactions

Low energy ionising photons only interact with the electrons of atoms, i.e. the interaction is quantum electro-dynamic (QED) in nature. Above a threshold energy, which is unique for every nuclide, photons can also produce nuclear reactions. A photon with energy sufficiently large to overcome the neutron separation energy (i.e. the binding energy of the most weakly bound neutron in the nucleus), may produce a (γ, n) reaction when absorbed by a nucleus. For most nuclei, the neutron separation energy is in the order of 7 MeV to 10 MeV.

Quite intense and energetic photoneutron production can be achieved in an electron accelerator where the bombardment of a target with energetic electrons produces intense *bremsstrahlung* with an energy distribution up to that of the incident electron energy. As the photon energy increases above the neutron separation energy, $\sigma_{(\gamma,n)}(E)$ increases by several orders of magnitude to a broad maximum of a few millibarns per nucleon at photon energies of approximately 20 MeV to 23 MeV for light nuclei ($A \lesssim 40$), or 13 MeV to 18 MeV for medium and heavy nuclei. This is called a *giant resonance* peak. The width of the giant resonance varies from about 10 MeV for light nuclei, to 3 MeV for heavy nuclei. Consequently, in medical or accelerator facilities that produce photons with energies above approximately 15 MeV, photoneutron production in the surrounding walls can lead to a significant neutron field, which should not be ignored in radiation safety assessments.

In many ionising photon shielding scenarios, the energies of the ionising photons are well below the threshold energy for (γ, n) reactions, so that photoneutron production is of no concern. Note, however, that a few light nuclides have low thresholds for photoneutron production via (γ, n) reactions. These nuclides are listed in Table 5.6.

Table 5.6: *Nuclides with low threshold energies for photoneutron production, i.e.* (γ, n) *nuclear reactions.*

Nuclide	**Threshold energy** (MeV)	**Nuclear reaction**
^{2}H	**2.225**	**$^{2}\mathrm{H}(\gamma, n)^{1}\mathrm{H}$**
^{6}Li	3.698	$^{6}\mathrm{Li}(\gamma, n+p)^{4}\mathrm{He}$
^{9}Be	1.665	$^{9}\mathrm{Be}(\gamma, n)^{8}\mathrm{Be}$
^{13}C	4.946	$^{13}\mathrm{C}(\gamma, n)^{12}\mathrm{C}$

Specific nuclides such as ^{9}Be, ^{2}D, ^{6}Li and ^{13}C have low neutron separation energies and will produce neutrons via (γ, n)-reactions at photon energies lower than the usual threshold energy of approximately 7-9 MeV, so that photons within the energy range of primary and secondary photons in the radiation field around several types of radiation sources, will be able to produce neutrons, should any of these light nuclides be present. As a result of (1) the low natural abundances in nature of the above 4 nuclides that readily produce neutrons in (γ, n)-reactions, as well as (2) the relatively low cross-sections for these (γ, n)-reactions, they do not normally play any significant role in shielding problems when ionising photon energies are below circa 8 MeV.

For most situations encountered in the incident photon energy range below circa 4 MeV, only photon-induced neutron production by ^{2}H will be of practical importance, because Be and Li have very low natural abundances, and also because the energy threshold for the reaction $^{13}\mathrm{C}(\gamma, n)$ is higher than the maximum energy of ionising photons emitted by radionuclides having half-lives more than a few hours.

Because the natural abundance of ^{2}H (deuterium) in the element H (hydrogen) is ~0.015%, the neutron field deep within a hydrogenous shield is often dependent on photo-neutron production in deuterium. This is all the more pronounced if the hydrogen is enriched in ^{2}H, as is the case with heavy water (D_2O) — in nuclear reactors moderated by heavy water, such as the Canadian CANDU reactors, the (γ, n) photoneutron production rate may not be neglected in accurate reactor calculations. An appreciable fraction of the ionising photons produced by (n, γ) reactions in hydrogenous shields around e.g. nuclear reactors or beam target stations at particle accelerator facilities, has an energy above the threshold of 2.225 MeV for the $^{2}\mathrm{H}(\gamma, n)^{1}\mathrm{H}$ neutron-production reaction, and can therefore produce photoneutrons. At medical accelerators where high-energy ionising photons are produced by *bremsstrahlung,* photoneutron production may not be neglected.

In the case of very *thick* shields composed of e.g. alternating layers of Fe and polyethylene — which contains small amounts of ^{2}H (natural abundance 0.015%) and ^{13}C (natural abundance 1.11%), will photo-neutrons, i.e. neutrons produced in (γ, n) reactions, make a non-negligible contribution to dose rates outside the shielding material. In the above type of shields, Fe produces energetic capture γ-rays with energies in the order of approximately 7 MeV when it

absorbs (mainly slow) neutrons. These high-energy ionising photons will readily produce neutrons in ^{2}H and ^{13}C via (γ, n) reactions.

In a situation where an intense beam of e.g. 40 MeV electrons are stopped in a tungsten alloy target, the reaction rate of (γ, n) reactions, i.e. the neutron production rate, can be very high when the bremsstrahlung in the energy range 20-30 MeV strikes practically any material. For such sources, shield design is quite a challenge — refer e.g. to the recent MSc dissertation by Mr Eric Chinaka (2014).

Figure 5.6 shows the ionising photons that are produced when ^{1}H, Fe and Pb capture thermal neutrons. The graph is based on simulations with MCNPX 2.7 (2011) using ENDF-B/7.0 cross-section data (2008), and shows the total ionising photon production in a 1 mm shell of pure ^{1}H, Fe and Pb, each having a nuclide number density of 0.01 barn^{-1} cm^{-1}.

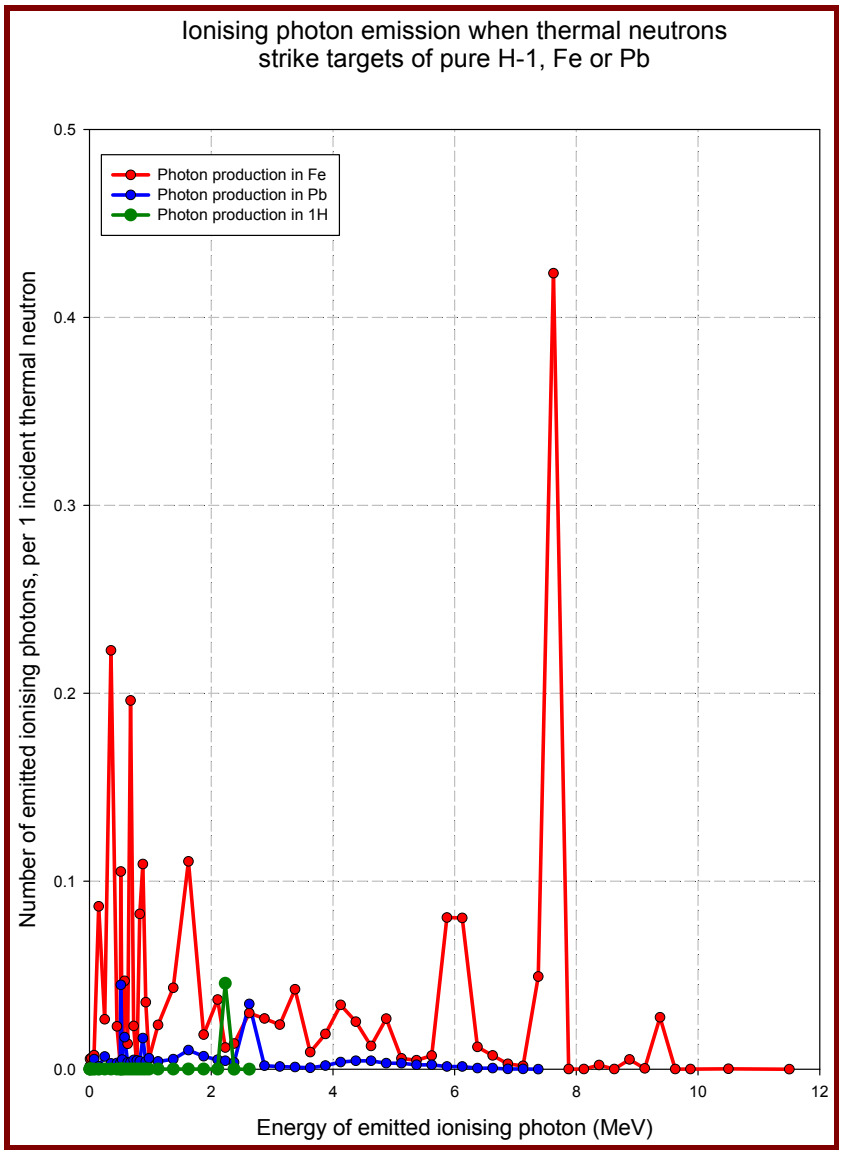

Figure 5.6: *Energies and yields of prompt γ-rays produced when* ^{1}H / *Fe* / *Pb* *capture thermal neutrons.*

Note in Figure 5.6 that Fe produces a relatively high abundance of high-energy photons upon thermal neutron capture. These high-energy photons will cause photo-neutron production via (γ, n) reactions in ^{2}H and ^{13}C in hydrocarbon layers of radiation shields such as | Fe | PE | shields, where PE $\equiv$ polyethylene, or | Fe | Wax | shields. In comparison, Pb produces a far lower yield of high-energy capture γ-rays, so that (γ, n) driven neutron production will be a non-issue in | Pb | Wax | shields.

View a steel/polyethylene | Fe | PE | Fe | PE | Fe | laminated radiation shield around a source of well thermalised neutrons as example. As can be seen from Figure 5.6, Fe will produce significant amounts of high-energy photons in (n, γ) reactions when capturing thermal neutrons. A large fraction of these photons will have energies well above the threshold energy of 2.225 MeV for the reaction ^{2}H (γ, n) ^{1}H, and also above the threshold energy of approximately 5 MeV for the ^{13}C(γ, n) reaction. The natural isotopic abundance of ^{2}H is 0.015%, and the natural isotopic abundance of ^{13}C is 1.07% The average cross-section for the ^{2}H (γ, n) ^{1}H neutron production reaction is about 2 mb. The average cross-section for the nuclear reaction ^{13}C(γ, n) ^{12}C is 1 mb in the energy region between 5 MeV and 10 MeV, 2 mb from 10 MeV to 20 MeV and 8 mb from 20 MeV to 30 MeV. As a result of these low cross-sections, the above two (γ, n)-reaction will only become important in thick laminated | Fe | PE | or | Fe | Wax | radiation shields. When such shields are designed, it is important to use a code and cross-section set that can model (γ, n) photonuclear reactions. MCNPX 2.7 and MCNP6 have this capability — make certain that this reaction option is activated.

Question
Why is it safe to irradiate food with ^{60}Co, but not with e.g. ^{24}Na or spent nuclear fuel?

Answer
Refer to the (γ, n) cross-section plots of ^{2}H and ^{13}C on page 358 and to the threshold energies for (γ, n) reactions listed in Table 5.6 on page 252.

The radionuclide ^{60}Co emits the following ionising photons — column 1 being the photon energy E and column 2 being the emission yield Y per nuclear transition.

E	Y
2.50569E+00	2.00000E-08
2.15857E+00	1.20000E-05
1.33249E+00	9.99826E-01
1.17323E+00	9.98500E-01
8.26100E-01	7.60000E-05
3.47140E-01	7.50000E-05
8.28816E-03	4.86742E-09
8.28784E-03	3.34900E-09
8.22459E-03	7.66065E-06
8.22229E-03	3.90686E-06
7.43578E-03	6.23882E-05
7.41782E-03	3.19463E-05

All food contains hydrogen, and a small fraction of hydrogen is ^{2}H, so that all photons with energies above circa 2.3 MeV will be capable of producing radionuclides in foodstuff. The highest energy gamma-photon emitted by the radioisotope ^{60}Co, with a non-negligible emission yield, has an energy of 1.332 MeV, which falls below the lowest threshold energy for a (γ, n)-reaction in any isotope. The only γ-photon emitted by ^{60}Co that can activate food (which contains $^{2}_{1}$H but usually no $^{9}_{4}$Be and practically no Li), is the 2.506 MeV photon, but its emission yield is very low at $y = 2 \times 10^{-8}$, and the only isotope in food that will be activated by this photon is ^{2}H which has a natural abundance of only 0.015% and a (γ, n) cross-section of circa 1 mb. Accordingly, food will not be measurably activated by neutrons produced in the food via (γ, n) reactions, when ^{60}Co is used as the irradiator isotope. In contrast, ^{24}Na emits a 2.754 MeV gamma photon with an emission yield of 0.99944 per nuclear transition; this energy is higher than the important threshold of 2.225 MeV for the reaction $^{2}\text{H}(\gamma, n)^{1}\text{H}$, so that (γ, n) reactions will take place, and the emitted neutron will activate the food, i.e. produce radionuclides in the food.

As a result, the most practical radionuclide to use in food irradiator facilities, is ^{60}Co. The radionuclide ^{137}Cs is less suitable that ^{60}Co because (1) caesium and its salts are soluble in water and poses a contamination hazard in the event of water leaks into the stainless-steel pins encapsulating the radioisotope, and (2) its maximum γ-energy is in the order of 0.66 MeV, so that the dose distribution in irradiated packages will be significantly worse than that obtained with ^{60}Co, which emits ionising photons at higher energies, which are attenuated less steeply, so that flatter dose distributions in irradiated product packages are obtained.

Spent nuclear fuel emits many ionising photons with $E > 2.225$ MeV, and these energetic ionising photons will cause neutron emission by (γ, n) interactions with the trace quantities of the isotope ^{2}H that is present in all food. Spent nuclear fuel also produces neutrons through (α, n) interactions; these neutrons will cause activation of the irradiated product, i.e. produce radionuclides in the food.

Laboratory neutron sources based on (γ, n)-reactions

The (γ, n) photoneutron production reaction mechanism can be used to produce laboratory neutron sources by intimately mixing a beryllium compound or beryllium metal powder with a radionuclide that emits high energy ionising photons. Alternatively, the encapsulated γ-emitting radionuclide can be surrounded by a beryllium-bearing shell. One of the most commonly used source of photo-neutrons, is an antimony-beryllium (Sb-Be) mixture, which has the advantage that it can easily be rejuvenated by exposing the source to reactor neutrons to transmute the stable ^{123}Sb into the radioactive ^{124}Sb ($T_{½} = 60.2$ days). Such antimony-beryllium (Sb-Be) sources typically emit approximately 30 neutrons per 10^{6} Bq of ^{124}Sb. Photoneutron sources emit reasonably mono-energetic neutrons. They are, however, quite dangerous to handle because typically 10^{4} ionising photons are emitted for every 1 neutron that is emitted.

The importance of (γ, n)-reactions at radiotherapy accelerators

At older generation, low energy radiotherapy installations where 2.3 MeV $\lesssim E_\gamma \lesssim$ 6 MeV, a low fluence-rate of neutrons can be produced by $^{1}\mathrm{H}(\gamma, n)^{2}\mathrm{H}$ reactions and $^{13}\mathrm{C}(\gamma, n)^{12}\mathrm{C}$ with the low concentrations of $^{2}\mathrm{H}$ and $^{13}\mathrm{C}$ in concrete, polymers, the human body, etc.

At radiotherapy installations where $E_\gamma \gtrsim 10$ MeV, a higher fluence-rate of neutrons can be produced by many (γ, n)-reactions, because the neutron separation energy for most nuclides are in the order of 7 MeV – 9 MeV. The photoneutron production cross-section usually has a broad peak in the energy range 15 MeV $\leq E_\gamma \leq$ 30 MeV. When E_γ exceeds circa 15 MeV, the neutron field can become quite intense and present a significant shielding problem.

Threshold photon energy per element for incidence of (γ, n)-reactions

Table 5.7 lists the energy thresholds for (γ, n)-reactions, by element, showing the limiting isotope, i.e. the isotope with the lowest energy threshold value. The elements are sorted from low to high threshold energies.

The element beryllium (i.e. $^{9}_{4}\mathrm{Be}$) can emit neutrons when it is struck by ionising photons with energies above 1.67 MeV. The element lithium can emit neutrons when it is struck by ionising photons with energies above 3.698 MeV. The small fraction of $^{17}\mathrm{O}$ that is present in oxygen, will emit neutrons when struck by ionising photons having an energy above 4.14 MeV. The small fraction of $^{13}_{6}\mathrm{C}$ that is present in natural carbon, can emit neutrons when it is struck by ionising photons with an energy above 4.95 MeV.

***Table 5.7**: The (γ, n)-reaction energy thresholds for a variety of nuclides encountered in engineering materials.*

Element	Limiting Nuclide	Threshold Energy (MeV)
Be	Be-9	1.67
H	H-2	2.22
Li	Li-6	3.70
O	O-17	4.14
C	C-13	4.95
W	W-183	6.19
Sn	Sn-119	6.49
Cd	Cd-113	6.54
Zr	Zr-93	6.73
Pb	Pb-207	6.74
Mo	Mo-97	6.82
Zn	Zn-67	7.05
Nb	Nb-94	7.23
Ag	Ag-108	7.27
Mg	Mg-25	7.33
Bi	Bi-209	7.46
Ta	Ta-181	7.58
Fe	Fe-57	7.65
K	K-40	7.80
Ni	Ni-61	7.82
Ca	Ca-43	7.93
Cr	Cd-53	7.94
Au	Au-197	8.07
Ti	Ti-49	8.14
Si	Si-29	8.47
S	S-33	8.64
Sb	Sb-123	8.97
Cu	Cu-65	9.91
Mn	Mn-55	10.23
Cl	Cl-37	10.31
Co	Co-59	10.45
N	N-14	10.55
V	V-51	11.05
Na	Na-23	12.42
Al	Al-27	13.06

How to read and use the above table - examples:

1. If photons with E > 1.67 MeV fall on beryllium, neutrons will be produced in (n, γ)-reactions with Be, and neutron activation becomes an issue. The neutron production rate can be appreciable, because all natural Be is in the form of the isotope ${}^{9}_{4}\mathrm{Be}$.

2. If photons with E > 4.14 MeV fall on oxygen, neutrons will be produced in (n,γ)-reactions with the tiny fraction of $^{17}_{8}\mathrm{O}$ present in oxygen, and neutron activation could become an issue.

3. If photons with E > 4.95 MeV fall on carbon, neutrons will be produced by in (n,γ)-reactions with the small fraction of $^{13}_{6}\mathrm{C}$ present in carbon, and neutron activation could become an issue.

4. If photons with E > 2.22 MeV fall on hydrogen in water, wax or polymers, neutrons will be produced in (n,γ)-reactions with the tiny fraction of $^{2}_{1}\mathrm{H}$ present in hydrogen, and neutron activation could become an issue.

5. From the viewpoint of the energy threshold for an undesired nuclear interaction that will produce undesired neutrons, aluminium is the least "worrisome" and most robust engineering material.

Assignment 5.5

1. Model the following with MCNPX6, using an F2 tally. Abbreviations have the following meanings. Use a point source and spherical geometry, with a simple variance reduction scheme, such as cell importance biasing.

NDR	=	Neutron dose rate
PDR	=	Photon Dose Rate
TDR	=	Total Dose Rate; TDR = NDR + PDR

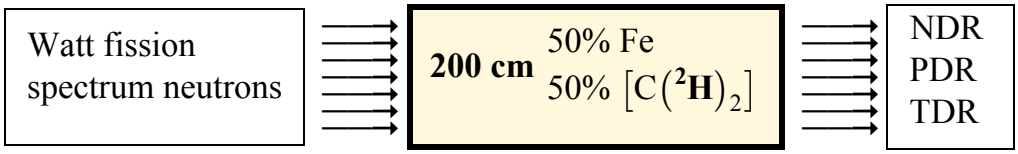

Run the following cases and compare the transmitted dose rate:

(a) MODE N P with photoneutron production turned **on**;

(b) MODE N P with photoneutron production turned **off**.

Quantify the importance of modelling (γ,n)-reactions in a fission reactor shielding medium containing a high energy (n,γ) ionising photon emitter such as Fe, and $^{2}_{1}\mathrm{H}$, which has a low threshold for (γ,n) neutron emission reactions. Is there a significant increase in the neutron fluence rate and the neutron dose rate at the exit side of the shield? Quantify the impact of modelling (γ,n) reactions on the NDR, PDR and TDR at the outer surface of the shield.

2. Use MCNP6 to check, by means of computational experiments, whether implementing ALL of the following steps will have a qualitatively significant impact on the results of

reactor neutronics calculations for a simple model of a heavy water cooled & moderated MTR. Investigate the impact on the integral parameter k_{eff} as well as on the thermal neutron fluence-rate, taken as

$$\int_{10^{-11}\,\text{MeV}}^{10^{-6}\,\text{MeV}} \phi(E)\,dE$$

in a D_2O pool surrounding the nuclear reactor, in a detector volume approximately 100 cm from the wall of the reactor.

(a) Switch on (γ, n) reactions in the PHYS:P card;

(b) Use cross-section sets that include photon production data;

(c) Run MCNP6 in | MODE N P | i.e. model neutron as well as photon transport;

(d) Model ionising photon emission by fission products, by specifying | **-102** | at the correct place in the PHYS:P card.

Note: The following recommended way to request fission product gamma-photon production, does not seem to work in MCNPX 2.7:

```
ACT       FISSION = ALL
          NONFISS = ALL
          DN      = BOTH
          DG      = LINES
          NAP     = 20
```

5.4.7 Neutrons from (α, n) reactions

Many compact laboratory neutron sources use energetic alpha particles from various radionuclides (called *emitters)* to induce (α, n) reactions in appropriate materials (called *converters)*. Light elements are used as converters, because the α-particles from radioisotopes can readily penetrate the relatively low nuclear Coulomb potential barrier of lighter nuclei.

Beryllium ($^{9}_{4}$Be) is the most efficient converter material for neutron production reactions, because its neutron separation energy is the lowest of all isotopes[17], and therefore emits the most energetic neutrons for a given incident α-particle energy.

Important (α, n) reactions are listed in Table 5.8.

[17] Removing a neutron from $^{9}_{4}$Be leaves $^{8}_{4}$Be, which is essentially two $^{4}_{2}\alpha$ particles; the radio-isotope $^{8}_{4}$Be disintegrates practically immediately into two $^{4}_{2}\alpha$ particles.

Table 5.8: *Important (α, n) reactions (Shultis & Faw, 2000: 88)[18].*

Target (converter)	**Natural abundance** (%)	**Nuclear reaction**	**Threshold energy** (MeV)
^{9}Be	100	$^{9}\text{Be}(\alpha, n)^{12}\text{C}$	exothermic
^{9}Be	100	$^{9}\text{Be}(\alpha, n)3\alpha$	2.272
^{18}O	0.205	$^{18}\text{O}(\alpha, n)^{21}\text{Ne}$	0.852
^{19}F	100	$^{19}\text{F}(\alpha, n)^{22}\text{Na}$	2.361

The nuclides ^{18}O and ^{19}F listed in Table 5.8 are of special interest, because they are responsible for neutron production in many areas of the nuclear fuel cycle. Alpha particles emitted by isotopes of uranium and plutonium, which are ubiquitous in the nuclear fuel cycle, range between energies approximately 4 MeV and 6 MeV. These energies are well above the threshold energies listed in Table 5.8, and can therefore cause (α, n) neutron production reactions in uranium & plutonium compounds such as UO_2, PuO_2, UF_4, and UF_6, because all fluorine consists of the stable isotope ^{19}F and because all oxygen contains about 0.205% ^{18}O. During uranium enrichment, α-particle emitting actinide isotopes are in the presence of fluorine, because uranium is in the chemical form UF_6 during enrichment in gas centrifuges. In the chemical form UO_2 as well as in aqueous solutions or suspensions, uranium is in the presence of oxygen, a small isotopic fraction (0.205%) of which is ^{18}O. Neutrons produced by (α, n) reactions are therefore important in UF_4, UF_6 as well as in UO_2, PuO_2, ThO_2 and all aqueous solutions and suspensions of uranium and plutonium. Note that all spent reactor fuel that contains O and F will produce neutrons by (α, n) reactions.

Important commercially available (α, n) sources are listed in Table 5.9.

Table 5.9: *Important commercially available (α, n) sources.*

Source	$T_{½}$	$\bar{E}_n$ (MeV)	**Maximum neutron yield per 10^6 primary alphas**
$^{241}\text{Am/Be}$	432 y	4.4	75 (to 100)
$^{226}\text{Ra/Be}$	1600 y	3.9	500

[18] Note: Reaction threshold energies in JANIS 4 differ from the threshold energies listed in this table. Reasons are unclear.

Neutrons emitted by (α, n) reactions have a well-defined maximum neutron energy.

Figure 5.7 shows the experimentally determined energy spectrum of a typical ^{241}Am-Be (α, n) neutron source (ISO Am-Be spectrum, year 2000 standard).

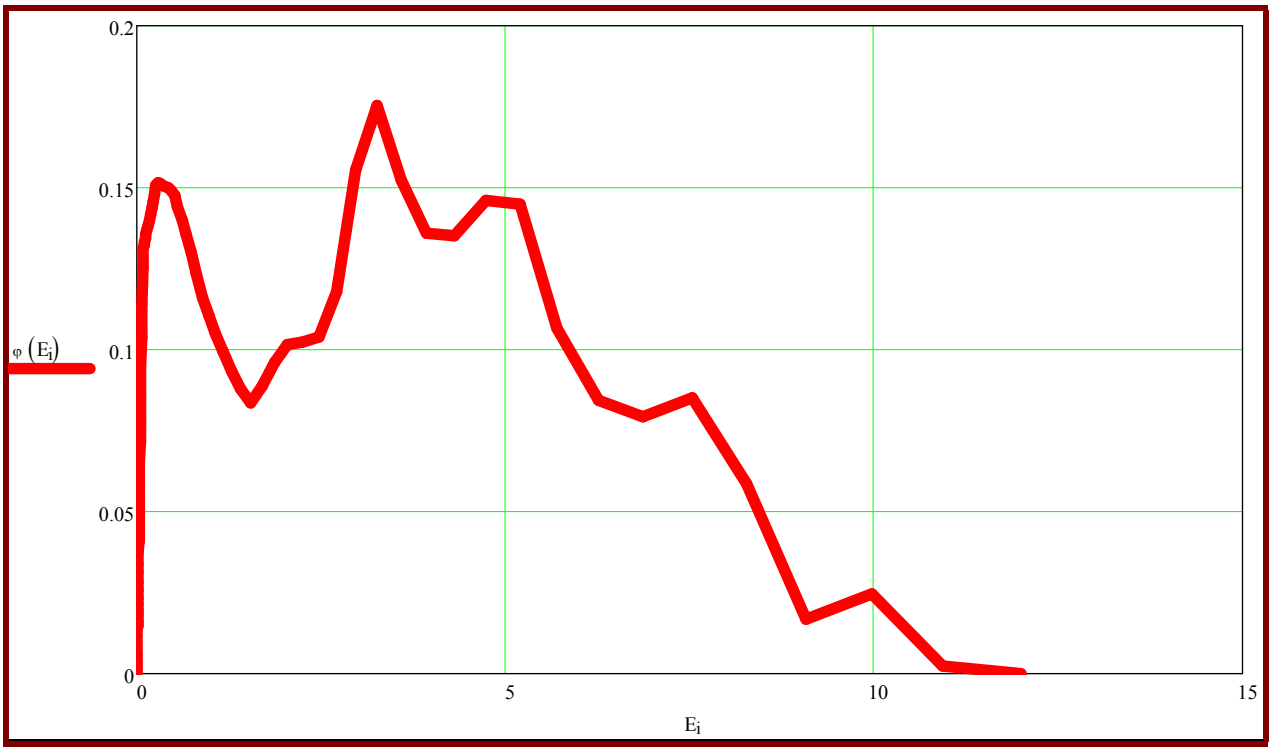

Figure 5.7: *The energy spectrum of a typical ^{241}Am-Be (α, n) source[19]. The neutron energy unit is MeV.*

Note that the maximum neutron energy from an ^{241}Am-Be (α, n) is just below 11 MeV, and that the average neutron energy is 4.2 MeV.

The following MathCAD worksheet shows a dose calculation for a ^{241}Am-Be (α, n) source.

Dose rate near 16 Ci Am-Be NEUTRON Source - New ISO 2000 Spectrum.xmcd

[19] The neutron energy spectrum of a given design of Am-Be source is supplied by the source manufacturer; the energy spectrum and neutron yield of every source design differs somewhat.

Assignment 5.6

1. Run MCNP6 with a SDEF PAR=A ENG=10 source definition, i.e. define a source emitting α-particles. Let these α-particles fall onto a ^{9}Be target. Construct a neutron tally. Let the code run in MODE A N P. Are neutrons detected in the tally?

An MCNPX 2.7.4 input file for a (futile) attempt to model an (α, n) source:

```
Attempt to simulate (alpha,n) reactions
c Cell Cards
1  1  -1.205E-3    -1          imp:a,n,p,e=1      $ Air
2  2  -1.84        -2  +1      imp:a,n,p,e=1      $ Be
3  1  -1.205E-3    -3  +2      imp:a,n,p,e=1      $ Surrounding Air
4  0                   +3      imp:a,n,p,e=0      $ UmWelt -- "EXTERNAL
VOID"
c ====================================================

c ====================================================
c Surface Cards
1  SPH 0  0  0      +1.0    $ AIR OR
2  SPH 0  0  0      +1.2    $ Be OR
3  SPH 0  0  0     +10.0    $ Outer AirShell OR; start of UmWelt
c ====================================================

c ====================================================
c Data Cards
c Mode: transport photons
mode a n p e
c source definition:
sdef par=a pos=0 0 0 erg=10
c
c Material definitions
m1      6000   -1.24E-4         $ Air, dry.  Density = 1.205E-03 g/cc
        7014   -0.755267        $ Air, dry.  Density = 1.205E-03 g/cc
        8016   -0.231781        $ Air, dry.  Density = 1.205E-03 g/cc
       18000   -0.012827        $ Air, dry.  Density = 1.205E-03 g/cc
c
m2      4009   -1               $ Be-9
c
phys:n   20
          0
          0
       -1001
          -1
           0
           0
phys:p   20
           0
           0
          -1
           1
           0
c
fc12 Tally = neutron fluence-rate at surface
```

```
f12:n  2
c
ctme 5
```

The MCNPX 2.7.4 output for the above futile attempt to model an (α, n) source, is as follows:

```
                    tally   12
      nps       mean      error    vov  slope    fom
   256000   0.0000E+00 0.0000 0.0000  0.0 0.0E+00
  3150881   0.0000E+00 0.0000 0.0000  0.0 0.0E+00
```

In other words, the as-supplied MCNPX 2.7.4, with its as-supplied MCNPDATA cross-section libraries, does not take into account (α, n) reactions in the "Table Physics" low-energy alpha-particle energy range — a deplorable fact.

2. Run MCNP6 with a `SDEF PAR=P ENG=10` source definition, i.e. define a source of 10 MeV incident photons. Let the high-energy photons strike a ^{9}Be target, which is surrounded by D_2O, i.e. heavy water. Ascertain whether neutrons are produced by (γ, n)-reactions.

The MCNP input file that models a (γ, n) source:

```
(gamma,n) reactions with MCNPX
c Cell Cards
1  1  -1.84        -1          imp:n,p=1      $ Be
2  2  -1.10        -2  +1      imp:n,p=1      $ Surrounding Air
3  0                  +2      imp:n,p=0      $ UmWelt -- "EXTERNAL VOID"
c ==================================================

c ==================================================
c Surface Cards
1  SPH 0  0  0     +20.0    $ Be OR
2  SPH 0  0  0     +50.0    $ D2O OR; start of UmWelt
c ==================================================

c ==================================================
c Data Cards
c Mode: transport photons
mode n p
c source definition:
sdef   par = p
       pos = 0 0 0
       erg = 10
c
c Material definitions
m1     4009      -1       $ Be-9
       nlib = 70c
       plib = 05p
c
m2     1002      +2       $ D in D2O
       8016      +1       $ O in D2O
       nlib = 70c
```

```
      plib = 05p
c
c ========
c
phys:n   20
          0
          0
      -1001
         -1
          0
          0
phys:p   20
          0
          0
         -1   $ Switch on (gamma,n) reactions
          1
          0
c
c ========
c **** Tally specs *******
fc12 Tally = neutron fluence-rate at surface
f12:n  1  2
c
c === RUNTIME CONTROLS ======
ctme 30
```

Result:

nps	mean	error	vov	slope	fom
8192000	8.4744E-06	0.0092	0.0002	10.0	4879
40960000	8.3628E-06	0.0041	0.0000	10.0	4837
102880839	8.3662E-06	0.0026	0.0000	10.0	4945

Conclusion: The "as supplied" version of MCNP6 does indeed model (γ, n) nuclear reactions, provided that this reaction is "switched on" in the phys: p card — consult the code manual.

5.4.8 An activation product that emits neutrons

The nuclide ^{17}N is produced in water-moderated nuclear reactors as well as in the circulating coolant water of radionuclide production beam target stations at particle accelerators, by an (n, p) reaction with ^{17}O, the natural abundance of which is 0.038%.

$$^{17}\mathrm{O}\,(n, p)\,^{17}\mathrm{N}.$$

The threshold energy for this (n, p) reaction is 8 MeV. The cross-section for this (n, p) reaction is quite small at approximately 5.2 μb (averaged over a prompt fission neutron

spectrum). The nuclide ^{17}N undergoes β^--transition with a halflife of $T_{½} = 4.4$ s, to produce ^{17}O in a highly excited state, which in turn transitions rapidly by ***neutron emission;*** the emitted neutrons have energies close to 1 MeV. Careful surveys with radiation detector instrumentation that can discriminate well between neutrons and ionising photons, may be able to detect small fluence-rates of neutrons emitted from circulating coolant in the above facilities.

Off-the-shelf radiation transport codes will generally not model this neutron-producing reaction pathway.

5.5 Sources of ionising photons

5.5.1 Radioactive sources that emit ionising photons

When radio-active nuclides transition, progeny nuclides are almost invariably left in excited states whose subsequent transition to lower energy states usually results in the emission of one or more gamma photons.

The present ICRP reference source for the ionising photon, electron and positron emissions by radionuclides, is ICRP-107. Note that not all compilations of radiation emissions are tailored for shielding calculations, because some leave out the 0.511 MeV annihilation photons produced by positron emitters. The ICRP-107 database has a GUI DBFE[20] called DECDATA, which runs under Windows on a PC. DECDATA Version 2.7 provides access to a nuclear decay database of 1252 radionuclide presented in ICRP Publication 107 entitled "Nuclear Decay Data for Dosimetric Calculations." The database contains the physical data needed in calculations of absorbed dose due to intake of, or exposure to, a radionuclide and members of its decay chain.

5.5.2 Prompt fission gamma photons

The fission process produces copious gamma photons, which may be classified as follows in terms of the time when they are emitted:

- If emission is within the first ~60 ns after the fission event, these gamma-photons are called *prompt fission gamma photons* (abbreviation: PFG);
- Ionising photons emitted from the radioactive transition of fission products, are sometimes termed "delayed fission gammas" (abbreviation: DFG). However, the preferred terminology is *ionising photons emitted by fission products* or, alternatively, *fission product gamma photons.*

For the fission of ^{235}U, the number of prompt fission gamma photons is approximately 8.13 per fission; their energies extend from $E = 0.1$ MeV to $E = 10.5$ MeV. The total emitted prompt fission gamma photon energy is 7.7 MeV per fission; the average prompt photon energy per fission is about 0.95 MeV.

Optional: Simple empirical fit to PFG spectrum

A reasonably acceptable analytical fit to the **prompt fission ionising photon** spectrum for ^{235}U, is (Shultis & Faw, 2000: 95):

---

[20] Graphical User Interface (GUI) serving as Data-Base Front-End (DBFE).

$$S_{p\gamma}(E) := 1.056 \cdot \begin{cases} 6.6 & \text{if } 0.1 < E < 0.6 \\ 20.2 \cdot \exp(-1.78 \cdot E) & \text{if } 0.6 < E < 1.5 \\ 7.2 \cdot \exp(-1.09 \cdot E) & \text{if } 1.5 < E < 10.5 \\ 0 & \text{otherwise} \end{cases} \tag{5.13}$$

where the energy E is expressed in MeV and the units of the fitting function is prompt fission gamma-photons per fission.

The average number of prompt fission photons emitted per fission event, is approximately

$$\int_0^{12} dE\, S_{p\gamma}(E) = 8.1$$

The approximate prompt fission photon spectrum for the fission of ^{235}U, as fitted by Eq. (5.13) is shown in Figure 5.8.

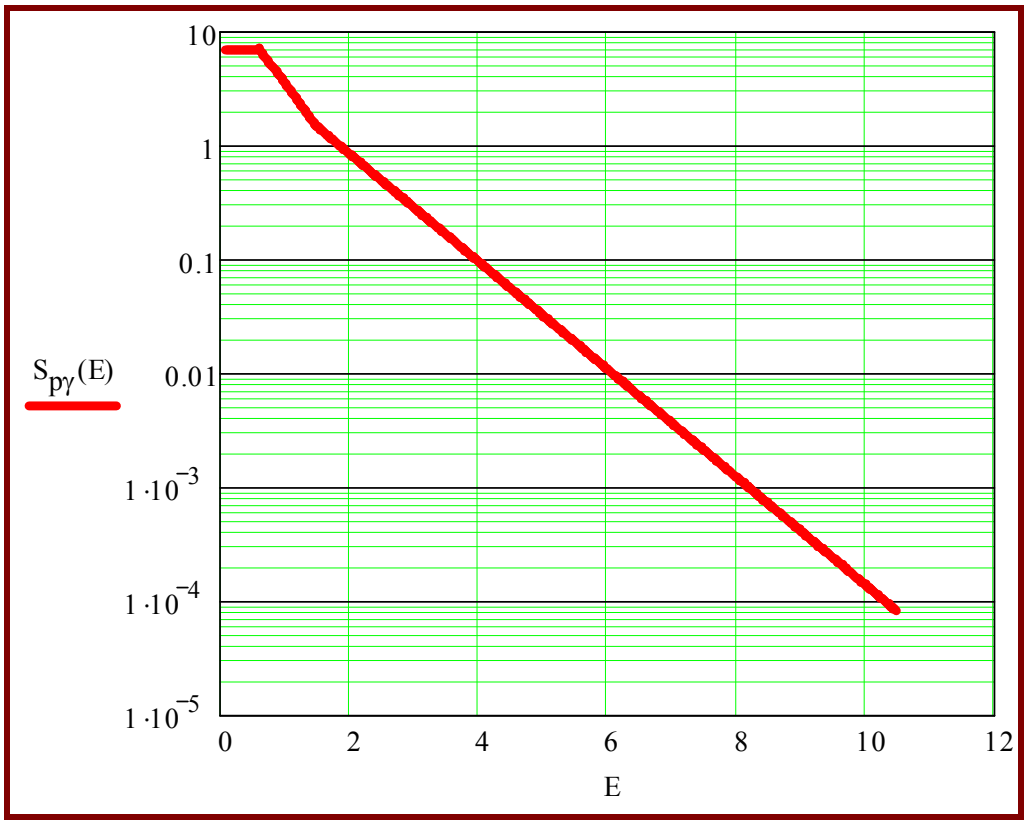

Figure 5.8: *The prompt fission photon spectrum for fission of ^{235}U, according to the fit of Eq. (5.13).*

The number of prompt fission ionising photons from ^{235}U is approximately 8 per fission; their energies extend from about $E = 0.1$ MeV to $E = 10.5$ MeV.

The prompt fission photon spectrum for other fissioning systems such as ^{233}U, ^{238}U and ^{239}Pu is similar to that of ^{235}U.

5.5.3 Ionising photons from fission products

With the widespread application of nuclear power, many shielding analysts regularly have to perform calculations of the ionising photon source-term presented by fission products produced in nuclear reactor fuel. The total energy of ionising photons produced after $t = 50$ ns after fission, is comparable to the energy released as prompt fission gamma photons. About 75% of the photon energy from fission products are released in the first 1000 seconds ($\approx$ 17 minutes) after fission (Shultis & Faw, 2000: 95).

A rough representation of the average energy spectrum of ionising photons produced by fission products from the fission of ^{235}U, for times up to 500 s after the fission, is the proportionality (Shultis & Faw, 2000: 95-96)

$$S_{d\gamma}(E) \propto \exp(-1.1E) \tag{5.14}$$

which is shown in Figure 5.9.

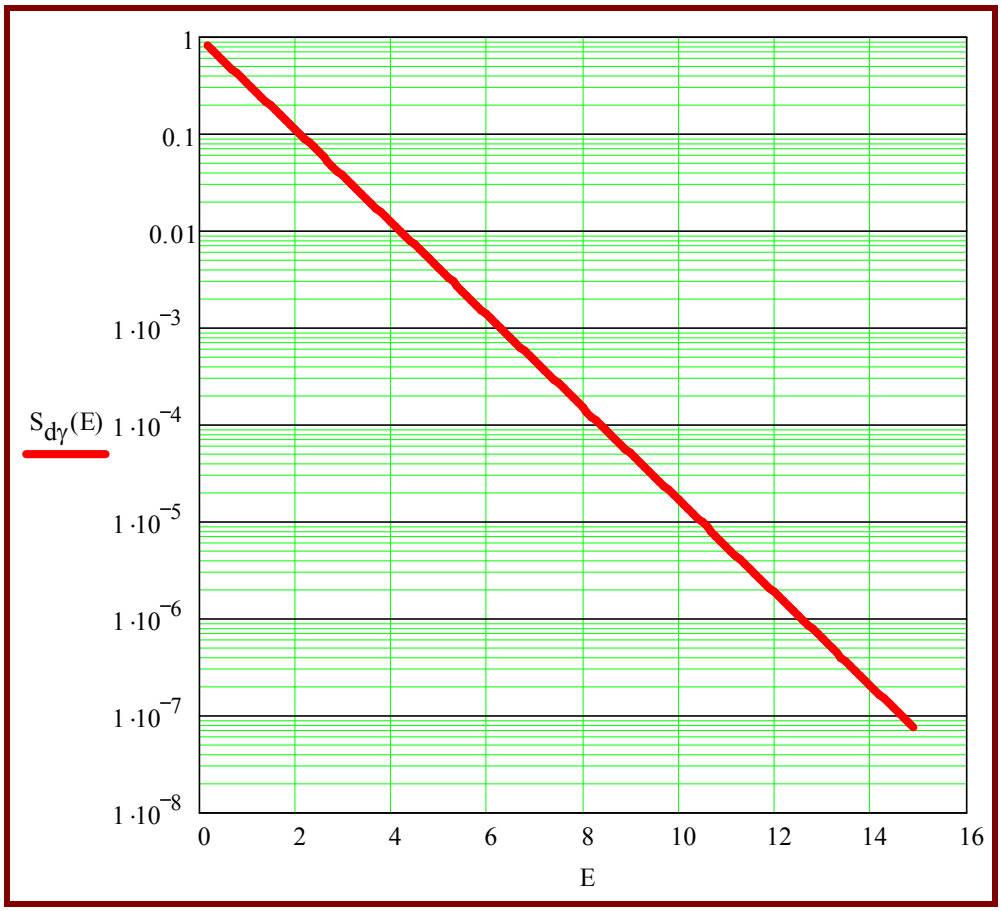

Figure 5.9: *Approximate representation of the average energy spectrum of ionising photons produced by ^{235}U fission products, for times up to 500 s after the fission event. The fit of Eq. (5.14) is illustrated here.*

Accurate measurements show a significantly more complex spectral shape for fission product gamma-photons, depicted in Figure 5.10.

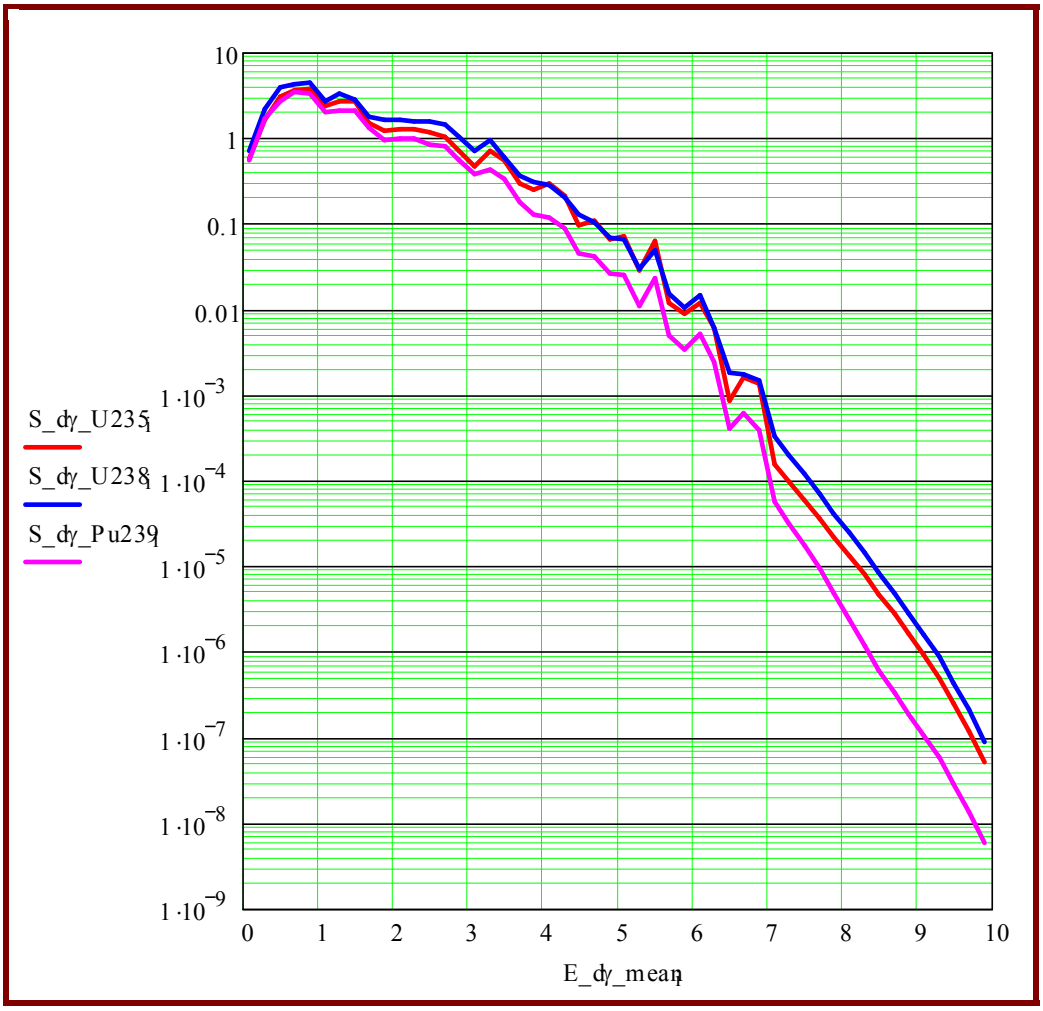

Figure 5.10: *Measured ionising photons spectra from fission products for three different fissioning nuclides — ^{235}U, ^{238}U and ^{239}Pu.*

Fission products formed from ^{238}U fission produce the highest yield of ionising photons, because the higher neutron excess in the parent nucleus leads to fission products with higher neutron excesses, that are more unstable than e.g. fission products from ^{233}U, which has a lower neutron excess — see Figure 5.10.

On average, a total of approximately 13 ionising photons are emitted per ^{235}U fission event — this includes both prompt and delayed fission gamma-photons. Even though more ionising photons than prompt fission neutrons (PFNs) are emitted per fission event, PFNs present the major shielding problem in nuclear reactor shield design, because neutrons are more penetrating, produce radionuclides by neutron activation reactions, and produce secondary ionising photons through e.g. (n,γ) reactions and from the de-excitation of nuclei excited in inelastic neutron scattering reactions.

The fission product photon energy spectrum emitted by spent nuclear fuel becomes "softer" (i.e. less energetic) with time after fission, because successive radioactive transition products

move closer and closer to the valley of β-stability, as the neutron excess is lowered and the $\left(\frac{\text{neutron}}{\text{proton}}\right)$-ratio for stability against β^--transition is approached.

As a general rule, ionising photons emitted by fission products are not very important in the shielding of a reactor operating under full power, because the radiation field is dominated by neutrons and the ionising photons are largely absorbed within the high-Z materials in the reactor core and pressure vessel wall. The consideration of fission product γ-rays in nuclear reactor shielding calculations increases the calculated total dose rate outside the reactor pressure vessel wall by less than ~1 % (Assignment: verify this un-referenced, unmotivated statement and correct it if necessary.) However, when spent fuel is removed from a reactor core, ionising photons emitted by fission products constitute the dominant ionising radiation type.

Note that MCNP5 can not (in 2013) automatically model ionising photons emitted by fission products, but that MCNPX 2.7 does have this capability. This option must be specifically turned on in the PHYS:p card by specifying the -102 option, or the -101 option if memory does not permit the more accurate -102 option.

PFG and DFG energy spectra from MCNPX simulations

A simulation with MCNPX 2.7 yielded an energy spectrum for ^{235}U PFGs shown in Figure 5.11.

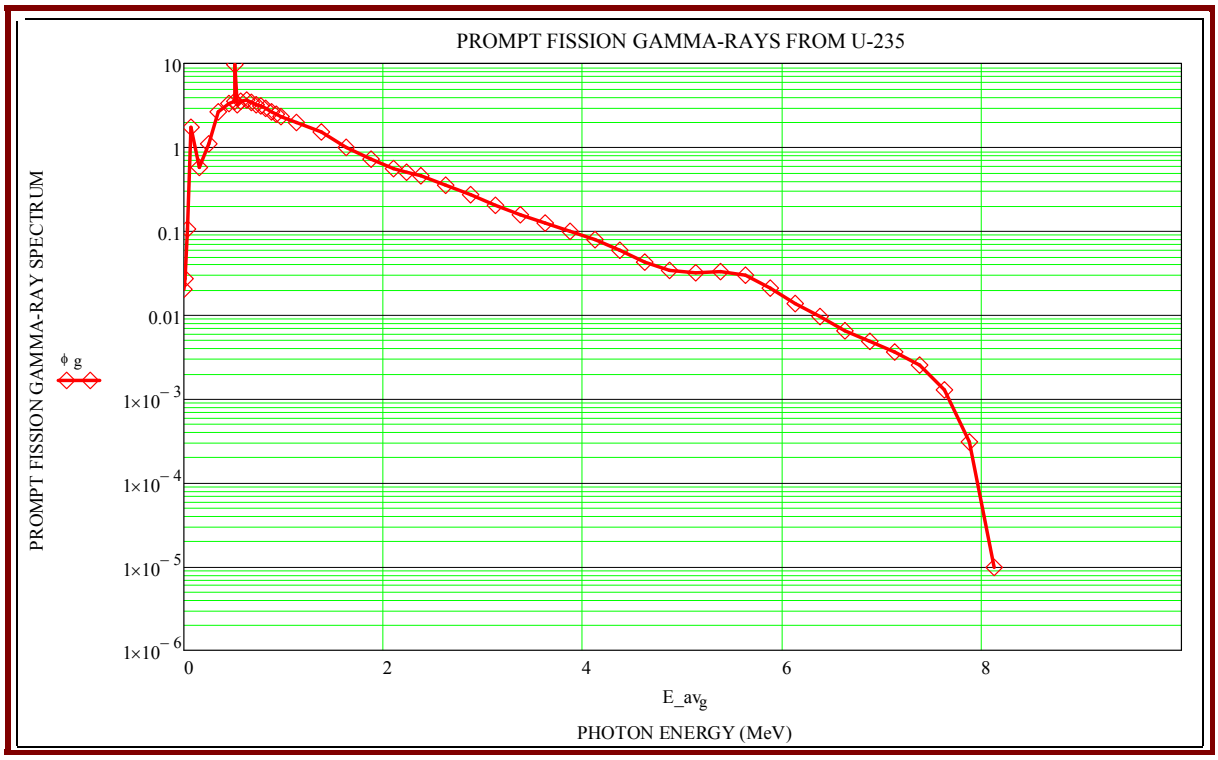

Figure 5.11: *Prompt fission gamma-photon spectrum, for fission of ^{235}U; the spectrum extends to a maximum photon energy of 8.25 MeV.*

A simulation with MCNPX 2.7 yielded an energy spectrum for ^{235}U fission product gamma-rays shown in Figure 5.12.

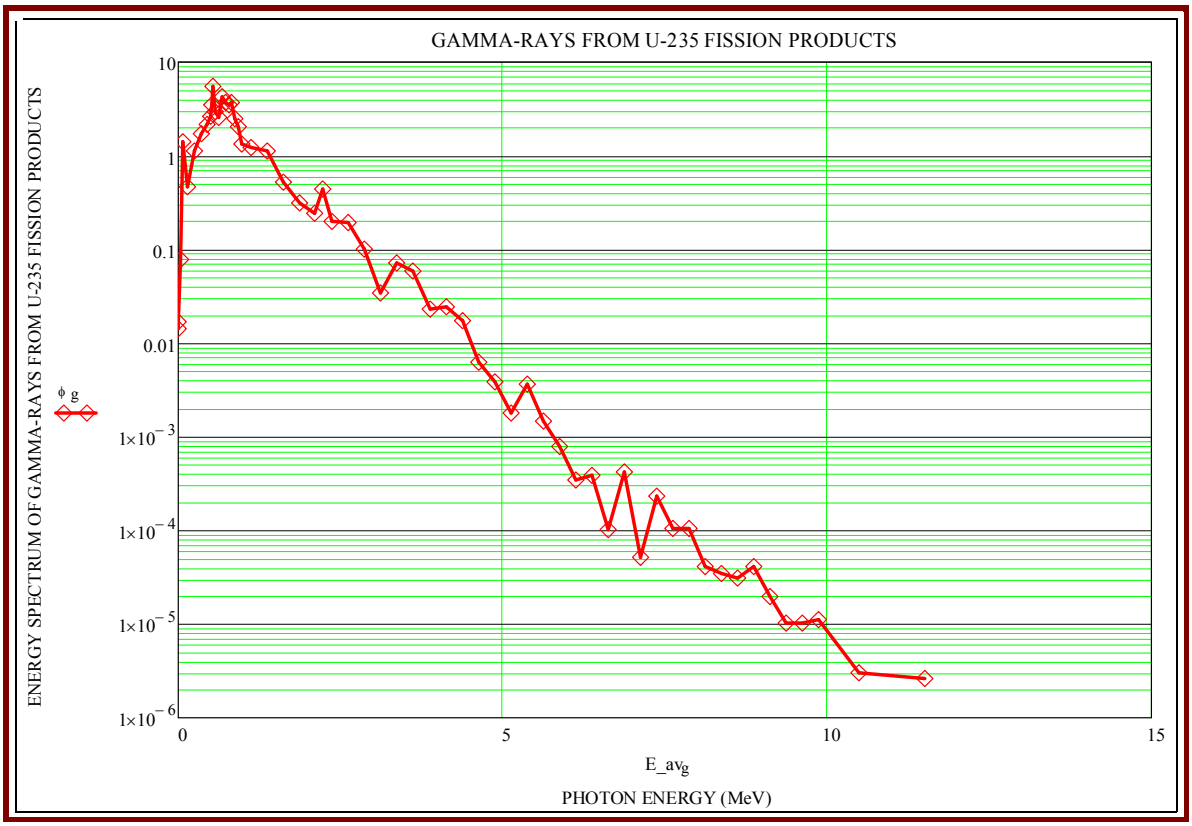

Figure 5.12: *Energy spectrum for ^{235}U fission product gamma-rays. The spectrum extends to a photon energy of 12 MeV.*

The MCNPX 2.7 simulation produced 4.4 prompt-fission gamma-photons and 3.23 fission-product gamma-photons per incident thermal neutron[21].

By comparing Figure 5.8 (page 267) with Figure 5.11, and Figure 5.10 (page 269) with Figure 5.12, and , it is clear that MCNPX 2.7 simulations predict the PFG and fission product gamma-photon spectra quite accurately.

Assignment 5.7

1. Run MCNPX 2.7 or MCNP6 with a point source of 10^{-9} MeV thermal neutrons embedded at the centre of a sphere of pure ^{235}U having a radius of approximately 0.1 cm. Switch OFF the production of "fission product gamma-rays" in the PHYS:p

[21] Note: It was also found that the ACT card specification does not work, but that the -102 specification on the "deprecated" PHYS:P physics card specification is still needed to produce gamma-rays from fission product, i.e. to activate the CINDER component of MCNPX 2.7.

physics card. Use an F1 tally along with an E energy bin card to obtain the photon energy spectrum on the outer surface of the ^{235}U sphere. The ionising photons that are detected will be largely prompt fission γ-photons. Graph and compare the prompt fission γ-spectrum with Figure 5.8 on page 267.

2. Run MCNPX 2.7 or MCNP6 with a point source of 10^{-9} MeV thermal neutrons embedded at the centre of a sphere of pure ^{235}U with a radius of about 0.1 cm. Switch ON the production of "fission product gamma-rays" with a $\boxed{-102}$ specification in the relevant entry on the PHYS:p card. Use an F1 tally along with an E energy bin card to obtain the photon spectrum on the outer surface of the ^{235}U sphere. Deduct the prompt ionising photon spectrum from the total ionising photons spectrum to obtain and graph the spectrum of the ionising photons emitted by fission products, i.e. the DFG spectrum. Graph and compare the spectrum with Figure 5.10 on page 269.

3. Repeat for ^{239}Pu and ^{233}U to obtain their prompt fission gamma-ray spectra.

4. Repeat for ^{239}Pu and ^{233}U to obtain their spectra of ionising photons emitted by fission products (i.e. PFG spectra).

Examples of the importance of ionising photons from fission products

1) When a nuclear reactor is operated at full power for some time, and is then is scrammed[22], the gamma photons from fission products initially produce about 7% of full power thermal energy. This energy production rate slowly diminishes with time. The amount of radioactive materials present in the reactor at the time of shutdown is dependent on the power levels at which the reactor operated and the amount of time spent at those power levels. The amount of decay heat is very significant; a nuclear reactor operated at full power for 3 or 4 days prior to shut down has much higher decay heat generation than a reactor operated at low power for the same period. A reactor operated at 3600 MW (thermal) for some days prior to being shut down, will produce approximately 252 MW of decay heat immediately after shutdown; if no cooling is present, this decay heat can melt certain types of reactor cores. The amount of decay heat produced in the reactor will exponentially decrease as more and more of the radioactive material decays to stable nuclides. Decay heat will decrease to about 2% of the pre-shutdown power level within the 1 hour after shutdown, and to 1% of pre-shutdown power levels within 1 day. Decay heat will continue to decrease, but the rate of decrease will diminish exponentially. Decay heat will be significant for months after the reactor is shut down. Failing to cool a water-cooled reactor core after shutdown will result in core damage. The decay heat $P_{\mathrm{D}}(t)$ produced at time t by all the fuel in a nuclear reactor fuel after months at full power P_{th}, after decay time t, is approximated quite well by the simple relationship

---

[22] "SCRAM" means to shut down a nuclear reactor by e.g. the insertion of control rods. SCRAM is an initialism for "Safety Control Rod Axe Man" — named after the crude reactivity control technique used in the historical 1942 Chicago football pavilion "critical pile." The man who stood ready with an axe to cut the rope holding the safety control rod, should things have gone wrong with the first "critical pile", repeatedly joked, "I am the **S**afety **C**ontrol **R**od **A**xe **M**an…" Therefore shutting down a nuclear reactor by insertion of control rods acquired the name "SCRAM."

$$P_{\mathrm{D}}(t) = (P_{\mathrm{th}})\, 0.062\, t^{-0.2} \tag{5.15}$$

where the unit of time t is seconds.

In many older generation nuclear reactors, which are not based on inherently safe design principles, this "decay heat" is enough to cause severe core damage for many days or even months following reactor shutdown, unless the heat is removed by circulating coolant covering the fuel assemblies; this heat must be dumped in a heat exchanger such as a steam generator. In the event of a LOCA or a LOHA, core damage can occur, so that a emergency reactor coolant injection system must be engineered to provide reactor core cooling in the event of a LOCA, LOHA or a LOFA[23].

2) Fission product gamma emission is very important in the design of spent fuel transport flasks as well as storage design for spent reactor fuel elements. The SCALE system, specifically the code ORIGEN-S in SCALE, is used to calculate the inventory of fission products, transuranic nuclides and activation products in nuclear reactor fuel. SCALE is a comprehensive modelling and simulation suite for nuclear safety analysis and design. The SCALE home page is **http://scale.ornl.gov** .

Important short-lived fission products are short-lived isotopes such as ^{131}I and ^{140}Ba. After approximately four months ^{141}Ce, ^{95}Zr/^{95}Nb, and ^{89}Sr represent the largest share of radioactive material. After two to three years, ^{144}Ce/^{144}Pr, ^{106}Ru/^{106}Rh, and ^{147}Pm constitute the bulk of the radioactivity. After a few years, the radiation is dominated by ^{90}Sr/^{90}Y and ^{137}Cs, whereas in the period between 10,000 and a million years it is ^{99}Tc that dominates. In the very long term, the residual radioactivity of the actinides will dominate in spent nuclear fuel.

The time dependence for the total gamma photon energy emission rate, $F_T(t)$ (MeV s^{-1} fission^{-1}) in spent nuclear reactor fuel, is often described by the simple formula,

$$F_T(t) = 1.4t^{-1.2} \text{ for } 10\,\mathrm{s} < t < 1 \text{ day}$$

where t is in seconds.

The decrease in photon energy emission, over the first 40 years, by fission products formed in a nuclear reactor that operated for a long time at a normalised power of 1 fission per second, is illustrated in Figure 5.13.

---

[23] Acronyms/initialisms related to loss of cooling accidents in water-cooled nuclear reactors:
LOCA = Loss of Coolant Accident;
LOHA = Loss of Heatsink Accident;
LOFA = Loss of Flow Accident.

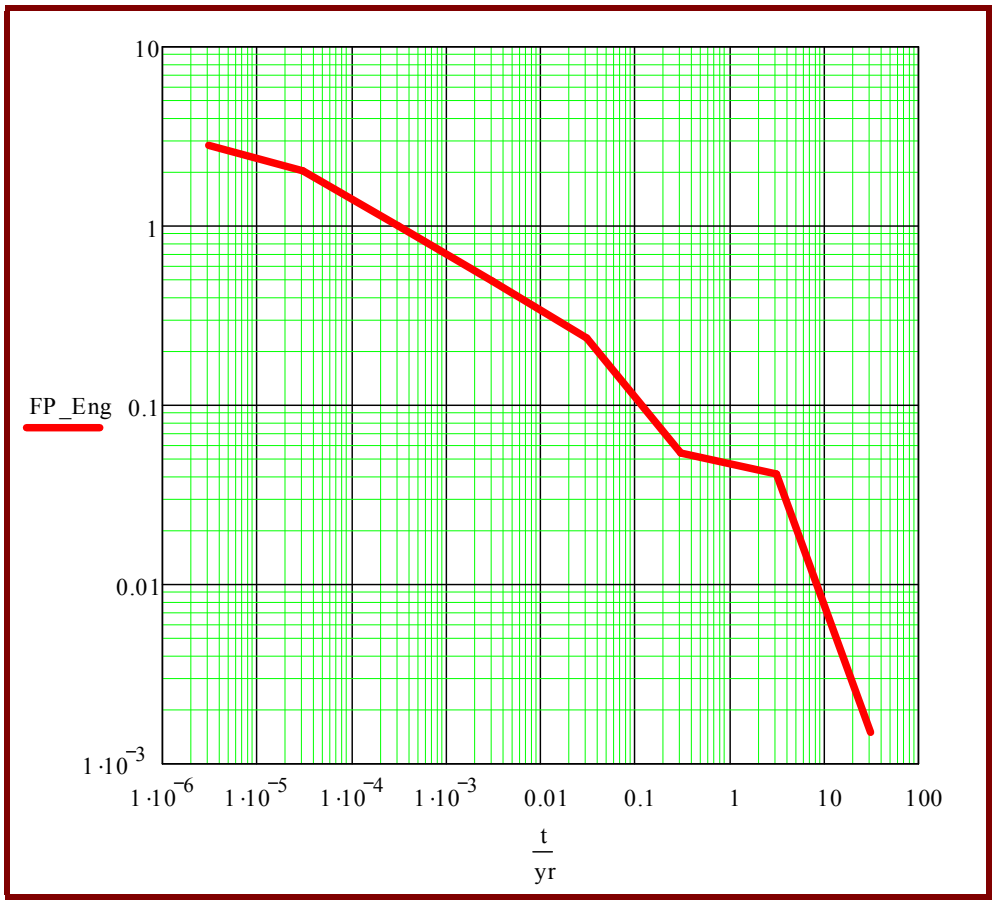

Figure 5.13: *The decrease in photon energy emission by fission products formed in a nuclear reactor that operated for a long time at a normalised power of 1 fission per second, over the first 40 years.*

Spent reactor fuel source term calculations

MCNPX 2.7 or MCNP6 can be used to calculate the isotopic inventory present in fissile material that underwent fission, i.e. burnup. To calculate burnup with a Monte Carlo Code such as MCNPX, has two major drawbacks: (1) The process is untenably slow on a PC, if the code only utilises a single core, and (2) MCNPX only calculates the nuclide inventory, and not the ionising photon emission spectrum. Monte Carlo burnup calculations are only practically viable when performed on a "supercomputer cluster."

A practical alternative is to use MCNP to calculate the multigroup neutron spectrum in the relevant material volume, and then use the ORIGEN-S burnup code in SCALE 6.1 (2011) to calculate the isotopic inventory of that material region, after a user-specified irradiation or power history.

Assignment 5.8

1. SCALE calculation: Assume that a Westinghouse 17×17 PWR fuel assembly (FA) contains 450 kg uranium, and that the initial enrichment grade is 4.75%. This FA is one of 157 FAs in the PWR. The total thermal reactor power is 3100 MW(th). Assume that the FA "sees" an averaged power. Calculate the isotopic inventory of the FA at a burnup of 60,000 $\frac{\text{MWD}}{\text{MTU}}$, given a capacity factor of 92%. Calculate the radionuclide inventory at several times up to 20 years after removal of the FA from the reactor. Also calculate the multigroup ionising photon emission spectrum in more than 30 energy groups, 20 years after removal of the FA from the reactor.

2. Use MCNPX to calculate the isotopic inventory in the following burnup scenario: A 100 cm $\times$ 100 cm $\times$ 15 cm high heap of U_3Si_2 powder ($\rho = 7.0\,\text{g}\,\text{cm}^{-3}$), 45% enriched in ^{235}U, is wetted by a 40% water ingress scenario, where the water does not displace the powder, but only displaces the air between the solid grains. A criticality accident lasting 1 second, follows, and 10^{16} fissions take place. Calculate the isotopic inventory 1 hour, 30 days and 1 year after the accident.

3. Repeat the above calculation by using MCNP to calculate the average neutron fluence-rate energy spectrum in the pile of uranic material, and pass this neutron fluence-rate spectrum to ORIGEN-S in SCALE 6.1 (2011) to calculate the isotopic inventory 1 hour, 30 days and 1 year after the accident. Also calculate the multigroup ionising photon source term at these times, in more than 30 energy groups.

4. Pass the above neutron fluence-rate spectrum to FISSPACT-2010 to calculate the isotopic inventory 1 hour, 30 days and 1 year after the accident. Also calculate the multigroup ionising photon source term in the maximum number of energy groups available in FISSPACT runs.

5. Quantitatively compare the results of the full Monte Carlo burnup calculation with the results of the hybrid burnup approach calculations (ORIGEN and FISSPACT). Is there at present any apparent benefit in using a full Monte Carlo burnup calculation?

5.5.4 Induced radioactivity: ionising photons from activation products

In this subsection, the focus is on particle accelerator facilities such as cyclotrons where mainly proton and light ion beams are accelerated.

Photons from neutron activation products

Neutrons in the energy range $E_n \in [0; 200\ \text{MeV}]$ may produce, *inter alia,* (n,γ)-, (n,p)-, (n,α)-, $(n,2n)$-, $(n,3n)$-, (n,np)- (n,Xn) and spallation reactions in materials. Product radionuclides from (n,γ) and (n,p) usually transition by the β^- mechanism, because these nuclei have an excess of neutrons. As a rule, beta transitions are followed by the emission of ionising photons when product nuclei de-excite.

Neutron activation, i.e. (n,X) reactions, may produce radionuclides; some of these nuclides may have significantly long half-lives. This is the reason why radionuclides are produced in the internal structures of nuclear reactors, in the primary reactor coolant, as well as in surrounding shielding and other structures, and also in particle accelerator components and shielding.

Ionising photons from proton activation products at a particle accelerator facility

High-energy protons produced at a particle accelerator facility, can cause a variety of nuclear reactions in materials. Product nuclides are normally deficient in neutrons, so that they will transition by positron transition (β^+) and electron capture (EC). Product nuclei de-excite by emitting ionising photons, while ionising photons with an energy of 0.511 MeV are produced when positrons combine with electrons, their antiparticle, and produce annihilation radiation. Radionuclides with halflives up to about 5.3 years are produced in significant activities in beamlines and beamline components — ^{60}Co ($T_{½} = 5.27$ yr) is usually the longest-lived activation radionuclide formed in steels.

At many cyclotron particle accelerator facilities, injector cyclotrons are used to pre-accelerate protons and other charged particles before injection into the main cyclotron. The low energy protons ($E_{max} \approx 8$ MeV) moving in the injector cyclotrons tend to produce the radionuclide ^{65}Zn in a loose form on the surface of the copper internals of injector cyclotrons. This loose ^{65}Zn can contaminate workers during maintenance work on the internal copper structures of the injector cyclotrons. In the high energy main cyclotron, the activation product ^{65}Zn is also produced in copper structures, but here it is deeply imbedded inside the copper by virtue of the deeper penetration distance of the higher energy protons into the copper. In most high-energy cyclotrons, loose ^{65}Zn contamination on copper structures are not found.

Table 5.10 summarises important activation nuclides formed in miscellaneous structures at proton accelerator facilities.

Table 5.10: *Residual radioactivity produced at proton accelerators — miscellaneous structures.*

Material	Radionuclides produced by activation
Lubricants	**Nuclide** / $T_{½}$: ^{3}H — 12.35 yr
Water	**Nuclide** / $T_{½}$: ^{3}H — 12.35 yr; ^{7}Be — 53.6 days; ^{11}C — 20.4 min; ^{13}N — 10.0 min; ^{15}O — 2.0 min
Air	**Nuclide** / $T_{½}$: ^{11}C — 20.4 min; ^{15}O — 2.0 min; ^{41}Ar — 1.8 h; ^{13}N — 10.0 min
Copper	**Nuclide** / $T_{½}$: ^{65}Zn — 244.06 days
Steels	**Nuclide** / $T_{½}$: ^{51}Cr — 27.703 days; ^{59}Fe — 44.495 days; ^{60}Co — 5.27 yr

Table 5.11 lists important radionuclides produced at proton accelerator facilities by (n,γ) reactions. Protons hit the beamline wall and targets, produce neutrons, which are subsequently slowed down, become thermalised and then produce these neutron activation products.

Table 5.11: *Residual radioactivity produced at proton accelerators by thermal neutron activation (Sullivan, 1992: 121).*

Parent nuclide	Natural abundance	σ	Active nuclide	$T_{½}$
^{23}Na	100	0.53	^{24}Na	15 h
^{40}Ar	99.6	0.61	^{41}Ar	1.8 h
^{44}Ca	2	0.70	^{45}Ca	165 d
^{50}Cr	4.3	17	^{51}Cr	28 d
^{55}Mn	100	13	^{56}Mn	2.6 h
^{59}Co	100	37	^{60}Co	5.3 a
^{63}Cu	69	4.5	^{64}Cu	13 h
^{64}Zn	49	0.46	^{65}Zn	245 d
^{121}Sb	57	6.1	^{122}Sb	2.8 d
^{123}Sb	43	3.3	^{124}Sb	60 d
^{133}Cs	100	31	^{134}Cs	2.1 a
^{151}Eu	48	8700	^{152}Eu	12 a
^{153}Eu	52	320	^{154}Eu	8 a
^{186}W	28	40	^{187}W	1 d

Table 5.12 lists important residual radionuclides produced in ground water and soil at proton accelerator facilities.

Table 5.12: *Residual radionuclides produced in ground water and soil at proton accelerators (Sullivan, 1992: 121).*

Radionuclide	$T_{½}$	Relative saturation activity (%)
^{7}Be	53 d	3.2
^{45}Ca	165 d	7.1
^{54}Mn	303 d	3.8
^{22}Na	2.6 a	11.9
^{60}Co	5.3 a	6.5
^{3}H	12.3 a	23.8
^{152}Eu	12 a	42.2
^{154}Eu	8.0 a	1.5

Induced radioactivity in cooling water at a particle accelerator facility

Water exposed to high-energy radiation will become radioactive. The major source of activated water will be cooling water from radionuclide production target bombardment stations, beam stops, collimators, magnets and other components requiring cooling water.

The short-lived positron emitters ^{11}C, ^{13}N and ^{15}O are produced in water at particle accelerator facilities. If they are released to the air, they mainly present an external dose hazard as a consequence of the 0.511 MeV annihilation photons produced. They seldomly present an inhalation hazard. The 0.511 MeV annihilation photons can produce high radiation fields around cooling water systems.

^{7}Be is longer-lived ($T_{½} = 53.6$ days) and can be removed from cooling water by ion-exchange resins. In some cases, the resin beds used to trap the ^{7}Be, become quite intense sources of exposure that may require shielding.

In specific accelerator applications, ^{17}N ($T_{½} = 4.17$ s), a neutron emitter, may be produced via the nuclear reaction $^{17}_{8}\mathrm{O}\ (n, p)\ ^{17}_{7}\mathrm{N}$ in cooling water. In the case of ^{17}N, the beta transition leads to the population of states in ^{17}O at excitation energies of 5.95 MeV, 5.39 MeV and 4.55 MeV. The neutron separation energy for ^{17}O is only 4.144 MeV. Therefore neutrons emission will take place; the neutrons will be emitted with discrete kinetic energies. The neutron production reaction is

$$^{17}_{7}\mathrm{N} \xrightarrow[\beta^-]{} {}^{17}_{8}\mathrm{O}^{*} + e^{-} + \overline{\nu} \rightarrow {}^{16}_{8}\mathrm{O} + {}^{1}_{0}n \tag{5.16}$$

Neutron dose rates should be surveyed if personnel access to areas close to cooling water

outlets from bombardment areas is possible. Because the natural abundance of ^{17}O is only 0.038%, ^{17}N rarely becomes a significant neutron source in coolant water.

^{3}H is the only long-lived radionuclide produced in coolant water that can not be removed by ion-exchange resins. Therefore, ^{3}H will continue to build up in a water system at a rate governed by the production rate, decay rate and removal rate.

Production of radioactive gasses and toxic gasses in air at a particle accelerator facility

The short-lived positron emitters,^{11}C, ^{13}N and ^{15}O are produced in the air inside accelerator vaults. They mainly present an external dose hazard as a consequence of the 0.511 MeV annihilation photons produced.

The most important toxic gasses produced in the air and materials in an accelerator vault, are ozone (O_3) and NO_x.

Comparison of lead and steel as shielding material around beamstops at a particle accelerator facility

Sullivan (1972) has shown that the dose rate from lead irradiated by high-energy protons decays as $t^{-1.4}$ if the irradiation time is short compared to the cooling time. This is significantly faster than the $t^{-1.0}$ dependence of the decrease in dose rate around proton-bombarded Fe in similar circumstances.

Sullivan also reports that for an irradiation time of 1 year and a cooling time of 1 month, the dose rate from proton-bombarded Pb was only one-fifth of that from steel.

Gabriel and Santoro (1972) showed that the use of a 100 mm thick lead shroud around an iron component irradiated by high-energy protons, lowers the residual dose rate after a cooldown time of 100 hours, by more than a factor 100, compared with the case where the lead shroud was absent (Gabriel & Santoro, 1972). For al irradiation and decay times considered, the lead collars substantially reduced the dose rate compared with that from the iron cylinder. In addition, the lowering of the dose rate with time is faster for the lead collar than for iron. However, this behaviour depends critically on the presence of impurities in the lead, especially antimony (Sb) — impure lead becomes more radioactive than pure Pb.

Low-activation concrete for nuclear power plants and particle accelerator facilities

In a nuclear power plant, the inner part of the biological shielding concrete surrounding the nuclear fission reactor, is classified as radioactive waste. This concrete is subject to thermal neutron fluence-rates above $\sim 3 \times 10^4$ cm^{-2} s^{-1}. Concrete used in storage casks for spent nuclear fuel that contains spontaneous fissioning nuclides such as ^{244}Cm, or strong (α, n) sources, also experiences a neutron fluence-rate.

The dominant long-lived residual radioisotopes induced in concrete by thermal neutron activation are, in order of importance,

- ^{152}Eu; $T_{½} = 13.54$ yr; produced from ^{151}Eu by an (n, γ) reaction;
- ^{154}Eu, with $T_{½} = 8.59$ years; produced from ^{153}Eu by an (n, γ) reaction.
- ^{60}Co, with $T_{½} = 5.27$ yr; produced from ^{59}Co by an (n, γ) reaction;

Note: The natural abundances of both stable europium isotopes, ^{151}Eu and ^{153}Eu, are close to 50%.

The above radionuclides present more than 99% of the long-term residual radioactivity in ordinary concrete in a nuclear reactor containment building. Far less important radionuclides induced in concrete, are ^{3}H and ^{55}Fe, which together typically represent less than 1% of the long-term residual radioactivity problem in ordinary concrete.

The best raw materials for low-activation concrete are simply materials low in both the elements Eu and Co. If possible, the Eu content should be below 0.01 ppm and the Co content below 0.1 ppm. Limestone found sandwiched between two beds of schalstein, is an excellent low-activation raw material for the production of nuclear-grade concrete.

Reference: see Kinno *et al.,* (2002).

Summary

Proton beams in the energy range $66 - 200$ MeV can induce a large variety of radionuclides in accelerator structures, cooling water and air inside radiation containment vaults.

After termination of beam-on conditions, dose rates will be dominated by induced radioactivity produced inside stainless-steel beamlines and copper beamstops.

Lead is significantly better than steel in reducing dose rates after beam cessation. It becomes less radioactive than steel, and its radioactivity falls of considerably faster than that of steel. Unless its cost, mass and inferior mechanical properties are prohibitive, Pb should be used as a shield for accelerator components when:

- The aim is to reduce personnel dose upon vault entry after termination of beam-on conditions.
- The shield is present during and after beam-on conditions.

If we assume a representative energy of approximately 1 MeV for ionising photons produced after termination of beam production, the use of 50 mm of Pb will reduce dose rates by as much as a factor 20 compared to the use of no shielding at all.

5.5.5 The production of ^{16}N in circulating coolant

In nuclear reactors, particle accelerators and other applications, coolant is circulated through a loop. When passing through the radiation field, radioactive activation products are formed. After exiting the radiation field, the activation products are no longer formed. The fluence rate of radiation "seen" by the coolant can be approximated as a cyclic step function. Radioactive decay of the activation product takes place continuously, whereas production of the activation product only takes place while it is inside the radiation producing device, i.e. where the value of ϕ is highest. In this section, an analysis of the production of the radionuclide ^{16}N in the coolant of a nuclear reactor is performed. This nuclide is produced by the nuclear reaction

$$^{16}_{8}\mathrm{O}\ (n,p)\,^{16}_{7}\mathrm{N} \tag{5.17}$$

from the ^{16}O isotope in the primary coolant of a pressurised water reactor (PWR). The half-life of ^{16}N is a short 7.13 seconds (ICRP-107), and it radiates ionising photons with energies and emission yields summarised in Table 5.13.

Table 5.13: *Energies and emission yields of ionising photons radiated by ^{16}N (ICRP-107, 2008).*

E (MeV)	Yield
8.86930E+00	7.600E-04
7.11515E+00	4.900E-02
6.91550E+00	3.800E-04
6.12863E+00	6.700E-01
2.82220E+00	1.300E-03
2.74150E+00	8.200E-03
1.95470E+00	3.800E-04
1.75490E+00	1.210E-03
9.86930E-01	3.400E-05
8.67700E-01	2.100E-06

It is seen that ^{16}N emits very high energy γ-radiation. The neutron activation product ^{16}N is produced by the high neutron fluence rate inside a water-cooled nuclear reactor; it presents radiation safety problems while the nuclear reactor is operating, because the energies of the emitted photons are exceptionally high. During reactor operation, ^{16}N presents a particular problem at heat exchangers in the primary coolant circuit, because a large volume of primary coolant is concentrated inside these heat-exchangers.

The energy dependence of the cross-section for the reaction $^{16}_{8}\mathrm{O}\ (n,p)\,^{16}_{7}\mathrm{N}$ is shown in Figure 5.14.

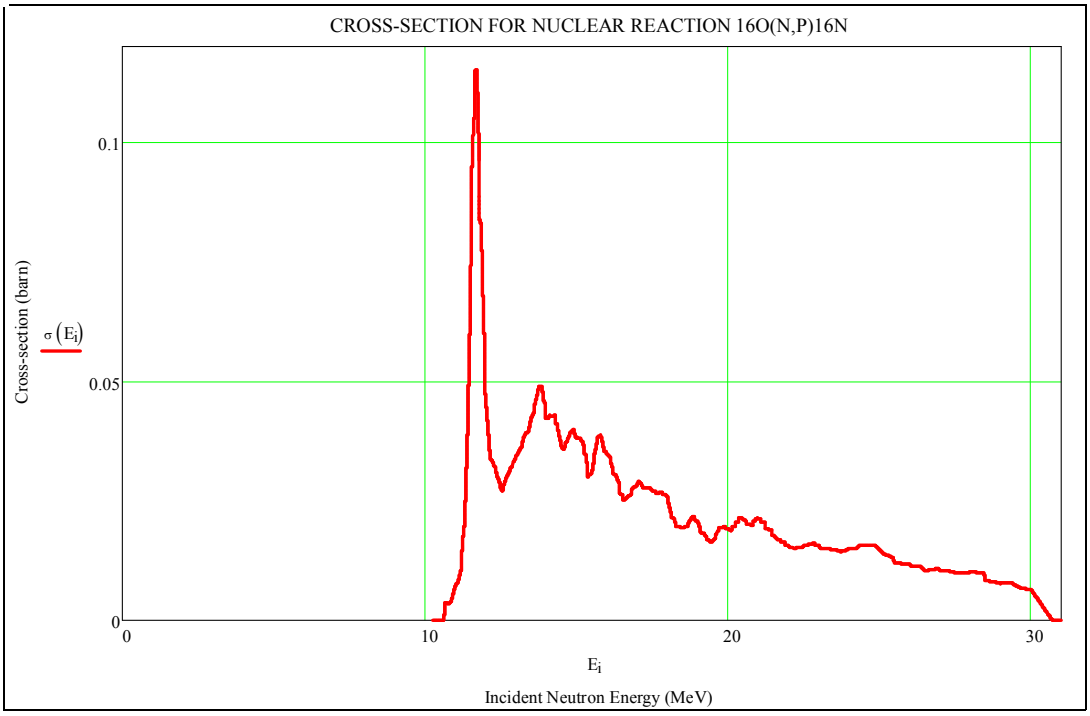

Figure 5.14: *The cross-section for the reaction* ${}^{16}_{8}O\ (n,p)\ {}^{16}_{7}N$ *(ENDF/B-7.1 cross-section data, from JANIS-3.4 (NEA, 2012)).*

The reaction has a threshold at $E_n = 10.245$ MeV.

In this subsection the following are presented:

- The differential equation for the production of an activation product;
- A numerical solution of the differential equation for the case of cyclic irradiation, i.e. in a closed loop with recirculation;
- An analytical solution for the case of cyclic irradiation;
- The determination of a fluence-weighted, 1-group cross-section for the neutron activation reaction, to enable the calculation of reaction rates.

Calculation of activation product source term in the heat exchanger

The activation and decay reaction by which the radionuclide ^{16}N is formed according to the activation reaction in (5.17), has the following general form,

$$N_1\ (n,X)\ N_2 \xrightarrow[\beta^-]{} \{\text{Stable product}\}$$

The symbols N_1 and N_2 designate the number of, respectively, the target nuclide ${}^{16}_{8}$O and the radioactive neutron activation product, ^{16}N. The symbol X specifies a general, unspecified reaction emission product — it can be a photon, proton, α-particle, etc. In the case at hand, it is a proton (p).

If effective one-group values for the fluence rate ϕ and the activation cross-section σ can be determined, the above activation & decay reaction will be described by the following two coupled ordinary differential equations,

$$\frac{dN_1(t)}{dt} = -N_1(t)\,\sigma_{TTL}\,\phi(t) \tag{5.18}$$

$$\frac{dN_2(t)}{dt} = +N_1(t)\,\sigma_{1\to 2}\,\phi(t) - \lambda_2 N_2(t) \tag{5.19}$$

The subscript "TTL" in the symbol σ_{TTL} in Eq. (5.18) designates "total transmutation loss." The cross section σ_{TTL} is the sum of all cross-sections that will deplete N_1 via transmutations. In other words, it quantifies the cross-section for the "burnup" of the target nuclide via all possible transmutation losses. We will in due course argue that σ_{TTL} can be assumed as 0 barn in the problem at hand.

Eqs. (5.18) and (5.19) must now be solved for the specific time-dependent form of the fluence rate, $\phi(t)$, that will be "seen" by the target nuclide when the coolant circulates through the active and inactive parts of the system. The time dependence of the neutron irradiation that the coolant "sees" as it cyclically moves through the reactor core, pipelines, the heat exchanger, the pump, etc., can be approximated by a cyclic step function, as shown in Figure 5.15.

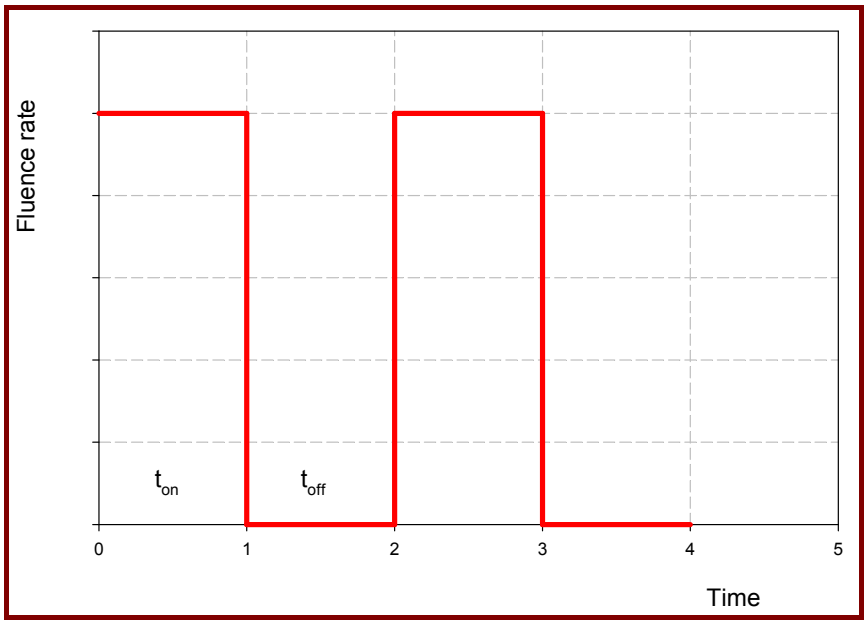

Figure 5.15: *Cyclic irradiation of coolant in cooling system.*

Mathematically, the cyclic step function is defined in terms of the "window function" W which, in turn, is defined in terms of the Heaviside unit step function. The "window function" $W(a,b,x)$ defines a window in the variable x on the interval $[a,b]$—it takes the value $1\ \forall\ x \in [a,b]$, and is 0 outside. It is defined in terms of the Heaviside unit step function, Φ,

$$W(a,b,x) = \Phi(x-a) - \Phi(x-b). \tag{5.20}$$

The time dependence of the fluence rate seen by a small pocket of circulating coolant, will approximately be,

$$\phi(t) = \phi_o \sum_{m=0}^{M} W[m(t_{\text{on}} + t_{\text{off}}), m(t_{\text{on}} + t_{\text{off}}) + t_{\text{on}}, t] \tag{5.21}$$

where t_{on} is the residence time of the coolant in the part of the system where it is irradiated by a fluence-rate, ϕ_o, which is assumed to be spatially and temporally uniform; t_{off} is the residence time of the coolant in the part of the system where it experiences negligible irradiation. The values of t_{on} and t_{off} depend on the total length of the loop, L_T, the length of the active part of the loop, L_A, the length of the inactive part of the loop, and the flow speed, v. The relationships are,

$$t_{\text{on}} = \frac{L_A}{v} \tag{5.22}$$

$$t_{\text{off}} = \frac{L_T - L_A}{v} \tag{5.23}$$

A typical numerical solution of differential Eqs. (5.18) and (5.19) is shown in Figure 5.16. The activity as a function of time, has a saw-tooth shape — while the coolant passes through the reactor, the activity of the radioactivation product is raised, and in the remainder of the flow loop, the activity drops as a result of radioactive transition.

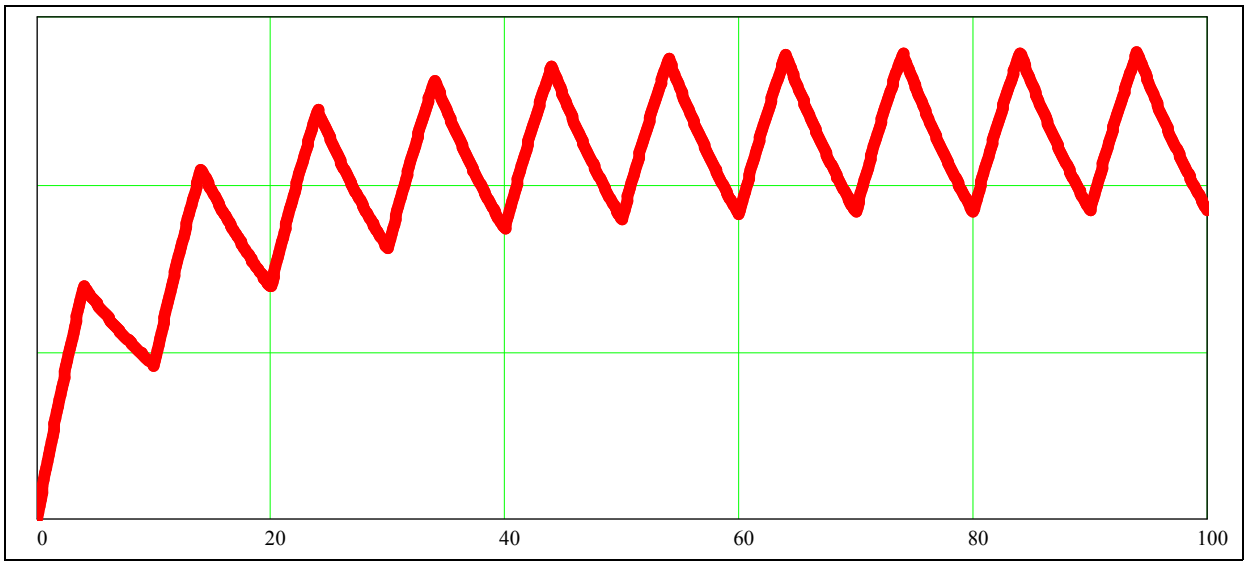

Figure 5.16: *Time dependence of a short-lived activation product such as ^{16}N in the primary cooling system of a nuclear reactor.*

After having been through the reactor core m times, before any subsequent decay of the activation product, the solution A_2 to differential Eqs. (5.18) and (5.19) is given by Eq. (5.24)

$$A_2^{\text{peak}} = \frac{N1_0\,\sigma\,\phi\,\lambda_2}{(\lambda_2 - \sigma_{TTL}\,\phi)}[\exp(-\sigma_{TTL}\,\phi\,t_{\text{on}}) - \exp(-\lambda_2 t_{\text{on}})] \times \left[\frac{\exp(-n\,\sigma_{TTL}\,\phi\,t_{\text{on}}) - \exp(-n\lambda_2(t_{\text{on}} + t_{\text{off}}))}{\exp(-\sigma_{TTL}\,\phi\,t_{\text{on}}) - \exp(\lambda_2(t_{\text{on}} + t_{\text{off}}))}\right]. \tag{5.24}$$

(Here, the defining relationship $A(t) = \lambda N(t)$ was used to transform from the number of atoms N to activity A.)

Eq. (5.24) will now be simplified step by step. The first simplification is to take $\sigma_{TTL} = 0$, because the total transmutation loss of the target nuclide in the circulating coolant will be practically zero.

Some pertinent facts are:

- $\sigma_{TTL} = [\sigma_{\text{All transmutations}}] - [\sigma_{\text{All zero-loss transmutations}}]$.
- Transmutation losses can be ignored because any "lost" coolant will be replenished by new water molecules from the primary coolant make-up system.
- As a result of the short 7.13 second halflife of the ^{16}N nucleus, the equilibrium concentration of ^{16}N will be extremely low relative to that of ^{16}O, so that the concentration of ^{16}O can be viewed as unaffected by the irradiation of the coolant in the active part of the loop.
- The short-lived product nuclide $^{16}_{7}$N in the $^{16}_{8}$O $(n, p)\,^{16}_{7}$N nuclear reaction, undergoes radioactive transition via β^--transition to the target nuclide $^{16}_{8}$O. In other words, this is a zero-loss reaction, because the radioactive transition of the product radionuclide $\left(^{16}\text{N}\right)$ almost immediately replenishes the target nuclide $\left(^{16}_{8}\text{O}\right)$.

Because there is essentially no depletion of target nuclide concentration as a result of transmutation losses, i.e. $\sigma_{TTL} \simeq 0$, Eq. (5.24) simplifies to

$$A_2^{\text{peak}} = N_{1_0}\,\sigma\,\phi\,[1 - \exp(-\lambda_2 t_{\text{on}})]\left[\frac{1 - \exp[-n\lambda_2(t_{\text{on}} + t_{\text{off}})]}{1 - \exp[\lambda_2(t_{\text{on}} + t_{\text{off}})]}\right]. \tag{5.25}$$

As a result of the short halflife of the ^{16}N product radionuclide, a steady state will be reached within as little as 3 flow cycles. The asymptotic behaviour of Eq. (5.25) in the limit $n \to \infty$, will be the equilibrium activity of ^{16}N when a packet of coolant exits the active region. Taking the limit $n \to \infty$ and dropping superficial subscripts, the steady-state expression for the

activity of a packet of coolant the moment it exits the irradiation region, is given by Eq. (5.26),

$$A_{\text{exit}} = N_0\,\sigma\,\phi\left[\frac{1-\exp(-\lambda t_{\text{on}})}{1-\exp(\lambda(t_{\text{on}}+t_{\text{off}}))}\right]. \tag{5.26}$$

If the flow speed of the coolant is v, and the length of piping from the exit of the reactor pressure vessel to the heat exchanger is L, the decay time will be $t_d = \frac{L}{v}$. The activity A_{hx} of the coolant in a part of the primary coolant loop that is reached at a time t_d after coolant exit from the reactor core, will therefore be given by Eq. (5.27)

$$A_{\text{hx}} = A_{\text{exit}} \times \exp(-\lambda t_d). \tag{5.27}$$

The activity of ^{16}N calculated using Eq. (5.27) can now be used to calculate a tally multiplication factor for dose-rate calculations with MCNP. The γ-photon spectrum that must be specified in the SDEF source definition specification of the code MCNP, will essentially be the EY-matrix of Table 5.13 on page 282. The first column of the EY-matrix is the line energies E_g of the emitted ionising photons, and these form the γ-spectrum's SI ("Source Information") card in the MCNP input data set. The second column of the EY-matrix is the corresponding emission yields Y_g of the emitted ionising photons, and these form the γ-spectrum's SP ("Source Probability") card in the MCNP input data set.

Determination of a fluence-weighted, 1-group cross-section for the neutron activation reaction $^{16}_{8}O\,(n,p)^{16}_{7}N$

The cross-section for the nuclear reaction $^{16}_{8}\text{O}\,(n,p)^{16}_{7}\text{N}$ is shown in Figure 5.14 on page 283; let this cross-section function be denoted as $\sigma(E)$. A typical thermal reactor neutron energy spectrum is shown in Figure 5.17; let this spectrum be denoted $\phi(E)$.

Figure 5.17: *A typical thermal reactor neutron energy spectrum $\phi(E)$, for calculating energy group averaged group cross-sections.*

The spectrum-weighted one-group cross-section for the nuclear reaction ${}^{16}_{8}\mathrm{O}\ (n,p)\ {}^{16}_{7}\mathrm{N}$ over the energy range 10^{-11} MeV to 20 MeV, calculates to the value in Eq. (5.28),

$$\sigma_{\mathrm{av}} = \frac{\displaystyle\int_{10^{-11}\ \mathrm{MeV}}^{20\ \mathrm{MeV}} dE\,\phi(E)\,\sigma(E)}{\displaystyle\int_{10^{-11}\ \mathrm{MeV}}^{20\ \mathrm{MeV}} dE\,\phi(E)} = 4.42 \times 10^{-4}\ \mathrm{barn}. \qquad (5.28)$$

To calculate the activity of ${}^{16}\mathrm{N}$ in a given point in the primary circuit of a nuclear reactor, step 1 is to calculate the average total neutron flux $\phi = \displaystyle\int_{10^{-11}\ \mathrm{MeV}}^{20\ \mathrm{MeV}} d\phi\,\phi(E)$ in the coolant passing through the core of a nuclear reactor. This value of ϕ, along with the above value of σ_{av} are then used in expressions for the activity of ${}^{16}\mathrm{N}$. From MCNP calculations by the author, using an OSMINT model of the SAFARI-1 core, the fast and thermal neutron fluence-rates averaged over 3 fuel assemblies, are given in Figure 5.18.

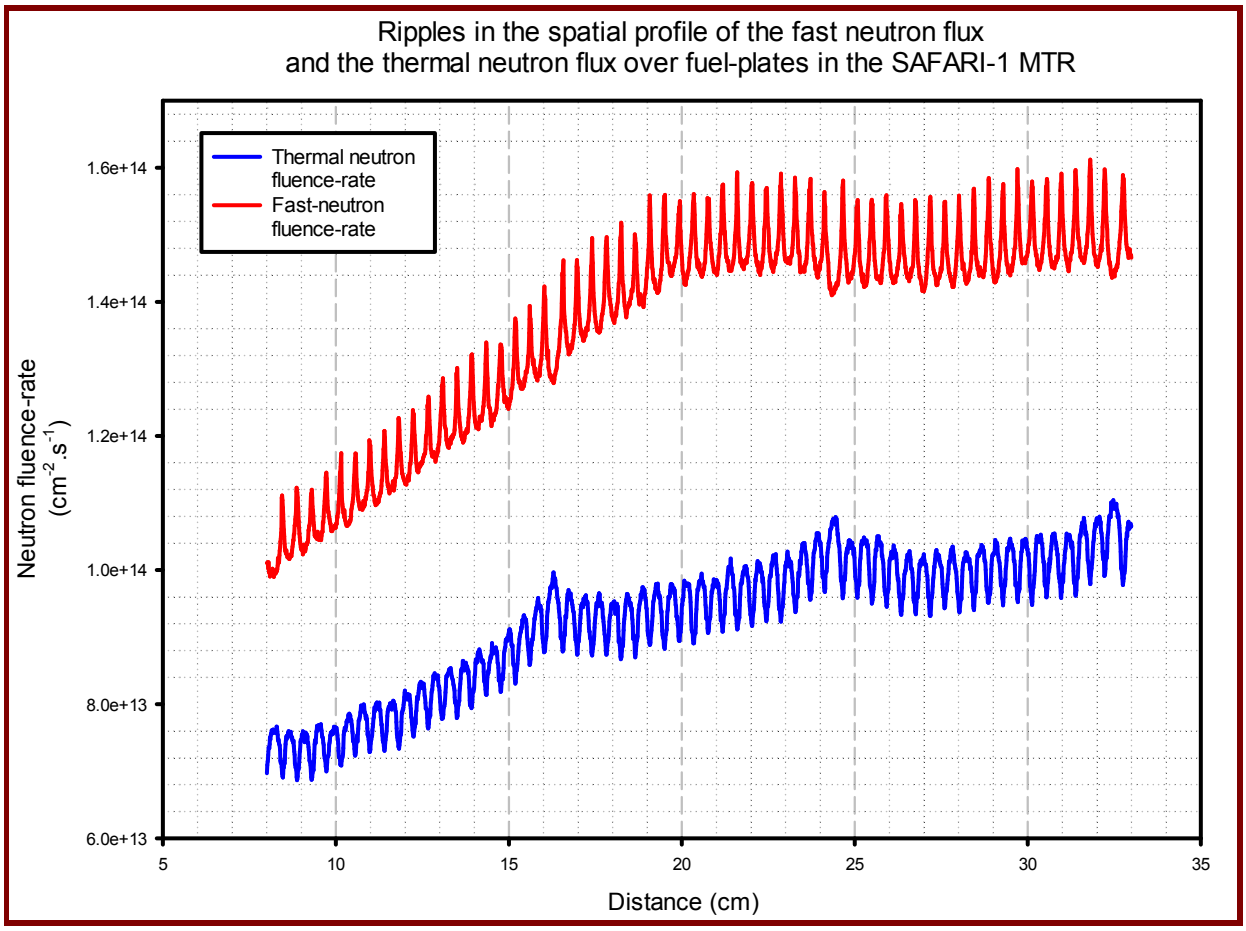

Figure 5.18: *Fast neutron flux and thermal neutron flux in and between fuel plates in the SAFARI-1 reactor core (MCNP calculation).*

The maximum fast plus thermal neutron fluence-rate is 2.6E14 $\text{cm}^{-2}\,\text{s}^{-1}$ and the average total fast plus thermal fluence-rate is 2.3E14 $\text{cm}^{-2}\,\text{s}^{-1}$. Unfortunately, the information from the historical calculation used to obtain Figure 5.18, contained no epithermal neutron fluence-rate, and it was therefore decided to approximate

$$\phi_n = \left\{ \int_{10^{-11}\ \text{MeV}}^{20\ \text{MeV}} d\phi\, \phi(E) \right\} = 3.0\text{E}14\ \text{cm}^{-2}\,\text{s}^{-1}$$

in Eq. (5.28).

Benchmarking: In order to obtain the measured values of the ^{16}N related dose rate in the Safari-1 pump room (0.3 mSv/h) and in the Safari-1 heat exchanger room (1.5 mSv/h) it was found that the calculated value of σ_{av} in Eq. (5.28) is too low. To meet the empirical benchmark dose rate values, σ_{av} had to be increased from the "theoretical" value of $\sigma_{\text{av}} = 3.1$ µb to a "fudged" value of $\sigma_{\text{av}} = 370$ µb. This large discrepancy of a factor 120 is not satisfactory.

The above calculation is performed in the following MathCAD worksheet:

Weighted Cross-Section - 16O_N_P_16N.xmcd

5.5.6 Annihilation photons from antiparticle-particle annihilation reactions

The positron is the anti-particle of the electron; matter and anti-matter fuses with the consequent production of annihilation radiation. Positrons, generated either from β^+ transition of radionuclides, or from pair production interactions induced by high energy photons, slow down in matter within approximately 10^{-10} seconds, and subsequently annihilate when they fuse with electrons. Two annihilation photons, each with energy 0.511 MeV, i.e. the rest-mass energy of an electron, are emitted.

The LHS of Figure 5.19 shows a beam of 25 MeV positrons striking a 30 cm $\times$ 30 cm $\times$ 30 cm block of tissue-equivalent material (TEM) with a mass-density of $\rho = 1.0\,\mathrm{g\,cm^{-3}}$. The RHS of Figure 5.19 shows the spatial distribution of the fluence-rate of ionising photons with $E_\gamma \simeq 0.511\,\mathrm{MeV}$. It is evident that the 0.511 MeV annihilation photons are produced in the region where the positrons are stopped and recombine with electrons.

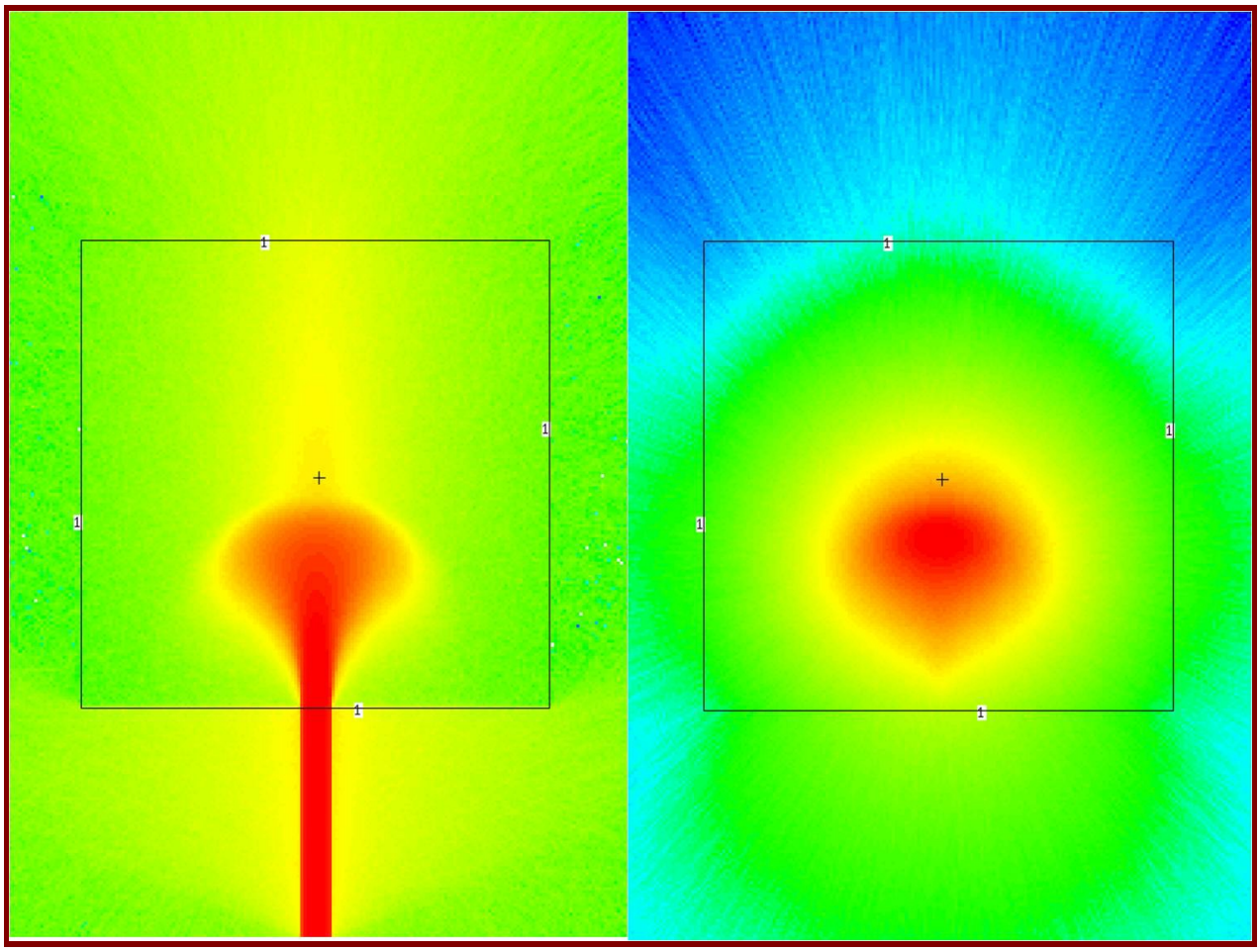

Figure 5.19:
LHS: A collimated beam of positrons strike a block of tissue-equivalent material (TEM).
RHS: 0.511 MeV annihilation photons are produced in the region where the positrons are stopped and recombine with electrons.

We observe that MCNPX 2.7 and MCNP6 does indeed model annihilation radiation production from positron transport in matter.

Assignment 5.9

1. Use MCNPX to investigate positron transport. Verify whether annihilation γ-photons with $E_\gamma = 0.511$ MeV are emitted when positrons stop in a material medium. Use the following input data set to check whether 0.511 MeV annihilation radiation photons are indeed produced when positrons are slowed down and stopped in matter. (This input data set was used to generate Figure 5.19.)

```
Particle beam of positrons
c Cell Cards
1  2  -1.00         -1        imp:n,p,h,e=1       $ TEM
2  1  -1.205E-3     -2  +1    imp:n,p,h,e=1       $ Air
3  0                   +2    imp:n,p,h,e=0       $ Umwelt
```

```
c ============================================================

c ============================================================
c Surface Cards
1  RPP  -15.0 +15.0    -15.0 +15.0    -15.0 +15.0    $ TEM BOUNDARY
2  RPP  -50.0 +50.0    -50.0 +50.0    -50.0 +50.0    $ Air BOUNDARY
c ============================================================

c ============================================================
c Data Cards
mode p e
sdef   par = -3
       erg = 10
       pos = 0  0 -30
       axs = 0  0  +1
       vec = 0  0  +1
       dir = +1
       ext = 0
       rad = d1
c
si1 h    0  1
sp1 d  -21  1
c
c Material definitions
m1      6000  -1.24E-4      $ Air
        7014  -0.755267     $ Air
        8016  -0.231781     $ Air
       18000  -0.012827     $ Air
c
m2      8016  -6.143E-01      $ Tissue-Equivalent Material (TEM)
        6000  -2.286E-01      $ Tissue-Equivalent Material (TEM)
        1001  -1.000E-01      $ Tissue-Equivalent Material (TEM)
        7014  -2.571E-02      $ Tissue-Equivalent Material (TEM)
       20000  -1.429E-02      $ Tissue-Equivalent Material (TEM)
       15031  -1.114E-02      $ Tissue-Equivalent Material (TEM)
       19000  -2.000E-03      $ Tissue-Equivalent Material (TEM)
       16000  -2.000E-03      $ Tissue-Equivalent Material (TEM)
       11023  -1.429E-03      $ Tissue-Equivalent Material (TEM)
       17000  -1.357E-03      $ Tissue-Equivalent Material (TEM)
       12000  -2.714E-04      $ Tissue-Equivalent Material (TEM)
       26000  -6.000E-05      $ Tissue-Equivalent Material (TEM)
c
c **** Physics Table *****
phys:p  20      $  Emax
         0      $  0 always
         0      $  0 always
        -1      $ -1 always
         1      $  1 ALWAYS
         0      $  0 Unless fission takes place, then -101 or -102
phys:e  20      $  Emax
c
c ==== Mesh Tally
tmesh
 rmesh11:e flux
  cora11   -20           +20
  corb11   -20   399i     +20
  corc11   -30   599i     +30
```

```
 rmesh21:p flux
  cora21   -20            +20
  corb21   -20   399i      +20
  corc21   -30   599i      +30
 rmesh31:p flux
  cora31   -20            +20
  corb31   -20   399i      +20
  corc31   -30   599i      +30
  ergsh31   0.500        0.520
endmd
c =====
ctme 1000
```

5.5.7 Characteristic x-rays

Characteristic x-rays are produced when excited atoms transition to lower electron energy states. Characteristic x-rays have with sharp line energies, and these characteristic ionising photon energies are the fingerprint of the atom or molecule in which they are excited. The term "x-ray" simply indicates the reaction mechanisms by which these photons originate; the bottom-line is that they are ionising photons. Their energies are typically in the sub-keV and lower keV range.

Question 5.10

1. Explain the difference between gamma-rays and x-rays.

   Answer: X-rays are ionising photons produced when energy transitions take place in atoms or molecules (these are characteristic x-rays), and when charged particles are stopped in matter to produce bremsstrahlung x-rays. Characteristic x-rays have characteristic, sharp, line energies that can be used to identify and quantify elements. Bremsstrahlung x-rays have broad energy spectra.

2. Can an x-ray ever have an energy higher than a gamma-ray?

   Answer: Yes, certainly. The upper energy of bremsstrahlung x-rays are determined by the upper energy of the charged particle stopped in matter.

5.5.8 *Bremsstrahlung* x-rays

When charged particles are rapidly slowed down and deflected by Coulomb interactions with nuclei, *bremsstrahlung* is produced. The intensity of *bremsstrahlung* production is roughly proportional to $\frac{Z^2}{M^2}$, where Z is the atomic number Z of the material wherein the radiation transport takes place, and M the mass of the interacting charged particle. It is clear that (1)

bremsstrahlung production will be higher for high-Z media than for low-Z media, and that (2) *bremsstrahlung* production will be far more intense when light charged particles such as electrons and positrons are slowed down compared to the slowing down of heavy charged particles such as alpha-particles and protons.

Example 5.1

A given charged particle will produce approximately $\left(\frac{82}{13}\right)^2 = 40$ times less *bremsstrahlung* in Al ($Z = 13$) than in Pb ($Z = 82$).

A given charged particle will produce approximately $\left(\frac{82}{4}\right)^2 = 420$ times less *bremsstrahlung* in Be ($Z = 4$) than in Pb ($Z = 82$).

The slowing down of electrons in a given material will produce approximately $\left(\frac{m_p}{m_e}\right)^2 \approx 3.3$ million times more *bremsstrahlung* than the slowing down of protons of the same energy.

The slowing down of electrons in a given material will produce approximately $\left(\frac{m_\alpha}{m_e}\right)^2 \approx 53$ million times more *bremsstrahlung* than the slowing down of α-particles of the same energy.

The energy of bremsstrahlung is determined by the maximum energy of the charged particles that produce the bremsstrahlung when slowing down. A 40 MeV electron beam stopped by e.g. a 3 mm thick tungsten target, will produce a broad energy spectrum of photons, ranging nearly to 40 MeV, i.e. the incident energy of the charged particles.

Figure 5.20 shows the energy spectrum of secondary ionising photons, principally bremsstrahlung, produced when a 40 MeV electron beam strikes a 3.5 mm thick tungsten (W) target.

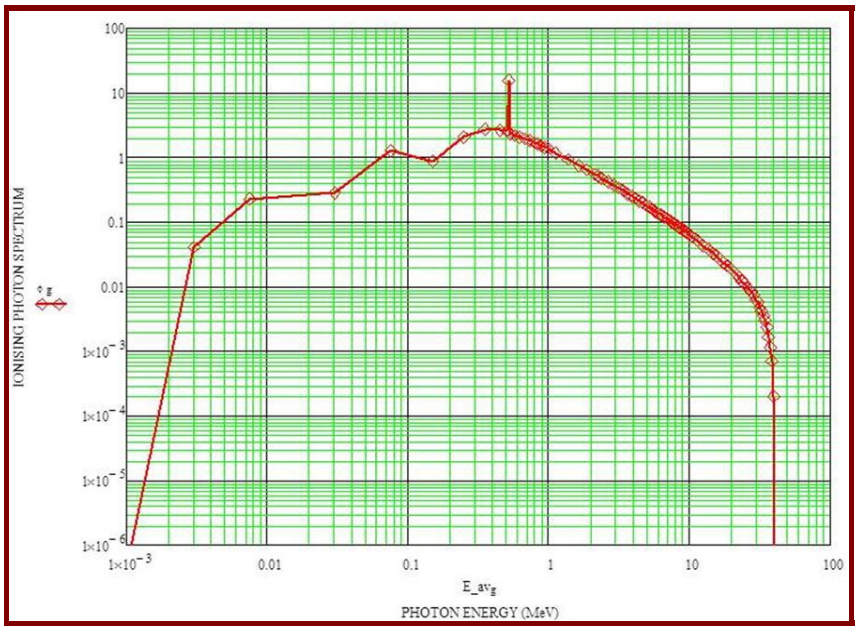

Figure 5.20: *Energy spectrum of bremsstrahlung produced when a 40 MeV electron beam strikes a 3.5 mm thick tungsten (W) target, i.e. a target just thick enough to stop practically all incident primary electrons.*

It is evident that the bremsstrahlung photons are produced in a continuous spectrum extending to an upper energy almost equal to that of the incident electrons. The prominent narrow peak at $E_\gamma = 0.511$ MeV is caused by an abundance of positron-electron annihilation photons.

When the 40 MeV electron beam strikes the 3.5 mm thick tungsten target, neutrons are produced as well. Whereas in the order of 10 ionising photons are produced per one incident 40 MeV electron, only approximately 0.005 neutrons are produced per incident 40 MeV electron; the maximum neutron energy is in the order of 12 MeV. These neutrons are produced by photonuclear interactions of energetic bremsstrahlung, i.e. by (γ, n)-reactions.

5.5.9 Gamma photons from inelastic scattering of neutrons

Gamma-photons from the inelastic scattering of neutrons are secondary photons that originate when neutrons are scattered inelastically, i.e. in (n, n')-reactions. The nucleus absorbs energy in the inelastic scattering process, and subsequently transitions to a stable state by emitting the excitation energy as ionising photons.

5.5.10 Conclusion

In order to accurately model radiation transport and to design effective shielding, step 1 is to accurately model the source-term. Energy spectra and production rates of the primary radiation must be known with good precision. The code MCNP can usually generate secondary radiation from primary radiation, so that the user normally only has to specify the primary radiation characteristics. In KCODE calculations with MCNP, it is not even necessary to specify the primary radiation characteristics.

Unfortunately, in 2013, MCNP still has many glaring shortcomings. In the low energy range, it does not produce protons from (n, p) reactions. Also in the low energy range, it does not produce neutrons from (α, n) reactions. In the simulations of the transport of low-energy alpha-particles through matter, all the ions of a certain kind seem to have exactly the same range, i.e. range straggling and energy straggling is not properly simulated, and it appears that lookup-tables instead of rigorous radiation transport is used.

Assignment 5.11

1. Consider the biological shield around a nuclear fission reactor. Which type of ionising radiation will be most important for the design of the biological shield (a) during reactor operation, and (b) when the reactor is shut down and opened during a refueling outage?

2. In KCODE calculations with MCNP, which particle spectra need to be supplied to the code to perform radiation shielding design calculations for the biological shield around a nuclear fission reactor.

3. Attempt to simulate the Rutherford scattering of a collimated beam of 8 MeV alpha-particles striking a 0.001 cm thick gold foil (Au; $\rho =$, using MCNPX. Run for e.g. 24 hours and plot a mesh tally to see if any alpha-particles had been scattered through large scattering angles. Any success?

5.6 Calculation of source strength

In this section, we present a number of practical examples of source strength determinations, for use in MCNP calculations.

5.6.1 Source strength of a nuclear fission reactor

It is easily shown that the fission neutron production rate (abbreviation: npr; units: neutrons per second) is given by

$$\text{npr} = \frac{\nu_{\text{av}}\, P_{\text{th}}}{\overline{E}_{\text{R}}}, \tag{5.29}$$

where P_{th} is the thermal power produced by the reactor, $\overline{E}_{\text{R}}$ is the average energy released per fission event (excluding neutrino energy) and ν_{av} is the average fission neutron yield. The above value of m is specified in the FM card as the tally multiplication factor (TMF) in MCNP calculations.

Assignment 5.12

1. A specific typical Generation II Westinghouse-type PWR, commissioned in 1984, produces approximately 2940 megawatt (thermal) per unit under full-power operating conditions. Assume that an average of 199 MeV of recoverable energy is released per fission, and that the average fission neutron yield is $\nu = 2.49$ neutrons per fission. Determine the total neutron production rate in the reactor core under full-power conditions, in the unit $[\,\text{s}^{-1}]$.

2. An Oak Ridge type MTR (Material Testing Reactor) operates at 20 MW (thermal power). Assume that an average of 201 MeV of recoverable energy is released per fission, and that the average fission neutron yield is $\nu = 2.51$ neutrons per fission. Determine the total neutron production rate in the reactor core under full-power conditions, in the unit $[\,\text{s}^{-1}]$.

5.6.2 Source strength in a radionuclide production beam target station at a particle accelerator facility

Suppose a 200 MeV proton beam current of I ampere is incident upon a copper target in which all the protons are stopped (a so-called stopping-length target).

Before the coming of age of MCNPX, the norm was to use measured yield curves — see e.g. Ryder (1982), to calculate the source strength of the neutrons produced by the protons via (p, n) and other neutron producing reactions. Since the coming of age of MCNPX, the above procedure need not be followed as primary methodology (but is still useful for QA checks of

results obtained with MCNPX). MCNPX has the ability to generate neutrons and ionising photons from proton interactions in copper. The primary proton beam is modelled, MCNPX is run in `mode h n p` and the code then generates neutrons and photons. As cross-section tables and nuclear models built into MCNPX improves, results should steadily improve every decade.

The following MCNPX SDEF statement defines a simple 200 MeV proton beam with a radius of 0.5 cm, incident in the $+z$ direction:

```
c Simple beam with 2 cm diameter travelling in +z direction
sdef   par = h
       erg = 200
       pos = 0  0 -20
       axs = 0  0  +1
       vec = 0  0  +1
       dir = +1
       ext = 0
       rad = d1
si1 h   0  0.5   $ Sampling of source point along radial coordinate
sp1 d -21  1   $ Probability of sampling of source point
```

MCNPX presents its results normalised to 1 source particle per second. The actual source strength is incorporated by multiplication with a so-called tally multiplication factor, which is specified in the input data set in an FM card. Suppose the beam current of the proton beam incident on a target, is 100 μA. This corresponds to

$$\frac{100\ \mu\text{A}}{q_e} = 6.242 \times 10^{14}\ \text{protons s}^{-1}$$

where q_e is the (absolute value of) the charge of an electron; the above value of $6.242 \times 10^{+14}$ must be used as FM tally multiplication factor in the MCNPX input data set, for F1, F2, F4 and F5 type tallies.

The general expression for the number op accelerated charged particles per second (cpps) having an electrical charge of $\{n|q_\text{e}|\}$, that are incident onto a target, is

$$\text{cpps} = \frac{I}{n|q_\text{e}|}$$

where I is the beam current and q_e is the elementary electrical charge on an electron. For a proton beam or an electron beam, $n = 1$ and for an α-particle beam, $n = 2$.

Note that with older radiation transport codes, one had to use empirically determined neutron & photon production spectra and yields for beam-on-target situations to calculate source terms. Thanks to all the physics built into the MCNP6 code and its associated cross-section libraries, this older methodology is no longer necessary. The user specifies the proton beam details and its source strength (protons per second impinging onto the target, and secondary particles such as neutrons, ionising photons and electrons are generated by the code as the transport process unfolds. Note, however, that the nuclear models built into MCNP6 only functions above a specific incident particle energy, so when "Table Physics" cross-section tables are missing

from the supplied cross-section data, the affected nuclear reactions will not be modelled in the transport simulation. For example, the as-supplied version of MCNPX 2.7.4 plus the as-supplied MCNPDATA, will not model (α, n)-reactions and (n, p)-reactions. The code user has to make an effort to obtain the desired "Table Physics" cross-section data sets and amend the XSDIR file to point to the correct cross-section data.

Assignment 5.13

1. A proton accelerator runs at a proton beam current of 150 μA. Determine the number of protons per second that will strike an isotope production target.

2. An α-particle accelerator runs at a beam current of 150 μA α-particles. Determine the number of α-particles per second that will strike a charged-particle radiotherapy calibration phantom.

5.6.3 Calculation of the source strength for a simple radionuclide

In this subsection, we assume that the ionising photons emitted by ^{60}Co is the source term of concern for envisaged MCNP calculations. As a first step, ^{60}Co is selected in ICRP-107 and the ionising photon EY-matrix is obtained; $E =$ photon energies and $Y =$ corresponding emission yields. Energies lower than 1 keV are truncated, i.e. only emission lines with $E \geq 1$ keV are retained in the EY-matrix. The energy column of this matrix now becomes the SI card in the MCNP input data set, while the yield column becomes the corresponding SP card in the MCNP input data set. Because the characteristic x-rays as well as the gamma-photons emitted by a radionuclide have sharp line energies, the SI card must specify *line* energies via the input parameter L. The EY-matrix for ionising photons emitted by ^{60}Co is therefore specified to MCNP as

```
#       SI4                 SP4
        L                   D
        2.50569E+00         2.00000E-08
        2.15857E+00         1.20000E-05
        1.33249E+00         9.99826E-01
        1.17323E+00         9.98500E-01
        8.26100E-01         7.60000E-05
        3.47140E-01         7.50000E-05
        8.28816E-03         4.86742E-09
        8.28784E-03         3.34900E-09
        8.22459E-03         7.66065E-06
        8.22229E-03         3.90686E-06
        7.43578E-03         6.23882E-05
        7.41782E-03         3.19463E-05
```

Inside MCNP, the SP card will be renormalised to add up to a value of 1. The as-specified values in the SP card can therefore not be used to specify the fact that approximately 2 ionising photons are emitted per 1 nuclear transition of ^{60}Co. This value, i.e. the sum $Y = \sum_{i=1}^{I} y_i$ of the ionising photon emission yields y_i, must be explicitly specified to MCNP by multiplying Y with the activity A, expressed in Bq, and inputting this value AY as the tally multiplication factor in the FM card. Suppose that the activity A of the ^{60}Co source is 1 Ci, i.e. $A = 3.7 \times 10^{10}$ Bq. The value of $Y = \sum_{i=1}^{I} y_i$ is $Y = 1.99859$, so that the tally multiplication factor TMF specified in the tally modification FM card will be

$$\begin{aligned} \text{TMF} &= A \times Y \\ &= \left(3.7 \times 10^{10}\right) \times (1.99859) \\ &= 7.39480 \times 10^{10}. \end{aligned}$$

5.6.4 Calculation of the source strength for the radionuclide ^{137}Cs

In this subsection, we assume that the ionising photons emitted by ^{137}Cs is the source term of concern for envisaged MCNP calculations. The radionuclide ^{137}Cs has a half-life of almost 30 years and transitions to the radionuclide ^{137m}Ba with emission matrix $(EY)_1$, which transitions in turn with a half-life of only 2.552 minutes, to the stable radionuclide ^{137}Ba, with the emission matrix $(EY)_2$. The branching ratio for the transition $^{137}\text{Cs} \rightarrow {}^{137m}\text{Ba}$ is 0.944, while the branching ratio for the transition $^{137m}\text{Ba} \rightarrow {}^{137}\text{Ba}$ is 1.000. Because the halflife of the daughter radionuclide ^{137m}Ba is many orders of magnitude shorter than that of the parent radionuclide, transition equilibrium will be reached within about $8 \times 2.552 \approx 20$ minutes, i.e. the activity of ^{137m}Ba will become $0.944 \times \{\text{activity of } {}^{137}\text{Cs}\}$ within less than half an hour. As a result, the EY matrixes of the two nuclides may be joined and manipulated as follows: the net or resultant EY emission matrix will be $(EY)_{\text{total}} = \text{stack}\begin{bmatrix} [E_1] & [Y_1] \\ [E_2] & [0.944 \times Y_2] \end{bmatrix}$. This total emission matrix $(EY)_{\text{total}}$ for this doublet of radionuclides, is the resultant EY matrix for the entire transition cascade of the $\{{}^{137}\text{Cs}; {}^{137m}\text{Ba}\}$ doublet. As before, photon energies lower than 1 keV, and their corresponding emission yields, are deleted from the resultant matrix, i.e. only emission lines with $E \geq 1$ keV are retained in the EY-matrix. The energy column of this matrix now becomes the SI card in the MCNP input data set, while the yield column becomes the corresponding SP card in the MCNP input data set. Because the characteristic x-rays as well as the gamma-photons emitted by a radionuclide have sharp line energies, the SI card must specify *line* energies via the input parameter L. The last complication that must be overcome in this and some other cases, is that many characteristic x-rays for ^{137}Cs and ^{137m}Ba have identical energies, so that these non-unique energy values must be replaced by a

consolidated single energy line with an emission yield that is the sum of all the emission yields of lines with identical energies. (A MS Excel VB-Script macro to perform this consolidation was developed by the author's son, and is available from the author.)

The *EY*-matrix for ionising photons emitted by the $\{^{137}Cs; ^{137m}Ba\}$ doublet, is specified to MCNP in the following format

```
#       SI4                 SP4
        L                   D
        6.61657E-01         8.471390E-01
        2.83500E-01         5.800000E-06
        3.74270E-02         2.039842E-04
        3.74270E-02         7.420630E-10
        3.74247E-02         1.063510E-04
        3.74247E-02         3.868900E-10
        3.73496E-02         1.072091E-05
        3.73469E-02         7.904943E-06
        3.72607E-02         1.476576E-03
        3.72607E-02         5.371580E-09
        3.72447E-02         7.579744E-04
        3.72447E-02         2.757400E-09
        3.66586E-02         5.281350E-05
        3.66586E-02         1.921280E-10
        3.66424E-02         3.891017E-05
        3.66424E-02         1.415490E-10
        3.63920E-02         6.951720E-03
        3.63920E-02         2.528930E-08
        3.63167E-02         3.587785E-03
        3.63167E-02         1.305180E-08
        3.22056E-02         3.753958E-02
        3.22056E-02         1.365630E-07
        3.18187E-02         2.038662E-02
        3.18187E-02         7.416340E-08
        5.93880E-03         1.219280E-05
        5.93650E-03         7.741801E-06
        5.86135E-03         7.424834E-07
        5.85863E-03         4.864460E-07
        5.77244E-03         8.345272E-05
        5.77244E-03         2.679920E-10
        5.75658E-03         5.226985E-05
        5.75658E-03         1.678540E-10
        5.60829E-03         3.862376E-08
        5.59191E-03         2.483315E-06
        5.52814E-03         3.904922E-04
        5.52814E-03         1.350160E-09
        5.44193E-03         2.642228E-07
        5.37394E-03         1.838770E-05
        5.22140E-03         3.424860E-08
        5.21911E-03         3.600728E-08
        5.20501E-03         6.318173E-06
```

```
5.17030E-03       5.589660E-06
5.15417E-03       3.741629E-06
5.14394E-03       6.382865E-04
5.14394E-03       2.234480E-09
5.14124E-03       7.142861E-05
5.14124E-03       2.500530E-10
5.05505E-03       2.355573E-07
5.03920E-03       2.445715E-07
4.98704E-03       4.040801E-05
4.98704E-03       1.414580E-10
4.90381E-03       3.599727E-04
4.90381E-03       1.155980E-09
4.82860E-03       2.326025E-04
4.82860E-03       7.469570E-10
4.82366E-03       2.417952E-03
4.82366E-03       8.360300E-09
4.57329E-03       1.846889E-06
4.45292E-03       4.036553E-03
4.45292E-03       1.413100E-08
4.43676E-03       4.556990E-04
4.43676E-03       1.595280E-09
4.35689E-03       1.203137E-04
4.35689E-03       4.159970E-10
4.18639E-03       2.233211E-06
4.11121E-03       2.405652E-06
3.97001E-03       4.195136E-04
3.97001E-03       1.468610E-09
```

Chapter 6:
The Shielding of Neutrons

6.1 Introduction

Introduction to neutron shielding

Neutrons are uncharged particles and can therefore penetrate very deeply into materials, so that strong neutron sources require very thick shields to lower dose rates to acceptable levels. Neutrons are of great importance in many shielding problems both from a biological and from radiation damage considerations. When neutrons interact with materials, they usually produce secondary types of ionising radiation such as ionising photons as a byproduct of inelastic scattering, i.e. (n, n')-reactions, as well as capture gamma photons from (n, γ) reactions, and may also transmute stable isotopes into radioactive ones when the stable isotopes e.g. capture a neutron to produce a radionuclide. Because neutrons are radiologically important, the accurate modelling of the source strength and the detailed energy spectrum and directional characteristics of the neutron source-term, is very important for shield design calculations.

Neutron energy range

Human-made neutron sources encountered in Africa (year 2013) produce neutrons in the range $E_n \in [0; 200\ \text{MeV}]$, so that attention will be restricted to this energy range.

6.2 Fundamental principles of neutron shielding

In this section we present a distilled set of neutron shielding principles.

Neutron shielding principle 1:
Slow neutrons down to make them easier to absorb

Figure 6.1 shows the energy dependence of the neutron absorption cross-section of ^{56}Fe (the most abundant isotope of Fe). In the low energy region, i.e. at neutron energies below the resonance threshold, absorption cross-sections are generally dominated by the (n, γ) reaction, and therefore have a $1/v$, i.e. a $1/\sqrt{\text{E}}$ dependence on the incident neutron energy E. This $1/\sqrt{E}$ shape of the curve at low energies, is representative of the energy dependence of $\sigma_{\text{abs}}(E)$, in the low neutron energy region, for most isotopes, especially those like Fe which is used in the structural materials of radiation shields. The general rule is that the lower a neutron's energy, the easier is it absorbed; to "get rid of" neutrons, the first step is to slow them down, because lowering its energy makes the neutron far easier to absorb & so to eliminate it from the radiation field. The secondary types of ionising radiation produced by neutron interactions in matter, such as e.g. photons via (n, γ) interactions, alpha particles via (n, α) reactions and protons via e.g. (n, p) and (n, np) reaction, are significantly easier to shield than

neutrons themselves. It therefore pays greatly to absorb neutrons in a shield; slowing neutrons down will make them more absorbable.

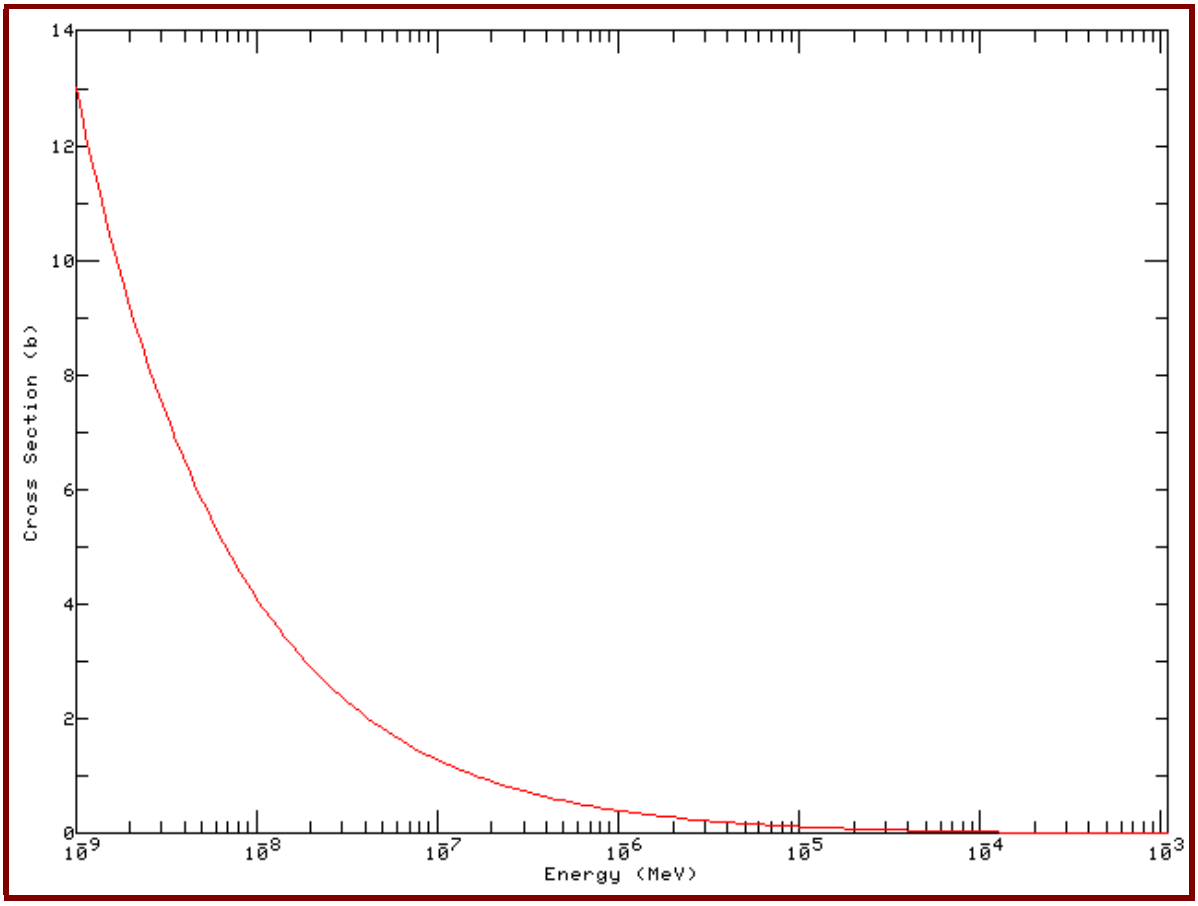

Figure 6.1: *Energy dependence of the cross-section $\sigma(E)$ for neutron absorption via the (n,γ) interaction mechanism with ^{56}Fe.*

A radiation shield is considered adequate when it lowers dose response functionals of the general form $R = \langle \phi, \mathfrak{R} \rangle$ to values that are below a given constraint. Because the response function $\mathfrak{R}(E)$ is fixed and generally is a steeply and monotonically rising function of particle energy, the only way to reduce the value of the response functional $R = \langle \phi, \mathfrak{R} \rangle$, is to reduce the value of the real function $\phi(E)$ on the personnel side of the shield, by (1) lowering the fluence-rate of high energy neutrons by scattering them to lower energies and (2) by removing neutrons them from the neutron field via (n,z)-reactions, where z denotes any exit-channel particle that is *not* a neutron. A particularly useful category of neutron removal reactions are (n,γ)-reactions, and their cross-sections generally rise as $\sigma_{(n,\gamma)} \propto \frac{1}{\sqrt{E}}$. So: to decrease the neutron fluence-rate ϕ, slow down the neutrons in order to absorb them easily.

There are two important facets to the ability of an isotope to slow down neutrons by scattering:

1. The ***cross-section*** $\sigma_s(E)$ of the scattering interaction that will lower neutron energy. The larger this cross-section, the more collisions there will be.

2. If such a scattering interaction takes place, what will be its ***kinematic effectiveness,*** i.e. what will be the values of, *inter alia:*

- The average lowering in the energy of the neutron, per collision;
- The number of collisions required to thermalise a neutron;
- The average angle the neutrons are scattered through;
- The maximum angle through which the neutron can be deflected per interaction.

The higher the kinematic effectiveness of neutron scattering, the greater the expectation value of the fractional energy loss per collision will be.

Neutron shielding principle 2: Slow neutrons down to make them less harmful

Figure 6.2 shows the energy dependence of the fluence-rate to dose-rate conversion function for neutrons, photons, protons and electrons.

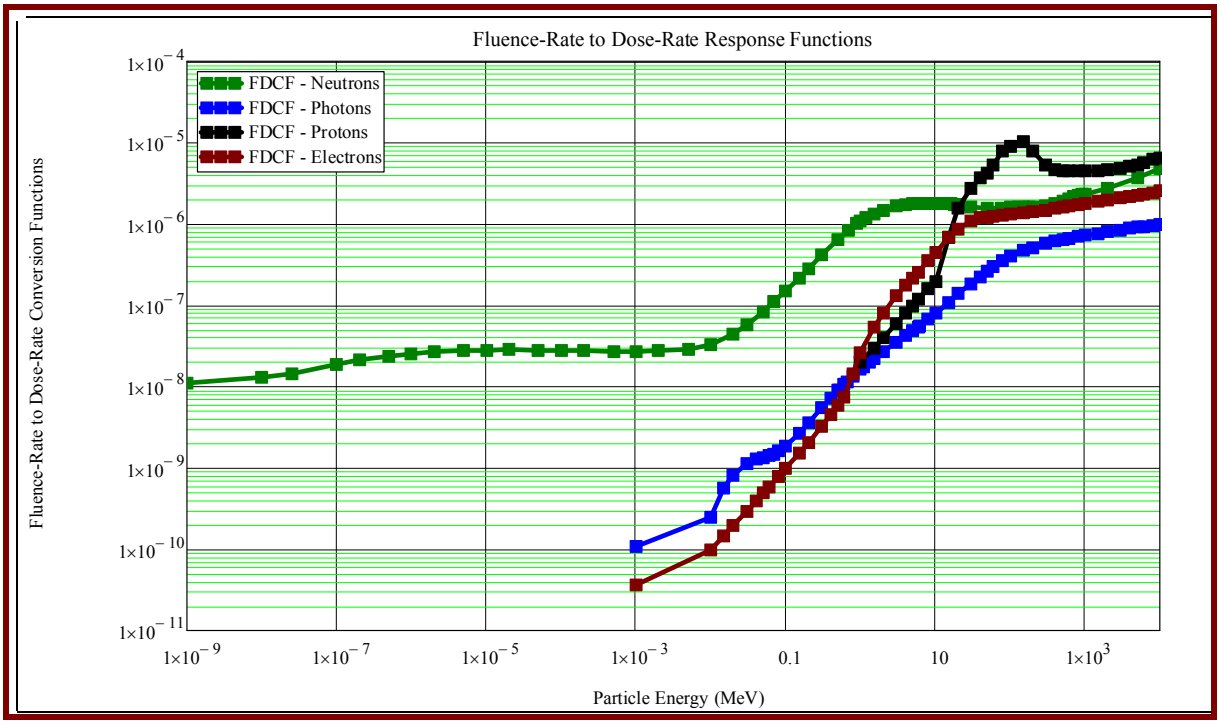

Figure 6.2: *Energy dependence for the response function $\mathfrak{R}_n(E_n)$ used to convert neutron fluence-rate $\phi_n(E)$ to equivalent or effective dose rate.*

Legend:

Neutrons
Photons
Electrons
Protons

It is clear that the harmfulness of neutrons will become less and less as their energy E decreases. For example: the cancer-induction potential of a given fluence-rate of thermal neutrons $\left(\overline{E}_{\text{thermal\_n}} \simeq 0.025 \text{ eV}\right)$, is nominally approximately 125 times less than that of the same fluence-rate of 10 MeV neutrons, because $\frac{\mathfrak{R}_n(E_n=0.025\,\text{eV})}{\mathfrak{R}_n(E_n=10\,\text{MeV})} \approx \frac{1}{125}$. The material damage

done by low-energy neutrons is also substantially less than the damage done by fast neutrons — damage functions for polymers are usually taken as the absorbed dose response function, which is in turn very similar to the response function for effective dose. Metals used near nuclear reactor cores are damaged by fast neutrons, which displace atoms from their crystalline lattice positions. The lower the neutron energy, the less harmful neutrons are; slowing down neutrons will make them less harmful to both people and materials such as electronic apparatus, metals and polymers. Detriment is therefore minimised by minimising the fast-neutron spectral component of the neutron fluence-rate function $\phi_n(E)$ in the spatial region of interest, and the principal way to achieve this is to slow down fast neutrons as effectively as possible.

A fundamental principle of effective neutron shielding follows from the above: Select shielding materials that will optimally slow neutrons down, because slow neutrons are (1) more easily absorbed and (2) less harmful to people and materials, than fast neutrons.

In this way, the fluence-rate function $\phi(E)$ will be lowered, especially in the high-energy region, so that dosimetric functionals of the general form $R = \langle \phi, \mathfrak{R} \rangle$ will have lower values.

Neutron shielding principle 3: Use shielding materials rich in ^{1}H to efficiently slow down neutrons with energies below circa 4 MeV, via elastic scattering

When a neutron having an incident energy below circa 10 MeV, scatters elastically off ^{1}H, it loses, on average, approximately 50% of its energy per elastic scattering event, because the mass of the neutron is practically the same as the mass of the single proton that constitutes the nucleus of ^{1}H. For elastic neutron scattering at energies where the scattering will be reasonably isotropic in the centre-of-mass system, $\mathcal{C}$, *^{1}H is the most efficient isotope to slow neutrons down by elastic scattering.* The number of successive elastic scattering events off a target nucleus with mass number A, that will be equally effective in slowing down neutrons, as a single elastic scattering of a neutron off ^{1}H, under the assumption of isotropic scattering in the centre-of-mass system, $\mathcal{C}$,is given by

$$n(A) = \frac{\log\left(\frac{1}{2}\right)}{\log\left(\frac{1+\alpha(A)}{2}\right)}, \tag{6.1}$$

where

$$\alpha(A) = \left(\frac{A-1}{A+1}\right)^2. \tag{6.2}$$

This dependence of the average kinematic efficiency of elastic scattering, on the mass number A of the scattering nucleus, is illustrated in Figure 6.3, which shows how many successive elastic scatterings off a nuclide with mass number A, is required to be equally as effective as a single elastic scattering off ^{1}H, in its ability to lower neutron energy.

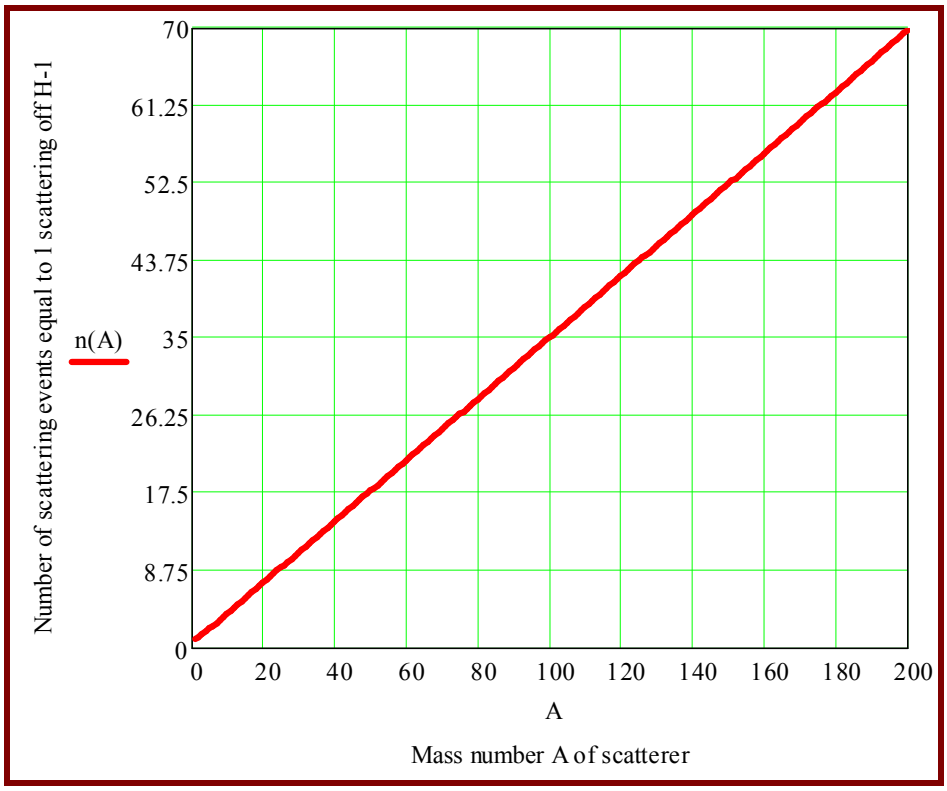

Figure 6.3: *The number of successive elastic scattering events off a target nucleus with mass number A, that will be equally effective in slowing down neutrons as a single elastic scattering of a neutron with ^1H.*

In the case of Pb (A $\approx$ 208), more than 70 elastic scattering interaction are required to reduce the neutron energy to 50% of its original value, which is the expectation value for the energy of the scattered neutron after just a single collision with ^{1}H. In the case of Fe ($A \approx 56$), approximately 20 elastic scatterings are required to reduce the neutron energy to 50% of its original value. It is clear that *heavy elements are quite inefficient at slowing down neutrons by elastic scattering;* ^{1}H is by far the most efficient isotope for reducing neutron energy via elastic scattering — the kinematic efficiency of elastic scattering by ^{1}H as a mechanism for neutron slowing down, is very high: the average energy loss for the neutron is 50% per elastic scattering event, provided that scattering is reasonably isotropic in the centre-of-mass system, C.

Neutron shielding principle 4:
The isotope ^{1}H is only able to effectively slow down neutrons with energies below about 4 MeV; when higher energy neutrons are to be shielded, a higher-Z element such as Fe must be included in the neutron shield to slow neutrons down via inelastic scattering

^{1}H has a relatively high cross-section for scattering neutrons with energies below approximately 0.1 MeV. Then the cross-section $\sigma(E_n)$ for elastic scattering by ^{1}H begins to fall steeply ("nose-dive") with increasing neutron energy, to become practically "useless" for incident neutron energies above approximately 10 MeV. Even though the kinematic effective-

ness of elastic scattering by ^{1}H will always be high (see Figure 6.3), at an average of 50% energy loss per scattering interaction, the low cross-section $\sigma(E_n)$ at higher neutron energies, makes hydrogenous shielding materials ineffective at higher incident neutron energies — this is clearly evident in Figure 6.4. Even though the scattering by ^{1}H is kinematically very efficient, *the probability for neutron scattering by ^{1}H becomes simply too low at high neutron energies.* In other words, when a fast neutron is scattered elastically by $^{1}_{1}$H, the slowdown is excellent, but the probability that the scattering will happen at all, falls to catastrophically low values at higher values of the incident neutron energy E_n.

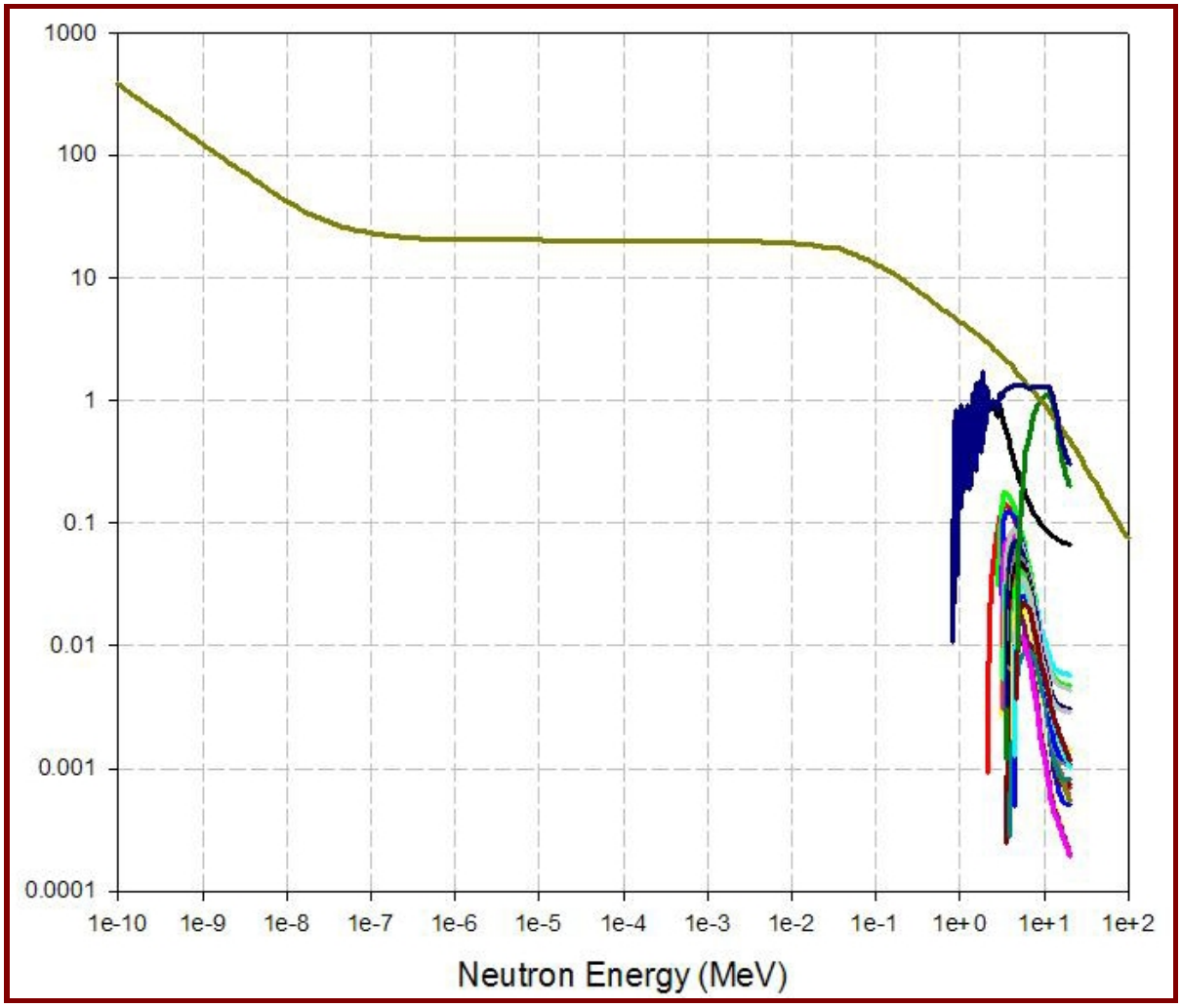

Figure 6.4: *The cross-section for neutron scattering by ^{1}H, and the cross-sections (excitation functions) for inelastic neutron scattering by Fe.*

Figure 6.5 shows greater detail of the elastic scattering cross-sections for ^{1}H and the inelastic scattering cross-sections for ^{56}Fe in the neutron energy region where the "excitation functions" i.e. the inelastic scattering cross-sections for ^{56}Fe, start to rise. The excitation of every discrete energy level in the ^{56}Fe nucleus by inelastic scattering of neutrons, has a characteristic threshold energy. The inelastic scattering cross-sections initially rise steeply, and then begin to fall, because other nuclear reaction mechanisms with neutrons, e.g. $(n, 2n)$, $(n, 3n)$, (n, p) (n, np) and (n, α) reactions with Fe, become *energetically possible* and therefore *compete* with inelastic neutron scattering.

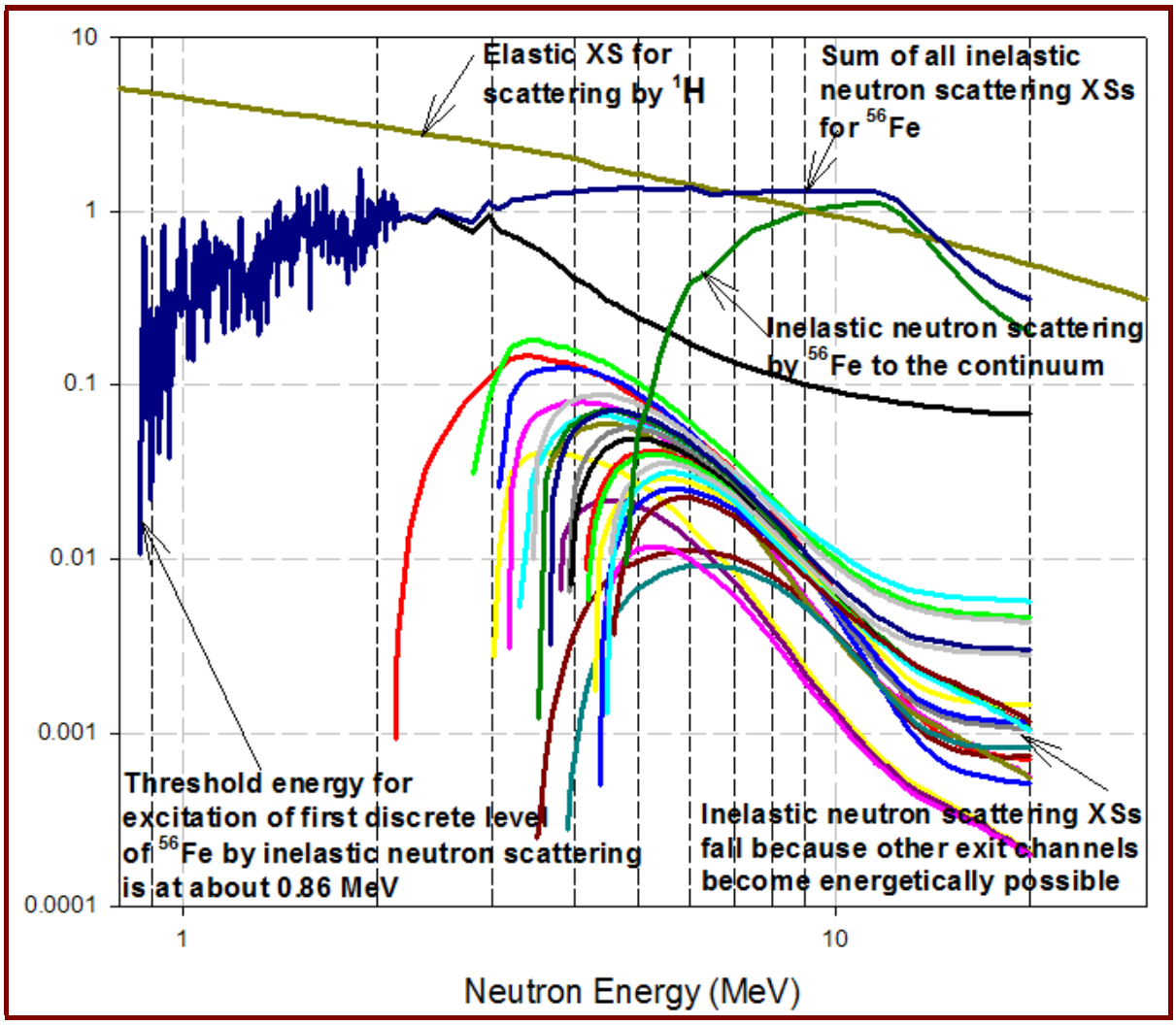

Figure 6.5: *Detail of the elastic scattering cross-section for ^{1}H (top curve starting at top left corner) and the inelastic scattering cross-sections for ^{56}Fe in the neutron energy region where the "excitation functions" i.e. the inelastic scattering cross-sections for ^{56}Fe, start to rise.*

Elements such as Fe are able to efficiently slow down neutrons with energies above approximately 1 MeV**, by inelastic scattering — this compensates for the steep fall in the elastic scattering cross-section of ^{1}H.**

Inelastic neutron scattering by materials such as Fe can make an important contribution to neutron slowing down, for neutrons with energies above ~1 MeV. Figure 6.6 shows the excitation functions, i.e. the energy dependences of the cross-sections for the excitation of the different energy levels in the ^{56}Fe nucleus — this is the most abundant isotope of iron in nature, and is therefore taken as being representative of iron. The excitation functions for inelastic scattering by Fe, exceed the magnitude of the elastic scattering cross-section for ^{1}H from approximately 5 MeV to about 18 MeV. Inelastic scattering by Fe is also kinematically quite efficient, as illustrated in Figure 6.6.

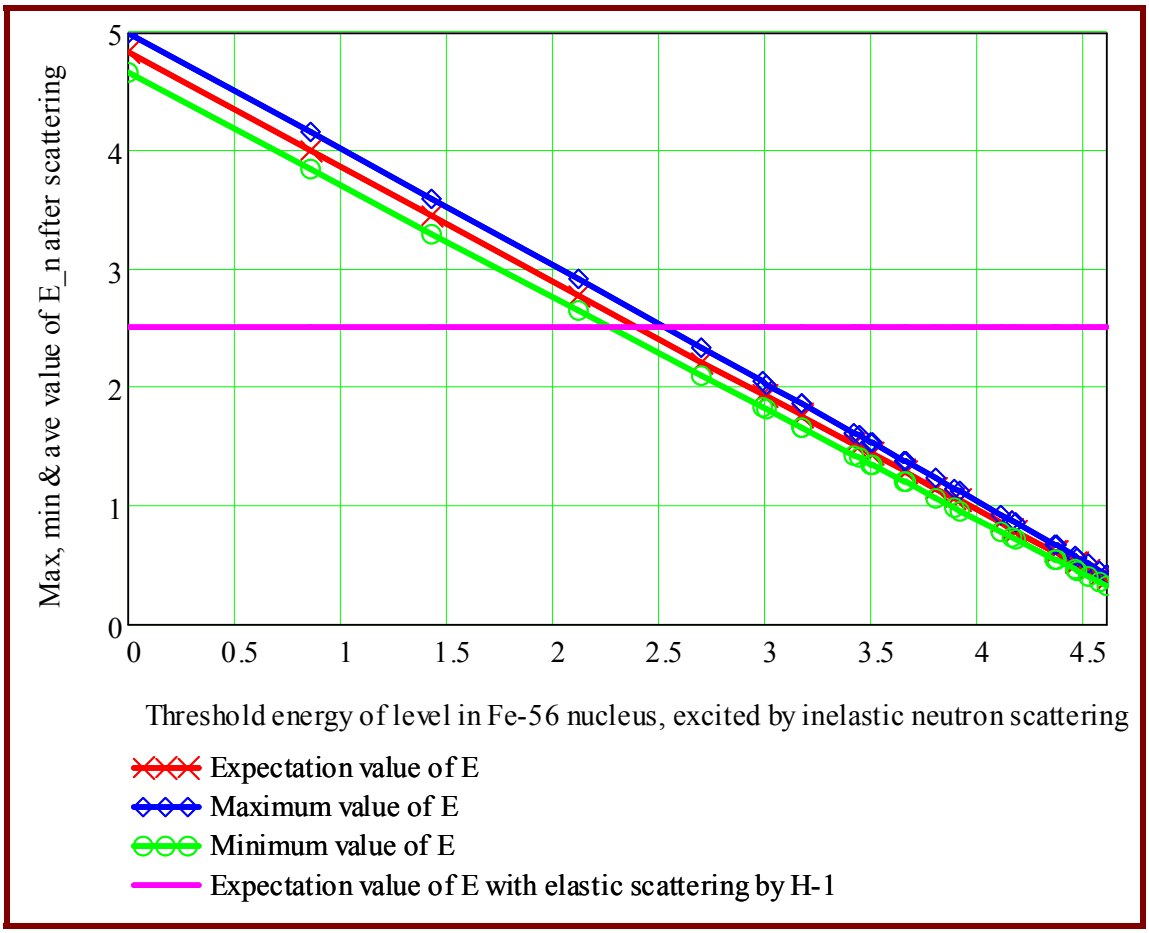

Figure 6.6: *The ability of ^{56}Fe to decrease the energy of an incident neutron with chosen incident energy of $E_n = 5$ MeV, in a single inelastic scattering interaction that excites a single discrete energy level in the ^{56}Fe nucleus, compared to the ability of a single elastic scattering interaction of a neutron by ^{1}H, to lower neutron energy.*

It is observed that inelastic scattering by Fe can, under specific conditions, be substantially more kinematically effective than elastic scattering by ^{1}H. Combined with the fact that (1) excitation cross-sections for inelastic scattering by Fe exceeds the cross-section for elastic scattering by ^{1}H, from about 5 MeV to 18 MeV, plus the fact that (2) many discrete energy levels in a nucleus can be excited in a single inelastic neutron scattering interaction, it is clear that an element such as Fe can make a substantial contribution to neutron slowing down — not by elastic scattering, but by inelastic scattering.

Conclusion: Effective neutron shields will typically operate as follows: High-Z elements such as Fe are used to slow down the high-energy neutrons in the incident neutron field, by inelastic neutron scattering. Such high-energy neutrons are outside the cross-sectional "grasp" of kinematically highly efficient elastic scattering by ^{1}H. The inelastic scattering by the high-Z element lowers neutron energy to within the energy range where ^{1}H has a proper cross-sectional "grip" on them and can efficiently slow them down to low energies, where they can be easily absorbed.

Neutron shielding principle 5:
Use isotopes with substantial (n,p), (n,α), (n,d), $(n,{}^3\mathrm{He})$ and (n,t) reaction cross sections to remove neutrons from the radiation field, and with substantial (n,np), (n,nd), (n,nt) $(n,n\alpha)$ and even $(n,2n)$ and $(n,3n)$ reaction cross-sections to help to remove neutrons from the radiation field, and to slow neutrons down

Nuclear reactions such as (n,p), (n,α), (n,d), (n,t) reactions, removes a highly penetrating, energetic neutron from the radiation field and replaces it with a minimally penetrating light ion. Nuclear reactions such as (n,np), (n,nd), (n,nt) and $(n,n\alpha)$ reactions, serve as highly effective neutron slowing down interactions, because the energy of the neutron in the exit channel will be significantly lower than that of the neutron in the entrance channel. Some of the above cross-sections for $^{56}_{26}$Fe are shown in Figure 6.7. The higher these cross-sections are, and the lower their threshold energies, the more they can contribute to neutron removal and slowing down.

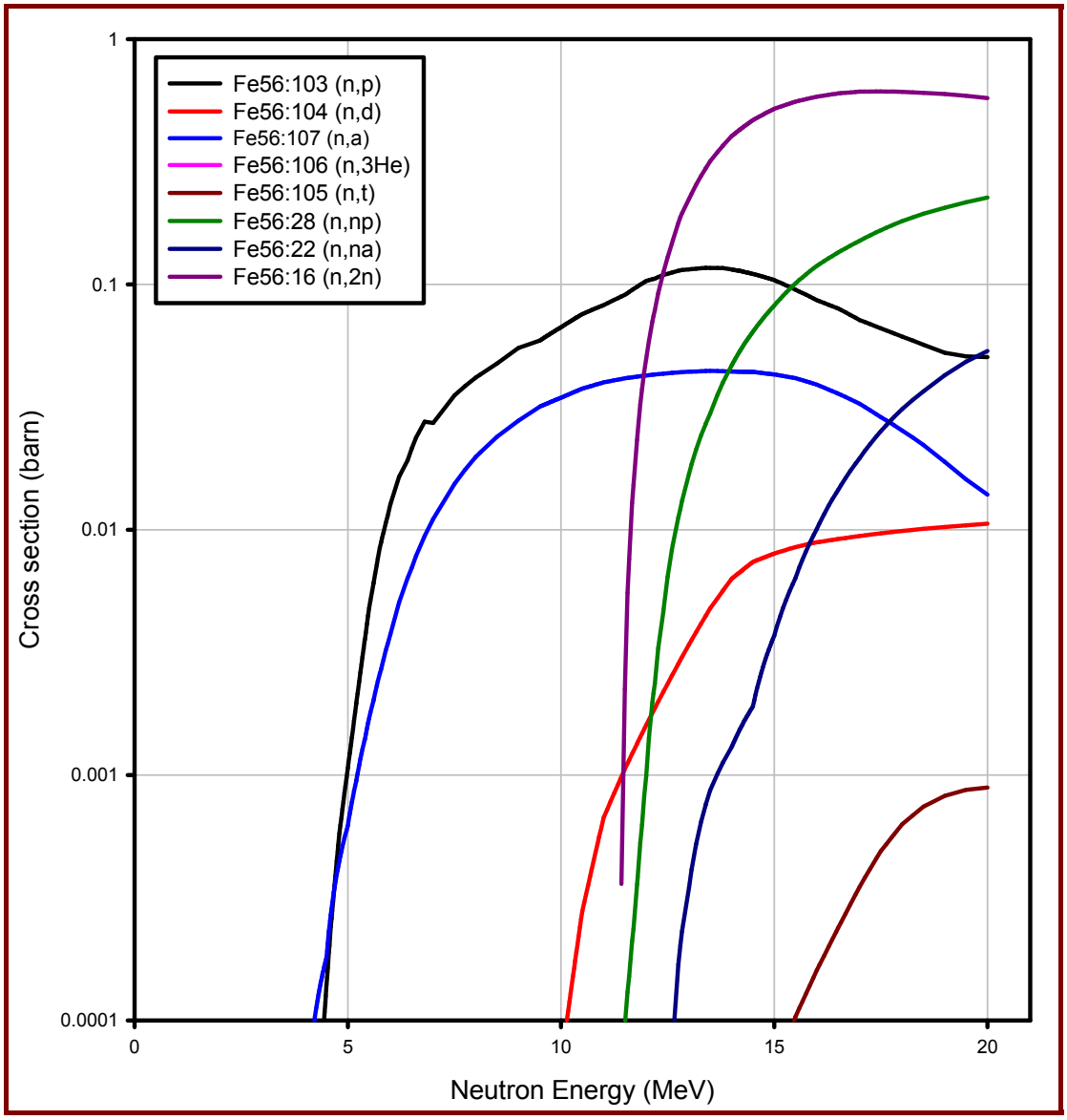

Figure 6.7: *Cross-sections for* (n,p), (n,α), (n,d), $(n,{}^{3}He)$, (n,t), (n,np), $(n,n\alpha)$ *and* $(n,2n)$ *nuclear reactions of neutrons with the dominant iron isotope,* ${}^{56}Fe$.

In $(n,2n)$ and $(n,3n)$ neutron nuclear reactions, which are always endo-thermic i.e. endo-ergic, energy conservation principles will ensure that the energy of the neutrons in the exit channel will be substantially lower than the neutron energy in the entrance channel. Therefore even these neutron multiplication reactions can contribute to neutron slowing down, and therefore to neutron attenuation.

Neutron shielding principle 6:
Use heavier elements such as e.g. C and Fe to scatter neutrons through large angles, i.e. to reflect neutrons

Heavy nuclides such as Fe are able to deflect neutrons through significantly larger angles than light isotopes such as ${}^{1}H$. These "large angle scatterers" such as Fe are valuable neutron *reflectors*. The average scattering angle of a neutron off ${}^{1}H$ is 48°, while the average

scattering angle of a neutron off a Fe nucleus, is close to 90° — use the formula on page 98. The isotope ^{1}H can not scatter neutrons through angles larger than 90° — only scattering angles between 0° and 90° are allowed, while heavier elements such as Fe can scatter a neutron through an angle as large as 180° in a single scattering interaction; all scattering angles between 0° and 180° are possible. Heavy elements such as Fe have a higher ability to turn a neutron back through a large scattering angle. This better backscattering property is valuable in neutron shielding, because reflection through large scattering angles will make it more difficult for the incident neutrons to penetrate through the shield, as Figure 6.8 illustrates.

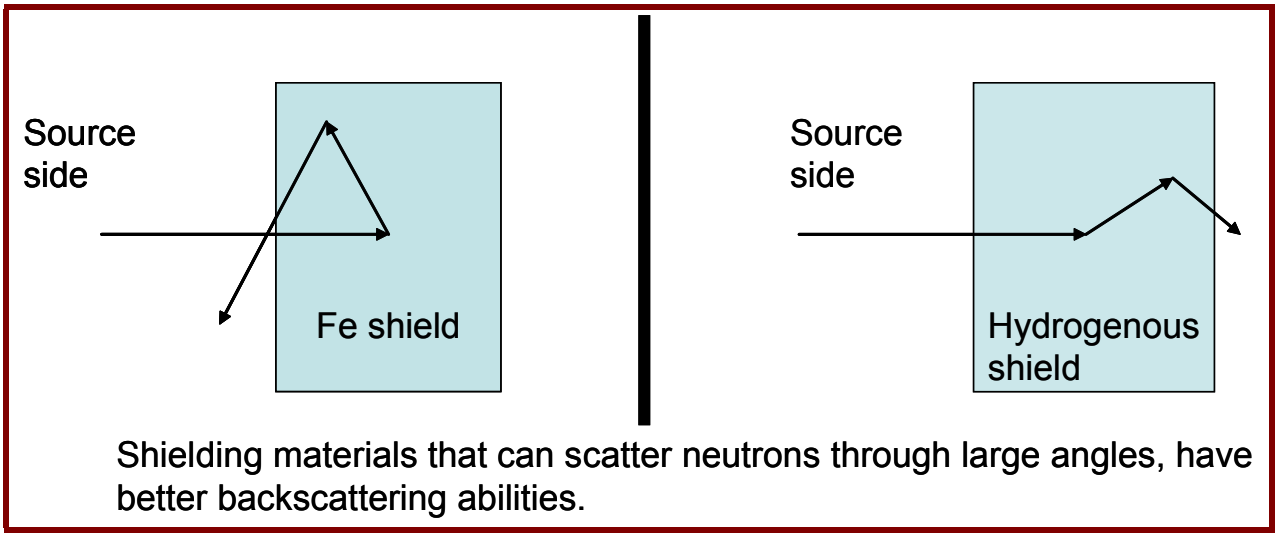

Figure 6.8: *Neutron shields that are able to scatter neutrons through large angles in a single scattering event, can make a valuable contribution to neutron shielding, by reflecting neutrons. Iron can scatter neutrons through angles as large as 180° in a single scattering interaction, and the average scattering angle is close to 90°. On the other hand, ^{1}H can only scatter neutrons through angles less than 90° in one scattering event, and the average scattering angle is 48°.*

Suppose a neutron is moving through a 100 cm thick shield composed mainly of $^{1}_{1}$H. Because scattering angles are below 90° and the expectation value of the scattering angle is 48°, the total path length traversed by the neutron before it emerges on the personnel side of the shield, may be significantly lower than for a Fe shield of a similar thickness, because neutron scattering angles in Fe may be as high as 180° and the expectation value of the scattering angle is almost 90°. Longer particle path lengths produce more collisions, and in materials such as Fe these collisions will be effective in slowing down neutrons having energies higher than the threshold energy for inelastic scattering or charged particle producing reactions.

Neutron shielding principle 7: Aggressively absorb radiation types z that produce significant yields of neutrons via (z, xn) reactions

As an example, we consider 40 MeV electrons producing bremsstrahlung ionising photons in a 3.3 mm thick tungsten target. A significant fraction of the ionising photon fluence rate is in the energy range above 10 MeV, where (γ, n)-reactions are possible in all isotopes. The shield optimisation problem may be stated as follows: Minimise the ***goal-functional,*** namely

the total dose rate on the personnel-side of the shield, under the imposed ***geometric constraint*** of a fixed maximum total shield thickness, plus the imposed ***economic constraint*** that only three engineering materials — Pb, Fe, borated paraffin wax — are available to the designer. Given the fact that ionising photons with $E_\gamma \geq 10$ MeV are able to produce neutrons, the first shielding layer on the source-side must be a relatively thick Pb shielding layer. This substantial Pb layer has the function of aggressively driving down the fluence-rate $\phi_{E_\gamma \geq 10\text{MeV}}$ of ionising photons having $E_\gamma \geq 10$MeV. In other words, the initial Pb shielding layer has to substantially lower the value of the integral

$$\int_{E_{\text{th}}}^{E_{\text{max}}} \phi_\gamma(\vec{\boldsymbol{x}}, E)\, dE$$

where E_{th} is the threshold energy where (γ, n)-reactions become important and E_{max} is the maximum energy that ionising photons will attain (40 MeV in the case under consideration).

In above shield, the echelon of radiation types capable of producing problematic secondary ionising radiation types, are as follows:

1	High energy ionising photons, i.e. $\phi_{E_\gamma \geq 10\text{ MeV}}$
2	Neutrons produced via (γ, n)-reaction
3	Low energy secondary photons produced via interactions of neutrons as well as high energy ionising photons

Only when $\phi_{E_\gamma \geq 10\text{MeV}}$ has been lowered to negligibly small values, so that the reaction rates for (γ, n) neutron producing reactions will be low, will it become productive to shift the goal to shield neutrons *per se.* If the shield designer fails to eliminate the radiation type highest in the echelon, but instead merely shields radiation types lower in the echelon, the high fluence-rate of radiation types higher up in the echelon will simply keep on producing a cascade of problematic ionising radiation types. In the case under assessment, if one does not all but eliminate the $\phi_{E_\gamma \geq 10\text{ MeV}}$ component of the radiation field as close to the source as possible, these high-energy ionising photons will simply keep on producing new neutrons.

Assignment:

In a given source-target configuration, a substantial fluence-rate of ionising photons having energies E_γ between 10 MeV and 30 MeV are produced. Which of the following shields, each constrained to be 100 cm thick, will be good and which shields will be inferior? Motivate your choice by explaining the function of each layer in the most optimal shield (i.e. delivering the lowest transmitted total dose rate on the personnel side) and, in contradistinction, the failures of the inferior shields.

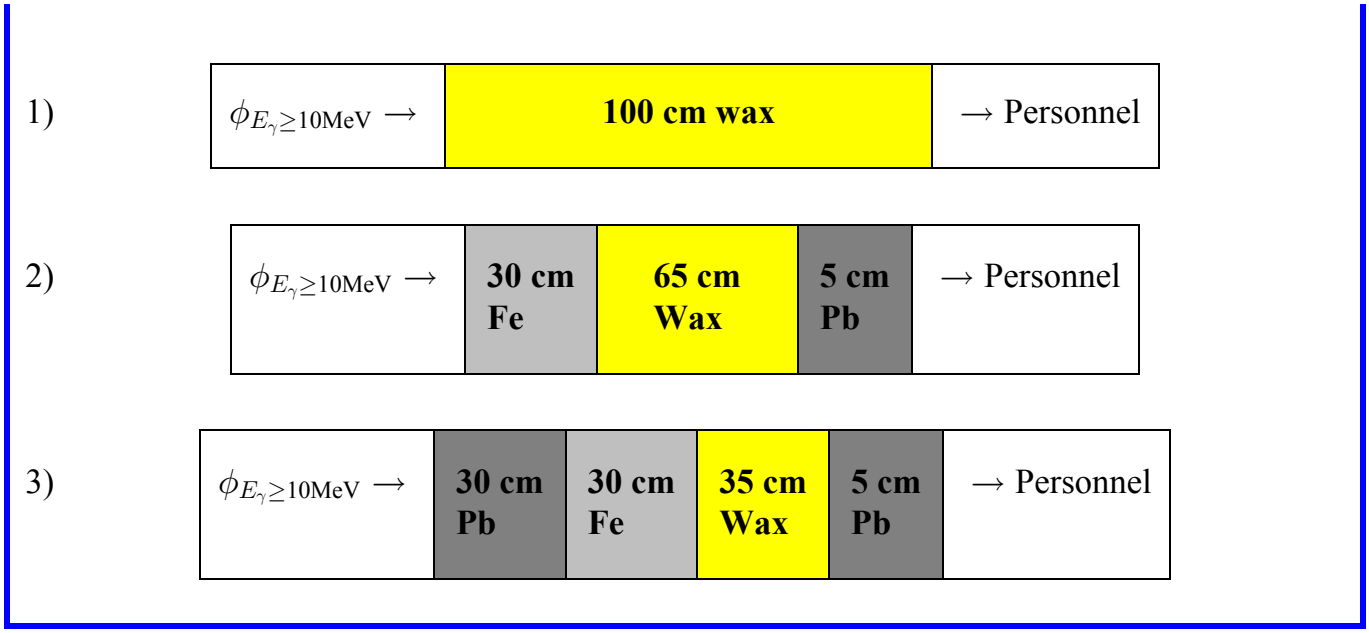

Neutron shielding principle 8:
Suppress the production of energetic ionising photons produced by thermal neutron capture reactions in a shield, by mixing a slow-neutron absorber such as boron carbide (B_4C) into the hydrogenous layer(s) of the shield

As a rule, the lower the energy of a neutron, the higher the value of the neutron absorption cross-section $\sigma_a(E)$ will be — see e.g. Figure 6.1 on page 304. Absorbing a neutron in a (n,γ)-reaction is good, because it "gets rid" of the neutron. However, if a high energy γ-photon is emitted when the neutron is absorbed in such a (n,γ)-reaction, this ionising photon will present a further shielding problem. High energy photons can also produce further neutrons via (γ,n)-reactions in isotopes such as ^{2}H — which are present in trace amounts in all hydrogenous materials. Figure 5.6 on page 253 shows the relative yields as well as the energies of the ionising photons produced when neutrons are absorbed in ^{1}H, Fe and Pb. Note in Figure 5.6 on page 253 that Fe produces a relatively high abundance of high-energy photons in (n,γ) reactions; ^{1}H produces 2.205 MeV γ-rays in the neutron capture reaction, $^1\text{H}\,(n,\gamma)\,^2\text{H}$. Lead (Pb) produces a low yield of capture gamma-photons from (n,γ)-reactions, making it an ideal shielding material for the outermost layer of a layered shield against a neutron source.

The cross-sections for (n,γ)-reactions are much higher for low energy neutrons than for high energy neutrons. Therefore one effective way to suppress the production of potentially problematic ionising photons from (n,γ)-reactions, is to suppress the slow-neutron fluence-rate ϕ by strongly absorbing slow neutrons. This is done by mixing a slow-neutron absorber such as e.g. boron carbide (B_4C) or ammonium pentaborate into the hydrogenous layers of a neutron shield. The thermal neutron absorption cross-section of ^{10}B, which has a natural abundance of circa 19.9% in boron, is 3844 barn at the reference thermal neutron energy of 0.0253 eV, a cross-section that is far bigger than the thermal neutron capture cross-section of Fe or ^{1}H. Mixing a carefully chosen percentage of e.g. boron carbide (B_4C) into the hydrogenous layers of a neutron shield will suppress the thermal neutron fluence-rate $\phi(E)$,

and therefore suppress the production rate of energetic capture γ-rays, which are given by reaction rate integrals of the type $\int dE\,\phi(E)\,\sigma(E)$.

The reaction mechanism by which ^{10}B absorbs neutrons, is

$$^{10}\mathrm{B}\,(n,\alpha)\,^{7}\mathrm{Li} + \gamma\ (0.48\ \mathrm{MeV}).$$

The ionising photons produced when ^{10}B captures a neutron, have an energy of only 0.48 MeV — far lower than the energies of the ionising photons produced when ^{1}H, Fe and Pb capture neutrons. Mixing boron carbide (B_4C) into a neutron shield, will suppress the slow neutron fluence-rate, and so lower the production of energetic ionising photons, whilst producing only a low energy ionising photon, which is quite easy to absorb.

Neutron shielding principle 9:
Suppress the production of radioactive neutron activation products by including a slow-neutron absorber such as boron carbide (B_4C) in the neutron shield

The use of a thermal neutron absorber such as boron carbide (B_4C) will lower the thermal neutron fluence-rate. The lowering of the thermal neutron fluence-rate can substantially reduce the reaction rates of all reactions having an elevated cross-section at low neutron energies, because reaction rates are proportional to,

$$\int dE\,\phi(E)\,\sigma(E).$$

In this way, mixing boron carbide (B_4C) into the shield, will suppress the production of radioactive neutron activation products such as e.g. ^{59}Fe, ^{60}Co, ^{28}Al, ^{51}Cr and ^{56}Mn, which are formed by (n,γ)-reactions. This will lower radiation levels that will be encountered during maintenance work in e.g. (1) radionuclide production vaults at a particle accelerator facility, (2) in regions inside the containment of a PWR close to the reactor, and (3) in regions close to the core of a MTR reactor.

Because it is rather impractical to mix the boron carbide (B_4C) into metallic layers, it is normally only mixed into the hydrogenous shield layers, i.e. the wax or polyethylene layers.

Assignment 6.1

1. How much "easier" is it for $^{10}_{5}$B to absorb a 1 eV neutron than a 7 MeV neutron via the (n,α) reaction mechanism, i.e. ENDF reaction type 107?

2. How much less biologically dangerous is a 1 keV neutron than a 10 MeV neutron?

3. Model the following spherical source/shield combinations with MCNP, using an F2 surface fluence-rate tally, for mono-energetic incident neutrons having energies of $E_n =$ | 1 | 1.5 | 2 | 2.5 | 3 | 4 | 4.5 | 5 | 5.5 | 6 | MeV.

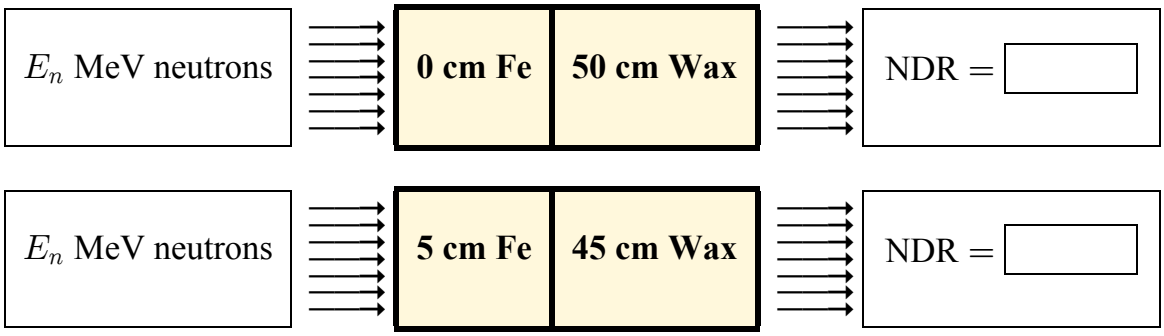

Ascertain the incident neutron energy for which the transmitted NDR becomes less with the thin Fe layer in place, compared to the result obtained with no Fe layer. This will enable one to pinpoint the approximate threshold value of the incident neutron energy from where a hydrocarbon shield needs to be complemented with the inelastic scatterer Fe.
(Important: for meaningful results, the standard error must be at least 5 times smaller than the magnitude of the perturbation being investigated.)

4. Repeat the "shielding material fingerprint" calculational experiments starting on page 324 and verify the amazing ability of a thick layer of Fe to lower the energy of 40 MeV incident neutrons and concentrate them in the energy range between about 1 keV and 0.9 MeV.

5. Repeat the "shielding material fingerprint" calculational experiments starting on page 324 and verify that materials such as wax, water and polyethylene are very poor at slowing down high-energy neutrons (e.g. 20 MeV neutrons).

6. Repeat the "shielding material fingerprint" calculational experiments starting on page 324 and verify that materials such as wax, water and polyethylene are very good at slowing down low energy neutrons, e.g. for $E_n = 0.7$ MeV

7. Model the following source/reflector combinations with MCNP, using an F1 surface current tally with a direction-cosine bin, and ascertain whether Be is indeed better than H_2O at reflecting neutrons:

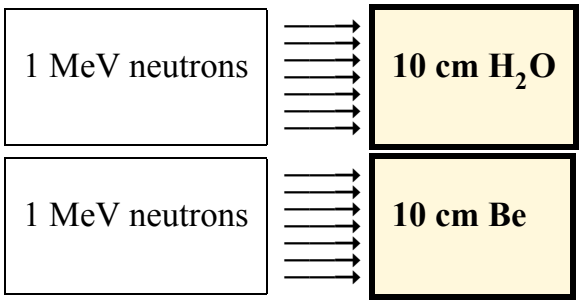

8. Model the following spherical source/shield combinations with MCNP, using an F2 surface fluence-rate tally

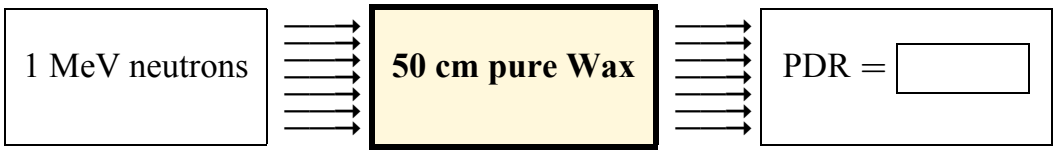

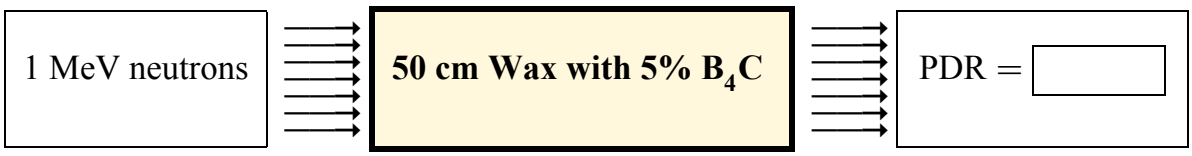

and quantify the ability of the B_4C to lower the photon dose rate on the personnel-side of the shield.

9. Model the following spherical source/shield combinations with MCNP, using an F2 surface fluence-rate tally

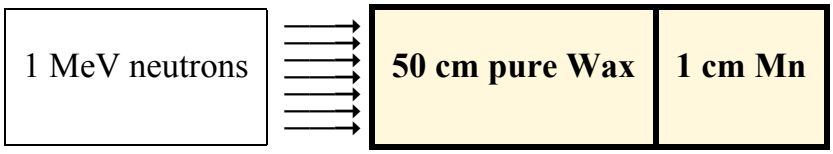

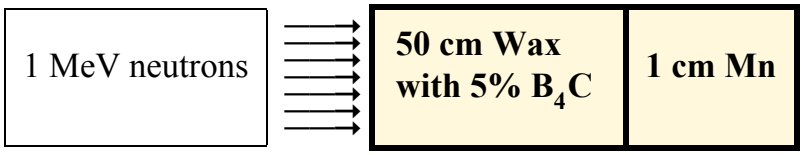

and quantify the ability of the B_4C to lower the reaction-rate of the neutron activation reaction ${}^{55}_{25}\mathrm{Mn}\,(n,\gamma)\,{}^{56}_{25}\mathrm{Mn}$.

6.3 Some neutron shielding materials

Hydrogenous materials such as paraffin wax, polyethylene and water are efficient neutron shields for neutron energies below circa 4 MeV, because the kinematic effectiveness of elastic scattering with ^{1}H is high, and the cross-section for this elastic scattering interaction remains reasonably high below approximately 4 MeV. The shortcomings of ^{1}H as neutron shielding material were stated above: (1) the cross section falls drastically at high neutron energies, (2) the scattering angle is forward peaked and (3) quite energetic capture 2.205 MeV γ-rays are emitted during the nuclear reaction ${}^{1}_{1}\mathrm{H}\,(n,\gamma)\,{}^{2}_{1}\mathrm{H}$. Further disadvantages of hydrogenous materials are that paraffin wax is flammable, water can leak and evaporate and causes corrosion in shields, while polyethylene can be damaged by high fluences of neutrons and lose its structural integrity.

Metals such as e.g. iron are valuable shielding materials against fast neutrons — both the inelastic scattering cross-section and the kinematic efficiency of inelastic neutron scattering by Fe are high enough to make this element quite useful in neutron shielding. These materials are also used to shield ionising photons. The radiation resistance of metals are very high, i.e. they are very resistant to damage by ionising radiation. Iron is particularly effective and reasonably economical for application in a neutron shield as one member of a set of complementary shielding materials, that constitute the neutron shield.

Boron is often incorporated into neutron shields — the natural abundance of the isotope ^{10}B is close to 19.9%, and the reference thermal neutron capture cross-section for this isotope of boron is quite high at 3844 barn. The isotope ^{10}B is an almost perfect $(1/v)$-absorber up to neutron energies of circa 4 MeV, and is therefore a broad-spectrum neutron absorber. This contrasts with e.g. the non-$(1/v)$ neutron absorber, cadmium, which only efficiently absorbs neutrons slower than the so-called "cadmium-cutoff" energy of 0.625 eV — see Figure 3.31 on page 133.

Boron carbide can be blended into aluminium to form BorAl, which is a useful neutron absorber in e.g. PWR fuel casks. In aqueous applications, BorAl tends to suffer from corrosion damage. It is practically impossible to alloy more than 3% boron into steels.

Cadmium has a high (n,γ) neutron capture cross section (2450 b at the reference thermal neutron energy) and is frequently used as a neutron absorber. Cadmium has the disadvantage of emitting energetic 9.05 MeV capture gamma photons, which themselves require shielding. The specific cadmium isotope having the high neutron absorption cross-section (20 730 barn) is ^{113}Cd, which has a natural abundance of 28.73%.
Cadmium is very toxic, so that its use should be restricted — using boron carbide (B_4C) or ammonium pentaborate as a slow neutron absorber, is far safer than using Cd. As explained above cadmium is a thermal neutron absorber, whereas the isotope ^{10}B is a wide energy range neutron absorber.

Concrete is often the shield material of choice for neutron sources, especially around nuclear reactors and accelerators. Concrete is never the best shielding material — in terms of the ability of a given shield thickness to maximally lower the transmitted dose rate — but have the benefits of being relatively cheap and also strong. One of the reasons why concrete is a

reasonable good neutron shielding material, is that it contains crystalline water. Thanks to this crystalline water, there is normally a substantial amount of ^{1}H present in concrete. The heavier elements in concrete can assist to slow down fast neutrons by inelastic scattering, and the ^{1}H in the concrete can effectively lower the energies of neutrons with energies below about 4 MeV, to thermal energies. Because its water content is vital to its neutron shielding abilities, concrete neutron shields must never be heated to temperatures above circa 65°, because that may cause a loss of crystalline water from the concrete.

As a result of the slow loss of crystalline water, the neutron shielding ability of concrete shields may slowly deteriorate over the first decade after the concrete had been cast. High temperatures will accelerate the rate of loss of moisture from concrete. In the design of a concrete neutron shield, shield design calculations must always be done for a reasonably "dried out" concrete composition in order to design a sufficiently robust shield that will not become inefficient e.g. 5 years after construction. Also note that the mass-density ρ of concrete may diminish from e.g., 2.55 to 2.35 over the first decade after construction; shield design calculations must be performed with due conservatism, using the post-dryout mass-density of the concrete.

Improved shielding concretes: Thermal neutron absorbers such as boron carbide (B_4C) can easily be added to concrete. Instead of making concrete from normal sand and stone, fine and coarse iron ore may be used to make magnetite concrete, which has a higher density than ordinary concrete, and better shielding abilities against ionising photons. A whole range of concrete types have been developed and tested for radiation shielding abilities — refer to Shultis & Faw (2000) as well as the different volumes of Robert G. Jaeger's reference work, *Engineering compendium on radiation shielding.*

6.4 The effect of the water content of concrete on its neutron shielding ability

Introduction

Ordinary concrete is a relatively cheap structural and radiation shielding material employed around e.g. nuclear fission reactors. Nuclear reactors produce neutrons and ionising photons, and these radiations must be shielded in order to limit dose rates. The shielding of neutrons as close to the radiation source as possible, also limit neutron activation problems, i.e. induced radioactivity is minimised.

Ordinary concrete consists of a mixture of Portland cement, sand and stones, which is mixed with water and allowed to harden. The isotope $^{1}_{1}H$ in the crystalline water that is chemically trapped in cured concrete, is a very important determinant of the neutron shielding ability of the concrete, because $^{1}_{1}H$ is kinematically highly effective in slowing fast neutrons down to low energies, where they can be easily absorbed.

Methodology

The Monte Carlo radiation transport code, MCNPX 2.7 was used to model a hypothetical point source emitting neutrons having a Watt prompt fission neutron energy spectrum. This neutron spectrum can be seen in Figure 5.3 on page 243. The isotropic source was surrounded by a 100 cm thick spherical concrete sphere, surrounded in turn by about 300 cm of a spherical air shell.

The effective dose rate on the outer surface of the concrete shell, was tallied using an MCNP `F2` surface fluence-rate tally, modified by the effective dose rate response function `DF[ ]2 IC=31 IU=2 FAC=1` for both the neutrons and the ionising photon tally.

The transmitted effective dose rates were calculated as a function of the water content of the concrete.

The effect of the water content of the concrete on the concrete density was taken into account.

Under the assumptions that the normal partial density in ordinary concrete is $0.013\ \mathrm{g\,cm^{-3}}$ (Shultis & Faw, 2000) and that the mass-density of concrete at the water content corresponding to a ${}^{1}_{1}\mathrm{H}$ partial density of $0.013\ \mathrm{g\,cm^{-3}}$ is $2.35\ \mathrm{g\,cm^{-3}}$ (Shultis & Faw, 2000), the mass-density of ordinary concrete as a function of its water content was calculated, and results are tabulated in Table 6.1.

Table 6.1: *Mass-density of ordinary concrete as a function of its water content.*

Partial density of $^{1}_{1}H$ in concrete $\left(\mathrm{g\,cm^{-3}}\right)$	**Mass-density of bulk concrete** $\left(\mathrm{g\,cm^{-3}}\right)$	**Percentage H_2O in concrete**
0.001	2.243	0.398
0.002	2.252	0.794
0.003	2.261	1.186
0.004	2.27	1.575
0.005	2.278	1.961
0.006	2.287	2.344
0.007	2.296	2.724
0.008	2.305	3.101
0.009	2.314	3.475
0.010	2.323	3.846
0.011	2.332	4.215
0.012	2.341	4.581
0.013	2.350	4.943
0.015	2.368	5.661
0.020	2.413	7.408
0.025	2.457	9.092
0.030	2.502	10.715

A simple variance reduction technique — population control via cell importance biasing — was used to obtain standard deviations for the Monte Carlo calculations below 1%, for runtimes of 240 minutes per case, for 17 discrete values of the water content of the concrete. The concrete shell was divided into layers to enable variance reduction via optimised cell-importances in MCNP — see Figure 6.9.

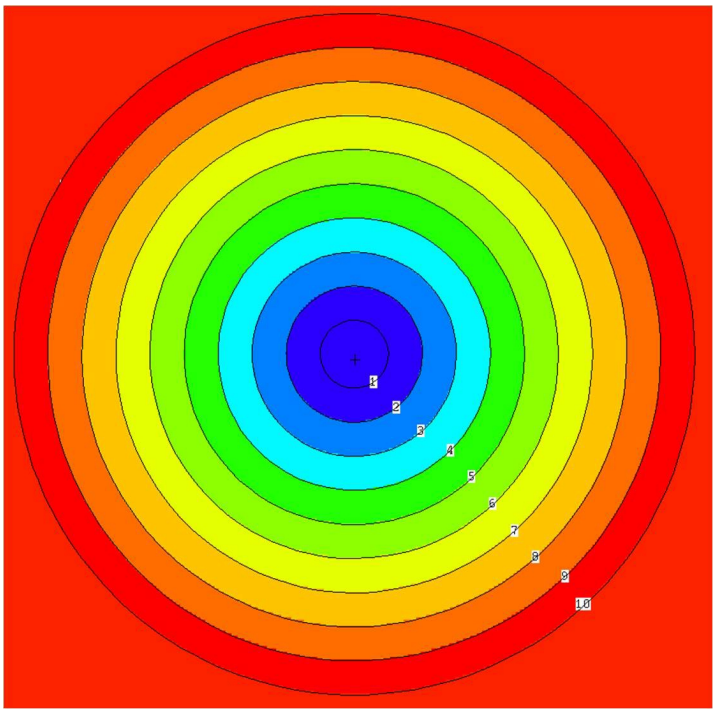

Figure 6.9: *Colour schematic of neutron population control via cell importance biasing — the neutron importance is increased in steps of less than a factor 3 from the inside to the outside of the shield.*

Results

The sensitivity of the neutron shielding ability of ordinary concrete, on its H_2O content, is shown in Figure 6.10.

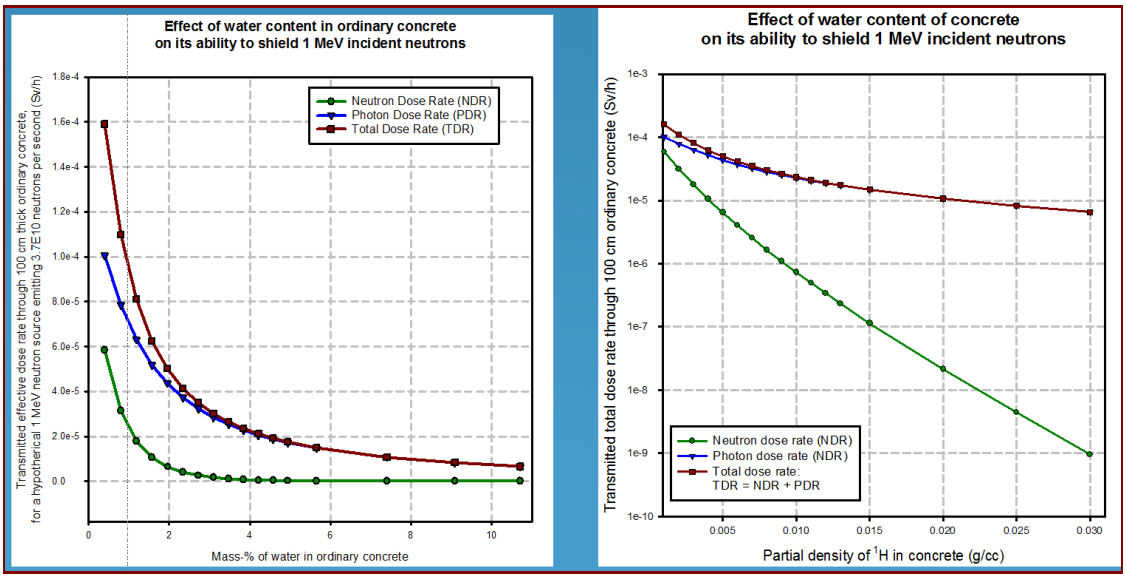

Figure 6.10: *The sensitivity of the neutron shielding ability of ordinary concrete, on its H_2O content.*
Note: The leftmost graph uses a linear vertical axis, while the graph on the far right employs a logarithmic vertical axis.

Conclusions

The dose rate lowering ability of a 100 cm thick concrete shield around a point source that emits neutrons having a Watt prompt fission neutron energy spectrum, can drop by a factor as much as 20, should the concrete loose all its crystalline water as a result of e.g. prolonged, severe overheating caused by high temperatures.

Concrete used for neutron shielding should be allowed to harden with a "wet cure" and can subsequently be painted with a waterproof paint, and should be kept cool, in order to minimise the loss of water from the concrete matrix. When used in neutron shielding applications, concrete should ideally retain at least 3% water. Neutron shielding concrete should be made from raw materials tested for their ability to retain a high water content.

From Figure 6.10 it is clear that ordinary concrete is not an optimal neutron shielding material. Its main advantages are its low cost and high compressive strength. Concrete is therefore employed in circumstances where space and mass are of no concern. Note that secondary ionising photons dominate the transmitted dose rate. High-density concrete such as magnetite, hematite and barytes concrete, are more optimal neutron shields, because they contain significantly more elements with high atomic numbers, which will absorb secondary ionising photons — an optimal neutron shield will tend to equalise the transmitted neutron and photon dose rates.

6.5 The characteristic "fingerprints" of Fe, Pb and paraffin wax as neutron shielding materials

A simple methodology was construed to determine the characteristic nature or "fingerprint" of a material as a neutron shield:

- Envelop a mono-energetic neutron point source emitting e.g. 40 MeV neutrons — i.e. a source of high-energy, mono-energetic neutrons — in a 100 cm thick spherical-symmetrical shell of a single shielding material such as either Fe, Pb or paraffin wax. Run MCNP to calculate the neutron energy spectrum as well as absorbed dose rates at the exit surface of the shield. Analyse the neutron energy spectrum as well as the transmitted dose rate to determine the "characteristic fingerprint" of the material as a shield against high-energy neutrons.

- Repeat the above for a mono-energetic neutron point source emitting e.g. 3 MeV neutrons — i.e. a source of low-energy neutrons to determine the "characteristic fingerprint" of the material as a shield against low-energy neutrons.

Analysis: Characteristic nature of Fe as shield against low-energy neutrons

For a 100 cm thick spherical Fe shield having a point source of 3 MeV neutrons at the centre of the sphere, the group-integrated multigroup neutron energy spectrum at the exit surface of the shield displayed in Figure 6.11, was obtained with an MCNPX 2.7 calculation using ENDF-B/7.0 cross-section data.

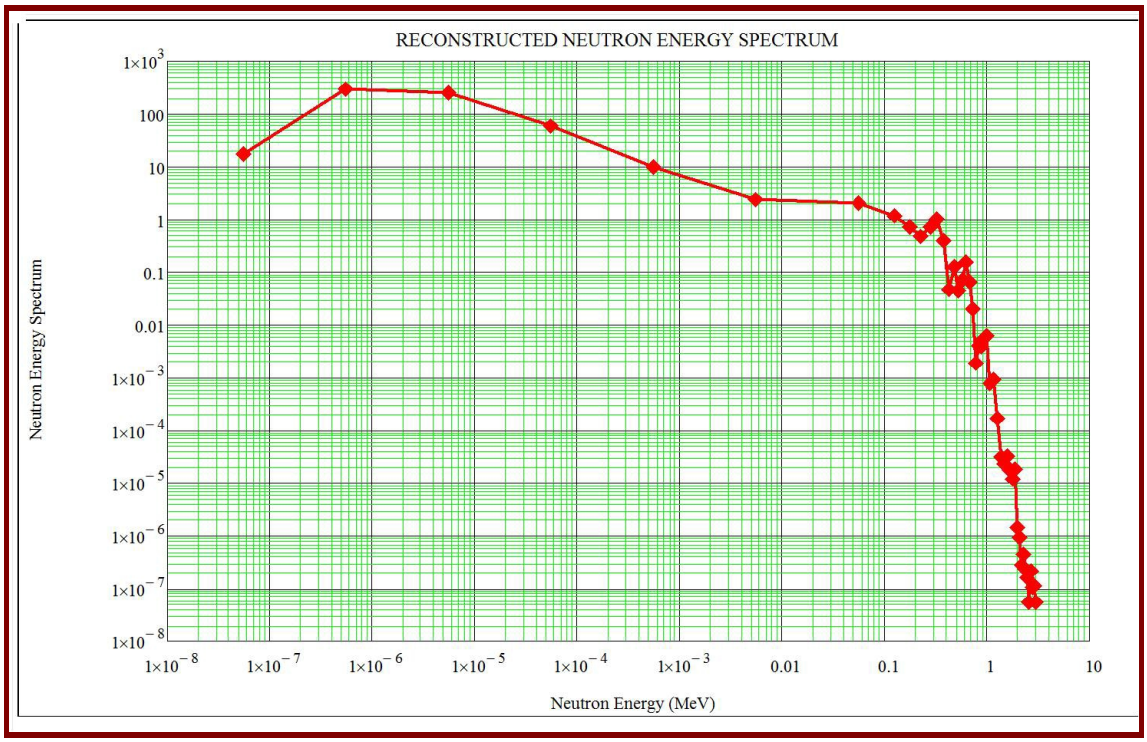

Figure 6.11: *Neutron energy spectrum at the exit side of a 100 cm thick Fe shield having a point source emitting 3 MeV neutrons at its centre.*

Results at the exterior surface of the 100 cm radius Fe sphere with a 3 MeV point source of neutrons at its centre, are as follows:

- $\frac{47}{100}$ neutrons reach the outer surface of the sphere for every neutron emitted at the centre of the sphere; neutron loss is negligible.
- $\frac{0.81}{100}$ ionising photons reach the surface of the Fe sphere for every neutron emitted at its centre; these are secondary ionising photons produced via (n, γ)-reactions and inelastic scattering of neutrons by Fe.
- *Percentage of neutrons slowed down to below 1 MeV: 99.94%.*
- *Percentage of neutrons with energies above 1 MeV: 0.06%.*
- *Average neutron energy:* $E_{av} = 0.157$ *MeV.*
- $NDR = 5.82E\text{-}13$ *Sv/hr for source strength of 1 n/s.*
- $PDR = 2.80E\text{-}15$ *Sv/hr for source strength of 1 n/s.*
- *Ratio* $\frac{NDR}{PDR} = 208$, *i.e. the NDR dominates outside the thick Fe sphere.*
- $E_{\gamma}^{\max} = 12$ MeV.

Analysis: The characteristic nature of Fe at attenuating high-energy neutrons

For a 100 cm radius spherical Fe shield with a point isotropic source of 40 MeV neutrons at its centre, the neutron energy spectrum on the outer surface of the sphere is shown in Figure 6.12; this was calculated with MCNPX 2.7 using ENDF/B-7.0 cross-section data.

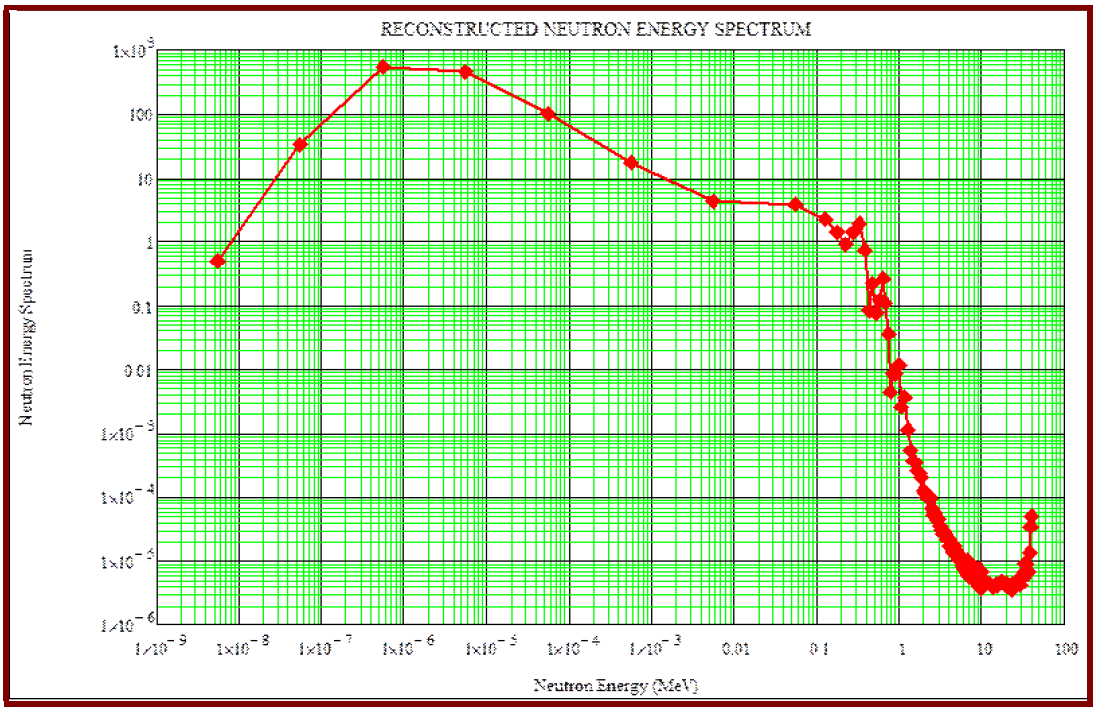

Figure 6.12: *Neutron energy spectrum at the outer surface side of a 100 cm thick spherical Fe shield with a point source of 40 MeV neutron at the centre of the Fe shield.*

Results at the exterior surface of the Fe sphere with a 40 MeV point source of neutrons at its centre, are as follows:

- $\frac{89}{100}$ neutrons reach the outer surface of the sphere for every neutron emitted at the centre of the sphere; neutron loss is negligible.
- $\frac{1.5}{100}$ ionising photons reach the surface of the Fe sphere for every neutron emitted at its centre; these are secondary ionising photons produced via (n, γ)-reactions and inelastic scattering of neutrons by Fe.
- Percentage of neutrons slowed down to below 1 MeV: 99.845%.
- Percentage of neutrons with energies above 1 MeV: 0.155%.
- Percentage of neutrons with energies above 2 MeV: 0.038%.
- Percentage of neutrons with energies above 3 MeV: 0.031%.
- Average neutron energy: $E_{\text{av}} = 0.166$ MeV.
- NDR = 1.11E-12 Sv/hr for source strength of 1 n/s.

- PDR = 5.16E-15 Sv/hr for source strength of 1 n/s.
- Ratio $\frac{\text{NDR}}{\text{PDR}} = 215$, i.e. the NDR clearly dominates outside a pure Fe sphere.
- $E_{\gamma}^{\max} = 12$ MeV.

Another noteworthy finding, is that Fe is incapable of efficiently moderating neutrons down to epi-thermal and thermal energies, because the only mechanism available to do this is elastic scattering, which is kinematically very inefficient. For a spherical Fe shield with a 100 cm radius, surrounding a 40 MeV point source at the origin, the percentage of the neutron fluence-rate $\phi(E)$ with $E_n < 1$ keV is only,

$$\frac{\int_0^{1\,\text{keV}} dE\,\phi(E)}{\int_0^{E_{\max}} dE\,\phi(E)} = 5.8\,\%$$

while the percentage of neutrons with $E_n < 1$ eV is only,

$$\frac{\int_0^{1\,\text{eV}} dE\,\phi(E)}{\int_0^{E_{\max}} dE\,\phi(E)} = 0.041\,\%,$$

i.e. Fe is very capable in slowing neutrons down to energies below 1 MeV, but is practically incapable of slowing neutrons down to thermal energies; Fe readily scatters neutrons into the approximate energy range $E_n \in [10\,\text{eV}; 1\,\text{MeV}]$, but not to lower energies.

Analysis: The characteristic abilities of different thicknesses of Fe at attenuating high-energy neutrons

For an incident mono-energetic neutron energy spectrum of 40 MeV neutrons, emitted isotropically from a point source at the centre of a spherical Fe shield with variable radii, the percentage of neutrons found in selected energy bands were calculated, and results are tabulated in Table 6.2. The analysis on neutron spectra generated in several very long MCNP runs, was performed using the following MathCAD worksheet,

Neutron Spectrum Analysis.xmcd

Table 6.2: *The ability of different thicknesses of iron to "soften" a "hard" incident neutron spectrum. Neutron spectrum assessment for mono-energetic incident neutrons, $E = 40$ MeV, after transport through different thicknesses of Fe. Using the MathCAD worksheet for spectrum analysis, the neutron spectrum $\phi(E)$ was reconstructed numerically, and then integrals are of the type, $\frac{\int_{E_1}^{E_2}\phi(E)\,dE}{\int_{0}^{Emax}\phi(E)\,dE}$ were evaluated.*

Fe thickness (cm)	Percentage neutrons with $E > 1$ MeV	Percentage neutrons with $E > 5$ MeV	Percentage neutrons with $E > 10$ MeV	Percentage ϕ_n with $E \leq 1$ MeV
10	61.1%	34.9%	31.3%	38.9%
20	34.4%	15.1%	13.2%	65.6%
30	17.9%	6.7%	5.8%	82.1%
40	8.9%	2.9%	2.5%	91.1%
50	4.4%	1.3%	1.1%	95.6%
60	2.1%	0.6%	0.5%	97.9%
80	0.5%	0.1%	0.09%	99.5%
100	0.16%	0.026%	0.022%	99.84%

The results in the second column of Table 6.2 clearly show that 40 cm thick Fe is able to moderate about 91% of incident 40 MeV neutrons to energies below 1 MeV, that 60 cm Fe is able to moderate approximately 98% of incident 40 MeV neutrons to energies below 1 MeV and that 100 cm Fe is able to moderate 99.84 % of incident 40 MeV neutrons to energies below 1 MeV. This ability of relatively thick Fe shields to practically "eliminate" fast neutrons from an incident neutron field, is quite spectacular and very valuable in radiation shield design.

Conclusions: The characteristic ability of Fe as a neutron shield

From these and other possible simulations using MCNP, it may be stated that the characteristic "fingerprint" of Fe for slowing down and shielding neutrons in the important energy range $E_n \in (1\,\text{MeV}, 200\,\text{MeV})$, is as follows:

- Fe is rather bad at shielding neutrons with $E_n \lesssim 1$ MeV, because it is very inefficient at slowing neutrons down via elastic scattering. The threshold energy for the excitation of first discrete energy level in the dominant Fe isotope, ^{56}Fe, via inelastic neutron scattering, lies at about 0.861 MeV. The element Fe can therefore not effectively slow down neutrons below about circa 0.861 MeV.

- Fe is an excellent shielding material for slowing down neutrons with $E \gtrsim 1$ MeV, because inelastic scattering by Fe is remarkably efficient at slowing neutrons down. Fe aggressively slows down neutrons above about 1 MeV, because the threshold energy for inelastic neutron scattering by the most abundant iron isotope, ^{56}Fe, lies at 0.861 MeV.

The neutron energy spectra in Figures 6.11 and 6.12 are practically identical, proving that the above is indeed the characteristic neutron shielding fingerprint of Fe: it is very good in lowering the energies of high energy neutrons to below 1 MeV, but it is unable to "finish the job" and there is a "build-up" of neutrons in the energy range $E_n \in (10 \text{ eV}, 1 \text{ MeV})$, and Fe is unable to "get rid of" the neutrons in this energy range by either slowing down or absorption.

Analysis: ability of Pb to shield low-energy neutrons

For a 100 cm thick spherical Pb shield having a point source of 3 MeV neutrons at the centre of the sphere, the group-integrated multigroup neutron energy spectrum at the exit surface of the Pb shield displayed in Figure 0.0, was obtained with an MCNPX 2.7 calculation using ENDF-B/7.0 cross-section data.

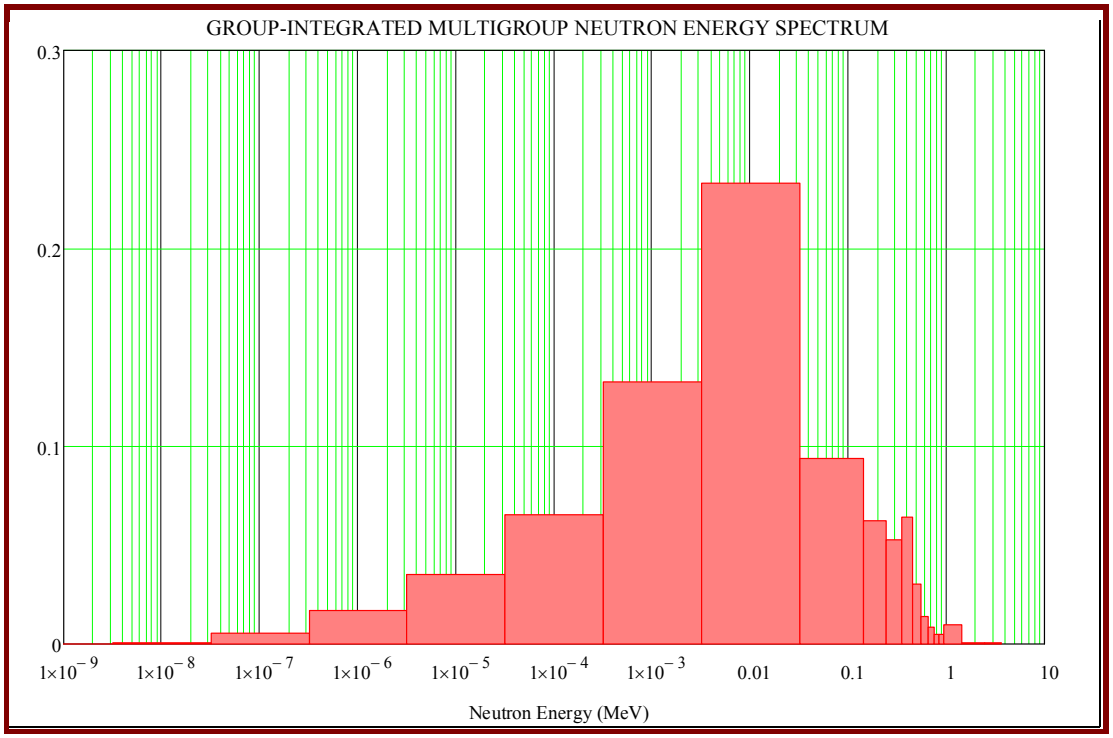

***Figure 6.13**: Neutron energy spectrum at the exit side of a 100 cm thick Pb shield having a point source emitting 3 MeV neutrons at its centre.*

Results at the exterior surface of the 100 cm radius Pb sphere with a 3 MeV point source of neutrons at its centre, are as follows:

- $\frac{83.2}{100}$ neutrons reach the outer surface of the sphere for every neutron emitted at the centre of the sphere; neutron loss is negligible. Main reason: the neutron absorption cross-section for Pb is low.

- $\frac{0.08}{100}$ ionising photons reach the surface of the Fe sphere for every neutron emitted at its centre; these are secondary ionising photons produced via (n,γ)-reactions and inelastic scattering of neutrons by Pb. Reasons: Pb produces less as well as les energetic capture γ-rays than Fe, and shields these ionising photons more strongly than does Fe.

- Percentage of neutrons slowed down to below 2 MeV: 99.89%.
  Percentage of neutrons with energies above 2 MeV: 0.11%.
  Conclusion: A very thick Pb shield practically eliminates high energy neutrons from the transmitted neutron energy spectrum, and concentrates neutrons into the energy band 0.1 eV to 2 MeV.

- *Average neutron energy:* $E_{av} = 0.125$ *MeV.*

- *NDR = 1.21E-12 Sv/hr for source strength of 1 n/s.*

- *PDR = 2.54E-16 Sv/hr for source strength of 1 n/s.*

- *Ratio* $\frac{NDR}{PDR} = 4756$*, i.e. the NDR dominates outside the thick Pb sphere.*

- $E_{\gamma}^{\max} \approx 7.3$ MeV.

Analysis: Ability of Pb to shield high energy neutrons

For a 100 cm radius spherical Pb shield with a point isotropic source of 40 MeV neutrons at its centre, the neutron energy spectrum on the outer surface of the Pb sphere is shown in Figure 6.14; this was calculated with MCNPX 2.7 using ENDF/B-7.0 cross-section data.

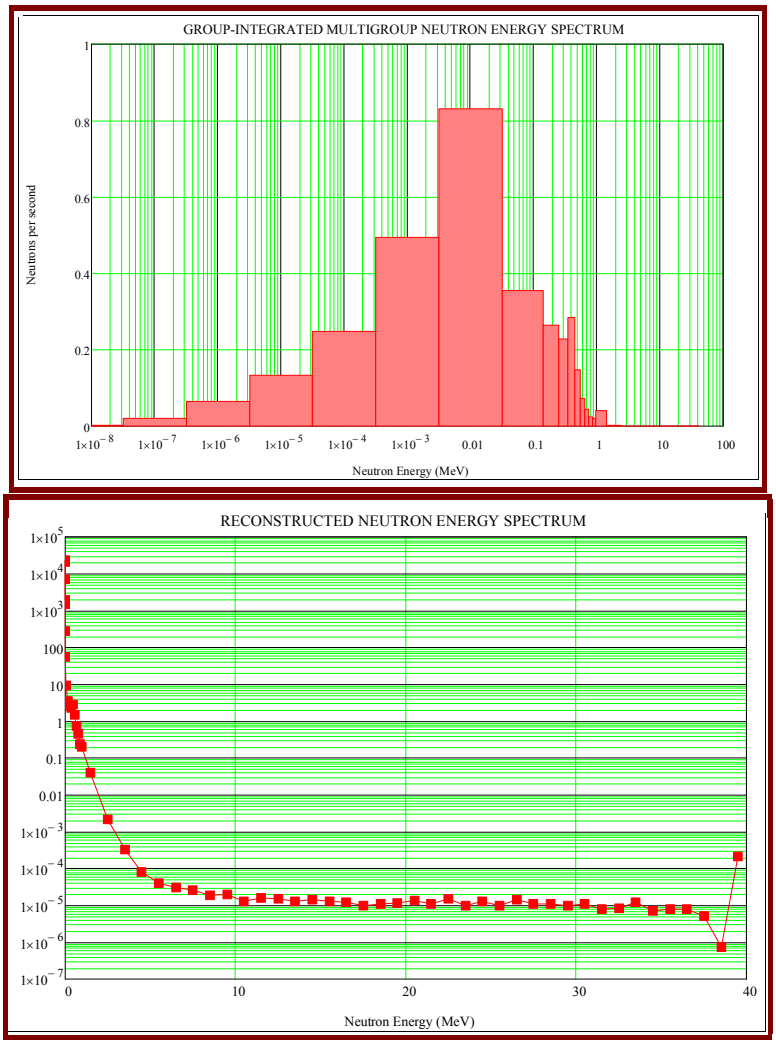

Figure 6.14: *Neutron energy spectrum at the outer surface side of a 100 cm thick spherical Pb shield with a point source of 40 MeV neutron at the centre.*

Results at the exterior surface of the 100 cm radius Pb sphere with a 40 MeV point source of neutrons at its centre, are as follows:

- 3.28 neutrons reach the outer surface of the sphere for every neutron emitted at the centre of the sphere; neutron loss is negligible. More neutrons reach the surface of the shield than are born at the centre of the sphere, because $(n, 2n)$ and $(n, 3n)$ neutron multiplication reactions are energetically possible in the high neutron energy range. The nuclei of Pb isotopes are not as stable as e.g. $^{56}_{26}$Fe, so that the threshold energies of $(n, 2n)$ and $(n, 3n)$ neutron multiplication reactions are lower, and their cross-sections tend to be higher than for $^{56}_{26}$Fe.

- $\frac{0.33}{100}$ ionising photons reach the surface of the Fe sphere for every neutron emitted at its centre; these are secondary ionising photons produced via (n, γ)-reactions and inelastic scattering of neutrons by Pb. Reasons: Pb produces less as well as less energetic capture γ-rays than Fe, and shields these ionising photons more strongly than does Fe.

- Percentage of neutrons slowed down to below 2 MeV: 99.85%
  Percentage of neutrons with energies above 2 MeV: 0.15%.
  Conclusion: A very thick Pb shield practically eliminates high energy neutrons from the transmitted neutron energy spectrum, and concentrates neutrons into the energy band 0.1 eV to 2 MeV.

- Average neutron energy: $E_{\text{av}} = 0.143$ MeV.

- NDR = 5.28E-12 Sv/hr for source strength of 1 n/s.

- PDR = 1.05E-15 Sv/hr for source strength of 1 n/s.

- Ratio $\frac{\text{NDR}}{\text{PDR}} = 5037$, i.e. the NDR dominates outside the thick Pb sphere.

- $E_{\gamma}^{\text{max}} = 11$ MeV.

Comparison: Abilities of Fe and Pb to moderate high-energy neutrons

Which material — Fe or Pb — has the best ability to moderate fast neutrons, so that a subsequent hydrogen-rich shield can easily shield the low-energy neutrons emerging from the first shield?

This question is answered by simulating the transport of fast incident neutrons through thick layers of Fe and Pb. This enables the characteristic "fingerprint-nature" of the shielding material to emerge clearly. Figure 6.15 shows the reconstructed energy spectra, $\phi(E)$ emerging from the outer surface of a spherical shell-shield, with thickness 100 cm, around an isotropic source of mono-energetic 40 MeV neutrons.

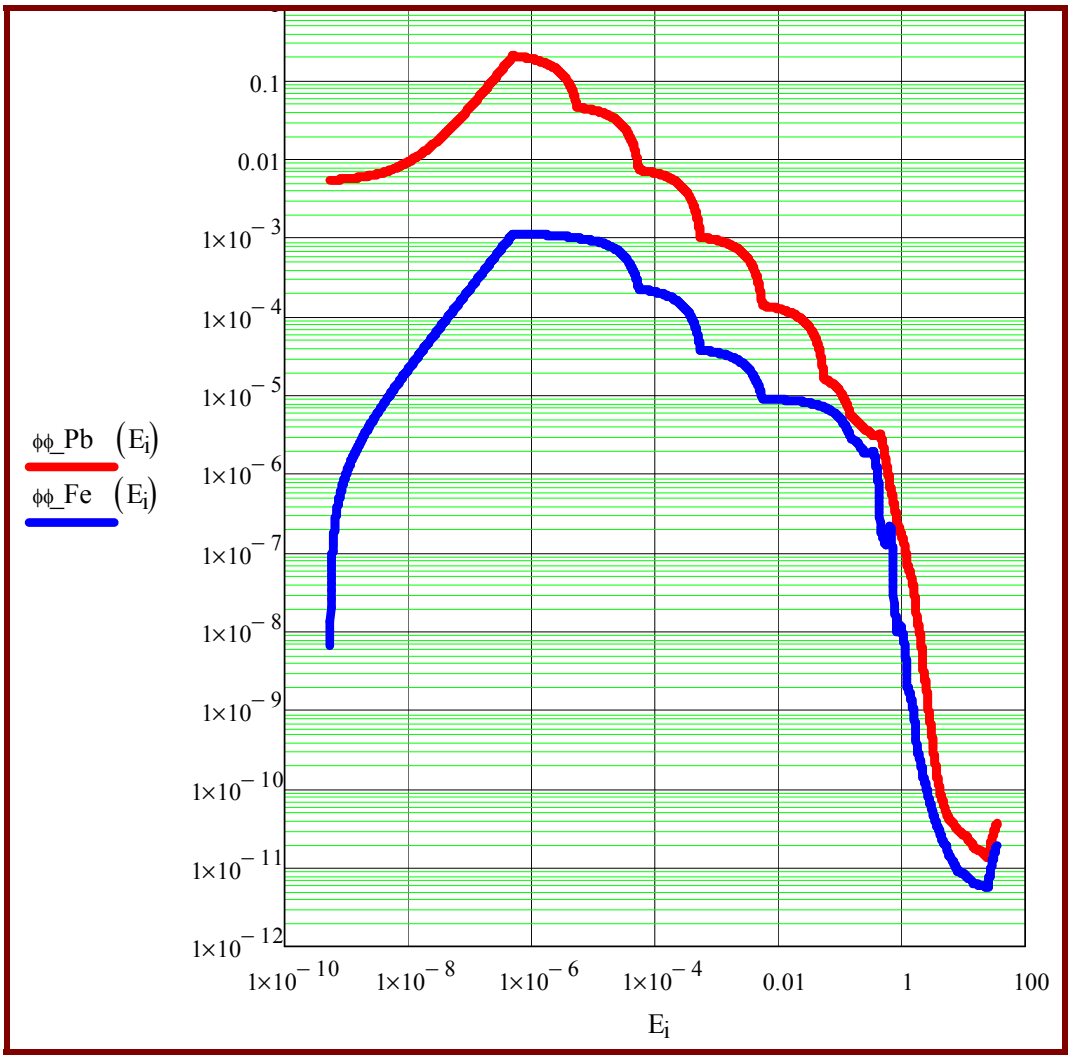

Figure 6.15: *Neutron energy spectra, $\phi(E)$, emerging from the outer surfaces of Pb and Fe spherical shell-shields, having thicknesses of 100 cm, around an isotropic source of mono-energetic 40 MeV neutrons.*

From Figure 6.15 and Table 6.4 it is clear that Fe is a substantially better neutron shield than Pb. Transmitted neutron fluence-rates and transmitted total dose rates at the exit side of a Fe shield are markedly lower than for a Pb shield. One of the reasons for this is that number density of Fe nuclei in an iron shield is almost 2.5 times higher than the number density of Pb nuclei in a Pb shield. Another reason is that the iron's cross-sections for the excitation of internal energy states of the nucleus via inelastic scattering, maintains higher, sustained values at high neutron energies. In contrast, excitation cross-sections for Pb have somewhat lower values and also a somewhat more pronounced inverse-U shape, i.e. $\cap$-shape, so that Pb is inferior as a moderator material for high-energy neutrons. This pronounced $\cap$-shape of the inelastic scattering excitation cross-section functions for Pb is the result of other exit channels opening up sooner for Pb nuclei than for Fe nuclei, because the larger Pb nuclei are less stable than the Fe nuclei in terms of nuclear binding energy per nucleon.

Analysis: Ability of paraffin wax to attenuate high-energy neutrons

Next, the characteristic ability of paraffin wax to attenuate high-energy neutrons is analysed. The incident neutron energy spectrum is mono-energetic, 40 MeV neutrons. Results are summarised in Table 6.3.

Table 6.3: *The ability of different thicknesses of paraffin wax to "soften" a "hard" incident neutron spectrum. Neutron spectrum assessment for mono-energetic incident neutrons, $E = 40$ MeV, after transport through different thicknesses of wax. Integrals are of the type,* $\frac{\int_{E_T}^{Emax} \phi(E)\, dE}{\int_{0}^{Emax} \phi(E)\, dE}$.

Wax thickness (cm)	**Percentage neutrons with** $E > 1$ MeV	**Percentage neutrons with** $E > 5$ MeV	**Percentage neutrons with** $E > 10$ MeV	**Percentage neutrons with** $E < 1$ keV
10	91.9%	87.1%	82.9%	3.9%
20	88.5%	82.1%	76.3%	5.8%
30	94.1%	86.2%	79.1%	7.3%
40	93.6%	85.2%	77.5%	7.8%
50	93.5%	84.7%	76.6%	8.2%
60	93.2%	84.1%	75.7%	8.4%
80	93.1%	83.9%	75.0%	8.6%
100	93.0%	83.4%	74.2%	9.2%

From Table 6.3 it is evident that wax is unable to effectively slow down fast neutrons. Even after having gone through a 100 cm thick wax shield, more than 83% of neutrons still have energies above 5 MeV. This is in strong contrast to a 100 cm radius sphere of iron, which slows down practically all fast neutrons ($E_n = 40$ MeV) with great ease.

Figure 6.16 shows the group-integrated neutron fluence-rate spectrum where it exits a 100 cm thick wax shield around a point source of 40 MeV neutrons. Many neutrons are "uncollided" and still have energies of 40 MeV. The spectrum shows the complete inability of materials such as wax, water and polyethylene to effectively slow down fast neutrons.

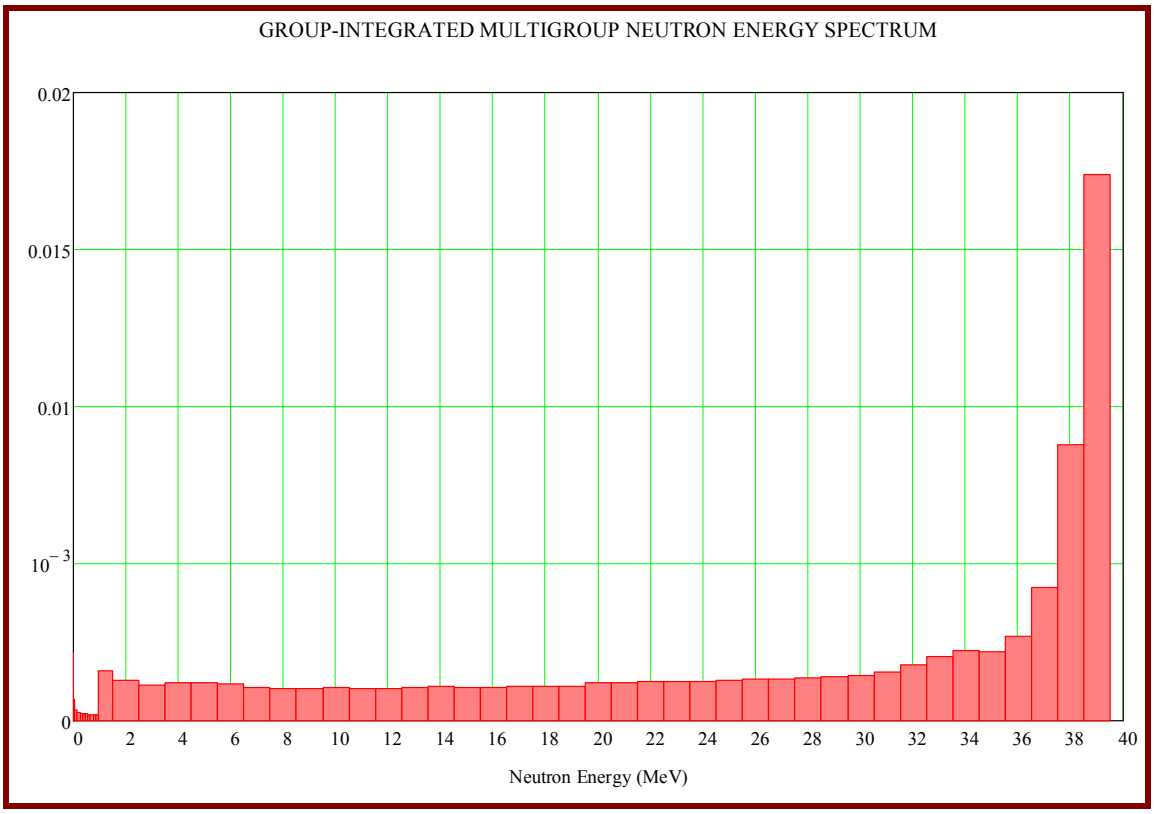

Figure 6.16: *Group-integrated neutron fluence-rate spectrum where it exits a 100 cm thick wax shield around a point source of 40 MeV neutrons.*

In Figure 6.16 it is evident that many neutrons remain "uncollided" and still have energies of 40 MeV. The spectrum shows the stark inability of materials such as wax, water and poly-ethylene to effectively slow down fast neutrons.

When the source is 40 MeV neutrons, and the radiation shield is a 100 cm radius paraffin wax sphere, with mass density $\rho = 0.92\ \mathrm{g\,cm^{-3}}$, a total of 0.284 ionising photons reach the outer surface, while 8.60E-02 neutrons reach the surface, for every neutron emitted at the centre of the sphere. The surface dose rate from neutrons is 1.64E-12 Sv/hr per neutron/s emitted at the centre of the sphere, which is 34.3 times higher than the surface dose rate from ionising photons, which is 4.77E-14 Sv/hr per neutron/s emitted at the centre of the sphere. The dose rate field outside the sphere will be dominated by neutrons when a 100 cm radius paraffin wax shield surrounds a source of 40 MeV neutrons.

Results at the exterior surface of the 100 cm radius paraffin wax sphere with a 40 MeV point source of neutrons at its centre, are as follows:

- $\frac{8.6}{100}$ neutrons reach the outer surface of the sphere for every 40 MeV neutron emitted at the centre of the sphere.
- $\frac{28.4}{100}$ ionising photons reach the surface of the paraffin wax sphere for every neutron emitted at its centre; these are secondary ionising photons produced via (n, γ)-reactions and inelastic scattering of neutrons by carbon nuclei in wax.

- Percentage of neutrons slowed down to below 2 MeV: 21 %
  Percentage of neutrons with energies above 2 MeV: 79 %.
  Conclusion: A very thick paraffin wax shield is incapable of effectively slowing down fast neutrons.
- Average neutron energy: $E_{\text{av}} = 21.4$ MeV.
- NDR = 1.64E-12 Sv/hr for source strength of 1 n/s.
- PDR = 4.77E-14 Sv/hr for source strength of 1 n/s.
- Ratio $\frac{\text{NDR}}{\text{PDR}} = 34.3$, i.e. the NDR dominates outside the thick paraffin wax sphere.
- $E_{\gamma}^{\text{max}} = 42$ MeV (probably nuclear bremsstrahlung from protons).

Analysis: Ability of paraffin wax to attenuate low energy neutrons

For the transport of 3 MeV neutrons through 100 cm wax, some of the original 3 MeV neutrons remain in the spectrum; most neutrons are found in the thermal and epithermal energy range. The transmitted neutron fluence-rate and neutron dose-rate are both extremely low. This shows that materials such as paraffin wax, water and polyethylene are excellent shielding materials against low-energy neutrons. The transmitted neutron energy spectrum is shown in Figure 6.17.

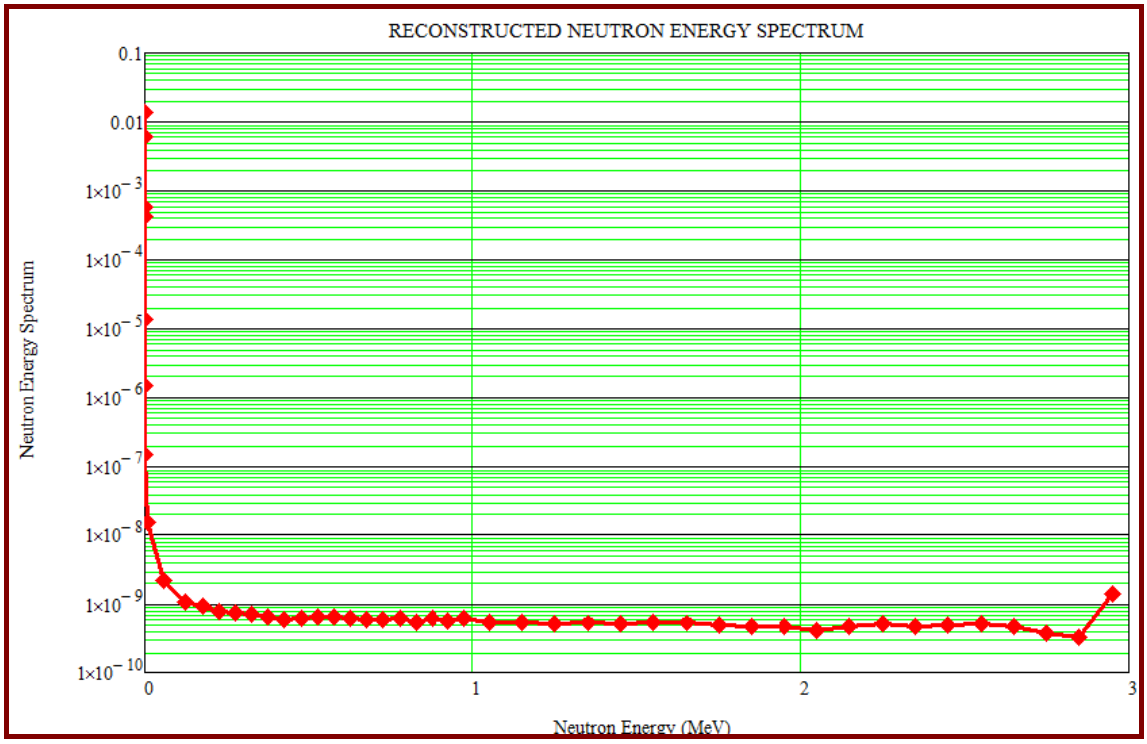

Figure 6.17: *Neutron energy spectrum on the outer surface of a paraffin wax sphere with a 100 cm radius with a neutron source emitting 3 MeV neutrons at the centre.*

Results at the exterior surface of the 100 cm radius paraffin wax sphere with a 3 MeV point source of neutrons at its centre, are as follows:

- 4.0E-09 neutrons reach the outer surface of the sphere for every 3 MeV neutron emitted at the centre of the sphere.
- $\frac{13.5}{100}$ ionising photons reach the surface of the paraffin wax sphere for every 3 MeV neutron emitted at its centre; these are secondary ionising photons produced via (n, γ)-reactions and inelastic scattering of neutrons by carbon nuclei in wax.
- Percentage of neutrons slowed down to below 2 MeV: 94.3 %
  Percentage of neutrons with energies above 2 MeV: 5.7 %.
  Percentage of neutrons with energies below 1 eV: 49.9 %.
  Conclusion: A very thick paraffin wax shield is good at slowing down low energy neutrons.
- Average neutron energy: $E_{\text{av}} = 0.28$ MeV.
- NDR = 1.0E-20 Sv/hr for source strength of 1 n/s.
- PDR = 1.46E-14 Sv/hr for source strength of 1 n/s.
- Ratio $\frac{\text{NDR}}{\text{PDR}} = 6.9\text{E-}7$, i.e. the PDR completely dominates outside the thick paraffin wax sphere. The surface dose rate from ionising photons is 1.44 million times higher than the surface dose rate from neutrons. In other words, secondary ionising photons completely dominate the radiation field when a very thick paraffin wax shield surrounds a source of low energy neutrons.
- $E_{\gamma}^{\text{max}} = 5$ MeV.

Conclusions: Neutron shielding characteristic "fingerprint" natures of Fe, paraffin wax and Pb

From the above, it is concluded that:

- An adequate thickness of iron has a very high ability to slow down fast neutrons to energies below about 0.9 MeV;
- Iron is unable to effectively shield neutrons with energies below about 0.9 MeV;
- Paraffin wax is unable to effectively shield neutrons with energies above approximately 4 MeV;
- Paraffin wax has an excellent ability to shield neutrons with energies below circa 4 MeV.

6.5.1 Dose rates on the outer surfaces of solid spheres of paraffin wax, Pb and Fe containing neutron sources

Table 6.4 lists calculated dose rates on the outer surfaces of solid spheres of paraffin wax, Pb and Fe containing 3 MeV and 40 MeV neutron sources emitting 1 neutron per second. The Monte Carlo code MCNPX 2.7 and ENDF/B-7.0 cross-section data were used in these calculations.

***Table 6.4**: Calculated dose rates on the outer surfaces of solid spheres of paraffin wax, Fe and Pb containing 3 MeV and 40 MeV neutron sources emitting 1 neutron per second.*

	Shielding Material		
	Paraffin wax	**Fe**	**Pb**
Neutron dose rate (Sv/hr) **for $E_n = 3$** MeV	1.01E-20	5.82E-13	1.21E-12
Neutron dose rate (Sv/hr) **for $E_n = 40$** MeV	1.64E-12	1.11E-12	5.28E-12
Photon dose rate (Sv/hr) **for $E_n = 3$** MeV	1.46E-14	2.80E-15	2.52E-16
Photon dose rate (Sv/hr) **for $E_n = 40$** MeV	4.77E-14	5.16E-15	1.07E-15

A number of conclusions can be drawn from Table 6.4. The transmitted dose rates for the shielding of 3 MeV and 40 MeV neutrons by Fe, are remarkably similar, differing by a factor les than 2, because Fe "concentrates" the neutrons in the energy range $E_n \in [1\text{ eV}; 1.5\text{ MeV}]$. We also observe that the element Fe is clearly a better neutron shielding material than Pb — for the given Fe shield, the transmitted dose rate is between 2 and 5 times lower than for the given Pb shield; the Fe shield will also be significantly lighter and cheaper than the Pb shield. When pure paraffin wax is used to shield low energy incident neutrons, the transmitted ionising photon dose rate is excessively high compared to the transmitted neutron dose rate, because the production rate of secondary 2.205 MeV ionising photons from ${}^{1}_{1}\text{H}(n,\gamma){}^{2}_{1}\text{H}$ nuclear reactions are high, and the low-Z atoms in paraffin wax are unable to effectively shield these secondary photons. Of the 3 materials under assessment, paraffin wax is clearly the most effective neutron dose rate attenuator for low energy incident neutrons, while Fe is the best shielding material for high energy neutrons.

6.6 The necessity for deploying *complementary shielding materials* against neutron sources

For incident neutron energies in the approximate energy range $E_n \in (0, 100\text{ MeV})$, Fe in isolation, is an inferior single-material shield; the Fe must always be complemented by a hydrogen-rich shielding material. ***Complementary shielding materials*** must be deployed to obtain a shield with an optimised dose rate reduction ability for a constrained shield thickness, because no single element is good in isolation as a neutron shield; materials must always be

used in well-chosen combinations in order to complement each other, to construct a truly effective neutron shield. For incident neutrons, a well-chosen combination of complementary shielding materials will always be a far better shield than a single-material shield.

The function of Fe in a composite neutrons shield containing selected complementary shielding materials, is to lower neutron energies via inelastic scattering to below about 1 MeV; the function of the hydrogen-rich material such as paraffin wax or polyethylene in the shield, is to further aggressively lower the energies these neutrons, slowed down by Fe into the energy band below about 1 MeV, to thermal and near-thermal energies, where neutron absorption can take place and where neutrons are biologically less dangerous. Materials such as Fe must be used when a significant fraction of the incident neutrons have energies above approximately 4 MeV, and materials such as paraffin wax or polyethylene must be used to thermalise the neutrons that have been slowed down by Fe to within the cross-sectional "reach" or "grasp" of ${}_{1}^{1}\mathrm{H}$. A strong low-energy neutron absorber that produces low-energy capture ionising photons, can then be used inside the hydrogenous material to absorb the thermalised neutrons with minimal production of problematic secondary ionising photons.

Chapter 7:
The Shielding of Ionising Photons

7.1 Introduction

In this chapter, we look at ionising photon interactions that are important from the perspective of the shielding of ionising radiation.

Just like neutrons, high-energy photons cause indirect ionisation when they pass through matter — photon interactions release charged particles, mainly electrons, which then deposit energy in the medium. Because neutrons and ionising photons are indirectly ionising, they can penetrate deeply into matter, and are often the two principal radiation types that have to be considered when designing shields to reduce levels of ionising radiation to safe values.

7.2 The photon energy range of primary interest

First, we determine the energy boundaries of the photons met in practical radiation shielding problems. First, we establish the upper energy boundary of practical interest.

- Ionising photons emitted by radionuclides normally have energies below 12 MeV — excited nuclei can de-excite by radiating photons in the approximate energy range $E \in (0, 12\ \text{MeV}]$.

- Ionising photons produced in operating nuclear reactors and in spent nuclear fuel do not have energies exceeding approximately 15 MeV.

- Secondary photons emitted after (n, γ) neutron capture reactions, typically have energies in the approximate energy range $E \in (0, 15\ \text{MeV}]$.

- Secondary photons emitted after the inelastic scattering of neutrons, typically have energies in the approximate energy range $E \in (0, 7\ \text{MeV}]$.

- In the case of electronic transitions in atoms, only photons with relatively low energies (sub-MeV) are emitted.

- The most important mechanism for the production of ionising photons having energies potentially in excess of circa 15 MeV, is *nuclear bremsstrahlung.* The deceleration of energetic, heavy, charged particles such as protons and α-particles in matter, produces *bremsstrahlung,* known as *nuclear bremsstrahlung*. At a particle accelerator where protons are e.g. accelerated to an energy of 200 MeV, nuclear *bremsstrahlung* will be produced where the proton beam strikes targets, and in this example, these *bremsstrahlung* photons can have energies close to the proton energy of 200 MeV. However, the cross-section for the production of nuclear *bremsstrahlung* is much lower than the cross-section for the production of *bremsstrahlung* with the slowing-down of electrons. The cross-section σ_{bs} for the production of *bremsstrahlung* when charged particles of mass m are decelerated in an element with atomic number Z, is

approximately proportional to,

$$\sigma_{\text{bs}} \propto \frac{Z^2}{m^2}. \tag{7.1}$$

The last of the two examples given below, show that nuclear *bremsstrahlung* is negligible.

Example 7.1

The deceleration of protons in an element produces $\left(\frac{1836}{1}\right)^2 \approx 3.3$ million times less *bremsstrahlung* than the attenuation of electrons in the same element.

Example 7.2

The deceleration of α-particles in an element produces $\left(\frac{7294}{1}\right)^2 \approx 53$ million times less *bremsstrahlung* than the attenuation of electrons in the same element.

- From Eq. (7.1) and the above examples, we conclude that nuclear *bremsstrahlung* may be ignored in practically all radiation shield design studies. The cross-section for this category of interaction is so low that the reaction rate of the production of such high-energy photons will be negligible.

- Suppose an electron accelerator has a maximum operating voltage of e.g. 40 MV. Then the *bremsstrahlung* photons produced from the interactions of the electrons produced by such an accelerator will have a maximum energy of 40 MeV.

In Africa, no electron accelerator can presently (2013) accelerate electrons to energies above approximately 40 MeV. Therefore 40 MeV is at present the maximum ionising photon energy at research institutes and industries in Africa.

We now establish the lower boundary of the energy region of interest. Photons with an energy below circa 1 keV have such a low penetrating ability that they may be ignored. We conclude that the photon energy region of primary interest in radiation shielding, is approximately

$$E \in [1\text{ keV}; 40\text{ MeV}]. \tag{7.2}$$

This then, is the incident photon energy range that the shield designer working on the African continent, has to consider. Shield designers working in the nuclear power industry only have to consider ionising photons in the energy range up to about 15 MeV.

7.2.1 Overview of photon interactions

Photons can interact with the atoms of a substance in 12 possible ways. These can be tabulated as in Table 7.1.

Table 7.1: *Interactions of photons (the Fano system of classification). Twelve combinations are possible, but only 4 combinations have practical importance.*

Interaction partner	Result of interaction
1. Electrons of atomic shell	A. Coherent scattering
2. Atomic nuclei	B. Incoherent scattering
3. Electric fields of atomic nuclei and of shell electrons	C. Total absorption
4. Meson fields of atomic nuclei	

The most important three processes in the photon energy range, $E \in [1\text{ keV}; 40\text{ MeV}]$ are:

1B **Incoherent scattering** with electrons of the atomic shell. This is called ***Compton scattering.***

1C Total absorption of the photon by the electrons of the atomic shell. This is called ***photo-electric absorption*** **(PEA).**

3C Total absorption of the photon in the electric fields of atomic nuclei and of shell electrons. An electron positron *pair* is produced. After slowing down, the positron combines with an electron. Both particles disappear and two photons are emitted. This process is known as ***pair production.***

The following category of reaction may become important, especially at photon energies above specific threshold values:

2C ***Photo-nuclear reactions****,* mainly (γ, n) reactions, may become important for selected isotopes at energies as low as 1.67 MeV, but generally only become important at photon energies above 8 MeV to 10 MeV. Specific isotopes for which the threshold energies E_γ for (γ, n) reactions are unusually low, are discussed in § 7.2 on page 357.

The following reaction is of minor importance and will not be considered further:

1A **Coherent scattering** of the photon with electrons of the atomic shell. This is called *Rayleigh scattering.* This category of photon interaction contributes negligibly to the attenuation of ionising photons.

In most cases, the transport, and hence the attenuation, of ionising photons are largely via three types of interactions — Compton scattering, photo-electric absorption and pair production. The relative contributions of the above interaction types to the attenuation of photons, depend on the atomic numbers of the elements in the shielding material, the density of the shielding material and the energy of the ionising photons. We shall now discuss the three important categories of photon interactions separately.

Whereas neutrons typically interact by strong interaction, photons typically undergo electromagnetic interaction in matter. Photo-nuclear reactions, mainly (γ, n) reactions, may become important above given photon threshold energies, though.

7.2.2 Nuclide number density and electron number density

To calculate the linear interaction coefficient μ of a given reaction, the microscopic cross-section σ (unit: barn) is multiplied by the number density N of the target particle:

$$\mu = N\sigma.$$

The volume unit barn.cm is a very convenient volume for the expression of number density N, because the product $N\sigma$ has the unit cm^{-1}. The product $N\sigma$ yields the linear interaction coefficient μ (unit: cm^{-1}). Let N_A signify Avogadro's number, $N_A = 6.023 \times 10^{23}$.

View a elemental material medium with atomic number Z, mass number A and mass density ρ. Let M_R be the molar mass of the element (unit: g.cm^{-1}). To a very good approximation,

$$M_R = A$$

and we can calculate the number density per unit volume as follows:

$$1 \text{ cm}^3 \text{ contains } \frac{\rho N_A}{M_R} \text{ atoms.}$$

$$\approx \frac{\rho N_A}{A} \text{ atoms}$$

$$\therefore 1 \text{ barn.cm contains} \approx \frac{10^{-24}\rho N_A}{A} \text{ atoms}$$

$$\therefore 1 \text{ barn.cm contains} \approx 10^{-24}\rho N_A\left(\frac{Z}{A}\right) \text{ electrons}$$

In summary: nuclide number density per unit volume, and electron number density per unit volume, are

$$N_{\text{atom}} \approx \frac{10^{-24}\rho N_A}{A} \quad \text{barn}^{-1}\,\text{cm}^{-1} \tag{7.3}$$

$$N_{\text{electron}} \approx 10^{-24}\rho N_A\left(\frac{Z}{A}\right) \quad \text{barn}^{-1}\,\text{cm}^{-1}$$

For the range of elements with $Z \geq 3$, the atomic mass number A ranges between $2Z$ and approximately $2.6Z$. This range is small, and the average value can be approximated to, say,

about $A \approx 2.2Z$. Substitute this into Eq. (7.3), to obtain,

$$N_{\text{atom}} \approx \frac{10^{-24}\rho N_A}{2.2Z} \quad \text{barn}^{-1}\,\text{cm}^{-1} \tag{7.4}$$

$$N_{\text{electron}} \approx \frac{10^{-24}\rho N_A}{2.2} \quad \text{barn}^{-1}\,\text{cm}^{-1}$$

7.2.3 Energy-dependence of the biological harmfulness of ionising photons

The energy dependence of the effective dose response function, $\mathfrak{R}_\gamma(E)$, for photons, is summarised in Figure 7.1.

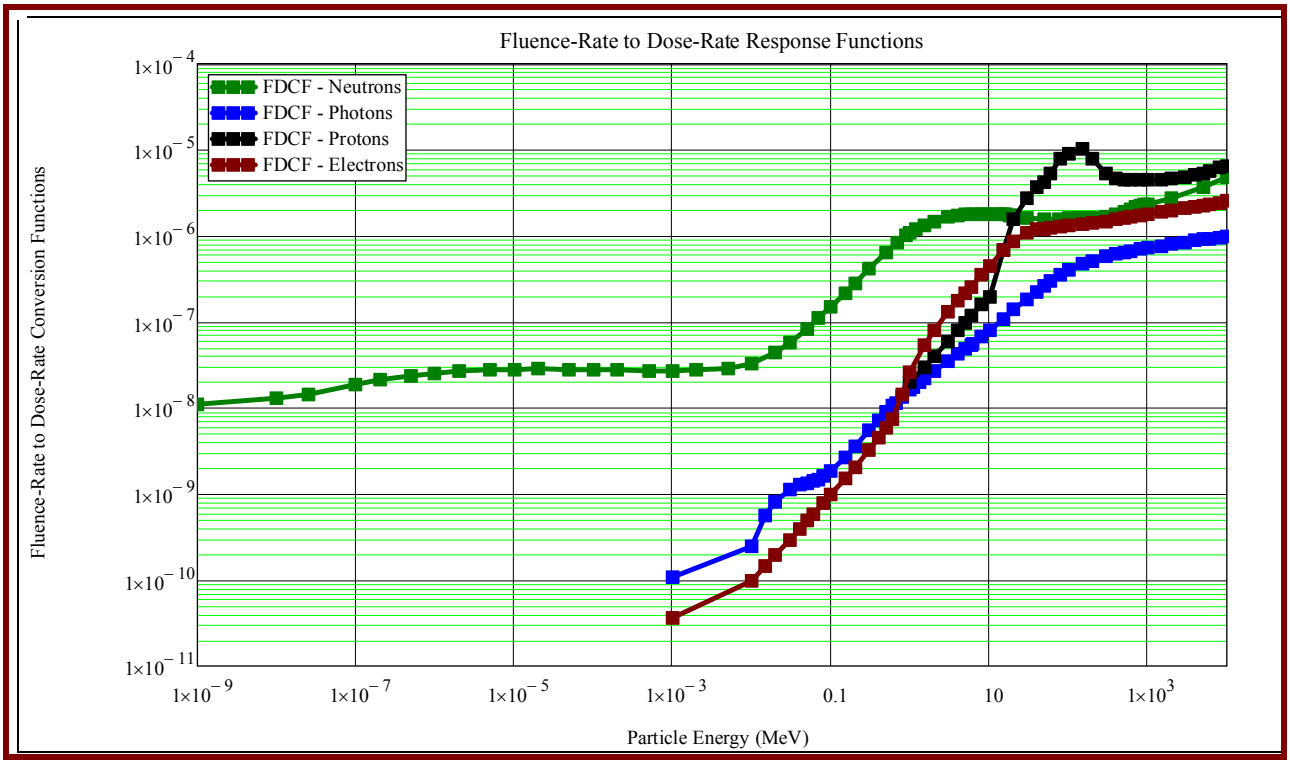

Figure 7.1: *Response functions $\mathfrak{R}(E)$ to calculate the effective dose $E = \int dE\,\mathfrak{R}(E)\Phi(E)$ for fluences $\Phi(E)$ of neutrons, photons, protons and electrons.*

From Figure 1.3 it can be seen that the effective dose response function for photons, $\mathfrak{R}_\gamma(E)$, increases monotonically with photon energy, from 1 keV to 10^4 MeV. We also see that, for the same fluence-rate and same incident energy, E, ionising photons are less harmful than other classes of ionising radiation.

The biological harmfulness of photons of various energies relative to that of a 0.01 MeV photon, is listed in Table 7.2.

Table 7.2: *Biological harmfulness of photons relative to that of a 0.01 MeV photon.*

Photon Energy E	$\frac{\mathfrak{R}_\gamma(E)}{\mathfrak{R}_\gamma(1\,\mathrm{MeV})}$
0.01 MeV	1.0
0.05 MeV	6.3
0.1 MeV	8.6
0.2 MeV	16.7
0.3 MeV	25.4
0.5 MeV	41.4
0.8 MeV	62.2
1 MeV	74.5
2 MeV	125
3 MeV	167
5 MeV	238
8 MeV	337
10 MeV	403
15 MeV	576
20 MeV	770

Conclusion: lowering photon energy will contribute to photon shielding, because a given fluence of low energy photons will contribute a considerably lower effective dose than the same fluence of high-energy photons. This principle of photon attenuation is analogous to one of the fundamental principles of neutron attenuation.

7.2.4 Energy-dependence of photon absorption cross-sections

Figure 7.2 shows the linear interaction coefficients μ for ionising photons, for a number of important elements and compounds.

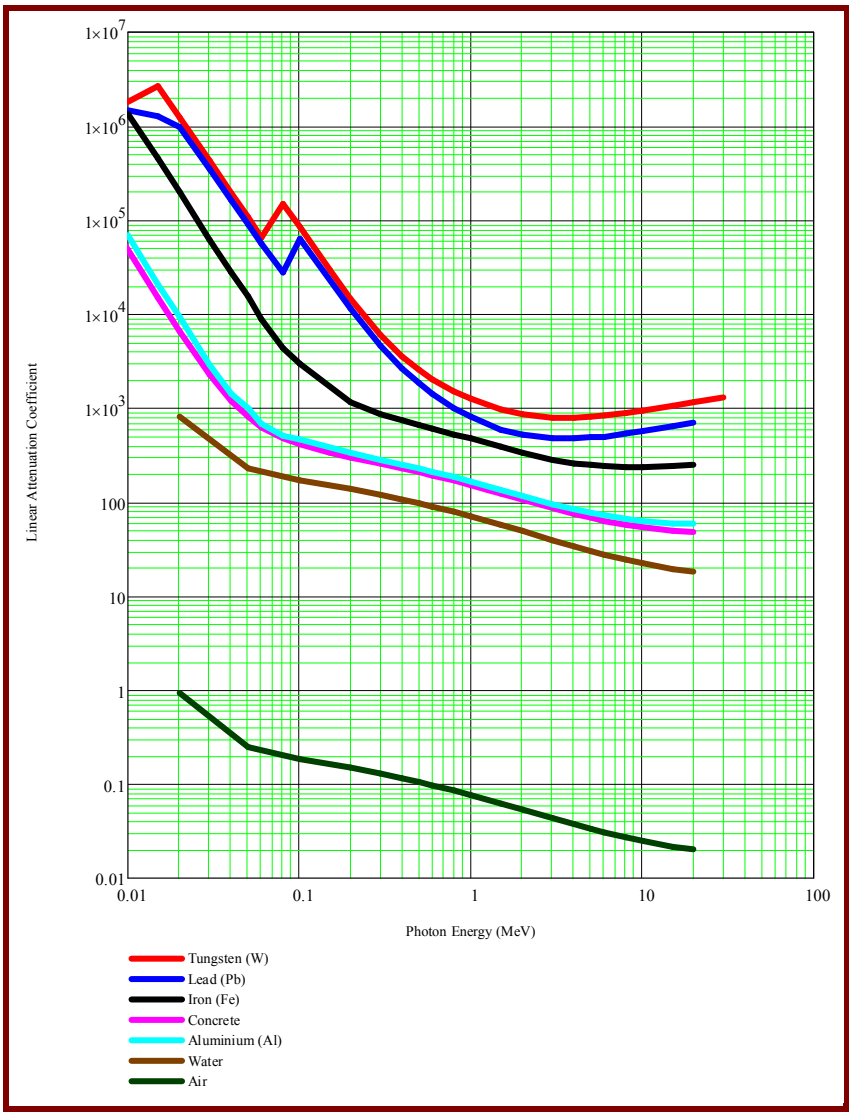

Figure 7.2: *Linear interaction coefficients μ for ionising photons, for a number of important elements and compounds.*

Note how much simpler photon interaction cross-sections are compared to neutron cross-sections. The underlying reason is that the Quantum ElectroDynamic (QED) interaction whereby ionising photons usually interact at energies below about 8 MeV, is far simpler than the Quantum ChromoDynamic (QCD) Strong Interaction between particles having a quark substructure, e.g. the neutron and the atomic nucleus. Photon interaction cross-sections differ only on the elemental level and not significantly at the isotopic level. In MCNP calculations for low-energy ionising photon transport, therefore, the material Fe is e.g. merely specified as 26000; there is no need to specify it in terms of its isotopes 26054, 26056, 26057 and 26058, as is the case for high-accuracy neutron transport runs.

It is clear that depleted uranium (DU), tungsten (W) and lead (Pb) are the best shielding materials against ionising photons. Steel is intermediate in its ionising photon shielding ability. Concrete and aluminium are approximately equal in their ionising photon shielding abilities, while water is quite a weak shield against ionising photons.

From Figures 7.1 (page 344) and 7.2 (page 346) we can immediately deduce an important principle of the shielding of ionising photons in the energy range under consideration: Lower photon energies in order to make the photon field biologically less harmful and also easier to absorb. The twin reasons for this are:

- The response function $\mathfrak{R}_{\gamma\_\text{effdos}}(E)$ for the effective dose from ionising photons, monotonically decreases as photon energy decreases.
- The general trend is that the linear interaction coefficient $\mu(E)$ for ionising photons, which measures the ability of shielding materials to interact with ionising photons and thereby lower their energy, increases as photon energy decreases.

In the next subsections, we shall show step-by-step that

$$\mu(E) \approx \mu_{\text{PEA}}(E) + \mu_{\text{CS}}(E) + \mu_{\text{PP}}(E) \tag{7.5}$$

and that $\mu(E)$ is maximised by selecting shielding materials so as to maximising their atomic number Z and their mass-density ρ.
In Eq. (7.5), the abbreviations have the following meanings:

PEA	$\equiv$	photo-electric absorption
CS	$\equiv$	Compton scattering
PP	$\equiv$	pair production

7.2.5 Rayleigh scattering (coherent scattering)

Reaction type 1A in Table 7.1 (page 342) is known as *coherent scattering*. The incident photon is scattered coherently by the bound electrons of an atomic shell. The electrons act collectively, and not individually; the electrons in the atom participate in a coherent manner in the scattering process. The coherent scattering of photons by atomic electrons is also known as *Rayleigh scattering*. This category of photon interaction contributes negligibly to the attenuation of ionising photons, because:

- ▷ The photon practically loses no energy, because the recoil momentum in the Rayleigh scattering is taken up by the atom as a whole, which is many thousands of times heavier than a single electron. The energy of the scattered photon is only slightly less than that of the incident photon: $E \simeq E'$. Practically no energy is transferred to the medium. The atoms are neither excited nor ionised, and only the direction of the photon is changed (Shultis & Faw, 2000: 43). Therefore an extremely low fraction of the energy of the photon will be lost.
- ▷ Deflection angles are small, i.e. the scattering is strongly forward-peaked. Example: When 1 MeV photons undergo coherent scattering off Fe, 75% are scattered within a cone with half-angle 4° (Shultis & Faw, 2000: 43).
- ▷ The cross-section for Rayleigh scattering is large only at energies where it is overshadowed by the cross-section for photoelectric absorption (Shultis & Faw, 2000: 43).

We see that coherent scattering has a minimal effect on photon energy and direction. Because it contributes so little to photon attenuation, coherent scattering is often ignored in the compilation of photon cross-section libraries for practical photon transport calculations.

7.2.6 Photo-electric absorption (PEA)

Reaction type 1C in Table 7.1 (page 342) is known as *photo-electric absorption* (PEA). This process involves the total absorption of the incident photon by the electrons of the atomic shell. The atomic electrons do not interact with the incident photon as free electrons, but as bound electrons; PEA is a reaction between the incident ionising photon and the *entire* atom (Marmier & Sheldon, 1969: 114; Shultis & Faw, 2000: 44).

The incident photon is absorbed, and the energy that is imparted to the atom causes the emission of a so-called photo-electron. The name "photo-electron" derives from the fact that the atom releases the electron after having absorbed a photon. Because the recoil energy of the atom is numerically negligible, the kinetic energy T of the ejected electron is related to the energy E_γ of the incident photon and the binding energy E_b of the ejected electron by the relationship

$$T_\mathrm{e} = E_\gamma - E_b \,.$$

K-shell electron binding energies E_K vary from 13.6 eV for hydrogen, to 7.11 keV for Fe and 88 keV for Pb, and 116 keV for U. As the energy of the incident photon drops below E_K, the cross-section drops suddenly. As E decreases further, the cross-section for PEA increases until the first L-edge is reached, at which energy the cross-section for PEA drops suddenly once again, then rises once more, and so on, for the remaining edges. These edges are clearly visible in Figure 7.9 on page 364. For light nuclei, K-shell electrons are responsible for almost all photoelectric interactions. For heavy nuclei, about 80% of photo-electric absorptions result in the ejection of a K-shell electron.

When the vacancy left by the photoelectron is filled with an electron from an outer shell, either characteristic fluorescence x-rays or Auger[24] electrons may be emitted. The majority of photo-electrons are emitted from innermost electron shell, i.e. the K-shell, i.e. the electron-shell with principal quantum number $N = 1$. As the vacancy left by the electron emitted as a photo-electron, is filled by an electron from an outer electron shell, either fluorescence characteristic x-rays or Auger electrons may be emitted. The probability of characteristic x-ray emission is expressed as the *fluorescent yield;* for the K-shell, the yield vary from 0.5% for $Z = 8$, to 96.5% for $Z = 90$. That is, Auger-electron emission has a high relative importance in low-Z elements, and a lower relative importance in higher-Z elements.

PEA is the dominant attenuation mechanism for photons having low energies. The microscopic cross-section $\sigma_\mathrm{PEA}(E)$ for the PEA of a photon with an incident energy E, by an

[24] If an electron in an outer shell of an atom makes a transition to a vacancy in an inner shell, an x-ray may be emitted having an energy equal to the difference in the binding energy between the two shells. Alternatively, this energy may be transferred to an electron, so that the energy difference is not transferred to an emitted x-ray photon, but to an emitted electron — such an electron is called an Auger electron.

atom with atomic number Z, follows the following approximate relationship over the energy range where photo-electric absorption is dominant (Marmier & Sheldon, 1969: 117; Shultis & Faw, 2000: 44; Shultis & Faw, 2002: 175):

$$\sigma_{\text{PEA}}(Z, E_\gamma) \propto \frac{Z^4}{(E_\gamma)^3} \,. \tag{7.6}$$

The large exponential power to which the atomic number Z is raised in Eq. (7.6), indicates why high-Z materials like lead, tungsten and depleted uranium are such excellent absorbers of low energy photons. The large exponential power to which the variable E is raised, indicates why the contribution of PEA to the attenuation of photons diminishes sharply with increasing photon energy, and increases sharply with a decrease in photon energy.

Because secondary ionising particles are emitted when PEA takes place, it is not a pure ionising photon absorption process. However, energy conservation considerations imply that the energies of all individual secondary photons will be far less than the energy of the original incident ionising photon. From Eq. (7.6), it follows that the cross-section for the photo-electric absorption of these less energetic photons will be considerably larger than the cross-section for the photo-electric absorption of the original photon. It is clear that a series of successive reactions will take place, and that every PEA reaction will further decrease the photon energy. Eventually, photon energies will become so low that it will be below the threshold for ionisation. At such low energies, the photons are, for all practical purposes, not biologically dangerous any more.

Linear interaction coefficient for photo-electric absorption

According to Eq. (7.6) on page 349,

$$\sigma_{\text{PEA}} \propto \frac{Z^4}{(E_\gamma)^3} \,. \tag{7.7}$$

Because

$$N_{\text{atom}} \approx \frac{10^{-24} \rho N_A}{2.2Z} \text{barn}^{-1}\,\text{cm}^{-1}$$

and $\mu = N\sigma$, it follows that

$$\mu_{\text{PEA}} \approx \frac{10^{-24}\rho N_A}{2.2Z}\frac{Z^4}{(E)^3} \tag{7.8}$$

$$\propto \frac{\rho Z^3}{(E)^3}$$

$$= \rho\left(\frac{Z}{E}\right)^3$$

$$\boxed{\mu_{\text{PEA}} \propto \rho Z^3}$$

7.2.7 Compton (incoherent) scattering

Incoherent or Compton scattering takes place when an incident photon interacts with an *individual* electron in an atom (as distinguished from the coherent interaction of a photon with all the electrons of an atom). In the energy range where incoherent scattering dominates, bound electrons may be assumed to interact as free particles (Marmier & Sheldon, 1969: 110).

In the energy region of interest, incoherent scattering may be treated as the elastic scattering of a photon from a free electron that is initially at rest.

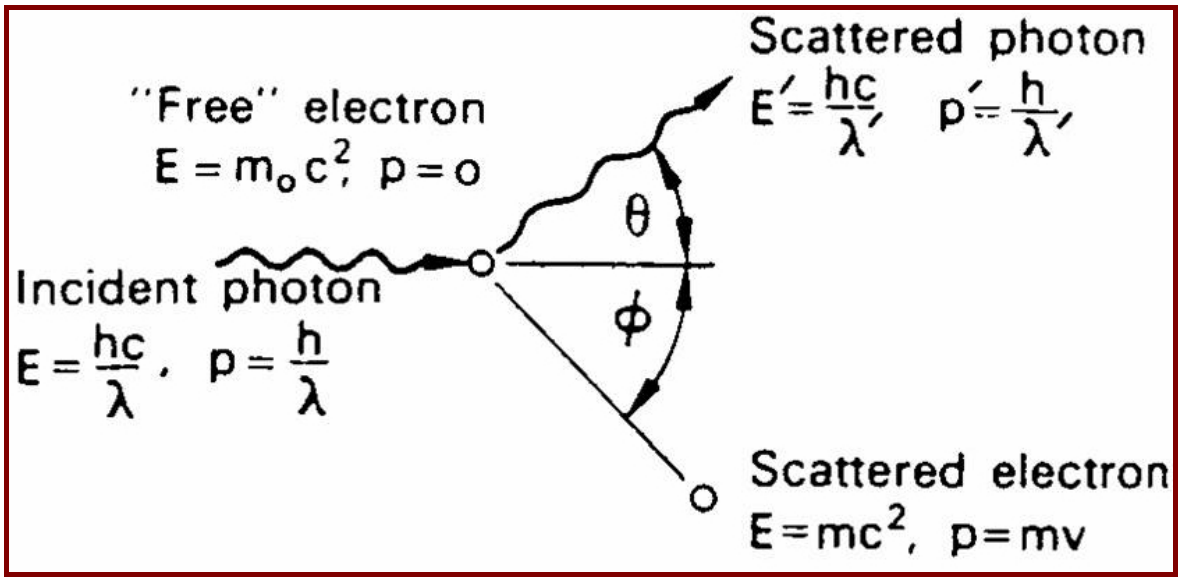

Figure 7.3: *Compton scattering: an elastic collision between a photon and an electron*

By starting from a mathematical statement of the conservation of energy and momentum, the following relationship between the energy E of the scattered photon and the energy E of the incident photon and the scattering angle θ, can be deduced (Knoll, 1979: 65):

$$E(E,\theta) = E\left(\frac{m_e c^2}{m_e c^2 + E(1-\cos(\theta))}\right). \tag{7.9}$$

In Eq. (7.9), m_e represents the rest mass of the electron, while c is the speed of light in a vacuum. The product $m_e c^2$ is the rest mass energy of the electron (0.511 MeV).

Figure 7.5 on page 360 shows that Compton scattering is an important mechanism for the lowering of photon energy for incident photons in the approximate energy ranges,

$$E_\gamma \in \left\{ \begin{array}{ll} [0.1\,\text{MeV}; 10\,\text{MeV}] & \text{for } Z \leq 20 \\ [0.2\,\text{MeV}; 8\,\text{MeV}] & \text{for } 20 < Z \leq 40 \\ [0.3\,\text{MeV}; 6\,\text{MeV}] & \text{for } 40 < Z \leq 60 \\ [0.5\,\text{MeV}; 5\,\text{MeV}] & \text{for } Z > 60 \end{array} \right\}. \tag{7.10}$$

The primary and secondary photon energies in most radiation shields largely fall in the energy ranges of Eq. (7.10). The cross-section for PEA is significant up to $E \sim 1\,\text{MeV}$. The threshold for pair production is at $E = 1.02\,\text{MeV}$, from where it rises with higher incident photon energies, tending to a plateau.

Compton scattering and pair production play roles in photon attenuation that are analogous to the role of the elastic and inelastic scattering of neutrons, in that it decreases the energy of the photon.

In Compton scattering, the incident photon is scattered through an angle θ (expressed in the laboratory system, $\mathcal{L}$) relative to the direction of incidence. All scattering angles ($0° < \theta < 180°$) are allowed kinematically. The photon transfers a fraction of its energy to the electron with which it collides. The angular distribution of photons that had undergone incoherent scattering, is approximated by the Klein-Nishina formula for the differential scattering cross-section. The details of the analysis are shown in the MathCAD worksheet

COMPTON.XMCD

Table 7.3 shows the ratio $\frac{\sigma(E,\theta=0)}{\sigma(E,\theta=\pi)}$ for Compton scattering at different incident photon energies. This is a measure of the increasingly forward angular bias of Compton scattering at higher incident photon energies E.

Table 7.3: *The ratio* $\frac{\sigma(E,\theta=0)}{\sigma(E,\theta=\pi)}$ *for selected incident photon energies.*

E (MeV)	$\frac{\sigma(E,\theta=0)}{\sigma(E,\theta=\pi)}$
0.1	1.8
0.2	2.7
0.5	5.3
1.0	9.4
2.0	17
3.0	25
4.0	33
5.0	40
8.0	65
10.0	80
15.0	120

It is evident that incoherent scattering becomes very anisotropic at high photon energies, i.e. angles of deflection become very small. The quantum-mechanics of the reaction dynamics of incoherent scattering cause the process to become highly anisotropic at incident energies in excess of about 0.5 MeV.

In the following MathCAD worksheet we investigate how the ability of Compton scattering to decrease the energy of the incident photon, depends on the scattering angle.

Compton.XMCD

Linear interaction coefficient for Compton scattering

$\sigma_{CS} \propto Z$

$N \propto \frac{\rho}{Z}$

$\mu_{CS} \propto \rho^1$

Compton scattering is an interaction of an incident photon with *individual* atomic electrons, which may be treated as free (unbound) electrons, because the photon energy is much higher than their binding energies. Because Compton scattering is a reaction with individual electrons, the cross-section $\sigma_{CS}(E)$ is independent of the element. Therefore the Compton cross-section per atom is linearly proportional to the number of electrons in the atom of the element, i.e.

$$\sigma_{CS} \propto Z \tag{7.11}$$

because in a (neutral) atom, the number of electrons equals the number of protons in the nucleus.

We will now derive an expression for the atomic number density N, i.e. the number of atoms per unit volume, of an element with atomic number Z and mass number A. One mole of the element has a mass of approximately A gram, where A is the mass number of the element. The mass-density of the element is ρ, so that A gram will have a volume of $V = \frac{A}{\rho}$. This volume will contain N_A atoms, where N_A is Avogadro's number, 6.022137×10^{23} mol^{-1}. Therefore the atomic number density per unit volume is $N = \frac{\rho}{A} N_A$. But, for all stable nuclides, A ranges between $1Z$ and approximately $2.6Z$, so that we may say that $A \propto Z$, so that

$$N \propto \frac{\rho}{Z}. \tag{7.12}$$

It follows that the linear interaction coefficient for Compton scattering, μ_{CS} (unit: cm^{-1}) for an element with atomic number Z and atomic mass A, is given by the proportionality,

$$\begin{aligned} \mu_{\text{CS}}(E) &= N\sigma \\ &\propto \left(\frac{\rho}{Z}\right) \times Z \\ &\propto \rho \end{aligned} \tag{7.13}$$

We conclude that, at a fixed photon energy E, the linear interaction coefficient μ_{CS} will only be proportional to the mass-density, ρ of the material medium through which the ionising photons propagate:

$$\boxed{\boldsymbol{\mu_{\text{CS}}(E) \propto \rho}}. \tag{7.14}$$

Application: At a given photon energy, the ratio between the linear interaction coefficient for Compton scattering by iron ($\rho \approx 7.8$ g.cm^{-3}) and water ($\rho \approx 1$ g.cm^{-3}), will be approximately $\frac{\mu_{\text{CS\_Fe}}}{\mu_{\text{CS\_water}}} = \frac{7.8 \text{ g.cm}^{-3}}{1.0 \text{ g.cm}^{-3}} = 7.8$.

Thompson scattering

Thomson scattering is the scattering of photons by free electrons in the classical limit. It is the low-energy limiting case of Compton scattering. Incoherent scattering is unimportant in this energy range, because the cross-section for photo-electric absorption will dominate in this energy region.

7.2.8 Pair production

The third of the three important reactions that make the dominant contribution to photon attenuation, is pair production (PP):

$$\gamma \longrightarrow \mathrm{e}^{+} + \mathrm{e}^{-}.$$

Pair production is treated in some detail in Marmier & Sheldon (1969: 122 — 146).

When the energy of a photon is more than twice the rest-mass energy $m_{\mathrm{e}}c^2$ (0.511 MeV) of an electron, i.e. in excess of 1.02 MeV, the formation of an electron-positron pair becomes energetically possible. As a result of the law on the conservation of linear momentum, pair production can only take place in the vicinity of a third particle that can recoil to take up linear momentum. This particle must have an electrical charge. This third particle is usually an atomic nucleus. As a result of the kinetic energy absorbed by the recoil particle, the threshold for pair production is not $2m_{\mathrm{e}}c^2$ any more, but:

$$E_{\mathrm{PP\_threshold}} = 2m_{\mathrm{e}}c^2\left[1 + \frac{m_{\mathrm{e}}}{M}\right], \tag{7.15}$$

where M is the mass of the recoil particle (Marmier & Sheldon, 1969: 123).

Pair production does not specifically have to take place in the vicinity of an atomic nucleus. There exists a very small probability that it will take place in the Coulomb-field of an electron, with the electron serving as the recoil particle. Because the experimentalist will observe three particle tracks in a cloud chamber, this process is called *triplet formation.* From Eq. (7.15) it follows that the threshold energy for triplet formation in the Coulomb field of an electron, is $4m_{\mathrm{e}}c^2$, i.e. 2.044 MeV.

The electron and positron are charged particles. They are slowed down by continuous Coulomb interactions in matter, as well as emission of *bremsstrahlung* photons (continuous-spectrum x-rays) by radiative slowing down, with energies far lower than that of the incident photon, are produced in the process. When the positron has lost most of its energy, it recombines with its anti-particle, namely a negatively charged electron (negatron). Both leptons disappear, and 2 or 3 *annihilation photons,* each of which has an energy equal to the rest-mass of the leptons, i.e. 0.511 MeV, are produced:

$$\mathrm{e}^{+} + \mathrm{e}^{-} \longrightarrow 2\gamma\,(0.511\ \mathrm{MeV})\,.$$
$$\mathrm{e}^{+} + \mathrm{e}^{-} \longrightarrow 3\gamma\,(0.511\ \mathrm{MeV})$$

When 2 annihilation photons are produced, they move in opposite directions, at an angle of approximately 180° in order to conserve linear momentum. When 3 annihilation photons are produced, they move apart in a set of directions that will also conserve linear momentum.

(Positronium: more about electron/positron annihilation: The annihilation of positrons with electrons is not quite as simple a process as sketched above. Like the proton and electron in a hydrogen atom, the electron-positron pair attract each other electrically, and form a mini-atom, in which the two leptons move around their common centre of mass. This 2-lepton-

atom has energy levels, but has no stable ground state, because positronium is unstable against matter-antimatter annihilation. The size of the positronium atom is double that of a hydrogen atom; this size is about $\frac{\hbar^2}{m_e(q_e)^2} \approx 53$ pm, where m_e is the mass of an electron, and q_e is the magnitude of the charge of an electron. In the positronium "atom", there is a small but finite chance of roughly $\left(\frac{1}{137}\right)^3 \approx 3.9 \times 10^{-7}$ that the wave functions of the positron and electron will overlap significantly; when this happens, matter-antimatter annihilation takes place. When positronium annihilates, 2 or 3 annihilation photons are emitted; these annihilation photons must move away in a set of directions that will ensure the conservation of linear momentum.

It is necessary to take into account the spins of the electron and positron that comprise positronium. The electron and positron have spin quantum numbers of $\pm\frac{1}{2}$, i.e. intrinsic angular momentum of $\pm\frac{1}{2}\hbar$. Two forms of positronium are found: in para-positronium the spins of the electron and positron are antiparallel, i.e. opposite: $\boxed{\downarrow \bullet}\boxed{\bullet \uparrow}$ In para-positronium, the opposite spins cancel each other to give a net spin of 0 for this form of positronium. In ortho-positronium, the spins point in the same direction: $\boxed{\uparrow \bullet}\boxed{\bullet \uparrow}$. In ortho-positronium, the spins point in the same direction, so that this form of positronium has a net spin of 1. When para-positronium with net spin 0 annihilates, two annihilation photons are produced, moving in opposite directions and having spins -1 and $+1$, so that the net spin and the net linear momentum of the photons are both 0, the same as the net spin 0 of para-positronium. When ortho-positronium with net spin 1 annihilates, there is no way in which 2 annihilation photons can have net spin 1. Therefore 3 annihilation photons are produced, moving in directions that ensure conservation of linear momentum, having spins -1, $+1$ and $+1$, so that the net spin of the 3 photons is 1, the same as the net spin 1 of ortho-positronium. The process of producing 3 annihilation photons is considerably slower than the production of 2 annihilation photons. The measured lifetime of para-positronium, $\boxed{\downarrow \bullet}\boxed{\bullet \uparrow}$, is 1.25E-10 s, while that of ortho-positronium, $\boxed{\uparrow \bullet}\boxed{\bullet \uparrow}$, is about 137 times longer.)

The cross-section for pair production dominates both PEA and Compton scattering in the high energy region. As a result, it is the dominant photon attenuation mechanism for photons with energy $E_\gamma \gtrsim 5$ MeV (Knoll, 1979: 67). We see that pair production can easily lower photon energies by an order of magnitude (e.g. from 5 MeV to 0.511 MeV). This final energy (0.511 MeV) falls right in the energy region where PEA dominates photon attenuation, especially in higher-Z materials. In this fashion, pair production can serve as the first event in the chain of interactions that will eventually degrade photon energy to a value below the threshold for ionisation. When photons reach such a low energy, they are highly absorbable and have also practically lost most of their ionising nature and biological hazard potential.

Above the threshold energy for pair production, the cross-section for pair production, $\sigma_{\text{PP}}(E, Z)$, is a function of the incident energy E and the atomic number Z of the attenuating medium. If we keep the incident energy E constant, we find that,

$$\sigma_{\text{PP}}(Z) \propto Z^2. \tag{7.16}$$

If we keep the variable Z constant, we find that $\sigma_{\text{PP}}(E)$ is zero below the threshold energy, then rises monotonically with E, tending to a plateau (Shultis & Faw, 2000)—see Figure 7.9 on page 364.

Incident energy (E) and atomic number (Z) regions where the different photon attenuation mechanisms dominate, are depicted in Figure 7.5 on page 360.

Linear interaction coefficient for pair-production

According to Eq. (7.16),

$$\sigma_{\text{PP}} \propto Z^2 \,.$$

According to Eq. (7.4) on page 344,

$$N_{\text{atom}} \approx \frac{10^{-24} \rho N_A}{2.2Z} \text{barn}^{-1}\,\text{cm}^{-1}$$

so that the linear interaction coefficient

$$\mu_{\text{PP}} = N_{\text{atom}}\, \sigma_{\text{PP}}$$

for pair production will be proportional to

$$\mu_{\text{PP}} \approx \frac{10^{-24} \rho N_A Z^2}{2.2Z}$$

$$\boxed{\propto \rho Z.} \tag{7.17}$$

7.2.9 Summary: Dependence of the linear interaction coefficient μ for the three dominant attenuation mechanisms for ionising photons, on Z and E

Ionising photons interact and lose energy by 3 principal mechanisms: photo-electric absorption (PEA), Compton scattering (CS) and pair production (PP). These three principal interactions of ionising photons and their linear interaction coefficients μ are summarised in Table 14.2.

Table 7.4: *The three principal interaction mechanisms of ionising photons, and their linear interaction coefficients.*

Interaction	**Cross-section σ**	**Nuclide number density of target N**	**Linear interaction coefficient μ**
Photo-electric absorption (PEA)	$\sigma_{\text{PEA}} \propto \frac{Z^4}{(E_\gamma)^3}$	$N \propto \frac{\rho}{Z}$	$\mu_{\text{PEA}} \propto \rho^1 Z^3$
Compton scattering (CS)	$\sigma_{\text{CS}} \propto Z$	$N \propto \frac{\rho}{Z}$	$\mu_{\text{CS}} \propto \rho^1$
Pair production (PP)	$\sigma_{\text{PP}} \propto Z^2$	$N \propto \frac{\rho}{Z}$	$\mu_{\text{PP}} \propto \rho^1 Z^1$

It follows clearly from Table 14.2 that there exists a simple recipe for maximising the efficiency of a photon shield: Maximise the atomic number Z and maximise the density ρ of the shielding material. The simplicity of this recipe is rooted in the predictable, systematically varying nature of the Hamiltonian for quantum electrodynamic interaction.

In the high photon-energy region, where pair production is dominant, both ρ and Z should be maximised with equal weight to maximise shield efficiency. In the low-energy region, where photo-electric absorption of photons is dominant, it pays significantly more to maximise Z than to maximise ρ. In the intermediate photon energy region, where Compton scattering dominates, the atomic number Z has very little effect on shield efficiency, and the parameter that should be maximised to maximise shield efficiency, is the mass-density ρ of the shield.

7.2.10 The Photonuclear effect: Neutron production by (γ, n)-reactions

The ***photonuclear effect*** consists of the absorption of a photon by a nucleus and the subsequent emission of nuclear reaction products. The most likely outcome is the emission of a single neutron, i.e. a (γ, n) reaction. Other possibilities are the emission of two or more neutrons and the emission of charged particles and ionising photons. The energy dependence of the photo-nuclear cross-section is characterised by a peak ~ 5 MeV wide at an energy located below ~ 30 MeV and above the threshold energy (typically ~ 5 to 15 MeV). As a result of [1] low cross-sections, [2] the high energy threshold and [3] the low abundance of sources that produce photons with energies above the threshold energy, the photonuclear effect is not very important in shield design calculations. However, when there is a substantial number of nuclides with very low threshold energies for photonuclear reactions, e.g.

deuterium and beryllium, in a very thick shield around a neutron or high-energy photon source, we can no longer ignore the photonuclear effect. (Question: why a neutron source too? Answer: When neutrons are attenuated, secondary ionising photons are produced by (n,γ) reactions and inelastic scattering.)

Cross-sections for photoneutron, i.e. (γ, n) reactions

Figure 7.4 shows the energy dependence of photo-neutron, i.e. (γ, n)-production cross-sections for the nuclides having particularly low energy thresholds for (γ, n) reactions: ^{9}Be, ^{2}H and the element Li.

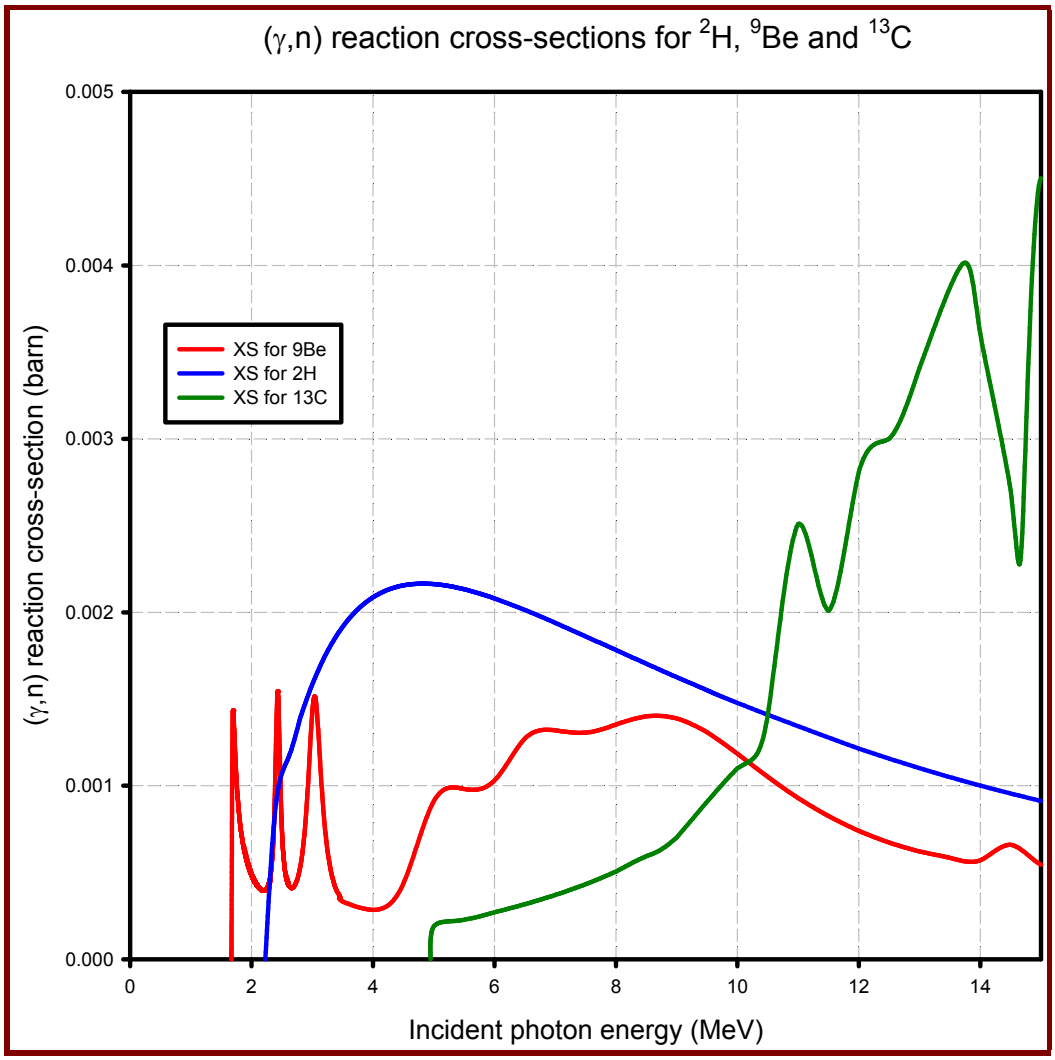

Figure 7.4: *Photoneutron (i.e. (γ, n)) production cross sections for ^{2}H, ^{9}Be and ^{13}C (JANIS 3.2, 2010). Neutron separation energies, and hence threshold energies for (γ, n) interactions, will generally be above about 7 MeV, but (γ, n)-reaction threshold energies are uncommonly low for the above isotopes, as a result of the low separation energy of the last neutron.*

The isotope ^{9}Be has an extremely low natural abundance. However, the natural abundance of the nuclide ^{2}H is not wholly insignificant, at 0.015%. Hydrogen, and therefore ^{2}H, is found in water and therefore in all living beings, and accordingly also in all food. The threshold energy

for the interaction $^{2}\mathrm{H}\,(\gamma, n)$ is in the order of 2.3 MeV. This explains why radionuclides emitting a significant amount of ionising photons with $E \gtrsim 2.3$ MeV may not be used in food preservation by irradiation — at energies above this threshold, neutrons will be produced in (γ, n)-reactions, and these neutrons — if produced in significant quantities — will cause radio-activation of the irradiated food via (n, X)-reactions. The radionuclide most widely used in food irradiation, is ^{60}Co, which emits practically no ionising photons above energy 1.332 MeV, which is well below photoneutron-producing, i.e. (γ, n) reaction threshold energies, so that food preservation by irradiation with ^{60}Co will cause negligible radio-activation of irradiated food.

Assignment 7.1

1. A package containing food undergoes irradiation with a 1 MCi ^{60}Co source. Assume that the chemical composition of the food is $\mathrm{H_{10}C_5O_2N_1}$ and that its density is 0.9 g cm^{-3}. Calculate the order of magnitude of the reaction rate of (γ, n)-reactions in the food.

2. A package containing food undergoes irradiation with a 1 MCi ^{24}Na source. Assume that the chemical composition of the food is $\mathrm{H_{10}C_5O_2N_1}$ and that its density is 0.9 g cm^{-3}. Calculate the order of magnitude of the reaction rate of (γ, n)-reactions in the food.

7.2.11 Photon attenuation coefficients

If we disregard unimportant photon attenuation mechanisms, we may express the photon mass interaction coefficient (i.e. μ/ρ) for a substance with molar mass M_A (unit: g.mol^{-1}) as:

$$\mu/\rho = \frac{N_{\text{Avogadro}}}{M_A}\left[\sigma_{\text{PEA}} + \sigma_{\text{incoherent}} + \sigma_{\text{coherent}} + \left(\sigma_{\text{PP}}^{\text{nucl}} + \sigma_{\text{PP}}^{\text{elec}}\right)\right]. \tag{7.18}$$

In this equation, N_{Avogadro} is Avogadro's number, while the superscripts “nucl” and “elec” in $\sigma_{\text{PP}}^{\text{nucl}}$ and $\sigma_{\text{PP}}^{\text{elec}}$ refer to pair production in the Coulomb field of a nucleus and an electron, respectively.

Incident energy and atomic number regions where the different photon interaction mechanisms dominate

Figure 7.5 shows the regions on the (Z, E_γ)-plane where a specific ionising photon interaction cross-section, $\sigma \in \{\sigma_{\text{PEA}}; \sigma_{\text{CS}}; \sigma_{\text{PP}}\}$ will have the largest value.

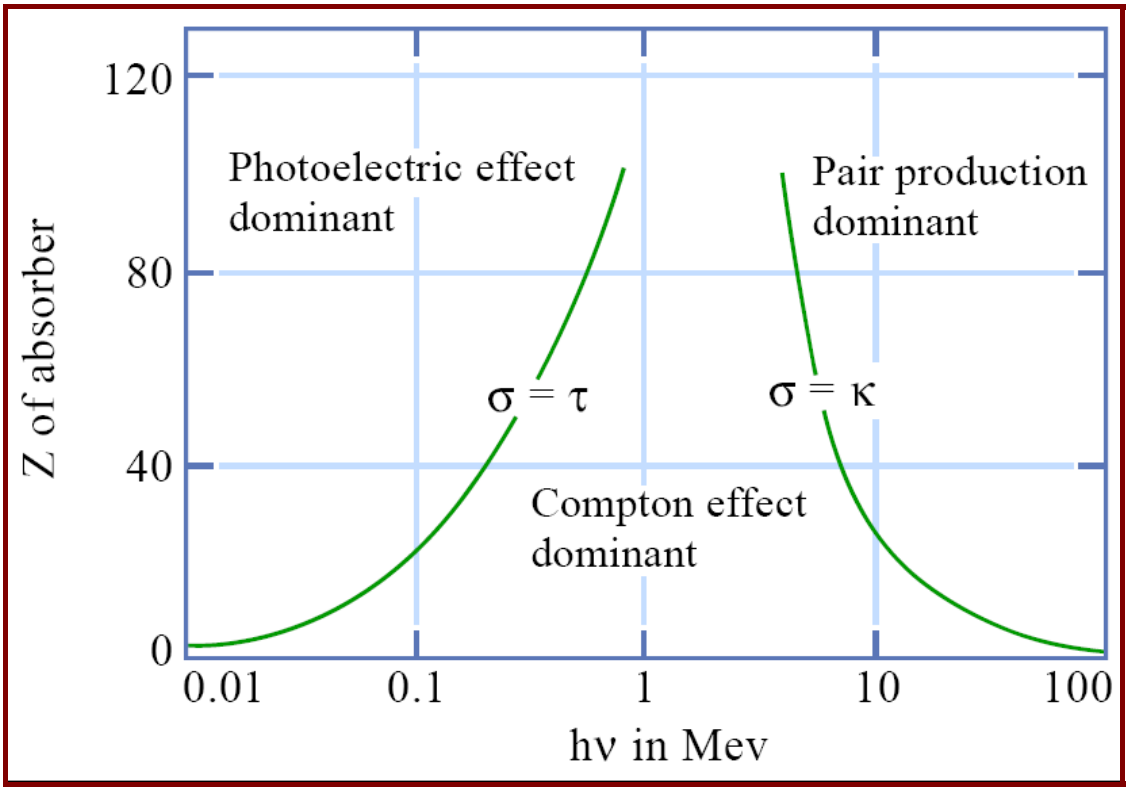

Figure 7.5: *The relative importance of the three major types of interaction mechanisms of ionising photons.*

The lines show the values of Z and $E = h\nu$ for which the two neighbouring effects are equal; the regions where each type of interaction is dominant, are also shown (Knoll, 1997: 67). PEA dominates in the low-energy region, incoherent (Compton) scattering dominates in the intermediate region, while pair production dominates in the high-energy region. On account of the approximate relationships $\mu_{\text{PEA}} \propto Z^3$ and $\mu_{\text{PP}} \propto \rho Z$, the energy region where Compton scattering dominates, diminishes as a function of the atomic number Z.

Photon interaction mechanisms for low-Z mixtures and compounds

Figures 7.6 and 7.7 show typical behaviour of the linear interaction coefficient for low-Z materials such as air and water. Compton scattering dominates over a wide incident photon energy range; pair production only dominates above $E_\gamma > 10$ MeV, while photo-electric absorption only dominates for $E_\gamma < 0.04$ MeV.

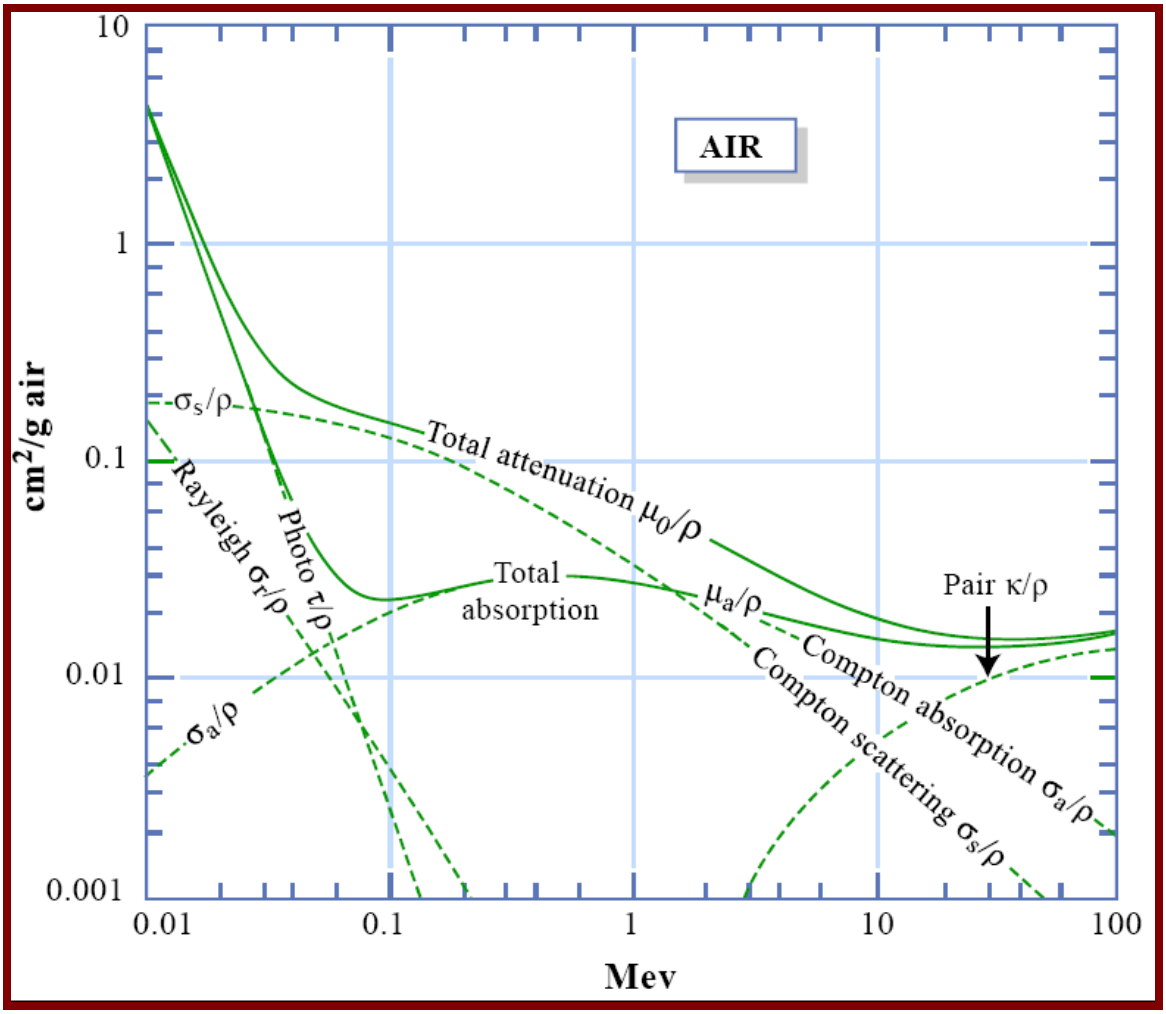

Figure 7.6: *Linear mass interaction coefficients for photon interactions in the low-Z material, air.*

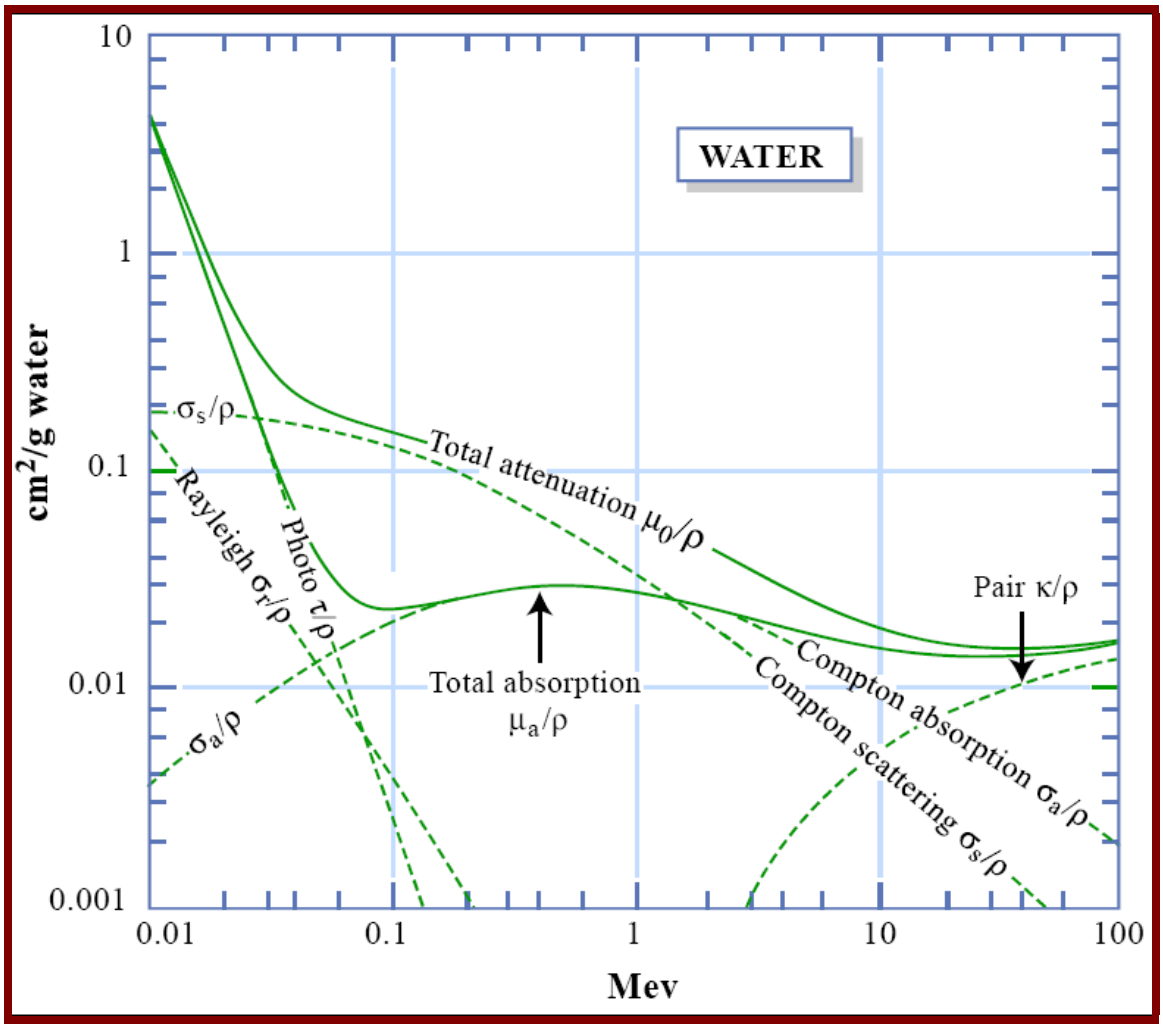

Figure 7.7: *Linear mass interaction coefficients for photon interactions in the low-Z material, water.*

Photon interaction mechanisms for a high-Z element

Figure 7.8 shows typical behaviour of the linear mass interaction coefficient for a high-Z material such as lead (Pb). Compton scattering only dominates over a narrow incident photon energy range; pair production dominates above $E_\gamma \gtrsim 4$ MeV, while photo-electric absorption dominates for $E_\gamma \lesssim 0.8$ MeV.

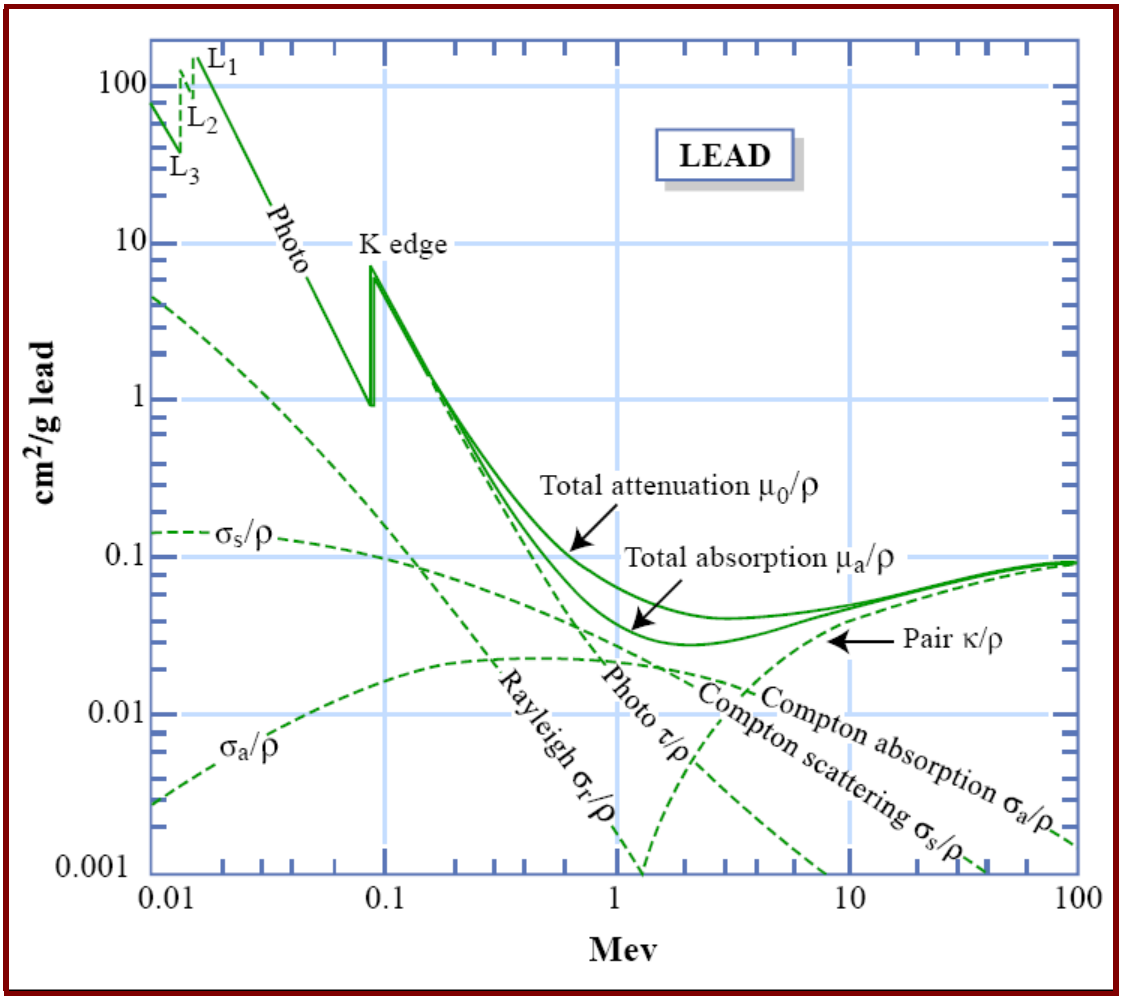

Figure 7.8: *The mass interaction coefficients for photon interactions in a high-Z material such as lead (Pb).*

Mass interaction coefficients

At STP, the density of water is 1.0 g cm^{-3}. At the operating temperature T and pressure P in a typical PWR, $\rho_{\text{water}} \approx 0.7$ g cm^{-3}. We see that it would be a bad practice to list values of μ in photon interaction coefficient databases, because the mass-density ρ of a specific material may vary over a considerable range. It is therefore more sensible to express the linear attenuation coefficient as

$$\mu = \rho\left(\frac{\mu}{\rho}\right) \tag{7.19}$$

where $\left(\frac{\mu}{\rho}\right)$ is called the mass interaction coefficient, having units $\text{cm}^2\,\text{g}^{-1}$. The density-independent values of $\left(\frac{\mu}{\rho}\right)$ are listed, per material and per photon energy, in the photon-interaction coefficient database. The density of the material, ρ, is specified in the input data file of the radiation transport code, and is then used in the code to calculate the linear interaction coefficient μ according to Eq. (7.19).

Figure 7.9 shows the mass interaction coefficients for ionising photon interaction in Pb; it was produced using ionising photon cross-section data available on the website,
http://physics.nist.gov/PhysRefData/

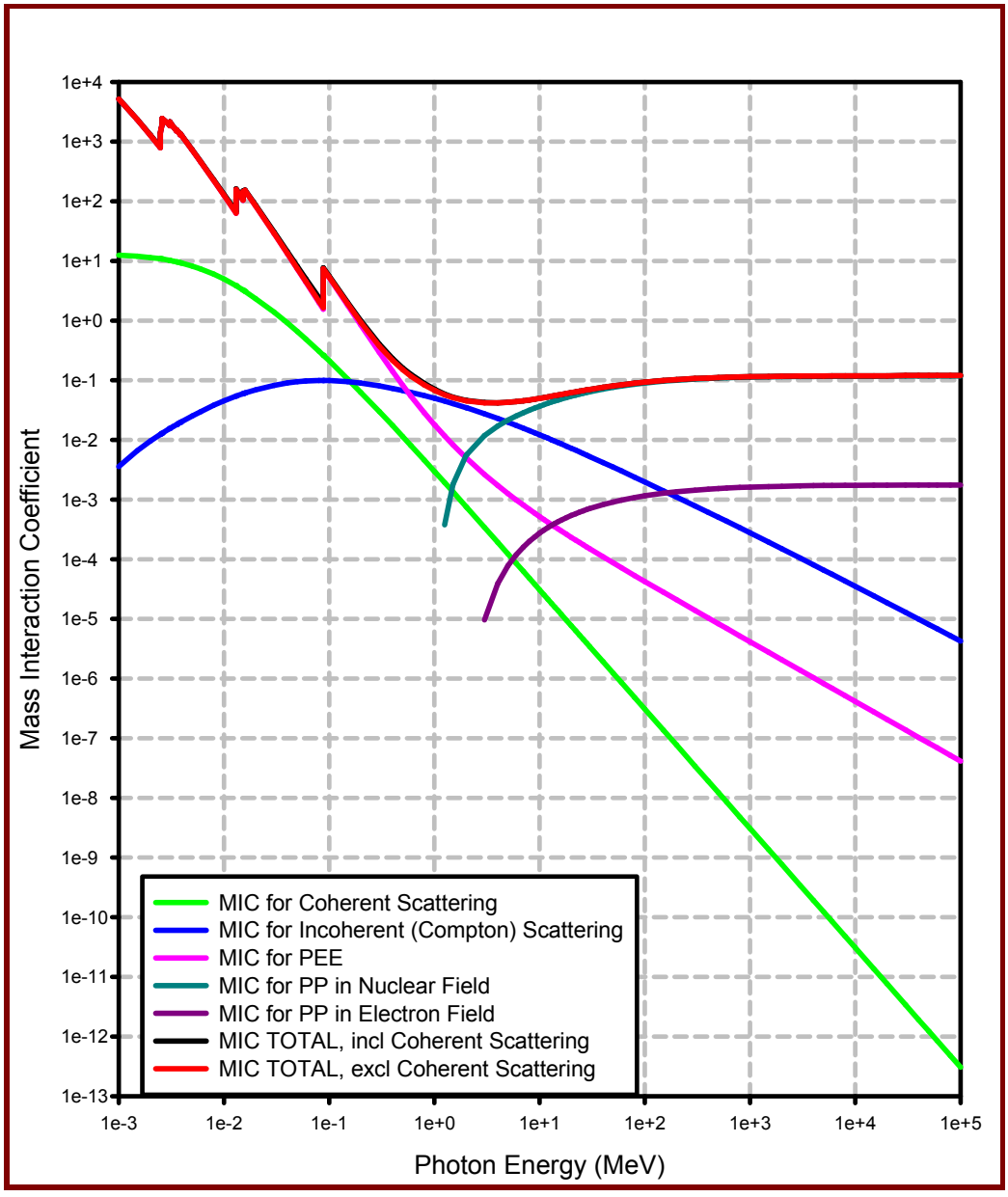

Figure 7.9: *Mass interaction coefficients for ionising photon interaction in Pb.*

Linear attenuation coefficients for common photon shielding materials

Figure 7.10 displays the linear interaction coefficients for a number of important shielding materials.

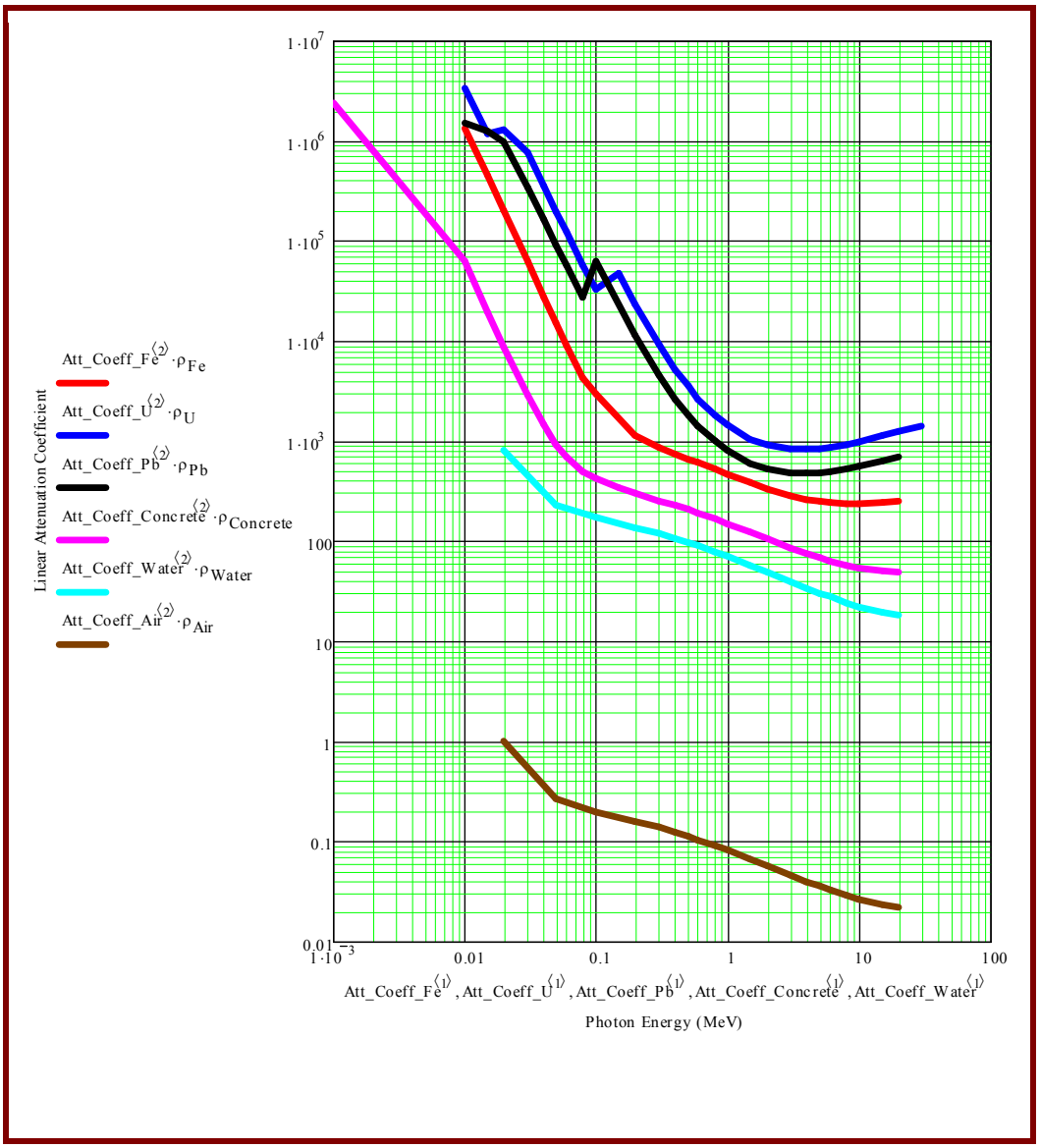

Figure 7.10: *Linear interaction coefficients for ionising photons in a number of important materials.*

7.2.12 Tenth-value thicknesses

For the effective shielding of ionising photons, the atomic number and density of an element should be as high as possible. Accordingly, lead (atomic number $Z = 82$; density $\rho = 11.3$ g cm^{-3}) is a particularly effective shield against ionising photons. Depleted uranium (atomic number $Z = 92$; density $\rho = 18.9$ g cm^{-3}) would be even more effective.

A convenient concept to use as an approximate measure of shielding effectiveness against ionising photons, is the ***tenth-value thickness.*** This is the thickness of material that will reduce the dose rate to $\frac{1}{10}$ of its original value. The tenth-value thicknesses for important radionuclides that emit ionising photons, and some common materials, are listed in Table 0.0.

Table 7.5:
The tenth value thickness for important shielding materials, and important radionuclides that emit ionising photons.

Material	ρ $(\mathrm{g\,cm^{-3}})$	Z	Tenth value thickness (cm)		
			^{60}Co	^{137}Cs	^{22}Na
Tungsten (W)	19.6	74	#3.5		
Lead (Pb)	11.35	82	4.5	2.3	3.4
Iron (Fe)	7.86	26	8.2	7.1	7.9
Aluminium (Al)	2.70	13	24	22	24
Concrete	2.35	-	27	25	26
Water (H_2O)	1.00	-	59	55	57

Example 7.3

Suppose you have to shield a ^{60}Co source with lead (Pb) to reduce the photon dose rate at a point outside the shield by a factor 1000 compared to what the dose rate would be at the same point in the absence of a shield. What thickness of lead is required to attain this *dose attenuation factor* of 1000? Because $1000 = 10^3 = 10 \times 10 \times 10$, three tenth-value thicknesses of lead, i.e. 3×4.5 cm $\approx$ 13 cm Pb will be required to achieve the desired dose attenuation factor. To achieve the same dose attenuation factor, one will require approximately 90 cm concrete or 200 cm water. Also note that the standard thickness of lead bricks is 5 cm, so that, in practice, one will have to construct a 15 cm lead shield if calculations indicate the need for a 13 cm lead shield.

7.2.13 Beware: thin shields can be very inefficient

Consider the example of the radionuclide ^{24}Na shielded by water. The tenth-value thickness is 81 cm, i.e. the dose-rate attenuation factor is 10 for a water shield of this thickness. Figure 7.11 shows that the reciprocal of the dose-rate attenuation factor, i.e. $\left(\frac{1}{\mathrm{DAF}}\right)$ is only about 2.3 for the first 40 cm of shielding material. The attenuation of ionising photons is near-

exponential and not linear with shield thickness. Using too thin a shield against ionising photons, can sometimes have almost no effect on the dose rate.

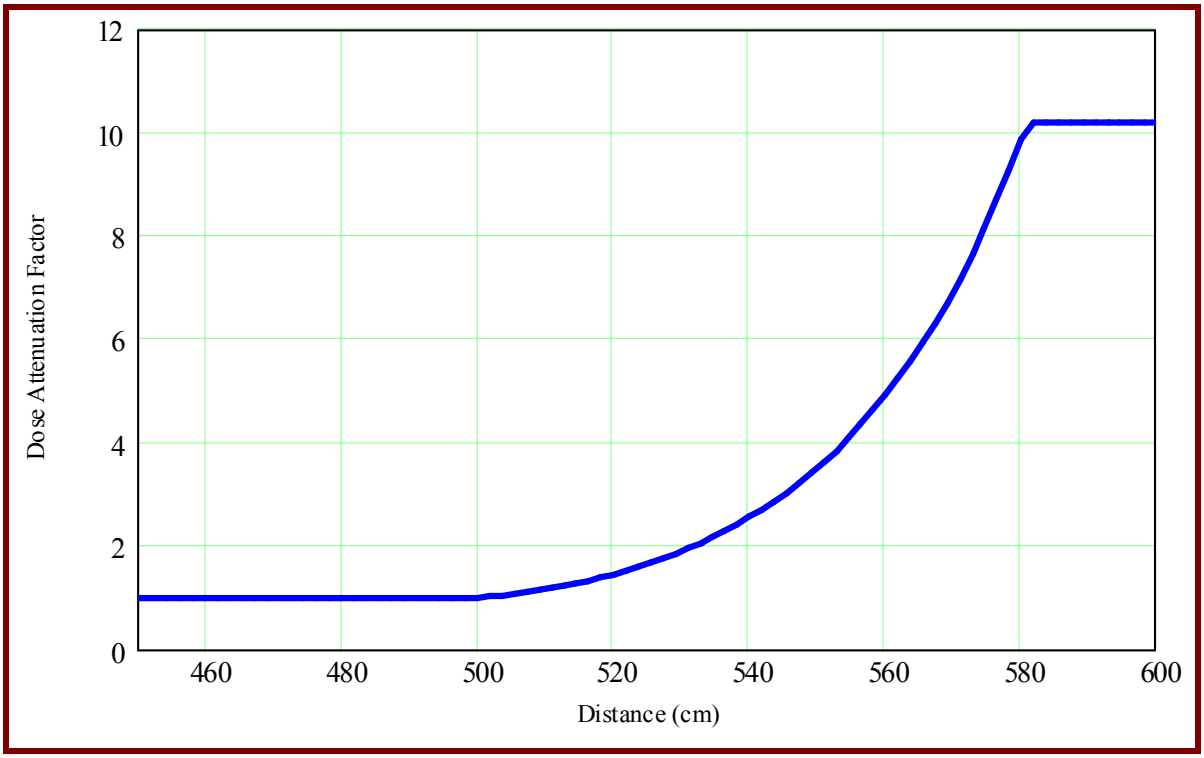

Figure 7.11: *Graph of* $\left(\frac{1}{DAF}\right)$ *for* ^{24}Na *photons, attenuated by water.*

The lesson learn from the above example is that employing too thin a radiation shield against ionising photons can be quite useless — dose rate reduction is a near-exponential function of shield thickness, and not a linear function.

Chapter 8: Complementary Shielding Materials; Principles of Shield Optimisation

8.1 Shield design principles for n/γ-sources: Complementary shielding materials

The need to use complementary shielding materials in neutron shields

In the above summary of the principles of neutron and ionising photon shielding, it became clear that there is no single shielding material that will be an optimal shield for low and high energy neutrons. Hydrogenous shielding materials such as paraffin wax are very good for slowing down neutrons with energies below about 3 MeV, by elastic neutron scattering. At higher energies the cross-section for elastic neutron scattering by ^{1}H becomes very low, and hydrogen-based shields become very "transparent" to neutrons. Another problem is that energetic capture γ-rays are produced when ^{1}H captures a (slow) neutron. Iron is good in slowing down faster neutrons by inelastic scattering, but is very bad as a neutron shield for neutron energies below the threshold energy for the excitation of the first discrete energy level by inelastic scattering (about 0.86 MeV). Iron and lead are also very capable in shielding ionising photons, but especially Fe produces energetic capture γ-rays when it absorbs (slow) neutrons. It becomes clear that a combination of paraffin wax, Fe, a thermal neutron absorber such as boron carbide (B_4C) and Pb, are needed to build a really effective shield against neutrons with a wide range of energies. These materials are called ***complementary shielding materials***, because they *complement* each other by compensating and making up for each other's weaknesses. Where the one shielding material is "weak" the other one is "strong." For neutrons, one must use complementary shielding materials to build an optimal shield. If the incident radiation field is a mixed n/γ-field, complementary shield materials must also be used for the construction of an effective shield. There is no single element that is in all respects an excellent shielding material throughout the energy domain of neutrons encountered at a nuclear reactor or a particle accelerator facility.

The optimisation of photon shielding is a trivial problem

If the incident radiation field consists only of ionising photons, the selection of materials for a shield of minimum thickness that must attenuate the radiation field to below a given dose rate, is a simple design problem. The atomic number, Z, and density, ρ, of the shield materials must simply be maximised, as is evident from Table 0.0. on page 0.

Terminology

The side of the shield from where the radiation comes, will be called the "source side" of the shield. The other side, where people will have to work, will be called the "personnel side" or

the “detector side” of the shield. This is illustrated below.

8.2 Shield optimisation

Shield optimisation problem

When neutrons are an important component of the source-term, complementary shielding materials are needed, because no single shielding material is good enough in isolation. The kind of shield optimisation problem that will be solved is: A given thickness is available to place shielding materials in. Given that four shielding materials are available, namely paraffin wax, boron carbide (B_4C), iron and lead, determine thicknesses and placements of these material layers that will minimise the transmitted dose rate for a given shield thickness.

Parametric shield optimisation

A technique that will be often used in this study, is parametric shield optimisation. A single material property is varied as parameter, and a radiation transport calculation is done for each shield configuration. The transmitted dose rate is plotted as a function of the material property that is varied as parameter, and the optimum is the material configuration where the transmitted dose rate is a minimum.

Suppose that 20 MeV neutrons fall onto a shield with a total thickness of 60 cm, and that the thickness of iron and paraffin wax that will minimise the dose rate on the personnel side of the shield, must be determined. Material thicknesses are varied is steps of, say 5 cm at a time. It is known that the iron will be best used on the source side, where it can slow down fast neutrons by inelastic scattering. It is also known that the paraffin wax will be best on the personnel side of the shield, because it can only slow neutrons down well if neutron energy has already been lowered to below about 3 to 4 MeV by inelastic scattering with Fe. The following calculational experiment is now performed: Start with a shield that is 100% steel. Now decrease steel thickness and increase wax thickness in small steps, e.g. 5 cm at a time. Do a radiation transport calculation for every shield configuration. Plot the transmitted dose rate as a function of the thickness percentage of Fe in the shield. For 20 MeV neutrons, the optimum will typically lie at about 70% Fe and 30% wax thickness. The systematic, step by step change in the material configuration of the shield, whilst keeping the overall shield thickness constant is illustrated in Figure 8.1.

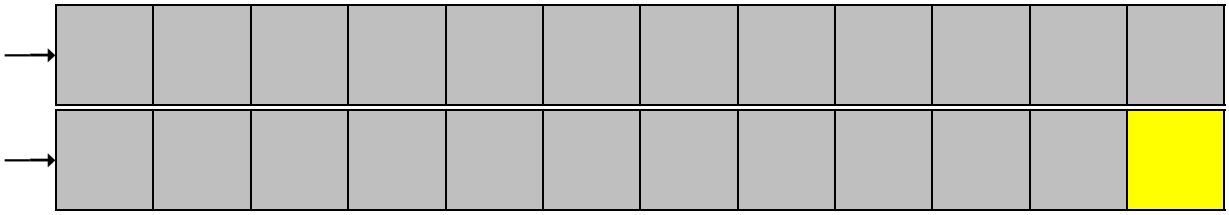

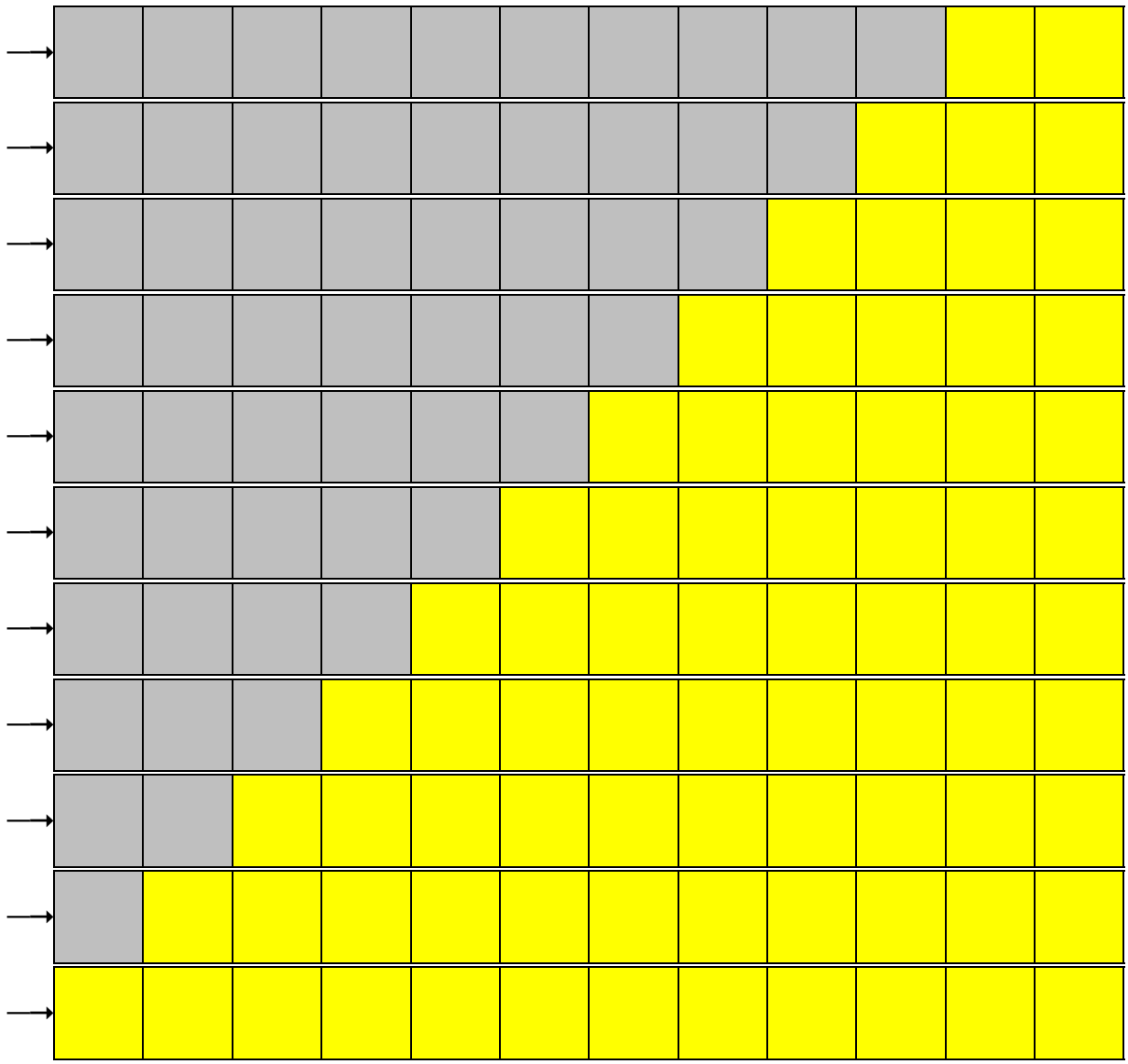

Figure 8.1: *Parametric shield optimisation study to determine optimal material thicknesses in a 2-layer Fe/wax shield.*

In a parametric shield optimisation study, one aspect of a shield is varied as parameter, and the transmitted dose rate is calculated for every material configuration. The optimal shield will transmit the lowest dose rate. The above illustration is for varying material composition in 5 cm steps. This is good enough far from the optimum, i.e. the turning point in the graph. Close to the optimum, variations must be finer, e.g. in 1 cm steps.

Step 2 of the optimisation study can now begin, once the optimal thickness of wax in the above Fe/wax shield is known. In step 2, the optimum is refined. Suppose the optimum for a 2-layer Fe/wax shield having a total thickness of 60 cm, is found to be 40 cm Fe followed by 20 cm wax. Now "swim" a 20 cm wax layer step-by-step through a 40 cm thick Fe layer, to determine the optimal position of the wax in a 3-layer Fe/wax/Fe shield, as illustrated in Figure 8.2.

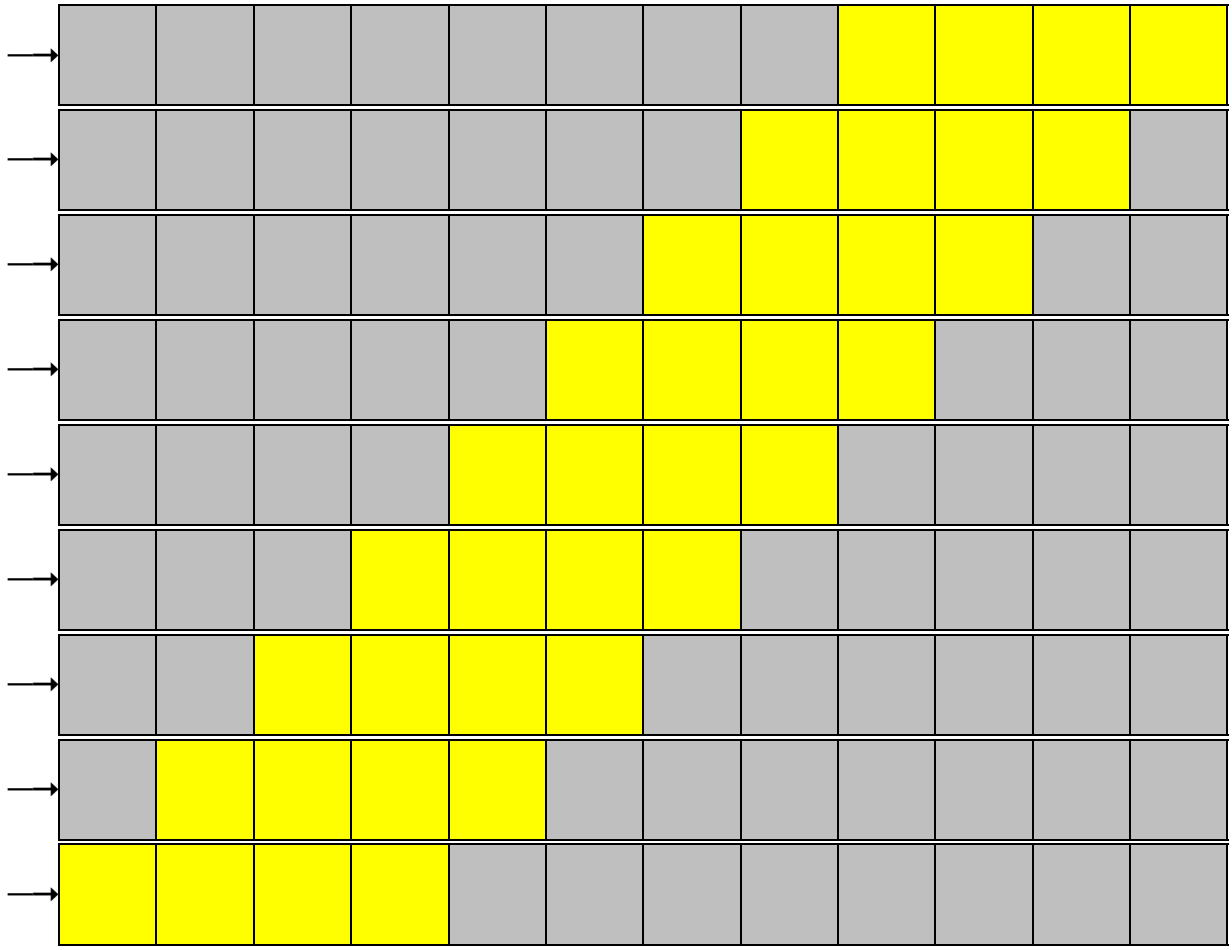

Figure 8.2: *Parametric shield optimisation study to determine the optimal position of a paraffin wax layer of a pre-determined thickness in a 3-layer Fe/wax/Fe shield.*

In this parametric shield optimisation study, one aspect of a shield is varied as parameter, and the transmitted dose rate is calculated for every material configuration. The optimal shield is that material configuration that will transmit the lowest dose rate. The above illustration is for varying material composition in 5 cm steps. This is good enough far from the optimum, i.e. the turning point in the graph. Close to the optimum, material variations must be finer, e.g. 1 cm steps.

After step 2 of the above optimisation study, perturbation analysis can be used once again to fine-tune the optimum material configuration. Once the optimal position of the wax layer, sandwiched inside the steel, has been determined, the outside Fe layer (i.e. on the personnel side of the shield) can e.g. be replaced by Pb. Optimal material thicknesses can then be fine-tuned by sets of parametric analyses. Furthermore, varying amounts of boron carbide (B_4C) can be added to the wax layer, and the influence of the percentage B_4C determined by a series of transport calculations. For economical reasons, the percentage B_4C will usually not be allowed to exceed about 5%. The shield designer works like a detective to determine the best shield, by performing systematic "experiments" using advanced, accurate radiation transport codes. If such experiments had to be done using blocks of shielding material and detectors, it would take very long and consume lots of expensive "beam time" at a particle accelerator or research reactor facility. The advantage of the availability of modern computers, radiation

transport codes and cross-section libraries is that one can quickly and conveniently perform these "experiments" by simulation.

8.3 Dose attenuation factor (DAF)

Refer to page 2 for the definition of this important measure of the performance of a shield against ionising radiation.

8.4 Suppression of the production of energetic capture γ-rays, by mixing a neutron absorber, boron carbide (B_4C), into a hydrogenous material

The neutron capture reactions ("radiative neutron-capture reactions"),

$$^{1}\mathrm{H} + n \rightarrow {}^{2}\mathrm{H} + \gamma\ (2.205\ \mathrm{MeV})$$

and

$$^{10}\mathrm{B}\ (n, \alpha)\ {}^{7}\mathrm{Li} + \gamma\ (0.48\ \mathrm{MeV})$$

are important in the design of neutron shielding. Neutron sources require *(inter alia)* hydrogenous materials for shielding. However, the first of the two reactions listed above, produces relatively energetic 2.2 MeV capture gamma-photons. In this way, secondary gamma radiation is produced in the shield. In thick hydrogenous shields, the transmitted ionising photon dose rate can exceed the transmitted neutron dose rate. The gamma-photons produced by the second capture reaction have energies with an energy of only 0.48 MeV, i.e. they are approximately 4.6 times less energetic than the capture gamma-photons produced when ^{1}H absorbs neutrons. A gamma-photon of energy 0.48 MeV is biologically about 3.3 times less dangerous than a 2.205 MeV photon. For a given material, it also follows from Eq. (8.0) that the ratio between the linear interaction coefficients for the photo-electric absorption of a 0.48 MeV photon and a 2.2 MeV photon, is

$$\frac{\mu_{\mathrm{PEA}}(0.48\ \mathrm{MeV})}{\mu_{\mathrm{PEA}}(2.205\ \mathrm{MeV})} = \left(\frac{2.205}{0.48}\right)^{3.5} \approx 200.$$

A photon with $E = 0.48$ MeV is therefore approximately 200 times more likely to be absorbed by photo-electric absorption than a photon with an energy of 2.205 MeV. Because it suppresses the production of high-energy secondary photons, B_4C (boron carbide) is often used in hydrogenous neutron shields. Figure 8.3 illustrates the boron neutron capture (BNC) reaction whereby ^{10}B captures a neutron, and Figure 3.43. shows the cross-section for the BNC nuclear reaction.

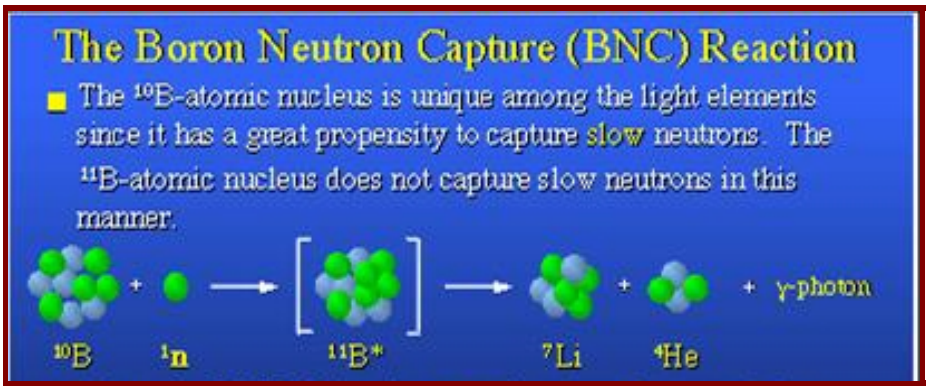

Figure 8.3: *The boron neutron capture reaction, $^{10}B\,(n,\alpha)\,^{7}Li + \gamma$ (0.48 MeV). The natural abundance of ^{10}B is 20%. Boron is often mixed into neutron shielding materials in order to suppress the emission of high-energy ionising photons as well as to suppress the fluence-rate of low-energy neutrons in order to minimise the reaction rates of neutron activation reactions.*

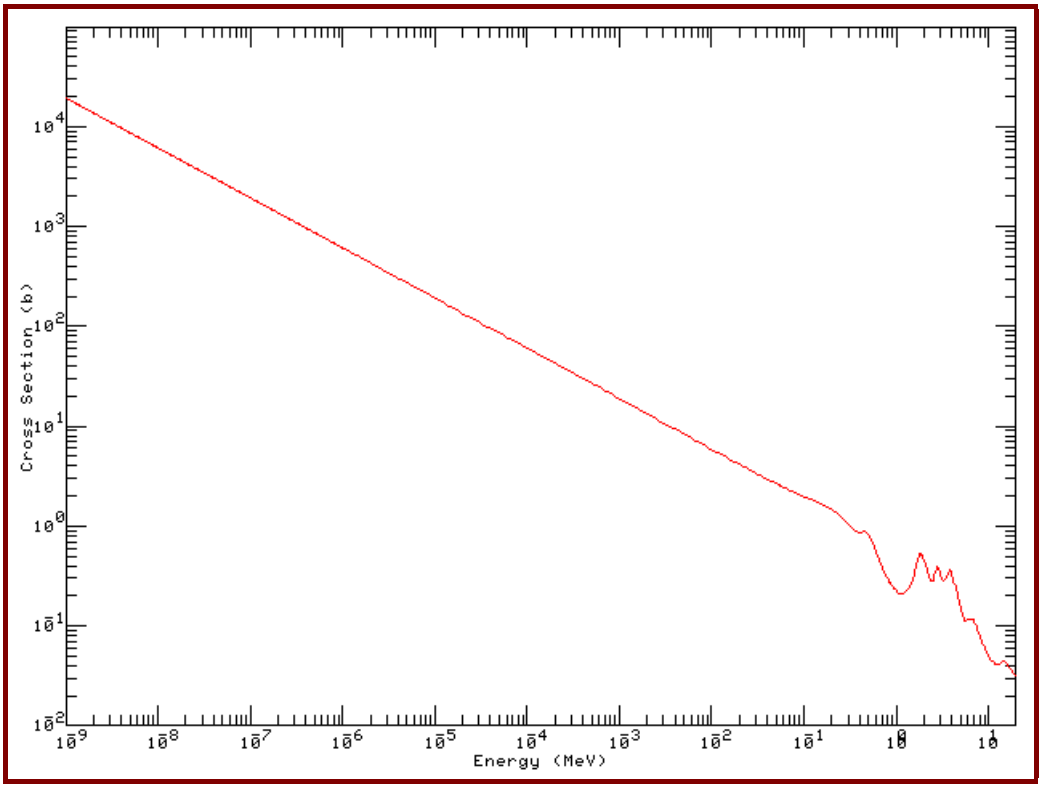

Figure 8.4: *Cross-section for the boron neutron capture reaction, $^{10}B\,(n,\alpha)\,^{7}Li + \gamma$ (0.48 MeV). Boron-10 is a very useful absorber of neutrons, especially slow neutrons. The gamma-photon emitted upon neutron capture, has a relatively low energy, and is quite easily absorbed. In this way, adding boron to a neutron shield suppresses the production rate of high-energy ionising photons.*

At the reference neutron speed of 2200 m.s^{-1}, the cross-section of the capture reaction $^{10}\mathrm{B}\,(n,\alpha)\,^{7}\mathrm{Li}$ is 3844 barn, while the cross-section for the reaction $^{1}\mathrm{H}\,(n,\gamma)\,^{2}\mathrm{H}$ (at the same reference neutron speed) is only 0.33 barn. The mixing ratio of B_4C in paraffin wax or polyethylene is determined by the requirement that the reaction rates, and accordingly, the linear interaction coefficients for the favourable and the unfavourable absorption reactions

should be related as follows:

$$\frac{\mu_{^{10}\mathrm{B}(n,\alpha)}}{\mu_{^{1}\mathrm{H}(n,\gamma)}} \approx 25.$$

By working from this principle, it is easy to show that the ideal volume percentage of B_4C in paraffin wax or polyethylene should be between circa 2.5 % and 5 %. In practice, we find that 90% of the advantage of adding 5% B_4C to a shield is obtained by adding only 3%. Because B_4C is very expensive, 5% B_4C is the highest mixing ratio that can normally be afforded in a bulk shielding material. The B_4C that is employed in the shield, should be in the form of an extremely fine powder in order to approximate a homogeneous mixture and produce the maximum benefit.

In view of neutron activation problems, i.e. the problem of induced radioactivity, other cheaper boron-containing compounds, e.g. borax (disodium tetraborate[25]), should not be used in the place of boron carbide — the borax molecule contains sodium, which is strongly activated by the neutron capture reaction $^{23}\mathrm{Na}(n,\gamma)^{24}\mathrm{Na}$; the latter radionuclide produces energetic ionising photons and has a $T_{½}$ of about 15 hours.

Percentage of the neutron absorber, boron carbide (B_4C), to mix into a hydrogenous material

Refer to Annexure B on page 505.

8.5 Typical cost-effective optimised neutron shields

Abbreviations

PE = polyethylene;
Wax = Paraffin wax.

Assumptions

If space and mass are of no concern, ordinary concrete is typically the shielding material of choice — e.g., in a PWR containment building.

In this section we assume that the space available for a shield is limited. The total shield thickness is constrained to a given value, while the project budget as well as mechanical considerations constrain the shield designer to select only from the following shielding materials:

- Low-alloy Fe;
- Low-alloy Pb;

[25] Typical chemical formula: hydrated $Na_2B_4O_7$.

- Paraffin wax;
- Boron carbide (B_4C) is available to mix into the was, in a mass ratio not exceeding 5% B_4C. A good alternative to B_4C is ammonium pentaborate.

Shield design issues are: which of the above materials must be deployed? In which order, from the source-side to the personnel-side of the shield? What is the optimal thickness of each material layer, given the constraint on total shield thickness?

Case 1: Incident neutron energy $E_n = 1$ MeV

The configuration of a typical neutron shield against incident neutrons with an energy spectrum restricted to $E_n \leq 1$ MeV, will be as follows:

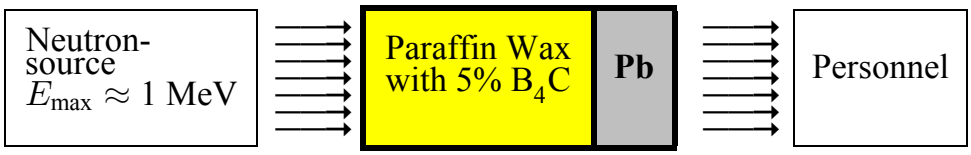

Explanation: The ^1_1H in the hydrogenous shield layer is very capable of thermalising the neutrons, because the cross-section for elastic scattering by ^1_1H is still usefully high at a neutron energy of 1 MeV. The kinematical efficiency of elastic scattering by ^1_1H is high, at an expectation value of a 50% reduction in the energy of the scattered neutron.

Case 2: Incident neutron energy E_n covers the range from 0 to approximately 20 MeV

The configuration of a typical neutron shield against incident neutrons with an energy spectrum that extends above 5 MeV to e.g. 20 MeV, will be as follows:

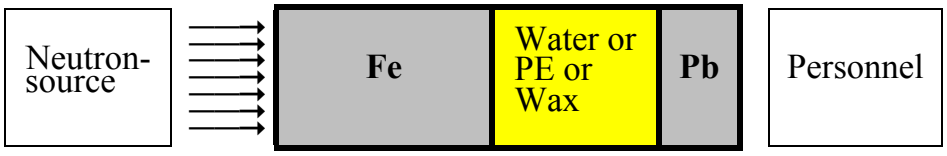

Explanation: The iron on the source side will typically constitute 50% – 70% of the total thickness of the shield, the hydrogenous layer 20% – 50% and the lead 0% – 5%. The optimal thicknesses will depend on the incident neutron spectrum, as well as the total thickness that is available for the shield. The iron slows down the neutrons with energies above circa 4 MeV via inelastic scattering, while the hydrogen-rich layer is able to very effectively slow down the neutrons with energies below approximately 4 MeV. The main function of the layer of lead on the personnel side of the shield, is to absorb ionising photons produced in the hydrogenous layer, and also to — when the neutron source is switched off by e.g. terminating target bombardment or shutting down the nuclear reactor — shield personnel, electronics and polymers against the ionising photons emitted by radioactive neutron activation products produced in the steel layer of the shield.

Case 3: Incident neutron energy 100 MeV $\leq E_n \leq$ 200 MeV

The configuration of a typical neutron shield against incident neutrons with an energy spectrum that falls mainly in the energy region above circa 100 MeV and below circa 200 MeV, will be as follows:

Explanation: The iron on the source side will typically constitute 80% – 90% of the total thickness of the shield, and the hydrogenous layer approximately 20% – 10%. No final Pb layer will be required, because the neutron dose rate will exceed the ionising photon dose rate on the detector side. The iron slows down the neutrons with energies above circa 4 MeV via inelastic scattering, and also removes neutrons from the radiation field via e.g. (n, p), (n, α), and (n, d) reactions, while the hydrogen-rich layer is able to very effectively slow down the neutrons with energies below approximately 4 MeV.

8.6 A typical cost-effective optimised radiation shield around an intense 40 MeV electron beam striking a tungsten target

Suppose that a 40 MeV electron beam strikes a 3.5 mm thick tungsten target. It will produce an intense ionising photon radiation field with an energy spectrum, averaged over the polar angle, as shown in Figure 5.20 on page 295. Suppose that these high-intensity, high-energy ionising photons strike mined kimberlite ore held in a hopper. The maximum (γ, n) nuclear reaction cross-section for most nuclides display a broad maximum in the photon energy region 18 MeV to 32 MeV, so that the bremsstrahlung photons produced by the 40 MeV electrons in the W target, will readily produce an intense neutron field wherever it strikes materials. To shield such a source, is quite a challenge. The best shielding strategy will be to first aggressively attenuate the high energy ionising photons by using a substantial thickness of Pb. Next, a thick layer of Fe must be deployed to further slow down the secondary neutrons produced by the primary high energy ionising photons. Next, a layer of paraffin wax containing e.g. 5% B_4C must be deployed. A final layer of e.g. 5 cm Pb may be required to attenuate capture γ-photons produced by neutron capture reactions in the Fe layer as well as in the hydrogenous layer.

The final radiation shield against the high-energy ionising photons will typically have the following configuration:

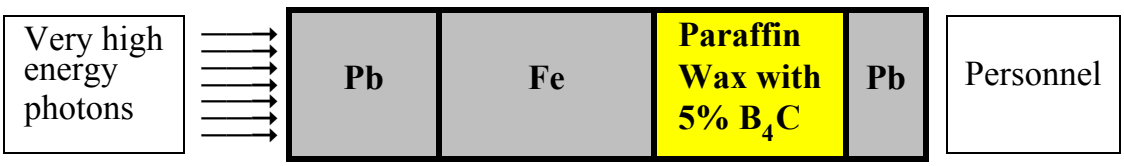

For an intense electron beam (e.g. $I = 1500$ mA), the required total shield thickness may be as thick as 100 cm. Extensive use of variance reduction methods will be required to optimise such a shield configuration. It will be advantageous to optimise a radiation shield having only 50% of the allowed total thickness, and then simply double the optimised thicknesses of every layer, in order to make the variance reduction task less challenging and time-consuming.

Chapter 9:
Monte Carlo Methods in Radiation Transport

If one could determine the exact path each particle makes and energies it assumes while passing through a medium in its random-walk fashion, one could, in principle, calculate many useful quantities by averaging over a large number of individual particle histories so as to minimise the stochastic effects of the individual particle interactions. For example, the probability that a particle in a certain energy range will be absorbed in a certain volume could be estimated by computing the proportion of all particles, in the specific energy group, that terminates in the specified volume. This concept of using a large number of particle histories, each of which is random in nature, to estimate some average particle behaviour, is the essential feature of the Monte Carlo method.

In Monte Carlo calculations, the particle tracks or histories are generated by simulating the random nature of the particle interactions with the medium. To do this, one requires mathematical expressions for the probability relationships which govern the track length of an individual particle between interaction points, the choice of an interaction type at each such point, the choice of a new energy and a new direction if the interaction is of a scattering type, and the possible production of additional particles. These are all stochastic variables. One needs a complete understanding of the physics of the various processes a particle undergoes in its lifetime from the time it is born in the source until it is either absorbed or leaves the system under consideration, in order to make selections of the specific values for these variables.

Monte Carlo methods are used in radiation transport applications such as shielding & detector response analysis & dosimetry. Monte Carlo refers to a statistical method wherein expected characteristics of particles (e.g. particle fluence) are estimated by sampling a large number of individual particle histories whose trajectories are simulated by a digital computer.

In some cases, there are equations that adequately describe the behaviour of such systems and that can be solved either analytically or numerically. Why the, resort to Monte Carlo methods?

The fundamental advantage of Monte Carlo techniques over deterministic techniques (i.e. numerical solutions to the Boltzmann transport equation (BTE)), is that Monte Carlo techniques more accurately represent the geometry and the nuclear data than deterministic techniques. Deterministic techniques require reasonably simple geometries for the numerical technique to work, and use the multigroup approximation to cross-section data. Monte Carlo techniques can handle complex geometries and continuous cross-section data (as well as simple geometry and multigroup data). The disadvantage of the Monte Carlo technique is that it is statistical in nature and does not provide an exact solution to the problem. All results represent estimates with associated uncertainties. Also, Monte Carlo techniques can be quite time-consuming on a computer if small uncertainties are required.

The relationship between Monte Carlo techniques and deterministic techniques is: deterministic techniques provide a highly exact solution to a significantly simplified

approximation of the problem, while Monte Carlo techniques provide an approximate solution to a highly exact representation of the problem.

When a neutron, e.g., traverses a material, it interacts with the constituent atoms of that material. These processes occur statistically in nature, with the probability of occurrence determined by a cross-section. Nobody can predict exactly how far one particle will travel in a material before interacting; however, one can predict the distribution of flight distances that a large number of those particles will have prior to their first interaction. Using "random" numbers, the digital computer can generate a statistical history of the life of each particle — a random walk analysis. That is, an individual particle may experience many scattering interactions before finally being absorbed or leaking from the system. Random numbers — a set of numbers which have no pattern and are sampled uniformly between 0 and 1, are used at each interaction to determine which process (fission, elastic scattering, etc.) occurs., how much energy is lost, what is the new direction of the particle (in the event of scattering), or how many neutrons are created in a fission event. The life of the particle begins at birth — either from an external (fixed) source of from a fission event, and ends with absorption or with a scattering event that moves the particle outside the region of interest. The events that occur during a particle's life, are tabulated and become the history of that particle. Because a single particle is not representative of the system, a number of histories must be evaluated to accurately describe what occurs.

Examples of Monte Carlo processes

A sequence of random numbers $0 < R_i < 1$ is used to produce a random distribution of quantities that simulate the problem at hand:

1. Determine the initial position where the neutron is emitted.

2. Use a random number to select E_n, based on $\chi(E)$, the energy distribution of fission neutrons.

3. Use the next random number(s) to determine the direction cosine(s) of the neutron's direction of movement.

4. Use the next random number to determine the location of the next collision site (the distance travelled depends on the total cross-section of the material medium.

5. Check the new position to determine if the particle has escaped (leaked) from the system. If it has, add 1 to the total leaked and go to step 1 & start another history with another neutron. If not, go to step 6.

6. Determine which type of interaction occurred at the new position, based on the next random number. Each type of interaction has an associated cross-section that determines the probability of occurrence:

    - If the interaction is scattering, then determine the new energy of the neutron after scattering using the next random number. Then GoTo step 3 & continue to follow the neutron, i.e. determine the direction in which the scattered neutron moves.

- If the interaction is absorption, GoTo step 1 and start a new neutron in the system.

- If the interaction is fission, use the average fission neutron multiplicity $\overline{\nu}$ to determine how many neutrons are created in this fission event and tabulate the total number of new neutrons that are created in this fission event, and tabulate the total number of new neutrons created. Also store the locations of the fission events with each of the new neutrons so that they can be started at this location in the next cycle (replaces step 1).

7. When a given set of histories has been completed — enough to provide acceptable statistical precision — evaluate the tally.

Monte Carlo terminology

Monte Carlo
A numerical analysis technique that uses random sampling to estimate the solution of a physical or mathematical problem.

Random numbers
In Monte Carlo methods, the process of deciding on a specific value of some stochastic variable is generally based on the selection of a random number in the interval $[0; 1]$. Random numbers are, in principle, an infinite set of numbers that are uniformly distributed from 0 to 1 and are independent. We actually use pseudorandom numbers — a deterministic reproducible sequence of numbers generated by a computer that satisfy statistical tests for randomness. Most Fortran, C and C++ compilers, as well as MathCAD, Maple, MatLAB and Mathematica, have built-in random number generators.

Monte Carlo weight
The number of physical particles w that a Monte Carlo particle represents.

Random walk
The random selection of events for a particle history.

History
The complete random walk of a Monte Carlo particle from its birth in the source to its death, including all progeny.

Monte Carlo track
A branch or subset of a history that can be obtained by physical events or by variance reduction techniques.

Score
Contribution from a track to a tally.

History score
Sum of all scores from 1 source particle's tracks.

Tally
The quantity we wish to estimate — the average score — obtained by summing all scores from all histories.

Relative error
Standard deviation of the mean of a tally, divided by the mean. The relative error indicates the precision of the tally, not its accuracy.

Importance
The expected score per unit weight of a track at a point in phase-space.

Fluence-rate
The product of particle density and particle speed. The sum of lengths of all Monte Carlo tracks per unit volume per unit time.

Fluence

$$\int_t dt\,(\text{FluenceRate})$$

If the MCNP source is in units of particles, the fluence tallies are fluence tallies. If the MCNP source is in units of particles per unit time, the fluence tallies are in fact fluence-rate tallies. Fluence has the units particles/cm^2.

Current
The number of particles crossing a surface in a given time in a given time interval and in a given direction interval.

Selection techniques for given stochastic variables

The way in which a random number between 0 and 1 is used to select an event from a **discrete probability distribution** is best explained by example. Consider the selection of whether a photon of a given energy will interact by the photoelectric effect (pe), Compton scattering (c) or pair production (pp) in a particular collision. The probabilities of the three available modes of interaction are defined as

$$\begin{aligned} p_1 &= \frac{\sigma_{pe}}{\sigma_t} \\ p_2 &= \frac{\sigma_c}{\sigma_t} \\ p_3 &= \frac{\sigma_{pp}}{\sigma_t} \end{aligned} \tag{9.1}$$

where $\sigma_t = \sigma_{pe} + \sigma_c + \sigma_{pp}$. Our discrete probability density function is normalised, because

$$\sum_{i=1}^{N} p_i = 1$$

where N is the number of interaction options ($N = 3$ in our example).

Suppose that $p_1 = 0.2,\ p_2 = 0.5,$ and $p_3 = 0.3.$ The index 1 denotes photoelectric absorption, the index 2 denotes Compton scattering and the index 3 denotes pair production; the reaction type is uniquely referenced by its integer index.

The discrete probabilities may be represented as shown in Figure 9.1.

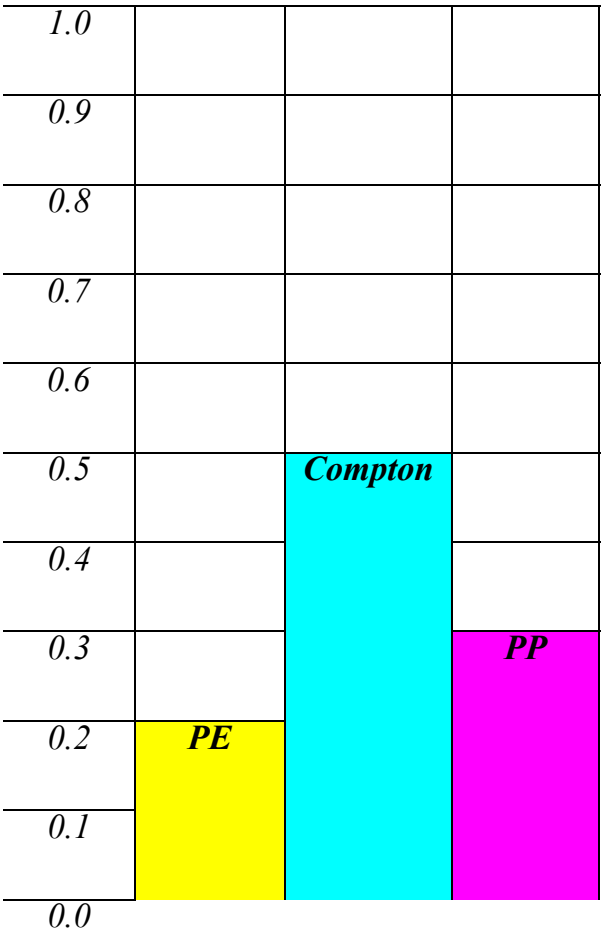

Figure 9.1: *A discrete probability-density function.*
(PE = Photoelectric effect; PP = Pair production.)

Let us now define the cumulative-probability distribution,

$$P_j = \sum_{i=1}^{j} p_i;\ j \leq N\,, \tag{9.2}$$

which gives the probability that interaction type i is less than or equal to j. In our example,

$$P_1 = p_1 = 0.2$$
$$P_2 = p_1 + p_2 = 0.7$$
$$P_3 = p_1 + p_2 + p_3 = 1.0.$$

If $j = 1$, $P_1 = 0.2$; if $j = 2$, $P_2 = 0.7$ and if $j = 3$, $P_3 = 1$. This is shown in Figure 9.5. We see that the summation (in general: integration) of the normalised probability density function yields a cumulative-probability distribution function which has values in the interval $[0; 1]$.

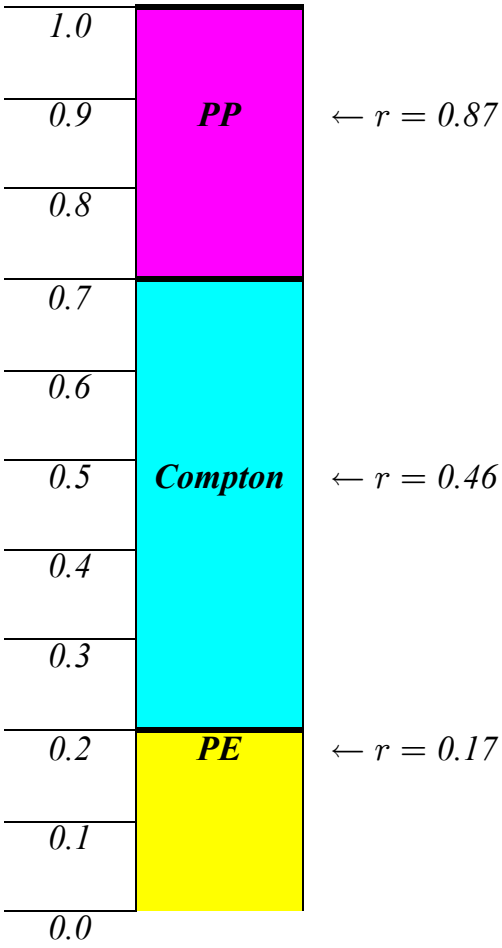

Figure 9.2: *Cumulative-probability distribution and selection of interaction type with random number r. Forming the cumulative probability-distribution function (cpdf) from a normalised probability-distribution function (pdf) defined on the interval $[a, b]$ provides a mapping from $[a, b]$ to the unit interval $[0, 1]$. If, e.g. $r = 0.17$, the chosen interaction will be photoelectric absorption; if $r = 0.46$, the chosen interaction will be Compton scattering, and if $r = 0.87$, the chosen interaction will be pair production.*
(Abbreviations: PE ≡ photoelectric absorption; PP ≡ pair production.)

Refer to Figure 9.2. If we generate a random number r in the interval $[0; 1]$ and set

$$r = P_j \tag{9.3}$$

then the type of interaction, denoted by j, is determined. The interaction is:

- Photoelectric (type 1) if $0 < r \leq P_1$, i.e. $0 < r \leq 0.2$,
- Compton (type 2) if $P_1 < r \leq P_2$, i.e. $0.2 < r \leq 0.7$,

and

- Pair production (type 3) if $P_2 < r \leq P_3$, i.e. $0.7 < r \leq 1.0$.

Because r is uniformly distributed on the unit interval $[0; 1]$, each type of interaction is sampled with probability p_1, p_2, or p_3. In a large number of samples, Compton scattering would, e.g., be selected in circa 50% of the cases, photo-electric absorption in 20% and pair production in 30%. The smaller the number of samples, the greater the degree of statistical fluctuations would be.

In view of the above example, we can now formalise the *method of selection from a discrete probability density function* as follows:

To select an event (uniquely referenced by its integer index) k randomly according to the probabilities p_i that event i will occur, a random number r is generated and then the k for which the expression

$$\sum_{i=1}^{k-1} p_i < r \leq \sum_{i=1}^{k} p_i \tag{9.4}$$

i.e.

$$P_{k-1} < r \leq P_k$$

holds, is selected.

(Note: $P_0 = 0$ by definition.)

We shall now extend this method to **continuous probability density distributions**. Consider a continuous *probability density function* (pdf), say $f(x)$. By definition, the probability of finding the variable x between x and $x + dx$, is the infinitesimal area $f(x)\,dx$. Accordingly, the probability that a randomly selected value of x is between x_1 and x_2, is given by the area under $f(x)$ bounded by x_1 and x_2:

$$P\{x_1 < x \leq x_2\} = \int_{x_1}^{x_2} dx\, f(x). \tag{9.5}$$

Let us now assume that x may be any value between the limits a and b, either of which may be $-\infty$ or $+\infty$, respectively. Corresponding to $f(x)$, there is a *cumulative probability distribution* $F(x)$, defined by

$$F(x) = \int_a^x f(x')\,dx'. \tag{9.6}$$

The probability that the randomly selected value of x is less than x_1, $P\{x < x_1\}$, is thus given by $F(x_1)$. It is easily seen that the function $F(x)$ is monotonically increasing with x if $f(x)$ is a normalised probability density function between a and b, with $F(a) = 0$ and $F(b) = 1$. *We see that F is a mapping from the interval $[a; b]$ to $[0; 1]$. Likewise, the inverse cumulative probability density function F^{-1} will be a mapping from $[0; 1]$ to $[a; b]$.*

In the Monte Carlo process it is necessary to generate random values of some variable, x (e.g. path length) which, from the physics of the particle interaction process, has some distribution $f(x)$. A histogram of the density per unit-interval on the x-axis, of a large number of such randomly generated x values, should approach $f(x)$ in shape. A major aspect of Monte Carlo calculations is the efficient generation of stochastic variables having a specified probability distribution.

Chapter 10:
Introduction to the Practical Use of the Monte Carlo Radiation Transport Code, MCNP

MCNP

MCNP is a general-purpose Monte Carlo radiation transport code for modelling the interaction of radiation with materials. MCNPX stands for Monte Carlo N-Particle extended. MCNP is fully three-dimensional in its modelling abilities. The latest nuclear cross-section libraries ship with the code, and the code includes physics models for particle types and energies where tabular data are not available.

MCNPX 2.7.0 (2011) is a Monte Carlo radiation transport code for modelling the interaction of radiation with matter, that is capable of tracking more than 2000 particle types. The forthcoming release of the code is MCNP6, which will probably be released before the end of 2014.

The "number-crunching" parts of MCNP are coded in Fortran-90, while the graphics-generation modules are coded in C++.

MCNPX can model 3-dimensional objects is space in exact or near-exact geometry. The code normally uses point-wise (or so-called "continuous") cross-section data, but can also use multigroup cross-section data. The cross-section data supplied with the code covers the photon energy range from 1 keV to 100 GeV, and the electron energy range from 1 keV to 1 GeV. Most cross-section data libraries shipped with the code covers the neutron energy range from 1E-11 MeV to 20 MeV, but some neutron cross-section libraries extend up to 150 MeV. When MCNPX is requested to model neutron transport at energies where cross-section tabulations are not supplied, the code switches over from using tabular cross-section data, to using nuclear models. This is called the cross-over from table physics to model physics. Using nuclear models in radiation transport instead of the actual evaluated cross-section data, is, of course, not as accurate as using measured, tabular cross-section data.

MCNP code execution

A number of instructions are available to determine how MCNP is to execute the particle tracking.

- NPS n: number of source particles n to be started.
- CTME t: CPU time t to be spent in the Monte Carlo run, in unit minutes.
- IMP: importance with which particles are to be tracked in a particular cell.

- MODE $x\ y\ z\ldots$: Determines which particles to track (default: track only neutrons).
- PRINT : Request printout of specific tabular simulation information in the output file.

In addition there are variance reduction options that can be used to improve the quality of the answer obtained in a given runtime, by forcing more particles to score in the tallies.

MCNP input data card organisation

An MCNP input file must contain descriptions of problem geometry, source and materials. The input file is organized as follows:

- **TITLE CARD**
- **CELL CARDS**
- Blank line
- **SURFACE CARDS**
- Blank line
- **DATA CARDS** — including Source Definition, Material specifications, Tally specification & Execution instructions.

The comment character, c␣, where ␣ indicates a space, is inserted at the beginning of a card to render that card a comment card. Note that at least one space must follow the c, which must be in column 1.

In any card, the first five characters are reserved for the "card name," i.e. the name of the instruction or specification. Lines may not be longer than 80 characters.

A dollar sign $ anywhere in a card changes everything to the right of the $ into an in-line comment.

MCNP cell and surface cards

MCNP enables the user to specify the problem geometry in a general manner, based on defining geometrical regions from all first and second degree surfaces and elliptical tori and then combining them with Boolean operators into cells. This is sometimes termed combinatorial geometry. Surfaces are defined in Surface Cards and Cells are defined in Cell Cards. Each cell is described by a cell number, a material number, a material density, combinatorial geometry parameters and a Cell Importance specification.

In the combinatorial geometry specification in the cell cards, a signed surface number stands for the region on the side of the surface where points have the indicated sense, in a Cartesian

coordinate system. The negative sign signifies a negative sense, while a plus sign signifies a positive sense. Cells are built up using the following Boolean operators:

- Intersection: space
- Union: colon
- Complement: #

Parentheses can be used to control the order of operations. The default order is complement, intersection, union. A number immediately after a complement operator is interpreted as a cell number, and is shorthand for the geometry specification of the corresponding cell.

Cell parameters may be defined appended to the cell description instead of as execution instructions. For example, neutron Importances and cell temperatures might be easier to cross check if they are given within the cell definition block.

Example

```
1   6   -7.2     (+1 -2):(3 -4)     imp:n=1
```

This cell card states that cell number 1 is the union of the spatial volume having a positive sense relative to surface 1, and a negative sense relative to surface two, with the spatial volume having a positive sense relative to surface 3 and a negative sense relative to surface 4. This cell is filled with material number 6, having a density of 7.2 $\mathrm{g\,cm^{-3}}$. Neutrons (and no other particle types) should be tracked, with an importance of 1.

MCNP data cards

The data card section in an MCNP input data set, includes the SDEF source definition card, the source information (SI) and source probability (SP) cards, the material composition cards, tally cards, dose response function cards, execution control cards, printout control cards, and more.

Definitions of radiation sources, which include specification of spatial extension, energy, direction and particle type, may be defined for a variety of sources. Sources that can be specified, are e.g. point sources, area sources, volume sources, multiple sources, etc. The energy of the source particles can be entered as an explicit value such as `erg = 2` or as a distribution, e.g. `erg = d1`, or as function of another variable, e.g.

```
pos = d1
erg = fpos d2
```

.

MCNP Tally types

An MCNP tally is the "answer" that is sought. The user can instruct MCNP to tally for particle fluence-rate across a surface or averaged over a cell volume; energy deposition tallies may also be specified. MCNP tallies are usually normalized to 1 starting particle. Some important tally types are summarised in Table 10.1.

Table 10.1: *Some MCNP tally types.*

Tally code	Description	Units
F1	Number of particles crossing a surface	Particles
F2	Fluence-rate at a surface	$\text{Particles}/\left(\text{cm}^2\ \text{s}\right)$
F4	Fluence-rate averaged in a cell	$\text{Particles}/\left(\text{cm}^2\ \text{s}\right)$
F5	Fluence-rate at a point or ring detector	$\text{Particles}/\left(\text{cm}^2\ \text{s}\right)$
F6	Energy deposition by a specific particle type	MeV/g
+F6	Total energy deposition by all particles	MeV/g

Experience has taught that F5 tallies sometimes do not converge well; tally types F1, F2, F4 and F6 form the backbone of results presented here.

Tally type F6 is very important for the calculation of absorbed doses. F6 tallies are reported in the unit MeV/g; with the correct tally multiplication factor applied, F6 tallies can report doses directly in the dose unit Gy, i.e. $\frac{\text{joule}}{\text{kg}}$. If the source strength is specified on the FM card in the unit particles per second, the unit of an F6 tally will be $\left(\frac{\text{MeV}}{\text{gm s}}\right)$. The multiplication factor that converts the unit $\left(\frac{\text{MeV}}{\text{gm s}}\right)$ to $\left(\frac{\text{joule}}{\text{kg s}}\right)$, i.e. $\left(\frac{\text{Gy}}{\text{hr}}\right)$, is

$$\left(\frac{\left(\frac{\text{MeV}}{\text{gm s}}\right)}{\left(\frac{\text{Gy}}{\text{hr}}\right)}\right) = 5.768 \times 10^{-7}$$

where we used the symbol gm for gram and hr for hour, to conform to the usage in MathCAD[26].

If the source strength is specified on the FM card in the unit of integral particle fluence, the unit of an F6 tally will be $\left(\frac{\text{MeV}}{\text{gm}}\right)$, and the multiplication factor that converts from the default MCNP units $\left(\frac{\text{MeV}}{\text{gm}}\right)$ to the required dose unit $\left(\frac{\text{joule}}{\text{kg}}\right)$, i.e. Gy, is

$$\left(\frac{\left(\frac{\text{MeV}}{\text{gm}}\right)}{\text{Gy}}\right) = 1.602 \times 10^{-10}.$$

[26] In MathCAD, the symbol h refers to Planck's constant, while g refers to the gravitational acceleration at the surface of the earth.

10.1 Discussion of a simple input data set for MCNP

A simple input data set for an MCNP calculation is now shown and explained.

```
Concrete Sphere with 100 Ci Co-60 Source inside
c Cell Cards
1  1  -1.2E-3    -1          imp:p=1      $ Vault Air
2  2  -2.35      -2  +1      imp:p=1      $ Concrete Shield
3  1  -1.2E-3    -3  +2      imp:p=1      $ Surrounding Air
4  0                 +3      imp:p=0      $ External Void = UmWelt
c ============================================================

c ============================================================
c Surface Cards
1  so  +150.0    $ INNER AIR OR
2  so  +200.0    $ CONCRETE OR
3  so  +300.0    $ Outer AirShell OR; start of UmWelt
c ============================================================

c ============================================================
c Data Cards
c Mode: transport photons
mode p
c source definition:
sdef     par = P
         pos = 0  0  0
         erg = D22
c
#        SI22               SP22
         L                  D
         2.505690E+00       2.000000E-08
         2.158570E+00       1.200000E-05
         1.332490E+00       9.998260E-01
         1.173230E+00       9.985000E-01
         8.261000E-01       7.600000E-05
         3.471400E-01       7.500000E-05
         8.288160E-03       4.867420E-09
```

```
        8.287840E-03       3.349000E-09
        8.224590E-03       7.660650E-06
        8.222290E-03       3.906860E-06
        7.435780E-03       6.238820E-05
        7.417820E-03       3.194630E-05
c
c
c Material definitions
c
M1      1000     -0.00100          $ H  in  Air
        6000     -0.01240          $ C  in  Air
        7000     -75.5267          $ N  in  Air
        8000     -23.1781          $ O  in  Air
       18000      -1.2827          $ Ar in  Air
c
c
M2      1000   -0.013     $ H in Ordinary Concrete
        8000   -1.165     $ O in Ordinary Concrete
       11000   -0.040     $ Na in Ordinary Concrete
       12000   -0.010     $ Mg in Ordinary Concrete
       13000   -0.108     $ Al in Ordinary Concrete
       14000   -0.740     $ Si in Ordinary Concrete
       16000   -0.003     $ S in Ordinary Concrete
       19000   -0.045     $ K in Ordinary Concrete
       20000   -0.196     $ Ca in Ordinary Concrete
       26000   -0.030     $ Fe Ordinary Concrete
c
c **** Tally specs *******
fc12 Tally = photon dose-rate at surfaces
f12:p  1  2
fm12   7.3948E+12      $ 100 Ci Co60 source
c  Units: Convert fluence-rate to Sv/hr
#        DE12            DF12
         1.00000E-3      1.08000E-10
         1.00000E-2      2.46600E-10
         1.50000E-2      5.61600E-10
         2.00000E-2      8.10000E-10
         3.00000E-2      1.12680E-9
```

```
4.00000E-2      1.26360E-9
5.00000E-2      1.33200E-9
6.00000E-2      1.40400E-9
7.00000E-2      1.48680E-9
8.00000E-2      1.59840E-9
1.00000E-1      1.86840E-9
1.50000E-1      2.69280E-9
2.00000E-1      3.60000E-9
3.00000E-1      5.43600E-9
4.00000E-1      7.20000E-9
5.00000E-1      8.89200E-9
5.11000E-1      9.07200E-9
6.00000E-1      1.04760E-8
6.62000E-1      1.14120E-8
8.00000E-1      1.34280E-8
1.00000E0       1.61640E-8
1.11700E0       1.76400E-8
1.33000E0       2.01240E-8
1.50000E0       2.20320E-8
2.00000E0       2.69280E-8
3.00000E0       3.51000E-8
4.00000E0       4.21200E-8
5.00000E0       4.82400E-8
6.00000E0       5.40000E-8
6.12900E0       5.47200E-8
8.00000E0       6.69600E-8
1.00000E1       7.92000E-8
1.50000E1       1.09080E-7
2.00000E1       1.37520E-7
3.00000E1       1.85040E-7
4.00000E1       2.23200E-7
5.00000E1       2.59920E-7
6.00000E1       2.95200E-7
8.00000E1       3.52440E-7
1.00000E2       3.96000E-7
1.50000E2       4.68000E-7
2.00000E2       5.14800E-7
3.00000E2       5.79600E-7
```

```
         4.00000E2       6.19200E-7
         5.00000E2       6.48000E-7
         6.00000E2       6.69600E-7
         8.00000E2       7.02000E-7
         1.00000E3       7.23600E-7
         1.50000E3       7.63200E-7
         2.00000E3       7.92000E-7
         3.00000E3       8.35200E-7
         4.00000E3       8.74800E-7
         5.00000E3       9.03600E-7
         6.00000E3       9.28800E-7
         8.00000E3       9.64800E-7
         1.00000E4       9.93600E-7
c
c =====
ctme 5
```

Line-by-line explanation of the MCNP input data set

```
Concrete Room with Co-60 Source
```

This is the title of the MCNP run. Problem title. Title card.

```
c Cell Cards
1  1  -1.29E-3   -1          imp:p=1      $ Vault Air
2  2  -2.35      -2  +1      imp:p=1      $ Concrete Shield
3  1  -1.29E-3   -3  +2      imp:p=1      $ Surrounding Air
4  0                 +3      imp:p=0      $ UmWelt
```

These are the cell cards. The cell cards can only be understood with reference to the surface card section, which follows the cell card section.

Cell 1 is composed of material number 1, which has a density of 1.29E-3 g cm^{-3} (negative densities mean quantity is mass-density in unit g cm^{-3} ; positive densities mean unit is number of atoms per barn.cm. Cell 1 consists of the volume inside surface 1. The importance (imp) of photons (p) inside cell 1, is 1. The $ sign signifies the beginning of an in-line comment; everything to the right of the $ sign, is only a comment.

Cell 2 is composed of material number 2, which has a density of 2.35 g cm^{-3} (negative densities mean quantity is mass-density with unit g cm^{-3} ; positive densities mean unit is number of atoms per barn.cm. Cell 2 consists of the intersection of all space outside surface 1 and inside surface 2. The importance (imp) of photons (p) inside cell 2, is 1. The $ sign signifies the beginning of an in-line comment; everything to the right of the $ sign, is only a comment.

Cell 3 is composed of material number 1, which has a density of 1.29E-3 g cm^{-3} (negative densities mean unit is mass-density in unit g cm^{-3} ; positive densities mean unit is number of atoms per barn.cm. Cell 3 consists of the intersection between all space outside surface 2 and inside surface 3. The importance (imp) of photons (p) inside cell 1, is 1. The $ sign signifies the beginning of an in-line comment; everything to the right of the $ sign, is only a comment.

Cell 4 is a void region with zero importance. The moment a particle enters this region, it is not tracked any more. The comment term, "UmWelt" is a nice, short, descriptive German word that means "the outside world." Some MCNP users call it the "graveyard" or the "external void."

It is not necessary at all to use explicit + signs as above, but it is a useful way of adding clarity to the input data set.

By looking at the surface cards, one now understands that cell 1 is an air-filled sphere with radius 150 cm. Cell 2 is a spherical shell consisting of ordinary concrete; it extends from 150 cm to 200 cm, i.e. the concrete thickness is 50 cm. Cell 3 is the air shell outside the concrete; it extends from radius 200 cm to radius 300 cm. Cell 4 is all space outside spherical radius 300 cm. Particles that enter into this region of space, are not followed (tracked) any more by the Monte Carlo code.

In a Monte Carlo radiation transport calculation, it is important to model a few hundred cm of air outside any shield, because radiation can be backscattered by the air to the "detector" i.e. "receiver" positions. Backscattering media such as walls of rooms, must usually be included in the problem geometry. Always model the problem geometry as realistically as possible.

```
c Surface Cards
1  so  +150.0    $ INNER AIR OR
```

```
2  so  +200.0    $ CONCRETE OR
3  so  +300.0    $ Outer AirShell OR; start of UmWelt
```

A blank line indicates the end of the cell cards and the beginning of the surface cards.

Surface 1 is a sphere (s) centred at the origin (o), hence the surface mnemonic `so`. The radius of surface 1 is 150 cm.

Surface 2 is a sphere (s) centred at the origin (o), hence the surface mnemonic `so`. The radius of surface 2 is 200 cm.

Surface 3 is a sphere (s) centred at the origin (o), hence the surface mnemonic `so`. The radius of surface 3 is 300 cm.

A blank line indicates the end of the surface cards and the beginning of the data cards.

A card starting with a `c` followed by at least 1 blank space, is a comment card.

```
c Mode: transport photons
mode p
```

Photons (particle type “p” in MCNPX or “2” in MCNP5) will be transported. This is the only particle that will be transported.

```
c source definition:
sdef     par = p
         pos = 0 0 0
         erg = d1
c
#        si1          sp1
         L            D
         1.332        1.000
         1.173        0.999
```

The source definition is: The source particle is the photon (p). The source is a point source located at position $x = 0, y = 0, z = 0$. The source energy, i.e. photon energy, is distributed as distribution (d) number 1, denoted as d1. The Source Information (SI) card number 1, i.e. the SI1 card, tells us that energy distribution d1 is a L(ine) distribution, i.e. that there are discrete photon energies. There are 2 discrete line energies in distribution d1: $E_1 = 1.173$ MeV and $E_2 = 1.332$ MeV. The Source Probability (SP) card SP1 states that, in source energy distribution d1, the photon with energy $E_1 = 1.173$ MeV is emitted with an emission yield $y_1 = 0.999$ photons per radioactive transition, while the photon with energy $E_2 = 1.332$ MeV is emitted with an emission yield of $y_2 = 1.000$ photons per radioactive transition event. The # indicates that the SI and SP cards will be specified vertically (in the interest of clarity)—that is, the # indicates that the data is organised in columns. Note that this neat # option only works in versions of MCNP released after ~2004.

```
c Material definitions
m1      7000  -0.79      $ N in dry AIR
        8000  -0.21      $ O in dry AIR
c
m2      1000  -0.013     $ H  in Ordinary Concrete
        8000  -1.165     $ O  in Ordinary Concrete
       11000  -0.040     $ Na in Ordinary Concrete
       12000  -0.010     $ Mg in Ordinary Concrete
       13000  -0.108     $ Al in Ordinary Concrete
       14000  -0.740     $ Si in Ordinary Concrete
       16000  -0.003     $ S  in Ordinary Concrete
       19000  -0.045     $ K  in Ordinary Concrete
       20000  -0.196     $ Ca in Ordinary Concrete
       26000  -0.030     $ Fe in Ordinary Concrete
```

Two materials are defined in this input data set. Material 1 is air, and material 2 is ordinary concrete. The ZAID identity code of an isotope is $(1000Z + A)$. However, this is a photon transport problem and photon energies are very low, far below the threshold for nuclear reactions. At such low energies, photons will only interact according to the laws of quantum electrodynamics, and interaction cross-sections will for all practical purposes only depend on the atomic number Z and not on the mass number, A. In other words, only the identity of the element is important; the specific isotope will not be important. Cross-sections will differ from element to element but not from isotope to

isotope. Example: for interactions by low energy ionising photons, the cross-sections for ^{54}Fe, ^{56}Fe, ^{57}Fe and ^{58}Fe will be identical, for all practical purposes. Therefore the ZAID (Z-A-Identity code) for an element will simply be $1000Z$, because only the atomic number Z and not the mass number A, will be relevant to the radiation transport. (Note that in neutron problems, this is not the case, so that the full ZAID must usually be specified for neutron problems. Note, too, that in neutron transport problems, a ZAID of e.g. 20000 indicates that the isotopic makeup of calcium is the natural abundance of Ca isotopes.)

The negative number following the ZAID, is the mass fraction of the material composed of that element. If the number was positive, it would have designated a number fraction and not a mass fraction.

Water, e.g., can be easily specified as

```
m1    1000 +2
      8000 +1
```

because its chemical formula is H_2O. Similarly, paraffin wax, having the approximate, representative chemical formula $C_{25}H_{52}$, can easily be specified as

```
m1     1000  +52
       6000  +25
```

Note: It is not necessary at all to use an explicit +sign as above, but it is a useful way of adding clarity to the input data set.

```
c Tally specification
fc12 Tally = photon dose-rate at surfaces
f12:p  1  2
fm12   7.4E12      $ 100 Ci source
```

The *tally* is the requested *result i.e. answer* calculated by MCNP. An F2 tally is a surface fluence-rate (older term: "flux") tally. The F2 tally card

```
f12:p  1  2
```

instructs the code MCNP to determine the fluence-rate, in unit $\mathrm{cm}^{-2}\,\mathrm{s}^{-1}$, of photons ("p") that cross surfaces 1 and 2. Note that the last number, i.e. the `2` in the tally name, `f12`, denotes the type of tally. An `F4` tally is a cell volume averaged fluence-rate tally. An `F6` tally is an energy deposition tally, and can be used to determine absorbed dose rate in e.g. the unit Gy/hr, with the appropriate unit conversion factor multiplied into the FM tally multiplication factor. The first number `1` in the tally designation `f12` is simply a counter. Tally designations such as `f12`, `f22`, `f32`, `f42`, `f52` etc will all be F2 tally types, i.e. surface fluence-rate tallies in unit $\mathrm{cm}^{-2}\,\mathrm{s}^{-1}$. It is best to read e.g. `f32` as "tally 3 of type 2" and not as "tally 32."

The `fc12` card is the "tally comment card", i.e. it is simply the "name" of tally `f12`; this tally comment line will be printed in the output data set where the tally results are given for tally `f12` (i.e. "tally 1 of type 2").

The `fm12` card is the tally multiplication card for tally `f12`. In this simple problem, it simply specifies the source activity in unit Bq, multiplied by the total source particle yield per radioactive transition. For a 100 Ci source of ^{60}Co, e.g., the tally multiplication factor is $A \times Y = \left(100 \times 3.7 \times 10^{10}\right) \times (1.000 + 0.999) \approx 7.4 \times 10^{12}$.

```
c  Units: Convert fluence-rate to Sv/hr
DF12   IC=31   IU=2   FAC=1
```

This is the fluence-rate to effective dose-rate response function, also known as the "flux-to-dose conversion factors." The first column contains the photon energies, and the second column contains the conversion factors (dose function values) to convert from fluence-rate to dose-rate in unit Sv/h.

Important: Every ~15 years, the ICRP recommends new sets of radiation weighting factors w_R and tissue weighting factors w_T. The new values of these weighting factors will have a small but definite effect on the values of the fluence-rate to dose-rate conversion factors, because these are calculated for expanded and aligned mono-energetic radiation fields incident upon anthropomorphic calculational phantoms, using codes such as MCNP, FLUKA, GEANT or EGS. Conclusion: one may not can not use the above conversion factors indefinitely. It is very important to continually monitor the scientific literature and the ICRP website for new dose conversion factors. Places to watch: New ANS/ANSI standards, the ICRP website as well as ICRP publications. Also the two journals *Radiation Protection & Dosimetry* and *Health Physics*. New conversion functions were published in (ICRP-116, 2010).

Here the user specifies which tables should be printed in the output file.

```
c === RUNTIME CONTROLS ======
ctme 45
```

Here it is specified that the code MCNP must execute for 45 minutes.

Study *AN MCNP PRIMER* by Shultis & Faw before progressing to the topics below.

Chapter 11:
Preparatory skills for using MCNP

11.1 Beginners beware: common pitfalls

Typical scenario: An MSc student doing a project in radiation transport, performs hundreds of lengthy MCNP calculations. It takes him 4 months of long hours and late-night work to generate results. However, the shield dimensions and material densities in all his input data sets are inaccurate up to 25%, and he also uses outdated cross-section sets and incorrect tally multiplication factors. All his results are therefore useless and must be discarded. All his work must be repeated, and because Monte Carlo calculations take a lot of time, this process will be frustratingly slow.

Conclusion: It is vital to make 100% certain that input data sets are accurate, because Monte Carlo codes require very long runtimes. Double-check every facet of your input data against engineering sketches before submitting long MCNP runs. Talk to experienced experts about the dimensions and material compositions and refine & hone your model before beginning lengthy calculations.

11.2 Mass Fractions and Number Fractions of Nuclides in UO_2, where the Uranium is Enriched

Use the supplied MathCAD worksheet to perform the following calculations:

Assume that $^{16}_{8}O$ is the only isotope of oxygen, and that only ^{235}U and ^{238}U are present in the uranium.

Q.1 Determine the mass-fractions of $^{16}_{8}O$, $^{235}_{92}U$ and $^{238}_{92}U$ in UO_2 with a mass-density of 10.8 $g\,cm^{-3}$, where the uranium is enriched to 4.75%.

Q.2 Determine the mass-fractions of $^{16}_{8}O$, $^{235}_{92}U$ and $^{238}_{92}U$ in UO_2 with a mass-density of 10.8 $g\,cm^{-3}$, where the uranium is enriched to 19.75%.

Q.3 Determine the mass-fractions of $^{16}_{8}O$, $^{235}_{92}U$ and $^{238}_{92}U$ in UO_2 with a mass-density of 10.8 $g\,cm^{-3}$, where the uranium is enriched to 45%.

Q.4 Determine the mass-fractions of $^{16}_{8}O$, $^{235}_{92}U$ and $^{238}_{92}U$ in UO_2 with a mass-density of 10.8 $g\,cm^{-3}$, where the uranium is enriched to 93.7%.

Q.5 Determine the number-fractions of $^{16}_{8}O$, $^{235}_{92}U$ and $^{238}_{92}U$ in UO_2 with a mass-density of 10.8 $g\,cm^{-3}$, where the uranium is enriched to 4.75%.

Q.6 Determine the number-fractions of $^{16}_{8}O$, $^{235}_{92}U$ and $^{238}_{92}U$ in UO_2 with a mass-density of 10.8 $g\,cm^{-3}$, where the uranium is enriched to 19.75%.

Q.7 Determine the number-fractions of $^{16}_{8}O$, $^{235}_{92}U$ and $^{238}_{92}U$ in UO_2 with a mass-density of 10.8 $g\,cm^{-3}$, where the uranium is enriched to 45%.

Q.8 Determine the number-fractions of $^{16}_{8}O$, $^{235}_{92}U$ and $^{238}_{92}U$ in UO_2 with a mass-density of 10.96 $g\,cm^{-3}$, where the uranium is enriched to 93.7%.

11.3 Mass Fractions and Number Fractions of Nuclides in U_3Si_2, where the Uranium is Enriched

Use the MathCAD worksheet

U3Si2 Wet - Isotopic Composition Calculator.xmcd

to perform the following calculations:

Assume that only ^{235}U and ^{238}U are present in the uranium.

Q.9 Determine the mass-fractions of Si, $^{235}_{92}U$ and $^{238}_{92}U$ in U_3Si_2 with a mass-density of 7.0 $g\,cm^{-3}$, where the uranium is enriched to 19.75%, for 0% water ingress.

Q.10 Determine the number-fractions of Si, $^{235}_{92}U$ and $^{238}_{92}U$ in U_3Si_2 with a mass-density of 7.0 $g\,cm^{-3}$, where the uranium is enriched to 19.75%, for 40% water ingress.

11.4 Mesh tally plot generation in MCNP

- Execute MCNP, specifying an input data file that contains a tmesh…endmd data block that defines the mesh tally. In the command-line, specify an explicit file-name for the "runtape" file, such as e.g. R=CASE01.R .
- Activate an X-Windows Server if necessary, to enable plotting to the screen under MS-Windows.
- Once the calculational run is finished, enter the following at the command prompt: MCNP Z R=CASE01.R . The "runtape" CASE01.R will now be read.
- A MCNP plot prompt will appear in the "DOS box" you are working in. Type PLOT after the **MCPLOT>** prompt, after having activated X-Windows Server .
- Maximise the plot window, switch off the surface and cell number display, adjust the scale, etc.
- Click on **tal** in lower right corner of plot window.
- Toggle **COLOR** to **COLOR tal** .
- If there are multiple mesh-tallies in the tmesh…endmd data block, click on **tal** and then as many times as is necessary on the **n** in lower right corner of the plot window, to select the specific mesh-tally that must be graphically displayed.
- **Redraw** .
- Use the interactive utility program GRIDCONV to convert the binary mdata mesh-tally data file to an ASCII file, if necessary.

Note: Regions of space without cell lines will not display properly on the plot.

Chapter 12:
Case Studies:
Radiation Shielding & Dose Distributions

12.1 Case Study RSDD-1: Point source in a room

A point source of 1 Ci (3.7E10 Bq) ^{60}Co is located at the centre of a room with ordinary concrete walls. The concrete thickness is 30 cm.
Approximate the problem in spherical-symmetrical geometry. Leave 150 cm of air between the point source and the inner surface of the concrete wall.

- Calculate the ionising photon fluence-rate on the outer surface of the concrete shield.
- Calculate the effective dose rate on the outer surface of the concrete shield.
- Calculate the photon energy spectrum where the photons enter into the inside of the concrete shield, and plot it as a histogram.
- Calculate the photon energy spectrum where it emerges from the outer concrete surface, and plot it as a histogram.
- Analyse the photon energy spectrum calculated by MCNP. Calculate the average photon energy $\langle E \rangle$ at the inner surface, as well as the average photon energy $\langle E \rangle$ at the outer surface of the concrete shield. Does the photon spectrum become "harder" or "softer" with transport through the concrete shield? Explain the observed phenomenon with reference to the physics of ionising photon interactions.
- Calculate the effective dose rate from a distance about 50 cm from the source, in steps of about 10 cm, up to a radius about 50 cm outside the outer surface of the concrete shielding wall. Plot the effective dose rate as a function of radius.
- On the same plot, also show what the dose rate would be with no concrete shield in place.
- Plot the dose attenuation factor (DAF) as a function of radius.

Solution: Case Study RSDD-1

The source definition cards need to specify a point source of ^{60}Co at the centre of the geometry. Photons must be transported, i.e. a `mode p` run must be performed.

```
mode p
sdef par=p erg=d1 pos=0 0 0
```

```
si1 L  1.173  1.332
sp1    0.999  1.000
```

The source definition (SDEF) is: The source particle is the photon (p). The source is a point source located at position $x = 0$, $y = 0$, $z = 0$, hence pos=0 0 0. The source energy, i.e. photon energy, is distributed as distribution (d) number 1, denoted as d1. The Source Information (SI) card number 1, i.e. the SI1 card, tells us that energy distribution d1 is a L(ine) distribution, i.e. that there are discrete photon energies. There are 2 discrete line energies in distribution d1: $E_1 = 1.173$ MeV and $E_2 = 1.332$ MeV. The Source Probability (SP) card SP1 states that, in source energy distribution d1, the photon with energy $E_1 = 1.173$ MeV is emitted with an emission yield $y_1 = 0.999$ photons per radioactive transition, while the photon with energy $E_2 = 1.332$ MeV is emitted with an emission yield of $y_2 = 1.000$ photons per radioactive transition event.

The surface cards are:

```
c Surface Cards
1  SO   +150.0     $ INNER AIR OR
2  SO   +180.0     $ CRT WALL OR
3  SO   +500.0     $ Outer AirShell OR; start of UmWelt
```

The cell cards are

```
c Cell Cards
1  1  -1.205E-3   -1        imp:p=1   $ Chamber Air
2  2  -2.35       -2   +1   imp:p=1   $ Concrete
3  1  -1.205E-3   -3   +2   imp:p=1   $ Surrounding Air
4  0                   +3   imp:p=0   $ UmWelt
```

A surface dose-rate tally is evaluated at surfaces 1 and 2. The tally result is multiplied by the activity of the source, in unit Bq $\times$ {total photon yield}.

```
fc12 Tally: photon effective dose-rate
f12:p  1   2
fm12   7.4E10      $ 1 Ci Co-60
```

Because a response function is defined with the same number as this tally's number, i.e. 12, i.e. tally 1 of type 2,

```
#      de12     df12
```

the interpolated response function will be calculated and the fluence-rate $\phi(E)$ will be "folded" with the response function $\Re(E)$ to calculate the dose rate integral,

$$R(r) = \int_{E_{\min}}^{E_{\max}} \phi(r, E)\, \Re(E)\, dE$$

The second tally specification is:

```
fc22 Photon fluence-rate & eng-spectrum tally
f22:p  1  2
e22    0.01  0.10  0.20  0.30  0.40  0.50  &
       0.60  0.70  0.80  0.90  1.00  1.10  &
       1.15  1.20  1.25  1.30  1.50
fm22   7.4E10
```

Explanation of tally 22: The designation 22 means "tally number 2 of type 2." A surface fluence-rate tally (type 2) is evaluated at surfaces 1 and 2. The tally result is multiplied by the activity of the source, in unit Bq, multiplied by the total photon yield per radioactive transition, i.e. $2 \times 3.7\text{E}10 = 7.4\text{E}10$. The spectrum is binned according to the energy partition specified in card e22. The lowest specified energy bin boundary in card E22 is 0.01 MeV. This specifies a lowest energy bin with lower energy E_{cut} and upper energy boundary 0.01 MeV, where E_{cut} is the energy below which photons are no longer transported, i.e. 0.001 MeV (default). The energy bin boundaries, plus the additional implicit lowest bin boundary, serves as integration boundaries for tallying to evaluate stochastic approximations to integrals of the form $\int_{E_{\text{low}}}^{E_{\text{high}}} \phi(E)\, dE$.

The complete input data set for MCNP is:

```
Point Source of Co-60 in a room
c Cell Cards
1  1   -1.205E-3   -1        imp:p=1   $ Chamber Air
2  2   -2.35       -2   +1   imp:p=1   $ Concrete
3  1   -1.205E-3   -3   +2   imp:p=1   $ Surrounding Air
4  0                    +3   imp:p=0   $ UmWelt

c Surface Cards
1  SO   +150.0     $ INNER AIR OD
2  SO   +180.0     $ CRT WALL OD
3  SO   +500.0     $ Outer AirShell OD; start of UmWelt

c Data Cards
mode p
c
sdef par=p erg=d1 pos=0 0 0
si1 L  1.173  1.332
sp1    0.999  1.000
c
c Material definitions
m1   6000  -1.24E-4    &   $ Air, dry.  Density = 1.205E-03 g/cc
     7000  -0.755267   &   $ Air, dry.  Density = 1.205E-03 g/cc
     8000  -0.231781   &   $ Air, dry.  Density = 1.205E-03 g/cc
    18000  -0.012827       $ Air, dry.  Density = 1.205E-03 g/cc
c
m2    1001  -0.013    &   $ Ordinary Concrete
      8016  -1.165    &   $ Ordinary Concrete
     11023  -0.040    &   $ Ordinary Concrete
     12000  -0.010    &   $ Ordinary Concrete
     13027  -0.108    &   $ Ordinary Concrete
```

```
    14000  -0.740    &   $ Ordinary Concrete
    16000  -0.003    &   $ Ordinary Concrete
    19000  -0.045    &   $ Ordinary Concrete
    20000  -0.196    &   $ Ordinary Concrete
    26000  -0.030        $ Ordinary Concrete
c
c **** Physics Table *****
phys:p   10   &   $     Emax
          0   &   $     0 always (generate el in MODE e calcs)
          0   &   $     0 always (Coherent/Thomson scattering on)
         -1   &   $    -1 always (photonuclear reaction on)
          1   &   $     1 always (1 = Doppler broadening off)
       -102       $  -102 ALWAYS
c
fc12 Tally: photon effective dose-rate
f12:p  1   2   3
fm12   7.4E10      $ 1 Ci Co-60
c
DF12   IC=31   IU=2   FAC=1c
c
fc22 Photon fluence-rate & eng-spectrum tally
f22:p  1  2  3
e22    0.01  0.10  0.20  0.30  0.40  0.50  0.60  0.70  0.80  0.90  &
       1.00  1.10  1.15  1.20  1.25  1.30  1.35  1.50
fm22   3.7E10
c ==== PRINT CONTROLS =====
PRINT 10 40 50 60 72 100 110 120 170 200
c === RUNTIME CONTROLS ======
ctme 10
```

The fluence-to-dose conversion function to convert photon fluence-rate to dose-rate, is specified as follows:

```
DF12   IC=31   IU=2   FAC=1c
```

Note that it is not necessary to specify isotopes in the material cards, because this is a photon transport problem. More care is needed to specify materials for neutron transport problems, because neutrons are hadrons on account of having a quark substructure, and therefore interact via the strong nuclear interaction, the Hamiltonian of which differs markedly from isotope to isotope, and not merely from element to element.

Results

The calculated effective dose rate at the outer surface of the concrete wall, is 1.44E-04 Sv/h, and the relative standard error is 0.0015. This indicates excellent problem convergence.

The calculated total photon fluence-rate at the outer surface of the concrete wall, is 1.49989E+04 $cm^{-2}\,s^{-1}$, and the relative standard error is 0.0017. This indicates excellent problem convergence.

On a unit lethargy scale, the photon energy spectrum looks as follows:

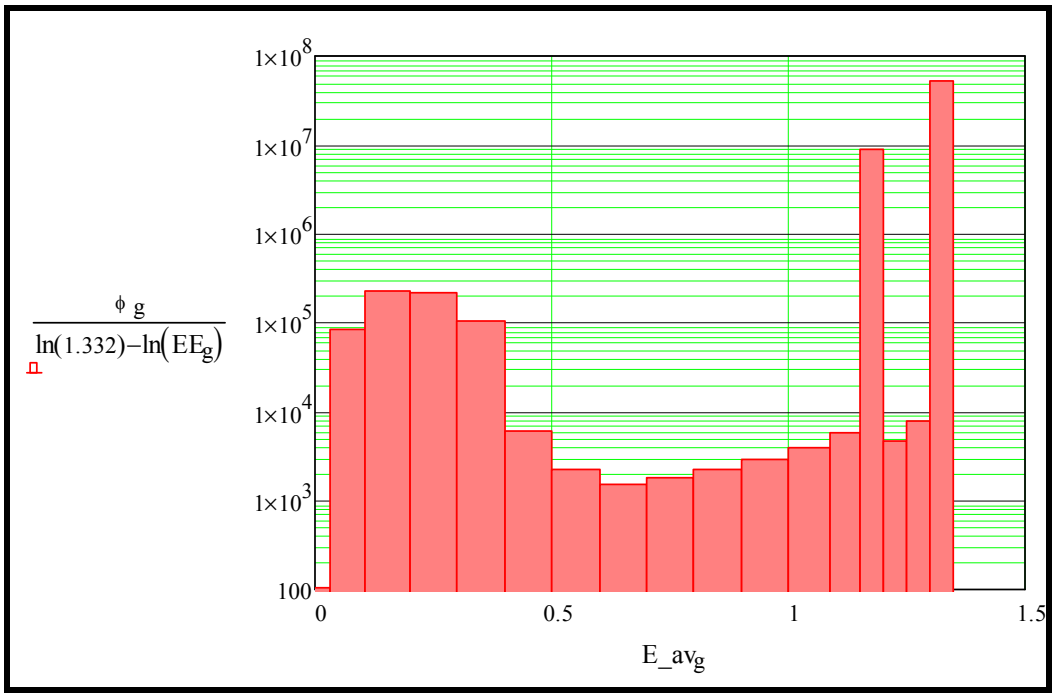

The source lines are still very prominent, but backscattering out of the concrete has contributed a sizable amount of low-energy photons.

The average photon energy (MeV) on the entrance side of the shield, is,

$$\frac{\int_{\min(EE)}^{\max(EE)} E\cdot\phi\phi\ (E)\ dE}{\int_{\min(EE)}^{\max(EE)} \phi\phi\ (E)\ dE} = 0.604$$

On the **exit side of the concrete,** the photon spectrum, in unit lethargy, looks as follows,

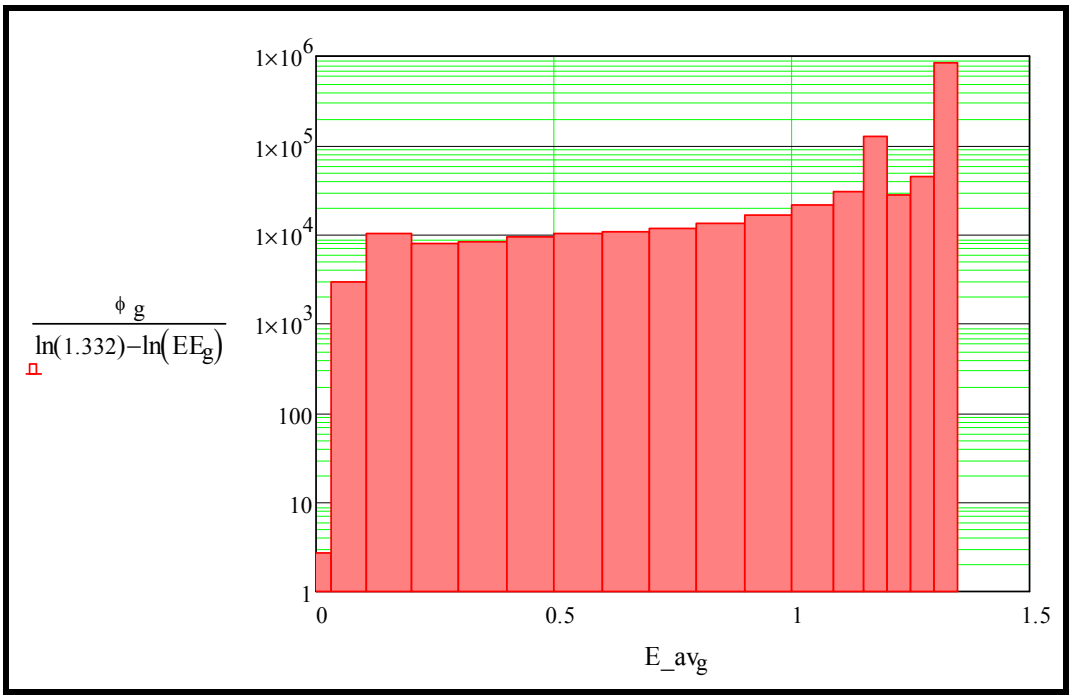

The two uncollided source peaks are less prominent than on the inside surface of the shield — many scattering interactions diminished the relative fluence-rate of uncollided photons.

The average photon energy (MeV) on the exit side of the shield, is slightly lower, at,

$$\frac{\int_{\min(EE)}^{\max(EE)} E\cdot\phi\phi\ (E)\ dE}{\int_{\min(EE)}^{\max(EE)} \phi\phi\ (E)\ dE} = 0.548$$

12.2 Case study RSDD-2: Ionising photon sources of different geometries in a room with concrete walls

There are various 3.7×10^{12} Bq (i.e. 100 Ci) sources of ^{60}Co present close to the centre of a rectangular room with internal dimensions 300 cm $\times$ 300 cm $\times$ 220 cm high. Roof, floor and walls are all 30 cm thick ordinary concrete.

Model the following source geometries, one by one, i.e. one after the other: Make Co the source material.

- Spherical source, $R = 4$ cm;
- Cylindrical source, $R = 2$ cm and $H = 10$ cm along the $+z$ direction;
- Rectangular source of 5 cm $\times$ 4 cm $\times$ 3 cm in the xyz directions, with the origin at the centre of the bottom face of the source volume.

Now calculate the following:

- The ***effective*** dose rate from ionising photons at (1) a point-tally and (2) in a tally-cell about 30 cm outside a chosen wall, opposite the source position.
- The ***absorbed*** dose rate from ionising photons in a tally-cell about 30 cm outside a chosen wall, opposite the source position.

Solution: Case Study RSDD-2

The cell cards and surface cards are:

```
1 1  -1.205e-3   -1  +5      IMP:P=1   $ AIR
2 2  -2.35       -2  +1      IMP:P=1   $ CRT
3 1  -1.205e-3   -3  +2  +4  IMP:P=1   $ AIR
4 3  -1.0        -4          IMP:P=1   $ TEHP
5 4  -8.746      -5          IMP:P=1   $ Cobalt sphere
6 0                  +3      IMP:P=0   $ VOID
c ============

c ============
c Surface cards
1 RPP  -150  +150     -150  +150     +0   +210
2 RPP  -180  +180     -180  +180    -30   +240
3 RPP  -900  +900     -900  +900   -900   +900
4 RCC  +200  0  0      0  0  170      +11.5
5 SPH  0 0 80   10
```

The source definition card for a cylindrical ^{60}Co volume-source with a height of 30 cm, the (x, y, z) coordinate of the base-centre at $(0, 0, 80)$ cm, and a radius of 10 cm is as follows:

```
c source definition: CYLINDRICAL VOLUME ALONG Z-AXIS
sdef  par=p erg=d3 cel=5  EFF=1E-9
      pos=0 0 80 axs=0 0 1  ext=d1  rad=d2
si1 h  0.0  30.0
sp1 d -21  0
si2 h  0.0   10
sp2 d -21  1
si3 L  1.173  1.332
sp3 d  0.999  1.000
```

The z-variable is sampled uniformly as $\frac{\partial}{\partial z}[V(r,z)] = \frac{\partial}{dz}\left(\pi z r^2\right) \propto z^{1-1} = z^0$, as per the power law specification `sp1 d -21  0`.
The radial variable r is sampled as $\frac{\partial}{\partial r}[V(r,z)] = \frac{\partial}{dr}\left(\pi z r^2\right) \propto r^{2-1} = r^1$, as indicated by the power law `sp2 d -21  1`.

The source definition card for a spherical ^{60}Co volume-source, with a radius of 10 cm and its origin at $(x, y, z) = (0, 0, 80)$ cm is as follows:

```
c source definition: SPHERICAL VOLUME SOURCE
sdef  par=p erg=d2
      pos=0 0 80  rad=d1
si1 h  0.0   10.0
sp1 d -21  2
```

```
si2 L  1.173  1.332
sp2 d  0.999  1.000
```

The radial variable r is sampled as $\frac{\partial}{\partial r}[V(r,z)] = \frac{\partial}{dr}\left(\frac{4}{3}\pi r^3\right) \propto r^{3-1} = r^2$, as indicated by the power law `sp2 d -21  2`.

The SDEF card for a Cartesian volume-source of spatially uniform intensity stretching from $x = -15$ cm to $x = +15$ cm, from $y = -15$ cm to $y = +15$ cm, and from $z = -15$ cm to $z = +15$ cm, is as follows:

```
c source definition: CARTESIAN VOLUME
sdef   par = p
       x   = d1
       y   = d2
       z   = d3
       erg = d4
si1 h  -15.0  +15.0
sp1 d  0  1
c
si2 h  -15.0  +15.0
sp2 d  0  1
c
si3 h  -15.0  +15.0
sp3 d  0  1
c
#      SI4      SP4
       L        D
       1.173    0.999
       0.999    1.000
```

The tally definitions are as follows:

```
c **** Tallies *******
c
fc15 Point tally for photon effective dose-rate
f15:p  +200  0  +80    +1   ND
fm15   7.4E12     $ 100 Ci Co-60
c
fc16 Tally: ABSORBED photon dose-rate
+f16  4
fm16  4.2661E6      $ 100 Ci Co-60, dose-rate in unit Gy/hr
c
c Mesh tally
tmesh
 rmesh11:p
  cora11  +179.9          +180
  corb11  -200      99i   +200
  corc11     0      74i   +300
endmd
```

Tally f15:p defines a point-detector located at $(x, y, z) = (200, 0, 80)$ cm, with an exclusion-radius of 1 cm and with (potentially confusing) superfluous printout suppressed via the ND specification. The tally multiplication factor ("TMF") of 7.4E12 is equal to the activity A of the radionuclide source, expressed in the unit Bq, multiplied by the total ionising photon emission yield of $\sum_i y_i = 1.999$ emissions per radioactive transition, i.e.

$$\text{Tally multiplication factor} = A \times \sum_i y_i \, .$$

Tally F16 specifies a cylinder-phantom outside the room. The tally number ends with "6" which signifies that it is an energy-deposition tally. The specification +f16 4 means that energy deposition by *all* particles inside the volume of cell 4 must be counted. The tally multiplication factor **4.2661E6 is** $\left[A \times \sum_i y_i \times c_d \right]$, where A is the activity of the radionuclide source in Bq, $\sum_i y_i$ is the total emission yield of ionising photons, and the conversion factor c_d converts from energy deposition rate expressed in the code MCNP's units of $\left(\frac{\text{MeV}}{\text{g.s}}\right)$, to the standard units $\left(\frac{\text{Gy}}{\text{hr}}\right)$ in which absorbed dose rate is normally reported; this conversion factor has the value $c_d = 5.768 \times 10^{-7}$. Note that $1\,\text{Gy} = 1\,\frac{\text{joule}}{\text{kg}}$.

The response function $\mathfrak{R}(E)$ is specified as follows:

```
DF15    IC=31    IU=2    FAC=1
```

Tally F15 is modified by this response function, because the tally number "15" is post-fixed to the DF. The specification IU=2 specifies that the response must be calculated in Sv/h, while IC=31 specifies that the ANS/ANSI 1991 fluence to dose function for Anterior-Posterior (AP) exposure geometry must be used.

Mesh-tally 11,

```
tmesh
 rmesh11:p
  cora11  +179.9        +180
  corb11  -200    99i   +200
  corc11     0    74i   +300
endmd
```

is a fluence-rate mesh tally in a rectangular, i.e. a Cartesian grid. This mesh-tally evaluates the dose rate profile across the outer surface of one wall in a rectangular grid. The mesh is in the yz-plane. In the x-direction, fluence-rates are evaluated over the last 1 mm of the outer part of the wall, stretching from $x = 179.9$ cm to 180.0 cm. In the y-direction, the mesh stretches from -200 cm to $+200$ cm and the mesh interval size is $\frac{(200-(-200))}{100}$ cm $= 4$ cm. In the z-

direction, the mesh stretches from 0 cm to +300 cm and the mesh interval size is $\frac{300}{75}$ cm = 4 cm.

The 2-D mesh-tally plot is obtained by running MCNPX, then typing MCNPX Z R = runtpe at the command line, and typing PLOT at the MCPLOT> prompt. To convert the binary mdata mesh-tally file produced by the code to an ASCII file, ready for importation into a graphics package, the interactive utility program GRIDCONV is executed.

12.3 Case study RSDD-3: Tenth-value thicknesses

Definition: The tenth-value thickness of a shielding material and a given source of ionising photons, is thát thickness of shielding material that will reduce the transmitted dose rate by a factor 10, compared to the reference case where there is no shielding material present.

Problem: Determine the tenth value thicknesses for the shielding of the ionising photons emitted by ^{60}Co, for the following shielding materials:

- U $\left(\text{Depleted Uranium (DU); } Z = 92; \rho = 18.9\ \text{g cm}^{-3}\right)$;
- W $\left(\text{Tungsten; } Z = 74; \rho = 19.6\ \text{g cm}^{-3}\right)$;
- Tungsten alloy containing 92% W and 8% Cu ($Z = 29$) by mass, having $\rho = 17.5$ g cm^{-3};
- Pb $\left(\text{Lead; } Z = 82; \rho = 11.35\ \text{g cm}^{-3}\right)$;
- Fe $\left(Z = 26; \rho = 7.86\ \text{g cm}^{-3}\right)$;
- Al $\left(Z = 13; \rho = 2.7\ \text{g cm}^{-3}\right)$;
- Ordinary concrete $\left(\rho = 2.35\ \text{g cm}^{-3}\right)$;
- Water $\left(\text{H}_2\text{O}; \rho = 1\ \text{g cm}^{-3}\right)$.

Solution: Case Study RSDD-3

Solution: Case Study RSDD-3

The complete input data set is as follows. A simple spherical-symmetrical geometry is used. The point source is surrounded by 100 cm air, which is surrounded by the shielding material. At about 200 cm from the source at the origin, there is a 1 cm thick layer of tissue-equivalent material (TEM), in which the absorbed dose rate is calculated. The tally specification **+f16 4** means that the total absorbed dose rate in cell 4, i.e. the TEM detector shell, will be determined by the F6 type tally, i.e. an energy deposition tally. The mass-density of the TEM detector is given a low value, so as not to perturb the fluence-rate excessively. The tally multiplication factor **fm12 1E6** is arbitrary, because only ratios between dose rates, and not the dose rate values *per se,* are important.

Note the blank line between the cell card section and the surface card section, and again between the surface card section and the data card section.

```
Tenth-Value Thickness ("TVT") Calculation
c Cell Cards
01    1    -1.205E-3    -1       imp:p=1   $ Air
02    6   -11.35        -2  +1   imp:p=1   $ Shield
```

```
03    1    -1.205E-3    -3  +2   imp:p=1   $ Air
04   10    -0.01        -4  +3   imp:p=1   $ TEM Detector
05    1    -1.205E-3    -5  +4   imp:p=1   $ Air
06    0                     +5   imp:p=0   $ UmWelt
c ======

c ======
c Surface Cards
01  so  200.0        $ OR, inner air
02  so  204.5        $ OR, Shield layer
03  so  299.5        $ OR, Air
04  so  300.5        $ OR, TEM Detector
05  so  350.0        $ OR, surrounding air layer
c ======

c ======
c Data Cards
c Mode: transport photons
mode p e
c source: Isotropic point source of photons at origin
sdef par=p erg=d1 pos=0 0 0
si1  L  1.173  1.332
sp1     0.999  1.000
c
c Material definitions
m1     6000    -1.24E-4             $ Air, dry.  Density = 1.205E-03 g/cc
       7000    -0.755267            $ Air, dry.  Density = 1.205E-03 g/cc
       8000    -0.231781            $ Air, dry.  Density = 1.205E-03 g/cc
      18000    -0.012827            $ Air, dry.  Density = 1.205E-03 g/cc
c
m2     1000    +2
       8000    +1                   $ Water
c
m3     1000    -0.013               $ Type 04 Ordinary Concrete
       8000    -1.165               $ Type 04 Ordinary Concrete
      11000    -0.040               $ Type 04 Ordinary Concrete
      12000    -0.010               $ Type 04 Ordinary Concrete
      13000    -0.108               $ Type 04 Ordinary Concrete
      14000    -0.740               $ Type 04 Ordinary Concrete
      16000    -0.003               $ Type 04 Ordinary Concrete
      19000    -0.045               $ Type 04 Ordinary Concrete
      20000    -0.196               $ Type 04 Ordinary Concrete
      26000    -0.030               $ Type 04 Ordinary Concrete
c
m4    13000    -1.0                 $ Aluminium (density = 2.7 g/cc)
c
m5    26000    -1.0                 $ Iron (density = 7.86 g/cc)
c
m6    82000    -1.0                 $ Lead (density = 11.35 g/cc)
c
m7    74000    -1.0                 $ Tungsten (density = 19.6)
c
m8    92000    -1.0                 $ Depleted Uranium (density = 18.9 g/cc)
c
m9    74000     -0.92               $ 92%W-8%Cu alloy
      29000     -0.08               $ 92%W-8%Cu alloy
c
m10    8000    -6.143E-01           $ TEM = Tissue-Equivalent Material
```

```
       6000    -2.286E-01           $ TEM = Tissue-Equivalent Material
       1000    -1.000E-01           $ TEM = Tissue-Equivalent Material
       7000    -2.571E-02           $ TEM = Tissue-Equivalent Material
      20000    -1.429E-02           $ TEM = Tissue-Equivalent Material
      15000    -1.114E-02           $ TEM = Tissue-Equivalent Material
      19000    -2.000E-03           $ TEM = Tissue-Equivalent Material
      16000    -2.000E-03           $ TEM = Tissue-Equivalent Material
      11000    -1.429E-03           $ TEM = Tissue-Equivalent Material
      17000    -1.357E-03           $ TEM = Tissue-Equivalent Material
      12000    -2.714E-04           $ TEM = Tissue-Equivalent Material
      26000    -6.000E-05           $ TEM = Tissue-Equivalent Material
c
c ====
fc16 Absorbed photon dose-rate in TEM Detector
+f16    4
fm12    1E6
c ====
PRINT  10  40  50  60  72  100  110  120  170  200
c
ctme 15
```

Tenth-value thickness calculations inevitably involve quite a bit of trial and error. Graphic representation of results will enable one to home in onto the correct value more quickly.

12.4 Case study RSDD-4: Dose rate around a steel drum filled with radioactive waste

There is 10 Ci of radioactive waste in a standard 210 litre RadWaste drum with a steel wall.

Drum dimensions & mass:

$H = 85$ cm
$R = 28$ cm
Steel thickness: 0.125 cm
Total mass of filled drum: 91 kg
Density of steel: 7.86 g cm^{-3}
Mass of empty drum: 19.5 kg.

Given: The fission product ^{137}Cs is the only radionuclide present in the drum. Assume that it is uniformly and homogeneously distributed in a CH_2 matrix, having a density calculable from the mass & dimensions of the drum. ^{137}Cs emits an ionising photon with $E_\gamma = 0.662$ MeV, with an emission yield of $Y = 0.85$.

Calculate the effective dose rate 10 cm from the outer surface of the drum, at the axial height $z = H/2$. (Important: Which type of F5 tally will you use?)

Solution: Case Study RSDD-4

```
RadWaste in a Drum
c CELL CARDS
1  3   -0.339       -1           IMP:P=1      $ CH2 drum-fill
2  2   -7.86        -2  +1       IMP:P=1      $ Steel wall of drum
3  4   -2.35        -3           IMP:P=1      $ Concrete floor
4  1   -1.205E-3    -4  +2 +3    IMP:P=1      $ Air surround
5  0                   +4       IMP:P=0      $ UmWelt
c ============

c ============
c Surface cards
1 RCC     0   0    0.125     0   0   +84.75   +27.875 $ Drum inner
2 RCC     0   0    0         0   0   +85      +28     $ Drum outer
3 RCC     0   0  -50         0   0   +50    +9000     $ Floor
4 RCC     0   0  -50         0   0 +9900    +9900     $ Air surround
c =============

c =============
c Data Cards
c Mode: transport photons
mode p
c source definition: CYLINDRICAL VOLUME ALONG Z-AXIS
sdef  par=p
      erg=d3
      cel=1
      pos=0 0 1
      axs=0 0 1
      ext=d1
```

```
      rad=d2
c
si1 h  0  85
sp1 d -21  0
c
si2 h  0  28
sp2 d -21  1
c
#       SI3         SP3
        L           D
        0.662       0.850
c =====
c Material definitions
m1      6000  -1.24E-4      $ Air, dry.  Density = 1.205E-03 g/cc
        7000  -0.755267     $ Air, dry.  Density = 1.205E-03 g/cc
        8000  -0.231781     $ Air, dry.  Density = 1.205E-03 g/cc
       18000  -0.012827     $ Air, dry.  Density = 1.205E-03 g/cc
c
m2     26000  +1            $ Fe, pure
c
m3      1000  +2            $ CH2
        6000  +1            $ CH2
c
m4      1000  -0.013        $ Concrete, ordinary, NBS type 04
        8000  -1.165        $ Concrete, ordinary, NBS type 04
       11000  -0.040        $ Concrete, ordinary, NBS type 04
       12000  -0.010        $ Concrete, ordinary, NBS type 04
       13000  -0.108        $ Concrete, ordinary, NBS type 04
       14000  -0.740        $ Concrete, ordinary, NBS type 04
       16000  -0.003        $ Concrete, ordinary, NBS type 04
       19000  -0.045        $ Concrete, ordinary, NBS type 04
       20000  -0.196        $ Concrete, ordinary, NBS type 04
       26000  -0.030        $ Concrete, ordinary, NBS type 04
c
c **** Tallies *******
c
fc15 Ring-tally: photon effective dose-rate
f15z:p  +42.5  +38  +1   ND    $ Ring-tally @ H = 42.5cm & R = 38cm
fm15    3.145E11              $ 10 Ci Cs-137
c
c ======
c  Fluence-rate to dose-rate conversion factors: photons
c  Convert fluence-rate to effective dose in Sv/hr
DF12  IU=2  FAC=1  IC=31
c
c === RUNTIME CONTROLS ======
ctme 30
```

Note that cell-rejection is used in the source-definition:

```
sdef  par=p erg=d3 cel=1
      pos=0 0 1   axs=0 0 1   ext=d1   rad=d2
si1 h  0  85
sp1 d -21  0
```

```
si2 h  0  28
sp2 d -21  1
```

Sampled points (z, r) are only accepted if they lie inside | cell 1 |. Therefore it does not matter that the sampling in the axial, i.e. the z-variable, stretches from 0 cm to 85 cm, instead of the correct 0.125 cm to 84.75 cm — z-values between 0 and 0.125 and between 84.75 and 85 will be rejected based on the cell-rejection criterion | cell = 1 |.

After having generated 22E6 source γ-photons, the problem converged to very high accuracy to an absorbed dose rate of | | Sv/h, i.e. | | mSv/h. The standard error is very low, the variance of the variance | vov | is | |, and the figure of merit | fom | has a good, high value.

To develop a feeling for the magnitude of a calculated dose rate, use the following chart, as well as the fact that the external natural background dose rate (from cosmic and terrestrial radiation) on the surface of the earth is approximately 0.11 μSv/h, i.e. 1.1E-7 Sv/h.

Staytime guidelines for radiation work

Dose rate @ eyes, chest, abdomen	Maximum worktime per day	Contact dose rate @ hands	Maximum worktime per day
10 µSv/h	10 hours	200 µSv/h	6 hours
20 µSv/h	5 hours	400 µSv/h	3 hours
30 µSv/h	3 hour 20 min	600 µSv/h	2 hours
40 µSv/h	2 hour 30 min	800 µSv/h	1.5 hours
50 µSv/h	2 hours	1 mSv/h	1.25 hours
70 µSv/h	1 hour 25 min	2 mSv/h	40 minutes
100 µSv/h	60 minutes	3 mSv/h	25 minutes
200 µSv/h	30 minutes	4 mSv/h	20 minutes
300 µSv/h	20 minutes	5 mSv/h	15 minutes
400 µSv/h	15 minutes	7 mSv/h	10 minutes
500 µSv/h	12 minutes	10 mSv/h	7.5 minutes
$\geq$ 1 mSv/h	RS job coverage	$\geq$ 15 mSv/h	RS job coverage
$\geq$ 2 mSv/h	RS to judge	$\geq$ 100 mSv/h	Work prohibited

Instructions

1. Important: This table does **NOT** apply to **PREGNANT radiation workers.**
   As a general rule, **pregnant radiation workers** may **NOT** work where dose rates are likely to exceed ~10 μSv/h.

2. Two dose rate measurements are needed to calculate the time budget for a day/shift. Reason: there are separate dose limits for "whole-body" dose and hand dose.

3. The dose rate on the left, in the "red" part of the table, refers to a measurement at the position of the trunk & abdomen.

4. The dose rate on the right, in the "blue" part of the table, refers to a measurement at the position of the hands.

5. Read off the two prescribed allowed work-times, using interpolation and sound judgement as necessary. Choose the more restrictive of the two work-times and do not exceed this.

The calculated dose rate 10 cm from the curved, cylindrical part of the outer surface of the RadWaste drum is [ ] mSv/h. Using the above table, it is seen that a registered radiation worker will normally NOT be allowed to come this close to the drum, because the dose rate is prohibitively high.

We conclude that a standard steel RadWaste drum containing 10 Ci, i.e. 3.7E11 Bq ^{137}Cs, will be surrounded by a dangerously high radiation field. In fact, such a high activity of ^{137}Cs may normally not be disposed of in a steel RadWaste drum, but only in a high-density concrete RadWaste drum with an inner stainless steel liner. Standard steel RadWaste drums are used for the disposal of Low Level Waste (LLW), while standard concrete drums are used for the storage and disposal of Intermediate Level Waste (ILW). Waste Acceptance Criteria (WAC) for RadWaste repositories such as Vaalputs, normally only accept steel RadWaste drums if the contact dose rate next to the drum is below 0.2 mSv/h, i.e. 200 µSv/h.

12.5 Case study RSDD-5: Dose rate around a high-density concrete drum filled with intermediate-level RadWaste (ILW)

An activity of 1 kCi, i.e. 3.7×10^{13} Bq, of RadWaste is stored inside a high-density concrete RadWaste drum, shown in Figure 1. Calculate the maximum effective dose rate 10 cm from the lateral surface of the concrete drum.

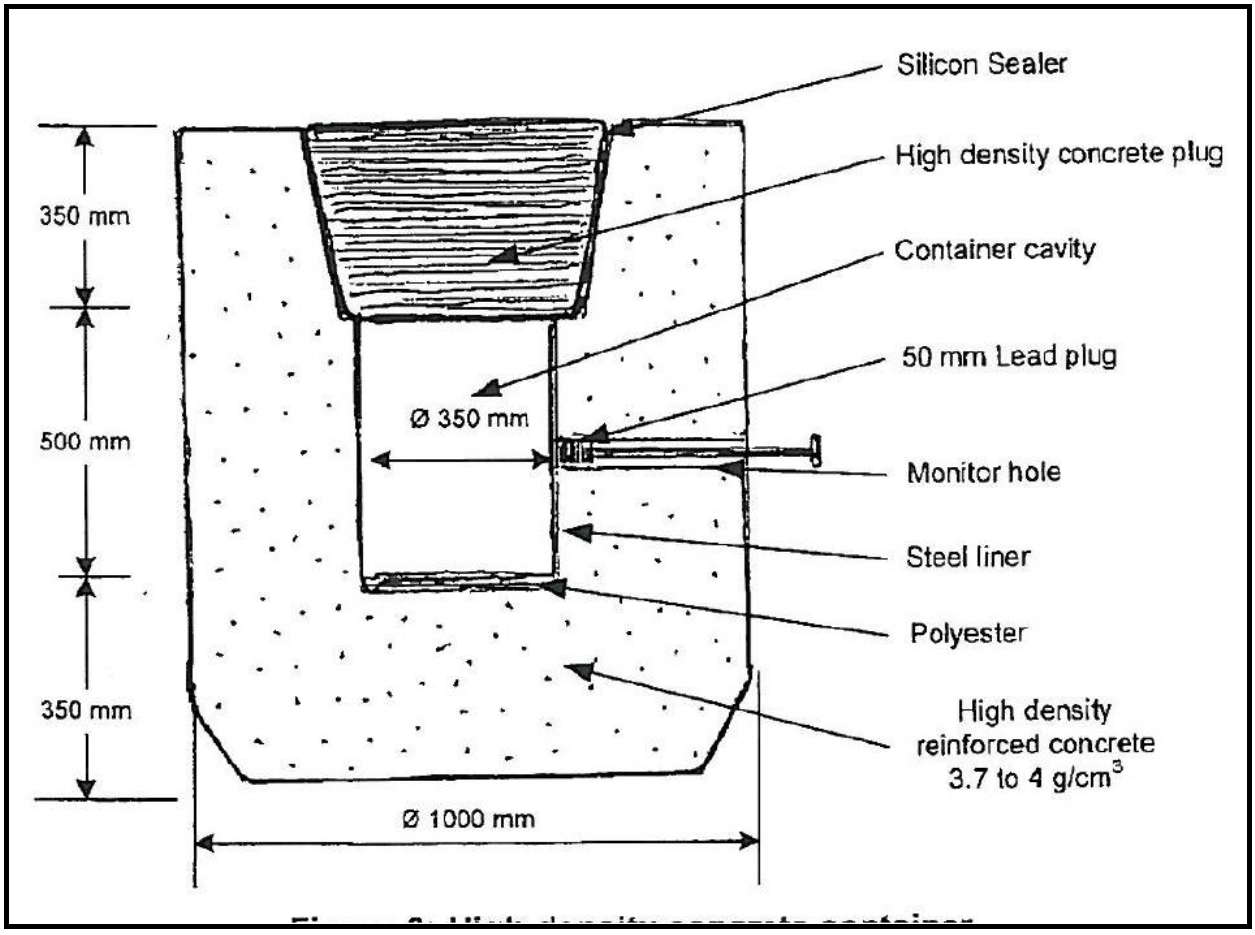

Figure 1: *Design of a high-density concrete RadWaste drum for ILW, as used by NTP at Necsa (2012).*

From Figure 1: The thickness of the high-density concrete shielding to the top and bottom of the rectangular circular cylinder (RCC) of radioactive content, is 35 cm. The lateral thickness of the high-density concrete is 32.5 cm. The height of the active RadWaste content in the drum is 50 cm, and its radius is $r = 17.5$ cm. The active RadWaste content stretches vertically from $z_1 = 35$ cm to $z_2 = 85$ cm.

Assume that the material composition of the drum-fill is CH_2 with a mass-density of $\rho = 0.9\ \mathrm{g\,cm^{-3}}$.

Assume that the radionuclide content of the drums is ^{131}I.

The RadWaste drum is constructed of high-density hematite concrete having a mass-density of $\rho = 3.61\ \mathrm{g\,cm^{-3}}$.

The ionising photon emissions by the radionuclide ^{131}I is as follows:

Table 12.1: *Line energy spectrum of ionising photons emitted by the radionuclide ^{131}I.*

```
c Photon Emissions of I-131
#       SI3                SP3
        L                  D
        7.2291E-01         1.7729E-02
        6.4272E-01         2.1732E-03
        6.3699E-01         7.1733E-02
        5.0300E-01         3.6030E-03
        4.0481E-01         5.4739E-04
        3.6449E-01         8.1700E-01
        3.5840E-01         1.6340E-04
        3.2579E-01         2.7370E-03
        3.2465E-01         2.1242E-04
        3.1809E-01         7.7615E-04
        3.0240E-01         4.7386E-05
        2.9580E-01         1.7974E-05
        2.8431E-01         6.1357E-02
        2.7250E-01         5.7762E-04
        2.3218E-01         3.1863E-05
        1.7721E-01         2.6961E-03
        8.5900E-02         8.9870E-07
        8.0185E-02         2.6226E-02
        3.4419E-02         1.1881E-03
        3.3624E-02         3.9231E-03
        3.3562E-02         2.0314E-03
        2.9782E-02         2.1712E-02
        2.9461E-02         1.1788E-02
        4.1100E-03         4.4925E-03
```

The total yield, $Y = \sum_{i=1}^{N} y_i$, of photon emission by ^{131}I, is $Y = 1.052763$ ionising photons per radioactive transition. Note that the value of Y must be used to calculate the correct tally multiplication factor for the FM card in MCNP input decks.

The material of the RadWaste drums, is high-density concrete with an assumed mass-density of $\rho = 3.61\ \mathrm{g\,cm^{-3}}$. The elemental composition of the high-density magnetite concrete, as specified in MCNP input data format, is:

```
m2      1000   -0.011   $ Mass fraction of H
        8000   -1.168   $ Mass fraction of O
       11000   -0.010   $ Mass fraction of Na
       12000   -0.033   $ Mass fraction of Mg
       13000   -0.083   $ Mass fraction of Al
       14000   -0.091   $ Mass fraction of Si
```

```
       20000    -0.250    $ Mass fraction of Ca
       26000    -1.893    $ Mass fraction of Fe
```

It was assumed that the air is dry; its mass-density was taken to be 1.205×10^{-3} g cm^{-3}; its material composition was specified as follows:

```
m4      6000     -1.24E-4      $ Mass fraction of C
        7000     -0.755267     $ Mass fraction of N
        8000     -0.231781     $ Mass fraction of O
       18000     -0.012827     $ Mass fraction of Ar
```

Reference: Website **http://en.wikipedia.org/wiki/Earth's_atmosphere** (website visited on 25 December 2014).

The complete input data set for the MCNP run is:

```
CONCRETE ILW RadWaste Drum
c Cell Cards
1    1   -0.60        -1              imp:p=1    $ Inner drum fill
2    2   -3.80        -2    +1        imp:p=1    $ Hematite CRT DrumMtl
3    3   -2.35        -3              imp:p=1    $ CRT Floor Slab
4    4   -1.205E-3    -4    +2   +3   imp:p=1    $ Air
5    0                      +4        imp:p=0    $ UmWelt
c ========================

c ========================
c Surface Cards
1  RCC    0    0  +35.0       0    0    +50.0        +17.5        $ Drum fill
2  RCC    0    0    0.0       0    0   +120.0        +50.0        $ Concrete drum
3  RCC    0    0  -30.0       0    0    +30.0       +9000.0       $ FloorSlab
4  RCC    0    0  -30.0       0    0 +9000.0        +9000.0       $ Air Surround
c ========================

c ========================
c Data Cards
mode p
c source definition: CYLINDRICAL VOLUME ALONG Z-AXIS
sdef    par=p
        erg=d3
        cel=1
        pos=0 0 0
        axs=0 0 1
        ext=d1
        rad=d2
c
si1 h  35  85
sp1 d -21  0
c
si2 h  0.0   17.5
sp2 d -21  1
c Photon Emissions of I-131
#       SI3               SP3
        L                 D
        7.2291E-01        1.7729E-02
        6.4272E-01        2.1732E-03
```

```
       6.3699E-01       7.1733E-02
       5.0300E-01       3.6030E-03
       4.0481E-01       5.4739E-04
       3.6449E-01       8.1700E-01
       3.5840E-01       1.6340E-04
       3.2579E-01       2.7370E-03
       3.2465E-01       2.1242E-04
       3.1809E-01       7.7615E-04
       3.0240E-01       4.7386E-05
       2.9580E-01       1.7974E-05
       2.8431E-01       6.1357E-02
       2.7250E-01       5.7762E-04
       2.3218E-01       3.1863E-05
       1.7721E-01       2.6961E-03
       8.5900E-02       8.9870E-07
       8.0185E-02       2.6226E-02
       3.4419E-02       1.1881E-03
       3.3624E-02       3.9231E-03
       3.3562E-02       2.0314E-03
       2.9782E-02       2.1712E-02
       2.9461E-02       1.1788E-02
       4.1100E-03       4.4925E-03
c
c Material definitions
m1      1000    +2          $ CH2
        6000    +1          $ CH2
c
m2      1000    -0.011      $ Hematite CRT
        8000    -1.168      $ Hematite CRT
       11000    -0.010      $ Hematite CRT
       12000    -0.033      $ Hematite CRT
       13000    -0.083      $ Hematite CRT
       14000    -0.091      $ Hematite CRT
       20000    -0.250      $ Hematite CRT
       26000    -1.893      $ Hematite CRT
c
m3      1000    -0.013      $ Type 04 Ordinary Concrete
        8000    -1.165      $ Type 04 Ordinary Concrete
       11000    -0.040      $ Type 04 Ordinary Concrete
       12000    -0.010      $ Type 04 Ordinary Concrete
       13000    -0.108      $ Type 04 Ordinary Concrete
       14000    -0.740      $ Type 04 Ordinary Concrete
       16000    -0.003      $ Type 04 Ordinary Concrete
       19000    -0.045      $ Type 04 Ordinary Concrete
       20000    -0.196      $ Type 04 Ordinary Concrete
       26000    -0.030      $ Type 04 Ordinary Concrete
c
m4      6000    -1.24E-4    $ Air, dry
        7000    -0.755267   $ Air, dry
        8000    -0.231781   $ Air, dry
       18000    -0.012827   $ Air, dry
c
c **** Tally definitions *******
fc15   Effective PDR
f15z:p   60    55   0.1
         60    60   1
         60    70   1
         60    80   1
```

```
         60    90   1
         60   100   1
         60   120   1
         60   150   1
         60   180   1
         60   200   1
         60   250   1
         60   300   1
         60   350   1
fm15   3.8952E13    $ 1 kCi I-131
c
c  Fluence-rate to dose-rate conversion factors: photons
c  Convert fluence-rate to effective dose in Sv/hr
DF15  IU=2  FAC=1  IC=31
c
PRINT 10 40 50 60 72 100 110 120 128 170 200
c
CTME 120
```

RESULT: Results between 4E-04 and 5E-4 Sv/h are acceptable.

12.6 Case study RSDD-6: Radioactive liquid in a pipe at a LWR

Following a LOCA (loss-of-coolant accident), which results in some core damage, the representative, normalised ionising photon energy-spectrum emitted by the coolant flowing in the reactor coolant pipes at a LWR is measured in a PASS (post-accident sampling system) and found to be as follows[27]:

#	SI3	SP3
	L	D
	0.055	2.12E-07
	0.25	3.42E-04
	0.55	4.96E-02
	0.85	8.73E-01
	1.5	7.43E-02
	2.5	2.36E-03
	3.5	1.30E-04
	4.5	2.24E-05
	5.5	3.19E-05
	6.5	4.13E-05
	7.5	6.37E-05
	8.5	1.09E-05
	9.5	9.56E-07
	10.5	5.66E-08
	11.5	9.44E-09

The total ionising photon yield is 8.48E+09 s^{-1} $litre^{-1}$.

Pipe specification:
Pipe ID: 30 cm
Pipe OD: 36 cm
Pipe steel: SS-304L

The pipe runs horizontally through a room with ordinary concrete walls, floor & roof 40 cm thick. The pipe centreline is 50 cm above the floor surface. The interior dimensions of the room are 300 cm × 300 cm × 240 cm high.

The pressure in the pipe is 4 bar and the temperature is 120 °C. From this the mass-density of the coolant water inside the pipe may be calculated as being $\boxed{0.9433}$ $g\,cm^{-3}$. (Hint: use EES[28] to perform this calculation.)

(a) Calculate the maximum dose rate at a point 40 cm from this pipe, 50 cm above the floor surface.

(b) Calculate the maximum dose rate at a point 30 cm outside the concrete wall, in an adjacent room.

---

[27] Note: these values are purely hypothetical and not realistic at all.

[28] EES ≡ Engineering Equation Solver.

Solution

```
LWR PIPE filled with post-LOCA Coolant
c Cell Cards
1  1  -1.205E-3    -2  +4        imp:p=1    $ Air in room
2  2  -2.35        -1  +2        imp:p=1    $ Concrete Wall
3  1  -1.205E-3    -3  +1        imp:p=1    $ Air outside Room
4  3  -8.00        -4  +5        imp:p=1    $ SS-304L Pipe Wall
5  4  -0.9433      -5            imp:p=1    $ Coolant in SS Pipe
6  0                  +3        imp:p=0    $ UmWelt -- "EXTERNAL VOID"
c ====================================================

c ====================================================
c Surface Cards
1  RPP -190  +190     -190  +190     -40  +280        $ Outer RPP for Concrete
2  RPP -150  +150     -150  +150      +0  +240        $ Inner RPP for Concrete
3  RPP -800  +800     -800  +800    -150  +950        $ Outer RPP for Air outside
room
c
4  RCC -150  +0  +50      +300  +0   +0        +18.0  $ Outer RCC for Pipe
5  RCC -150  +0  +50      +300  +0   +0        +15.0  $ Inner RCC for Pipe
c ====================================================

c ====================================================
c Data Cards
c Mode: transport photons
mode  p
sdef  par = p
      pos = 0 0 0
      axs = 1 0 0
      ext = d1
      rad = d2
      erg = d3
c
si1 h  -150  +150          $ Extent of sampling of Axial coordinate
sp1 d  -21 0               $ Sampling pattern in axial dimension
c
si2 h   0   +15            $ Extent of sampling in radial coordinate
sp2 d -21 1                $ Sampling pattern in radial dimension
c
#    SI3       SP3          $ Gammas from Coolant
     L         D            $ Gammas from Coolant
     0.055     2.12E-07     $ Gammas from Coolant
     0.25      3.42E-04     $ Gammas from Coolant
     0.55      4.96E-02     $ Gammas from Coolant
     0.85      8.73E-01     $ Gammas from Coolant
     1.5       7.43E-02     $ Gammas from Coolant
     2.5       2.36E-03     $ Gammas from Coolant
     3.5       1.30E-04     $ Gammas from Coolant
     4.5       2.24E-05     $ Gammas from Coolant
     5.5       3.19E-05     $ Gammas from Coolant
```

```
     6.5       4.13E-05     $ Gammas from Coolant
     7.5       6.37E-05     $ Gammas from Coolant
     8.5       1.09E-05     $ Gammas from Coolant
     9.5       9.56E-07     $ Gammas from Coolant
    10.5       5.66E-08     $ Gammas from Coolant
    11.5       9.44E-09     $ Gammas from Coolant
c
c Material definitions
m1     6000   -1.24E-4       $ Air
       7000   -0.755267      $ Air
       8000   -0.231781      $ Air
      18000   -0.012827      $ Air
c
m2     1000   -0.013         $ Concrete, ordinary, NBS type 04
       8000   -1.165         $ Concrete, ordinary, NBS type 04
      11000   -0.040         $ Concrete, ordinary, NBS type 04
      12000   -0.010         $ Concrete, ordinary, NBS type 04
      13000   -0.108         $ Concrete, ordinary, NBS type 04
      14000   -0.740         $ Concrete, ordinary, NBS type 04
      16000   -0.003         $ Concrete, ordinary, NBS type 04
      19000   -0.045         $ Concrete, ordinary, NBS type 04
      20000   -0.196         $ Concrete, ordinary, NBS type 04
      26000   -0.030         $ Concrete, ordinary, NBS type 04
c
m3     6000   -0.03          $ SS-304L
      14000   -0.60          $ SS-304L
      15000   -0.02          $ SS-304L
      16000   -0.03          $ SS-304L
      24000  -19.00          $ SS-304L
      25000   -1.70          $ SS-304L
      26000  -68.62          $ SS-304L
      28000  -10.00          $ SS-304L
c
m4     1000   +2             $ LWR Coolant
       8000   +1             $ LWR Coolant
c
c ========
c **** Tally specs *******
fc15 Photon Dose Rate Tally
f15:p    0   +76   +50    1    ND
         0  +230   +50    1    ND
fm15  1.798E12
c
c Fluence-rate to dose-rate conversion factors: photons
c Convert fluence-rate to effective dose in Sv/hr
DF15  IU=2  FAC=1  IC=31
c
c === RUNTIME CONTROLS ======
PRINT
ctme 10
```

12.7 Case study RSDD-7: Concrete shield design for an insect irradiator facility using a 20 kCi ^{60}Co source

Geometry modelling for insect irradiator facility shield design. Production of mesh tally plot for the dose rates in the insect sterilisation irradiator.

Introductory overview of *variance reduction* techniques that can be applied to get statistically meaningful results more quickly.

Solution: Case study RSDD-7

12.8 Case study RSDD-8: Radionuclide production hotcell shielding design

Model a 1 Ci ^{22}Na source located at the centre of a radionuclide production hotcell with inner dimensions,

$X_{\min} = 0$ cm
$X_{\max} = 75$ cm
$Y_{\min} = -50$ cm
$Y_{\max} = +50$ cm
$Z_{\min} = 0$ cm
$Z_{\max} = +100$ cm.

The hotcell walls are made of Pb ($\rho = 11.35$ g cm^{-3}) and the wall thickness is 10 cm on 5 sides, and 15 cm on the front side, where radiochemical technicians will stand while working. On the front side of the hotcell is a lead-glass window. Take the lead-glass composition as

```
m4      8000   +2        $ Lead Glass
       14000   +1        $ Lead Glass
       82000   +1        $ Lead Glass
```

and its density as 5.2 g cm^{-3}. The lead-glass is flush with the inside wall of the Hot-cell, and has a thickness of 30 cm, i.e. it will protrude 15 cm outside the outer face of the front of the hotcell. It is 42 cm wide, and 30 cm high. Its $Z_{\min}$ is 60 cm above the floor of the inside of the hotcell.

```
15  RPP   +75.0  +105.0    -21.0   +21.0    +60.0   +90.0  $ Lead-Glass
```

The ^{22}Na source is cylindrical with $H = 2$ cm and $R = 1$ cm. This radionuclide is dissolved in water, so that the source material is essentially pure water.

Obtain a photon fluence-rate mesh-tally plot over the frontal face of the hotcell. The hotcell is filled with air and surrounded by air.

Use GRIDCONV to convert the binary mesh tally output data to an ASCII file, read the ASCII file into a plotting package such as ORIGEN or SIGMAPLOT and plot a colour-contour of the dose rate distribution across the front face of the hotcell, where the radiochemical technician will stand.

Solution (point source case)

```
Particle beam of protons incident upon a 30cm x 30cm x 30cm wax block
c Cell Cards
1   1  -1.205E-3   -1                  imp:p=1    $ Air inside Hot-Cell
2   2  -11.35      -2   +1   +3        imp:p=2    $ Lead
12  1  -1.205E-3  -99   +2   +3  +4    imp:p=3    $ Air outside Hot-Cell
15  4  -5.2        -3                  imp:p=2    $ LeadGlassWindow
20  3  -0.1        -4                  imp:p=3    $ TEM Tally Cell
50  0                  +99             imp:p=0    $ UmWelt
c =====
```

```
c =====
c Surface Cards
1   RPP    +0.0   +75.0    -50.0   +50.0     +0.0  +100.0   $ Inner Box
2   RPP   -10.0   +90.0    -60.0   +60.0    -10.0  +110.0   $ Outer Box
3   RPP   +75.0  +105.0    -21.0   +21.0    +60.0   +90.0   $ LeadGlass
4   RPP  +110.0  +120.0    -60.0   +60.0    -10.0  +110.0   $ TEM Tally Cell
99  RPP  -300.0  +300.0   -300.0  +300.0    -100.0 +300.0   $ Outer AirBox
c =====

c =====
c Data Cards
mode p
sdef par = p
     pos = 45 0 5
     erg = d1
si1 L  1.27   0.511    $ Energies
sp1 D  0.999  1.8292   $ Emission Yields
c
c Material definitions
c
m1     6000    -1.24E-4         $ Air
       7000    -0.755267        $ Air
       8000    -0.231781        $ Air
      18000    -0.012827        $ Air
c
m2    82000    -1.0             $ Lead
c
m3     8000    -6.143E-01       $ TEM
       6000    -2.286E-01       $ TEM
       1000    -1.000E-01       $ TEM
       7000    -2.571E-02       $ TEM
      20000    -1.429E-02       $ TEM
      15000    -1.114E-02       $ TEM
      19000    -2.000E-03       $ TEM
      16000    -2.000E-03       $ TEM
      11000    -1.429E-03       $ TEM
      17000    -1.357E-03       $ TEM
      12000    -2.714E-04       $ TEM
      26000    -6.000E-05       $ TEM
c
m4     8000    +2               $ LeadGlass
      14000    +1               $ LeadGlass
      82000    +1               $ LeadGlass
c
c **** Physics Table *****
c
phys:p    10      $     Emax
           0      $     0 always (generate el in MODE e calcs)
           0      $     0 always (Coherent/Thomson scattering on)
          -1      $    -1 always (photonuclear reactions on)
           1      $     1 always (1 = Doppler broadening off)
           0      $     0 normally, but -101 for delayed gammas from FissProds)
c
c Tally Definitions ===
fc16 Photon Absorbed Dose Rate in TEM Cell
f16:p  20
fm16   6.036E4        $ 1 Ci Source, output in Gy/hr
```

```
c
fc26  Total Absorbed Dose Rate in TEM Cell
+f26   20
fm26   6.036E4        $ 1 Ci Source, output in Gy/hr
c
c Mesh Tally ====
tmesh
 rmesh11:p flux
   cora11   +106.0  +107.0
   corb11   -80.0  158i  +80.0
   corc11   -20.0  138i  +120.0
endmd
fm11   6.036E4        $ 1 Ci Source, output in Gy/hr
c ==== PRINT CONTROLS =====
PRINT  10  40  50  60  72 100 110 120 170 200
c === RUNTIME CONTROLS ======
ctme 10
```

12.9 Case study RSDD-9: Shield design for a ^{252}Cf spontaneous fission source

A ^{252}Cf source emits prompt fission neutrons via spontaneous fission. The activity of the source is 1 Ci. The source is in the chemical form $^{252}CfO_3$, and has a mass-density $\rho = 6\ \mathrm{g\,cm^{-3}}$. The active source radius is 2.5 cm. The spherical source is inside a SS-304 canister shell having a wall thickness of 0.15 cm.

For ^{252}Cf, the spontaneous fission probability per radioactive transition is 3.1%. The radionuclide ^{252}Cf has a half-life of 2.645 years. It transitions by α-particle emission (96.9%) and SF — spontaneous fission — (3.1%). It emits $\nu = 3.768$ neutrons per fission on average.

Design a Fe/Wax/Pb shield that will attenuate the transmitted dose rate on the outer surface of the shield to just below 100 μSv/h. Model the problem in spherical-symmetrical geometry.

References

SPENCER RR, GWIN R & INGLE RW. 1982. *A Measurement of the Average Number of Prompt Neutrons from Spontaneous Fission of Californium-252.* Journal of Nuclear Science & Engineering, 80: 603 (1982).

BRUNSON GS (Jr.). 1982. *Multiplicity and Correlated Energy of Gamma Rays Emitted in the Spontaneous Fission of Californium-252.* Ph.D. Thesis, University of Utah, Utah, USA.

Solution

```
Cf-252 Source
c Cell Cards
1   1       -6.0     -1          imp:n,p=1     $ 252CfO3
2   2       -7.9     -2   +1     imp:n,p=1     $ SS-304L
3   3       -7.86    -3   +2     imp:n,p=1     $ Fe
4   4       -0.92    -4   +3     imp:n,p=1     $ Wax
5   5      -11.30    -5   +4     imp:n,p=1     $ Pb
6   6  -1.205E-03    -6   +5     imp:n,p=1     $ Air
7   0                   +6     imp:n,p=0     $ UmWelt
c ==========================

c ==========================
c Surface Cards
1  so        2.5    $ OR: Cf-252
2  so        2.65   $ OR: SS-304 Canister
3  so       45.0    $ OR: Fe
4  so       70.0    $ OR: Wax
5  so       75.0    $ OR: Pb
6  so      900.0    $ OR: Air
c ==========================
```

```
c ==========================
c Data Cards
mode n p
c
sdef   par=n
       cell=1
       pos=0 0 0
       rad=d1
       erg=d2
c

si1    0.0   2.5
sp1   -21    2
c

sp2    -3    1.18  1.03419
c
c Material definitions
m1    98252    +1             $ 252CfO3
       8016    +3             $ 252CfO3
c
m2     6000    -0.03          $ SS-304L
      14028    -0.5532        $ SS-304L
      14029    -0.0282        $ SS-304L
      14030    -0.0186        $ SS-304L
      15031    -0.02          $ SS-304L
      16000    -0.03          $ SS-304L
      24050    -0.827         $ SS-304L
      24052   -15.920         $ SS-304L
      24053    -1.805         $ SS-304L
      24054    -0.448         $ SS-304L
      25055    -1.70          $ SS-304L
      26054    -3.980         $ SS-304L
      26056   -62.925         $ SS-304L
      26057    -1.468         $ SS-304L
      26058    -0.213         $ SS-304L
      28058    -6.776         $ SS-304L
      28060    -2.642         $ SS-304L
      28061    -0.116         $ SS-304L
      28062    -0.371         $ SS-304L
      28064    -0.095         $ SS-304L
c
m3    26054    +5.8           $ Iron
      26056   +91.7           $ Iron
      26057    +2.2           $ Iron
      26058    +0.3           $ Iron
c
m4     1001   +52             $ Paraffin wax
       6000   +25             $ Paraffin wax
c
m5    82206   +24.1           $ Lead
```

```
      82207   +22.1           $ Lead
      82208   +52.4           $ Lead
c
m6     6000    -1.24E-4       $ Air, dry
       7014    -0.755267      $ Air, dry
       8016    -0.231781      $ Air, dry
      18000    -0.012827      $ Air, dry
c =====
c
c KCODE SPECS
kcode  1E6  0.4  50  150
c
c =====
c
c **** Physics Table *****
c
phys:n    30      $     Emax
           0      $     0 always
           0      $     0 always
       -1001      $ -1001 always
          -1      $    -1 always (mix + match)
c
phys:p    30      $     Emax
           0      $     0 always (generate el in MODE e calcs)
           0      $     0 always (Coherent/Thomson scattering on)
          -1      $    -1 always (photonuclear reactions on)
           1      $     1 always (1 = Doppler broadening off)
        -101      $     0 normally, but -101 for accurate delayed gamma
production from fission products)
c =====
PRINT
c =====
c **** Tally Specs *******
c
fc12   Neutron Effective Dose Rate
f12:n  5
fm12   4.322E9
c
fc22   Photon Effective Dose Rate
f22:p  5
fm22   4.322E9
c
c =========
c  Fluence-rate to dose-rate conversion factors for neutrons
#      de12                df12
       1.0000000E-09       5.5620000E-09
       1.1623200E-09       1.1153900E-08
       1.3509900E-09       1.1188600E-08
       1.5702900E-09       1.1228900E-08
       1.8251800E-09       1.1275800E-08
       2.1214500E-09       1.1330300E-08
       2.4658100E-09       1.1393700E-08
```

```
2.8660700E-09       1.1467400E-08
3.3312900E-09       1.1553000E-08
3.8720400E-09       1.1652500E-08
4.5005600E-09       1.1768100E-08
5.2311000E-09       1.1902500E-08
6.0802200E-09       1.2058800E-08
7.0671800E-09       1.2240400E-08
8.2143400E-09       1.2451400E-08
9.5477200E-09       1.2696800E-08
1.1097500E-08       1.2898500E-08
1.2898900E-08       1.3093100E-08
1.4992700E-08       1.3319200E-08
1.7426300E-08       1.3582000E-08
2.0255000E-08       1.3887500E-08
2.3542900E-08       1.4242600E-08
2.7364400E-08       1.4536200E-08
3.1806300E-08       1.4792000E-08
3.6969100E-08       1.5089400E-08
4.2970000E-08       1.5435100E-08
4.9945100E-08       1.5836800E-08
5.8052300E-08       1.6303800E-08
6.7475400E-08       1.6846600E-08
7.8428200E-08       1.7477500E-08
9.1158900E-08       1.8210800E-08
1.0595600E-07       1.8863700E-08
1.2315500E-07       1.9278500E-08
1.4314600E-07       1.9760700E-08
1.6638200E-07       2.0321100E-08
1.9338900E-07       2.0972500E-08
2.2478100E-07       2.1346100E-08
2.6126800E-07       2.1661400E-08
3.0367700E-07       2.2027800E-08
3.5297100E-07       2.2453700E-08
4.1026600E-07       2.2948700E-08
4.7686100E-07       2.3524100E-08
5.5426600E-07       2.3895900E-08
6.4423600E-07       2.4180900E-08
7.4881000E-07       2.4512200E-08
8.7035900E-07       2.4897300E-08
1.0116400E-06       2.5323100E-08
1.1758500E-06       2.5535900E-08
1.3667200E-06       2.5783300E-08
1.5885700E-06       2.6070800E-08
1.8464200E-06       2.6405000E-08
2.1461400E-06       2.6660100E-08
2.4945100E-06       2.6793900E-08
2.8994200E-06       2.6949400E-08
3.3700600E-06       2.7130100E-08
3.9171000E-06       2.7340200E-08
4.5529400E-06       2.7584300E-08
5.2919800E-06       2.7779100E-08
6.1509900E-06       2.7847200E-08
```

```
7.1494300E-06       2.7926200E-08
8.3099400E-06       2.8018100E-08
9.6588300E-06       2.8125000E-08
1.1226700E-05       2.8160800E-08
1.3049000E-05       2.8174000E-08
1.5167200E-05       2.8189200E-08
1.7629100E-05       2.8206900E-08
2.0490700E-05       2.8222800E-08
2.3816900E-05       2.8214800E-08
2.7682900E-05       2.8205600E-08
3.2176400E-05       2.8194800E-08
3.7399400E-05       2.8182200E-08
4.3470100E-05       2.8167700E-08
5.0526300E-05       2.8150900E-08
5.8727900E-05       2.8133100E-08
6.8260700E-05       2.8112600E-08
7.9341000E-05       2.8088600E-08
9.2219800E-05       2.8060800E-08
1.0718900E-04       2.8028500E-08
1.2458800E-04       2.7990900E-08
1.4481200E-04       2.7947200E-08
1.6831800E-04       2.7896400E-08
1.9564000E-04       2.7837400E-08
2.2739700E-04       2.7765500E-08
2.6430800E-04       2.7681400E-08
3.0721100E-04       2.7583600E-08
3.5707900E-04       2.7469900E-08
4.1504000E-04       2.7337700E-08
4.8241100E-04       2.7184100E-08
5.6071700E-04       2.7144000E-08
6.5173400E-04       2.7144000E-08
7.5752500E-04       2.7144000E-08
8.8048800E-04       2.7144000E-08
1.0234100E-03       2.7149900E-08
1.1895300E-03       2.7191800E-08
1.3826200E-03       2.7240400E-08
1.6070500E-03       2.7297000E-08
1.8679100E-03       2.7362700E-08
2.1711200E-03       2.7469900E-08
2.5235400E-03       2.7622200E-08
2.9331700E-03       2.7799100E-08
3.4092900E-03       2.8004800E-08
3.9626900E-03       2.8243900E-08
4.6059200E-03       2.8521800E-08
5.3535700E-03       2.8982200E-08
6.2225700E-03       2.9695500E-08
7.2326300E-03       3.0524500E-08
8.4066500E-03       3.1488200E-08
9.7712400E-03       3.2608200E-08
1.1357300E-02       3.4305900E-08
1.3200900E-02       3.6356700E-08
1.5343700E-02       3.8740300E-08
```

```
        1.7834300E-02       4.1510900E-08
        2.0729200E-02       4.4838800E-08
        2.4094000E-02       4.9078500E-08
        2.8005000E-02       5.4006300E-08
        3.2550900E-02       5.9871900E-08
        3.7834600E-02       6.6814700E-08
        4.3976000E-02       7.4884500E-08
        5.1114300E-02       8.4324400E-08
        5.9411300E-02       9.5674700E-08
        6.9055100E-02       1.0886700E-07
        8.0264300E-02       1.2407800E-07
        9.3293000E-02       1.4174500E-07
        1.0843700E-01       1.6219900E-07
        1.2603800E-01       1.8589800E-07
        1.4649700E-01       2.1344400E-07
        1.7027700E-01       2.4473100E-07
        1.9791700E-01       2.8095000E-07
        2.3004300E-01       3.2175100E-07
        2.6738400E-01       3.6906900E-07
        3.1078700E-01       4.2263200E-07
        3.6123400E-01       4.7984000E-07
        4.1987100E-01       5.4633300E-07
        4.8802500E-01       6.2362100E-07
        5.6724300E-01       7.0377000E-07
        6.5931900E-01       7.9492600E-07
        7.6634100E-01       8.9132500E-07
        8.9073500E-01       9.9656200E-07
        1.0353200E+00       1.1020400E-06
        1.2033800E+00       1.1894200E-06
        1.3987100E+00       1.2714600E-06
        1.6257600E+00       1.3520300E-06
        1.8896500E+00       1.4318300E-06
        2.1963900E+00       1.5012600E-06
        2.5529100E+00       1.5667100E-06
        2.9673000E+00       1.6428000E-06
        3.4489600E+00       1.6892100E-06
        4.0088100E+00       1.7391500E-06
        4.6595300E+00       1.7649200E-06
        5.4158700E+00       1.7843900E-06
        6.2949900E+00       1.7938600E-06
        7.3168100E+00       1.7964000E-06
        8.5044900E+00       1.7982200E-06
        9.8849600E+00       1.8000000E-06
        1.1489500E+01       1.7973200E-06
        1.3354500E+01       1.7866500E-06
        1.5522300E+01       1.7691600E-06
        1.8041900E+01       1.7418700E-06
        2.0970500E+01       1.7067200E-06
        2.4374400E+01       1.6780500E-06
        2.8331000E+01       1.6448200E-06
c
c  Response Function for Eff Dose: photons
```

```
#       de22              df22
        1.00000E-03       1.08000E-10
        1.00000E-02       2.46600E-10
        1.50000E-02       5.61600E-10
        2.00000E-02       8.10000E-10
        3.00000E-02       1.12680E-09
        4.00000E-02       1.26360E-09
        5.00000E-02       1.33200E-09
        6.00000E-02       1.40400E-09
        7.00000E-02       1.48680E-09
        8.00000E-02       1.59840E-09
        1.00000E-01       1.86840E-09
        1.50000E-01       2.69280E-09
        2.00000E-01       3.60000E-09
        3.00000E-01       5.43600E-09
        4.00000E-01       7.20000E-09
        5.00000E-01       8.89200E-09
        5.11000E-01       9.07200E-09
        6.00000E-01       1.04760E-08
        6.62000E-01       1.14120E-08
        8.00000E-01       1.34280E-08
        1.00000E+00       1.61640E-08
        1.11700E+00       1.76400E-08
        1.33000E+00       2.01240E-08
        1.50000E+00       2.20320E-08
        2.00000E+00       2.69280E-08
        3.00000E+00       3.51000E-08
        4.00000E+00       4.21200E-08
        5.00000E+00       4.82400E-08
        6.00000E+00       5.40000E-08
        6.12900E+00       5.47200E-08
        8.00000E+00       6.69600E-08
        1.00000E+01       7.92000E-08
        1.50000E+01       1.09080E-07
        2.00000E+01       1.37520E-07
c =====
```

Need for variance reduction:

Model in spherical symmetry:

0.5 MeV neutron source surrounded by 100 cm wax.

Tally for flux on outer surface of wax.

Wax density $\rho = 0.92\ \mathrm{g\,cm^{-3}}$. Chemical formula of paraffin wax: $C_{25}H_{52}$.

Run for 2 minutes.

Tally result = ?
Statistical error = ?
Conclusion regarding the need for variance reduction = ?

12.10 Case study RSDD-10: Shield design for a radionuclide-production target bombardment station at a particle accelerator facility

A radionuclide production beam target station at a proton accelerator facility requires a local shield to shield the neutrons and ionising photons produced when the intense proton beam strikes the target. At the facility under assessment, a 100 μA, 66 MeV proton beam strikes a stopping-length copper target.

Given: Iron, paraffin wax, boron carbide (B_4C) and lead is available.

Problem: Design a reasonably optimal radiation shield.

Solution: Case study RSDD-10

Reference document, available as a PDF file:

> KUPI, TG. 2007. *Radiation Shield Design Verification and Optimisation for two Radionuclide Production Beam Target Stations, using the Monte Carlo Radiation Transport Code, MCNPX.* NorthWest University (Mafikeng Campus), South Africa.

12.11 Case study RSDD-11: Radiation streaming through a large penetration in the concrete floor at a particle accelerator facility

At a particle accelerator facility, a 100 μA, 200 MeV proton beam strikes a copper ($\rho = 8.92\ \mathrm{g\,cm^{-3}}$) Faraday-cup beamstop inserted into the beamline to temporarily stop the proton beam. A high fluence-rate of neutrons and ionising photons are produced by nuclear reactions of the high-energy protons in the copper, as well as by secondary nuclear reactions. Two metres away from the beamstop, at an angle of 90 degrees relative to the proton beam direction, there is a penetration through the floor of the vault, to a vault situated in the basement. The floor thickness is 100 cm ordinary concrete ($\rho = 2.35\ \mathrm{g\,cm^{-3}}$); the radius of the circular penetration is 30 cm. Calculate the following:

- The neutron fluence-rate entering into the underfloor vault, at the bottom of the penetration, as well as the neutron energy spectrum.
- The ionising photon fluence-rate entering into the underfloor vault, at the bottom of the penetration, as well as the photon energy spectrum.
- The absorbed neutron dose rate, calculated for tissue-equivalent detector material, at the bottom of the penetration into the underfloor vault.
- The absorbed photon dose rate, calculated for tissue-equivalent detector material, at the bottom of the penetration into the underfloor vault.

Hint: Use the code SRIM (**www.srim.org**) to calculate the required thickness of the copper beamstop, and to estimate the lateral spread of the beam in the copper. Use these results to define the dimensions for the RCC that serves as beamstop in the Monte Carlo simulation.

Solution: Case study RSDD-11

#

12.12 Case study RSDD-12: The impact of the water content of ordinary concrete on its ability to shield neutrons

Introduction

Ordinary concrete is a relatively cheap structural and shielding material employed around e.g. nuclear reactors. Nuclear reactors produce neutrons and ionising photons, and these radiations must be shielded in order to limit dose rates in regions where electronic equipment are deployed, as well as in regions where radiation workers must perform tasks. The shielding of neutrons as close to the radiation source as possible, also limit neutron activation problems, i.e. induced radioactivity is minimised.

Ordinary concrete consists of a mixture of Portland cement, sand and stones, mixed with water and allowed to harden.

The isotope ^{1}H in the crystalline water that is chemically trapped in cured concrete, is a very important determinant of the neutron shielding ability of the concrete, because ^{1}H is kinematically highly effective in slowing fast neutrons down to low energies, where they can be easily absorbed.

The aim of this section is to present results that show how sensitive the shielding ability of ordinary concrete is to its water content.

Methodology

The Monte Carlo radiation transport code, MCNPX 2.7 was used to model a hypothetical point source emitting mono-energetic neutrons of energy $E_n = 1$ MeV. The source was surrounded by a spherical air cavity with a radius of 100 cm, which was in turn surrounded by a 100 cm thick concrete shell, in turn surrounded by air on the outside.

The effective dose rate on the outer surface of the concrete shell, was tallied using an MCNP type F2 surface-fluence tally, modified by the effective dose rate response functions for both neutrons and (secondary) ionising photons.

The effect of the water content of the concrete on the concrete density was taken into account.

A simple variance reduction technique – population control via cell importance biasing – was used to obtain standard deviations for the Monte Carlo calculations below 1%, for runtimes of 120 minutes per case, for 17 discrete values of concrete water content.

The transmitted effective dose rates were calculated as a function of the water content of the concrete.

Table 12.2: *Density and water content of ordinary concrete, at various states of hydration.*

Partial density of ^{1}H in concrete ($g.cm^{-3}$)	Mass-density of bulk concrete ($g.cm^{-3}$)	Percentage H_2O in concrete
0.001	2.243	0.398
0.002	2.252	0.794
0.003	2.261	1.186
0.004	2.27	1.575
0.005	2.278	1.961
0.006	2.287	2.344
0.007	2.296	2.724
0.008	2.305	3.101
0.009	2.314	3.475
0.010	2.323	3.846
0.011	2.332	4.215
0.012	2.341	4.581
0.013	2.350	4.943
0.015	2.368	5.661
0.020	2.413	7.408
0.025	2.457	9.092
0.030	2.502	10.715

A partial density of 0.013 $g\,cm^{-3}$ for ^{1}H, and a mass-density of 2.35 $g\,cm^{-3}$ is "normal" for ordinary concrete (Shultis & Faw, 2000). Higher partial densities of H_2O represent "highly hydrated" concrete, and lower partial densities of H_2O represent dried-out concrete. In the first 2 weeks after casting, the H_2O content of ordinary concrete will typically be in the order of 10% (m/m). In the subsequent decade, the percentage of H_2O in the concrete will typically become lower and lower, eventually stabilising around 5% (m/m). Should the ordinary concrete be exposed to temperatures above approximately 70 °C, crystalline water in the concrete matrix will be lost and the H_2O content could drop to values lower than circa 3.5% (m/m).

Modelled geometry

A spherical shell of 100 cm concrete surrounds a sphere of air with a radius of 100 cm. At the centre is an isotropic point source of 1 MeV neutrons.

The concrete shell was divided into layers to enable variance reduction via optimised cell-importances in MCNP.

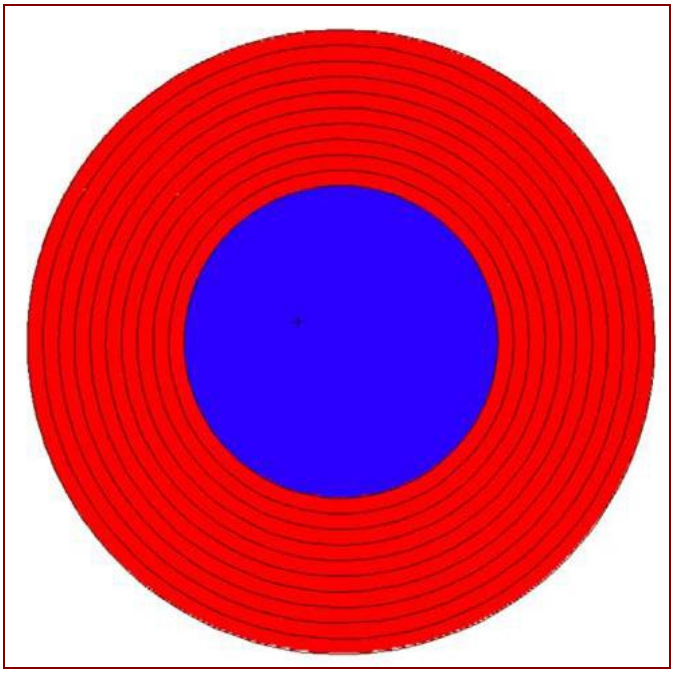

Results: Sensitivity of the neutron shielding ability of ordinary concrete, on its H_2O content

The transmitted dose rates as a function of the water content in ordinary concrete, is shown in Figures 12.2 and 12.3.

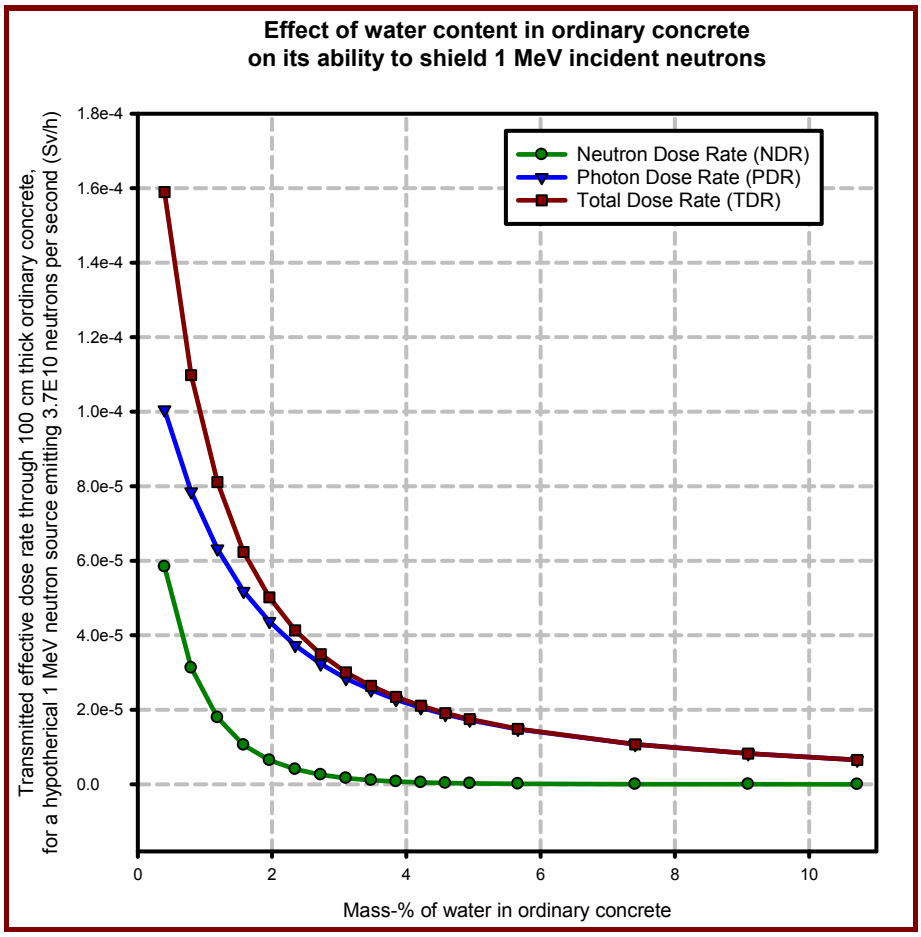

Figure 12.2: *Sensitivity of the neutron shielding ability of ordinary concrete, on the mass-% of H_2O in the concrete.*

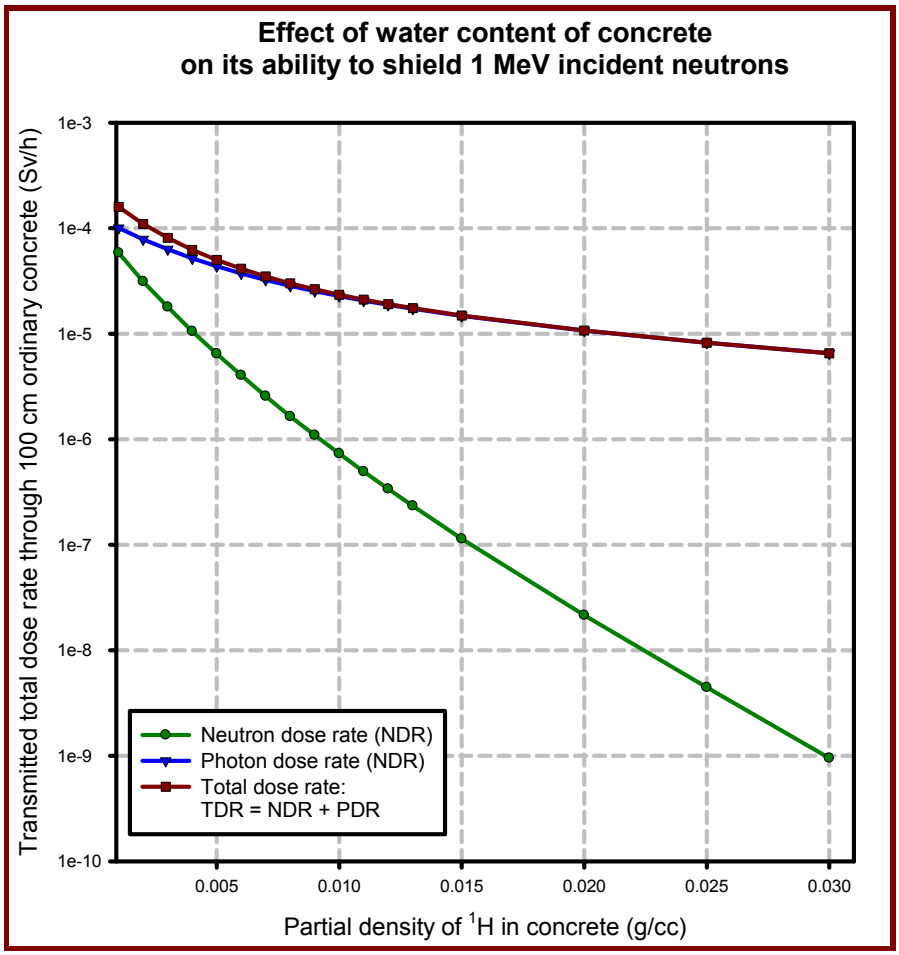

Figure 12.3: *Sensitivity of the neutron shielding ability of ordinary concrete, on the partial density of ^{1}H in the concrete.*

Note: Figure 12.2 uses a linear vertical axis, while Figure 12.3 employs a logarithmic vertical axis.

Conclusions

The ability of a 100 cm thick concrete shield around a source that emits 1 MeV neutrons, to lower the total effective dose rate, will drop by a factor of about 20, should the concrete loose all its crystalline water as a result of e.g. prolonged, severe overheating caused by high temperatures.

Concrete used for neutron shielding should be allowed to harden with a "wet cure" and can subsequently be painted with a waterproof paint, and should be kept cool, in order to minimise the loss of water from the concrete matrix.

Neutron shielding concrete should be made from raw materials tested for their ability to retain a high water content at the temperatures that may be encountered during operations. Some ores have the ability to retain high partial densities of ^{1}H at temperatures above 200 °C.

When concrete will be employed as a neutron shield, shield design calculations must always be performed for a dried-out, "old" concrete containing e.g. only 3% H_2O (m/m). If this is not

done, shields could be under-designed and dose rates will be excessively high once the concrete had dried out.

It is clear that ordinary concrete is not an optimal neutron shielding material; it is therefore only employed where space and mass are of no concern. Note how secondary ionising photons, generated by e.g. (n,γ) reactions, dominate the transmitted total dose rate (TDR). High-density concretes such as magnetite, hematite and barytes concrete, are more optimal neutron shields, because they contain significant percentages of elements such as Fe ($Z = 26$) and Ba ($Z = 56$) with high atomic numbers Z. The high-Z elements in the high-density concretes will be better able to absorb secondary ionising photons than e.g. Ca ($Z = 20$). One characteristic of many optimised neutron shields is that such a shield will tend to equalise the transmitted neutron and photon dose rates. The fact that the transmitted PDR is much larger than the transmitted NDR for ordinary concrete, is a tell-tale sign that this is a non-optimal shielding material.

12.13 Case study RSDD-13: Detailed profile of energy absorption in a tissue-equivalent material (TEM) struck by a beam of photons

When a beam of photons travelling through vacuum or air, strike a material such as tissue-equivalent material (TEM), a polymer, etc., charged particle equilibrium (cpe) is only established a few millimetres into the body being struck by the photon beam. To get a true

Beware of the results of an F6:P tally in small cells when running a photon or photon/electron problem. Photon heating numbers include the energy deposited by electrons generated during photon collisions, but assume that the electron energy is deposited locally. In a cell where the majority of the electrons lose all of their energy before exiting that cell, this is a good approximation. However, if the cell is thin and/or a large number of electrons are created near the cell boundary, these electrons could carry significant energy into the neighbouring cell. For this situation, the F6:P tally for the cell in which the electrons were created would be too large. For accurate results, run the problem in **MODE p e** and use an **F6:e** tally instead, which provides an accurate tally of electron energy deposition within a cell.

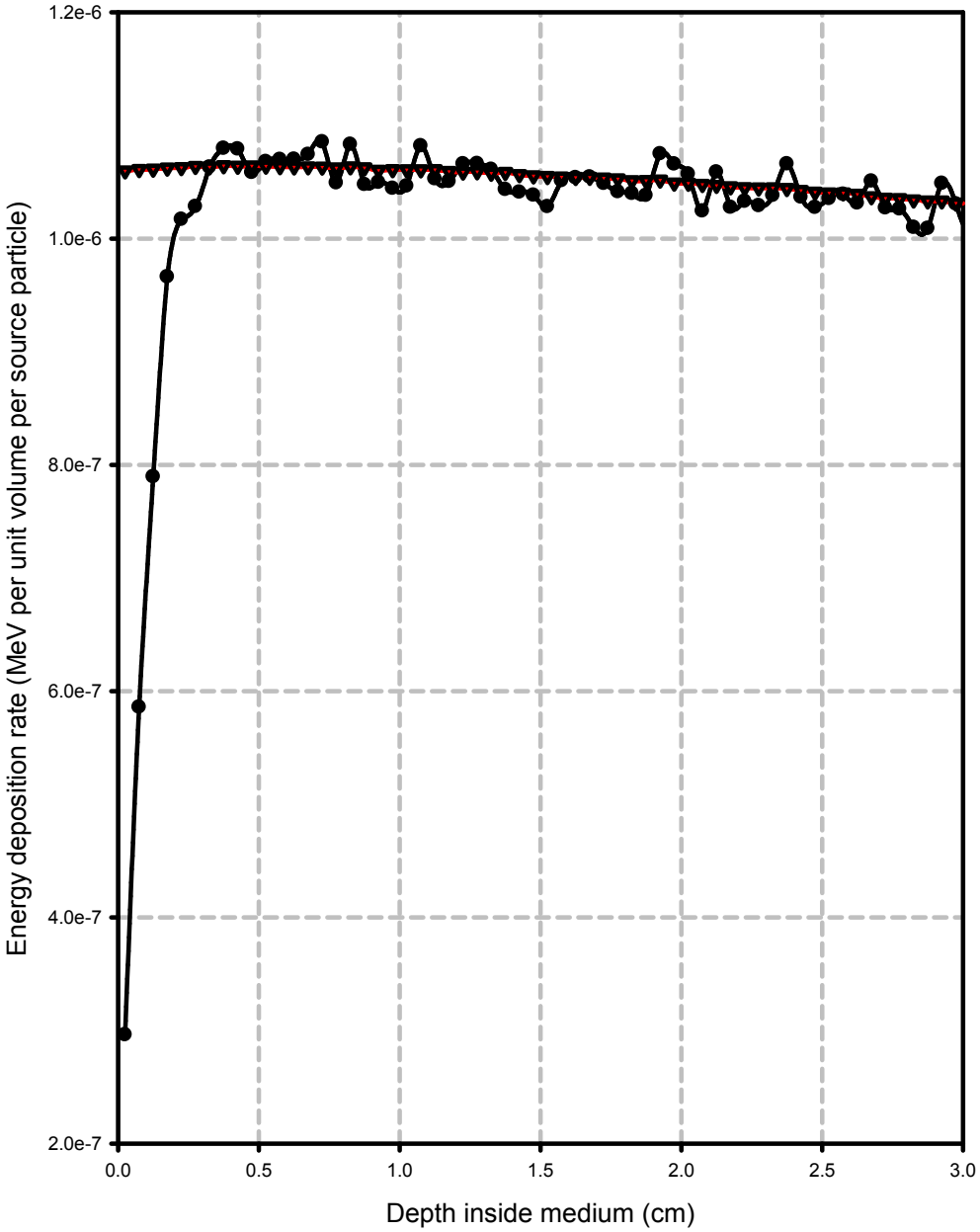
1.2e-6
1.0e-6
8.0e-7
6.0e-7
4.0e-7
2.0e-7
Energy deposition rate (MeV per unit volume per source particle)
0.0
0.5
1.0
1.5
2.0
2.5
3.0
Depth inside medium (cm)

12.14 Case study RSDD-14: Medical physics problem — energy deposition around a small seed of a radionuclide used as an implant for prostate-cancer control

Calculate the absorbed dose distributions around a point source of ^{103}Pd in equilibrium with its radioactive transition product, ^{103m}Rh. Activity of ^{103}Pd: 1 GBq.

Use the photon and electron emission data on page 0.

First model the ionising photon source, and run MCNP in MODE p e. Next, model the electron source, and again run MCNP in MODE p e.

Solution: Case study RSDD-14:

The MCNP input data set for the photon source term, is:

```
Energy deposition by ionising photons emitted by 103Pd & 103mRh
c Cell Cards
01   1  -1.0     -1       imp:p,e=1     $ Seed
02   1  -1.0     -2  +1   imp:p,e=1     $ Water
03   1  -1.0     -3  +2   imp:p,e=1     $ Water
04   1  -1.0     -4  +3   imp:p,e=1     $ Water
05   1  -1.0     -5  +4   imp:p,e=1     $ Water
06   1  -1.0     -6  +5   imp:p,e=1     $ Water
07   1  -1.0     -7  +6   imp:p,e=1     $ Water
08   1  -1.0     -8  +7   imp:p,e=1     $ Water
09   1  -1.0     -9  +8   imp:p,e=1     $ Water
10   1  -1.0    -10  +9   imp:p,e=1     $ Water
11   1  -1.0    -11 +10   imp:p,e=1     $ Water
12   1  -1.0    -12 +11   imp:p,e=1     $ Water
13   1  -1.0    -13 +12   imp:p,e=1     $ Water
14   1  -1.0    -14 +13   imp:p,e=1     $ Water
15   1  -1.0    -15 +14   imp:p,e=1     $ Water
16   1  -1.0    -16 +15   imp:p,e=1     $ Water
17   1  -1.0    -17 +16   imp:p,e=1     $ Water
18   1  -1.0    -18 +17   imp:p,e=1     $ Water
19   1  -1.0    -19 +18   imp:p,e=1     $ Water
20   1  -1.0    -20 +19   imp:p,e=1     $ Water
21   1  -1.0    -21 +20   imp:p,e=1     $ Water
22   1  -1.0    -22 +21   imp:p,e=1     $ Water
23   1  -1.0    -23 +22   imp:p,e=1     $ Water
24   1  -1.0    -24 +23   imp:p,e=1     $ Water
25   1  -1.0    -25 +24   imp:p,e=1     $ Water
26   1  -1.0    -26 +25   imp:p,e=1     $ Water
27   1  -1.0    -27 +26   imp:p,e=1     $ Water
28   1  -1.0    -28 +27   imp:p,e=1     $ Water
29   1  -1.0    -29 +28   imp:p,e=1     $ Water
30   1  -1.0    -30 +29   imp:p,e=1     $ Water
31   0          +30       imp:p,e=0     $ UmWelt

c Surface Cards
```

```
01  SPH   0.0   0.0   0.0   +1.0E-6 $
02  SPH   0.0   0.0   0.0   +2.0E-6 $
03  SPH   0.0   0.0   0.0   +5.0E-6 $
04  SPH   0.0   0.0   0.0   +8.0E-6 $
05  SPH   0.0   0.0   0.0   +1.0E-5 $
06  SPH   0.0   0.0   0.0   +2.0E-5 $
07  SPH   0.0   0.0   0.0   +3.0E-5 $
08  SPH   0.0   0.0   0.0   +4.0E-5 $
09  SPH   0.0   0.0   0.0   +5.0E-5 $
10  SPH   0.0   0.0   0.0   +6.0E-5 $
11  SPH   0.0   0.0   0.0   +7.0E-5 $
12  SPH   0.0   0.0   0.0   +8.0E-5 $
13  SPH   0.0   0.0   0.0   +9.0E-5 $
14  SPH   0.0   0.0   0.0   +1.0E-4 $
15  SPH   0.0   0.0   0.0   +2.0E-4 $
16  SPH   0.0   0.0   0.0   +5.0E-4 $
17  SPH   0.0   0.0   0.0   +8.0E-4 $
18  SPH   0.0   0.0   0.0   +1.0E-3 $
19  SPH   0.0   0.0   0.0   +2.0E-3 $
20  SPH   0.0   0.0   0.0   +5.0E-3 $
21  SPH   0.0   0.0   0.0   +8.0E-3 $
22  SPH   0.0   0.0   0.0   +1.0E-2 $
23  SPH   0.0   0.0   0.0   +2.0E-2 $
24  SPH   0.0   0.0   0.0   +5.0E-2 $
25  SPH   0.0   0.0   0.0   +8.0E-2 $
26  SPH   0.0   0.0   0.0   +0.1    $
27  SPH   0.0   0.0   0.0   +0.2    $
28  SPH   0.0   0.0   0.0   +0.5    $
29  SPH   0.0   0.0   0.0   +0.8    $
30  SPH   0.0   0.0   0.0   +1.0    $

c Data Cards
c Mode: transport photons and electrons (p e)
mode p e
c **** Physics Table *****
phys:p 100   &   $  Emax
         0   &   $  0 always
         0   &   $  0 always
         0   &   $ -1 always
         1       $  1 ALWAYS
phys:e 100   &   $  Emax
         0   &   $  0 always
         0   &   $  0 always
         0   &   $  0 always
         0   &   $  0 always
         1   &   $  1 always
         1   &   $  1 always
         1   &   $  1 always
         1   &   $  1 always
         0       $  0 always
c source definition:
sdef par=p erg=d3 pos=0 0 0
si3 L  0.4971   0.3574    0.03975  0.02317  0.02317  0.02272  &
       0.02272  0.0227    0.0227   0.02022  0.02022  0.02008  &
       0.02007  0.003147  0.00285  0.0027
sp3    0.00004  0.000221  0.0007   0.00198  0.0174   0.00751  &
       0.066    0.00396   0.0348   0.04269  0.375    0.0225   &
       0.198    0.00129   0.0161   0.0181
```

```
c
c ==== Material definitions ====
m1    1000 +2      8000  +1                  $ Water
c
c ==== Tally Specifications ====
fc16 Photon F6 Energy Deposition Tally. Unit: Gy/hr per 1 Bq Pd-103.
f16:p  1   2   3   4   5   6   7   8   9  10   &
      11  12  13  14  15  16  17  18  19  20   &
      21  22  23  24  25  26  27  28  29  30
fm16   5.768E-7  $ Gy/hr per 1 Bq Pd-103
c
fc26 Electron F6 Energy Deposition Tally.  Unit: Gy/hr per 1 Bq Pd-103.
f26:e  1   2   3   4   5   6   7   8   9  10   &
      11  12  13  14  15  16  17  18  19  20   &
      21  22  23  24  25  26  27  28  29  30
fm26   5.768E-7  $ Gy/hr per 1 Bq Pd-103
c
c ==== MESH TALLY =======
tmesh
SMesh3 total
    cora3  1.0E-3 98i  +1.0E+0
    corb3  0.001       +180.0
    corc3  0.001       +360.0
endmd
c ==== PRINT CONTROLS =====
PRINT 10 40 50 60 72 100 110 120 170 200
c ==== RUNTIME CONTROLS =====
ctme 1200
```

The input data set for the electron source term, is:

```
Energy deposition by electrons emitted by 103Pd & 103mRh
01  1  -1.0     -1      imp:p,e=1     $ Seed
02  1  -1.0     -2  +1  imp:p,e=1     $ Water
03  1  -1.0     -3  +2  imp:p,e=1     $ Water
04  1  -1.0     -4  +3  imp:p,e=1     $ Water
05  1  -1.0     -5  +4  imp:p,e=1     $ Water
06  1  -1.0     -6  +5  imp:p,e=1     $ Water
07  1  -1.0     -7  +6  imp:p,e=1     $ Water
08  1  -1.0     -8  +7  imp:p,e=1     $ Water
09  1  -1.0     -9  +8  imp:p,e=1     $ Water
10  1  -1.0    -10  +9  imp:p,e=1     $ Water
11  1  -1.0    -11 +10  imp:p,e=1     $ Water
12  1  -1.0    -12 +11  imp:p,e=1     $ Water
13  1  -1.0    -13 +12  imp:p,e=1     $ Water
14  1  -1.0    -14 +13  imp:p,e=1     $ Water
15  1  -1.0    -15 +14  imp:p,e=1     $ Water
16  1  -1.0    -16 +15  imp:p,e=1     $ Water
17  1  -1.0    -17 +16  imp:p,e=1     $ Water
18  1  -1.0    -18 +17  imp:p,e=1     $ Water
19  1  -1.0    -19 +18  imp:p,e=1     $ Water
20  1  -1.0    -20 +19  imp:p,e=1     $ Water
21  1  -1.0    -21 +20  imp:p,e=1     $ Water
22  1  -1.0    -22 +21  imp:p,e=1     $ Water
23  1  -1.0    -23 +22  imp:p,e=1     $ Water
```

```
24  1  -1.0     -24 +23  imp:p,e=1     $ Water
25  1  -1.0     -25 +24  imp:p,e=1     $ Water
26  1  -1.0     -26 +25  imp:p,e=1     $ Water
27  1  -1.0     -27 +26  imp:p,e=1     $ Water
28  1  -1.0     -28 +27  imp:p,e=1     $ Water
29  1  -1.0     -29 +28  imp:p,e=1     $ Water
30  1  -1.0     -30 +29  imp:p,e=1     $ Water
31  0           +30      imp:p,e=0     $ UmWelt

c Surface Cards
01  SPH   0.0   0.0   0.0   +1.0E-6 $
02  SPH   0.0   0.0   0.0   +2.0E-6 $
03  SPH   0.0   0.0   0.0   +5.0E-6 $
04  SPH   0.0   0.0   0.0   +8.0E-6 $
05  SPH   0.0   0.0   0.0   +1.0E-5 $
06  SPH   0.0   0.0   0.0   +2.0E-5 $
07  SPH   0.0   0.0   0.0   +3.0E-5 $
08  SPH   0.0   0.0   0.0   +4.0E-5 $
09  SPH   0.0   0.0   0.0   +5.0E-5 $
10  SPH   0.0   0.0   0.0   +6.0E-5 $
11  SPH   0.0   0.0   0.0   +7.0E-5 $
12  SPH   0.0   0.0   0.0   +8.0E-5 $
13  SPH   0.0   0.0   0.0   +9.0E-5 $
14  SPH   0.0   0.0   0.0   +1.0E-4 $
15  SPH   0.0   0.0   0.0   +2.0E-4 $
16  SPH   0.0   0.0   0.0   +5.0E-4 $
17  SPH   0.0   0.0   0.0   +8.0E-4 $
18  SPH   0.0   0.0   0.0   +1.0E-3 $
19  SPH   0.0   0.0   0.0   +2.0E-3 $
20  SPH   0.0   0.0   0.0   +5.0E-3 $
21  SPH   0.0   0.0   0.0   +8.0E-3 $
22  SPH   0.0   0.0   0.0   +1.0E-2 $
23  SPH   0.0   0.0   0.0   +2.0E-2 $
24  SPH   0.0   0.0   0.0   +5.0E-2 $
25  SPH   0.0   0.0   0.0   +8.0E-2 $
26  SPH   0.0   0.0   0.0   +0.1    $
27  SPH   0.0   0.0   0.0   +0.2    $
28  SPH   0.0   0.0   0.0   +0.5    $
29  SPH   0.0   0.0   0.0   +0.8    $
30  SPH   0.0   0.0   0.0   +1.0    $

c Data Cards
c Mode: transport photons and electrons (p e)
mode p e
c **** Physics Table *****
phys:p 100   &   $  Emax
         0   &   $  0 always
         0   &   $  0 always;
         0   &   $ -1 always;
         1       $  1 ALWAYS
phys:e 100   &   $  Emax
         0   &   $  0 always
         0   &   $  0 always
         0   &   $  0 always
         0   &   $  0 always
         1   &   $  1 always
         1   &   $  1 always
         1   &   $  1 always
```

```
         1   &   $  1 always
         0       $  0 always
c source definition:
sdef par=e erg=d3 pos=0 0 0
si3 L  3.975E-02  3.925E-02  3.675E-02  3.660E-02  3.634E-02  &
       2.220E-02  1.953E-02  1.953E-02  1.683E-02  1.683E-02  &
       1.653E-02  3.059E-03  3.052E-03  2.753E-03  2.275E-03  &
       2.270E-03  2.265E-03
sp3     2.53E-02   1.47E-01   4.24E-01   3.00E-01   5.44E-03  &
        5.79E-03   4.65E-02   5.29E-03   1.13E-01   1.29E-02  &
        9.75E-02   3.26E-02   2.80E-02   2.70E-01   2.30E-01  &
        6.17E-01   5.31E-01
c
c ==== Material definitions ====
m1    1000 +2      8000  +1                $ Water
c
c ==== Tally Specifications ====
fc16 Secondary Photon Eng dep. Unit: Gy/hr per 1 Bq Pd-103.
f16:p  1   2   3   4   5   6   7   8   9  10   &
      11  12  13  14  15  16  17  18  19  20   &
      21  22  23  24  25  26  27  28  29  30
fm16   5.768E-7  $ Convert to SI units
c
fc26 Electron F6 Eng dep Tally.  Unit: Gy/hr per 1 Bq Pd-103.
f26:e  1   2   3   4   5   6   7   8   9  10   &
      11  12  13  14  15  16  17  18  19  20   &
      21  22  23  24  25  26  27  28  29  30
fm26   5.768E-7  $ Convert to SI units
c
c ==== MESH TALLY =======
tmesh
SMesh3 total
    cora3  1e-6  998i   1e-1
    corb3  0.001       +180.0
    corc3  0.001       +360.0
endmd
c ==== PRINT CONTROLS =====
PRINT 10 40 50 60 72 100 110 120 170 200
c ==== RUNTIME CONTROLS =====
ctme 3000
```

Dose distributions around a point source of ^{103}Pd in equilibrium with its transition product, ^{103m}Rh, has been calculated with the Monte Carlo radiation transport programme, MCNP. Energies of emitted particles were taken from ICRP-107.

Figure 12.4 shows, on a linear dose rate axis scale, that the dose rate close to a ^{103}Pd/^{103m}Rh source is dominated by energy deposition by electrons. Figure 12.5 employs a logarithmic scale for the vertical dose rate axis to highlight the detailed contributions of different modes of energy deposition. An F6 energy deposition tally in the code MCNP was used to obtain these results.

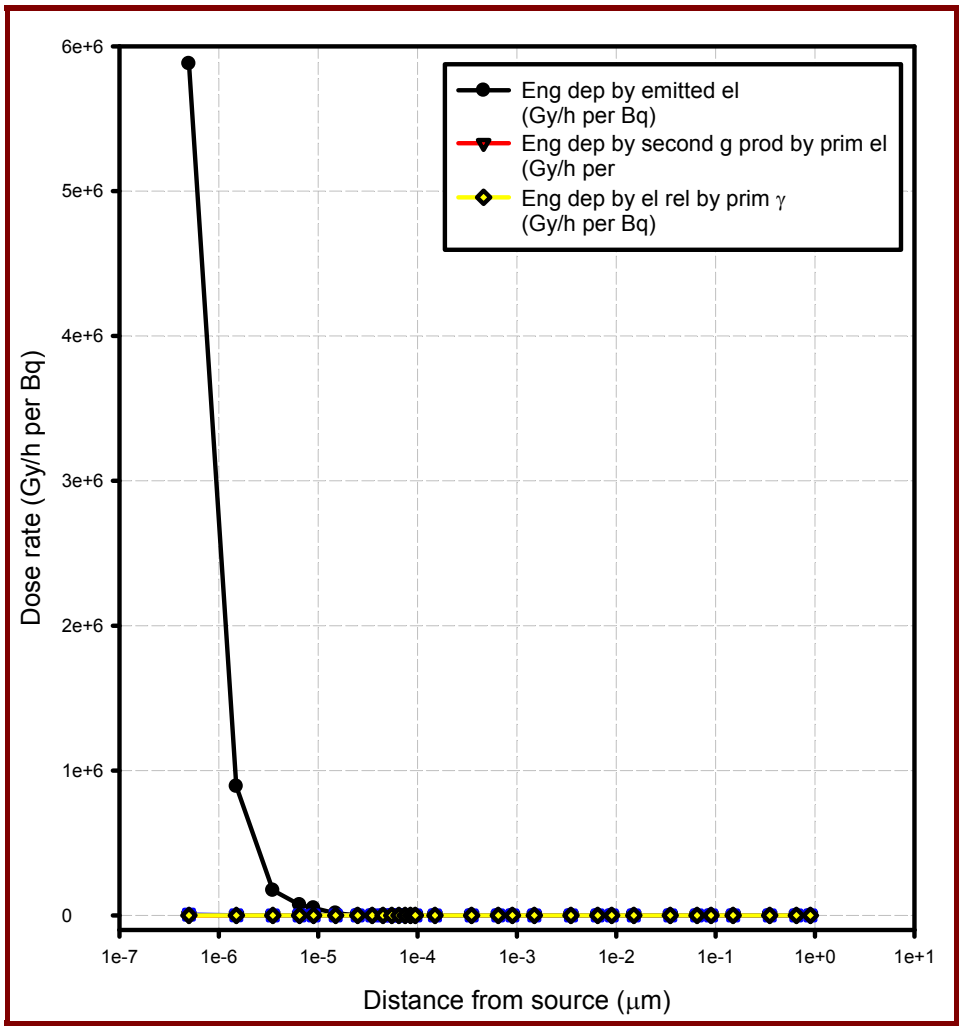

Figure 12.4: *The dose rate close to a $^{103}Pd/^{103m}Rh$ source is dominated by energy deposition by electrons. More than 99% of energy is deposited within a distance of about 0.2 μm from the point source, which is quite small compared to the dimensions of a mitochondrion in a typical animal cell.*

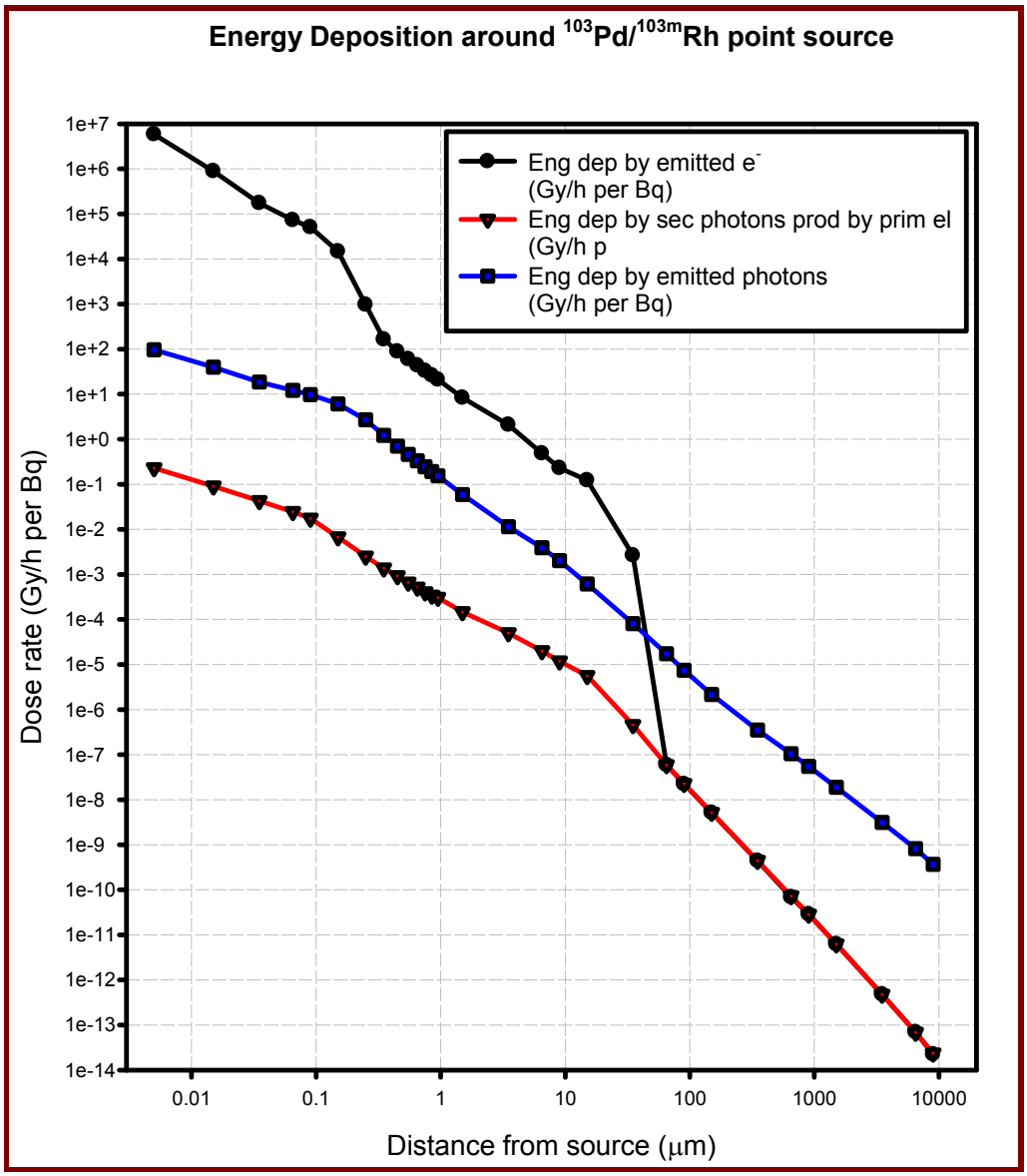

Figure 12.5: *The dose rate close to a $^{103}Pd/^{103m}Rh$ source is dominated by energy deposition by electrons up to a distance of about 50 μm. About 99.9% of the dose is deposited within a radius of 0.5 μm from the source, i.e. damage will be concentrated within the mitochondrion if the chelate that contains the ^{103}Pd is concentrated inside the mitochondria of the prostate cancer cells.*

The percentage energy deposition within a given radius R around a point source of $^{103}Pd/^{103m}Rh$,

$$\frac{\int_0^R D(r)\,dr}{\int_0^\infty D(r)\,dr}$$

where $D(r)$ is the absorbed dose rate at radius r, is summarised in Table 12.3.

Table 12.3: *Percentage energy deposition within a given radius around a point source of* $^{103}Pd/^{103m}Rh$.

Radius (μm)	**Percentage energy deposition within radius**
0.1	95.44%
0.2	99.36%
0.3	99.85%
0.5	99.92%
1.0	99.95%
5.0	99.99%

12.15 Case study RSDD-15: A beam of 200 MeV protons incident upon a block of tissue-equivalent material (TEM)

A beam of 200 MeV protons is incident upon a 30 cm × 30 cm × 30 cm block of tissue-equivalent material (TEM).

Use the mesh-tally capability of MCNP to make 2-D plots of the following:

- Proton fluence-rate
- Neutron fluence-rate
- Photon fluence-rate
- Total energy deposition, i.e. the total absorbed dose rate

Solution: Case study RSDD-15

```
Particle beam of protons incident upon a 30cm x 30cm x 30cm wax block
c Cell Cards
1  2  -0.92      -1       imp:n,p,h=1       $ Paraffin Wax
2  1  1.29E-3    +1  -2   imp:n,p,h=1       $ Air
3  0             +2       imp:n,p,h=0       $ Umwelt

c Surface Cards
1  RPP  -15.0 +15.0 -15.0 +15.0 -15.0 +15.0    $ Wax
2  RPP  -50.0 +50.0 -50.0 +50.0 -50.0 +50.0    $ Air

c Data Cards
c Mode: transport protons, neutrons and photons
mode h n p
c Simple proton beam with 2 cm diameter travelling in +z direction
sdef par=h erg=200    &
     pos=0  0  -30    &
     axs=0  0  1      &
     vec=0  0  1      &
     dir=1            &
     ext=0            &
     rad=d1
si1 h 0.0  1.0    $
sp1   -21  1      $
c
c Material definitions
m1   7014  -0.79     8016  -0.21        $ Air at STP
m2   1001  -0.1486   6000  -0.8514      $ Paraffin wax C(n)H(2n+2)
c
c **** Physics Table *****
phys:n  200    &   $     Emax
          0    &   $     0 always
          0    &   $     0 always
      -1001    &   $ -1001 always (analog production of delayed neutrons from
```

```
fission using models when libraries are missing)
          -1    &    $     -1 always (mix & match)
           0    &    $      0 always
           0         $      0 always
phys:p   200    &    $      Emax
           0    &    $      0 always (generate el in MODE e calcs)
           0    &    $      0 always (Coherent/Thomson scattering on)
          -1    &    $     -1 always (photonuclear reaction on)
           1    &    $      1 always (1 = Doppler broadening off)
           0         $      0 usually but -102 for delayed gamma production.
phys:e   200    &    $      Emax
           0    &    $      0 always
           0    &    $      0 always
           0    &    $      0 always
           0    &    $      0 always
           1    &    $      1 always
           1    &    $      1 always
           1    &    $      1 always
           1    &    $      1 always
           0         $      0 always
phys:h   200    &    $      Emax
           0    &    $      0 always
          -1    &    $     -1 always
           j    &    $      j always
           0    &    $      0 always
           j    &    $      j always
           0         $      0 always
c
c ==== Mesh Tally
tmesh
 rmesh1:h flux
  cora1   -2.0         +2.0
  corb1  -30.0  239i   +30.0
  corc1  -30.0  239i   +30.0
c rmesh3 total
c   cora3   -2.0         +2.0
c   corb3  -30.0  119i   +30.0
c   corc3  -30.0  119i   +30.0
endmd
c ==== PRINT CONTROLS =====
PRINT  10  40  50  60  72 100 110 120 170 200
c === RUNTIME CONTROLS ======
ctme 90
```

The cards

```
tmesh
 rmesh1:h flux
  cora1   -2.0         +2.0
  corb1  -30.0  239i   +30.0
  corc1  -30.0  239i   +30.0
endmd
```

The cards

```
tmesh
  rmesh3 total
    cora3   -2.0        +2.0
    corb3  -30.0  119i  +30.0
    corc3  -30.0  119i  +30.0
endmd
```

Note that no $ inline comment statements may appear inside a tally mesh block.

Some mesh tally plots that were generated for the proton beam stopped in the block of paraffin wax, are shown below in Figures 12.6 to 12.9.

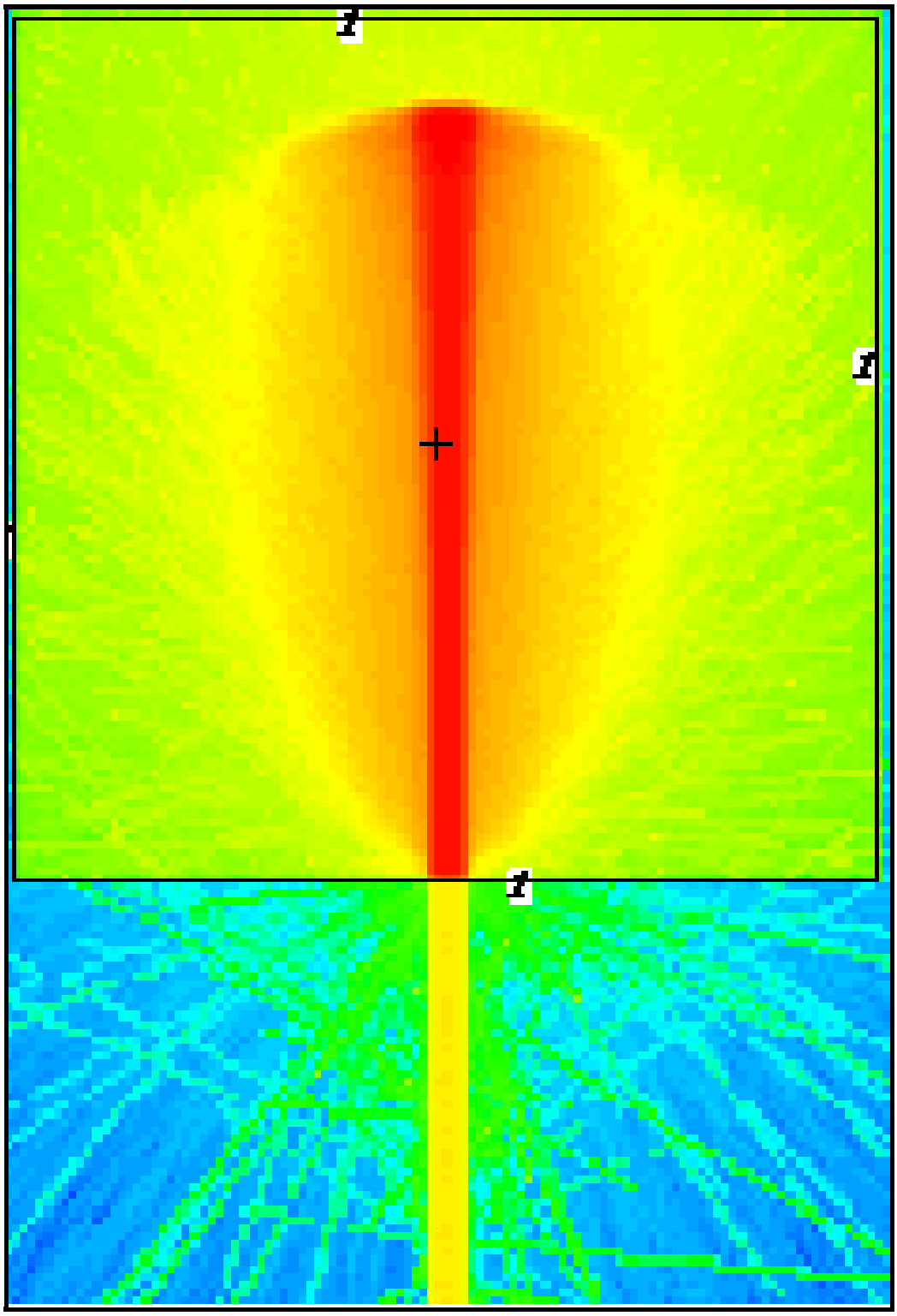

Figure 12.6: *Total energy deposition mesh tally for a 200 MeV proton beam stopped in a block of paraffin wax.*

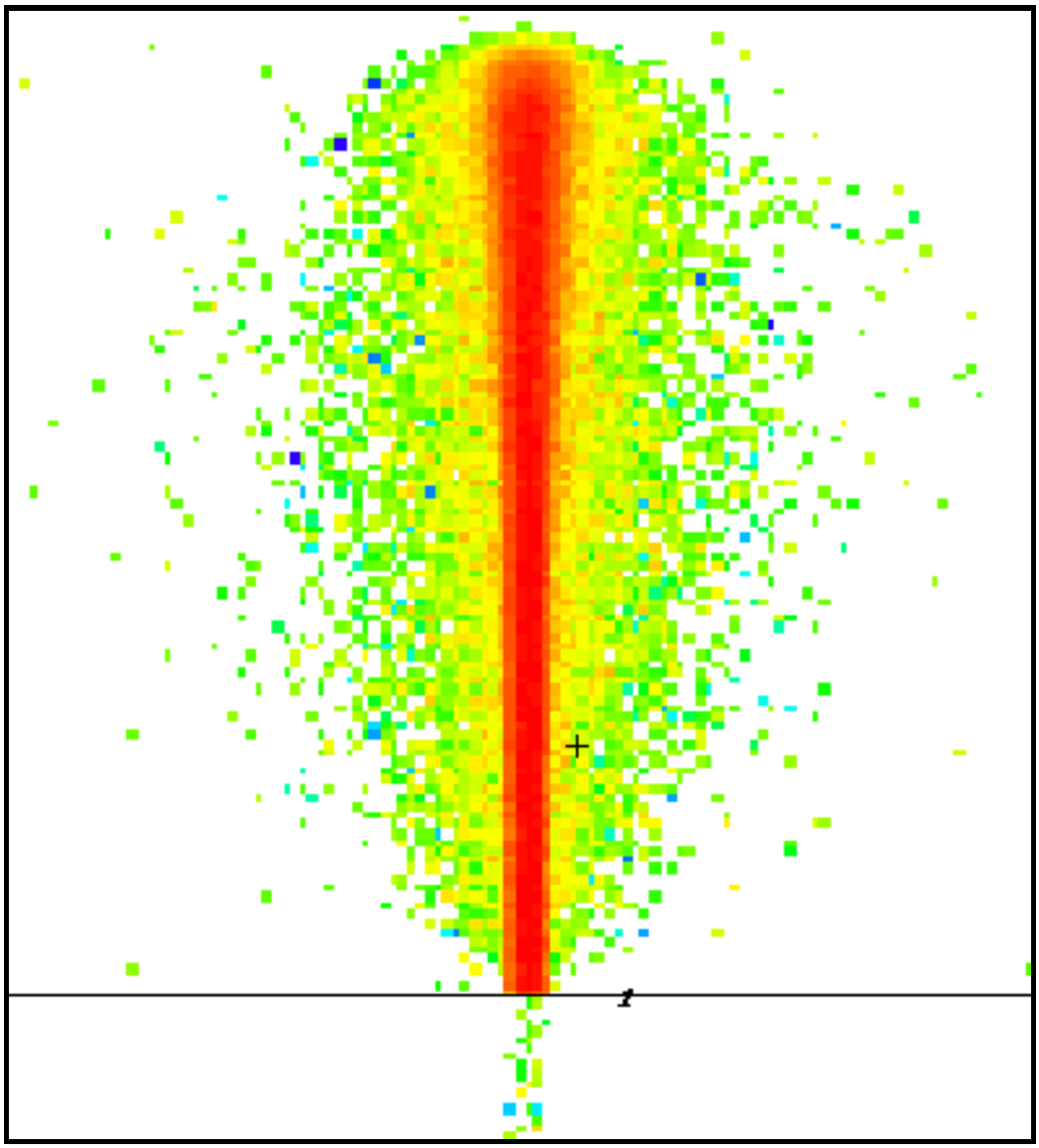

Figure 12.7: *Energy deposition by recoils, for a 200 MeV proton beam stopped in a block of paraffin wax.*

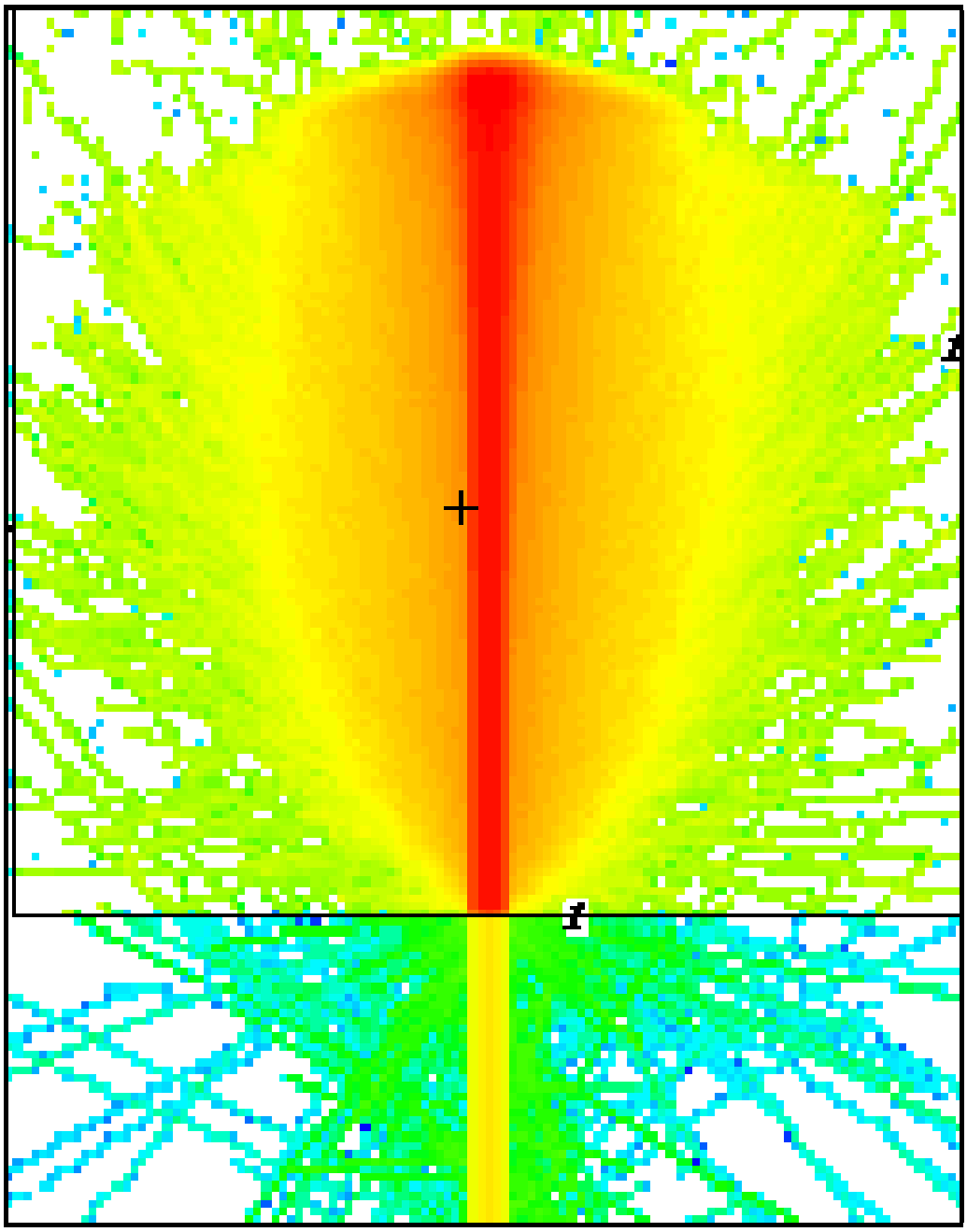

Figure 12.8: *Energy deposition by ionisation, for a 200 MeV proton beam stopped in a block of paraffin wax.*

Generating ASCII data files with the utility GRIDCONV

Next, the use of the utility program, GRIDCONV, which is shipped with MCNPX, was illustrated. The binary mesh tally data file was converted to ASCII format (TECPLOT) and then imported into the SigmaPlot plotting package to produce the contour plot shown in Figure 12.9.

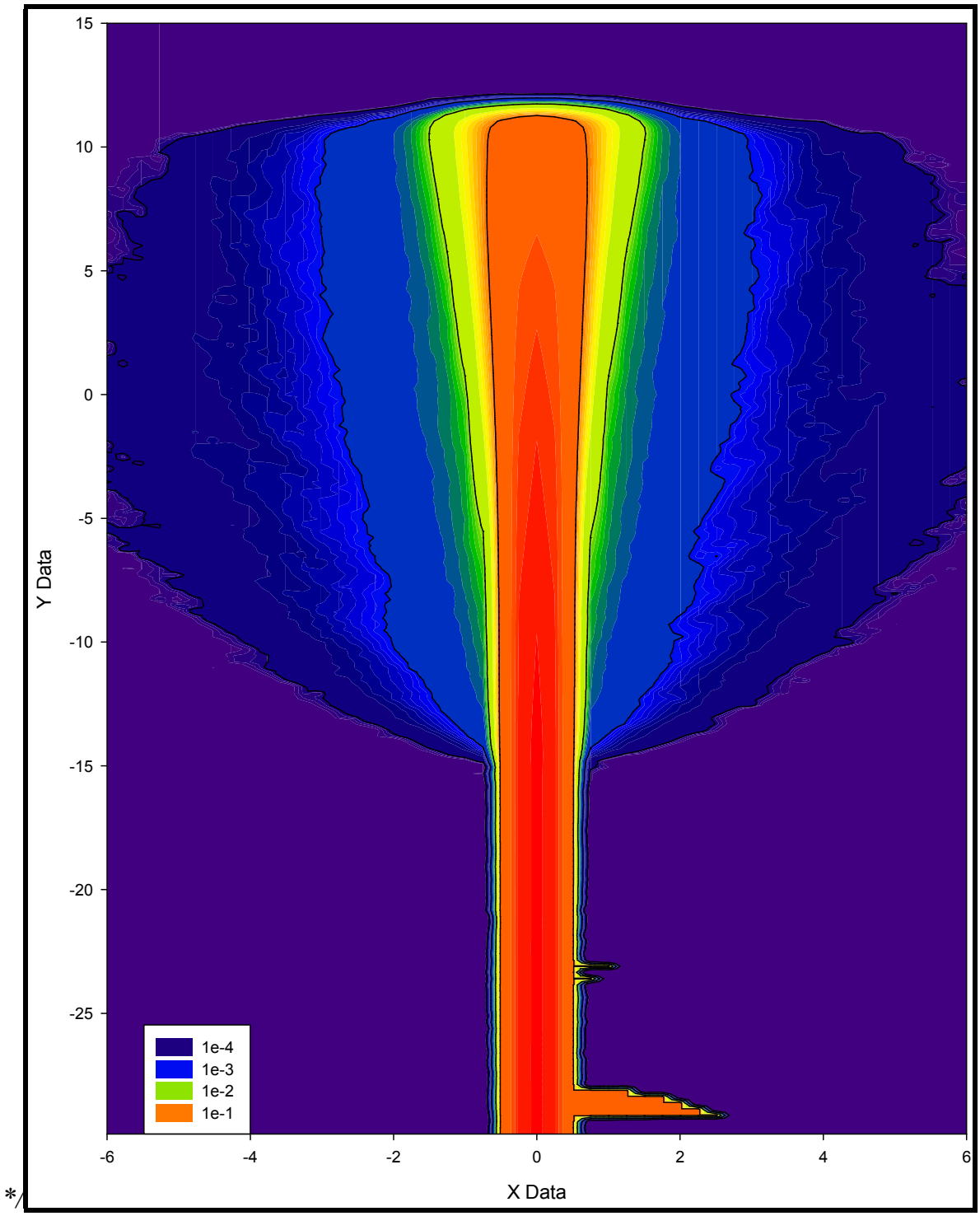

Figure 12.9: *Contour plot of proton fluence-rate when a 200 MeV proton beam is stopped in a block of paraffin wax.*

12.16 Case study RSDD-16: Shield design for a radionuclide target bombardment station at a particle accelerator facility

A radionuclide production beam target station at a proton accelerator facility requires a local shield to shield the neutrons and ionising photons produced when the intense proton beam strikes the target. At the facility under assessment, a 100 μA, 66 MeV proton beam strikes a stopping-length copper target.

Given: Iron, paraffin wax, boron carbide (B_4C) and lead is available.

Problem: Design a reasonably optimal radiation shield.

Solution: Case Study RSDD-16

The input data set is shown below.

```
HBTS-2 Shield Design, Real Shield, Proton Beam & Tally Tori
c Cell Cards
01    1    -8.92             -01     imp:h=1 imp:n,p=1       $ Cu Target
02    2    -1.21E-3    +01   -02     imp:h=1 imp:n,p=1       $ Air
03    3    -7.86       +02   -03     imp:h=0 imp:n,p=1       $ Fe Shield
04    4    -0.93787    +03   -04     imp:h=0 imp:n,p=1       $ Paraffin Wax
05    4    -0.93787    +04   -05     imp:h=0 imp:n,p=1       $ Paraffin Wax
06    4    -0.93787    +05   -06     imp:h=0 imp:n,p=2       $ Paraffin Wax
07    4    -0.93787    +06   -07     imp:h=0 imp:n,p=3       $ Paraffin Wax
08    4    -0.93787    +07   -08     imp:h=0 imp:n,p=4       $ Paraffin Wax
09    4    -0.93787    +08   -09     imp:h=0 imp:n,p=8       $ Paraffin Wax
10    4    -0.93787    +09   -10     imp:h=0 imp:n,p=15      $ Paraffin Wax
11    4    -0.93787    +10   -11     imp:h=0 imp:n,p=20      $ Paraffin Wax
12    4    -0.93787    +11   -12     imp:h=0 imp:n,p=30      $ Paraffin Wax
13    4    -0.93787    +12   -13     imp:h=0 imp:n,p=50      $ Paraffin Wax
14    4    -0.93787    +13   -14     imp:h=0 imp:n,p=90      $ Paraffin Wax
15    4    -0.93787    +14   -15     imp:h=0 imp:n,p=110     $ Paraffin Wax
16    4    -0.93787    +15   -16     imp:h=0 imp:n,p=150     $ Paraffin Wax
17    4    -0.93787    +16   -17     imp:h=0 imp:n,p=250     $ Paraffin Wax
18    4    -0.93787    +17   -18     imp:h=0 imp:n,p=400     $ Paraffin Wax
19    4    -0.93787    +18   -19     imp:h=0 imp:n,p=600     $ Paraffin Wax
20    4    -0.93787    +19   -20     imp:h=0 imp:n,p=800     $ Paraffin Wax
21    3    -7.86       +20   -21     imp:h=0 imp:n,p=800     $ Fe shell, structural
22    5   -11.35       +21   -22     imp:h=0 imp:n,p=800     $ Lead
23    3    -7.86       +22   -23     imp:h=0 imp:n,p=800     $ Fe shell, structural
c
24    2    -1.21E-3    +23  -999
                       #201 #202 #203
                       #204 #205 #206
                       #207 #208 #209
                       #210          imp:h=1 imp:n,p=900     $ Air
c
201  7    2.00E-03   -101       imp:h=1 imp:n,p=900    $ Tally-torus for polar angle (°) =     0.0
202  7    2.00E-03   -102       imp:h=1 imp:n,p=900    $ Tally-torus for polar angle (°) =    10.0
203  7    2.00E-03   -103       imp:h=1 imp:n,p=900    $ Tally-torus for polar angle (°) =    30.0
```

```
204  7    2.00E-03   -104        imp:h=1 imp:n,p=900    $ Tally-torus for polar angle (°) =    45.0
205  7    2.00E-03   -105        imp:h=1 imp:n,p=900    $ Tally-torus for polar angle (°) =    60.0
206  7    2.00E-03   -106        imp:h=1 imp:n,p=900    $ Tally-torus for polar angle (°) =    90.0
207  7    2.00E-03   -107        imp:h=1 imp:n,p=900    $ Tally-torus for polar angle (°) =   120.0
208  7    2.00E-03   -108        imp:h=1 imp:n,p=900    $ Tally-torus for polar angle (°) =   135.0
209  7    2.00E-03   -109        imp:h=1 imp:n,p=900    $ Tally-torus for polar angle (°) =   150.0
210  7    2.00E-03   -110        imp:h=1 imp:n,p=900    $ Tally-torus for polar angle (°) =   180.0
c
300  0                 +999         imp:h,n,p=0             $ UmWelt
c ============================================================================

c ============================================================================
c Surface Cards
01   RCC      0.0     0.0  +88.0    0.0     0.0    +1.0
           +1.5                                            $ OR: Copper target
02   RCC      0.0     0.0  +48.0    0.0     0.0   +80.0
          +40.0                                            $ OR: Inner Air cavity
03   RCC      0.0     0.0  +23.0    0.0     0.0 +130.0
          +65.0                                            $ OR: Inner Fe Layer
c = = = = = = = = = =
04   RCC      0.0     0.0  +22.0    0.0     0.0 +132.0
          +66.0                                            $ OR: Wax & 3% B4C Layer
01
05   RCC      0.0     0.0  +21.0    0.0     0.0 +134.0
          +67.0                                            $ OR: Wax & 3% B4C Layer
02
06   RCC      0.0     0.0  +20.0    0.0     0.0 +136.0
          +68.0                                            $ OR: Wax & 3% B4C Layer
03
07   RCC      0.0     0.0  +19.0    0.0     0.0 +138.0
          +69.0                                            $ OR: Wax & 3% B4C Layer
04
08   RCC      0.0     0.0  +18.0    0.0     0.0 +140.0
          +70.0                                            $ OR: Wax & 3% B4C Layer
05
09   RCC      0.0     0.0  +17.0    0.0     0.0 +142.0
          +71.0                                            $ OR: Wax & 3% B4C Layer
06
10   RCC      0.0     0.0  +16.0    0.0     0.0 +144.0
          +72.0                                            $ OR: Wax & 3% B4C Layer
07
11   RCC      0.0     0.0  +15.0    0.0     0.0 +146.0
          +73.0                                            $ OR: Wax & 3% B4C Layer
08
12   RCC      0.0     0.0  +14.0    0.0     0.0 +148.0
          +74.0                                            $ OR: Wax & 3% B4C Layer
09
13   RCC      0.0     0.0  +13.0    0.0     0.0 +150.0
          +75.0                                            $ OR: Wax & 3% B4C Layer
10
14   RCC      0.0     0.0  +12.0    0.0     0.0 +152.0
          +76.0                                            $ OR: Wax & 3% B4C Layer
11
15   RCC      0.0     0.0  +11.0    0.0     0.0 +154.0
          +77.0                                            $ OR: Wax & 3% B4C Layer
12
16   RCC      0.0     0.0  +10.0    0.0     0.0 +156.0
          +78.0                                            $ OR: Wax & 3% B4C Layer
```

```
13
17  RCC     0.0    0.0   +9.0   0.0    0.0 +158.0
          +79.0                                          $ OR: Wax & 3% B4C Layer
14
18  RCC     0.0    0.0   +8.0   0.0    0.0 +160.0
          +80.0                                          $ OR: Wax & 3% B4C Layer
15
19  RCC     0.0    0.0   +7.0   0.0    0.0 +162.0
          +81.0                                          $ OR: Wax & 3% B4C Layer
16
20  RCC     0.0    0.0   +6.0   0.0    0.0 +164.0
          +82.0                                          $ OR: Wax & 3% B4C Layer
17
21  RCC     0.0    0.0   +5.0   0.0    0.0 +166.0
          +83.0                                          $ OR: Steel shell
(structural)
22  RCC     0.0    0.0   +1.0   0.0    0.0 +174.0
          +87.0                                          $ OR: Pb
23  RCC     0.0    0.0    0.0   0.0    0.0 +176.0
          +88.0                                          $ OR: Steel shell
(structural)
c = = = = = = = = = =
101  SPH   0.0  0.0     238.0      10.0                    $ Tally-sphere for polar angle (°) =    0.0
102  TZ    0.0  0.0   235.721    26.047       3.5       3.5     $ Tally-torus for polar angle (°) =   10.0
103  TZ    0.0  0.0   217.904    75.000       5.0       5.0     $ Tally-torus for polar angle (°) =   30.0
104  TZ    0.0  0.0   194.066   106.066       7.1       7.1     $ Tally-torus for polar angle (°) =   45.0
105  TZ    0.0  0.0   163.000   129.904       8.7       8.7     $ Tally-torus for polar angle (°) =   60.0
106  TZ    0.0  0.0    88.000   150.000      10.0      10.0     $ Tally-torus for polar angle (°) =   90.0
107  TZ    0.0  0.0    13.000   129.904       8.7       8.7     $ Tally-torus for polar angle (°) =  120.0
108  TZ    0.0  0.0   -18.066   106.066       7.1       7.1     $ Tally-torus for polar angle (°) =  135.0
109  TZ    0.0  0.0   -41.904    75.000       5.0       5.0     $ Tally-torus for polar angle (°) =  150.0
110  SPH   0.0  0.0     -62.0      10.0                    $ Tally-sphere for polar angle (°) =  180.0
c = = = = = = = = = =
999 RCC     0.0    0.0  -900.0   0.0    0.0 +2E3  +900.0       $ Boundary: Outer medium & UmWelt
c ===============================================================================

c ===============================================================================
c Data Cards
c Mode: transport protons, neutrons and photons
mode h n p
c source: Simple Proton beam in y-direction
sdef   par=h erg=66
       pos=0  0 +70
       axs=0  0   1
       vec=0  0   1
       dir=1
       ext=0
       rad=d1
si1 h 0.0  0.5      $ Beam radius sampling limits
sp1   -21  1        $ Beam radius sampling probability
c
c ==================================
c Material definitions
m1     29063   +69.17
       29065   +30.83                                  $ Copper Target
m2      6000   -1.24E-4          $ Air, dry.  Density = 1.205E-03 g/cc
        7014   -0.755267         $ Air, dry.  Density = 1.205E-03 g/cc
        8016   -0.231781         $ Air, dry.  Density = 1.205E-03 g/cc
```

```
      18000   -0.012827          $ Air, dry.  Density = 1.205E-03 g/cc
m3    26054   +5.8                    $ Iron
      26056  +91.7                    $ Iron
      26057   +2.2                    $ Iron
      26058  +0.3                     $ Iron
m4     1001      -1.4416E-01          $ Paraffin wax  3% B4C
       6012      -8.3237E-01          $ Paraffin wax  3% B4C
       5010      -4.3274E-03          $ Paraffin wax  3% B4C
       5011      -1.9152E-02          $ Paraffin wax  3% B4C
m5    82206   +24.1                     $ Lead
      82207   +22.1                     $ Lead
      82208   +52.4                     $ Lead
m6     1001  -0.013                   $ Type 04 Ordinary Concrete
       8016  -1.165                   $ Type 04 Ordinary Concrete
      11023  -0.040                   $ Type 04 Ordinary Concrete
      12000  -0.010                   $ Type 04 Ordinary Concrete
      13027  -0.108                   $ Type 04 Ordinary Concrete
      14000  -0.740                   $ Type 04 Ordinary Concrete
      16000  -0.003                   $ Type 04 Ordinary Concrete
      19000  -0.045                   $ Type 04 Ordinary Concrete
      20000  -0.196                   $ Type 04 Ordinary Concrete
      26000  -0.030                   $ Type 04 Ordinary Concrete
m7     8016  -6.143E-01               $ Human tissue
       6000  -2.286E-01               $ Human tissue
       1001  -1.000E-01               $ Human tissue
       7014  -2.571E-02               $ Human tissue
      20000  -1.429E-02               $ Human tissue
      15031  -1.114E-02               $ Human tissue
      19000  -2.000E-03               $ Human tissue
      16000  -2.000E-03               $ Human tissue
      11023  -1.429E-03               $ Human tissue
      17000  -1.357E-03               $ Human tissue
      12000  -2.714E-04               $ Human tissue
      26000  -6.000E-05               $ Human tissue
c =======
c **** Physics Table *****
phys:n 200      $  Emax
         0      $  0 always
         0      $  0 always
        -1      $ -1 always
        -1      $ -1 always
         0      $  0 always
         0      $  0 always
c
phys:p 200      $  Emax
         0
         0
        -1
         1
c
phys:e 200      $  Emax
         0      $  0 always
         0      $  0 always
         0      $  0 always
         0      $  0 always
         1      $  1 always
         1      $  1 always
         1      $  1 always
```

```
         1      $  1 always
         0      $  0 always
c
phys:h 200      $  Emax
         0      $  0 always
        -1      $ -1 always
         j      $  j always
         0      $  0 always
         j      $  j always
         0      $  0 always
c
c =============
c
fc14 Neutron fluence rate spectrum in Fe layers adjacent to wax layer
f14:n 3 21
e14  1e-8 9log 1e2
fm14 6.24151e14
c
c =============
c
fc24 Photon fluence-rate spectrum in Fe layers adjacent to wax layer
f24:p 3 21
e24  0.01 0.1  0.4  0.5  1.0   2.0   2.3
     3.0  4.0  5.0  6.0  7.0   8.0  10.0  100.0
fm24 6.24151e14
c
c =============
c
fc34 Photon fluence-rate spectrum in outer wax layer
f34:p 20
e34  0.01 0.1  0.4  0.5  1.0   2.0   2.3
     3.0  4.0  5.0  6.0  7.0   8.0  10.0  100.0
fm34 6.24151E14
c
c =============
c
fc54 Neutron fluence-rate & spectrum in TallySpheres
f54:n  201  202  203  204  205  206  207  208  209  210
e54  1e-8 9log 1e2
fm54 6.24151E14
c
c =============
c
fc64 Photon fluence-rate & spectrum in TallySpheres
f64:p  201  202  203  204  205  206  207  208  209  210
e64  0.01 0.1  0.2  0.3  0.4   0.5   1.0   1.5    2.0  2.3  2.5
     3.0  4.0  5.0  6.0  7.0   8.0   9.0  10.0  100.0
fm64 6.24151E14
c
c =============
c
fc76 Tally neutron absorbed dose rate
f76:n  201  202  203  204  205  206  207  208  209  210
fm76 3.6E8
c
c =============
c
fc86 Tally photon absorbed dose rate
```

```
f86:p  201  202  203  204  205  206  207  208  209  210
fm86 3.6E8
c
c =============
c
fc96 Tally total absorbed dose rate
+f96   201  202  203  204  205  206  207  208  209  210
fm96 3.6E8
c
c =============
c
c << Mesh Tally >>
tmesh
 CMesh11:n flux
  cora11     0.0  148i   +150.0
  corb11  -100.0  374i   +276.0
  corc11                 +360.0
 CMesh21:p flux
  cora21     0.0  148i   +150.0
  corb21  -100.0  374i   +276.0
  corc21                 +360.0
 CMesh31:n dose  31  3  2  6.24151E14
  cora31     0.0  148i   +150.0
  corb31  -100.0  374i   +276.0
  corc31                 +360.0
 CMesh41:p dose  31  3  2  6.24151E14
  cora41     0.0  148i   +150.0
  corb41  -100.0  374i   +276.0
  corc41                 +360.0
endmd
c ==============
PRINT 10 40 50 60 72 100 110 120 170 200
c ==============
ctme 9900
```

12.17 Case study RSDD-17: Cell importance biasing technique

The aim of cell importance biasing is to keep the particle population as constant as possible in each cell.

When particles cross over from a cell with an IMPortance of e.g. 1 to a cell with an IMPortance of e.g. 2, the particle is split in 2 particles, each with a statistical weight of only $\frac{1}{2}$ of what it was before.

When 2 particles cross over from a cell with an IMPortance of e.g. 2 to a cell with an IMPortance of e.g. 1, then 1 of the 2 particles will be "killed" and the statistical weight of the remaining particle will be multiplied by a factor 2.

The splitting of particles is called ***importance splitting,*** and the "killing" of particles is called "Russian roulette."

In the example below, it is clear that the importance biasing in the above problem managed to keep the neutron population reasonably constant or "flat" as these particles traversed the successive, embedded layer of the shield.

```
neutron activity in each cell
        cell    tracks     population
     1     1       10211       7049459
     2     2    18884788       7215135
     3     3    22901069       7628344
     4     4    13565132       7638577
     5     5    10264078       7714774
     6     6    14650769      12151404
     7     7    15061044      12406502
     8     8    13354020      11453793
     9     9    17406152      15213687
    10    10    21079093      17827315
    11    11    18188431      15361900
    12    12    17855181      15389589
    13    13    19886940      17318002
    14    14    24634843      20782070
    15    15    21510367      18128761
    16    16    21915270      18944538
    17    17    28694171      24837115
    18    18    38013228      31874554
    19    19    49723367      38617448
    20    20    60513537      40851989
    21    21    53643811      34766610
    22    22    39629295      34323712
    23    23    29347678      26584877
    24    24    35311463      27766705
    25   201      168870        168819
    26   202      549849        549081
    27   203     1222012       1220035
```

```
    28   204       893795       891679
    29   205      1438514      1435105
    30   206      2260120      2254042
    31   207       623844       621953
    32   208       151579       150886
    33   209       137277       136877
    34   210        20357        20347
```

How does one generate reasonably optimal cell importances, such as e.g.

```
imp:h=1  imp:n=1   imp:p=1
imp:h=1  imp:n=1   imp:p=1
imp:h=0  imp:n=1   imp:p=1
imp:h=0  imp:n=1   imp:p=1
imp:h=0  imp:n=1   imp:p=1
imp:h=0  imp:n=2   imp:p=1
imp:h=0  imp:n=3   imp:p=1
imp:h=0  imp:n=4   imp:p=1
imp:h=0  imp:n=8   imp:p=1
imp:h=0  imp:n=10  imp:p=1
imp:h=0  imp:n=20  imp:p=1
imp:h=0  imp:n=30  imp:p=1
imp:h=0  imp:n=50  imp:p=1
imp:h=0  imp:n=90  imp:p=1
imp:h=0  imp:n=100 imp:p=1
imp:h=0  imp:n=150 imp:p=1
imp:h=0  imp:n=250 imp:p=1
imp:h=0  imp:n=400 imp:p=1
imp:h=0  imp:n=600 imp:p=1
imp:h=0  imp:n=800 imp:p=1
imp:h=0  imp:n=800 imp:p=1
imp:h=0  imp:n=800 imp:p=1
```

Step 1 is to guess importances, or simply run with all importances 1. Run for e.g. 60 minutes. Then copy the cell | population | or | tracks entering | results for e.g. neutrons and for photons from the output data set. Copy these into a spreadsheet containing formulas for optimising the importances. Copy the optimal importances back into the input data set, run the problem, and repeat the process for a few times. Separate importances for neutrons and photons should be calculated in some cases.

12.18 Case study RSDD-18: Calculation of Fluence to Dose Conversion Factors for Neutrons and Ionising Photons, based on a Simple Cylindrical Phantom

Introduction

In this case-study, approximate fluence-to-absorbed dose-rate conversion factors will be calculated.

In dose and dose rate calculations for many radiation protection applications, it is necessary to calculate the effective dose rate to a human standing at a specific position in a radiation area whilst e.g. performing a task that exposes him/her to a dose of ionising radiation. Calculating the effective doses at a single point in space is often not a very good estimate of the effective dose received by the worker, because the human body occupies a substantial volume of space, and different parts of the body are at different distances from the radiation source. Using a very accurate, complex anthropomorphic calculational voxel phantom for the calculation of effective doses, and applying ICRP tissue weighting factors as well as ICRP radiation weighting factors in the calculation of the effective dose, is at present far too complex for most routine radiation protection related calculations.

We here investigate the viability of using a simple cylindrical phantom, composed of uniform tissue-equivalent material (TEM) with a density of 1 g/cm3, a height of 170 cm and a mass of 70 kg, for the calculation of the effective dose from neutron and ionising photon radiation fields, in the energy range up to 20 MeV. The Monte Carlo particle transport code MCNPX-2.6.0 (2008), developed at Los Alamos National Laboratories (LANL) in the USA, was used to determine fluence-to-dose conversion factors (FDCFs). These FDCFs are compared with ANSI/ANS (1991) FDCFs for Anterior-Posterior (AP) exposure geometry for a more geometrically faithful anthropomorphic calculational phantom. Broad, parallel beams of incident neutrons and photons, at a range of mono-energetic incident energies, were used to irradiate the simple cylinder-phantom.

Methodology

The simple cylindrical phantom is assumed to be composed of uniform tissue equivalent material (TEM) with a density of 1 g.cm^{-3}; the elemental composition of this TEM was taken as the weighted average of the composition of all the human body's tissues and organs. Following accepted data for the average built of a human, we used a phantom of height 170 cm and mass 70 kg to represent an average human. This represents a fairly radical simplification of the geometry and spatial dependence of material composition of an actual human body. (A complete model of a humanoid phantom consists of all organs and tissues such as the liver, bones, bone marrow, stomach, liver, heart, kidneys, lungs, etc.)

Monte Carlo simulations of broad, parallel beam irradiation of the simple cylinder phantom for incident mono-energetic neutrons and photons were performed using MCNPX-2.6.0. Calculations were run in MODE n p e, i.e. secondary particles were transported. A +F6

total energy deposition tally was used to calculate the absorbed dose rate D to the phantom, at many mono-energetic incident particle energies. For photons and neutrons, the tissue weighting factors w_T were ignored, because our phantom is a homogenous right circular cylinder (RCC). For neutrons, the fluence-rate to absorbed dose rate conversion factors (FDCF) were multiplied by the w_R function for neutrons shown on page 28; for photons, the w_R function is trivial, because it is 1 at all energies (ICRP 2007). The ratio $\left(\frac{w_R \times (\text{absorbed dose rate})}{(\text{incident fluence-rate})}\right)$ is then taken as an approximation of the fluence-rate to effective dose rate conversion function.

MCNP model

Data set for e.g. 10 MeV neutrons:

```
FDCF Calculation
c Cell Cards
01  1  -1.00E-0    -1         imp:n,p,e=1    $ Phantom
02  0              +1   -2    imp:n,p,e=1    $ Void
12  0              +2         imp:n,p,e=0    $ UmWelt

c Surface Cards
01  RCC    0.0   0.0 -85.0     0.0   0.0 170.0    11.4485  $ Phantom
02  so   900.0                                             $ OR: Inner Void

c Data Cards
mode n p e
c Parallel beam with large diameter, travelling in +y direction
sdef    par=n
        erg=10.0
        pos=0 -100   0
        axs=0    1   0
        vec=0    1   0
        dir=1
        ext=0
        rad=d1
si1 h 0.0  120.0      $ Sampling of source point along radial coordinate from
R.min to R.max
sp1   -21  1          $ Probability of sampling of source point in radial
dimension: power law: r**1 (disk/cyl)
c
c Material definitions
m1     1001  -1.000E-01        $ TEM
       6000  -2.286E-01        $ TEM
       8016  -6.143E-01        $ TEM
       7014  -2.571E-02        $ TEM
      20000  -1.429E-02        $ TEM
      15031  -1.114E-02        $ TEM
      19000  -2.000E-03        $ TEM
      16000  -2.000E-03        $ TEM
      11023  -1.429E-03        $ TEM
      17000  -1.357E-03        $ TEM
      12000  -2.714E-04        $ TEM
      26000  -6.000E-05        $ TEM
c
c **** Physics Table *****
```

```
phys:h 100    &    $  Emax
          0    &    $  0 always
         -1    &    $ -1 always
          j    &    $  j always
          0    &    $  0 always
          j    &    $  j always
          0         $  0 always
phys:n 100         $  Emax
          0        $  0 always
          0        $  0 always
         -1        $ -1 always
         -1        $ -1 always
          0        $  0 always
          0        $  0 always
phys:p 100         $  Emax
          0        $ 0 always
          0        $ 0 always
         -1        $ -1 always
          1        $  1 always
phys:e 100         $  Emax
          0        $  0 always
          0        $  0 always
          0        $  0 always
          0        $  0 always
          1        $  1 always
          1        $  1 always
          1        $  1 always
          1        $  1 always
          0        $  0 always
c
c **** Tally definitions *******
fc16  TOT_ABS_DR in TEM Phantom
+f16  1
fm16  5.768E-7
c
PRINT 10 40 50 60 72 100 110 120 170 200
c
ctme 120
```

Results

The FDCFs calculated for the simple cylinder-phantom are quite useful, because they compare reasonably well with the ANSI/ANS (1991) standard FDCFs for AP exposure.

Neutron FDCFs calculated for the cylinder phantom must be multiplied by the ICRP radiation weighting factor function $w_R(E)$ in order to calculate FDCFs for the effective dose.

Photon FDCFs calculated with the cylinder phantom need to be multiplied with an empirical correction factor between about 1.25 and 1.30 in order to agree well with the ANSI/ANS (1991) FDCFs.

"Correction factors" which are a function of particle energy, can be calculated for both neutrons and photons to generate a "dose factor" {DE DF}-function for MCNP calculations,

which will correct results obtained for the simple cylinder phantom to agree well with the ANSI/ANS (1991) FDCFs, for +F6 type energy-deposition tallies used in MCNP runs.

The FDCF function obtained for neutrons, is shown in Figure 12.10.

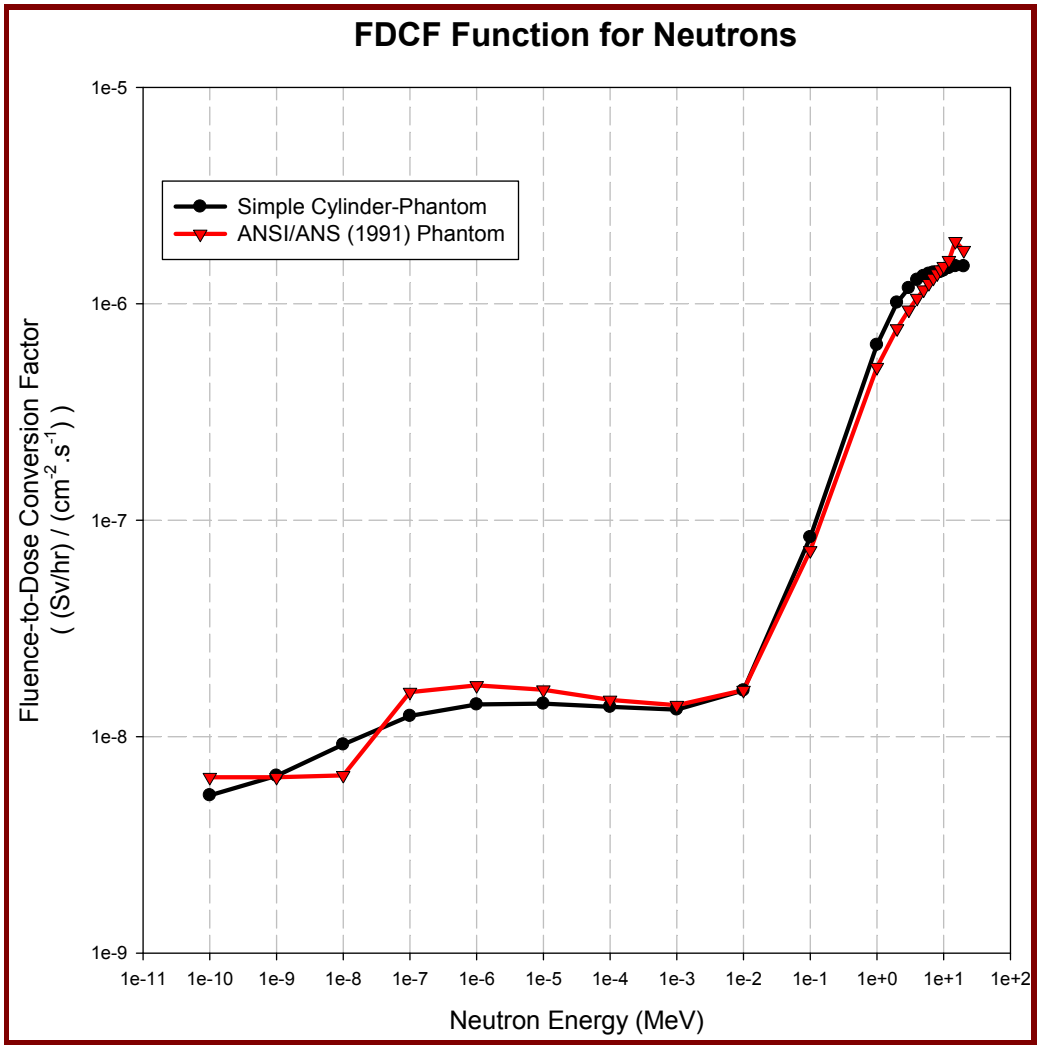

Figure 12.10: *Comparison of the 1991 ANS/ANSI FDCFs with FDCFs for neutrons, obtained with a simple cylinder-phantom.*

The FDCF function obtained for ionising photons, is shown in Figure 12.11.

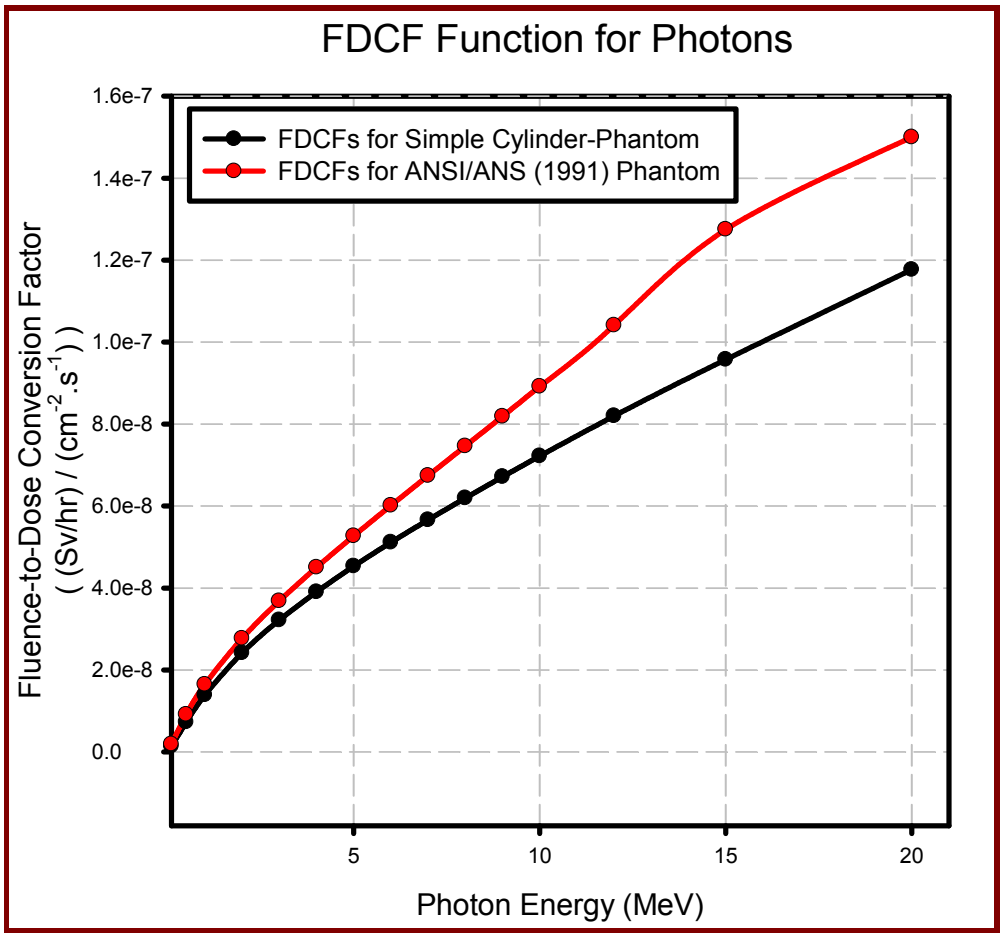

Figure 12.11: *Comparison of the 1991 ANS/ANSI FDCFs with FDCFs for ionising photons obtained with a simple cylinder-phantom.*

Conclusions

A simple cylinder-phantom can be used to represent the human body in effective dose rate calculations with the Monte Carlo code MCNP, provided that readily determined energy-dependent correction factors are applied.

12.19 Case study RSDD-19: Pipe with radioactive contamination on inside surface

A helium-filled stainless steel 304L pipe with wall thickness 2 cm and ID 30 cm, runs horizontally through the centre of a concrete cubicle at a PBMR reactor plant. The height of the pipe centreline above the floor level is 60 cm. The helium temperature is 800 °C and its pressure is 40 bar. According to the program EES, the density of the helium gas under these conditions is $\rho = 1.79 \times 10^{-3}\,\mathrm{g\,cm^{-3}}$. The concrete walls and floor are constructed of ordinary concrete, type 04. The thickness of the concrete wall, floor & roof is 50 cm. The pipe is 500 cm long. The room's inner dimensions are: RPP of 500 cm × 500 cm × 300 cm high. The room is filled with dry air, having $\rho = 1.205 \times 10^{-3}\,\mathrm{g\,cm^{-3}}$. A fairly uniform 1 mm thick carbon coating, with a density of 0.8 $\mathrm{g\,cm^{-3}}$, has formed on the inside of the SS-304L pipe, and the activity per unit mass is 1 MBq per gram. The ionising photon energy spectrum and emission yield of ionising photons is as follows:

E	Y
0.1	0.05
0.3	0.09
0.5	0.12
0.7	0.21
0.8	0.22
1.0	0.31
1.5	0.44
2.0	0.36
2.5	0.12
3.0	0.02
4.0	0.01

Calculate the dose received by a human standing 40 cm from the pipe for 20 minutes, during maintenance work.

Solution

```
PIPE at PBMR, Carbon Coating on inside
c Cell Cards
1  1  -1.205E-3    -2  +7  +4    imp:p,e=1    $ Air in room
2  2  -2.35        -1  +2        imp:p,e=1    $ Concrete Wall
3  1  -1.205E-3    -3  +1        imp:p,e=1    $ Air outside Room
4  3  -8.00        -4  +5        imp:p,e=1    $ SS-304L Pipe Wall
5  4  -0.8         -5  +6        imp:p,e=1    $ Graphite coating inside SS-pipe
6  5  -1.79E-3     -6            imp:p,e=1    $ Helium inside pipe
7  6  -1.0         -7            imp:p,e=1    $ TEM Phantom
8  0                  +3        imp:p,e=0    $ UmWelt -- "EXTERNAL VOID"
c ================================================

c ================================================
c Surface Cards
1  RPP -300  +300    -300  +300   -50  +350      $ Outer RPP for Concrete
```

```
2  RPP -250  +250    -250  +250    +0  +300      $ Inner RPP for Concrete
3  RPP -400  +400    -400  +400  -150  +450      $ Outer RPP for Air outside room
c
4  RCC -250  +0  +60    +500  +0   +0       +17.0  $ Outer RCC for Pipe
5  RCC -250  +0  +60    +500  +0   +0       +15.0  $ Inner RCC for Pipe
6  RCC -250  +0  +60    +500  +0   +0       +14.9  $ Inner RCC for Carbon layer
c
7  RCC   +0 +55   +0      +0  +0 +170       +11.5   $ Cylinder Phantom
c ================================================

c ================================================
c Data Cards
c Mode: transport photons
mode p e
sdef  par = p
      pos = 0 0 0
      axs = 1 0 0
      vec = 1 0 0
      ext = d1
      rad = d2
      erg = d3
      eff = 0.1
si1 h  -250  +250      $ Extent of sampling of Axial coordinate
sp1   -21  0           $ Sampling in axial dimension
si2 h  +14.9   +15.0   $ Extent of sampling in radial coordinate
sp2   -21  1           $ Sampling in radial dimension
si3 L  0.1   0.3   0.5   0.7   0.8   1.0   1.5   2.0   2.5   3.0   4.0
sp3    0.05  0.09  0.12  0.21  0.22  0.31  0.44  0.36  0.12  0.02  0.01
c
c Material definitions
m1     6000   -1.24E-4       $ Air
       7000   -0.755267      $ Air
       8000   -0.231781      $ Air
      18000   -0.012827      $ Air
c
m2     1000   -0.013         $ Concrete, ordinary, NBS type 04
       8000   -1.165         $ Concrete, ordinary, NBS type 04
      11000   -0.040         $ Concrete, ordinary, NBS type 04
      12000   -0.010         $ Concrete, ordinary, NBS type 04
      13000   -0.108         $ Concrete, ordinary, NBS type 04
      14000   -0.740         $ Concrete, ordinary, NBS type 04
      16000   -0.003         $ Concrete, ordinary, NBS type 04
      19000   -0.045         $ Concrete, ordinary, NBS type 04
      20000   -0.196         $ Concrete, ordinary, NBS type 04
      26000   -0.030         $ Concrete, ordinary, NBS type 04
c
m3     6000   -0.03          $ SS-304L
      14000   -0.60          $ SS-304L
      15000   -0.02          $ SS-304L
      16000   -0.03          $ SS-304L
      24000  -19.00          $ SS-304L
      25000   -1.70          $ SS-304L
      26000  -68.62          $ SS-304L
      28000  -10.00          $ SS-304L
      42000   -1.0E-88       $ SS-304L
c
m4     6000   -1.0           $ Graphite / Carbon Coating inside pipe
C
```

```
m5     2000   -1.0           $ Helium
c
m6     8000   -6.143E-01     $ Tissue-Equivalent Material (TEM)
       6000   -2.286E-01     $ Tissue-Equivalent Material (TEM)
       1000   -1.000E-01     $ Tissue-Equivalent Material (TEM)
       7000   -2.571E-02     $ Tissue-Equivalent Material (TEM)
      20000   -1.429E-02     $ Tissue-Equivalent Material (TEM)
      15000   -1.114E-02     $ Tissue-Equivalent Material (TEM)
      19000   -2.000E-03     $ Tissue-Equivalent Material (TEM)
      16000   -2.000E-03     $ Tissue-Equivalent Material (TEM)
      11000   -1.429E-03     $ Tissue-Equivalent Material (TEM)
      17000   -1.357E-03     $ Tissue-Equivalent Material (TEM)
      12000   -2.714E-04     $ Tissue-Equivalent Material (TEM)
      26000   -6.000E-05     $ Tissue-Equivalent Material (TEM)
c
c ========
c **** Tally specs *******
fc16   Tally = photon dose-rate at surfaces
+f16   7
fm16   3.9433E3
c
fc26   Tally = photon dose-rate at surfaces
f26:p  7
fm26   3.9433E3
c
fc36   Tally = photon dose-rate at surfaces
f36:e  7
fm36   3.9433E3
c
c === RUNTIME CONTROLS ======
PRINT
ctme 10
```

12.20 Case study RSDD-20: The characteristic "fingerprint"-nature of shielding materials against neutrons

Determine the characteristic "fingerprint"-nature of (1) Fe and (2) paraffin wax for the shielding of neutrons. Perform calculations first for e.g. 1 MeV neutrons and then for e.g. 40 MeV neutrons. Model in simple spherical-symmetrical geometry. Look at the transmitted neutron dose rate, the ionising photon dose rate as well as the neutron energy spectrum and the energy spectrum of secondary ionising photons.

Solution to Case Study 20

The conceptual methodology and results of this investigation are reported starting on page 324.

The MCNP input data file for a typical investigation for the "fingerprint" characterisation of a shielding material, is quite simple and an example is:

```
Wax shield with point neutron source at centre
c Cell Cards
01  1  -1.205E-3       -1    imp:n=1       imp:p=1   $ Air
02  2  -0.92      +1   -2    imp:n=2       imp:p=1   $ Paraffin Wax
03  2  -0.92      +2   -3    imp:n=5       imp:p=1   $ Paraffin Wax
04  2  -0.92      +3   -4    imp:n=25      imp:p=1   $ Paraffin Wax
05  2  -0.92      +4   -5    imp:n=125     imp:p=1   $ Paraffin Wax
06  2  -0.92      +5   -6    imp:n=625     imp:p=1   $ Paraffin Wax
07  2  -0.92      +6   -7    imp:n=3125    imp:p=1   $ Paraffin Wax
08  2  -0.92      +7   -8    imp:n=15625   imp:p=1   $ Paraffin Wax
09  2  -0.92      +8   -9    imp:n=78125   imp:p=1   $ Paraffin Wax
10  2  -0.92      +9   -10   imp:n=390625  imp:p=1   $ Paraffin Wax
11  2  -0.92     +10   -11   imp:n=1953125 imp:p=1   $ Paraffin Wax
12  2  -0.92     +11   -12   imp:n=9765625 imp:p=1   $ Paraffin Wax
13  0            +12         imp:n,p=0               $ Umwelt
c =====

c =====
c Surface Cards
01  so   010.00    $ inner Air cavity OR
02  so   020.00    $ Wax Layer 1  OR
03  so   030.00    $ Wax Layer 2  OR
04  so   040.00    $ Wax Layer 3  OR
05  so   050.00    $ Wax Layer 4  OR
06  so   060.00    $ Wax Layer 5  OR
07  so   070.00    $ Wax Layer 6  OR
08  so   080.00    $ Wax Layer 7  OR
09  so   090.00    $ Wax Layer 8  OR
10  so   100.00    $ Wax Layer 9  OR
11  so   110.00    $ Wax Layer 10 OR
12  so   120.00    $ Air OR
c =====

c =====
c Data Cards
```

```
c Mode: transport protons, neutrons and photons
mode n p
c source: Isotropic point source of neutrons at origin.
sdef par=n erg=1 pos=0 0 0
c
c Material definitions
m1      6000    -1.24E-4        $ Air, dry.  Density = 1.205E-03 g/cc
        7014    -0.755267       $ Air, dry.  Density = 1.205E-03 g/cc
        8016    -0.231781       $ Air, dry.  Density = 1.205E-03 g/cc
       18000    -0.012827       $ Air, dry.  Density = 1.205E-03 g/cc
c
m2      1001    +52
        6000    +25        $ Paraffin wax C(n)H(2n+2)
c
c **** Physics Table *****
c
phys:n    20      $     Emax
           0      $     0 always
           0      $     0 always
       -1001      $ -1001 always
          -1      $    -1 always (mix   match)
           0      $     0 always
           0      $     0 always
phys:p    20      $     Emax
           0      $     0 always (generate e in MODE e calcs)
           0      $     0 always (Coherent/Thomson scattering on)
          -1      $    -1 always (photonuclear reaction on)
           1      $     1 always (1 = Doppler broadening is off)
           0      $     0 normally, but -101 or -102 for delayed gamma production.
c
fc32 Tally on neutron fluence-rate of outermost wax surface
f32:n  11
e32    1e-11  1e-9  1e-8  1e-7  1e-6  1e-5  1e-4  1e-3  1e-2
       0.1    0.2   0.3   0.4   0.5   0.6   0.7   0.8   0.9
       1.0    1.5   2.0   3.0   4.0   5.0
       6.0    7.0   8.0   9.0  10.0  11.0  12.0
       13.0  14.0  15.0  16.0  17.0  18.0  19.0
       20.0  25.0  30.0  35.0  40.0  45.0  50.0  55.0
       60.0   70.0  80.0
fm32  3.7E10   $ 1 Ci
c
fc12 Tally on photon fluence-rate at cell surface
f12:p 11
e12    1e-2  0.1  0.2  0.3  0.4  0.5  0.6  0.7  0.8  0.9
        1.0  1.1  1.2  1.3  1.4  1.5  1.6  1.7  1.8  1.9
        2.0  2.1  2.2  2.3  2.4  2.5  2.6  2.7  2.8  2.9
        3.0  3.1  3.2  3.3  3.4  3.5  3.6  3.7  3.8  3.9
        4.0  4.1  4.2  4.3  4.4  4.5  4.6  4.7  4.8  4.9
        5.0  5.1  5.2  5.3  5.4  5.5  5.6  5.7  5.8  5.9
        6.0  6.1  6.2  6.3  6.4  6.5  6.6  6.7  6.8  6.9
        7.0  7.1  7.2  7.3  7.4  7.5  7.6  7.7  7.8  7.9
        8.0  8.1  8.2  8.3  8.4  8.5  8.6  8.7  8.8  8.9
        9.0  9.1  9.2  9.3  9.4  9.5  9.6  9.7  9.8  9.9
       10.0
       11.0
       12.0
       13.0
       14.0
```

```
       15.0
fm12 3.7E10  $ 1 Ci
c
c === RUNTIME CONTROLS ======
ctme 1200
```

12.21 Case study RSDD-21: Writing utility preprocessing code to help generate MCNP input data sets

Problem at hand: Industrial irradiator with source rack — modelling the source rack pin by pin, for 100 ^{60}Co pins.

Case Study 21: Solution

Refer to the .F90 codes in the supplied data-DVD.

Chapter 13:
Case Studies:
Nuclear Criticality Safety

Study material: Nuclear Criticality Safety

KNIEF, RA. 1986. *Nuclear Criticality Safety — Theory and Practice.* American Nuclear Society (ANS).

Critical Dimension of Systems Containing ^{235}U, ^{239}Pu, and ^{233}U. Report LA-10860-MS, REFSET, Unclassified, Volumes I-III, Los Alamos National Laboratory.

Assignment 13.1

1. Use MCNP to model an unreflected sphere of pure ^{235}U in air. Determine the radius that will give $k_{\text{eff}} \approx 1$. What is the mass and volume of the sphere?

2. Use MCNP to model an unreflected sphere of pure ^{233}U in air. Determine the radius that will give $k_{\text{eff}} \approx 1$. What is the mass and volume of the sphere?

3. Use MCNP to model an unreflected sphere of pure ^{239}Pu in air. Determine the radius that will give $k_{\text{eff}} \approx 1$. What is the mass and volume of the sphere?

4. A layer of loose, non-sintered UO_2 powder, enriched in ^{235}U to 19.75%, having a density of $3.5\,\text{g}\,\text{cm}^{-3}$, covers the bottom of a 210 litre process vessel having right circular cylinder (RCC) geometry. Inner radius (IR) = 28.5 cm; Inner height = 85.4 cm. Steel wall thickness: 0.36 cm. Density of steel: $7.86\,\text{g}\,\text{cm}^{-3}$. The process vessel is suspended in air.

   (a) Determine the UO_2 thickness, covered by air, that will give $k_{\text{eff}} \approx 0.85$.

   (b) Now fill the drum with water up to a height 30 cm above the top of the UO_2 powder layer. Determine the new value of k_{eff}.

   (c) Now stir the UO_2 & water together into a homogenous mixture and determine the new value of k_{eff}.

   (d) Draw generalised conclusions.

5. A layer of loose, non-sintered UO_2 powder, enriched in ^{235}U to 19.75%, having a density of $3.5\,\text{g}\,\text{cm}^{-3}$, covers the bottom of a steel vessel having rectangular circular cylinder (RCC) geometry. Inner radius (IR) = 20 cm; Inner height = 50 cm. Steel wall thickness: 0.2 cm. Density of steel: $7.86\,\text{g}\,\text{cm}^{-3}$. The vessel is suspended in air.

(a) Determine the UO_2 thickness, covered by air, that will give $k_{\text{eff}} \approx 0.98$.

(b) Now place this vessel on an ordinary concrete floor and calculate the new value of k_{eff}.

(c) Now allow for water ingress into the drum so that the water covers the UO_2 layer to the top of the drum, with the water also moving into the granular UO_2 layer to make up 10% of its volume, without affecting the partial density of the UO_2. Calculate the new value of k_{eff}.

(d) Draw generalised conclusions from the viewpoint of nuclear criticality safety.

Assignment 13.2

1. Calculate k_{eff} for a bare $^{239}_{94}\text{Pu}$ sphere with radius $r = 4.90$ cm. The density of plutonium is 19.8 g cm^{-3}, and the mass of this sphere will be approximately 10 kg. Show that k_{eff} is just below 1 when the ^{239}Pu sphere is surrounded by air.

2. Calculate k_{eff} for a $^{239}_{94}\text{Pu}$ sphere with radius $r = 4.90$ cm, reflected by 30 cm light water. What is the effect of the reflector on the criticality, i.e. on the value of k_{eff} for the system?

3. Calculate k_{eff} for a bare ^{235}U sphere with radius $r = 8.5$ cm. The density of uranium is 18.9 g cm^{-3}, and the mass of this sphere will be approximately 52 kg.

4. Calculate k_{eff} for a bare ^{235}U sphere with radius $r = 8.5$ cm, reflected by 30 cm light water. What is the effect of the neutron-reflector on the criticality, i.e. on the value of k_{eff} for the system?

5. What will be the effect if a nearly critical sphere of fissile material is accidentally submerged in a large volume of water?

6. Change the ^1H_2O (light water) to ^2H_2O, i.e. "heavy water" and describe the effect on k_{eff} as well as on the cycle execution time. What is the reason?

7. Next, change the surrounding medium back to light water but add a significant amount of ^{10}B to the H_2O medium, and describe the effect on the speed of the calculation.

8. Next, envelop the nearly critical ^{239}Pu sphere in a 100 cm thick surrounding beryllium shell. What is the value of k_{eff} now? What happens to the speed of the calculation?

Solution: Typical nuclear criticality safety investigation with MCNP

(a) The input data set is as follows:

```
Bare Plutonium Sphere
C Cell cards
1     1    -19.8           -1         imp:n=1      $ Pu-239
2     2    -1.205E-03      -2   +1    imp:n=1      $ Air
c 2   3    -1.205E-03      -2   +1    imp:n=1      $ Water into which Pu ball drops
3     0                          +2   imp:n=0      $ UmWelt
c ====================================================

c ====================================================
C Surface cards
1 so     4.9
2 so   500.0
c ====================================================

c ====================================================
c Data cards
mode n
c Criticality Control Cards
kcode 1E4  1.0   10   30
ksrc  0 0 0    1 0 0   0 1 0   0 0 1   1 1 0   0 1 1   1 0 1   1 1 1
c
c Materials Cards
m1    94239   -1            $ Pure plutonium Pu-239 metal
c
m2     6000  -1.24E-4       $ Air, dry
       7014  -0.755267      $ Air, dry
       8016  -0.231781      $ Air, dry
      18000  -0.012827      $ Air, dry
c
m3     1001  +2             $ Water
       8016  +1             $ Water
mt3 Lwtr.60t
```

The surface cards

```
C Surface cards
1 so     4.9
2 so   500.0
```

define a sphere with a radius of 4.9 cm, surrounded by an outer sphere with radius 500 cm.

The cell cards

```
C Cell cards
1   1    -19.8           -1         imp:n=1      $ Pu-239
2   2    -1.205E-03      -2   +1    imp:n=1      $ Air
3   0                          +2   imp:n=0      $ UmWelt
```

specifies that the volume inside surface 1 is filled with ^{239}Pu, with a given mass-density. This Pu sphere is surrounded by a thick air volume, outside of which is the UmWelt, where particles are no longer tracked (importance is zero).

The criticality calculation control card

```
kcode 1E4  1.0   20   50
```

states that 1E4 source neutrons will be generated per cycle, that the initial guess for k_{eff} is 1.0, that the results of the first 20 cycles will be ignored, and that a total of 50 cycles will be executed to arrive at a good estimate for k_{eff}.

Note that in real-world calculations, the above specification should be e.g.

```
kcode 1E6  1.0   20   50
```

in order to obtain a more accurate, trustworthy result for k_{eff}. It is more fruitful to increase the number of source-neutrons per cycle than to increase the number of cycles — study the concept "Shannon entropy" in information theory.

A couple of initial fission-neutron generation points are specified at the following set of (x, y, z) values. This simply initialises the fission chain reaction problem. The code will now internally generate thousands of fission events, and after a few cycles, the fission reaction distribution will converge to the "fundamental mode" of the fissioning system. These initial source points function akin to striking a match to light a fire in a pile of wood — soon, the fire will spread throughout the pile of wood, no matter where the match was initially struck to light the fire. If you put fire to the pile of wood at multiple places, the fire will spread faster. For this reason, we "light the neutronic fission fire" at more than one point.

```
ksrc  0 0 0    1 0 0   0 1 0   0 0 1   1 1 0   0 1 1   1 0 1   1 1 1
```

If one models a nuclear fission reactor in which fuel assemblies are used, it will be best to use a SDEF definition that envelops the entire spatial region containing fissile material. The most true-to-nature source neutron energy specification is

```
sdef par=n erg=d3…
```

with the source probability i.e. neutron energy spectrum specification

```
sp3  -3  0.988  2.249
```

which defines a Watt prompt fission neutron energy spectrum

$$S(E) = \exp\left(\frac{-E}{0.988}\right) \sinh\left(\sqrt{2.249E}\right) \tag{13.1}$$

b) Calculate k_{eff} for a bare pure ^{235}U sphere with radius $r = 8.5$ cm. The density of uranium is 18.9 g cm^{-3}, and the mass of this sphere will be approximately 52 kg.

Now drop this nearly critical ^{235}U sphere into a large volume of water. What is the value of k_{eff} now? What happens to the speed of the calculation?

Solution: Case Study 0b

Similar in principle to the ^{239}Pu problem.

13.1 Case study NCS-1: Nearly critical slab of fissile material, approached by a human

Model a slab of ^{235}U that is 170 cm high and 30 cm wide. Determine the slab thickness that will result in a k_{eff} of about 0.97. Now add a stylised humanoid phantom with slab-dimensions 170 cm high, 30 cm wide and 13.7 cm thick, to the model. (With a material density of 1 g cm^{-3}, the slab-phantom will have a mass of approximately 70 kg, which is realistic.) The material composition must be tissue-equivalent material (TEM). Perform a criticality calculation with the humanoid phantom about 100 cm away from the ^{235}U slab. Repeat the criticality calculation for the slab-phantom right up against the ^{235}U slab. Use the calculated value of k_{eff} to show how a human body can serve as a neutron moderator & reflector so that human proximity to nearly critical configurations of under-reflected, under-moderated slightly subcritical fissile material, may cause a criticality accident.

Solution: Case Study NCS-1

```
HEU Cylinder with approaching humanoid
c Cell cards
1  1  -18.74      -1                imp:n=1     $ HEU Metal as Cylinder
2  2   -1.0       -2                imp:n=1     $ Humanoid
3  3   -2.35      -3                imp:n=1     $ Concrete floor
4  4   -1.2E-3    -4  #1  #2  #3     imp:n=1     $ Air
5  0              +4                imp:n=0     $ UmWelt

c Surface cards
1 RPP    -03.3  +03.3     -20.0  +20.0      0.0  +170.0     $ HEU in Slab
2 RPP   +400.0 +440.0     -20.0  +20.0      0.0  +170.0     $ Human -- FAR from HEU
c 2 RPP     +3.4  +43.4     -20.0  +20.0      0.0  +170.0     $ Human -- CLOSE to HEU
3 RPP   -500.0 +500.0    -500.0 +500.0    -50.0    +0.0     $ Concrete floor -- THICK
4 RPP   -510.0 +510.0    -510.0 +510.0   -100.0  +500.0     $ Air (dry)

c Data cards
c Criticality Control Cards
kcode  1E4          $ nsrck = Number of source histories per cycle. (DEFAULT=1000)
       1.0          $ rkk   = Initial guess for k_eff. (DEFAULT=1.0)
       50           $ ikz   = Cycles to be skipped before beginning tally.(DEFAULT=30)
       100          $ kct   = Number of cycles to be done. (DEFAULT=ikz+100)
ksrc  0 0   5   0 0  10   0 0  20    0 0  30
      0 0  40   0 0  50   0 0  60    0 0  70
      0 0  80   0 0  90   0 0 100    0 0 110
      0 0 120   0 0 130   0 0 140    0 0 150
      0 0 160   0 0 165                  $ Source Points
c Materials Cards
m1    92235    -93.0                   $ HEU Metal
      92238     -7.0                   $ HEU Metal
c
m2     8016    -6.143E-01   6000  -2.286E-01   1001  -1.000E-01       $ Human tissue
       7014    -2.571E-02  20000  -1.429E-02  15031  -1.114E-02       $ Human tissue
      19000    -2.000E-03  16000  -2.000E-03  11023  -1.429E-03       $ Human tissue
      17000    -1.357E-03  12000  -2.714E-04  26000  -6.000E-05       $ Human tissue
mt2 lwtr.60t
```

```
c
m3     1001    -0.013       8016  -1.165      11023  -0.040          $ Concrete, ordinary
      12000    -0.010      13027  -0.108      14000  -0.740          $ Concrete, ordinary
      16000    -0.003      19000  -0.045      20000  -0.196          $ Concrete, ordinary
      26000    -0.030                                                $ Concrete, ordinary
c
m4     7014    -0.75             $ Air, dry
       8016    -0.23             $ Air, dry
      18000    -1.4              $ Air, dry
```

Chapter 14:
Case Studies: Nuclear Reactor Modelling — Introduction

The End

Annexure A: Reference Material

Constants & Equations

$\pi = 3.14159265$

$e = 2.71828183$

$1u = 1.660539 \times 10^{-27}$ kg

1 eV $= 1.60219 \times 10^{-19}$ joule

$c = 2.99792458 \times 10^{+8}$ m s^{-1}

$m\left({}^{1}\mathrm{H}\right) = 1.007825032u$

$m_p = 1.0072678745u$

$m_n = 1.008664916u$

Planck's constant: $h = 6.626 \times 10^{-34}$ J s

Boltzmann constant: $k = 1.381 \times 10^{-23}\ \frac{\mathrm{m^2\,kg}}{\mathrm{K\,s^2}}$

Avogadro's number: $N_A = 6.022 \times 10^{+23}$ mole^{-1}

1 Curie $= 3.7 \times 10^{+10}$ Bq, i.e. $3.7 \times 10^{+10}$ s^{-1}.

Magic numbers of nucleons: 2, 8, 20, 28, 50, 82 & 126; semi-magic number: 40.

$$\frac{-\hbar^2}{2m}\nabla^2\psi(\vec{r}) + U(\vec{r})\psi(\vec{r}) = E\psi(\vec{r}) \tag{A.1}$$

$$B(Z,A) = \left[Zm\left({}^{1}\mathrm{H}\right) + Nm_n - m\left({}^{A}_{Z}X\right)\right]c^2 \tag{A.2}$$

$$R = R_0 A^{1/3} \tag{A.3}$$

where $R_0 = 1.2$ fm

$$V = \frac{4}{3}\pi R^3 \tag{A.4}$$

$$B(A,Z) = [a_v A] + \left[a_s A^{2/3}\right] + \left[a_c \frac{Z^2}{A^{1/3}}\right] + \left[a_a \frac{(N-Z)^2}{4A}\right] + \left[a_p \frac{\delta}{A^{1/2}}\right] \tag{A.5}$$

$$T_{½}(E_\alpha) = C \exp\left(\frac{A}{\sqrt{E_\alpha}}\right) \tag{A.6}$$

$$\Delta p \, \Delta x \geq \frac{\hbar}{2} \tag{A.7}$$

$$\Delta E \, \Delta t \geq \frac{\hbar}{2} \tag{A.8}$$

$$\lambda = \frac{\ln(2)}{T_{½}} \tag{A.9}$$

$$A(T_{½}, M_R) = \frac{\ln(2)\, N_A}{T_{½}\, M_R} \tag{A.10}$$

$$M(A, T_{½}, A) = \left(\frac{T_{½}\, M_R}{\ln(2)\, N_A}\right) A \tag{A.11}$$

$$v = c\sqrt{1 - \frac{1}{\left(1 + \frac{T}{mc^2}\right)^2}}, \tag{A.12}$$

$$E = h\nu \tag{A.13}$$

$$\begin{aligned} p &= \frac{h}{\lambda} \\ &= \frac{h\nu}{c} \end{aligned} \tag{A.14}$$

$$E(m,p) = \sqrt{m^2c^4 + p^2c^2} \tag{A.15}$$

$$E(m,p) = mc^2 \text{ for } p = 0 \tag{A.16}$$

$$E(m,p) = pc \text{ for photons } (m=0) \tag{A.17}$$

$$p(m,v) = mc\sqrt{\left[\left(\frac{1}{1-\frac{v^2}{c^2}}\right)-1\right]} \tag{A.18}$$

$$T(m,v) = mc^2\left(\frac{1}{\sqrt{\left(1-\frac{v^2}{c^2}\right)}}-1\right) \tag{A.19}$$

$$v(m,T) = c\sqrt{1-\left[\frac{1}{\left(1+\frac{T}{mc^2}\right)^2}\right]} \tag{A.20}$$

$$\frac{1}{\sqrt{1-\frac{v^2}{c^2}}} = \sqrt{\left(1+\frac{p^2}{m^2c^2}\right)} \tag{A.21}$$

$$\frac{1}{\sqrt{1-\frac{v^2}{c^2}}} = 1+\frac{T}{mc^2} \tag{A.22}$$

$$p(m,T) = \frac{\sqrt{2mc^2T+T^2}}{c} \tag{A.23}$$

$$\begin{aligned} \lambda(p) &= \frac{h}{p} \\ \lambda(m,v) &= \frac{h}{mv}\sqrt{\left(1-\frac{v^2}{c^2}\right)} \\ \lambda(m,T) &= \frac{hc}{\sqrt{T^2+2Tmc^2}} \end{aligned} \tag{A.24}$$

$$\left.\frac{dE}{dx}\right|_{\text{ionisation}} = \text{LET}_{\text{ionisation}} \propto \frac{z^2\,Z}{v} \tag{A.25}$$

$$I_{BS} \propto \frac{z^2\,Z^2}{m^2} \tag{A.26}$$

$$\phi = \frac{A(\tau_I,\tau_C)}{N_T\,\sigma\,(1-e^{-\lambda\tau_I})\,e^{-\lambda\tau_C}}. \tag{A.27}$$

$$E_{\text{av}} = \frac{3}{2} kT \tag{A.28}$$

$$^{10}\text{B}\,(n,\alpha)\,^{7}\text{Li} + \gamma\ (0.48\ \text{MeV}) \tag{A.29}$$

$$^{1}\text{H} + \text{n} \rightarrow {}^{2}\text{H} + \gamma\ (2.205\ \text{MeV}) \tag{A.30}$$

$$\overbrace{\vec{\nabla}\cdot\widehat{\Omega}\,\psi(E,\widehat{\Omega},\vec{x})}^{\text{Leakage term}} + \overbrace{\Sigma_t(E,\vec{x})\,\psi(E,\widehat{\Omega},\vec{x})}^{\text{Outscattering term}} =$$

$$\overbrace{\int_0^\infty dE' \int_{\widehat{\Omega}'} d\widehat{\Omega}'\ \Sigma_s(E'\rightarrow E, \widehat{\Omega}'\rightarrow\widehat{\Omega},\vec{x})\,\psi(E',\widehat{\Omega}',\vec{x})}^{\text{Inscattering term}} + \overbrace{Q(E,\widehat{\Omega},\vec{x})}^{\text{Source-term}}. \tag{A.31}$$

Reference Tables

Table 1: *Periodic Table of the elements.*

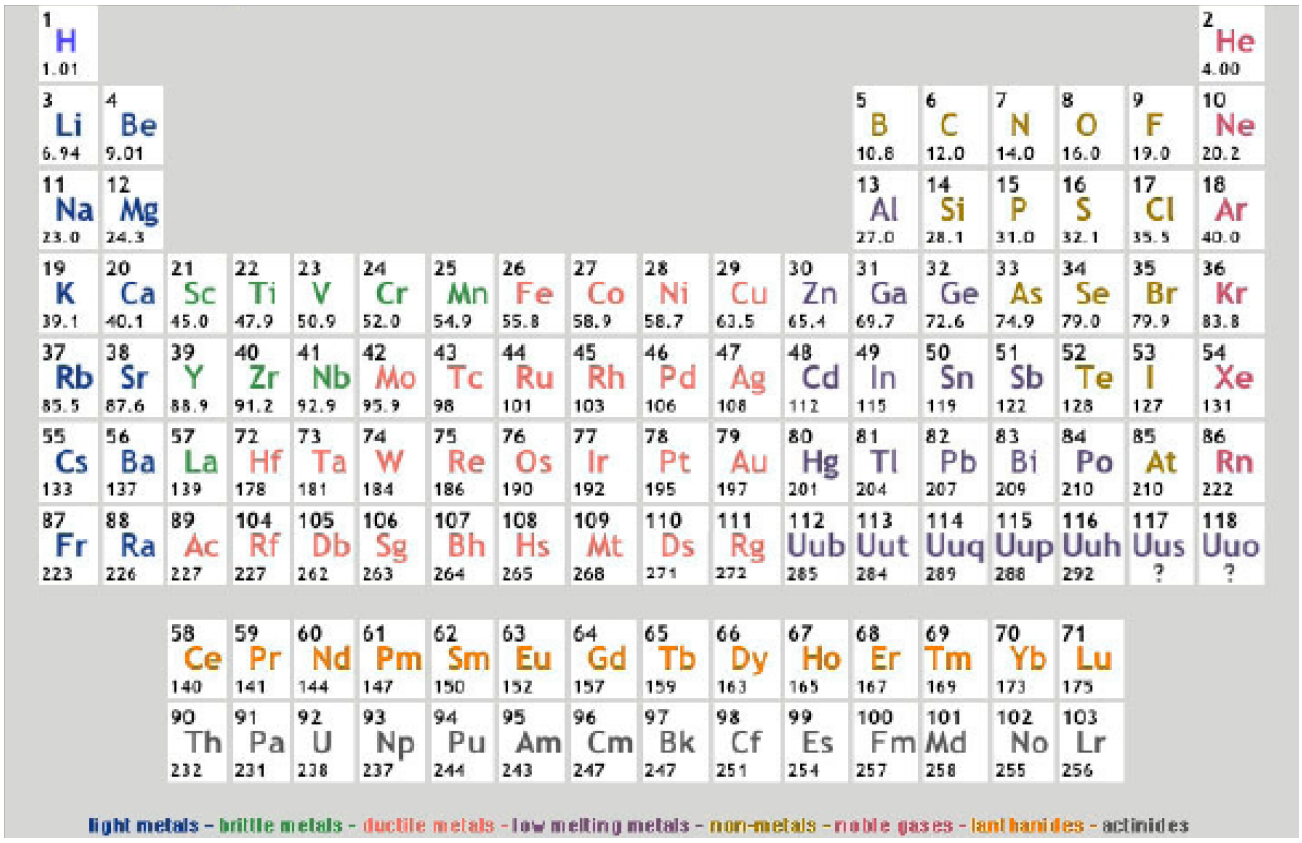

Table 2: *Mass-densities of selected materials.*

Material	**Mass-Density** $(\mathrm{g\,cm^{-3}})$
Water at STP	1.0
Aluminium (Al)	2.7
Iron (Fe)	7.86
Stainless Steels	8.0
Copper (Cu)	8.9
Molybdenum (Mo)	10.2
Tungsten (W)	19.6
Tungsten-Copper alloys	circa 17.0
Tungsten-Nickel-Copper alloys	circa 17.8
Lead (Pb)	11.35
Lead-Antimony-Tin alloys	11.0
Uranium (U)	18.9

Annexure B:
The Amount of Boron Carbide (B_4C) to Mix into Hydrogenous Shielding Materials

Qualitatively, it is well known that it is beneficial to mix a thermal neutron absorber such as boron carbide (B_4C) into the hydrogenous layer of a neutron shield. In this subsection, a quantitative answer is sought for the important question: what mass percentage of a thermal neutron absorber should be mixed into the hydrogenous layer of the shield? It is shown that a mixing ratio (mass-percentage) between about 2.5% and 5% B_4C in paraffin wax, will serve its intended purpose well.

At the reference thermal neutron speed of 2200 m.s^{-1}, the cross-section of the capture reaction $^{10}\mathrm{B}\,(n,\alpha)\,^{7}\mathrm{Li}$ is 3837 barn, while the cross-section for the reaction $^{1}\mathrm{H}\,(n,\gamma)\,^{2}\mathrm{H}$ (at the same reference neutron speed) is only 0.332 barn. The mixing ratio of B_4C in paraffin wax or polyethylene is determined by the requirement that the reaction rates, and accordingly, the linear interaction coefficients for the favourable and the unfavourable absorption reactions should be related as follows:

$$\frac{\mu_{(^{10}\mathrm{B}\,(n,\alpha))}}{\mu_{(^{1}\mathrm{H}\,(n,\gamma))}} \gtrsim 25$$

where the linear interaction coefficient μ is the product of nuclide number density N and the cross-section σ. By working from this principle, it can be shown that the ideal volume percentage of B_4C in paraffin wax or polyethylene should be between above circa 2.5%. Transport calculations with a code such as MCNP shows that, for a typical bulk shield, 90% of the advantage of adding 5% B_4C to a shield is obtained by adding only 3%. Because B_4C is very expensive, 5% B_4C is the highest mixing ratio that can normally be afforded in poorer countries. The B_4C that is employed in the shield, should be in the form of an extremely fine powder in order to approximate a homogeneous mixture and produce the maximum benefit.

A quantitative result for a sensible mass% of the thermal neutron absorber B_4C to mix into the paraffin wax layer of a neutron shield was derived and used to calculate all mass fractions and nuclide number densities for the paraffin wax & B_4C layers modelled for the assessments of local radiation shields around radionuclide production beam target stations at a particle accelerator facility.

Let $f_{(\mathrm{B_4C})}$ be the mass fraction of B_4C in the paraffin wax layer of a shield. Then the mass fraction of paraffin wax will be $f_{\mathrm{wax}} = \left(1 - f_{(\mathrm{B_4C})}\right)$.

The mass densities of the two constituent materials in the shield, are.

$$\rho_{(\mathrm{B_4C})} = 2.52 \text{ g cm}^{-3}$$

$$\rho_{\mathrm{wax}} = 0.92 \text{ g cm}^{-3} \quad . \tag{14.32}$$

The relative molar masses, Mr, of the elements in the mixture, are,

$$\begin{aligned} M_r(H) &= 1.00794 \text{ g mole}^{-1} \\ M_r(\text{C}) &= 12.0107 \text{ g mole}^{-1} \\ M_r(\text{B}) &= 10.811 \text{ g mole}^{-1} \quad . \end{aligned} \tag{14.33}$$

The relative molar masses, Mr, of the two molecules in the mixture, i.e. B_4C and $H_{52}C_{25}$ (the nominal chemical formula for typical paraffin wax), are,

$$\begin{aligned} Mr_{(\text{B}_4\text{C})} &= \left(4 \times Mr_{(\text{B})} + 1 \times Mr_{(\text{C})}\right) \text{ g mole}^{-1} \\ &= 55.255 \text{ g mole}^{-1} \\ Mr_{(\text{H}_{52}\text{C}_{25})} &= \left(52 \times Mr_{(\text{H})} + 25 \times Mr_{(\text{C})}\right) \text{ g mole}^{-1} \\ &= 352.68 \text{ g mole}^{-1} \end{aligned} \tag{14.34}$$

The linear interaction coefficients for the absorption of neutrons by ^{10}B and ^{1}H, are,

$$\begin{aligned} \mu_{(^{10}\text{B}\,(n,\alpha))} &= N_{(^{10}\text{B})} \times \sigma_{(^{10}\text{B}\,(n,\alpha))} \\ \mu_{(^{1}\text{H}\,(n,\gamma))} &= N_{(\text{H})} \times \sigma_{(^{1}\text{H}\,(n,\gamma))} \quad . \end{aligned} \tag{14.35}$$

The ratio between the above two linear interaction coefficients must be made $\frac{\mu_{(^{10}\text{B}\,(n,\alpha))}}{\mu_{(^{1}\text{H}\,(n,\gamma))}} \gtrsim 25$ by mixing an adequate amount of boron carbide (B_4C) into the hydrogenous medium.

The listed neutron absorption cross-sections of ^{10}B and ^{1}H at the reference thermal neutron speed of 2200 m/s, are,

$$\begin{aligned} \sigma_{(^{10}\text{B}\,(n,\alpha))} &= 3837 \text{ barn} \\ \sigma_{(^{1}\text{H}\,(n,\gamma))} &= 0.332 \text{ barn} \, . \end{aligned} \tag{14.36}$$

The problem of calculating how much boron carbide (B_4C) to add to the paraffin wax to ensure that $\frac{\mu_{(^{10}\text{B}\,(n,\alpha))}}{\mu_{(^{1}\text{H}\,(n,\gamma))}} \gtrsim 25$ is therefore essentially reduced to deriving expressions for $N_{(^{10}\text{B})}$ and $N_{(^{1}\text{H})}$. In transport calculations, the nuclide number densities, or, alternatively, the mass fractions of all the important isotopes present in the paraffin wax & B_4C layer, must be known. It is therefore also necessary to calculate $N_{(^{11}\text{B})}$ and $N_{(\text{C})}$. Note that some carbon in the mixture will be in B_4C, while other carbon will be in the $H_{52}C_{25}$. These number densities will be calculated separately and then added to give the total number density of carbon in the mixture.

The natural abundance of ^{10}B is 19.9%, while that of ^{11}B is 10.1%. The natural abundances of ^{1}H and ^{12}C will be assumed as 100% for the purposes of this calculation.

The number densities of the different isotopes in the mixture are given by,

$$
\begin{aligned}
N_{(^{10}\mathrm{B})} &= 4 \times 0.199 \times N_A \times \left(\frac{\rho_{\mathrm{mix}} \times f_{(\mathrm{B_4C})}}{Mr_{(\mathrm{B_4C})}} \right) \\
N_{(^{11}\mathrm{B})} &= 4 \times 0.801 \times N_A \times \left(\frac{\rho_{\mathrm{mix}} \times f_{(\mathrm{B_4C})}}{Mr_{(\mathrm{B_4C})}} \right) \\
N_{(\mathrm{C\_in\_B_4C})} &= 1 \times N_A \times \left(\frac{\rho_{\mathrm{mix}} \times f_{(\mathrm{B_4C})}}{Mr_{(\mathrm{B_4C})}} \right) \\
N_{(\mathrm{C\_in\_wax})} &= 52 \times N_A \times \left(\frac{\rho_{\mathrm{mix}} \times f_{(\mathrm{wax})}}{Mr_{(\mathrm{wax})}} \right) \\
N_{(\mathrm{H})} &= 25 \times N_A \times \left(\frac{\rho_{\mathrm{mix}} \times f_{(\mathrm{wax})}}{Mr_{(\mathrm{wax})}} \right) \\
N_{(\mathrm{C})} &= N_{(\mathrm{C\_in\_B_4C})} + N_{(\mathrm{C\_in\_wax})}
\end{aligned}
\tag{14.37}
$$

where N_A is Avogadro's number and ρ_{mix} denotes the net density of a paraffin wax & boron carbide mixture.

The following expression gives the net density ρ_{mix} of a paraffin wax & boron carbide mixture,

$$
\frac{1}{\rho_{\mathrm{mix}}} = \frac{f_{\mathrm{wax}}}{\rho_{\mathrm{wax}}} + \frac{f_{(\mathrm{B_4C})}}{\rho_{(\mathrm{B_4C})}}
$$

so that

$$
\rho_{\mathrm{mix}} = \frac{1}{\left(\frac{f_{\mathrm{wax}}}{\rho_{\mathrm{wax}}} \right) + \left(\frac{f_{(\mathrm{B_4C})}}{\rho_{(\mathrm{B_4C})}} \right)} \,. \tag{14.38}
$$

Note from Figure 14.1 that ρ_{mix} is not a linear function of the mass fraction of boron carbide B_4C in the mixture.

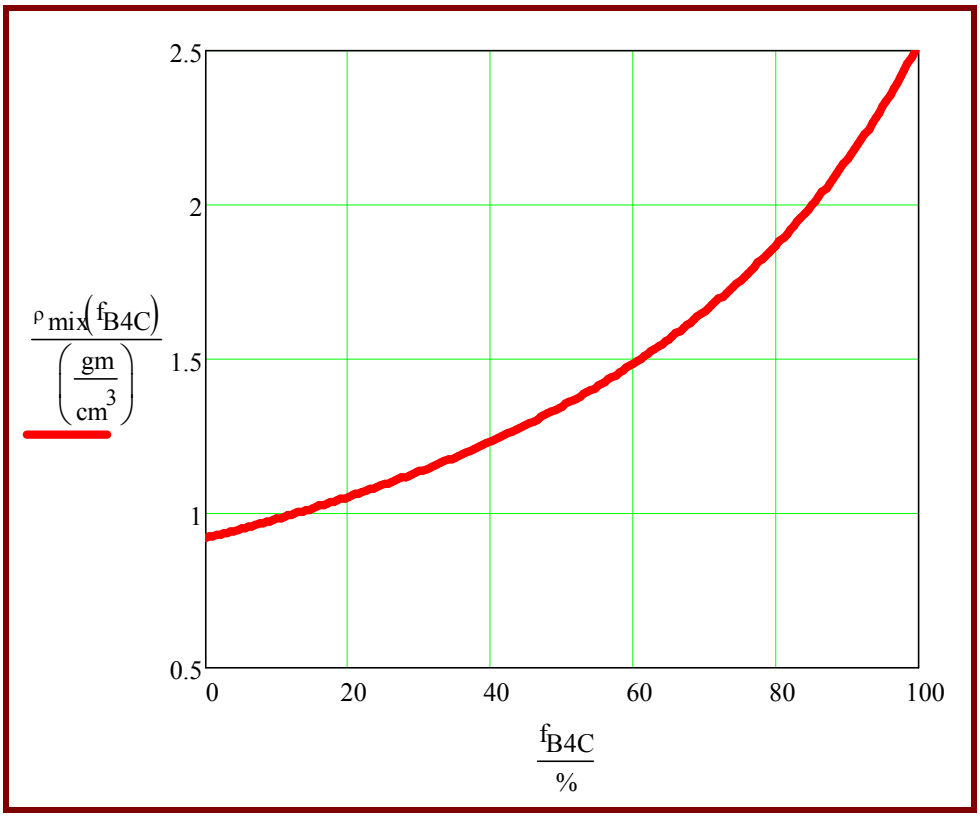

Figure 14.1: *Net density ρ_{mix} of a mixture of paraffin wax and boron carbide (B_4C), as a function of the mass fraction of B_4C in the mixture.*

Table 14.3 lists the nuclide number densities of the important isotopes in a mixture of paraffin wax and boron carbide (B_4C); these were calculated using the MathCAD worksheet displayed on page 514.

Table 14.3: *Nuclide number densities of the important isotopes in a mixture of paraffin wax and boron carbide (B_4C), calculated with Eq. (14.37) on page 507.*

Mass% B4C	NND(H)	NND (Carbon)	NND(B-10)	NND(B-11)	Mass-density of mixture
0	8.17E-02	3.93E-02	0.00E+00	0.00E+00	9.20E-01
0.5	8.15E-02	3.93E-02	4.00E-05	1.61E-04	9.23E-01
1	8.14E-02	3.92E-02	8.03E-05	3.23E-04	9.26E-01
1.5	8.12E-02	3.92E-02	1.21E-04	4.87E-04	9.29E-01
2	8.11E-02	3.92E-02	1.62E-04	6.51E-04	9.32E-01
2.5	8.09E-02	3.92E-02	2.03E-04	8.16E-04	9.35E-01
3	8.08E-02	3.91E-02	2.44E-04	9.83E-04	9.38E-01
3.5	8.06E-02	3.91E-02	2.86E-04	1.15E-03	9.41E-01
4	8.05E-02	3.91E-02	3.28E-04	1.32E-03	9.44E-01
4.5	8.03E-02	3.91E-02	3.70E-04	1.49E-03	9.47E-01
5	8.02E-02	3.91E-02	4.12E-04	1.66E-03	9.50E-01
5.5	8.00E-02	3.90E-02	4.55E-04	1.83E-03	9.53E-01
6	7.98E-02	3.90E-02	4.98E-04	2.00E-03	9.56E-01
6.5	7.97E-02	3.90E-02	5.41E-04	2.18E-03	9.60E-01
7	7.95E-02	3.90E-02	5.85E-04	2.35E-03	9.63E-01
7.5	7.93E-02	3.89E-02	6.29E-04	2.53E-03	9.66E-01
8	7.92E-02	3.89E-02	6.73E-04	2.71E-03	9.69E-01
8.5	7.90E-02	3.89E-02	7.17E-04	2.89E-03	9.72E-01
9	7.88E-02	3.89E-02	7.62E-04	3.07E-03	9.76E-01
9.5	7.87E-02	3.88E-02	8.07E-04	3.25E-03	9.79E-01
10	7.85E-02	3.88E-02	8.52E-04	3.43E-03	9.82E-01

The linear interaction coefficients for the two competing thermal neutron absorption reactions in a wax/B_4C mixture, namely $^{10}\mathrm{B}\,(n,\alpha)$ and $^{1}\mathrm{H}\,(n,\gamma)$, as calculated with the MathCAD worksheet on page 514, are shown in Figure 14.2.

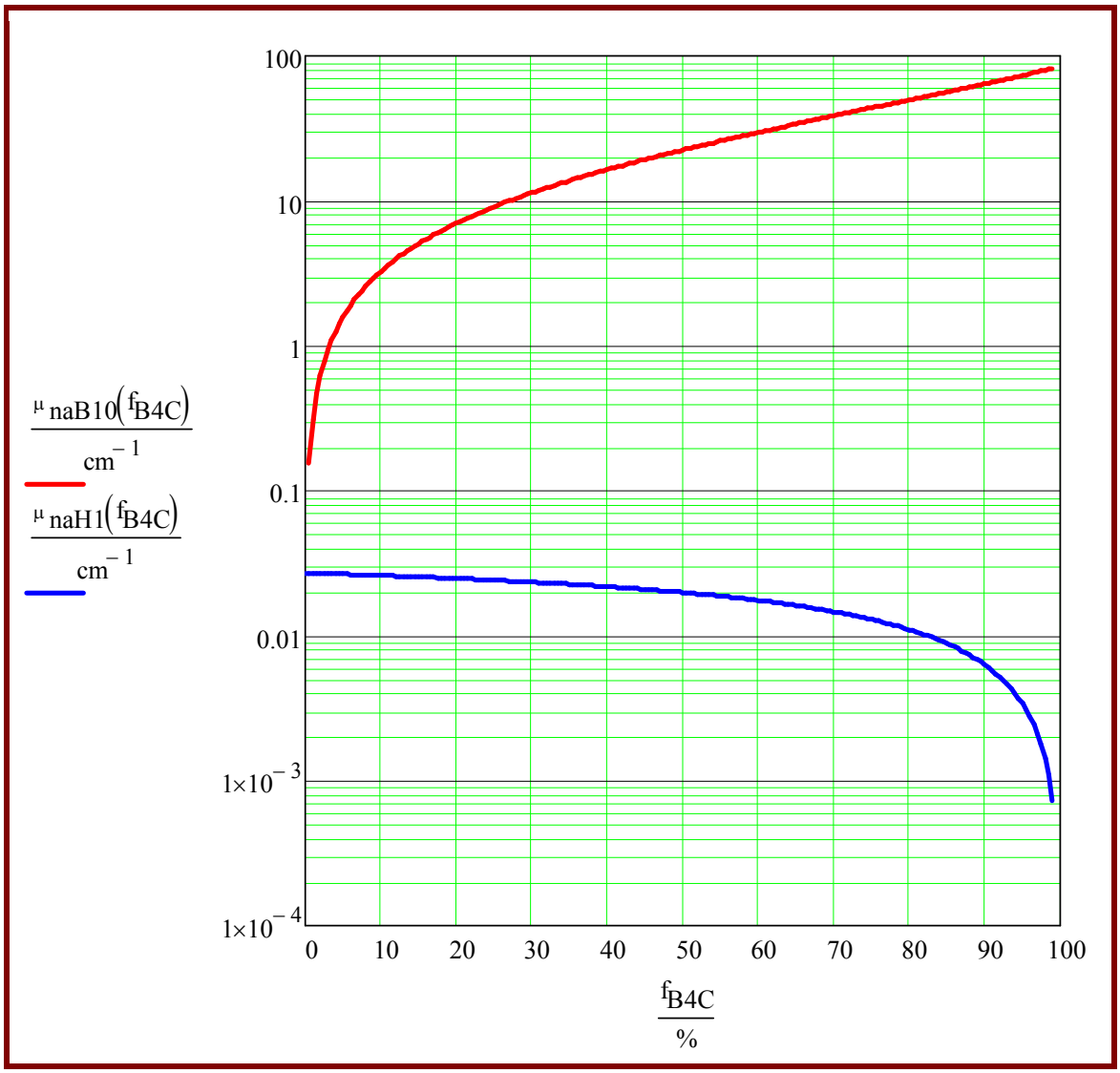

Figure 14.2: *The linear interaction coefficients* $\mu_{(^{10}B\,(n,\alpha))}$ *and* $\mu_{(^{1}H\,(n,\gamma))}$ *for the two competing thermal neutron absorption reactions in a wax/*B_4C *mixture, namely* $^{10}B(n,\alpha)$ *and* $^{1}H\,(n,\gamma)$.

Using the MathCAD worksheet on page 514, the ratio $\frac{\mu_{(^{10}B\,(n,\alpha))}}{\mu_{(^{1}H\,(n,\gamma))}}$ as a function of the mass fraction B_4C in the paraffin wax, is plotted in Figure 14.3 and listed in Table 14.4. This ratio expresses how much more likely thermal neutron absorption by ^{10}B will be, relative to thermal neutron absorption by ^{1}H, for different mass-fraction mixing ratios of B_4C in paraffin wax. Mixing is assumed to be perfectly homogenous, i.e. the finite grain size of the boron carbide powder is ignored.

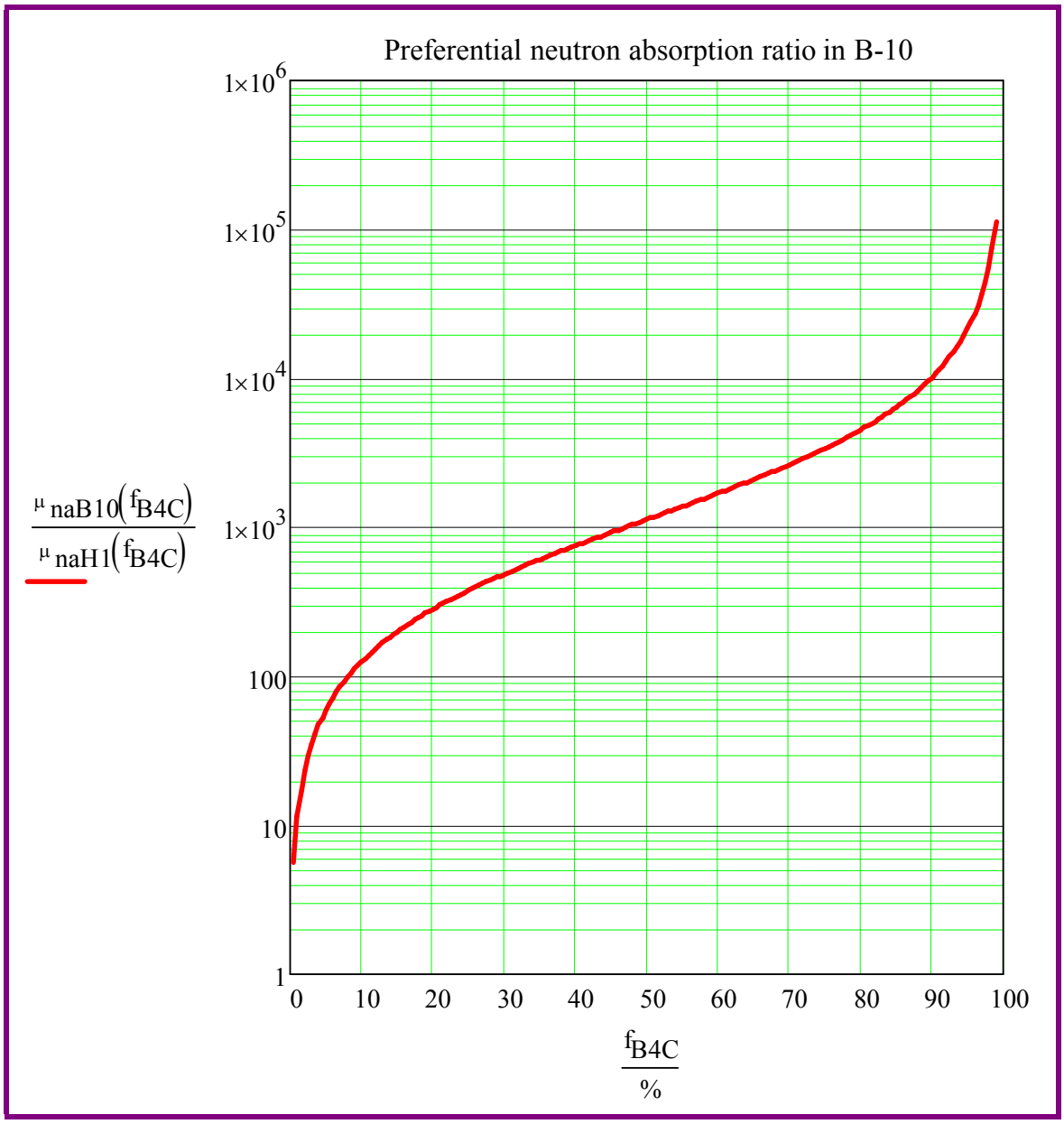

Figure 14.3: *Graph of how much more likely thermal neutron absorption by ^{10}B will be, relative to thermal neutron absorption by ^{1}H, for different mass-fraction mixing ratios of B_4C in paraffin wax.*

Table 14.4: *Table of how much more likely thermal neutron absorption by ^{10}B will be, relative to thermal neutron absorption by ^{1}H, for different mass-fraction mixing ratios of B_4C in paraffin wax.*

Mass% B4C	$\frac{\mu_{naB10}(f_{B4C})}{\mu_{naH1}(f_{B4C})}$
0.00	0.00
0.50	5.67
1.00	11.41
1.50	17.20
2.00	23.05
2.50	28.95
3.00	34.92
3.50	40.96
4.00	47.05
4.50	53.21
5.00	59.43
5.50	65.72
6.00	72.08
6.50	78.50
7.00	84.99
7.50	91.56
8.00	98.19
8.50	104.90
9.00	111.68
9.50	118.54
10.00	125.47

At a mixing ratio of 2.5% B_4C in paraffin wax, the ratio $\frac{\mu_{(^{10}B(n,\alpha))}}{\mu_{(^{1}H(n,\gamma))}} \approx 29$; at a mixing ratio of 3% B_4C in wax, the ratio $\frac{\mu_{(^{10}B(n,\alpha))}}{\mu_{(^{1}H(n,\gamma))}} \approx 35$; at a mixing ratio of 5% B_4C in wax, the ratio $\frac{\mu_{(^{10}B(n,\alpha))}}{\mu_{(^{1}H(n,\gamma))}} \approx 59$, and at a mixing ratio of 10% B_4C in wax, the ratio $\frac{\mu_{(^{10}B(n,\alpha))}}{\mu_{(^{1}H(n,\gamma))}} \approx 125$.

It is evident that the ideal mixing ratio of B_4C in wax will be between 2.5% and 5% for most applications in a bulk shield.

Codes such as MCNP require either the nuclide number densities of the mass fractions of the isotopes in a medium in its material specification cards. It is therefore important to derive expressions for the mass fractions of the important isotopes in a mixture of paraffin wax and boron carbide (B_4C); the first step is to derive the following expressions for the partial

densities D of the isotopes, which will typically be expressed in the unit g cm^{-3},

$$\begin{aligned} D_{(\mathrm{H})} &= N_{(\mathrm{H})}\, Mr_{(\mathrm{H})}\, m_{\mathrm{amu}} \\ D_{(\mathrm{C})} &= N_{(\mathrm{C})}\, Mr_{(\mathrm{C})}\, m_{\mathrm{amu}} \\ D_{(^{10}\mathrm{B})} &= N_{(^{10}\mathrm{B})}\, Mr_{(^{10}\mathrm{B})}\, m_{\mathrm{amu}} \\ D_{(^{11}\mathrm{B})} &= N_{(^{11}\mathrm{B})}\, Mr_{(^{11}\mathrm{B})}\, m_{\mathrm{amu}} \end{aligned} \qquad (14.39)$$

where m_{amu} is an atomic mass unit.

The total density of the mixture is $\sum_i D_i$, and should be equal to ρ_{mix}. The mass fractions of the different isotopes in the mixture, are, $\frac{D_{(\mathrm{H})}}{\sum_i D_i}$, $\frac{D_{(\mathrm{C})}}{\sum_i D_i}$, $\frac{D_{(^{10}\mathrm{B})}}{\sum_i D_i}$ and $\frac{D_{(^{11}\mathrm{B})}}{\sum_i D_i}$, which are equivalent to $\frac{D_{(\mathrm{H})}}{\rho_{\mathrm{mix}}}$, $\frac{D_{(\mathrm{C})}}{\rho_{\mathrm{mix}}}$, $\frac{D_{(^{10}\mathrm{B})}}{\rho_{\mathrm{mix}}}$ and $\frac{D_{(^{11}\mathrm{B})}}{\rho_{\mathrm{mix}}}$. The above formulas were coded into a MathCAD worksheet on page 514, and were used to generate mass fractions for the MCNP transport calculations.

Table 14.5 lists the mass fractions of the important isotopes in a mixture of paraffin wax and boron carbide (B_4C), as calculated with the MathCAD worksheet on page 514.

Table 14.5: *The mass fractions of the important isotopes in a mixture of paraffin wax and boron carbide.*

Mass% B4C	Mass fraction, H	Mass fraction, C	Mass fraction, B-10	Mass fraction, B-11	Mass-density of mixture
0	1.49E-01	8.51E-01	0.00E+00	0.00E+00	9.20E-01
0.5	1.48E-01	8.48E-01	7.21E-04	3.19E-03	9.23E-01
1	1.47E-01	8.45E-01	1.44E-03	6.38E-03	9.26E-01
1.5	1.46E-01	8.42E-01	2.16E-03	9.58E-03	9.29E-01
2	1.46E-01	8.39E-01	2.88E-03	1.28E-02	9.32E-01
2.5	1.45E-01	8.36E-01	3.61E-03	1.60E-02	9.35E-01
3	1.44E-01	8.32E-01	4.33E-03	1.92E-02	9.38E-01
3.5	1.43E-01	8.29E-01	5.05E-03	2.23E-02	9.41E-01
4	1.43E-01	8.26E-01	5.77E-03	2.55E-02	9.44E-01
4.5	1.42E-01	8.23E-01	6.49E-03	2.87E-02	9.47E-01
5	1.41E-01	8.20E-01	7.21E-03	3.19E-02	9.50E-01
5.5	1.40E-01	8.17E-01	7.93E-03	3.51E-02	9.53E-01
6	1.40E-01	8.13E-01	8.65E-03	3.83E-02	9.56E-01
6.5	1.39E-01	8.10E-01	9.38E-03	4.15E-02	9.60E-01
7	1.38E-01	8.07E-01	1.01E-02	4.47E-02	9.63E-01
7.5	1.37E-01	8.04E-01	1.08E-02	4.79E-02	9.66E-01
8	1.37E-01	8.01E-01	1.15E-02	5.11E-02	9.69E-01
8.5	1.36E-01	7.97E-01	1.23E-02	5.43E-02	9.72E-01
9	1.35E-01	7.94E-01	1.30E-02	5.75E-02	9.76E-01
9.5	1.34E-01	7.91E-01	1.37E-02	6.06E-02	9.79E-01
10	1.34E-01	7.88E-01	1.44E-02	6.38E-02	9.82E-01

The MathCAD worksheet used to calculate the nuclide number densities in a B_4C/wax mixture, is shown below.

NND B-10 B-11 C-12 and H-1 in Wax B4C mix.xmcd

Annexure C
Approximate Semi-Analytical Methods in Radiation Transport: Point Kernel Integration

C.1 Introduction

Point kernel integration represents a drastic simplification of radiation transport. It is used with great success for a wide variety of photon shielding problems. (It is less successful for solving neutron shielding problems.) In essence, this method amounts to initially neglecting the inscattering integral of the Boltzmann Transport Equation (BTE). This means that scattering is not considered, and that the medium is viewed as purely absorbing in nature. A solution for the simplified problem is obtained and then multiplied by a *buildup factor* which corrects for the initial neglect of the contribution of scattered radiation to the response at the point of interest. The term "buildup" refers to the buildup of scattered radiation in the material region between the source and detector positions.

C.2 Uncollided or unscattered radiation

Consider a uniform, isotropic, homogenous medium of infinite dimensions, having a total interaction coefficient μ. A single radiation quantum is produced at the origin ($x = 0$) and moves in the x direction.

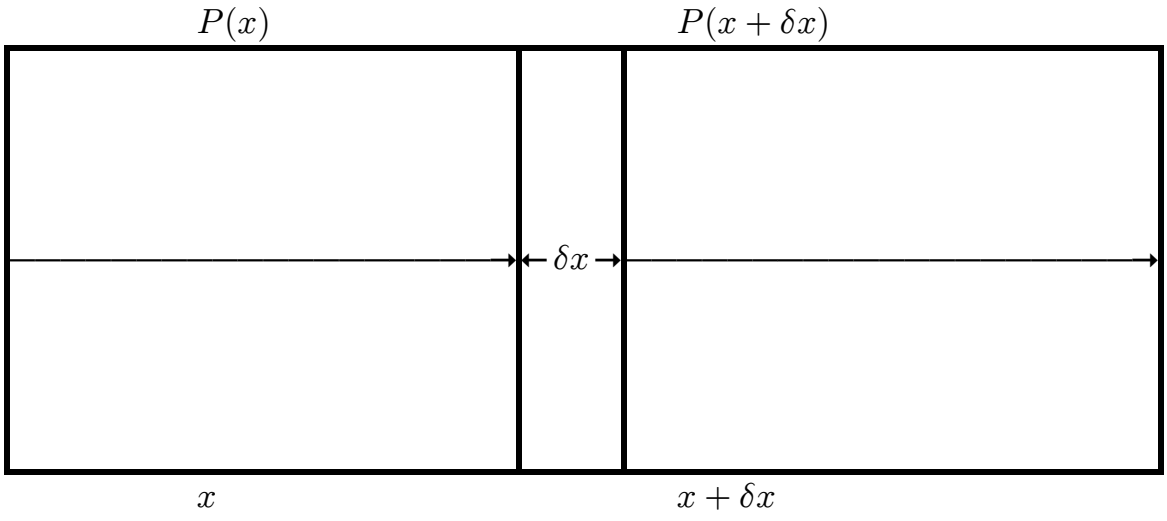

Let $P(x)$ be the probability that the quantum will move a distance x without any interaction. The probability that the quantum of radiation will react the point $x + \delta x$ without interaction is $P(x + \delta x)$, where δx is small. Let μ_t be the linear interaction coefficient for the medium at the energy under consideration.

Because we ignore scattering and consider the medium to be purely absorbing in nature, we assume $\mu_t \equiv \mu_{\text{abs}}$ and call it the linear attenuation coefficient. To simplify notation, the subscript of μ is now dropped.

According to the definition of linear interaction coefficient, the probability for the interaction of a single particle in the infinitesimal distance δx, is $\mu\delta x$. The probability of a reaction not taking place, is therefore $(1 - \mu\delta x)$. The probability of the quantum reaching $x + \delta x$ without interaction, is the product of the probability that it will reach x without interaction, multiplied by the probability that the particle will traverse the additional infinitesimal distance δx without interaction. Accordingly,

$$P(x + \delta x) = [P(x)]\,(1 - \mu\delta x).$$

By using the definition of a derivative, we obtain the differential equation

$$\frac{dP(x)}{dx} = -\mu P(x). \tag{C.1}$$

By using the initial condition $P(0) = 1$, it follows that the number of particles that will penetrate to depth x without interaction, is

$$P(x) = e^{-\mu x}. \tag{C.2}$$

We see that the uncollided radiation is attenuated exponentially.

This expression was derived for a single particle. We now apply this result to 1 a parallel beam and 2 a point source.

If a **mono-energetic parallel beam of neutral radiation quanta** moves in the x-direction, crossing the y–z plane with initial fluence-rate $\phi_{\text{uncoll}}(0)$, the fluence-rate that will penetrate to depth x with no interaction (i.e. uncollided), will be,

$$\begin{aligned} \phi_{\text{uncoll}}(x) &= \phi_{\text{uncoll}}(0)\,P(x) \\ &= \phi_{\text{uncoll}}(0)\,e^{-\mu x} \end{aligned} \tag{C.3}$$

The response $R_{uncoll}(x)$ from particles that have not interacted, will be

$$\begin{aligned} R_{\text{uncoll}}(x) &= \left\langle \phi_{\text{uncoll}}(0)\,e^{-\mu x}, \mathfrak{R} \right\rangle \\ &= R_{\text{uncoll}}(0)\,e^{-\mu x} \qquad , \end{aligned} \tag{C.4}$$

because $R_{\text{uncoll}} = \mathfrak{R}\,\phi_{\text{uncoll}}$.

(Remark: In pre-graduate physics courses, it is often stated that neutral radiation such as ionising photons are exponentially attenuated. The above treatment makes it clear that this approximation is only rigorously true for uncollided radiation quanta. Once non-absorbing interactions, i.e. scattering, is considered, radiation transport is not quite as simple as it is sometimes set forth in general textbooks.)

We now apply the result in Eq. (C.3) to a point source in a homogenous medium. Consider a **mono-energetic, isotropic point source of neutral particles** having a source strength of S quanta per unit time. The fluence-rate $\phi_{\text{uncoll}}(r)$ of particles at radius r that will move through a unit surface of a sphere with radius r, multiplied by the probability that the radiation quanta will traverse the distance r without interactions, will be

$$\begin{aligned}\phi_{\text{uncoll}}(r) &= \frac{S}{4\pi r^2}\,P(r)\\ &= \frac{S}{4\pi r^2}\,\exp(-\mu r)\end{aligned} \tag{C.5}$$

The response $R_{\text{uncoll}}(r)$ contributed by the uncollided radiation quanta will be

$$\begin{aligned}R_{\text{uncoll}}(r) &= \left\langle \phi_{\text{uncoll}}(r)\,e^{-\mu r}, \mathfrak{R}\right\rangle\\ &= \frac{S\,\mathfrak{R}}{4\pi r^2}\,e^{-\mu r}.\end{aligned} \tag{C.6}$$

where $\mathfrak{R}$ is the value of the response function at the given photon energy.

If the point source is in a vacuum, $\mu = 0$, so that $e^{-\mu r} = 1$, and $R_{\text{uncoll}}(r) = \frac{S\,\mathfrak{R}}{4\pi r^2}$. Notice that the fluence-rate and dose rate decrease as $\frac{1}{r^2}$ as the distance from the source is increased. This decrease op the fluence-rate and dose-rate with increasing distance is sometimes referred to as *geometric attenuation.*

In the case of a non-homogenous medium, the linear interaction coefficient is a function of x, so that the solution to differential Eq. (1.11) on page 15 will be,

$$P(x) = \exp\left(-\int_0^x dx'\,\mu(x')\right). \tag{C.7}$$

If we replace the product μx in the above attenuation equations with

$$\int_0^x dx'\,\mu(x'),$$

we obtain the general result for a general, non-homogenous medium.

In the special case of a piecewise-homogeneous, laminated shield, $\mu(x)$ is a step function. Consider the following partition of the spatial interval $[0; x]$ in I contiguous sub-intervals by the points

$$0 = x_1 < x_2 < \ldots < x_i < \ldots < x_{I+1} = x.$$

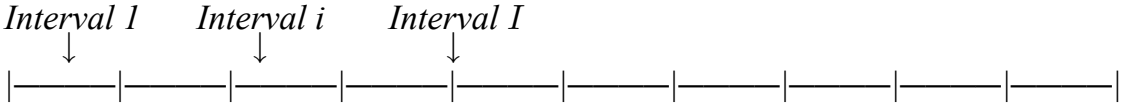

x_1 x_2 x_i x_{i+1} x_{I+1}
0 x

In each sub-interval (zone) i, the material composition is invariant/homogenous. Then,

$$\mu(x) = \sum_{i=1}^{I} \mu_i \, W(x_i, x_{i+1}, x)$$

where W is the "window function" defined in Eq. (2.6) on page 56. By using the linearity of the integral operator, i.e. the fact that an integral of a sum equals a sum of integrals, it follows that

$$\int_0^x dx' \, \mu(x') = \sum_{i=1}^{I} \mu_i \, \Delta x_i$$

where

$$\Delta x_i = (x_{i+1} - x_i) = t_i$$

is the thickness of layer i. If we replace the product μx in the attenuation equations for a homogenous material medium, by the sum $\sum_{i=1}^{I} \mu_i \, \Delta x_i$, we obtain the general result for a laminated heterogeneous medium. If the source is placed at $x' = 0$ and the detector at $x' = x$, the integral $\int_0^x dx' \, \mu(x')$ or the sum $\sum_{i=1}^{I} \mu_i \, \Delta x_i$ will represent the total mean free paths between the source and the detector. This dimensionless quantity is termed the *total optic path length,* ξ.

Poly-energetic point source

See Shultis & Faw (2000: 159-160)

Assignment C.1

1. Derive an expression for the half-value thickness, $x_{½}$, that is required to required to reduce the uncollided radiation response to $\frac{1}{2}$ of its original value.

2. Derive an expression for the tenth-value thickness, $x_{(\frac{1}{10})}$, that is required to required to reduce the uncollided radiation response to $\frac{1}{10}$ of its original value.

(See Shultis & Faw (2000: 157).)

Mean free path

Next, an expression for the mean free pathlength that a radiation quantum moves, is derived.

The probability that a particle will have a path-length between x and $x + dx$, is

$$P(x) - P(x + dx) = \mu e^{-\mu x}\, dx.$$

This is a probability distribution or probability density function. The mean free path λ of a radiation quantum in an infinite homogenous medium will be the expectation value of x, with weighting function the probability density function for path length:

$$\langle x \rangle = \frac{\int_0^\infty dx\, x\, (\mu e^{-\mu x})}{\int_0^\infty dx\, (\mu e^{-\mu x})}$$

$$\Rightarrow \lambda = \frac{1}{\mu} \tag{C.8}$$

The mean free path is an information-rich, convenient unit of length in the discipline of neutral particle transport. The physical distance can e.g. be expressed in terms of

$$\frac{x}{\lambda} = x\mu,$$

i.e. the number of mean free paths, also called the *optical path length.*

C.3 Photon buildup factor

In the previous subsection, we derived rigorous expressions for the **uncollided** or **unscattered** fluence-rate and **uncollided** or **unscattered** response. These expressions do not hold for the real fluence-rate and response, because the contribution of scattering to particle transport was neglected in their derivation. Now we show how the buildup factor formalism is applied to correct computed results for this omission.

Whatever the photon source and the attenuating medium, the energy spectrum of the total photon fluence-rate $\phi(\vec{\boldsymbol{r}}, E)$ at some point of interest defined by the position vector $\vec{\boldsymbol{r}}$ may be divided into two components. The *unscattered* component $\phi^0(\vec{\boldsymbol{r}}, E)$ consists of just those photons that have reached $\vec{\boldsymbol{r}}$ from the source without having experienced any interactions in the attenuating medium. The *scattered* component $\phi^s(\vec{\boldsymbol{r}}, E)$ consists of source photons scattered one or more times, as well as secondary photons such as X-rays and annihilation gamma-photons. Accordingly, the dose or detector response $R(\vec{\boldsymbol{r}})$ at the point of interest $\vec{\boldsymbol{r}}$

may be divided into unscattered (primary) and scattered (secondary) components, $R^0(\vec{\boldsymbol{r}})$ and $R^s(\vec{\boldsymbol{r}})$. The buildup factor $B(\vec{\boldsymbol{r}})$ is defined as the ratio of the total dose to the unscattered response. The unscattered response can be calculated with relative ease, as indicated above. Thus

$$B\left(\vec{\boldsymbol{r}}\right) \equiv \frac{R(\vec{\boldsymbol{r}})}{R^0(\vec{\boldsymbol{r}})} = \frac{R^0(\vec{\boldsymbol{r}}) + R^s(\vec{\boldsymbol{r}})}{R^0(\vec{\boldsymbol{r}})} = 1 + \frac{R^s(\vec{\boldsymbol{r}})}{R^0(\vec{\boldsymbol{r}})}. \tag{C.9}$$

The responses may be evaluated using response functions, so that the buildup is defined as

$$B\left(\vec{\boldsymbol{r}}\right) = 1 + \frac{\int dE\ \mathfrak{R}(E)\ \phi^s(\vec{\boldsymbol{r}}, E)}{\int dE\ \mathfrak{R}(E)\ \phi^0(\vec{\boldsymbol{r}}, E)}. \tag{C.10}$$

in which the integrations are over all possible E. From the last equation it follows that it is necessary to associate with buildup factors the nature of the source, the nature of the attenuating medium, and the nature of the response. (The nature of the source and the attenuating medium determines $\phi^s(\vec{\boldsymbol{r}}, E)$ and $\phi^0(\vec{\boldsymbol{r}}, E)$.)

It is clear that,

$$R = R^0\, B.$$

Because of the comparative ease of calculating the unscattered response R^0, we can readily find the total detector response if we have data for the buildup factors for the situation under consideration.

Because

$$\begin{aligned} R^s &= R - R^0 \\ &= (B-1)R^0 \end{aligned}$$

we observe that the buildup factor B can never be less than unity.

Buildup factors are calculated as follows: The transport equation is solved rigorously, by means of deterministic transport methods or a Monte Carlo simulation, to calculate the total fluence-rate $\phi(\vec{\boldsymbol{x}}, E)$ as well as the unscattered fluence-rate, $\phi^0(\vec{\boldsymbol{x}}, E)$. The buildup factors are calculated from Eq. (C.10).

Note that in the multigroup approximation, Eq. (C.10) becomes

$$B_i = \frac{\sum_{g=1}^{G} \overline{\mathfrak{R}}_g\, \phi_{\text{tot}_{g,i}}}{\sum_{g=1}^{G} \overline{\mathfrak{R}}_g\, \phi_{\text{uncoll}_{g,i}}}.$$

The necessity for large tables of data has been greatly reduced by the fact that photon cross sections (above the K-edge energies) are smooth functions of source energy and of atomic charge number of the attenuating medium. This property of photon cross sections implies that buildup data are needed only for a few selected values of source energies and elemental types, plus a few common mixtures or compounds. Accurate interpolation for other energies or materials is then possible. Moreover, buildup factors are smooth functions of distance (in terms of the mean-free-path length (mfp)) and therefore only a few selected mfp values between 0 and the greatest optical distance of practical importance, are needed. Thus, again, accurate interpolation for other distances is possible.

Only a few types of dosimetric responses are of major interest: absorbed dose in the shielding medium, tissue absorbed dose, and effective dose. In the case of photons, the buildup factors are usually quite similar for these various types of response, and, as an approximation, one may often be substituted for another if the responses are expected to be nearly equal.

The buildup factor approach for photon attenuation calculations should not be used without a careful consideration of the specific problem under consideration. Complexities and difficulties are discussed in more detail below.

C.4 Empirical approximations for point-source buildup factors

A great deal of effort has been directed toward the approximation of buildup factors by mathematical functions which can be used directly in calculations. These efforts have dealt almost exclusively with buildup factors for point-isotropic and monoenergetic sources in infinite media. Two forms of approximation have been in use for many years: the *Taylor form* and the *Berger form.* Because both forms still see wide application in computer codes used in engineering practice, they are presented here although they are outdated. The form of choice today should be the *geometric progression* form.

Let ξ be the geometrical, rectilinear distance which radiation has to travel through all non-vacuum regions of a radiation shield. Let μ be the linear interaction coefficient for the energy of interest. We know that the buildup factor is a function of the total optical path length, $\mu\xi$. In order to simplify the integration process, an analytical function is fitted to $B(\mu\xi)$ ($\xi \equiv$ "thickness traversed"); this function's coefficients will obviously be different for every energy group.

- ***Taylor approximation***

  This approximation to the buildup factor has the form

$$B(E_0, \mu\xi) \simeq \sum_{i=1}^{I} A_i \, e^{-\alpha_i \mu\xi}, \tag{C.11}$$

  in which the parameters A_i and α_i depend on E_0, the attenuating medium, and the type of response. Usually, $I = 2$ or 3. The advantage of the Taylor approximation is that it yields point kernels that are readily analytically integrable.

- ***Berger's formula***

  This approximation to the buildup factor is in the form

$$B(E_0, \mu\xi) \simeq 1 + a\mu\xi\, e^{+b\mu\xi} \tag{C.12}$$

  where ξ is the distance traversed. The parameters a and b depend on E_0, the attenuating medium, and the type of response. This formula also fits in reasonably well with analytical point-kernel calculations. Furthermore, the formulation is such that the contribution from the unscattered radiation is provided by the first term while the second term determines the in-scattered contribution. Even though only two parameters are involved, it is about as accurate as Taylor's 3-parameter formula. Berger buildup parameters are used in the point-kernel photon shielding code PELSHIE (RSICC CCC-202[29]).

- ***Polynomial formula***

$$B = \sum_{i=0}^{N} a_i (\mu\xi)^i \tag{C.13}$$

  Usually, $N = 3$; this provides reasonable accuracy up to 20 mean-free-path lengths. Capo's polynomial fit to buildup factor data is available as a (bad!) option in the code QAD-CGGP.

The above buildup formulae are inaccurate for deep penetration problems. For certain energies and distances, errors may be as great as 50%. Since the advent of powerful digital computers, there is no need to use the above simple approximations to the buildup factor any more; the following formula is to be preferred:

- ***The geometric progression approximation***

An extraordinarily precise formulation, called the *geometric progression approximation* of the buildup factor, was developed in the late 1980s. The geometric progression (GP) approximation is a 5-parameter function, and is the only known function that can fit all existing buildup factor data to an accuracy of $\pm 3\%$ over the entire range of material, penetration depth and energy parameters. The code QAD-CGGP (RSICC CCC-493) contains the option to use GP buildup factors. The GP approximation has the form

$$\begin{aligned} B(E, \mu\xi) &= 1 + (b-1)\,\frac{[K(E,\xi\mu)]^{\mu\xi} - 1)}{(K(E,\xi\mu) - 1)} \quad \text{for} \quad K(E,\xi\mu) \neq 1 \\ &= 1 + (b-1)\,\mu\xi \quad \text{for} \quad K(E,\xi\mu) = 1 \end{aligned} \tag{C.14}$$

---

[29] This is an abbreviation for: RSICC, Computer Codes Collection number 202.
RSICC = Radiation Safety Information Computational Center, Oak Ridge National Laboratory, Tennessee, USA.

where

$$K(E,\mu\xi) = c\cdot(\mu\xi)^a + d\cdot\left(\frac{\tanh\left(\frac{\mu\xi}{X_k}-2\right)-\tanh(-2)}{(1-\tanh(-2))}\right) \tag{C.15}$$

and

$$\begin{aligned} E &\equiv \text{source energy} \\ \mu\xi &\equiv \text{the source-detector distance in mean free paths} \\ b &\equiv \text{the buildup factor for 1 mean free path}^{30}. \end{aligned}$$

The constants a, c, d and X_k are four other parameters dependent on the photon energy, the attenuating medium, and the nature of the response. The variation of K with depth of penetration represents photon dose buildup as well as the change in the shape of the photon spectrum relative to the form at 1 mfp. The spectrum at 1 mfp determines the value of b.

We now look at a few factors that can complicate point-kernel photon attenuation calculations that uses the buildup factor formalism.

C.5 Point-kernel application of buildup factors

For a volume-distributed source of monoenergetic photons $S_V(\vec{\boldsymbol{r}}_s)$ of energy E_0, the dose from uncollided photons at some position $\vec{\boldsymbol{r}}$ is

$$R^0(\vec{\boldsymbol{r}}) = \int_{V_s} dV\ \frac{S_V(\vec{\boldsymbol{r}}_s)\,\mathfrak{R}(E_0)}{4\pi|\vec{\boldsymbol{r}}_s-\vec{\boldsymbol{r}}|^2}\,e^{-l} \tag{C.16}$$

where the integration is over all source locations and l is the optical thickness between $\vec{\boldsymbol{r}}_s$ and $\vec{\boldsymbol{r}}$, namely

$$l = \int_0^{|\vec{\boldsymbol{r}}_s-\vec{\boldsymbol{r}}|} ds\,\mu(s),$$

with s measured along a straight line from $\vec{\boldsymbol{r}}_s$ to $\vec{\boldsymbol{r}}$. To correct for the buildup of scattered radiation, an appropriate buildup factor is included in the integrand of Eq. (C.16). If an infinite-medium point-source buildup factor is used and the medium is of uniform composition but possibly of variable density, the total dose at $\vec{\boldsymbol{r}}$ is

$$\begin{aligned} R(\vec{\boldsymbol{r}}) &= \int_{V_s} dV\ \frac{S_V(\vec{\boldsymbol{r}}_s)\,\mathfrak{R}(E_0)}{4\pi|\vec{\boldsymbol{r}}_s-\vec{\boldsymbol{r}}|^2}\,B(E_0,l)\,e^{-l} \\ &\equiv \int_{V_s} dV\ S_V(\vec{\boldsymbol{r}}_s)\,G(\vec{\boldsymbol{r}}_s,\vec{\boldsymbol{r}}). \end{aligned} \tag{C.17}$$

[30] In other words, b is a material-dependent fitting parameter.

Here

$$G(\vec{\boldsymbol{r}}_s, \vec{\boldsymbol{r}}) \equiv \frac{S_V(\vec{\boldsymbol{r}}_s)\, \mathfrak{R}(E_0)}{4\pi|\vec{\boldsymbol{r}}_s - \vec{\boldsymbol{r}}|^2}\, B(E_0, l)\, e^{-l}$$

is the response Green's function or point kernel that gives the dose at $\vec{\boldsymbol{r}}$ contributed by a photon emitted isotropically at $\vec{\boldsymbol{r}}_s$.

From this approximate result, it is seen that the total dose at $\vec{\boldsymbol{r}}$ from radiation emitted isotropically from $\vec{\boldsymbol{r}}_s$ depends only on the material properties along a line between $\vec{\boldsymbol{r}}_s$ and $\vec{\boldsymbol{r}}$ and on the distance between these two points. This approximation, based on the infinite-medium point-source buildup factor, is sometimes called *ray theory,* indicative that the total dose is determined simply by the material and distance along the ray joining source and detector points. In many situations it is an excellent approximation; it is widely used in photon shielding calculations.

Disk source

Problem specification:
Consider the infinitesimally thin, uniform disk source shown in the figure below.
Source strength: S photons $\text{cm}^{-2}\,\text{s}^{-1}$;
Photon energy: 1 MeV (mono-energetic);
Angular distribution of photon emission: isotropic;
Density of shielding material: ρ g cm^{-3};
Mass attenuation coefficient of shielding material: μ_m $\text{cm}^2\,\text{g}^{-1}$. (Note that $\mu = \rho\mu_m$.)
Thickness of shield: t cm.
Radius of disk: r_0 cm.
The setup is located in air; ignore the attenuation of the radiation in air.
Distance from origin to detector: z_0.
The origin is at the centre of the disk source.

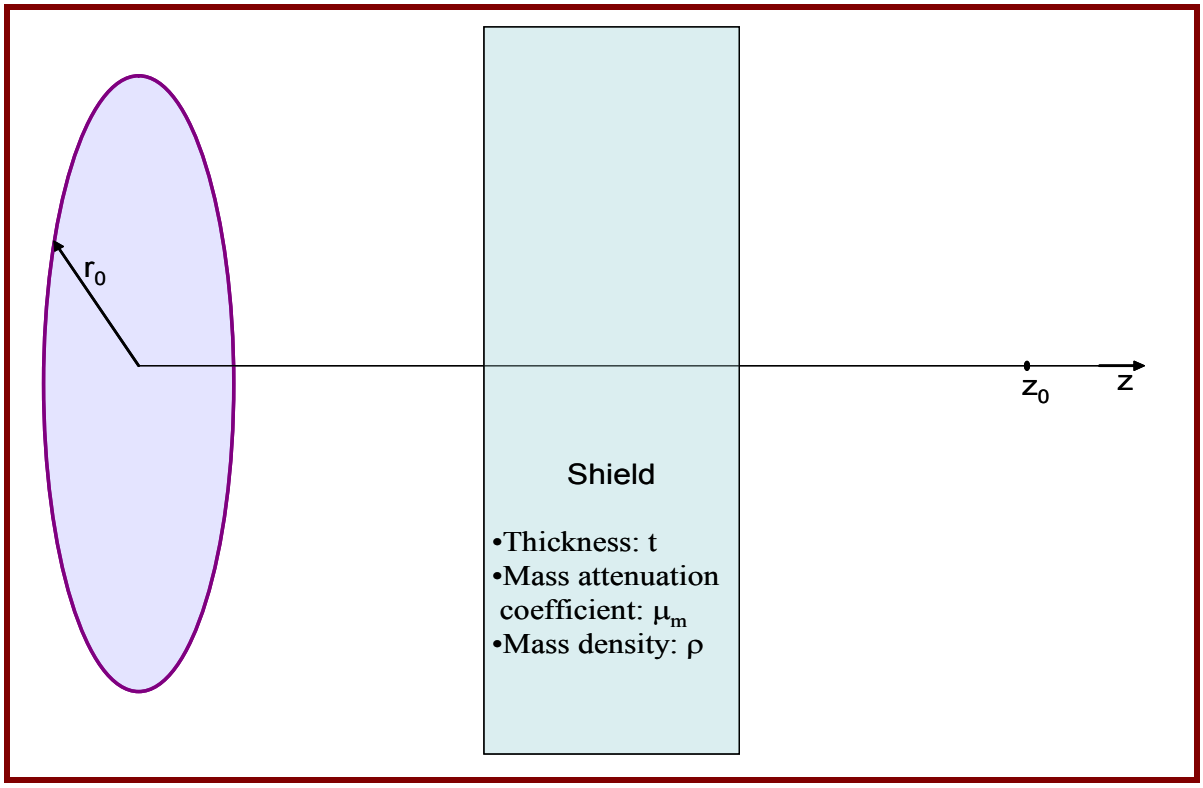

(a) Show that the point kernel for particles that do not interact, i.e. uncollided particles, is given by

$$dR_{\text{uncoll}} = \frac{\mathfrak{R} S r\,dr}{2(r^2+z_0^2)} \exp\left(-\rho\mu_m t \frac{\sqrt{r^2+z_0^2}}{z_0}\right)$$

where $r \in [0; r_0]$.

(b) Express the dose rate at the point z_0, contributed by uncollided radiation quanta, as a definite integral.

(c) Use the 2-parameter Berger buildup factor formalism,

$$B(\mu\xi) = B(\rho\mu\xi) = 1 + \beta_1 \rho\mu\xi \, e^{\beta_2 \rho\mu\xi},$$

where ξ is the distance that the photons move through the shield, to obtain an analytical expression for the total dose rate, R_{tot}.

(d) Assume that the shielding material is Pb, i.e. $\rho = 11.35$ g cm^{-3}, $\mu_m = 6.752 \times 10^{-2}$ cm^2 g^{-1}, $\beta_1 = 0.2604$ and $\beta_2 = 10^{-5}$.
Mono-energetic photons with $E = 1$ MeV are radiated isotropically. Let the source strength per unit area be $S = 10^{10}$ cm^{-2} s^{-1}.
For 1 MeV photons, $\mathfrak{R} = 1.65 \times 10^{-8} \left(\frac{\text{sievert h}^{-1}}{\text{cm}^{-2}\,\text{s}^{-1}} \right)$.
Let $z_0 = 100$ cm.
Draw a graph for R_{uncoll} and R_{tot} for:

(i) $r_0 = 10$ cm, and t that varies in 1 mm steps from 0 cm to 10 cm;

(ii) $t = 10$ cm, and r_0 that varies in 1 cm steps from 1 cm to 100 cm.

Solution:

(a) View an infinitesimal ring element with radius r and thickness dr. Divide this ring element azimuthally into infinitesimal area elements such that each is subtended by an angle $d\varphi$.

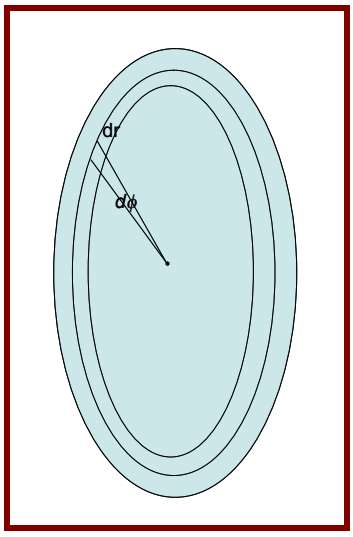

The area of the infinitesimal area element of the planar disk source, will be $dA = dr\, r d\varphi$, so that its infinitesimal source strength will be $dS = S\, dA = S\, r\, dr\, d\varphi$. According to the point-kernel approximation, $S\, r\, dr\, d\varphi$ photons per second will be emitted isotropically from the infinitesimal area around the point $(z, r, \varphi) = (0, r, \varphi)$. Photons emitted in an infinitesimal area around this point, will move a distance

$$\xi = t \sec(\eta) = t \frac{\sqrt{r^2 + z_0^2}}{2}$$

through the shield.

The product $\rho\mu_m$ gives the linear interaction coefficient μ.

Thanks to azimuthal symmetry, the integral over the variable φ has the value 2π.

- Solution to questions (b) — (d): refer to the following MathCAD worksheet:

DISK.XMCD

Demonstration

The lecturer demonstrates and explains the use of a MathCAD worksheet to model the transport of photons from the following point sources:

a. 3.7×10^{10} photons with $E = 10$ MeV;

b. 3.7×10^{10} photons with $E = 2$ MeV;

c. 3.7×10^{10} photons with $E = 0.5$ MeV;

through the following shields:

a. 10 cm Pb

b. 10 cm Fe

c. 10 cm water

d. 10 cm air.

The students explain results on the basis of the three most important attenuation mechanisms for ionising photons.

Example: Plane source

1) View the source-shield-detector arrangement below. The three homogenous and uniform blocks reach to infinity in the x and y directions. The z-axis is shown on the sketch. Zone 1 is a uniform, isotropic, mono-energetic volume source with source strength S photons.cm^{-3} s^{-1}. The detector is just to the right of zone 3, on the z-axis. The fluence to response conversion factor at the given photon energy is $\mathfrak{R}$.

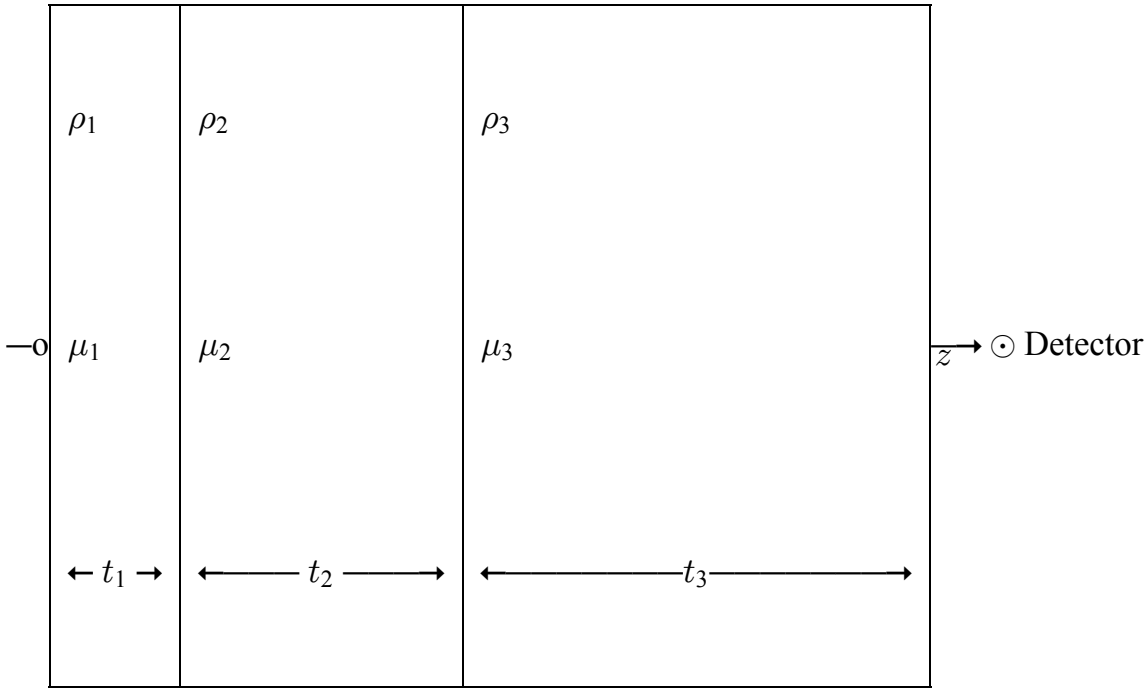

Show that, if the two-parameter Berger formula for dose buildup is used, the dose rate at the detector position will be:

$$R_{tot} = \int_{-\infty}^{\infty} dx \int_{-\infty}^{\infty} dy \int_{0}^{t_1} dz \, \frac{\mathfrak{R} S \exp\left(\sum_{i=1}^{3} (-\mu_{m_i} \rho_i \xi_i)\right)}{4\pi \left[x^2 + y^2 + (t_1 + t_2 + t_3 - z)^2\right]} \left(1 + \beta_1 \mu_{m_B} \rho_{m_B} \xi_B \exp(\beta_2 \mu_{m_B} \rho_{m_B} \xi_B)\right),$$

where

$$\xi_1 = (t_1 - z)\sec(\theta)$$

$$\xi_2 = t_2 \sec(\theta)$$

$$\xi_3 = t_3 \sec(\theta)$$

$$\xi_B = (t_1 + t_2 + t_3 - z)\sec(\theta)$$

$$\sec(\theta) = \frac{\sqrt{x^2 + y^2 + (t_1 + t_2 + t_3 - z)^2}}{t_1 + t_2 + t_3 - z}$$

Assume that the shielding material in zone 3 has the dominant influence on the spectrum of the transmitted photons, and select appropriate values for ρ_B and μ_B.

Suppose the three material zones are surrounded by air. Why will the use of infinite medium buildup factors lead to an overestimation of the buildup?

Further example of point kernel dose rate calculations

Photon Shielding - PointKernel - Point Source.xmcd

Bibliography

(Note: Excellent articles and books are preceded by a ♥ sign.)

♥AKHIEZER, NI & GLAZMAN, IM. 1961. *Theory of Linear Operators in Hilbert Space.* Volume I. New York: F. Ungar. 147 p.

ANSI/ANS 6.1.1. 1991. *Neutron and Gamma-Ray Flux-to-Dose-Rate Factors.* #.

CHINAKA, E. 2014. Radiation Shielding Analysis and Optimisation for the Mineral-PET Kimberlite Sorting Facility Using the Monte Carlo Calculation Code MCNPX. MSc Dissertation, University of Johannesburg, Johannesburg, South Africa.

CRANBERG, L, FRYE, G, NERESON, N & ROSEN, L. 1956. *Fission Neutron Spectrum of* ^{235}U. Physics Review, 103: 662.

DÖRSCHEL, B, SCHURICHT, V, & STEUER, J. 1996. *The Physics of Radiation Protection.* Ashford, Kent: Nuclear Technology Publishing. ISBN 1 870965 42 6.

♥DUPREE SA & FRALEY SK. 2001. *A Monte Carlo Primer: A Practical Approach to Radiation Transport.* Springer.

♥DUPREE SA & FRALEY SK. 2004. *Monte Carlo Primer: Volume 2.* Springer.

♥DUDERSTADT, JJ & HAMILTON, LJ. 1976. *Nuclear Reactor Analysis.* New York: Wiley. 650 p. ISBN 0-471-22363-8.

FERRARI & PELLICCIONI. 1998. *Fluence to Dose Equivalent Conversion Data and Effective Quality Factors for High Energy Neutrons.* Radiation Protection Dosimetry, Vol. 76, No. 4, pp. 215 – 224.

FISHMAN, G. 2003. *Monte Carlo.* Springer.

♥GLASSTONE, S & SESONKE, A. 1994. *Nuclear Reactor Engineering.* New York: Van Nostrand. 805 p. ISBN 0-442-30449-8.

GOORLEY, T (ed.). 2004. *MCNP Criticality Primer II: Criticality Calculations with MCNP5: A Primer.* Los Alamos National Laboratory, X-5. Report LA-UR-04-0294.

♥HENRY, AF. 1975. *Nuclear Reactor Analysis.* Cambridge, Massachusetts: MIT Press. 547 p. ISBN 0-262-08081-8.

IAEA. 1988. *Radiological Safety Aspects of the Operation of Proton Accelerators.* Vienna: International Atomic Energy Agency. Technical Reports Series No. 283. ISBN 92-0-125188-2.

ICRP. 2007. *The 2007 Recommendations of the ICRP.* Annals of ICRP, Publication 103, Elsevier.

ICRP. 2010. Conversion Coefficients for Radiological Protection Quantities for External Radiation Exposures. ICRP Publication 116, Annals of the ICRP 40 (2–5).

♥JAEGER, RG, ed. 1968. *Engineering Compendium on Radiation Shielding. Volume I: Shielding Fundamentals and Methods.* New York: Springer-Verlag. 537 p.

♥JAEGER, RG, ed. 1975. *Engineering Compendium on Radiation Shielding. Volume II: Shielding Materials and Design.* New York: Springer-Verlag. 436 p.

♥JAEGER, RG, ed. 1970. *Engineering Compendium on Radiation Shielding. Volume III: Shield Design and Engineering.* New York: Springer-Verlag. 478 p.

KINNO, M; KIMURA, K & NAKAMURA, T. 2002. *Raw Materials for Low-Activation Concrete Neutron Shields.* Journal of Nuclear Science and Technology, Volume 39, No. 12, p. 1275 – 1280 (December 2002).

KNOLL, GF. 2010. *Radiation Detection and Measurement.* 4th edition. Wiley. 860 p. ISBN-10: 0470131489, ISBN-13: 978-0470131480.

MADLAND, DG. 1982. *New Fission Neutron Spectrum Representation for ENDF.* Report LA-9285-MS (ENDF-321). Los Alamos: Los Alamos National Laboratory. 21 p.

MADLAND, DG. 1988. *Improved Calculation of the Prompt Fission Neutron Spectrum from the Spontaneous Fission of ^{252}Cf.* (In Proceedings of the International Conference on Nuclear Data for Science and Technology, May & June 1988, Mito, Japan. CONF-880546-10.

MADLAND, DG. 1988. *Theory of Neutron Emission in Fission.* (In The proceedings of the American Nuclear Society Conference, "Fifty Years with Nuclear Fission," April 26-28. CONF-8804213-2. Los Alamos: Los Alamos National Laboratory.

MADLAND, DG. & NIX, J.R. 1982. *New Calculation of Prompt Fission Neutron Spectra and Average Prompt Neutron Multiplicities.* Nuclear Science and Engineering, 81: 213-271.

MÄRTEN, H. 1988. *Theoretical Models and Computer Programs for the Calculation of Prompt Fission Neutron Spectra.* (In Proceedings of an Advisory Group on Nuclear Theory for Fast Neutron Nuclear Data Evaluations, held in Beijing, China, 12-16 October 1987. Vienna, Austria: IAEA. p. 148-160.)

MÄRTEN, H. & SEELIGER, D. 1985. *Measurement and Theoretical Calculation of the ^{252}Cf Spontaneous-Fission Spectrum.* (In Proceedings of an International Conference on Nuclear Standard Reference Data, Geel, Belgium. Vienna: IAEA. p. 255-261.)

MÄRTEN, H, RICHTER, D & SEELIGER, D. 1985. *On the Mechanism of Fission Neutron Emission.* (In Proceedings of the XV-th International Symposium on Nuclear Physics. Dresden: Akademie der Wissenschaften der DDR. p. 1-17.)

MCNPX Version 2.6.0 USER'S MANUAL. 2008. Report LA-CP-07-1473. MCNPX Version 2.6.0. Pelowitz, DB editor.

PÁZSIT. 1992. A simple derivation of the neutron transport equation. *Nuclear Science & Engineering*: **112**, 369–374 (1992)).

RYDER R. 1982. *Neutron production from proton and deuterons.* Daresbury Laboratory, Technical Memorandum DL/NUC/TM 60A, Daresbury, UK. **www.srs.ac.uk**

RSICC CCC-746. 2011. *MCNPX 2.7.0: Monte Carlo All-Particle Transport Code System and MCNPDATA.* Radiation Safety Information Computational Center, Oak Ridge National Laboratories, USA.

SHULTIS KJ & FAW, ER. 2000. *Radiation Shielding.* American Nuclear Society.

♥SHULTIS JK & FAW RE. 2006. *An MCNP Primer.*

VAN ROOYEN, TJ. 2004. *Protection of Electronic Apparatus against Damage by Ionising Radiation.* iThemba LABS, PO Box 722, Somerset West, 7129.

WALSH, R.L. 1989. *Spin-Dependent Calculation of Fission Neutron Spectra and Fission Spectrum Integrals for Six Fissioning Systems.* Nuclear Science and Engineering, 102: 119-133.

WATT, B.E. 1952. *Energy Spectrum of Neutrons from Thermal Fission of* ^{235}U. Physical Review, 87: 1037.

□